Dissertation zur Erlangung des Doktorgrades
der Fakultät für Chemie und Pharmazie
der Ludwig-Maximilians-Universität München

Synthesis, Characterization and Quantum-Chemical Analysis of bent and linear $\{CoNO\}^8$ Nitrosyls

Jens Popp
aus
Celle, Deutschland

2023

Erklärung

Diese Dissertation wurde im Sinne von § 7 der Promotionsordnung vom 28. November 2011 von Herrn Prof. Dr. Peter Klüfers betreut.

Eidesstattliche Versicherung

Diese Dissertation wurde eigenständig und ohne unerlaubte Hilfe erarbeitet.

München, den 23.10.2023

Jens Popp

Dissertation eingereicht am: 03.11.2023

1. Gutachter: Prof. Dr. Peter Klüfers

2. Gutachter: Prof. Dr. Hans-Christian Böttcher

Mündliche Prüfung am: 28.11.2023

Table of Contents

List of Figures

List of Tables

List of Schemes and Equations

Schemes

Equations

Abbreviations

Arg	arginine
ATR	attenuated total reflection
BASF	batch scale factor
BCP	bond critical point
Bn	benzyl
calcd.	calculated
CASSCF	complete active space self-consistent field
cGMP	cyclic guanosine monophosphate
Cit	citrulline
CPCM	conductor-like polarizable continuum model
CShM	continous-shape measures
Cy	cyclohexyl
DCD	Dewar–Chatt–Duncanson model/event
DCM	dichloromethane
DFT	density-functional theory
DMSO	dimethyl sulfoxide
DNA	desoxyribonucleic acid
DNIC	dinitrosyl iron complex
EDTA	ethylenediaminetetraacetate
EFO	effective fragment orbital
EOS	effective oxidation state
equiv.	equivalent(s)
Et	ethyl
FMN	flavin mononucleotide
GC	guanylate cyclase
GS	ground state
HSAB	hard and soft Lewis acids and bases
^{i}Pr	isopropyl
IR	infrared
ISOR	isotropic restraint
L	ligand (uncharged)
M	metal center

m	medium (IR spectroscopy)
Me	methyl
NAD	nicotinamide adenine dinucleotide
NADP	nicotinamide adenine dinucleotide phosphate
NOHLA	N^{ω}-hydroxy-L-arginine
NOR	nitric oxide reductase
NOS	nitric oxide synthase
obs.	observed
OC-6	octahedron (hexacoordinated)
Ph	phenyl
PLI	photoinduced linkage isomerism
QTAIM	quantum theory of atoms in molecules
R	organic ligand residue, complex fragment (in dinuclear species)
RIJCOSX	'resolution of the identity' approximation – 'chain of spheres' algorithm
RNS	reactive nitrogen species
ROS	reactive oxygen species
s	strong (IR spectroscopy)
SARC	segmented all-electron relativistically contracted
SNP	sodium nitroprusside
SPY-5	square pyramid (pentacoordinated)
T-4	tetrahedron (tetracoordinated)
TBPY-5	trigonal bipyramid (pentacoordinated)
Tf	triflyl
TFVC	topological fuzzy Voronoi cells
THF	tetrahydrofuran
TZVP	triple-zeta valence polarization
TZVPP	triple-zeta valence with two sets of polarization functions
UV/Vis	ultraviolet/visible
vOC-5	vacant octahedron (pentacoordinated)
vs	very strong (IR spectroscopy)
vTBPY-4	vacant trigonal bipyramid (tetracoordinated)
vw	very weak (IR spectroscopy)
w	weak (IR spectroscopy)
X	anionic ligand, halogen atom, counterion
ZORA	zeroth-order regular approximation

Conventions

- The shape of the coordination compounds is described with the IUPAC polyhedral symbols.[1]

- All molecular structures are presented with the same ORTEP color code: boron (pearl), bromine (maroon), carbon (gray), chlorine (green), cobalt (pink), fluorine (turquoise), hydrogen (white), iodine (purple), nitrogen (blue), oxygen (red), phosphorus (orange), sulfur (yellow). Atoms of disordered moieties are depicted in lighter colors.

- The hydrogen bond pattern of the crystalline compounds is described with the decriptors $X_d^a(n)$ as defined by graph-set analysis.[2,3] The number of atoms (n) that are involved in the respective ring pattern *X* is specified in parentheses. The number of hydrogen bond acceptors (a) is denoted as superscript and the number of hydrogen bond donors as subscript (d).

Overview of ligands and their abbreviations

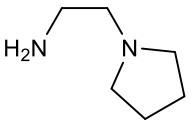

2-aepyrr

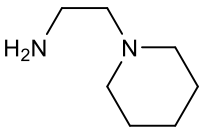

2-aepip

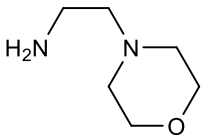

2-aemor

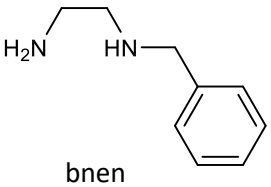

bnen

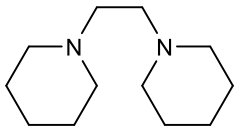

dpipe

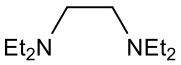

teen

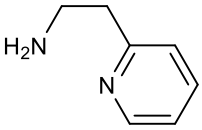

2-aepy

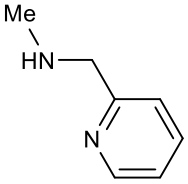

mampy

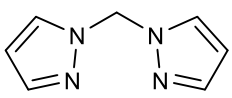

bpm

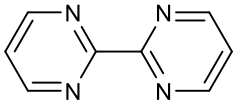

bpym

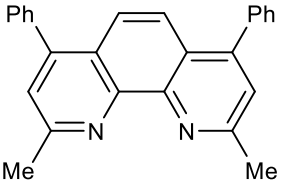

dmdpphen

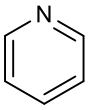

py

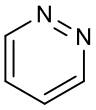

pydz

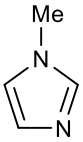

mim

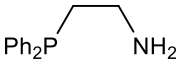

2-aedpp

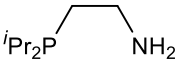

2-aedip

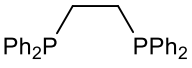

dppe

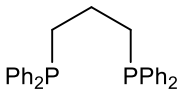

dppp

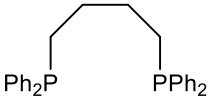

dppb

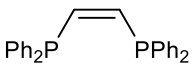

dppv

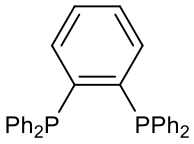

dppbz

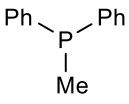

PMePh$_2$

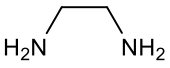

en

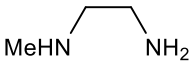

men

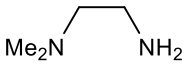

N,*N*-dmen

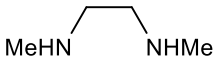

N,*N*′-dmen

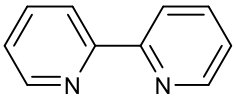

bpy

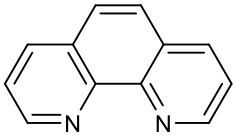

phen

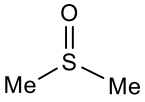

dmso

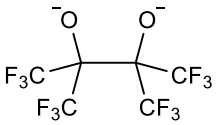

fpin

Molecular counterions:

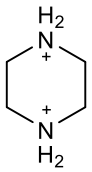

$ppzH_2^{2+}$

Names of all abbreviated ligands and ions mentioned in this work

acac	acetylacetonate
2-aedip	(2-aminoethyl)diisopropylphosphane
2-aedpp	(2-aminoethyl)diphenylphosphane
2-aemor	*N*-(2-aminoethyl)morpholine
2-aepip	*N*-(2-aminoethyl)piperidine
2-aepy	2-(2'-aminoethyl)pyridine
2-aepyrr	*N*-(2-aminoethyl)pyrrolidine
bpdap	bis((2-pyrrolyl)methylidene)-1,3-diaminopropane
bme-dach	*N*,*N*'-bis(2-mercaptoethyl)-1,4-diazacycloheptane
bnen	*N*-benzylethylenediamine
bpm	bis(1-pyrazolyl)methane
bpy	2,2'-bipyridine
bpym	2,2'-bipyrimidine
diars	1,2-bis(dimethylarsino)benzene
dmdpphen	2,9-dimethyl-4,7-diphenyl-1,10-phenanthroline
N,*N*-dmen	*N*,*N*-dimethylethylenediamine
N,*N*'-dmen	*N*,*N*'-dimethylethylenediamine
dmgH	*N*,*N*'-dimethylglyoximate (monoanion)
dmpe	1,2-bis(dimethylphosphino)ethane
dmphen	2,9-dimethyl-1,10-phenanthroline
dmso	dimethyl sulfoxide
doen	3,8-dimethyl-4,7-diazadeca-3,7-diene-2,9-dionedioximate (dianion)
dpipe	1,2-dipiperidinoethane
dppa	bis(diphenylphosphino)amine
dppb	1,4-bis(diphenylphosphino)butane
dppbz	1,2-bis(diphenylphosphino)benzene
dppe	1,2-bis(diphenylphosphino)ethane
dppp	1,3-bis(diphenylphosphino)propane

dppv	*cis*-1,2-bis(diphenylphosphino)ethene
edta	ethylenediaminetetraacetate (tetraanion)
en	ethylenediamine
esal	*N*-ethylsalicylideneiminate
fpin	perfluoropinacolate (dianion)
mampy	*N*-methyl-2-(aminomethyl)pyridine
mdtc	*N*,*N*-dimethyldithiocarbamate
men	*N*-methylethylenediamine
mim	*N*-methylimidazole
$ppzH_2^{2+}$	piperazinium (dication)
py	pyridine
pydz	pyridazine
tacn	1,4,7-triazacyclononane
tc	tropocoronand (dianion)
teen	*N*,*N*,*N*′,*N*′-tetraethylethylenediamine
tmc	*N*,*N*′,*N*′′,*N*′′′-tetramethylcyclam
tmen	*N*,*N*,*N*′,*N*′-tetramethylethylenediamine
tpp	tetraphenylporphyrinate (dianion)
trmen	*N*,*N*,*N*′-trimethylethylenediamine

Overview of numbered compounds

Classes 1–3: Perfluoropinacolatocobalt nitrosyls

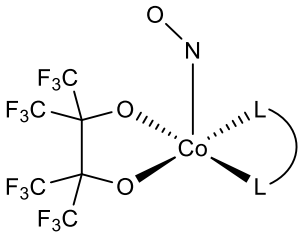

[Co(fpin)(L)(NO)]

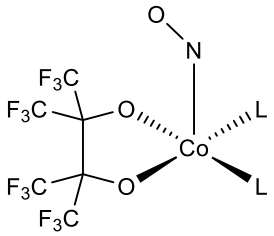

[Co(fpin)(L)$_2$(NO)]

1

a [Co(2-aepyrr)(fpin)(NO)]

b [Co(2-aepip)(fpin)(NO)]

c [Co(2-aemor)(fpin)(NO)]

d [Co(bnen)(fpin)(NO)]

e [Co(dpipe)(fpin)(NO)]

f [Co(fpin)(NO)(teen)]

g [Co(2-aepy)(fpin)(NO)]

h [Co(fpin)(mampy)(NO)]

i [Co(bpm)(fpin)(NO)]

j [Co(bpym)(fpin)(NO)]

k [Co(dmdpphen)(fpin)(NO)]

l [Co(fpin)(NO)(py)$_2$]

m [Co(fpin)(NO)(pydz)$_2$]

n [Co(fpin)(mim)$_2$(NO)]

2

a [Co(2-aedpp)(fpin)(NO)]

b [Co(2-aedip)(fpin)(NO)]

3

a [Co(dppe)(fpin)(NO)]

b [Co(dppp)(fpin)(NO)]

c [Co(dppb)(fpin)(NO)]

d [Co(fpin)(NO)(PMePh$_2$)$_2$]

Class 4: *trans*-Bis(diamine)cobalt nitrosyls

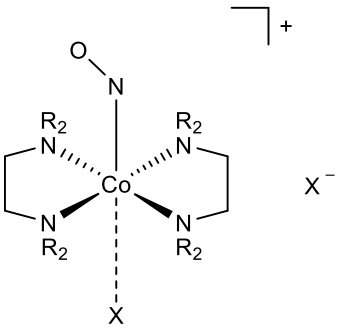

trans-[Co(NO)(R-en)$_2$(X)]X

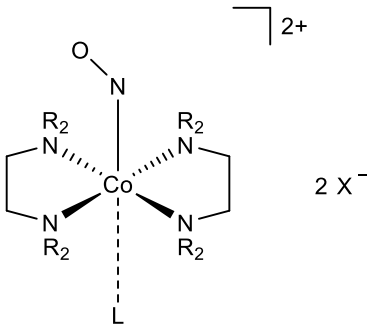

trans-[Co(L)(NO)(R-en)$_2$]X$_2$

4

a *trans*-[Co(ClO_4)(en)$_2$(NO)]ClO_4

b *trans*-[CoCl(en)$_2$(NO)]Cl

c *trans*-[Co(en)$_2$I(NO)](ClO_4)$_{0.6}$I$_{0.4}$

d *trans*-[Co(en)$_2$(NO)(NO_3)]NO_3

e *trans*-[Co(BF_4)(en)$_2$(NO)]BF_4

f *trans*-[Co(dmso-κ*O*)(en)$_2$(NO)](ClO_4)$_2$

g *trans*-[Co(ClO_4)(men)$_2$(NO)]ClO_4

h *trans*-[Co(ClO_4)(*N*,*N*-dmen)$_2$(NO)]ClO_4

i *trans*-[Co(BF_4)(*N*,*N*-dmen)$_2$(NO)]BF_4

j *trans*-[Co(ClO_4)(*N*,*N*′-dmen)$_2$(NO)]ClO_4

k *trans*-[Co(BF_4)(*N*,*N*′-dmen)$_2$(NO)]BF_4

l *trans*-[Co(bnen)$_2$(NO)(NO_3)]NO_3

Classes 5+6: Bis(diphosphane)- and dihalogenidodiphosphane-cobalt nitrosyls

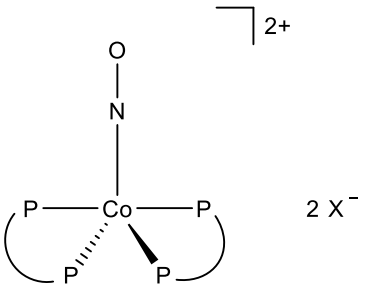

$[Co(L)_2(NO)]X_2$

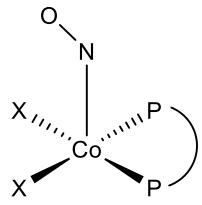

$[Co(L)(NO)(X)_2]$

5

a $[Co(dppe)_2(NO)](ClO_4)_2$

a' $[Co(dppe)_2(NO)](BF_4)_2$

b $[Co(dppa)_2(NO)](ClO_4)_2$

c $[Co(dppv)_2(NO)](ClO_4)_2$

c' $[Co(dppv)_2(NO)](BF_4)_2$

d $[Co(dppbz)_2(NO)](ClO_4)_2$

6

a $[CoCl_2(dppe)(NO)]$

a' $[CoBr_2(dppe)(NO)]$

b $[CoCl_2(dppp)(NO)]$

c $[CoCl_2(dppv)(NO)]$

c' $[CoBr_2(dppv)(NO)]$

d $[CoCl_2(dppbz)(NO)]$

d' $[CoBr_2(dppbz)(NO)]$

Class 7: Further cobalt nitrosyls and hyponitrite complexes

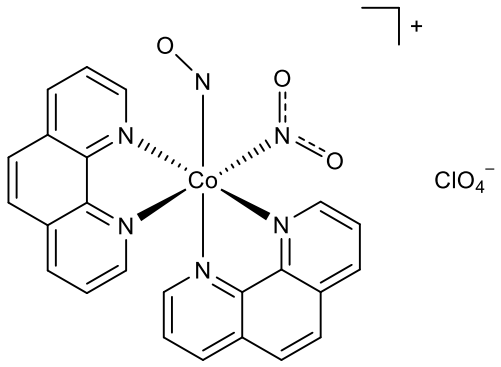

+ Λ enantiomer

rac-cis-[Co(NO)(NO_2-κ*N*)(phen)$_2$]ClO_4

7a

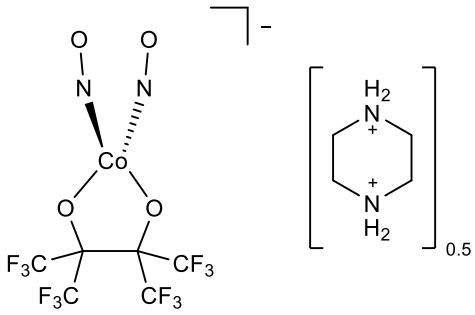

$(ppzH_2)_{0.5}$[Co(fpin)$(NO)_2$]

7b

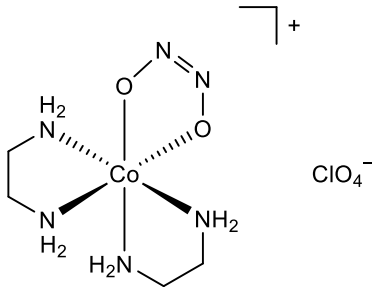

+ Λ enantiomer

rac-[Co(en)$_2$(*cis*-N_2O_2-κ^2*O*,*O*′)]ClO_4

7c

1 Introduction

Nitric oxide is a compound with a checkered history. For a long time, it was regarded only as an air pollutant, being involved in the formation of acid rain,[4–7] various types of cancer[8,9] and contributing to the depletion of the ozone layer.[10–13] In the late 1970s, the biological relevance of nitric oxide was discovered. It was found to play a role in a variety of physiological processes, acting as a blood-pressure regulator[14,15] and secondary messenger.[16,17] Furthermore, it was found to be involved in the human immune system,[18–20] exhibiting antimicrobial and even tumoricidal activity.[21–23] These findings led to a revival of the compound in scientific research. Due to its significance, nitric oxide was declared ''molecule of the year'' by *Science* magazine in 1992,[24,25] followed by the founding of the ''Nitric Oxide Society'' in 1996 in order to promote research on this compound in all academic fields.[26] In 1998, Furchgott, Ignarro and Murad were awarded the Nobel Prize in Physiology or Medicine ''for their discoveries concerning nitric oxide as a signalling molecule in the cardiovascular system''.[27]

1.1 General properties of nitric oxide

Formed in a highly endothermic reaction, nitric oxide represents the simplest oxide of nitrogen. Large amounts of nitric oxide are produced as an intermediate in the Ostwald process, the most common industrial method for the synthesis of nitric acid from ammonia. For laboratory use, several synthetic routes are known, most of them involving the reduction of nitrite in the presence of acid. NO of high purity can be generated by reacting sodium nitrite with iodide or iron(II) salts in sulfuric acid.[28]

$$N_2 + O_2 \rightleftarrows 2NO \qquad \Delta_r H^{\ominus} = 180.62\ \mathrm{kJ\,mol^{-1}}$$

Scheme 1.1: Reaction of nitrogen and oxygen to nitric oxide.[28]

In life sciences, NO adducts of amino acids, such as *S*-nitrosocysteine, as well as nitrosamine compounds such as *N*-nitrosopyrrolidine are used as a nitric oxide source for biochemical experiments.[29,30] At room temperature, the compound is a colorless gas and highly toxic despite its poor water solubility ($1.93–1.95 \times 10^{-6}\ \mathrm{mol\,cm^{-3}\,atm^{-1}}$), the latter being due to its low dipole moment of $5.29 \times 10^{-31}\ \mathrm{C\,m}$.[31,32] On contact with air, it reacts immediately to NO_2, recognizable by the formation of brown fumes. With halogens, it forms products of the composition NOX, such as nitrosyl chloride (NOCl).[28] Because of its odd number of fifteen electrons, nitric oxide is a free radical. It is best described by the resonance structures depicted in Scheme 1.2.

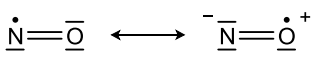

Scheme 1.2: Resonance structures of nitric oxide.[28]

As in the molecular orbital (MO) diagram in Figure 1.1, the unpaired electron is located in one of the two degenerate 1π* orbitals. The 2σ (HOMO−1) and 1π* (HOMO) frontier orbitals can be used to form bonding and antibonding interactions with d orbitals of transition metals, leading to a stabilization of said electron in the resulting metal nitrosyl complexes. In the case of the 2σ orbital, a σ-type bond with the metal's symmetrically matching e orbitals can be formed. The two 1π* orbitals each can form a π bond with the t_2 orbitals of the metal center. Due to the larger lobes of the relevant MOs being located on the nitrogen atom, the nitrosyl ligand usually coordinates via the κN-binding mode under normal conditions.[33]

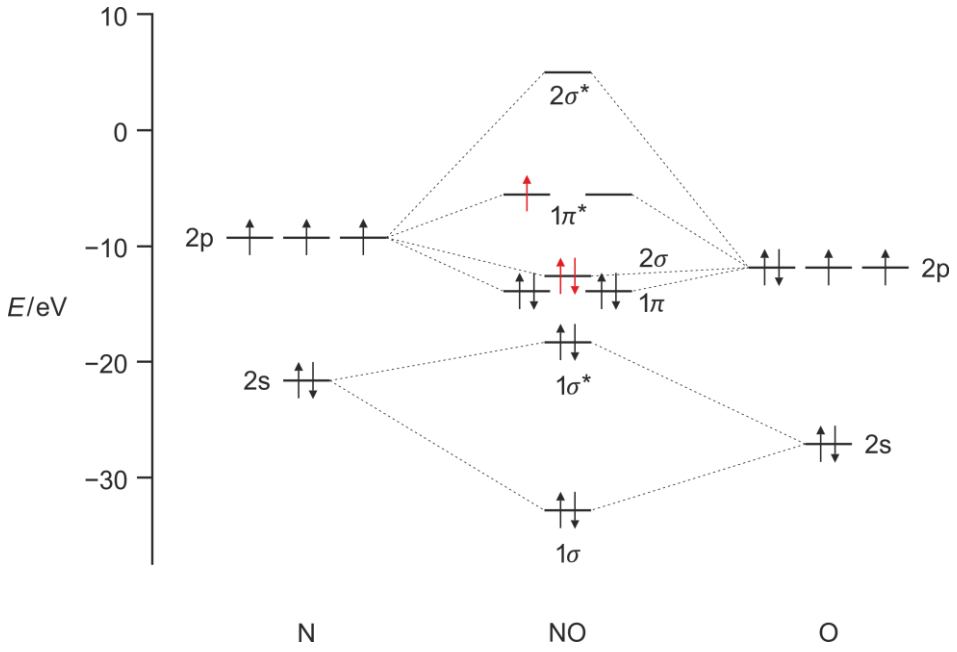

Figure 1.1: Molecular orbital (MO) diagram of nitric oxide, adopted from Ref.[33]. The α- and β-spin electrons are symbolized by up- and down-arrows, respectively. Electrons involved in the formation of dative bonds to the metal center are highlighted in red. As an alternative numbering, the MOs shown in the diagram are also commonly labeled (in order of increasing energy) as 1σ, 2σ, 1π, 3σ, 2π and 4σ.

Due to its radical character, nitric oxide is a highly reactive species. When coordinating to a metal, it can either be oxidized to the nitrosonium cation NO^+ or reduced to the nitroxyl anion NO^-. Both ions are isoelectronic with several species of high relevance in coordination chemistry: NO^+ is isoelectronic with N_2, CO and CN^-, while NO^- is isoelectronic with O_2. Uncharged $NO^\bullet$ can be considered isoelectronic with O_2^+.[34] This redox activity, together with the fact that the oxidation states of the metal center and the nitrosyl ligand cannot be determined unequivocally by direct physical measurement, lead to nitric oxide being referred to as a so-called ''non-innocent ligand''. This means that for a given MNO moiety, it is not possible to determine whether this entity exists as $M–NO^0$, $M^-–NO^+$ or $M^+–NO^-$ in the complex.[35–37] To overcome this problem, Enemark and Feltham introduced a notation in which the nitrosyl complex is described as an $\{M(NO)_x\}^n$ fragment, with *x* being the number of NO ligands binding to the metal and *n* the sum of the metal's d electrons and 1π* electrons of the nitrosyl ligand.[38] Besides

the different oxidation states, terminally bonded nitric oxide can also adapt various bond angles relative to the metal center. Prior to this work, as a general consensus, it became common to assign linearly bonded nitric oxide as $^{1}NO^{+}$ and strongly bent (around 120°) as $^{1}NO^{-}$, regardless of the coordinating metal and its electronic configuration. For the former, this is based on the notion that, due to its isoelectronicity with carbon monoxide, NO^{+} enables π backbonding to the metal center and, thus, will favor a linear coordination. Hence, with more obtuse angles, other oxidation states such as $^{2}NO^{0}$ (bond angles around 140°) and $^{3}NO^{-}$ (160°–180°) are expected.[34,39] Spectroscopic and structural characteristics can be used in order to gain insights into the electronic state of nitrosyl complexes. More precisely, the infrared band of the N–O stretching vibration, the M–N and N–O bonds as well as the M–N–O bond angle provide information for determining the nitrosyl binding mode.[34] Since the structural data are usually obtained by X-ray crystallography, there is often a need for suitable crystallization methods in addition to the usual development of new synthetic methods for obtaining novel compounds. As can be seen in Figure 1.2, according to the consensus mentioned above, the geometry of the MNO fragment determines the binding interactions that occur: In a linear entity, a σ bond is generated due to the donation of electron density from the nitrosyl ligand's 2σ orbital into the d_{z^2} orbital of the metal. In addition to this σ basicity, the $1\pi^*$ orbitals can act as electron donors or acceptors with the matching d_{xz} and d_{yz} orbitals, forming either two π bonds or, in the case of a bent MNO moiety, one π interaction and one σ bond with a strong d_{z^2} participation of the metal. For complex species consisting of NO^{+} linearly bound to an electron-rich metal center, the nitrosyl ligand also acts as a π acid, causing strong backdonation from the metal atom's d_{xz} and d_{yz} orbitals into the ligand's $1\pi^*$ orbitals.[34,38,39]

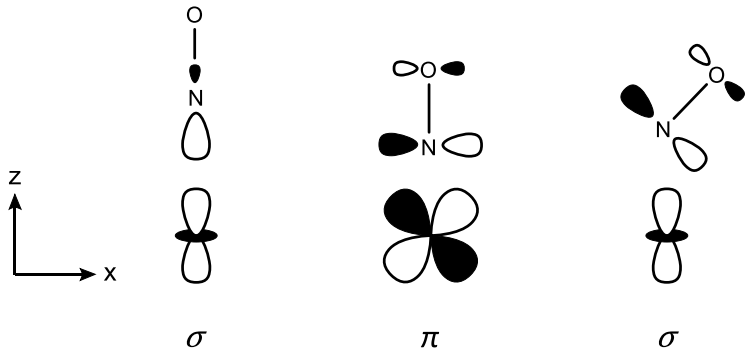

Figure 1.2: Possible interactions involved in metal-nitrosyl bonding. **Left:** σ bond ($2\sigma + d_{z^2}$), **middle:** π bond(s) ($1\pi^*_{xz} + d_{xz}$ and $1\pi^*_{yz} + d_{yz}$). These bonds and the previously mentioned σ interaction apply to a linear MNO moiety. **Right:** σ bond ($1\pi^*_{yz} + d_{z^2}$) in a bent MNO moiety.[34,38,39]

Although most known nitrosyl complexes contain terminally bonded NO, compounds with one or more nitrosyl ligands bridging up to three metal centers have been discovered as well.[40,41] While the NO entity usually binds via the nitrogen atom to the metal center, some nitrosyl complexes have shown the ability to change to κO (isonitrosyl)- or $\kappa^2 N,O$ (side-on)-binding mode upon irradiation with light in

the range of 350 nm to 580 nm.[42,43] If metastable below a certain temperature, these excited states can be observed using IR spectroscopy, differential scanning calorimetry, and even photocrystallography.[44,45] This phenomenon, called photoinduced linkage isomerism (PLI), was first detected for sodium nitroprusside (SNP), $Na_2[Fe(CN)_5(NO)]\cdot 2H_2O$.[46,47] Following this discovery, other metal nitrosyl complexes with Ru, Os, Mo, Ni and Pt were also found to show this behavior.[48,49] Since the linkage isomers of a PLI-active compound differ in their absorptive properties and photorefractive characteristics, such complexes have been considered candidates for new forms of information storage and other optical applications.[50]

1.2 Biological relevance and pharmacology of nitric oxide

As mentioned earlier, besides its image as an air pollutant and use in inorganic chemistry, nitric oxide was also found to be of significant biological relevance. Initially, it was recognized only as a signaling molecule in the cardiovascular system of mammals.[51–53] Produced in endothelial cells by NO synthases (NOS), nitric oxide is generated enzymatically via oxidation of L-arginine to L-citrulline (Scheme 1.3).[54] In this context, the NO released in blood vessels activates guanylate cyclase (GC), causing it to produce cyclic guanosine monophosphate (cGMP). This in return initiates the relaxation of the surrounding smooth muscle tissue, subsequently increasing the blood flow and lowering vascular pressure. This mechanism of action also provided an explanation for the long known vasodilatative action of heart medications such as sodium nitroprusside as well as organic nitro and nitrate compounds such as amyl nitrite and nitroglycerin. While SNP was shown to directly liberate NO in solution, the latter first react with SH groups to *S*-nitrosothiols which then decompose under release of nitric oxide.[53] By nitrosylating thiol groups in enzymes and other proteins, nitric oxide can regulate their activity and function. Like its role as a vasodilatator, it was later found that this mechanism is not limited to the cardiovascular system, but also occurs in brain tissues.[55] Being a radical in its free, neutral form, NO can also act as an antioxidant, scavenging other harmful radicals such as reactive oxygen species (ROS). As such, it was found to terminate chain reactions that occur during lipid peroxidation (the breakdown of lipids by ROS that cause damage to the cell membrane).[56] However, it should be noted that besides these beneficial functions, the role of nitric oxide in biological systems is not just purely positive, but rather double-edged. Being a reactive species itself due to its radical character, nitric oxide is also capable of causing oxidative stress and damage to cells. It can react with superoxide radicals ($O_2^{\bullet -}$) to form peroxynitrite ions (ONO_2^-) which can damage lipids, proteins and DNA bases, provoking cell death by necrosis. In addition, peroxynitrite is also able to induce apoptosis via caspase activation.[57] Moreover, the use of NO as a vasodilatating drug can come with drawbacks as well: When inhaled, it coordinates to hemoglobin, oxidizing the iron(II) center to iron(III) in the process. The resulting methemoglobin cannot carry oxygen, therefore reducing its overall availability in the body and creating

severe complications. The application of gaseous NO is primarily used for the treatment of pulmonary hypertension in neonates, where usual dosages of up to 40 ppm have been found to create significant levels of methemoglobin in the blood, making nitric oxide therapy the subject of ongoing research.[58]

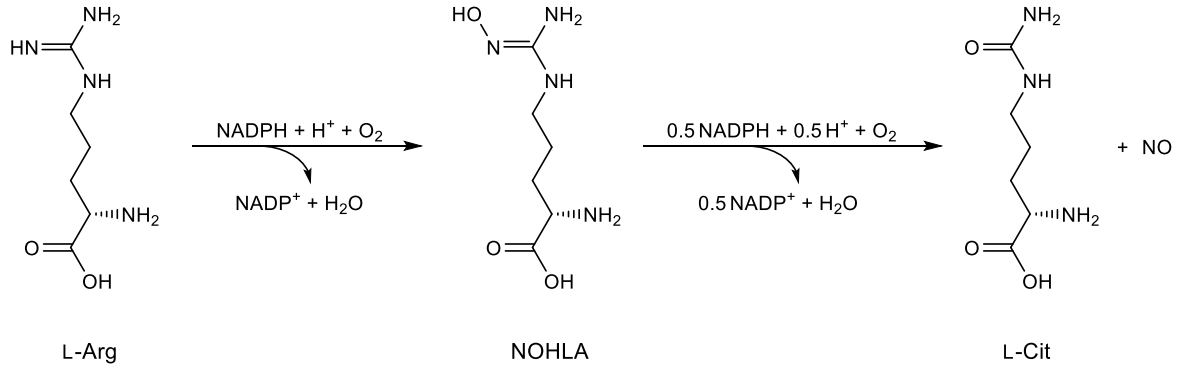

Scheme 1.3: Endogenous synthesis of NO catalyzed by nitric oxide synthase (NOS): oxidation of L-arginine (L-Arg) to L-citrulline (L-Cit) with N^{ω}-hydroxy-L-arginine (NOHLA) as intermediate.[54]

This dual behavior of NO was also observed for its role in immune response. Under resting conditions, it was found to act as an anti-inflammatory agent by initiating a negative feedback loop that suppresses cytokine production.[59] On the other hand, activated macrophages have been shown to produce NO in order to enhance chemokine production, therefore maintaining the inflammatory response. It is believed that the effect of nitric oxide on this response depends on its (spatial) concentration in the cell: low NO levels seem to promote inflammation, while high levels help to clear it.[60] This duality is also observed for the relationship between nitric oxide and cancer. Over the last two decades, plenty of evidence was found that NO plays a critical role in regulating the hallmarks of cancer. This means that the control and outcome of processes such as tumor growth, angiogenesis (development of blood vessels for its supply), metastasis and evasion of tumor apoptosis depend on the spatial and temporal concentration of nitric oxide as well as on its source. The compound initiates tumor-enhancing or -suppressing responses that are mediated by cGMP-dependent processes or protein modifications (such as *S*-nitrosylation or nitration). Other cancer hallmarks such as inflammation and genome instability are influenced as well.[61] In the latter case, NO reacts with superoxide or molecular oxygen to form reactive nitrogen species (RNS) that can deaminate bases of the DNA, causing potentially carcinogenic mutations.[62,63] The species generated in this process include nitrogen dioxide (NO_2) and dinitrogen trioxide (N_2O_3), the latter being formed by reaction with another equivalent of nitric oxide. As mentioned before, the reaction of NO with ROS can also lead to peroxynitrite, which, in turn, can form other RNS such as nitrite (by reaction with thiols) or nitrate (via CO_2-catalyzed isomerization with nitrosoperoxocarbonate $ONOOCO_2^-$ as an intermediate). Alternatively, peroxynitrite can be broken down by CO_2 into NO_2 and $CO_3^{\bullet -}$.[64,65] Deamination of a DNA base will result in the substitution of an amino group for a keto function, transforming cytosine, adenine, guanine and 5-methylcytosine to uracil, hypoxanthine, xanthine and thymine, respectively.[62]

In addition to the abovementioned functions that nitric oxide performs in mammals, it also plays an important role in other organisms such as bacteria, plants or insects. For example, as a defense against microbes, mammalian macrophages treat the pathogens simultaneously with NO and H_2O_2. Upon reaction with metalloproteins in the cell membrane (mainly iron-sulfur clusters), nitric oxide is converted to nitrite and metal ions from the active site are released into the bacterium, where they react with hydrogen peroxide to yield ROS that can damage the microbial DNA.[66] Another defense mechanism uses NO to poison the bacterium's purine metabolism in order to prevent proliferation.[67] As a detoxifying strategy, many pathogenic species have developed nitric-oxide-reducing enzymes which catalyze the two-electron reduction of two NO equivalents to less toxic nitrous oxide (N_2O) and water (Scheme 1.4).[54] Other organisms such as denitrifying bacteria, archaea, some protozoa and fungi also use NO reductases (NOR) in their anaerobic breathing process.[68,69] The ability of some microorganisms to consume nitric oxide is also exploited in industry: In the so-called BioDeNOx process, nitrogen oxides (NO_X) are removed from fossil flue gases with the help of denitrifying bacteria. In order to scavenge nitric oxide from the waste gas, the exhaust is first treated with an aqueous solution of iron(II) chelates, with EDTA being the most commonly used ligand for this purpose. Complex species such as $[Fe(edta)]^{2-}$ bind nitric oxide very effectively and the resulting $[Fe(edta)(NO)]^{2-}$ is then subsequently processed into harmless N_2 in a bioreactor. However, since $[Fe(edta)]^{2-}$ can easily be oxidized to the corresponding iron(III) species by O_2 from the flue gas, the bacteria need to be fed a substrate such as ethanol or glucose in order to regenerate the ferrous complex and sustain the process.[33,70] In a modification of the procedure, the bioreactor is replaced with a chemical one so that the collected NO can be used to synthesize useful chemical products such as, for example, oximes.[71]

$$2NO + 2e^- + 2H^+ \xrightarrow{NOR} N_2O + H_2O$$

Scheme 1.4: Two-electron reduction of NO to nitrous oxide (N_2O) catalyzed by nitric oxide reductase (NOR). The different classes of NORs use various co-factors as electron source, including NADH, NADPH and $FMNH_2$.[33]

However, nitric oxide does not always pose a threat to bacteria. Recently, the bacterium *Kuenenia stuttgartiensis* was found to grow on NO by coupling anaerobic ammonium oxidation (anammox) with nitric oxide reduction. Anammox species usually couple the reduction of nitrite with ammonium oxidation, resulting in the formation of nitrate and molecular nitrogen with nitric oxide and hydrazine as intermediates. However, by using the process mentioned above, *K. stuttgartiensis* can grow without nitrite and produces only N_2.[72] Since anammox bacteria have been estimated to be responsible for about 50 % of all atmospheric dinitrogen emissions, nitric oxide represents an important intermediate in this process of the biological nitrogen cycle.[73] The other major process involving NO in this context is the transformation of nitrite to N_2 by denitrifying bacteria. The gaseous nitrogen generated by these two processes is then made accessible to plants by nitrogen-fixating soil bacteria.[74] In plants themselves, nitric oxide acts mainly against oxidative stress (e.g. ROS), but also as a signaling molecule.[75] As for the role of NO in insects, little research has been done compared to that on mammals, bacteria

and plants. So far, it was found to be involved in the immune response of some insect species. In addition, some blood-sucking insects such as bed- and kissing bugs were shown to use nitric oxide's vasodilatative effect in order to increase the blood flow in their host. When piercing into a vessel, they first inject nitrophorines in the blood. In these NO-loaded Fe^{III} heme proteins, nitric oxide is only weakly bound to the metal center, much more weakly than in analogous Fe^{II} heme enzymes such as GC or NOR. Moreover, the bond strength also depends on the pH: stored in the insect's glands at pH ≈ 5, NO binds about ten times more tightly to the ferric center than in the blood of the host at pH > 7. Hence, when injected, NO dissociates into the blood stream, causing the vessel to dilate.[76]

1.3 Structural and IR-spectroscopic properties of {CoNO}^{8} complexes

Most cobalt nitrosyls can be described as {CoNO}^{8} according to the Enemark–Feltham notation. Prior to this work, with the exception of just a few compounds, all of the so far structurally characterized complexes feature a distinctly bent CoNO moiety. Together with the often observed diamagnetic behavior, this led to low-spin d^6-cobalt(III) and $^1NO^-$ as predominant oxidation-state assignment for these species. While the largest subset of recorded crystal structures comprises metalloporphyrin complexes, such data were also collected for a variety of {CoNO}^{8} compounds with non-biological ligands.[77] Besides N_4-ligation as the most common environment, among others, coordination with oxygen, sulfur, phosphorus and arsenic ligands is known as well (see Figures 1.3 and 1.4). For complexes with $(N/O/S)_4$- and $N_2(O/S)_2$-ligation, a square pyramidal shape is usually found. In addition to this, also a few octahedral species such as $[Co(NO)(NH_3)_5]^{2+}$ and *trans*-$[Co(Cl/ClO_4)(en)_2(NO)]^+$ have been described. As a peculiarity, they show a significant *trans* effect, i.e. a much greater Co–L bond length for the ligand *trans* to NO compared to those in the equatorial plane.[78–80] In the case of the phosphorus and arsenic derivatives, a trigonal bipyramidal geometry is observed for most complexes. Moreover, linear Co–N–O angles close to 180° are found in some structures such as $[CoI_2(NO)(PMe_3)_2]$ and $[Co(diars)_2(NO)]^{2+}$ (see Table 1.1 for an overview). However, other {CoNO}^{8} species with P_2X_2- or As_4-ligation feature the bent nitrosyl moiety, but at an angle that is slightly more obtuse than the usual value. Examples include $[CoCl_2(NO)(PMe_3)_2]$ and *trans*-$[Co(diars)_2(NO)(SCN\text{-}\kappa N)]^+$.[81,82] Within the group of P_2X_2-derivatives, additional structural irregularities were discovered: the halogenido compounds $[Co(Br/Cl)_2(NO)(PMePh_2)_2]$ both show disorder of the nitrosyl ligand, with NO bonded linearly in the major disorder form of the bromido complex while coordinating at a more acute angle in the major form of the chlorido derivative.[83]

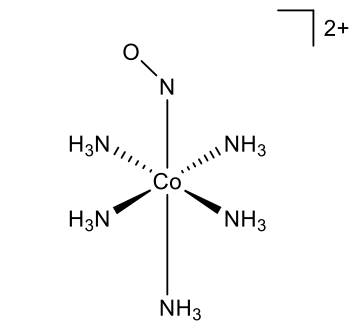

$[Co(NH_3)_5(NO)]Cl_2$

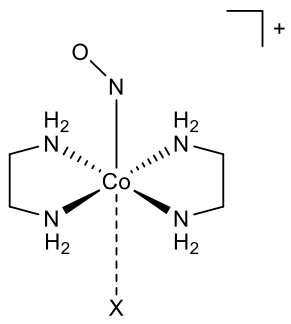

trans-$[Co(en)_2(NO)(X)]ClO_4$
X = ClO_4, Cl

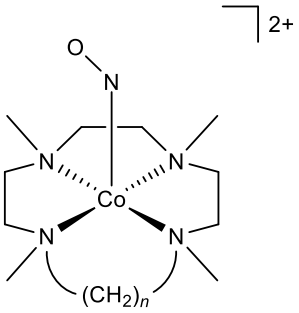

$[Co(NO)(12\text{-tmc})](ClO_4)_2$ $n = 2$
$[Co(NO)(13\text{-tmc})](ClO_4)_2$ $n = 3$

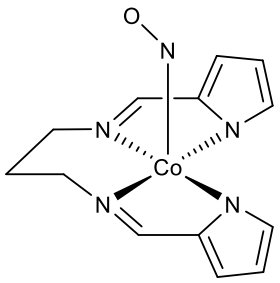

[Co(bpdap)(NO)]

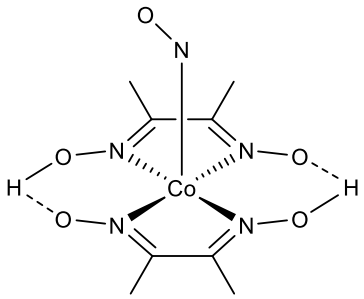

$[Co(dmgH)_2(NO)]$

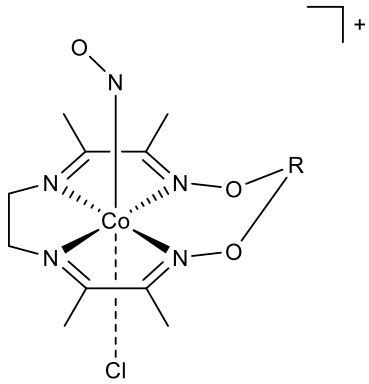

$[Cl(NO)Co(\mu\text{-doen})(R)]BPh_4$
R = $Mg(H_2O)(Me_3tacn)$

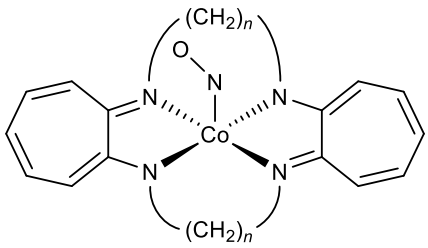

$[Co(tc\text{-}3,3)(NO)]$ $n = 3$
$[Co(tc\text{-}4,4)(NO)]$ $n = 4$

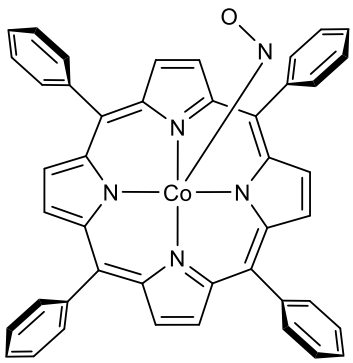

[Co(NO)(tpp)]

Figure 1.3: Overview of some structurally characterized $\{CoNO\}^8$ complexes with N_4-ligation. For clarity, the species are depicted without counterions and non-cobalt fragments. For references and information on structural and IR-spectroscopic parameters, see Table 1.1.

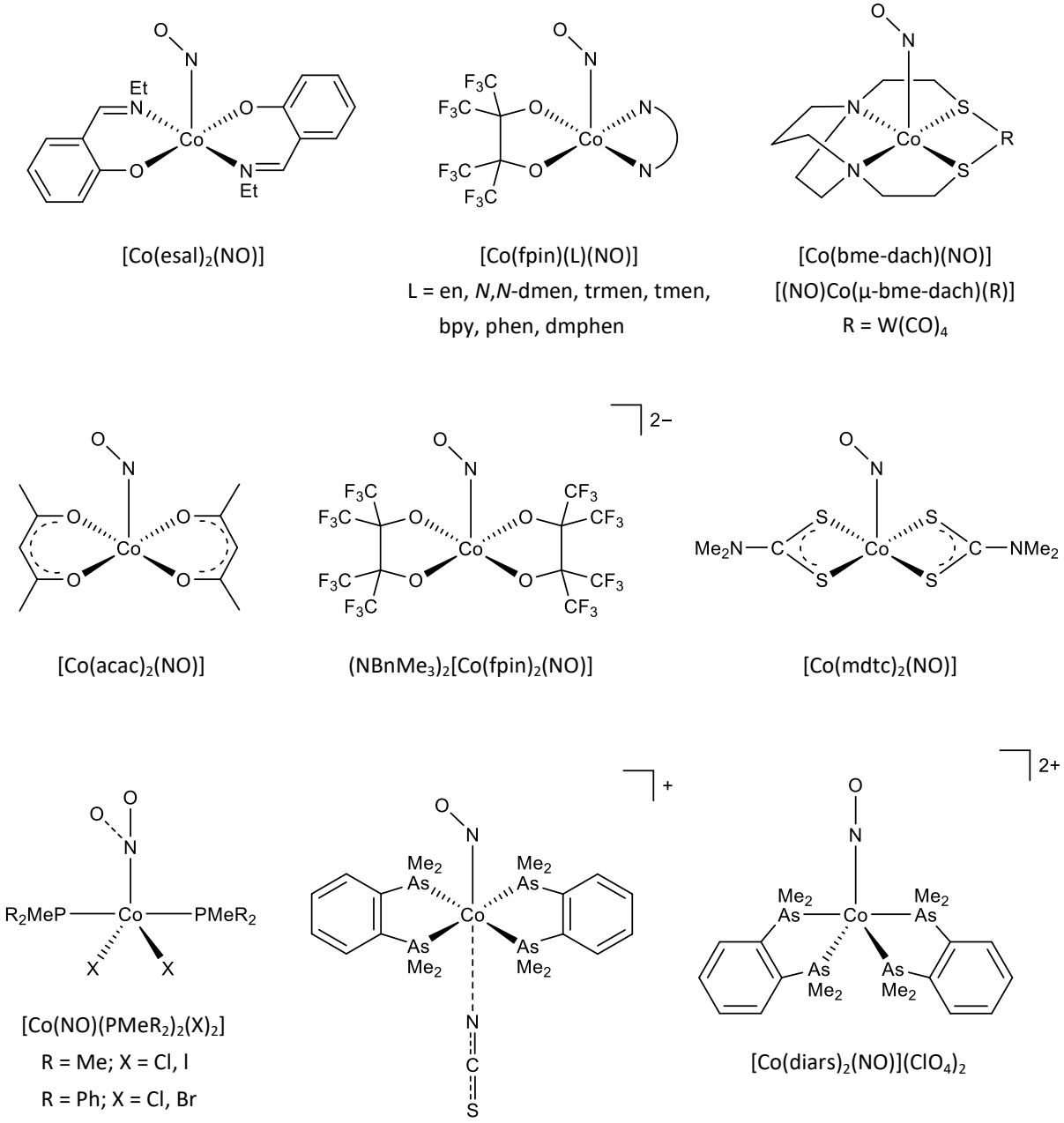

Figure 1.4: Overview of some structurally characterized $\{CoNO\}^8$ complexes with N_2O_2-, O_4-, N_2S_2-, S_4-, P_2X_2- or As_4-ligation. For clarity, the species are depicted without counterions and non-cobalt fragments. For references and information on structural and IR-spectroscopic parameters, see Table 1.1.

As for the infrared N–O stretching vibration of the nitrosyl ligand, a trend can be observed in that the vast majority of complexes with a strongly bent CoNO moiety comes at around 1600 cm^{-1} to 1700 cm^{-1} while species with a linear entity show nitrosyl stretches at slightly higher energies around 1770 cm^{-1} to 1850 cm^{-1} (see Table 1.1). However, it should be noted that data on (partly) linear $\{CoNO\}^8$ complexes is scarce, as only four such compounds have been crystallized to date.[81–83]

Table 1.1: X-ray and IR data of select structurally characterized $\{CoNO\}^8$ compounds.

	N–O/Å	Co–N/Å	∡Co–N–O/°	$\tilde{\nu}$/cm^{-1}	Ref.
$[Co(NH_3)_5(NO)]Cl_2$	1.154	1.871	119.0	1620 [d]	78,84
trans-$[Co(ClO_4)(en)_2(NO)]ClO_4$ [a]	1.15	1.805	122.7	1663 [e]	80,85
trans-$[CoCl(en)_2(NO)]ClO_4$	1.109	1.820	124.4	1611 [e]	79,85
$[Co(12\text{-}tmc)(NO)](ClO_4)_2$	1.155	1.7844	128.50	1712 [f]	86
[Co(bpdap)(NO)]	1.1551	1.7890	125.97	1645 [d]	87
$[Co(dmgH)_2(NO)]$ [b]	1.110	1.800	128.5	1641 [e]	88,89
$[Cl(NO)Co(\mu\text{-}doen)(R^1)]BPh_4$	1.149	1.856	122.1	1636 [g]	90
[Co(tc-3,3)(NO)]	1.137	1.785	127.3	1656 [d]	91
[Co(tc-4,4)(NO)] [a]	1.151	1.779	128.9	1584 [d]	91
[Co(NO)(tpp)] [a]	1.01	1.833	135.2	1689 [d]	92
$[Co(esal)_2(NO)]$	1.16	1.738	129	1645 [e]	93
[Co(*N*,*N*-dmen)(fpin)(NO)]	1.165	1.799	126.6	1667 [g]	94,95
[Co(fpin)(NO)(phen)]	1.161	1.825	122.1	1702 [g]	94,95
[Co(bme-dach)(NO)]	1.187	1.787	123.8	1603 [h]	96
$[(NO)Co(\mu\text{-}bme\text{-}dach)(R^2)]$	1.21	1.80	123.1	1638 [h]	96
$[Co(acac)_2(NO)]$	1.163	1.820	120.4	1675 [d]	97,98
$(NBnMe_3)_2[Co(fpin)_2(NO)]$	1.185	1.793	120.6	1638 [g]	95,99
$[Co(mdtc)_2(NO)]$ [a]	1.112	1.746	135.7	1630 [e]	100
$[CoCl_2(NO)(PMe_3)_2]$ [a,c]	0.88	2.00	129.0	1637, 1725 [e]	81
$[CoI_2(NO)(PMe_3)_2]$	1.024	1.706	179.6	1753 [e]	81
$[CoCl_2(NO)(PMePh_2)_2]$ [a,c]	1.106	1.721	156.9	1655, 1771 [h]	83
$[CoBr_2(NO)(PMePh_2)_2]$ [a,c]	1.055	1.706	171.9	1771, 1664 [h]	83
tr.-$[Co(diars)_2(NO)(SCN\text{-}\kappa N)]SCN$ [c]	1.18	1.87	132.3	1587, 1561 [i]	82
$[Co(diars)_2(NO)](ClO_4)_2$	1.16	1.68	178	1852 [i]	82

[a] Disorder of the nitrosyl ligand. The given structural data refers to the major disorder form.

[b] Structural values calculated as mean of three discrete entities in the unit cell.

[c] Split band of the NO vibration in the IR spectrum. The band with the higher relative intensity is listed first.

[d] KBr disk, [e] nujol mull, [f] MeCN solution, [g] ATR, [h] DCM solution, [i] nujol mull between KBr disks.

Non-cobalt fragments: R^1: $Mg(H_2O)(Me_3tacn)$, R^2: $W(CO)_4$.

1.4 Current perception of the bonding situation in {CoNO}^{8} species

The abovementioned interpretation of bent {CoNO}^{8} entities as Co^{III}–$^1NO^-$ pairs is a widely accepted consensus within the coordination chemistry community.[101–104] On the other hand, linear nitrosyls of transition metals are often found to resemble the shape of their carbonyl and cyanido counterparts, and since NO^+ is isoelectronic to CO and CN^-, a linear MNO moiety seems to reflect the binding of NO^+ as a typical σ-donor-π-acceptor ligand. However, the validity of this claim should be questioned for several reasons. First, cobalt(III) species were found to be almost exclusively octahedral for *N*/*O*-coordination, since only this geometry allows for a large ligand field stabilization energy of −24 Dq at maximum field splitting. An exception to this are complexes such as metalloporphyrins, in which the metal center is sterically shielded by a tetradentate ligand.[94] One explanation for the pentacoordination of {CoNO}^{8} nitrosyls involves the compounds *trans*-$[Co(Cl/ClO_4)(en)_2(NO)]ClO_4$ in which the ligand *trans* to NO binds to the metal at a distance that exceeds the usual Co^{III}–Cl/O bond lengths by about 0.3 Å. In this context, the *trans* influence of the $^1NO^-$ ligand as a strong σ-donor and weak π-acceptor is big enough to leave the sixth coordinating position unoccupied.[79,80] However, the structure of the perchlorato derivative suffers from a disorder of the nitrosyl ligand, which makes rationalization of its bonding situation difficult due to an unreliable Co–N–O bond angle and imprecisely determined Co–N and N–O distances. Other cases of disordered {CoNO}^{8} structures not allowing for a clear assessment of the nitrosyl bonding include compounds such as $[Co(NO)(NH_3)_5]Cl_2$, which was initially found to be linear, but in a more recent determination of the crystal structure proved to be bent with a fourfold disorder of the NO ligand.[78,105,106] Similar problems with disorder or unreliable ellipsoids of the nitrosyl ligand were encountered in the X-ray analyses of the phosphorus and arsenic complex species $[Co(Cl/I)_2(NO)(PMe_3)_2]$, $[Co(Br/Cl)_2(NO)(PMePh_2)_2]$ and $[Co(diars)_2(NO)](ClO_4)_2$, therefore leaving the very small class of linear {CoNO}^{8} compounds with no unambiguously solved crystal structure.[81–83] This represents the second point of criticism for the derivation of the nitrosyl ligand's charge from the Co–N–O angle: Most of the known {CoNO}^{8} crystal structures are poorly solved, thus leaving this general consensus on a speculative basis. As of 2021, there are fewer than two dozen well-defined structures of such compounds that allow for an in-depth discussion of the nitrosyl moiety's bonding situation.[94] The concept of unquestioningly categorizing all nitrosyl complexes with linearly- and bent bonded nitric oxide into NO^+ respectively NO^- was also extended to the IR analysis of such compounds. In the case of {CoNO}^{8}, nitrosyl stretching vibrations at lower wavenumbers in the range around 1600 cm^{-1} to 1700 cm^{-1} are assigned to Co^{III}–NO^- while IR stretches around 1800 cm^{-1} are associated with Co^{I}–NO^+.[101,102,104] Furthermore, this questionable mindset has also found its way into the instructions for determining the oxidation state of metal nitrosyls published a few years ago by the International Union of Pure and Applied Chemistry.[103,107,108]

1.5 Aim of this work

As was shown in Section 1.4, the assignment of charges and oxidation states in metal nitrosyl complexes based on the M–N–O bond angle or infrared nitrosyl stretch remains problematic, since this consenus is founded on the generalization that such compounds resemble the bonding situation of their related carbonyl and cyanido derivatives due to the isoelectronicity of their ligands. In the case of $\{CoNO\}^8$ compounds, there are only a few well-solved crystal structures that can be used as a reliable basis for discussing these issues. Therefore, the main goal of this thesis was to prepare and crystallize further bent and linear $\{CoNO\}^8$ complexes in order to provide well-solved crystal structures and analyze their bonding situation. For this purpose, the structures presented in this work all comply with a set of defined quality criteria: a) No, or at least well-solved disorder of the nitrosyl ligand (meaning that a disordered NO moiety can be refined anisotropically by splitting the position of nitrogen in order to generate two separate N–O entities); b) No unreliable ellipsoids that are either stretched along the N–O bond or largely expanded normal to this axis (the latter being an indicator for disorder of the oxygen atom); c) No unreliable N–O distances shorter than 1.10 Å. Together with the recorded IR nitrosyl stretches, the newly gained structural and spectroscopic data were used as input for quantum-chemical calculations on the compounds, including DFT structural optimization, QTAIM charge analysis and the assignment of effective oxidation states (EOS). Hence, the overall aim of this work was to re-assess the correlation between structure and bonding in $\{CoNO\}^8$ complexes based on more reliable crystallographic data and modern theoretical methods.

Severall compounds served as starting points for the synthesis of the novel cobalt nitrosyls presented in this work. Inspired by Riggenmann, who already succeeded in preparing a series of bent pentacoordinated $\{CoNO\}^8$ complexes with the composition [Co(fpin)(L)(NO)] that bear several diamines and *N*-heterocycles as co-ligands, a first objective was to extend this product class by creating further derivatives with other *N*-ligands, but using also phosphanes. The structurally similar $[Co(fpin)_2(NO)]^{2-}$ was recently shown by Klüfers *et al.* to not fit into the abovementioned framework, since it was found to be a Co^{I}–NO^{+} pair.[99] The class of hexacoordinated *trans*-$[Co(en)_2(NO)(X)]^{+}$ species, first synthesized by Feltham *et al.*,[85] should also be extended, not only by varying the diamine co-ligand, but also by incorporating other anionic and uncharged ligands in the position *trans* to NO. Another objective was the structural characterization of $[Co(L)_2(NO)]^{2+}$ compounds. Showing unusually high nitrosyl stretches at around 1800 cm^{-1} similar to the linear $[Co(diars)_2(NO)]^{2+}$ (1852 cm^{-1}),[82] these complexes have long been known to literature in bulk form, but could never be crystallized.[109] Finally, since the analysis of the monophosphane species $[Co(NO)(PR_3)_2(X)_2]$ has proven to be difficult due to the aforementioned occurrence of disorders and split nitrosyl bands,[81,83] the synthesis of new $\{CoNO\}^8$ products of the related type $[Co(L)(NO)(X)_2]$ with diphosphanes as co-ligands was attempted in order to gain a better insight into the bonding situation of this class of cobalt nitrosyls.

2 Results

2.1 Perfluoropinacolatocobalt nitrosyls with diamines and aromatic *N*-heterocycles as co-ligands

Crystalline $\{CoNO\}^8$ compounds with perfluoropinacolate and several nitrogen-bearing mono- and bidentate co-ligands (**1a–k**) were synthesized by using a modified procedure originally developed by Riggenmann:[94,95] In a Schlenk tube under an atmosphere of argon, cobalt(II) triflate was dissolved in a methanolic $(NBnMe_3)_2(fpin)$ stock solution followed by the addition of the respective co-ligand. All reagents were used in stoichiometric ratios. To assist dissolution, a certain amount of a polar organic solvent (MeOH, acetone or THF) was added. The argon atmosphere was then changed with gaseous nitric oxide, immediately turning the reaction mixture dark brown. Crystallization of the nitrosyl compounds was almost exclusively achieved by isothermal diffusion of the solvent into DMSO. For this purpose, the solution was transferred to one compartment of a two-chambered Schlenk tube, with the other chamber being filled with DMSO. The separating glass wall only extended to about half the length of the tube to allow for slow evaporation of the solvent. The batch was then stored under argon at room temperature. With some co-ligands, however, the solution of the respective nitrosyl complex will lose NO when stored under argon, which can be observed as a clearly visible brightening of the previously dark solution over the course of a few minutes. In such cases, the introduction of nitric oxide was carried out directly in the two-chambered Schlenk tube previously loaded with DMSO in order to enable crystallization under NO atmosphere. The single-crystalline nitrosyl compounds are obtained as brown blocks, platelets or needles within a few days, forming on the glass wall and / or in the mother liquor. They cannot be redissolved in common alcohols. Stored under argon, they are stable for several months. This even applies to the compounds that could only be crystallized under NO atmosphere.

The ability of some nitrosyl compounds to lose NO under inert gas atmosphere was further investigated. For this purpose, argon was bubbled at a defined rate through a freshly prepared solution of the complex for ten minutes while monitoring the brightening of the solution. It was found that those nitrosyls with co-ligands bearing *N*-heterocyclic aromatic systems would lose NO rapidly over a period of one to eight minutes, with considerable brightening of the solution to a color similar to that before NO introduction. Further nitrosyls showed slow decay with only slight brightening of the complex batch (see Table 2.1 for a complete overview of this compound class). Upon repeated exposure to NO, the argon-purged solution of such an unstable nitrosyl would immediately revert to its typical dark brown color, restoring the nitrosyl species. This cycle of nitrosyl formation and decay can be repeated multiple times, as shown below for the example of [Co(bpym)(fpin)(NO)] (**1j**), which was monitored by time-resolved in-situ IR spectroscopy (Figure 2.1). First, the formation of the nitrosyl complex is indicated by the emergence of the N–O stretching vibration at 1700 cm^{-1} upon introduction

of nitric oxide at 4:30 min, reaching its maximum about five minutes later. With subsequent argon purge starting at 12:00 min, the simultaneous decay of this absorption band is observed. The highest rate of decay is observed within the first eight minutes of bubbling, with the band reaching a plateau at about 29:00 min. After reintroduction of NO at 35:00 min, this absorption increases again within five minutes to a maximum similar to that of the first one.

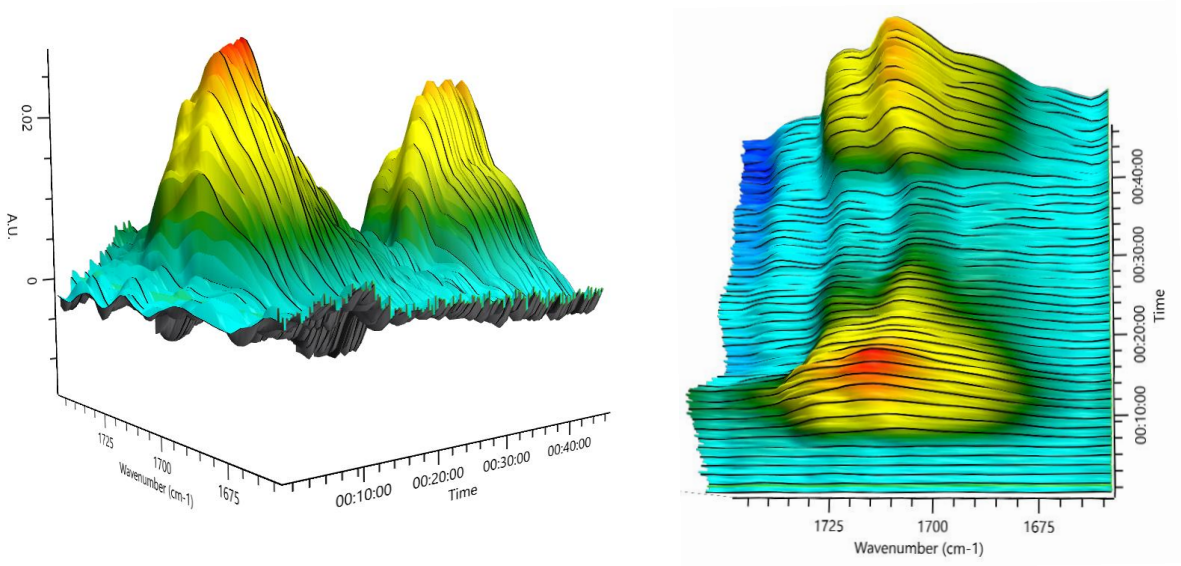

Figure 2.1: Three-dimensional plot of the time-resolved in-situ IR spectrum (**left:** side view, **right:** top view) of the formation of [Co(bpym)(fpin)(NO)] (**1j**), subsequent decay upon argon purge and regeneration under NO. All measurements are relative to a background spectrum of the reaction mixture prior to NO introduction, taken at 3:10 min. The precursor mixture consisted of a 40 mM methanolic $Co(NO_3)_2 \cdot 6\,H_2O$ solution, stoichiometric amounts of $fpinH_2$ and bpym and two equivalents of NEt_3.

X-ray diffraction of the single-crystalline products revealed a new library of electroneutral, fivefold-coordinated nitrosyls with the formula [Co(fpin)(L)(NO)] or, in the case of the monodentate co-ligands, $[Co(fpin)(L)_2(NO)]$ (**1a–n**, see Table 2.1). In each compound, the two chelating ligands are bent toward each other, resulting in a distortion of the coordination geometry, which can be best described as a distorted square pyramid according to Alvarez's continous-shape measures (CShM) calculations.[110, 111] In every specimen, the nitrosyl ligand is located at the apical position. The complex species closest to an ideal square pyramid (**1i**, **1j**, **1l**), as well as the most distorted one (**1k**), all possess *N*-heterocyclic aromatic co-ligands. All shape measures deviate from the Berry path. A detailed geometrical classification of the crystal structures within the range of relevant five-vertex polyhedra is given in Figure 2.2. These reference polyhedra comprise of the ideal, undistorted square pyramid (*SPY*-5), trigonal bipyramid (*TBPY*-5) and vacant octahedron (*vOC*-5). The latter differs from a *SPY*-5 geometry in that the metal center lies in the pyramid's basal L_4 plane, resulting in a planar CoL_4 moiety.[110]

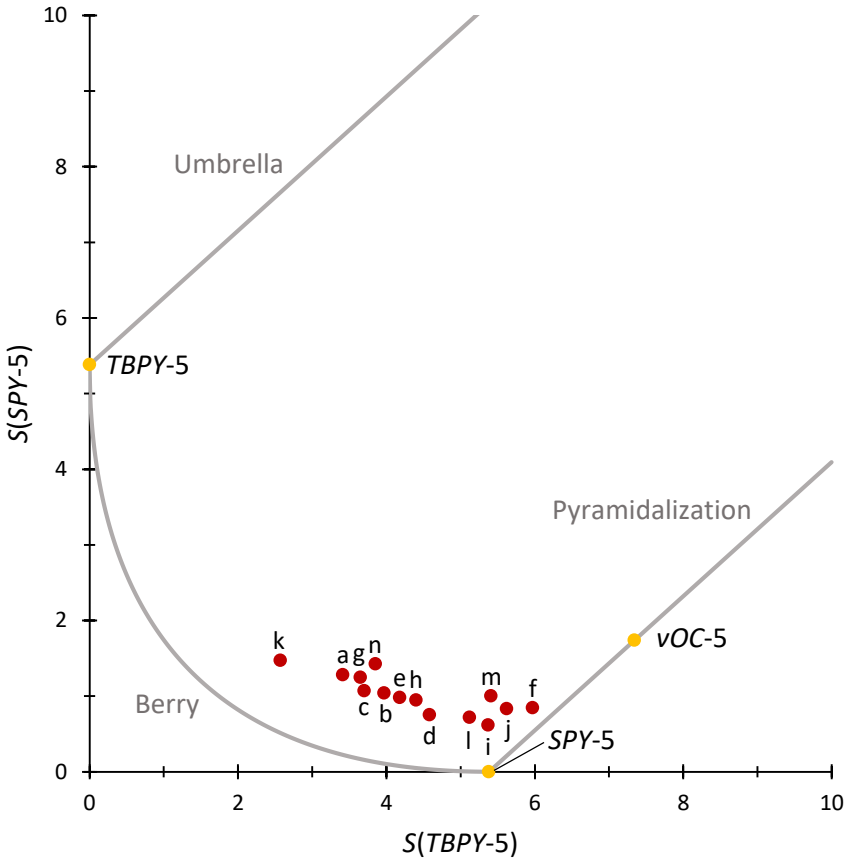

Figure 2.2: CShM map of compounds **1a–n** (red data points) for fivefold-coordinated species, based on the X-ray structural data of the crystalline products. Ideal, undistorted polyhedra (yellow data points): trigonal bipyramid (*TBPY*-5) at (0, 5.382), square pyramid (*SPY*-5) at (5.382, 0) and vacant octahedron (*vOC*-5) at (7.344, 1.740). The solid gray lines mark the Berry path (pseudorotation), the umbrella distortion [112, 113] (''folding'' of the equatorial plane in *TBPY*-5 along the unique axis) and the pyramidalization path (movement of the central metal in *SPY*-5 from the pyramid's center to its basal plane), respectively. For the compound **1i**, only the first entity in the asymmetric unit (see Figure 2.12) is plotted, since its CShM values do not differ significantly from those of the second entity. The values of the latter (**1i**†) are listed in Table 7.23 in the appendix.

In all structures, the CoNO moiety is bent at an angle ranging from 122.1° (**1j**) to 126.4° (**1e**), with the nitrosyl ligand pointing away from the CF_3 groups of the perfluoropinacolate and the organic side group(s) of the respective co-ligand. The Co–N bond is between 1.786 Å (**1d**) and 1.824 Å (**1j**) long, the N–O bond is ranging from 1.151 Å (**1f**) to 1.176 Å (**1a**). The majority of the structures exhibit a non-disordered nitrosyl moiety with only one complex molecule in the asymmetric unit. The infrared stretching vibration of the nitrosyl ligand is within a range from 1643 cm^{-1} (**1a**) to 1704 cm^{-1} (**1i**). It is striking that complexes with co-ligands containing an *N*-heterocyclic aromatic system exhibit a higher vibrational frequency and slightly longer Co–N bond compared to those with saturated side groups. A complete overview of the structural and vibrational data of the nitrosyl moieties is given in Table 2.1. With these findings, all the compounds of class **1** match Riggenmann's related cobalt nitrosyls with perfluoropinacolate and *N*,*N*'-ligands. His pioneering work focused on the synthesis and characte-

rization of fpin nitrosyls bearing ethylenediamine and its methylated derivatives (from men to tmen) as well as aromatic *N*-heterocyclic ligands such as phenanthroline, bipyridine and 2,9-dimethylphenanthroline. Their Co–N–O angles range between 121.2° and 126.6°, the Co–N bond ranges from 1.793 Å to 1.825 Å and for the N–O bond, lengths between 1.156 Å and 1.185 Å were found.[94, 95]

Table 2.1: X-ray and IR data of the crystalline {CoNO}^{8} compounds **1a–n** related to the CoNO moiety and loss of NO upon argon bubbling in solution. Decomposition of the nitrosyl species was rated as not occurring (–), slow (•), moderate (••) or rapid (•••).

1		N–O/Å	Co–N/Å	∡Co–N–O/°	$\tilde{\nu}$/cm^{-1}	NO loss
a	[Co(2-aepyrr)(fpin)(NO)]	1.176	1.787	123.8	1643	–
b	[Co(2-aepip)(fpin)(NO)]	1.172	1.792	123.8	1644	–
c	[Co(2-aemor)(fpin)(NO)]	1.169	1.788	125.2	1658	•
d	[Co(bnen)(fpin)(NO)]·S^1	1.176	1.786	125.4	1659	•
e	[Co(dpipe)(fpin)(NO)]	1.171	1.798	126.4	1660	•
f	[Co(fpin)(NO)(teen)] [a]	1.162	1.800	125.3	1655	•
g	[Co(2-aepy)(fpin)(NO)]	1.169	1.804	123.8	1683	•
h	[Co(fpin)(mampy)(NO)]·S^1 [b]	1.153	1.796	123.0	1673, 1653	–
i	[Co(bpm)(fpin)(NO)] [c]	1.166	1.814	122.4	1704	•••
j	[Co(bpym)(fpin)(NO)]·S^2	1.158	1.824	122.1	1692	••
k	[Co(dmdpphen)(fpin)(NO)]	1.161	1.809	125.5	1701	••
l	[Co(fpin)(NO)(py)$_2$]	1.173	1.807	123.8	1682	••
m	[Co(fpin)(NO)(pydz)$_2$]	1.168	1.807	122.4	1693	•••
n	[Co(fpin)(mim)$_2$(NO)]	1.167	1.809	123.1	1671	•••

[a] Disorder of the nitrosyl ligand. The given structural data refer to the major disorder form.
[b] Split band of the NO vibration in the IR spectrum. The band with the higher relative intensity is listed first.
[c] Mean structural data of the two entities in the asymmetric unit.
Co-crystallized solvents: S^1: DMSO, S^2: MeOH.

Plots of the crystal structures of **1a–n** are shown on the next pages. In compounds with co-ligands bearing an unsubstituted amino group, classical hydrogen bonds are formed between said moiety and one alkoxido group of the perfluoropinacolate from the neighboring complex. A pair of two such bonds forms a cyclic motif, as seen for example in **1b** (Figure 2.3), which are described by the descriptor $R_2^2(8)$ according to graph-set analysis [2, 3] (–N2–H721···O2^i–Co1^i–N2^i–H721^i···O2–Co1– in the unary graph

set). With partial substitution on the amino group (**1d+h**), also hydrogen bonds to the oxygen atom of the co-crystallized DMSO are built. Details on all classical hydrogen bonds occurring in the crystal structures are listed in Table 2.2.

Furthermore, non-classical hydrogen bonds occur between the aliphatic and aromatic C–H groups of the respective co-ligand and the perfluoropinacolate (O, F) as well as the nitrosyl moiety (N, O). Compared to the classic interactions, they represent the majority of hydrogen bonds in all compounds of this class. As can be seen in Figure 2.3, they also form intramolecular ring motifs such as $S_1^1(5)$ (–C9–H92···O3–Co1–N3– in the unary graph set). For a complete overview of all non-classical hydrogen bonds in the crystalline compounds of class **1**, see Table 7.16 in the appendix.

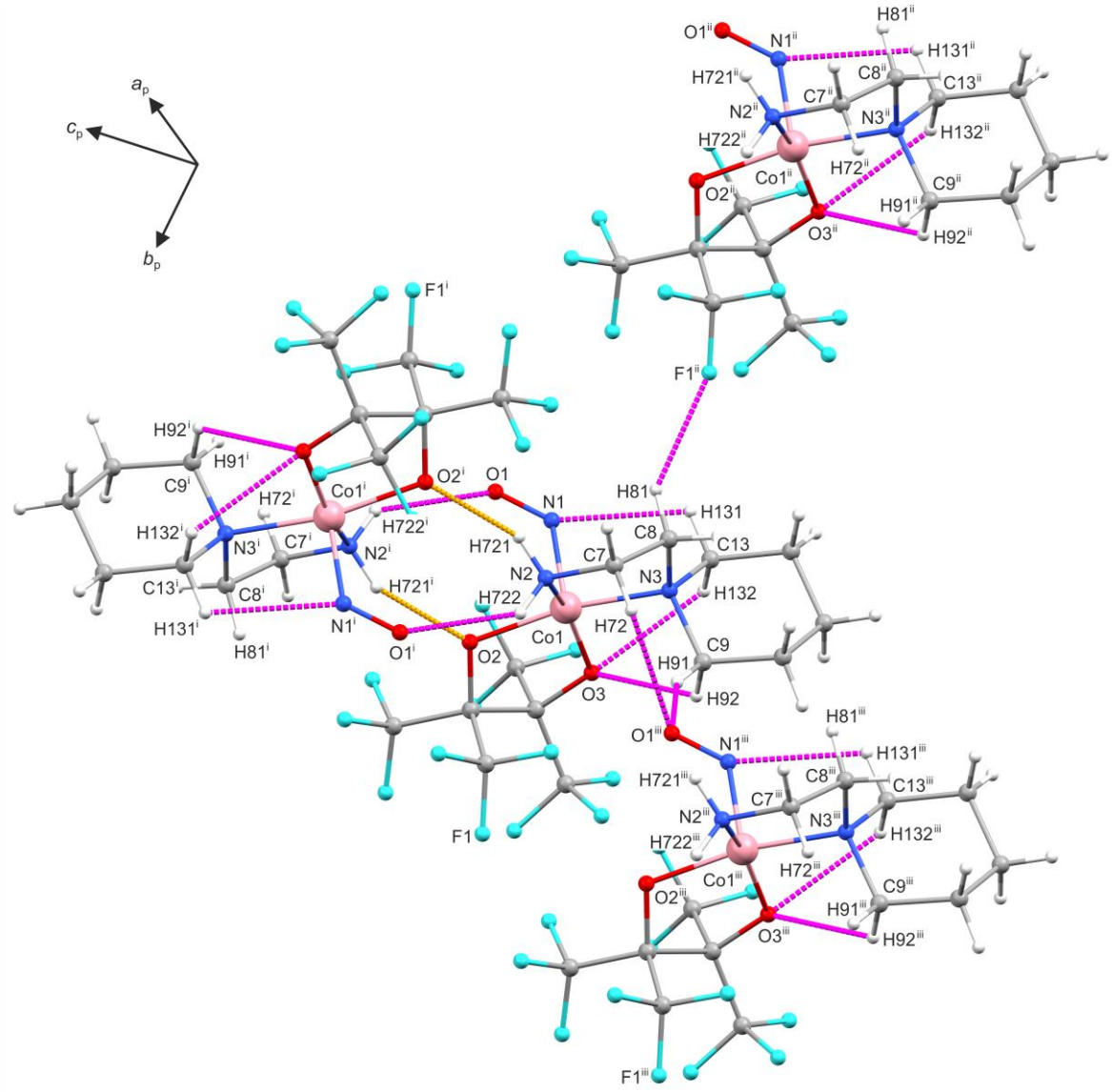

Figure 2.3: Plot of the pattern of classical (dashed yellow lines) and non-classical (dashed violet lines) hydrogen bonds in crystals of **1b**. Symmetry codes: [i] 1–*x*, 1–*y*, 1–*z*; [ii] *x*, –1+*y*, *z*; [iii] –1+*x*, *y*, *z*.

Table 2.2: Distances and angles of classical hydrogen bonds in crystalline compounds of class **1**. The standard deviation of the last decimal digit is given in parentheses. Values without a standard deviation refer to hydrogen atoms calculated on idealized positions, riding on their parent atoms.

1	D–H···A	*d*(D–H)/Å	*d*(H···A)/Å	*d*(D···A)/Å	∢(D–H···A)/°
a	N2–H721···O2^{i}	0.91	2.14	2.931(3)	145
b	N2–H721···O2^{i}	0.91	2.13	2.941(4)	148
c	N2–H721···O2^{i}	0.91	2.07	2.883(3)	149
d	N2–H721···O2^{ii}	0.91	2.02	2.891(3)	161
	N3–H73···O4^{i}	1.00	1.97	2.907(3)	155
g	N2–H721···O2^{i}	0.88(3)	2.19(3)	3.042(2)	163(2)
h	N2–H72···O4^{iii}	1.00	1.84	2.824(4)	167
j	O4–H84···N5^{iv}	0.79(4)	2.34(4)	3.072(2)	156(3)

Symmetry codes: ^{i} 1−*x*, 1−*y*, 1−*z*; ^{ii} 1−*x*, −*y*, 1−*z*; ^{iii} −1+*x*, *y*, *z*; ^{iv} 1+*x*, *y*, *z*.

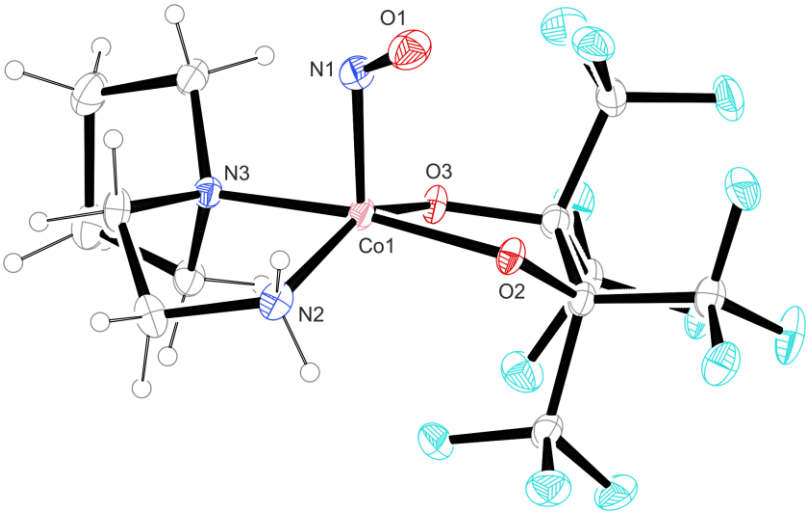

Figure 2.4: ORTEP plot of [Co(2-aepyrr)(fpin)(NO)] in crystals of **1a**. Thermal ellipsoids drawn at 50 % probability level at 102 K. Interatomic distances (Å) and bond angles (°) with the standard deviation of the last decimal digit given in parentheses: Co1–N1 1.787(2), Co1–N2 1.968(2), Co1–N3 1.971(2), Co1–O2 1.902(2), Co1–O3 1.851(2), N1–O1 1.176(3), Co1–N1–O1 123.8(2), N2–Co1–O3 152.34(8), N3–Co1–O2 171.29(8), N2–Co1–N3 86.8(1), O2–Co1–O3 86.24(7), N2–Co1–O2 93.00(8), N3–Co1–O3 89.90(9), N1–Co1–N2 96.9(1), N1–Co1–N3 93.6(1), N1–Co1–O2 95.04(9), N1–Co1–O3 110.76(9).

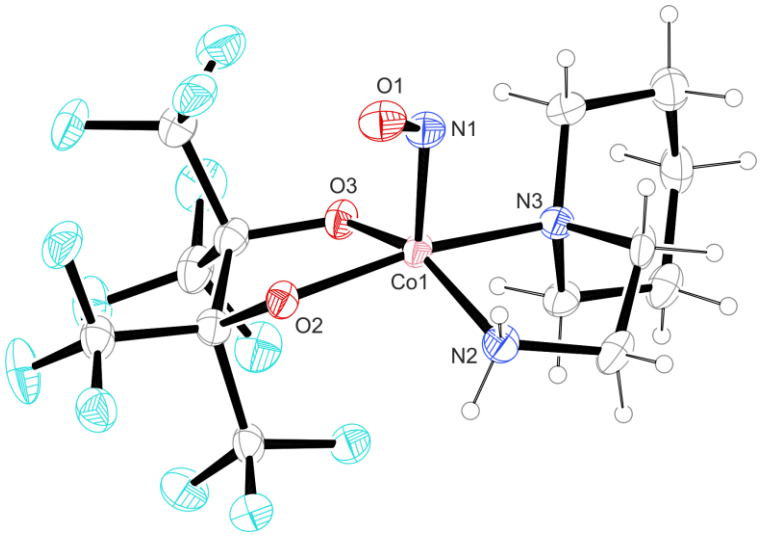

Figure 2.5: ORTEP plot of [Co(2-aepip)(fpin)(NO)] in crystals of **1b**. Thermal ellipsoids drawn at 50 % probability level at 102 K. Interatomic distances (Å) and bond angles (°) with the standard deviation of the last decimal digit given in parentheses: Co1–N1 1.792(3), Co1–N2 1.962(3), Co1–N3 1.986(3), Co1–O2 1.906(3), Co1–O3 1.857(3), N1–O1 1.172(5), Co1–N1–O1 123.8(3), N2–Co1–O3 154.6(1), N3–Co1–O2 169.1(1), N2–Co1–N3 86.7(1), O2–Co1–O3 85.7(1), N2–Co1–O2 92.6(1), N3–Co1–O3 90.3(1), N1–Co1–N2 96.1(2), N1–Co1–N3 94.7(1), N1–Co1–O2 96.2(1), N1–Co1–O3 109.2(1).

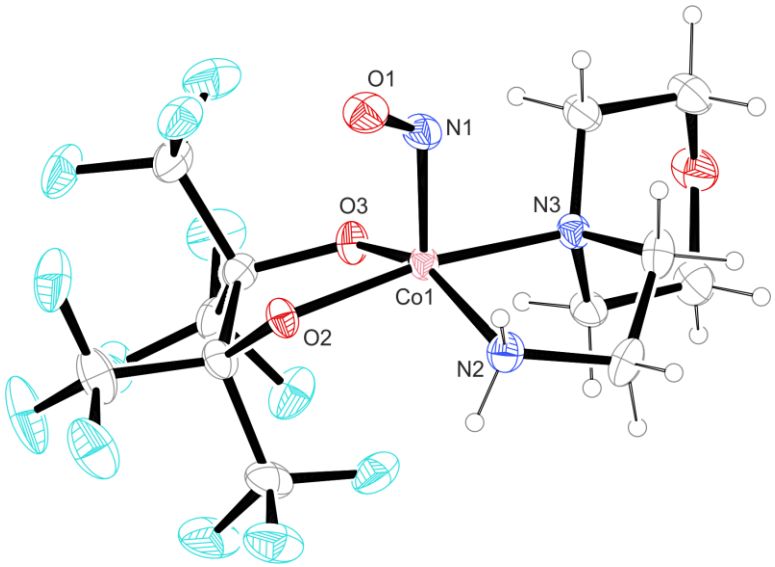

Figure 2.6: ORTEP plot of [Co(2-aemor)(fpin)(NO)] in crystals of **1c**. Thermal ellipsoids drawn at 50 % probability level at 105 K. Interatomic distances (Å) and bond angles (°) with the standard deviation of the last decimal digit given in parentheses: Co1–N1 1.788(2), Co1–N2 1.958(2), Co1–N3 1.995(2), Co1–O2 1.902(2), Co1–O3 1.857(2), N1–O1 1.169(2), Co1–N1–O1 125.2(1), N2–Co1–O3 153.54(8), N3–Co1–O2 169.68(8), N2–Co1–N3 86.73(7), O2–Co1–O3 85.66(7), N2–Co1–O2 91.86(7), N3–Co1–O3 91.04(7), N1–Co1–N2 97.64(8), N1–Co1–N3 93.27(8), N1–Co1–O2 97.05(7), N1–Co1–O3 108.82(8).

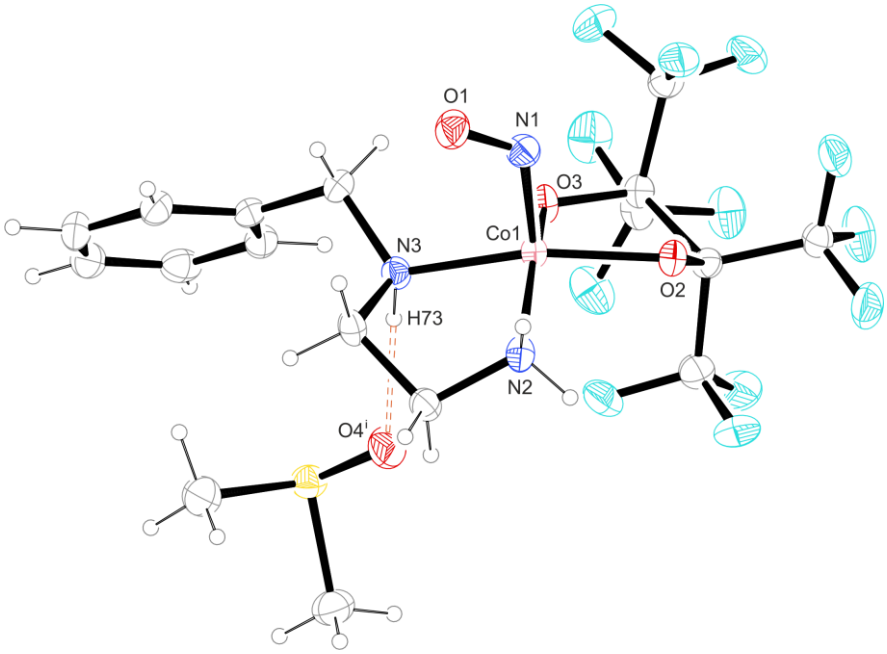

Figure 2.7: ORTEP plot of [Co(bnen)(fpin)(NO)]·DMSO in crystals of **1d**·DMSO. Thermal ellipsoids drawn at 50 % probability level at 103 K. Interatomic distances (Å) and bond angles (°) with the standard deviation of the last decimal digit given in parentheses: Co1–N1 1.786(2), Co1–N2 1.963(3), Co1–N3 1.994(2), Co1–O2 1.903(2), Co1–O3 1.863(2), N1–O1 1.176(3), H73–O4^{i} 1.97, Co1–N1–O1 125.4(2), N2–Co1–O3 155.47(8), N3–Co1–O2 165.10(7), N2–Co1–N3 85.69(8), O2–Co1–O3 86.06(8), N2–Co1–O2 93.82(9), N3–Co1–O3 88.26(8), N1–Co1–N2 96.5(1), N1–Co1–N3 98.21(9), N1–Co1–O2 96.64(8), N1–Co1–O3 107.85(9). Symmetry code: ^{i} 1–*x*, 1–*y*, 1–*z*.

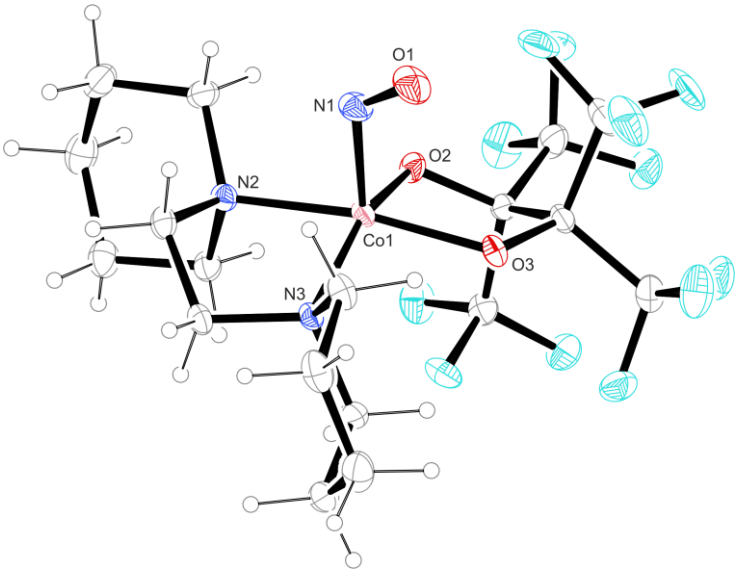

Figure 2.8: ORTEP plot of [Co(dpipe)(fpin)(NO)] in crystals of **1e**. Thermal ellipsoids drawn at 50 % probability level at 102 K. Interatomic distances (Å) and bond angles (°) with the standard deviation of the last decimal digit given in parentheses: Co1–N1 1.798(2), Co1–N2 1.988(1), Co1–N3 2.030(2), Co1–O2 1.885(1), Co1–O3 1.880(1), N1–O1 1.171(2), Co1–N1–O1 126.4(1), N2–Co1–O3 169.15(6), N3–Co1–O2 155.78(6), N2–Co1–N3 86.96(6), O2–Co1–O3 85.62(5), N2–Co1–O2 91.58(6), N3–Co1–O3 91.30(6), N1–Co1–N2 92.10(7), N1–Co1–N3 98.82(7), N1–Co1–O2 105.40(6), N1–Co1–O3 98.75(6).

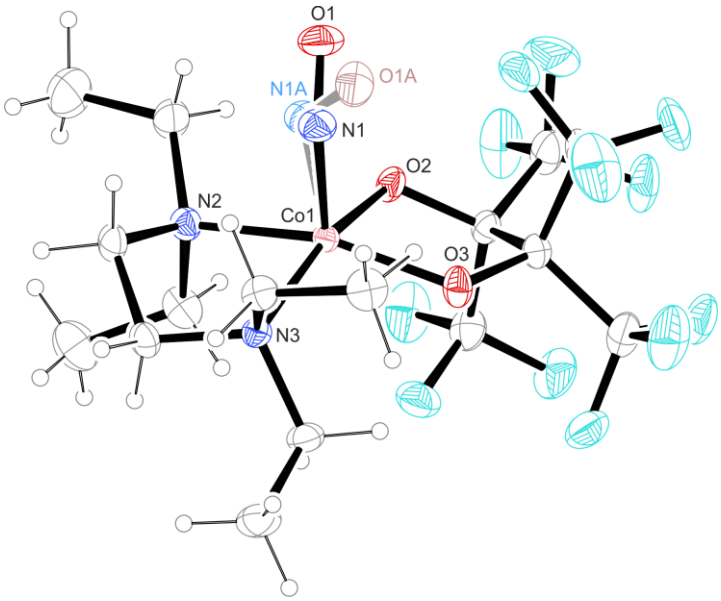

Figure 2.9: ORTEP plot of [Co(fpin)(NO)(teen)] in crystals of **1f**. The nitrosyl moiety of the minor disorder form (23 %) is depicted in light colors. Thermal ellipsoids are drawn at 50 % probability level at 173 K. Interatomic distances (Å) and bond angles (°) with the standard deviation of the last decimal digit given in parentheses: Co1–N1 1.800(4), Co1–N1A 1.793(1), Co1–N2 2.015(1), Co1–N3 2.053(1), Co1–O2 1.885(1), Co1–O3 1.873(1), N1–O1 1.162(5), N1A–O1A 1.151(1), Co1–N1–O1 125.3(4), Co1–N1A–O1A 124.7(1), N2–Co1–O3 162.23(6), N3–Co1–O2 164.50(6), N2–Co1–N3 87.09(6), O2–Co1–O3 85.17(5), N2–Co1–O2 91.04(5), N3–Co1–O3 91.94(5), N1–Co1–N2 97.0(1), N1–Co1–N3 93.5(1), N1–Co1–O2 102.0(1), N1–Co1–O3 100.7(1).

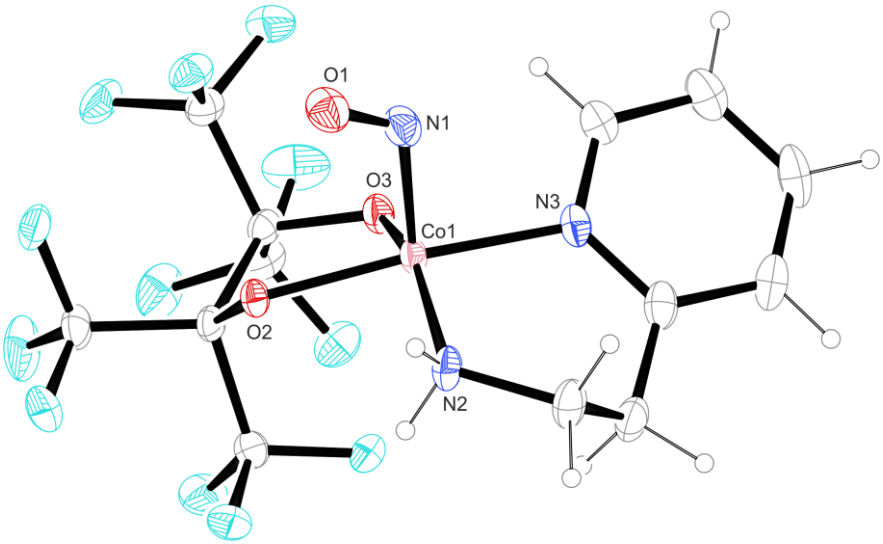

Figure 2.10: ORTEP plot of [Co(2-aepy)(fpin)(NO)] in crystals of **1g**. Thermal ellipsoids drawn at 50 % probability level at 102 K. Interatomic distances (Å) and bond angles (°) with the standard deviation of the last decimal digit given in parentheses: Co1–N1 1.804(2), Co1–N2 1.960(2), Co1–N3 1.957(2), Co1–O2 1.895(1), Co1–O3 1.865(2), N1–O1 1.169(2), Co1–N1–O1 123.8(1), N2–Co1–O3 153.66(7), N3–Co1–O2 169.94(6), N2–Co1–N3 95.41(7), O2–Co1–O3 85.87(6), N2–Co1–O2 88.19(6), N3–Co1–O3 86.77(7), N1–Co1–N2 98.61(7), N1–Co1–N3 92.87(7), N1–Co1–O2 95.88(6), N1–Co1–O3 107.51(7).

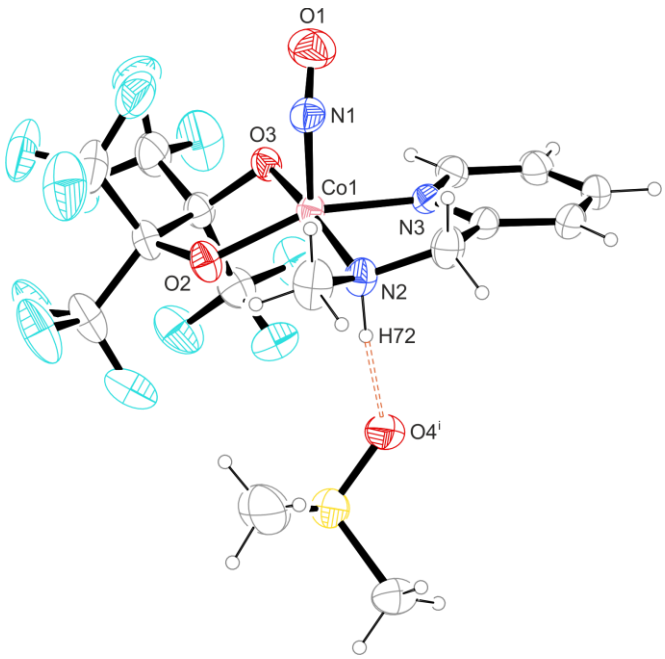

Figure 2.11: ORTEP plot of [Co(fpin)(mampy)(NO)]·DMSO in crystals of **1h**·DMSO. Thermal ellipsoids drawn at 50 % probability level at 173 K. Interatomic distances (Å) and bond angles (°) with the standard deviation of the last decimal digit given in parentheses: Co1–N1 1.796(3), Co1–N2 1.953(3), Co1–N3 1.934(3), Co1–O2 1.865(3), Co1–O3 1.883(2), N1–O1 1.153(5), H72–O4^{i} 1.84, Co1–N1–O1 123.0(2), N2–Co1–O3 169.1(1), N3–Co1–O2 157.4(1), N2–Co1–N3 83.3(1), O2–Co1–O3 85.9(1), N2–Co1–O2 92.6(1), N3–Co1–O3 94.0(1), N1–Co1–N2 93.8(1), N1–Co1–N3 96.1(1), N1–Co1–O2 106.4(1), N1–Co1–O3 97.0(1). Symmetry code: ^{i} −1+*x*, *y*, *z*.

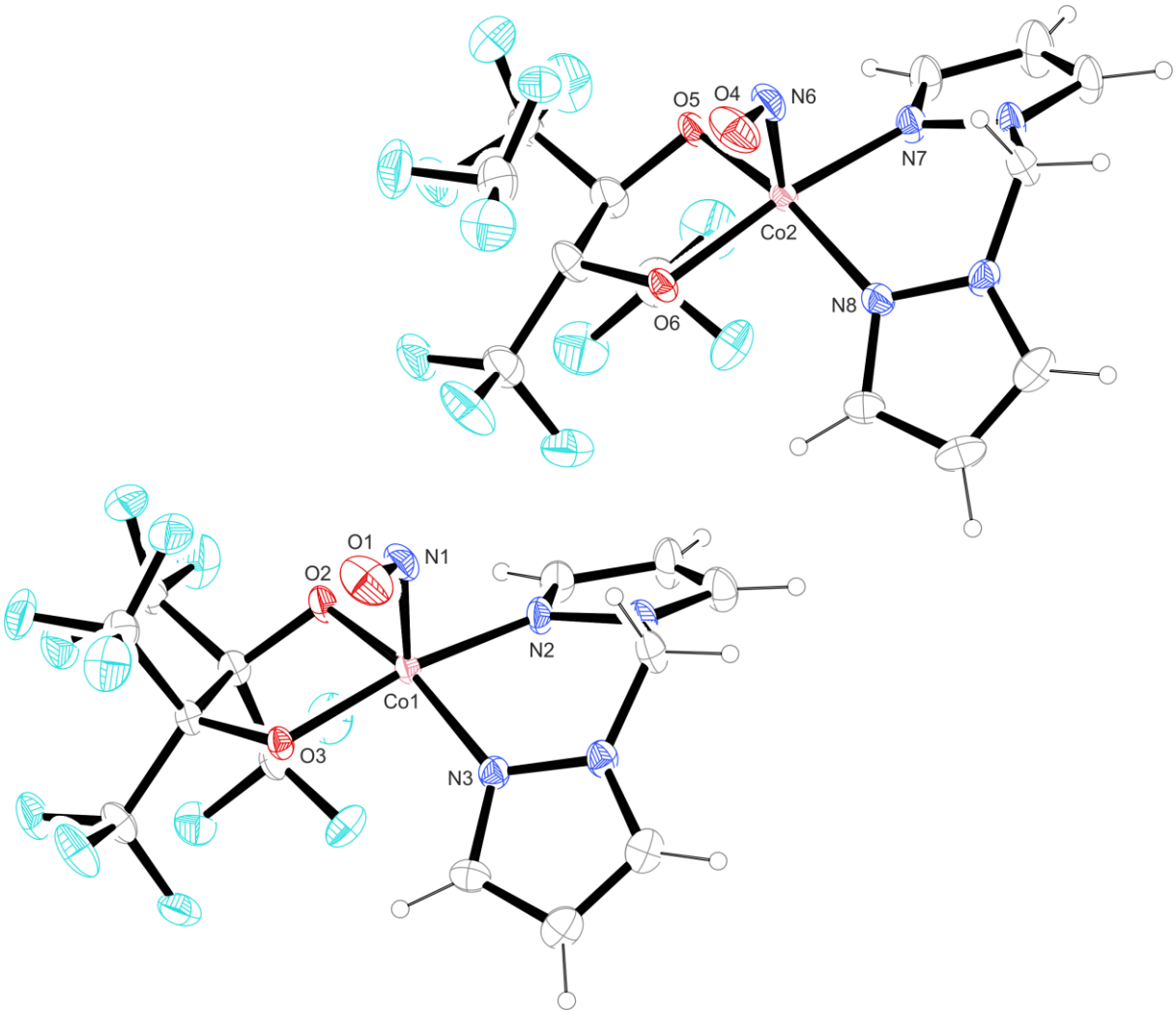

Figure 2.12: ORTEP plot of [Co(bpm)(fpin)(NO)] in crystals of **1i**. Thermal ellipsoids drawn at 50 % probability level at 102 K. Interatomic distances (Å) and bond angles (°) with the standard deviation of the last decimal digit given in parentheses: **left molecule (1i):** Co1–N1 1.819(6), Co1–N2 1.936(6), Co1–N3 1.934(5), Co1–O2 1.878(3), Co1–O3 1.869(4), N1–O1 1.172(8), Co1–N1–O1 121.5(5), N2–Co1–O3 166.3(2), N3–Co1–O2 161.7(2), N2–Co1–N3 89.7(2), O2–Co1–O3 86.3(2), N2–Co1–O2 90.1(2), N3–Co1–O3 89.6(2), N1–Co1–N2 96.4(2), N1–Co1–N3 97.2(2), N1–Co1–O2 101.0(2), N1–Co1–O3 97.2(2); **right molecule (1i^{t}):** Co2–N6 1.808(6), Co2–N7 1.943(6), Co2–N8 1.923(5), Co2–O5 1.871(4), Co2–O6 1.873(4), N6–O4 1.160(7), Co2–N6–O4 123.3(5), N7–Co2–O6 166.8(2), N8–Co2–O5 161.1(2), N7–Co2–N8 89.5(2), O5–Co2–O6 86.1(2), N7–Co2–O5 90.4(2), N8–Co2–O6 89.7(2), N6–Co2–N7 96.0(2), N6–Co2–N8 97.0(2), N6–Co2–O5 101.8(2), N6–Co2–O6 97.2(2).

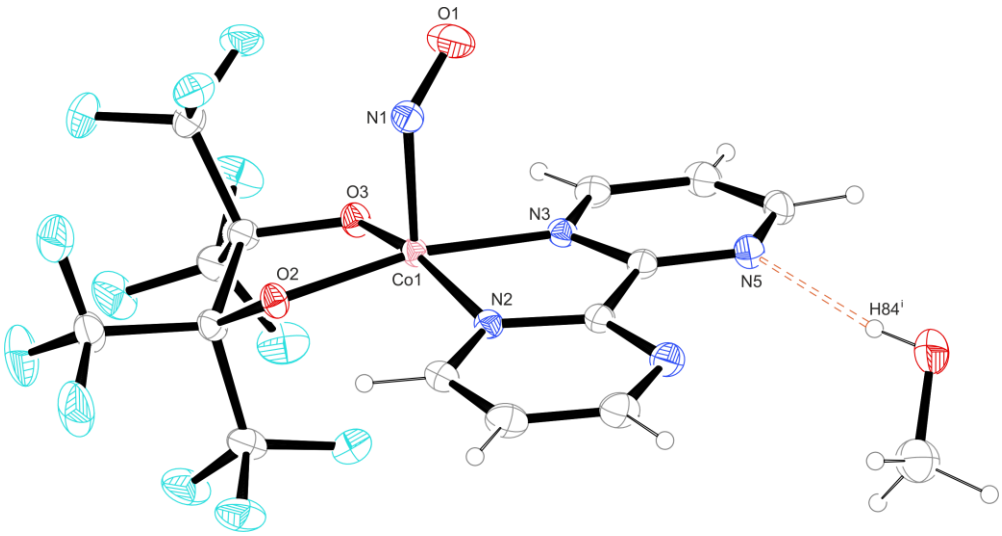

Figure 2.13: ORTEP plot of [Co(bpym)(fpin)(NO)]·MeOH in crystals of **1j**·MeOH. Thermal ellipsoids drawn at 50 % probability level at 103 K. Interatomic distances (Å) and bond angles (°) with the standard deviation of the last decimal digit given in parentheses: Co1–N1 1.824(2), Co1–N2 1.940(1), Co1–N3 1.920(2), Co1–O2 1.872(1), Co1–O3 1.847(1), N1–O1 1.158(2), H84^{i}–N5 2.34(3), Co1–N1–O1 122.1(1), N2–Co1–O3 163.82(6), N3–Co1–O2 168.43(6), N2–Co1–N3 82.52(6), O2–Co1–O3 86.99(6), N2–Co1–O2 94.63(6), N3–Co1–O3 92.70(6), N1–Co1–N2 95.72(6), N1–Co1–N3 94.28(6), N1–Co1–O2 97.17(6), N1–Co1–O3 100.06(5). Symmetry code: ^{i} −1+*x*, *y*, *z*.

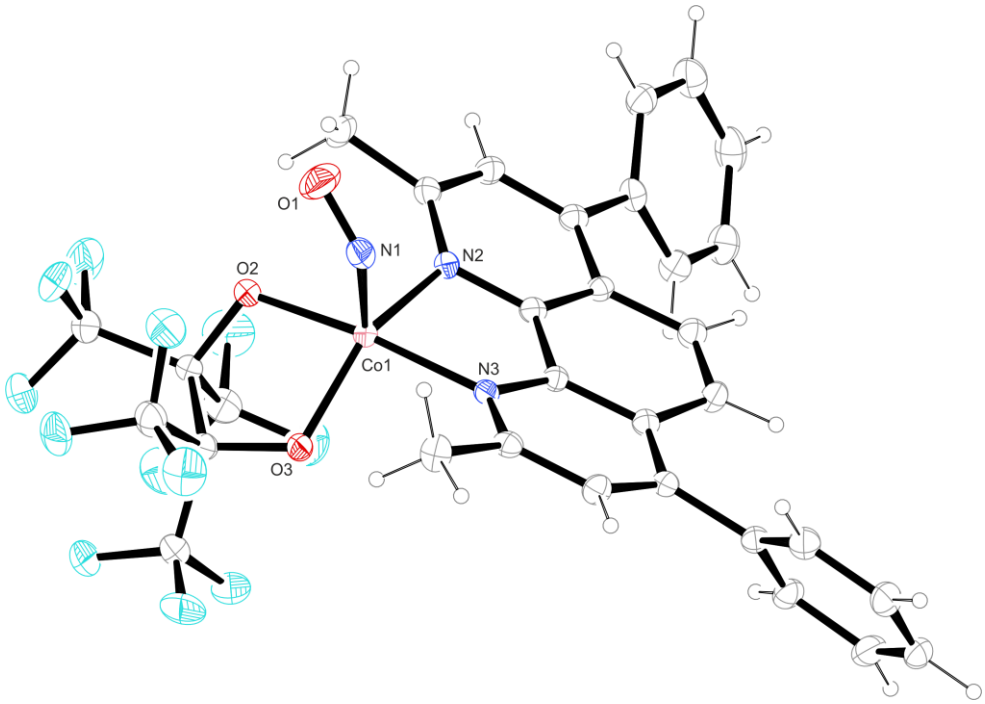

Figure 2.14: ORTEP plot of [Co(dmdpphen)(fpin)(NO)] in crystals of **1k**. Thermal ellipsoids drawn at 50 % probability level at 102 K. Interatomic distances (Å) and bond angles (°) with the standard deviation of the last decimal digit given in parentheses: Co1–N1 1.809(3), Co1–N2 1.974(3), Co1–N3 1.953(3), Co1–O2 1.884(2), Co1–O3 1.873(3), N1–O1 1.161(4), Co1–N1–O1 125.5(2), N2–Co1–O3 147.0(1), N3–Co1–O2 171.6(1), N2–Co1–N3 83.1(1), O2–Co1–O3 84.8(1), N2–Co1–O2 96.4(1), N3–Co1–O3 91.0(1), N1–Co1–N2 102.8(1), N1–Co1–N3 94.4(1), N1–Co1–O2 93.9(1), N1–Co1–O3 110.0(1).

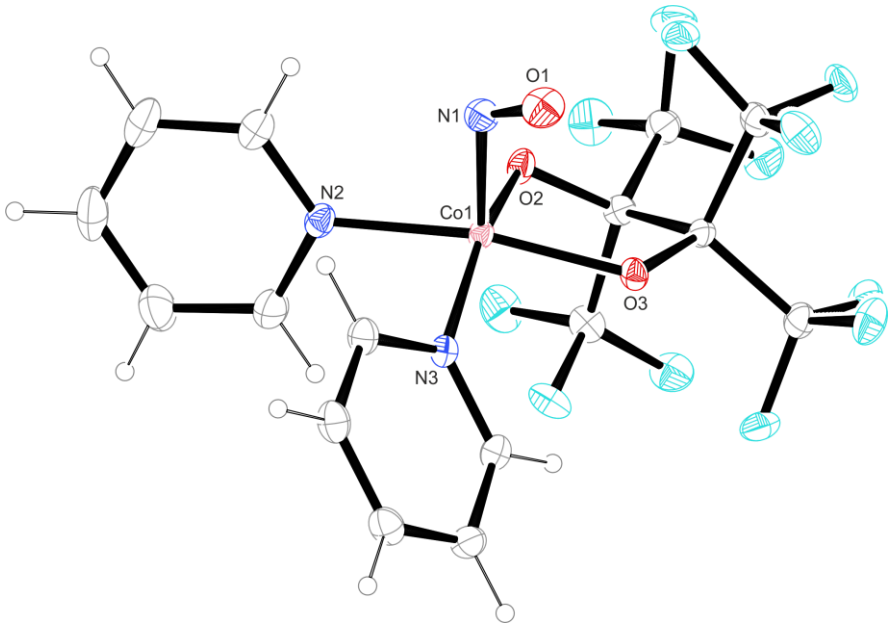

Figure 2.15: ORTEP plot of [Co(fpin)(NO)(py)$_2$] in crystals of **1l**. Thermal ellipsoids drawn at 50 % probability level at 100 K. Interatomic distances (Å) and bond angles (°) with the standard deviation of the last decimal digit given in parentheses: Co1–N1 1.807(2), Co1–N2 1.964(2), Co1–N3 1.955(2), Co1–O2 1.885(2), Co1–O3 1.872(2), N1–O1 1.173(2), Co1–N1–O1 123.8(1), N2–Co1–O3 166.88(7), N3–Co1–O2 160.28(7), N2–Co1–N3 89.93(7), O2–Co1–O3 86.14(6), N2–Co1–O2 90.35(7), N3–Co1–O3 89.16(7), N1–Co1–N2 94.91(7), N1–Co1–N3 97.01(7), N1–Co1–O2 102.61(7), N1–Co1–O3 98.20(7).

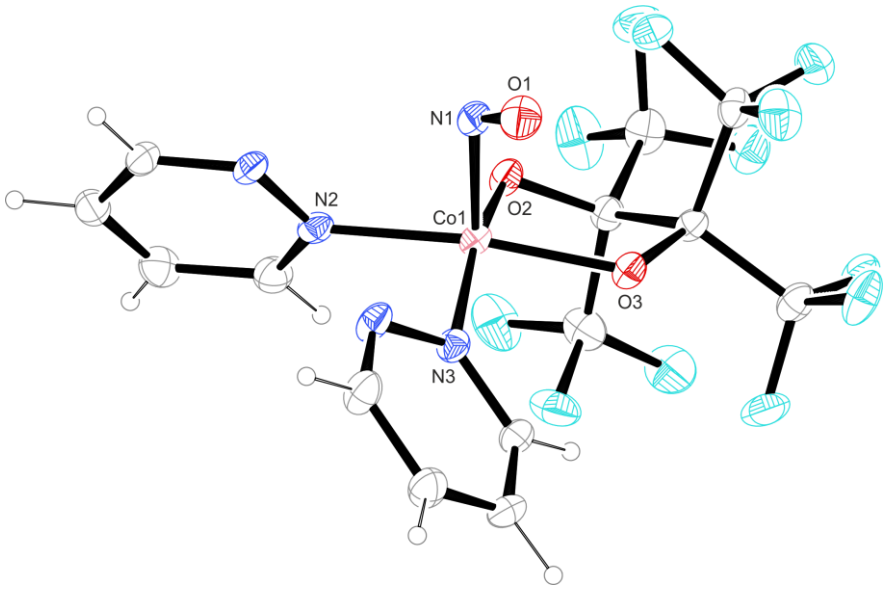

Figure 2.16: ORTEP plot of [Co(fpin)(NO)(pydz)$_2$] in crystals of **1m**. Thermal ellipsoids drawn at 50 % probability level at 100 K. Interatomic distances (Å) and bond angles (°) with the standard deviation of the last decimal digit given in parentheses: Co1–N1 1.807(3), Co1–N2 1.949(2), Co1–N3 1.934(2), Co1–O2 1.885(2), Co1–O3 1.872(2), N1–O1 1.168(4), Co1–N1–O1 122.4(2), N2–Co1–O3 169.01(9), N3–Co1–O2 162.4(1), N2–Co1–N3 93.39(8), O2–Co1–O3 85.93(8), N2–Co1–O2 89.25(8), N3–Co1–O3 88.32(9), N1–Co1–N2 92.9(1), N1–Co1–N3 93.8(1), N1–Co1–O2 103.4(1), N1–Co1–O3 97.8(1).

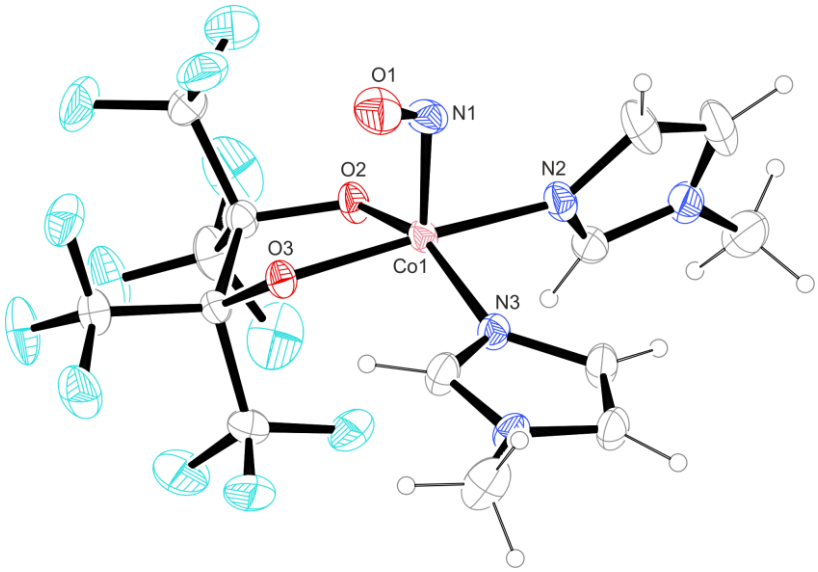

Figure 2.17: ORTEP plot of [Co(fpin)$(mim)_2$(NO)] in crystals of **1n**. Thermal ellipsoids drawn at 50 % probability level at 173 K. Interatomic distances (Å) and bond angles (°) with the standard deviation of the last decimal digit given in parentheses: Co1–N1 1.809(1), Co1–N2 1.943(2), Co1–N3 1.943(1), Co1–O2 1.863(1), Co1–O3 1.898(1), N1–O1 1.167(2), Co1–N1–O1 123.1(1), N2–Co1–O3 170.63(5), N3–Co1–O2 155.15(6), N2–Co1–N3 92.84(6), O2–Co1–O3 85.36(5), N2–Co1–O2 87.04(5), N3–Co1–O3 91.76(6), N1–Co1–N2 94.20(7), N1–Co1–N3 94.22(6), N1–Co1–O2 110.59(5), N1–Co1–O3 93.59(5).

2.2 Perfluoropinacolatocobalt nitrosyls with aminoethyl-substituted phosphanes as co-ligands

Using the previously described method, two crystalline $\{CoNO\}^8$ compounds [Co(fpin)(L)(NO)] with perfluoropinacolate and *P*,*N*-ligands were synthesized. As with the phosphorus-free analogs, the brown crystals of **2a+b** are insoluble in common alcohols and can be stored under argon. They show no signs of NO loss in solution when treated with argon. Both crystal structures are similar to those of class **1** with regard to the Co–N and N–O bond lengths, showing similar N–O stretching vibrations as well. For a complete overview, see Table 2.3.

Table 2.3: X-ray and IR data of the crystalline $\{CoNO\}^8$ compounds **2a+b** related to the CoNO moiety and loss of NO upon argon bubbling in solution. Decomposition of the nitrosyl species was rated as not occurring (–).

2		N–O/Å	Co–N/Å	∡Co–N–O/°	$\tilde{\nu}$/cm^{-1}	NO loss
a	[Co(2-aedpp)(fpin)(NO)]·0.5S [a]	1.171	1.783	129.6	1653	–
b	[Co(2-aedip)(fpin)(NO)]	1.138	1.783	132.3	1649	–

[a] Mean structural data of the two entities in the asymmetric unit.
Co-crystallized solvent (S): MeOH.

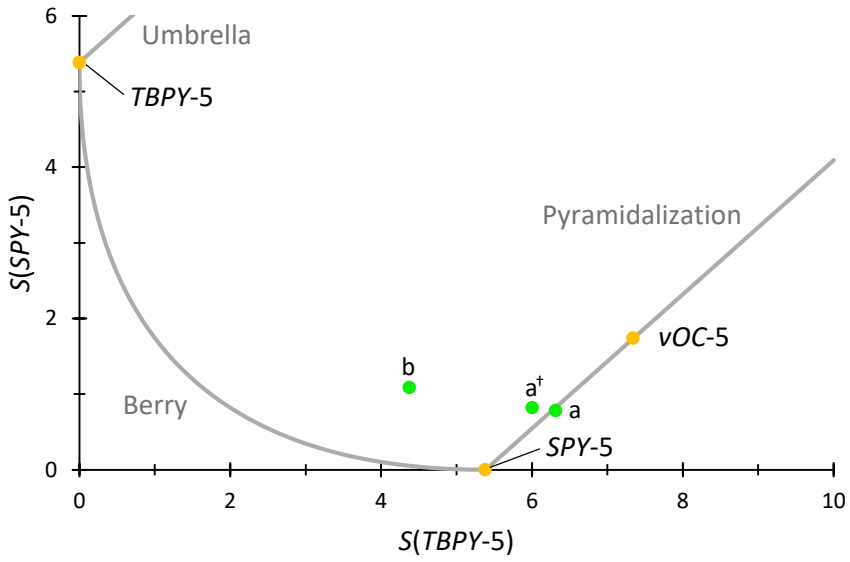

Figure 2.18: CShM map of compounds **2a+b** (green data points) for fivefold-coordinated species, based on the X-ray structural data of the crystalline products. For the compound **2a**, the CShM values of both entities in the asymmetric unit (**2a** and **2a**$^+$, see Figure 2.19) are plotted. Ideal, undistorted polyhedra (yellow data points) as reference. The solid gray lines mark the Berry path, the umbrella distortion and the pyramidalization path, respectively.

The compounds possess a molecular structure similar to **1a–n**, featuring a bent CoNO moiety and a coordination geometry which can be best described as distorted-square pyramidal in terms of CShM calculations (Figure 2.18). However, the Co–N–O angle in **2a+b** is slightly greater than in the class **1** species.

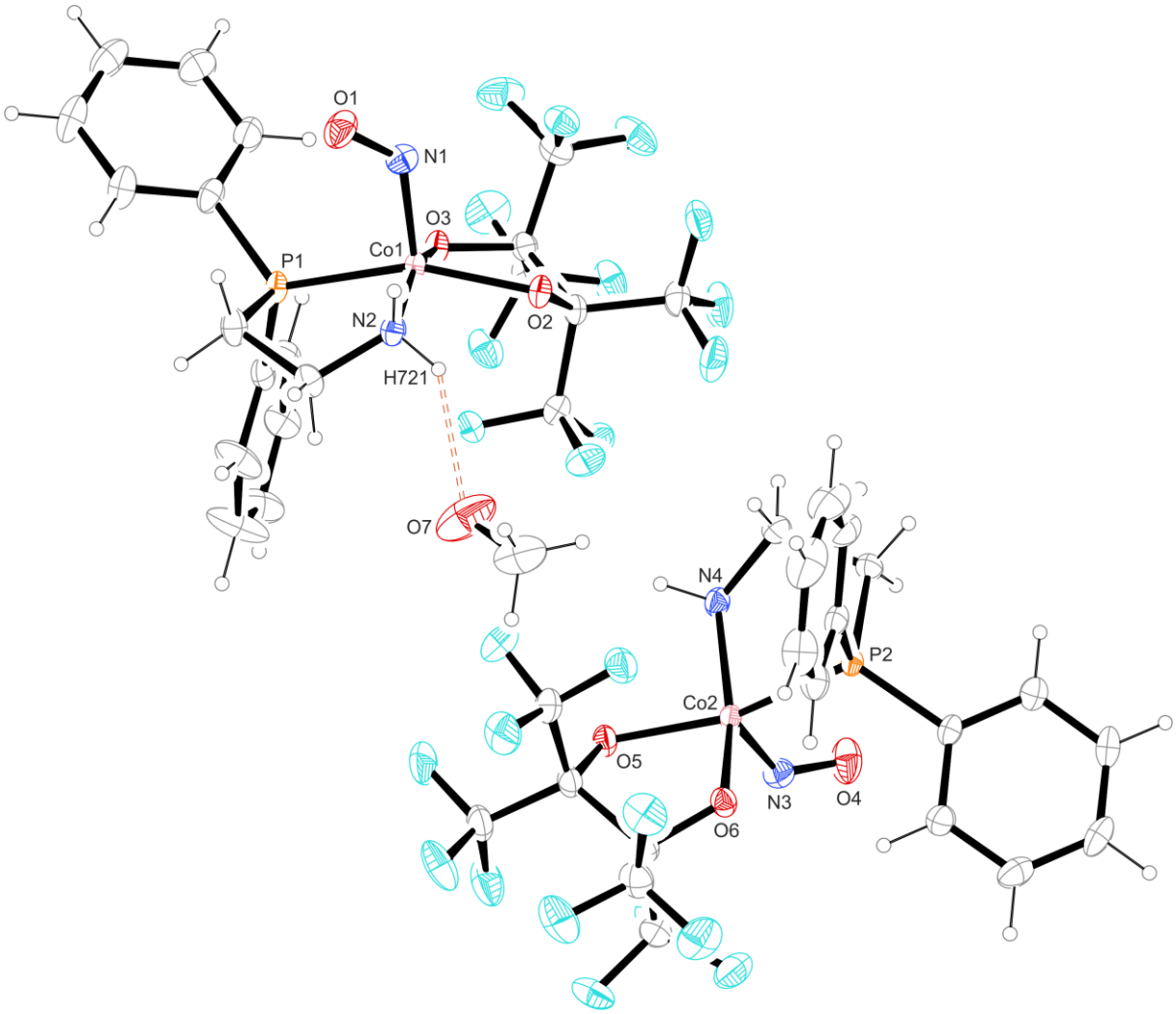

Figure 2.19: ORTEP plot of [Co(2-aedpp)(fpin)(NO)]·0.5 MeOH in crystals of **2a**·0.5 MeOH. Thermal ellipsoids drawn at 50 % probability level at 102 K. Due to the chosen perspective, the hydrogen atoms H741 and H87 are obscured in the plot by their respective parent atoms N4 and O7. Interatomic distances (Å) and bond angles (°) with the standard deviation of the last decimal digit given in parentheses: **left molecule (2a):** Co1–N1 1.777(2), Co1–N2 1.978(1), Co1–P1 2.1732(5), Co1–O2 1.936(1), Co1–O3 1.871(1), N1–O1 1.175(2), H721–O7 2.29, Co1–N1–O1 129.3(2), N2–Co1–O3 158.73(6), P1–Co1–O2 158.01(4), N2–Co1–P1 86.53(4), O2–Co1–O3 85.61(5), N2–Co1–O2 90.46(5), P1–Co1–O3 89.34(4), N1–Co1–N2 94.72(7), N1–Co1–P1 96.54(6), N1–Co1–O2 105.41(7), N1–Co1–O3 106.49(6); **right molecule (2a†):** Co2–N3 1.788(2), Co2–N4 1.978(1), Co2–P2 2.1865(5), Co2–O5 1.948(1), Co2–O6 1.873(1), N3–O4 1.166(3), Co2–N3–O4 129.8(2), N4–Co2–O6 158.55(6), P2–Co2–O5 159.92(4), N4–Co2–P2 85.58(4), O5–Co2–O6 85.27(5), N4–Co2–O5 90.15(5), P2–Co2–O6 91.57(4), N3–Co2–N4 95.65(7), N3–Co2–P2 97.41(7), N3–Co2–O5 102.53(8), N3–Co2–O6 105.80(7).

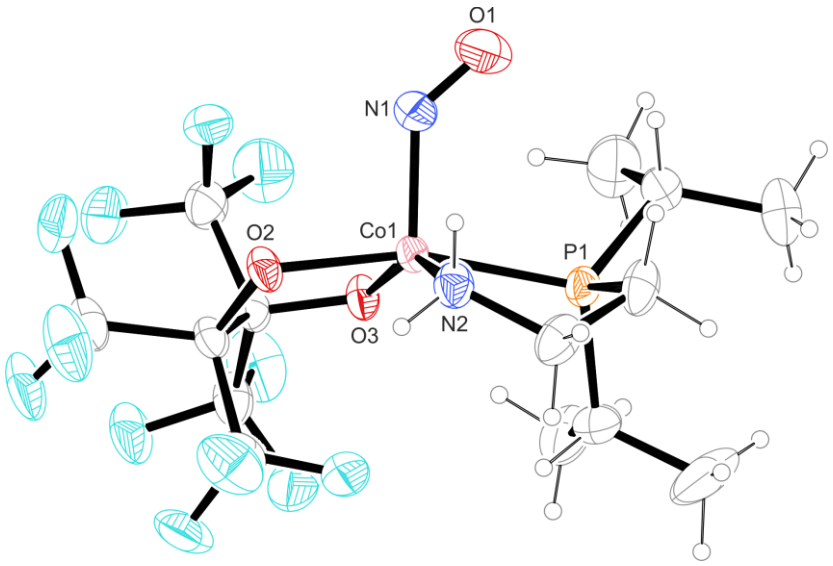

Figure 2.20: ORTEP plot of [Co(2-aedip)(fpin)(NO)] in crystals of **2b**. Thermal ellipsoids drawn at 50 % probability level at 173 K. Interatomic distances (Å) and bond angles (°) with the standard deviation of the last decimal digit given in parentheses: Co1–N1 1.783(2), Co1–N2 1.984(2), Co1–P1 2.2226(7), Co1–O2 1.937(1), Co1–O3 1.878(1), N1–O1 1.138(3), Co1–N1–O1 132.3(2), N2–Co1–O3 151.32(7), P1–Co1–O2 163.28(5), N2–Co1–P1 85.75(5), O2–Co1–O3 85.09(5), N2–Co1–O2 87.46(7), P1–Co1–O3 93.61(4), N1–Co1–N2 100.11(7), N1–Co1–P1 99.62(6), N1–Co1–O2 96.60(7), N1–Co1–O3 108.24(7).

As with the analogs of class **1**, the crystal structures **2a+b** feature classical hydrogen bonds between the amino group of the co-ligand and the adjacent perfluoropinacolate, forming cyclic motifs of the type $R_2^2(8)$. A detailed overview of all occurring classical hydrogen bonds is given below in Table 2.4. For the non-classical hydrogen bonds, which also form patterns similar to those of the diamine compounds, see Table 7.17 in the appendix.

Table 2.4: Distances and angles of classical hydrogen bonds in crystalline compounds of class **2**. The standard deviation of the last decimal digit is given in parentheses. Values without a standard deviation refer to hydrogen atoms calculated on idealized positions, riding on their parent atoms.

2	D–H···A	*d*(D–H)/Å	*d*(H···A)/Å	*d*(D···A)/Å	∢(D–H···A)/°
a	N2–H721···O7	0.91	2.29	3.045(3)	140
	N2–H722···O2^{i}	0.91	2.09	2.957(2)	158
	N4–H741···O5^{ii}	0.91	1.99	2.865(2)	160
b	N2–H721···O2^{iii}	0.91	2.00	2.847(2)	154

Symmetry codes: ^{i} 1−*x*, 1−*y*, −*z*; ^{ii} 2−*x*, 1−*y*, 1−*z*; ^{iii} −1+*x*, *y*, *z*.

2.3 Perfluoropinacolatocobalt nitrosyls with mono- and diphosphanes as co-ligands

The third subclass of newly synthesized perfluoropinacolatocobalt compounds consists of four penta-coordinated {CoNO}^{8} complexes with mono- and diphosphanes as co-ligands (**3a–d**). Being IR-spectroscopically similar concerning their N–O stretch, the crystal structures do not differ significantly from those of classes **1+2** either. However, the CoNO moiety in the phosphane complexes is even more obtuse-angled than in **2a+b**. Like the other subclasses, the crystalline compounds of class **3** cannot be redissolved in common alcohols and are storable under inert gas for several months. In solution, they are stable against NO loss. A complete overview of the compound class is given in Table 2.5. For the synthesis of **3d**, the general crystallization procedure had to be modified in such a way that the precursor solution was treated only briefly with nitric oxide and the gas atmosphere changed back to argon afterwards. In this case, a prolonged exposure to excess NO resulted in an almost complete decoloration of the previously dark brown solution, probably due to the formation of the phosphane oxide, which would not form a nitrosyl complex under the given reaction conditions.

Table 2.5: X-ray and IR data of the crystalline {CoNO}^{8} compounds **3a–d** related to the CoNO moiety and loss of NO upon argon bubbling in solution. Decomposition of the nitrosyl species was rated as not occurring (–).

3		N–O/Å	Co–N/Å	∢Co–N–O/°	$\tilde{\nu}$/cm^{-1}	NO loss
a	[Co(dppe)(fpin)(NO)]	1.168	1.779	134.4	1645	–
b	[Co(dppp)(fpin)(NO)]	1.153	1.783	134.5	1652	–
c	[Co(dppb)(fpin)(NO)]	1.162	1.789	133.0	1654	–
d	[Co(fpin)(NO)(PMePh$_2$)$_2$] [a]	1.142	1.770	135.5	1644	–

[a] Mean structural data of the two entities in the asymmetric unit.

According to CShM calculations, all structures exhibit a distorted square pyramidal coordination geometry (see Figure 2.21). With regards to their degree of distortion, the compounds of class **3** show an overall higher deviation from the ideal *SPY*-5 coordination than the nitrosyls of classes **1+2**. They also exhibit a greater deviation from the ideal trigonal bipyramidal geometry than most compounds of the other two subclasses. Plots of the crystal structures of **3a–d** are depicted on the next pages. A list of the non-classical H-bonds occurring in this compound class is given in Table 7.18 in the appendix.

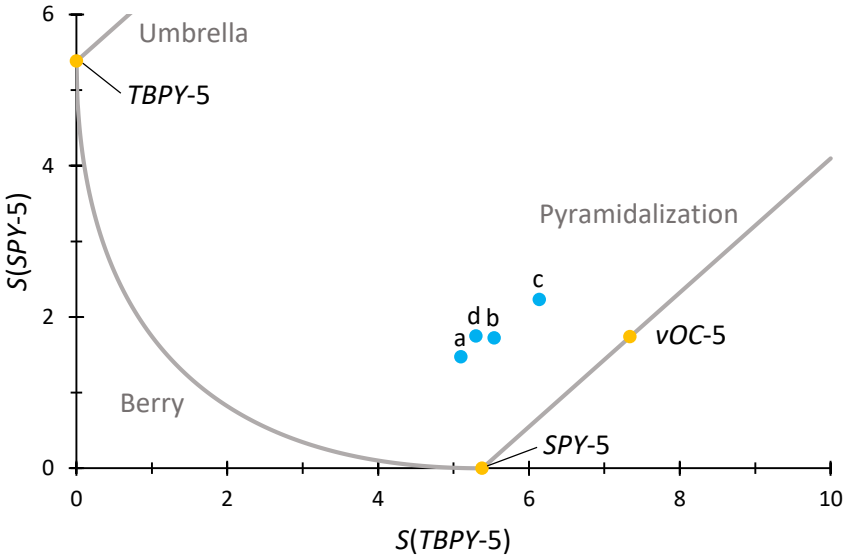

Figure 2.21: CShM map of compounds **3a–d** (blue data points) for fivefold-coordinated species, based on the X-ray structural data of the crystalline products. Ideal, undistorted polyhedra (yellow data points) as reference. The solid gray lines mark the Berry path, the umbrella distortion and the pyramidalization path, respectively. For the compound **3d**, only the first entity in the asymmetric unit (see Figure 2.25) is plotted, since its CShM values do not differ significantly from those of the second entity. The values of the latter (**3d'**) are listed in Table 7.23 in the appendix.

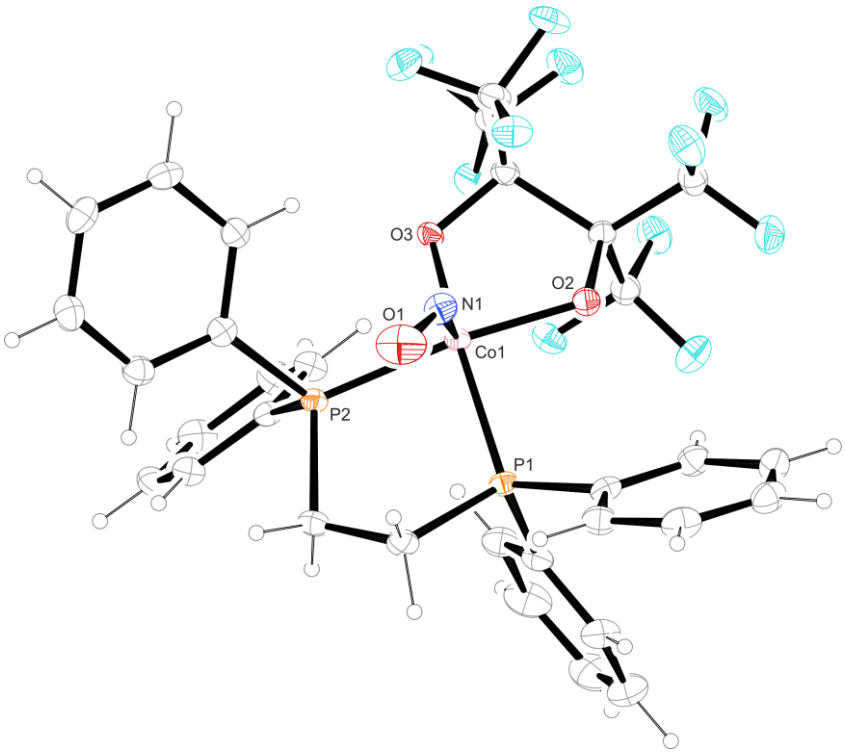

Figure 2.22: ORTEP plot of [Co(dppe)(fpin)(NO)] in crystals of **3a**. Thermal ellipsoids drawn at 50 % probability level at 102 K. Interatomic distances (Å) and bond angles (°) with the standard deviation of the last decimal digit given in parentheses: Co1–N1 1.779(2), Co1–P1 2.1910(6), Co1–P2 2.2095(7), Co1–O2 1.898(1), Co1–O3 1.907(1), N1–O1 1.168(3), Co1–N1–O1 134.4(2), P1–Co1–O3 155.63(5), P2–Co1–O2 166.63(5), P1–Co1–P2 86.25(2), O2–Co1–O3 85.20(6), P1–Co1–O2 89.88(4), P2–Co1–O3 93.08(5), N1–Co1–P1 92.87(7), N1–Co1–P2 94.24(6), N1–Co1–O2 98.74(7), N1–Co1–O3 111.46(8).

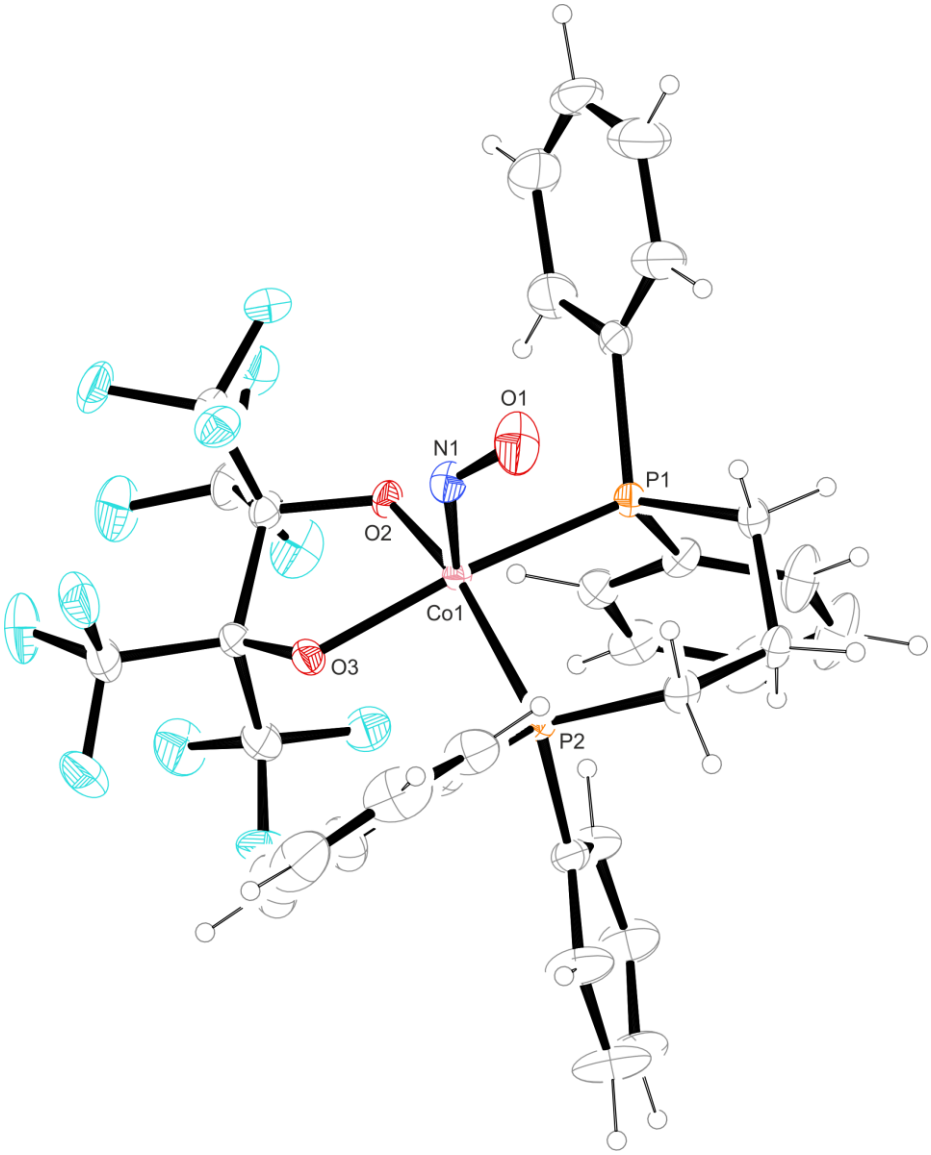

Figure 2.23: ORTEP plot of [Co(dppp)(fpin)(NO)] in crystals of **3b**. Thermal ellipsoids drawn at 50 % probability level at 102 K. Interatomic distances (Å) and bond angles (°) with the standard deviation of the last decimal digit given in parentheses: Co1–N1 1.783(2), Co1–P1 2.2249(5), Co1–P2 2.2144(6), Co1–O2 1.897(1), Co1–O3 1.919(1), N1–O1 1.153(3), Co1–N1–O1 134.5(2), P1–Co1–O3 164.67(5), P2–Co1–O2 155.42(5), P1–Co1–P2 94.61(2), O2–Co1–O3 84.31(6), P1–Co1–O2 87.09(4), P2–Co1–O3 88.06(5), N1–Co1–P1 94.21(7), N1–Co1–P2 93.67(7), N1–Co1–O2 110.69(8), N1–Co1–O3 100.69(8).

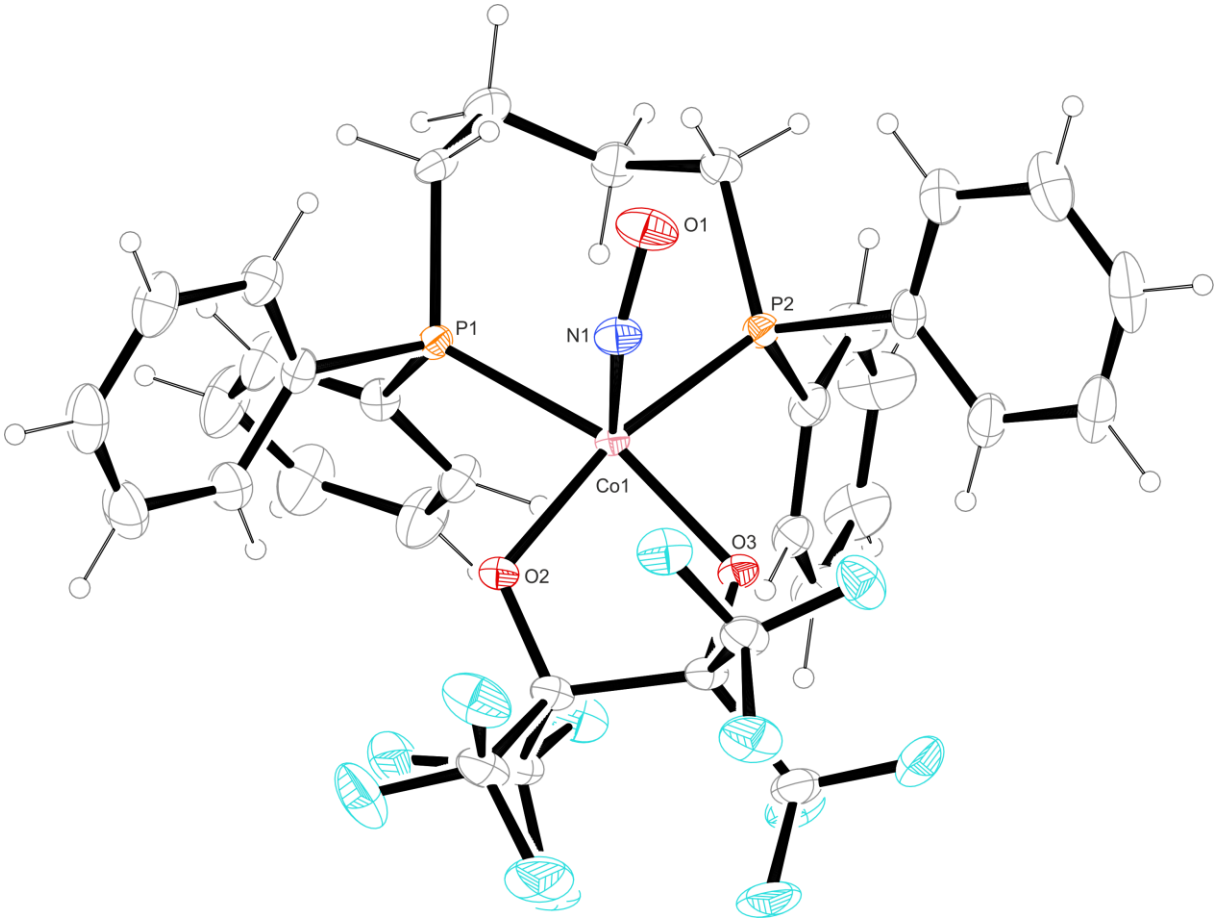

Figure 2.24: ORTEP plot of [Co(dppb)(fpin)(NO)] in crystals of **3c**. Thermal ellipsoids drawn at 50 % probability level at 102 K. Interatomic distances (Å) and bond angles (°) with the standard deviation of the last decimal digit given in parentheses: Co1–N1 1.789(2), Co1–P1 2.2476(6), Co1–P2 2.2382(6), Co1–O2 1.925(1), Co1–O3 1.891(1), N1–O1 1.162(3), Co1–N1–O1 133.0(2), P1–Co1–O3 155.76(5), P2–Co1–O2 163.85(5), P1–Co1–P2 98.97(2), O2–Co1–O3 83.86(6), P1–Co1–O2 86.60(5), P2–Co1–O3 85.03(5), N1–Co1–P1 91.61(7), N1–Co1–P2 94.18(7), N1–Co1–O2 100.85(8), N1–Co1–O3 112.04(8).

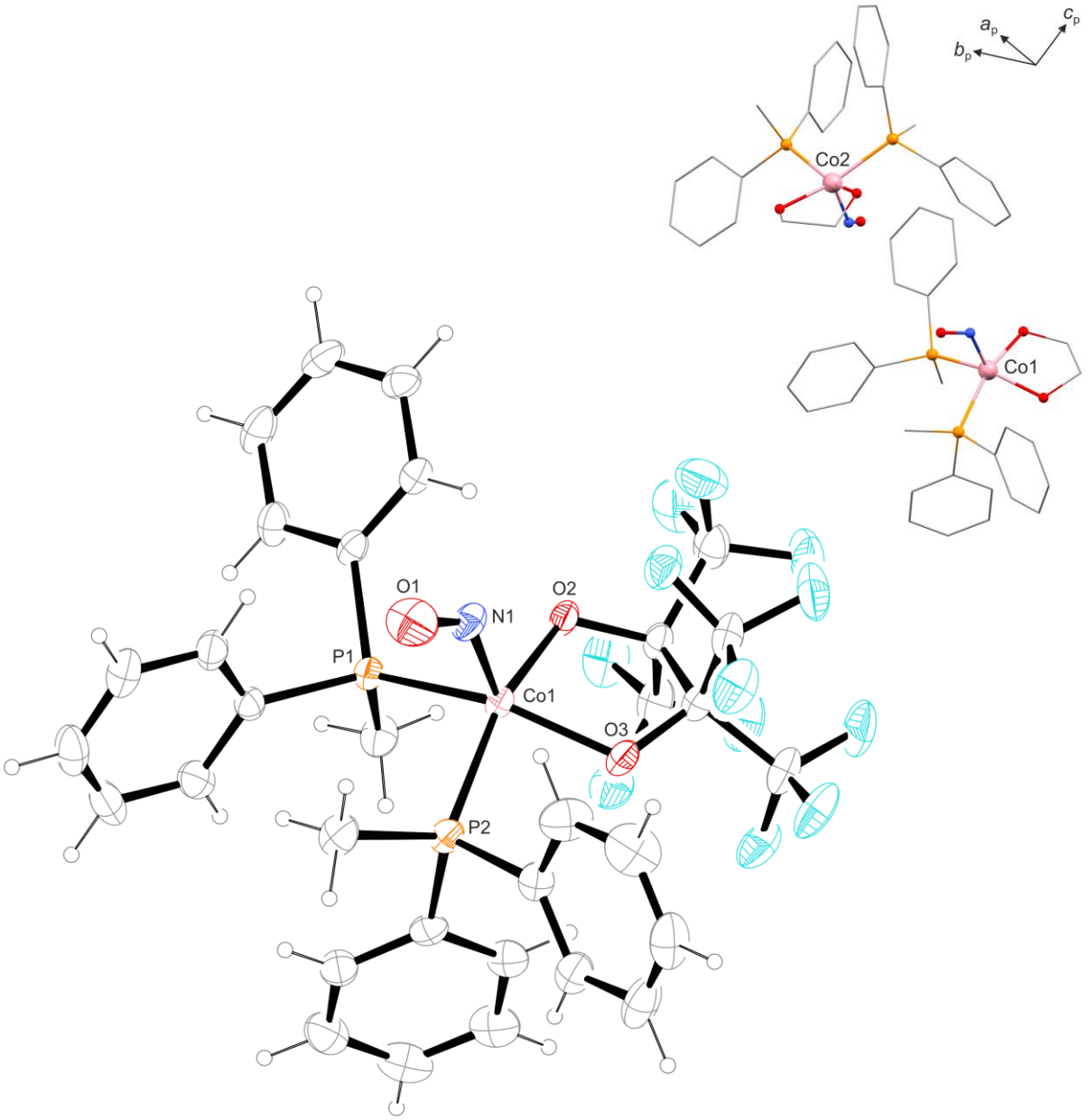

Figure 2.25: Left: ORTEP plot of [Co(fpin)(NO)($PMePh_2$)$_2$] in crystals of **3d**. For clarity, only one entity in the asymmetric unit is depicted. Thermal ellipsoids are drawn at 50 % probability level at 173 K. Interatomic distances (Å) and bond angles (°) with the standard deviation of the last decimal digit given in parentheses: **First molecule (3d, pictured):** Co1–N1 1.774(3), Co1–P1 2.2400(9), Co1–P2 2.226(1), Co1–O2 1.916(2), Co1–O3 1.887(2), N1–O1 1.155(4), Co1–N1–O1 134.7(2), P1–Co1–O3 150.27(8), P2–Co1–O2 160.85(8), P1–Co1–P2 97.34(4), O2–Co1–O3 84.0(1), P1–Co1–O2 85.10(8), P2–Co1–O3 84.66(8), N1–Co1–P1 96.06(9), N1–Co1–P2 97.0(1), N1–Co1–O2 101.7(1), N1–Co1–O3 113.2(1); **Second molecule (3d†, not shown):** Co2–N2 1.765(3), Co2–P3 2.218(1), Co2–P4 2.231(1), Co2–O5 1.914(2), Co2–O6 1.887(2), N2–O4 1.129(4), Co2–N2–O4 136.2(2), P3–Co2–O6 149.37(8), P4–Co2–O5 159.73(8), P3–Co2–P4 97.91(4), O5–Co2–O6 83.5(1), P3–Co2–O5 86.35(8), P4–Co2–O6 82.93(8), N2–Co2–P3 96.35(9), N2–Co2–P4 96.0(1), N2–Co2–O5 103.3(1), N2–Co2–O6 114.1(1). The ORTEP plot of the second entity is given in the appendix (Figure 7.47). **Right:** Plot of the asymmetric unit in **3d**. For clarity, hydrogen atoms and CF_3 groups are omitted. Furthermore, all remaining organic groups are depicted as wireframe.

2.4 Bis(diamine)cobalt nitrosyls with anionic and neutral co-ligands in *trans* position

With the use of DMSO as an antisolvent in the previously described crystallization method, a new series of eleven crystalline $\{CoNO\}^8$ compounds was synthesized. They feature a distorted octahedral structure consisting of two (in some cases *N*-substituted) ethylenediamine ligands in the equatorial plane, with NO and another monodentate co-ligand occupying the apical positions. The products have the composition *trans*-$[Co(NO)(R\text{-}en)_2(X)]X$ or *trans*-$[Co(L)(NO)(R\text{-}en)_2]X_2$, depending on the co-ligand's charge. The first members of this class were derived from *trans*-$[Co(ClO_4)(en)_2(NO)]ClO_4$ (**4a**) by reacting an acetonic solution of this complex with lithium chloride, iodide or nitrate in order to replace the coordinating perchlorate with the respective counteranion. Addition of the lithium salt induced precipitation of the product complex from the solution as a brown solid. Like the synthesis of the bis(perchlorate) precursor, this procedure was originally developed by Feltham *et al.*, who already assigned one of the perchlorate anions in **4a** to the coordination sphere of cobalt.[85]

The first crystal structure of the precursor compound was published by Johnson *et al.*, showing a disorder of the nitrosyl ligand that was solved by refinement with a fixed N–O bond length of 1.15 Å for both NO entities and plotted with thermal ellipsoids drawn at only 16 % probability level.[80] While the original structure was recorded from crystals that were grown from a methanolic bulk solution by slow cooling, it was now found that they can also be obtained from an aqueous solution of the bulk product using the DMSO method. That way, it was possible to redetermine the structure of **4a** with higher quality and resolution (see Figure 2.26). In comparison to the reported structure, the new one exhibits slightly longer Co–N bonds of 1.817 Å and 1.826 Å (reference: 1.803 Å and 1.805 Å) as well as longer N–O distances with lengths of 1.160 Å and 1.172 Å. The Co–O distance to the *trans* perchlorate appears slightly shorter (2.331 Å vs. 2.360 Å in the reference). For the angle of the bent CoNO moiety, values of 122.0° and 121.0° are observed, compared to 122.0° and 122.7°. Like all class **4** products described in this chapter, the crystal structure of this compound features an extensive network of classical hydrogen bonds between the amino groups of the ethylenediamine ligands and the respective adjacent counterions. In **4a**, each amino moiety forms three H-bonds to oxygen atoms of the perchlorate ions (see Table 2.6). A plot of the pattern is given in Figure 2.27. Cyclic ring motifs consisting of intramolecular H-bonds occur, such as $S_1^1(6)$ (–N4–H742 ···$O3^{iv}$–$Cl1^{iv}$–$O2^{iv}$–Co1– in the unary graph set), as well as intermolecular bonds, such as in $R_2^2(8)$ (–N2–H721···$O8^{i}$–$Cl2^{i}$–$O7^{i}$···H741–N4–Co1– in the binary graph set) or $R_4^4(8)$ (···H722···$O5^{i}$···H742···$O3^{iv}$···$H722^{vi}$···$O5^{iv}$···$H742^{vi}$···$O3^{i}$··· in the quarternary graph set). Besides that, non-classical interactions between the C–H groups and counterions and between NH_2 groups and NO are formed as well (see Table 7.19 for all compounds of this class). For the newly synthesized crystals, the IR stretch of the NO moiety was found at 1657 cm^{-1}, which is in good agreement with the value of 1663 cm^{-1} reported by Feltham.[85]

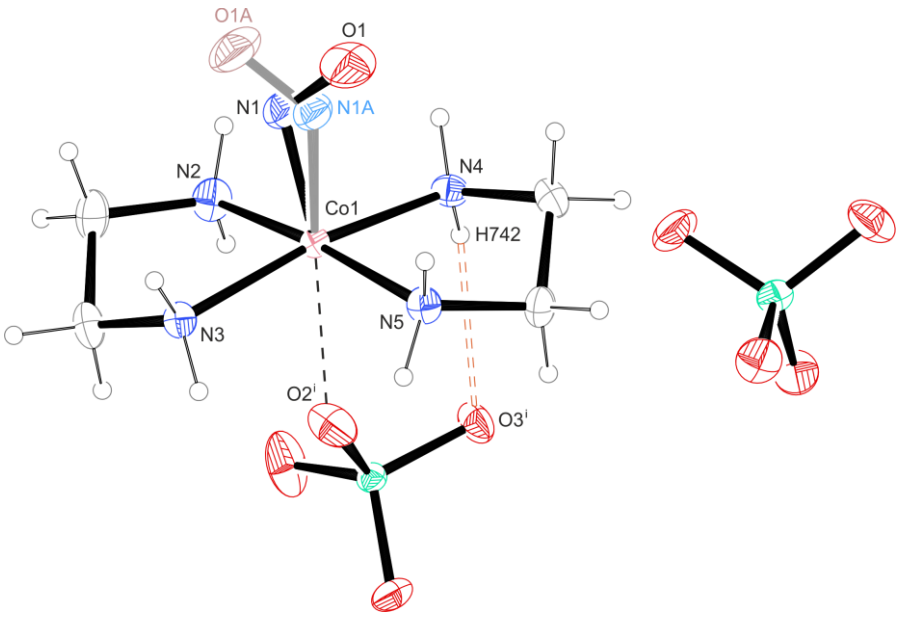

Figure 2.26: ORTEP plot of *trans*-[Co(ClO_4)(en)$_2$(NO)]ClO_4 in crystals of **4a** grown by isothermal solvent diffusion into DMSO. The nitrosyl moiety of the minor disorder form (32 %) is depicted in light colors. Thermal ellipsoids drawn at 50 % probability level at 101 K. Interatomic distances (Å) and bond angles (°) with the standard deviation of the last decimal digit given in parentheses: Co1–N1 1.817(6), Co1–N1A 1.826(1), Co1–O2^{i} 2.331(2), Co1–N2 1.961(2), Co1–N3 1.986(2), Co1–N4 1.969(2), Co1–N5 1.975(2), N1–O1 1.160(7), N1A–O1A 1.172(1), H742–O3^{i} 2.36, Co1–N1–O1 122.0(4), Co1–N1A–O1A 121.0(1), N1–Co1–O2^{i} 170.7(4), N2–Co1–N5 171.6(1), N3–Co1–N4 169.2(1), N2–Co1–N3 84.90(8), N4–Co1–N5 85.46(8), N2–Co1–N4 92.58(8), N3–Co1–N5 95.52(8), N1–Co1–N2 89.9(3), N1–Co1–N3 92.6(2), N1–Co1–N4 97.9(2), N1–Co1–N5 98.5(3), O2^{i}–Co1–N2 90.67(9), O2^{i}–Co1–N3 78.18(8), O2^{i}–Co1–N4 91.38(8), O2^{i}–Co1–N5 81.21(9). Symmetry code: ^{i} −1+*x*, *y*, *z*.

Table 2.6: Distances and angles of classical hydrogen bonds in crystals of **4a** grown by isothermal solvent diffusion into DMSO. The standard deviation of the last decimal digit is given in parentheses. Values without a standard deviation refer to hydrogen atoms calculated on idealized positions, riding on their parent atoms.

D–H···A	*d*(D–H)/Å	*d*(H···A)/Å	*d*(D···A)/Å	∢(D–H···A)/°
N2–H721···O8^{i}	0.91	2.11	2.999(3)	164
N2–H722···O3^{i}	0.91	2.37	3.099(3)	137
N2–H722···O5^{i}	0.91	2.48	3.093(3)	125
N3–H731···O4^{ii}	0.91	2.31	2.779(3)	112
N3–H731···O6^{iii}	0.91	2.25	3.018(3)	141
N3–H732···O9^{ii}	0.91	2.25	3.129(3)	163

Symmetry codes: ^{i} 1−*x*, 1−*y*, 1−*z*; ^{ii} −½+*x*, ½−*y*, ½+*z*; ^{iii} *x*, *y*, 1+*z*; ^{iv} −1+*x*, *y*, *z*.

Table 2.6, continued.

D–H···A	*d*(D–H)/Å	*d*(H···A)/Å	*d*(D···A)/Å	∢(D–H···A)/°
N4–H741···O7^{i}	0.91	2.16	3.065(3)	174
N4–H742···O3^{iv}	0.91	2.36	3.147(3)	145
N4–H742···O5^{i}	0.91	2.47	3.080(3)	125
N5–H751···O3^{ii}	0.91	2.53	3.285(3)	141
N5–H751···O4^{ii}	0.91	2.59	2.950(3)	104
N5–H752···O8^{ii}	0.91	2.16	3.059(3)	170

Symmetry codes: ^{i} 1−*x*, 1−*y*, 1−*z*; ^{ii} −½+*x*, ½−*y*, ½+*z*; ^{iii} *x*, *y*, 1+*z*; ^{iv} −1+*x*, *y*, *z*.

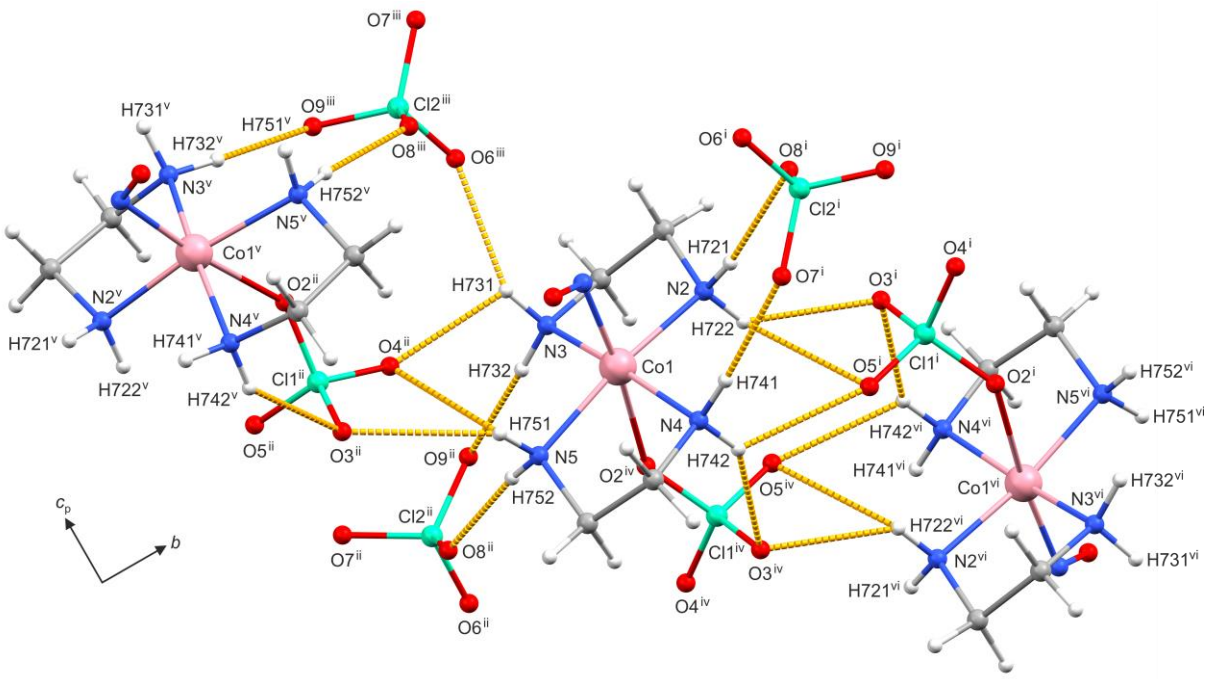

Figure 2.27: Plot of the pattern of classical hydrogen bonds (dashed yellow lines) in crystals of **4a** with view along [$\bar{1}$00]. The crystals were grown by isothermal solvent diffusion into DMSO. For clarity, only the nitrosyl moieties of the major disorder form (68%) are depicted. Symmetry codes: ^{i} 1−*x*, 1−*y*, 1−*z*; ^{ii} −½+*x*, ½−*y*, ½+*z*; ^{iii} *x*, *y*, 1+*z*; ^{iv} −1+*x*, *y*, *z*; ^{v} ½+*x*, ½−*y*, ½+*z*; ^{vi} −*x*, 1−*y*, 1−*z*.

The first X-ray structure of a derivative of **4a** was recorded by Snyder *et al.*, who crystallized the chlorido analog *trans*-[CoCl(en)$_2$(NO)]ClO$_4$ from a cold-saturated aqueous solution.[79] Contrary to the precursor compound, the nitrosyl moiety in the chlorido complex is not disordered. The reported distances for the N–O and Co–N bond are 1.109 Å and 1.820 Å, respectively. The CoNO moiety is bent at an angle of 124.4°. With a distance of 2.575 Å, the Co–Cl bond is even longer than the analogous Co–O bond in **4a**. However, infrared data were only provided for the bulk product, with the nitrosyl stretch reported to be at 1611 cm^{-1}. The complex was synthesized as a dichloride salt as well, using cobalt(II) chloride as educt (bulk: 1635 cm^{-1}).[85] As an alternative to these procedures, it has now been found that this species can also be crystallized reproducibly by isothermal diffusion of an aqueous bulk solution into DMSO, yielding it as *trans*-[CoCl(en)$_2$(NO)]Cl·H$_2$O (**4b**·H$_2$O). Compared to the product known from the literature, the crystal structure of the dichloride compound (Figure 2.28) exhibits longer N–O and Co–N distances of 1.154 Å and 1.830 Å, respectively. With a length of 2.6135 Å, the Co–Cl bond is longer as well. The CoNO moiety has an angle of 123.5°. The N–O stretch was found to be at 1629 cm^{-1}. As can be seen in Figure 2.29, the co-crystallized water molecules are linking both the coordinating and non-binding chloride ions as well as the amino groups of neighboring complexes via classical hydrogen bonds. Structural details on all H-bonds occurring in **4b**·H$_2$O are given in Table 2.7.

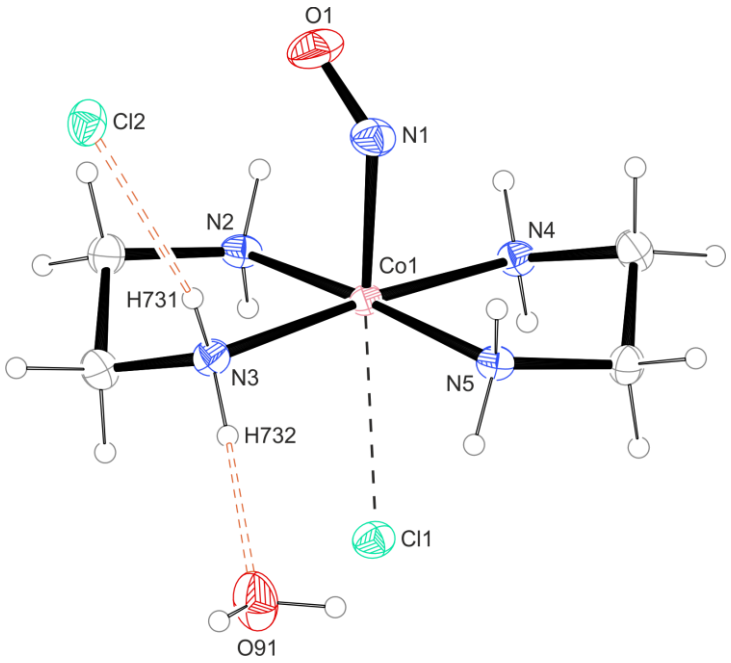

Figure 2.28: ORTEP plot of *trans*-[CoCl(en)$_2$(NO)]Cl·H$_2$O in crystals of **4b**·H$_2$O. Thermal ellipsoids drawn at 50 % probability level at 102 K. Interatomic distances (Å) and bond angles (°) with the standard deviation of the last decimal digit given in parentheses: Co1–N1 1.830(2), Co1–Cl1 2.6135(7), Co1–N2 1.958(2), Co1–N3 1.976(3), Co1–N4 1.972(3), Co1–N5 1.978(2), N1–O1 1.154(4), H731–Cl2 2.40, H732–O91 2.06, Co1–N1–O1 123.5(2), N1–Co1–Cl1 173.8(1), N2–Co1–N5 174.8(1), N3–Co1–N4 173.9(1), N2–Co1–N3 85.7(1), N4–Co1–N5 85.9(1), N2–Co1–N4 92.4(1), N3–Co1–N5 95.6(1), N1–Co1–N2 95.3(1), N1–Co1–N3 95.1(1), N1–Co1–N4 90.8(1), N1–Co1–N5 89.7(1), Cl1–Co1–N2 90.93(8), Cl1–Co1–N3 85.48(8), Cl1–Co1–N4 88.83(8), Cl1–Co1–N5 84.12(8).

Table 2.7: Distances and angles of classical hydrogen bonds in crystals of **4b**·H_2O. The standard deviation of the last decimal digit is given in parentheses. Values without a standard deviation refer to hydrogen atoms calculated on idealized positions, riding on their parent atoms.

D–H···A	*d*(D–H)/Å	*d*(H···A)/Å	*d*(D···A)/Å	∢(D–H···A)/°
N2–H721···Cl2^{i}	0.91	2.61	3.430(3)	150
N2–H722···Cl1^{ii}	0.91	2.48	3.351(3)	160
N3–H731···Cl2	0.91	2.40	3.271(3)	160
N3–H732···O91	0.91	2.06	2.961(4)	172
N4–H741···Cl2^{i}	0.91	2.38	3.267(3)	165
N4–H742···O91^{ii}	0.91	2.43	3.333(4)	171
N5–H752···Cl1^{iii}	0.91	2.51	3.305(3)	147
O91–H911···Cl1^{iii}	0.82(3)	2.31(3)	3.117(3)	168(3)
O91–H912···Cl2^{iv}	0.81(3)	2.33(3)	3.104(3)	160(3)

Symmetry codes: ^{i} 1−*x*, −½+*y*, 1−*z*; ^{ii} 1−*x*, −½+*y*, −*z*; ^{iii} 1−*x*, ½+*y*, −*z*; ^{iv} 2−*x*, ½+*y*, 1−*z*.

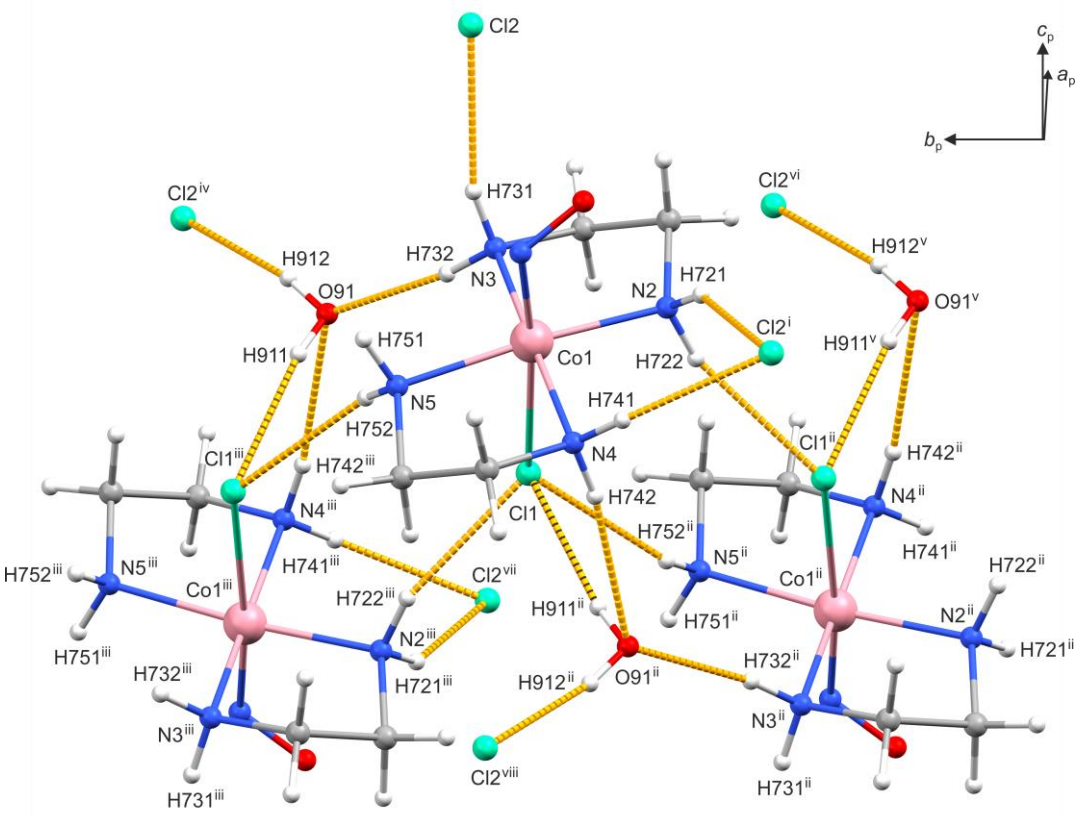

Figure 2.29: Plot of the pattern of classical H-bonds (dashed yellow lines) in crystals of **4b**·H_2O. Symmetry codes: ^{i} 1−*x*, −½+*y*, 1−*z*; ^{ii} 1−*x*, −½+*y*, −*z*; ^{iii} 1−*x*, ½+*y*, −*z*; ^{iv} 2−*x*, ½+*y*, 1−*z*; ^{v} *x*, −1+*y*, *z*; ^{vi} 2−*x*, −½+*y*, 1−*z*; ^{vii} *x*, *y*, −1+*z*; ^{viii} −1+*x*, *y*, −1+*z*.

Apart from the chlorido derivative, no crystal structures of other halogenido analogs of **4a** have been published to date. By using the DMSO method, it was now possible to crystallize the iodido species in the same way as **4a** and **4b**·H_2O, yielding it as *trans*-$[Co(en)_2I(NO)](ClO_4)_{0.6}I_{0.4}$ (**4c**). The crystal structure is depicted in Figure 2.30. While the coordination site *trans* to the NO ligand is fully occupied by iodide, the non-coordinating perchlorate ion was only partially replaced. The nitrosyl ligand is disordered, exhibiting N–O distances of 1.152 Å and 1.127 Å and Co–N bond lengths of 1.832 Å and 1.829 Å. The Co–I bond is 3.0477 Å long. For the CoNO moiety, bond angles of 121.9° and 122.2° are found, similar to **4a+b**. The nitrosyl stretching vibration was recorded at 1632 cm^{-1}. In comparison, for the reported bulk product *trans*-$[Co(en)_2I(NO)]ClO_4$ by Feltham *et al.*, a value of 1654 cm^{-1} has been published.[85] Attempts to obtain single crystals of the bromido anlog were unsuccessful (reported N–O stretching vibration of bulk *trans*-$[CoBr(en)_2(NO)]ClO_4$: 1640 cm^{-1}).[85]

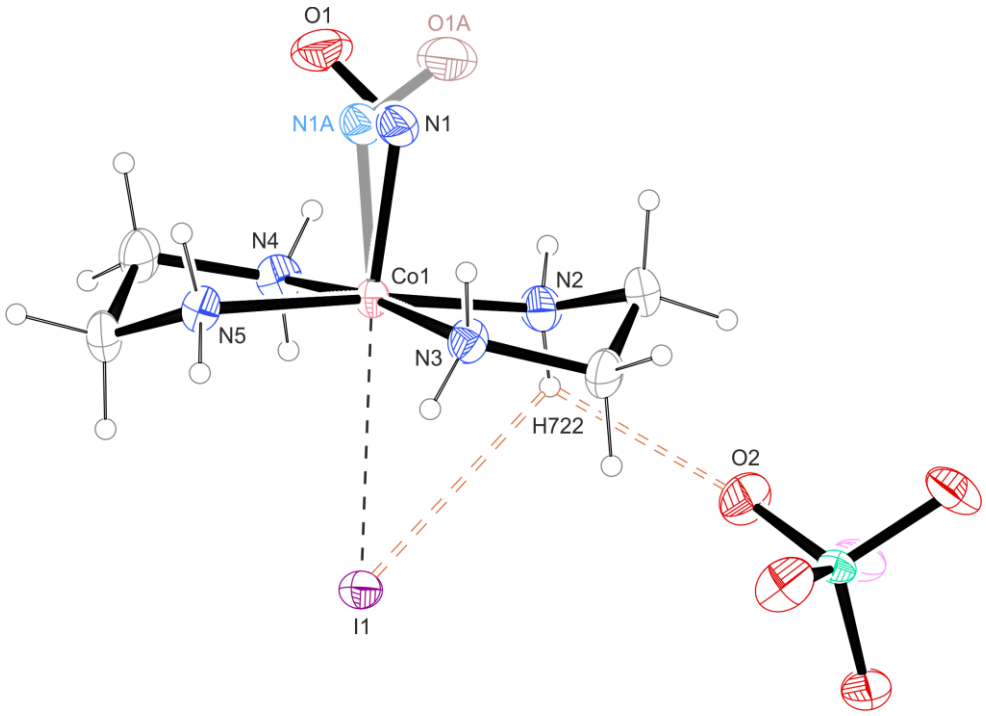

Figure 2.30: ORTEP plot of *trans*-$[Co(en)_2I(NO)](ClO_4)_{0.6}I_{0.4}$ in crystals of **4c**. The nitrosyl moiety of the minor disorder form (16 %) and the non-coordinating iodide ion partially disordered with the perchlorate are depicted in light colors. Thermal ellipsoids drawn at 50 % probability level at 103 K. Interatomic distances (Å) and bond angles (°) with the standard deviation of the last decimal digit given in parentheses: Co1–N1 1.832(3), Co1–N1A 1.829(2), Co1–I1 3.0477(4), Co1–N2 1.968(2), Co1–N3 1.979(2), Co1–N4 1.950(2), Co1–N5 1.974(2), N1–O1 1.152(4), N1A–O1A 1.127(2), H722–I1 3.04, H722–O2 2.57, Co1–N1–O1 121.9(2), Co1–N1A–O1A 122.2(2), N1–Co1–I1 173.5(1), N2–Co1–N5 173.36(8), N3–Co1–N4 173.23(9), N2–Co1–N3 85.74(7), N4–Co1–N5 85.66(7), N2–Co1–N4 93.12(7), N3–Co1–N5 94.71(7), N1–Co1–N2 90.2(1), N1–Co1–N3 90.5(1), N1–Co1–N4 96.2(2), N1–Co1–N5 96.4(1), I1–Co1–N2 85.94(6), I1–Co1–N3 83.96(9), I1–Co1–N4 89.30(6), I1–Co1–N5 87.52(6).

Table 2.8: Distances and angles of classical hydrogen bonds in crystals of **4c**. The standard deviation of the last decimal digit is given in parentheses. Values without a standard deviation refer to hydrogen atoms calculated on idealized positions, riding on their parent atoms.

D–H···A	*d*(D–H)/Å	*d*(H···A)/Å	*d*(D···A)/Å	∢(D–H···A)/°
N2–H721···O2^{i}	0.91	2.09	2.978(3)	166
N2–H721···I2^{i}	0.91	2.98	3.862(4)	165
N2–H722···I1	0.91	3.04	3.509(2)	114
N2–H722···O2	0.91	2.57	3.246(4)	132
N3–H731···I1^{ii}	0.91	2.93	3.697(2)	143
N3–H732···O4^{iii}	0.91	2.32	3.116(4)	147
N4–H741···O4^{i}	0.91	2.12	2.990(3)	160
N4–H741···I2^{i}	0.91	2.94	3.820(4)	162
N4–H742···I1^{iv}	0.91	2.81	3.597(2)	146
N5–H751···O5^{v}	0.91	2.43	3.083(3)	129
N5–H752···O3^{iii}	0.91	2.43	3.219(4)	145
N5–H752···O4^{iii}	0.91	2.42	3.269(3)	154
N5–H752···I2^{iii}	0.91	2.98	3.881(4)	173

Symmetry codes: ^{i} 1−*x*, 1−*y*, 1−*z*; ^{ii} ½+*x*, ½−*y*, ½+*z*; ^{iii} −½+*x*, ½−*y*, ½+*z*; ^{iv} −*x*, 1−*y*, 1−*z*; ^{v} *x*, *y*, 1+*z*.

A plot of the classical hydrogen bond pattern is given in Figure 2.31. In addition to intermolecular ring motifs, also one intramolecular ring occurs, which can be described as $S_1^1(4)$ (–N2–H722···I1–Co1– in the unary graph set). The non-coordinating iodide ions disordered with the perchlorates are integrated into the H-bond network as well. In part, they bind to the same donors as the perchlorate ions located at their sites. A detailed overview of all classical hydrogen bonds in **4c** is given in Table 2.8. Similar to the chlorido analog, no non-classical hydrogen bonds are found between the diamine ligands and the halogenide ions (see Table 7.19). Instead, such interactions are formed with the perchlorate ion, similar to those in the bis(perchlorate) precursor.

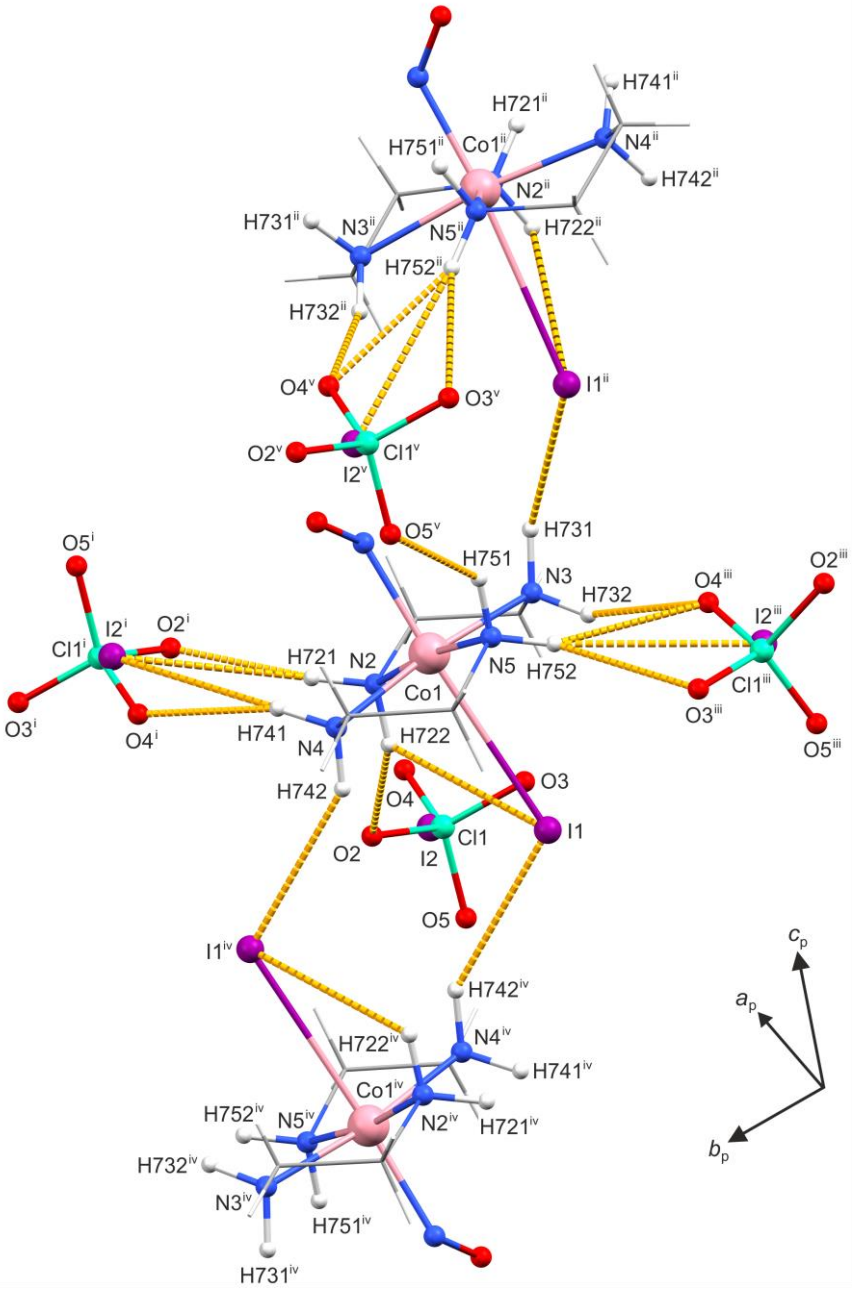

Figure 2.31: Plot of the pattern of classical hydrogen bonds (dashed yellow lines) in crystals of **4c**. For clarity, only the nitrosyl moieties of the major disorder form (84 %) are depicted. Furthermore, the organic ligand residues are depicted as wireframe. Symmetry codes: [i] 1−*x*, 1−*y*, 1−*z* ; [ii] ½+*x*, ½−*y*, ½+*z* ; [iii] −½+*x*, ½−*y*, ½+*z* ; [iv] −*x*, 1−*y*, 1−*z* ; [v] *x*, *y*, 1+*z*.

By using the respective lithium salt, the nitrato derivative of **4a** can be obtained as well. Feltham *et al.* reported a nitrosyl stretch at 1643 cm^{-1} for *trans*-$[Co(en)_2(NO)(NO_3)]ClO_4$ in the bulk.[85] The first crystal structure of the complex was recorded by Ampßler, who obtained *trans*-$[Co(en)_2(NO)(NO_3)]NO_3$ (**4d**) from a cold NO-saturated 1:2 solution of cobalt(II) nitrate and ethylenediamine. For this methanolic reaction mixture, a nitrosyl stretch at 1653 cm^{-1} was published. However, an infrared spectrum of the solid was not recorded.[94] As an alternative route, it was now found that single crystals of **4d** can be obtained reproducibly in larger quantities by isothermal diffusion of an aqueous bulk solution into dimethyl sulfoxide. The bulk product used for this recrystallization was synthesized via Feltham's procedure. In accordance with the cited values, the N–O stretch for crystalline **4d** is found at 1636 cm^{-1}. X-ray analysis of the crystals obtained by the DMSO method revealed that they are structurally identical to the product synthesized by Ampßler (Figure 2.32).

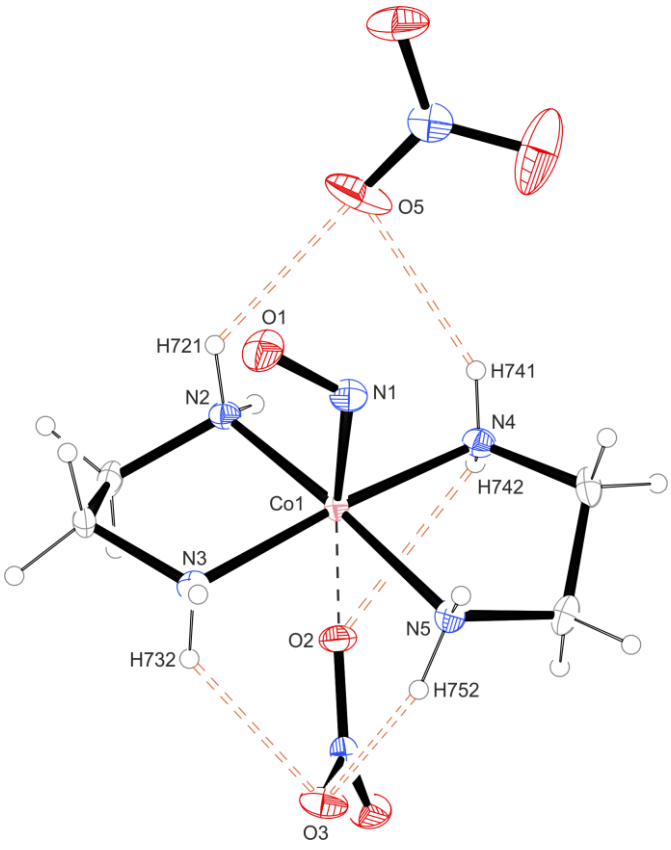

Figure 2.32: ORTEP plot of *trans*-$[Co(en)_2(NO)(NO_3)]NO_3$ (**4d**) based on structural data from Ref.[94]. Thermal ellipsoids are drawn at 50 % probability level at 105 K. Interatomic distances (Å) and bond angles (°) with the standard deviation of the last decimal digit given in parentheses: Co1–N1 1.820(3), Co1–O2 2.304(2), Co1–N2 1.953(3), Co1–N3 1.960(3), Co1–N4 1.973(3), Co1–N5 1.980(3), N1–O1 1.173(4), H721–O5 2.33(4), H732–O3 2.42(3), H741–O5 2.38(4), H742–O2 2.50(4), H752–O3 2.25(3), Co1–N1–O1 121.3(2), N1–Co1–O2 174.4(1), N2–Co1–N5 172.2(1), N3–Co1–N4 172.1(1), N2–Co1–N3 85.3(1), N4–Co1–N5 85.4(1), N2–Co1–N4 93.6(1), N3–Co1–N5 94.6(1), N1–Co1–N2 95.5(1), N1–Co1–N3 96.0(1), N1–Co1–N4 91.9(1), N1–Co1–N5 92.3(1), O2–Co1–N2 84.78(9), O2–Co1–N3 89.7(1), O2–Co1–N4 82.5(1), O2–Co1–N5 87.4(1).

In the published structure, the nitrosyl ligand is well ordered, with N–O and Co–N distances of 1.173 Å and 1.820 Å, respectively. Similar to **4a**, the Co–O distance to the coordinating nitrate ion is 2.304 Å long. For the CoNO moiety, a bond angle of 121.3° is found.[94] Looking at the pattern of classical hydrogen bonds shown in Figure 2.33, two intramolecular ring motifs can be identified: $S_1^1(4)$ (–N4–H742···O2–Co1– in the unary graph set) and $S_2^1(6)$ (–N3–H732···O3···H752–N5–Co1– in the binary graph set). A detailed overview of all classical hydrogen bonds is given in Table 2.9. Contrary to all of the previously mentioned compounds of this class, in **4d**, these interactions by far outnumber the non-classical hydrogen bonds, with only one such bond occurring between a diamine's C–H group and the nitrato ligand. Details on this interaction are listed in Table 7.19.

Table 2.9: Distances and angles of classical hydrogen bonds in crystals of **4d** based on structural data from Ref.[94]. The standard deviation of the last decimal digit is given in parentheses.

D–H···A	*d*(D–H)/Å	*d*(H···A)/Å	*d*(D···A)/Å	∢(D–H···A)/°
N2–H721···O4^{i}	0.84(4)	2.44(3)	3.073(3)	134(3)
N2–H721···O5	0.84(4)	2.33(4)	2.907(4)	127(2)
N2–H722···O6^{ii}	0.85(4)	2.17(4)	2.988(4)	164(3)
N3–H731···O4^{iii}	0.79(3)	2.41(4)	3.075(3)	143(3)
N3–H732···O3	0.87(3)	2.42(3)	3.117(4)	137(3)
N3–H732···O7^{iv}	0.87(3)	2.53(3)	3.249(4)	140(3)
N4–H741···O5	0.81(4)	2.38(4)	3.094(4)	148(3)
N4–H742···O2	0.87(4)	2.50(4)	2.831(4)	104(3)
N4–H742···O6^{ii}	0.87(4)	2.27(4)	2.929(4)	133(3)
N5–H751···O3^{iii}	0.80(4)	2.45(4)	3.159(4)	149(3)
N5–H751···O7^{v}	0.80(4)	2.58(4)	3.193(4)	134(3)
N5–H752···O3	0.90(4)	2.25(3)	2.941(4)	134(3)

Symmetry codes: ^{i} ½–*x*, –½+*y*, –½+*z*; ^{ii} 1–*x*, 1–*y*, ½+*z*; ^{iii} –*x*, 1–*y*, –½+*z*; ^{iv} ½–*x*, –½+*y*, ½+*z*; ^{v} –½+*x*, ³⁄₂–*y*, *z*.

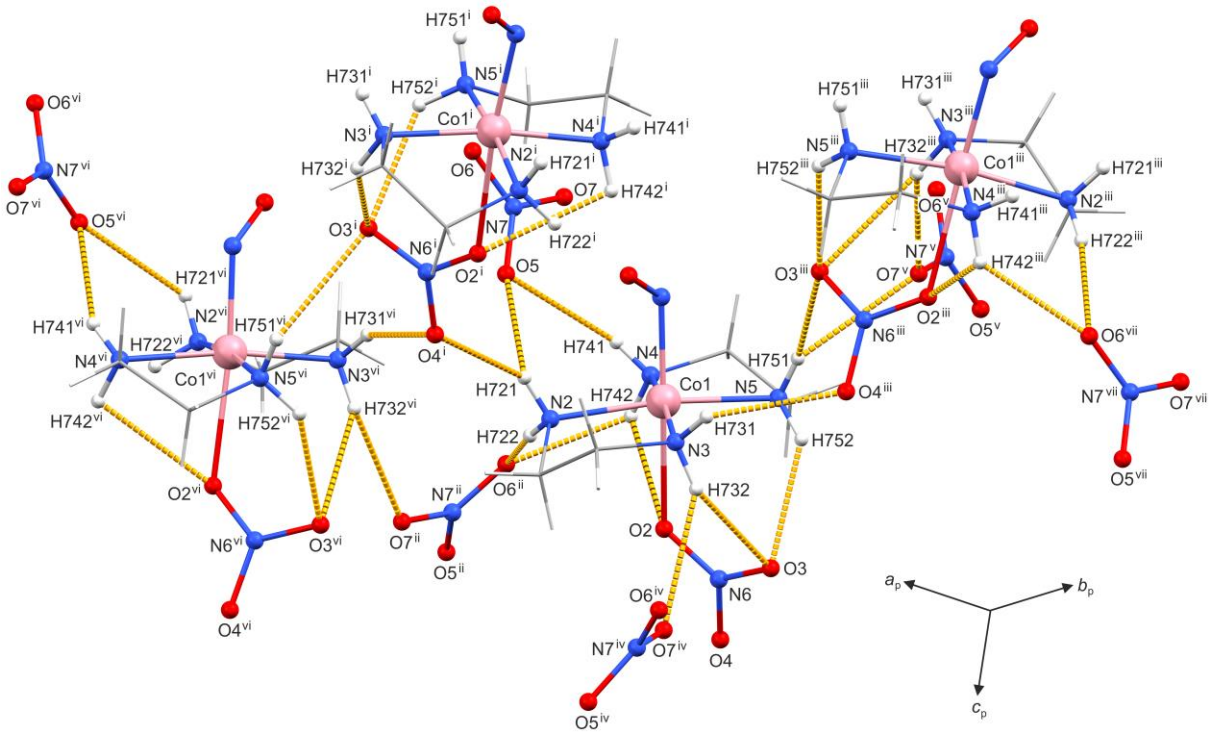

Figure 2.33: Plot of the pattern of classical hydrogen bond (dashed yellow lines) in crystals of **4d** based on structural data from Ref.[94]. For clarity, the organic ligand residues are depicted as wireframe. Symmetry codes: i ½−*x*, −½+*y*, −½+*z*; ii 1−*x*, 1−*y*, ½+*z*; iii −*x*, 1−*y*, −½+*z*; iv ½−*x*, −½+*y*, ½+*z*; v −½+*x*, ³⁄₂−*y*, *z*; vi ½+*x*, ½−*y*, *z*; vii −1+*x*, *y*, *z*.

Deviating from the aforementioned ligand-exchange procedure, further novel nitrosyl complexes of this compound class were synthesized directly without the use of a precursor. By reacting the respective cobalt salt and ligand with NO, *trans*-[Co(BF_4)$(en)_2$(NO)]BF_4 (**4e**) was obtained from methanol using the DMSO crystallization method. As it can be seen in the crystal structure (Figure 2.34), the spatial orientation of both tetrafluoroborate ions in the asymmetric unit strongly resembles the arrangement of the perchlorate ions in the analogous **4a**, therefore forming an almost identical pattern of classical hydrogen bonds (Figure 2.35). As expected, the H···F interactions in **4e** (Table 2.10) are slightly shorter than the analogous H···O bonds in **4a**. Both compounds also exhibit a similar pattern of non-classical hydrogen bonds (see Table 7.19). Furthermore, it can be seen that **4e** crystallizes isotypical to **4a**. This means that both compounds crystallize in the same space group ($P2_1/n$) and have similar lattice parameters (e.g. **4a:** a = 7.7695 Å, β = 104.291° vs. **4e:** a = 7.6626 Å, β = 104.552°). Like in the bis(perchlorate) product, the nitrosyl ligand in **4e** is disordered, with N–O distances of 1.143 Å and 1.131 Å and Co–N bond lengths of 1.824 Å and 1.804 Å. With a length of 2.326 Å, the Co–F bond is more similar to the analogous Co–O bond in **4a** than the corresponding Co–X bonds of the halogenido derivates. The CoNO moiety is bent in the usual range, angles of 121.6° and 121.5° are observed. The nitrosyl stretch was recorded at 1659 cm^{-1}.

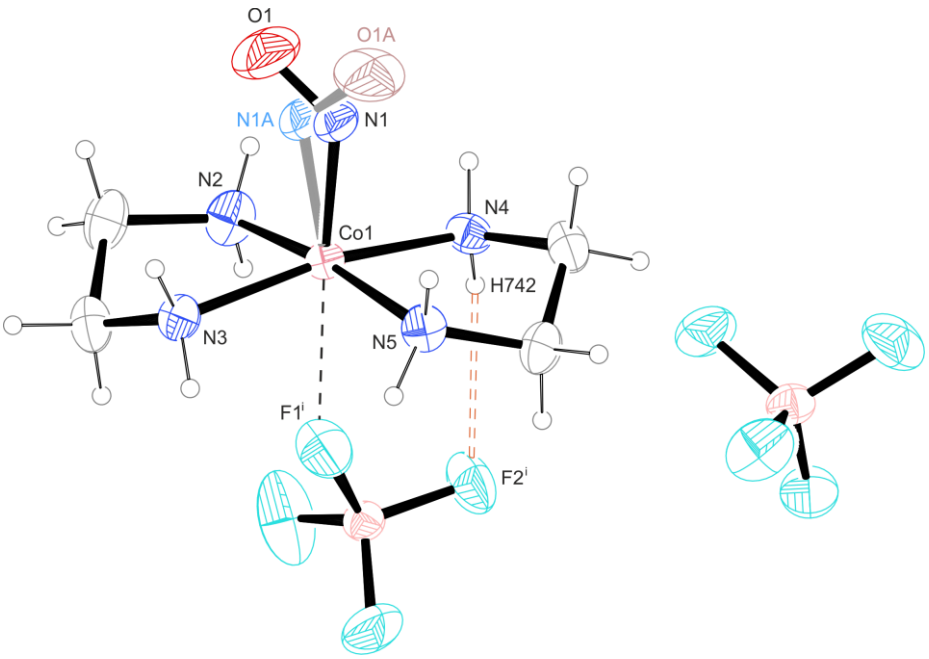

Figure 2.34: ORTEP plot of *trans*-[Co(BF_4)$(en)_2$(NO)]BF_4 in crystals of **4e**. The nitrosyl moiety of the minor disorder form (48 %) is depicted in light colors. Thermal ellipsoids drawn at 50 % probability level at 173 K. Interatomic distances (Å) and bond angles (°) with the standard deviation of the last decimal digit given in parentheses: Co1–N1 1.824(9), Co1–N1A 1.804(9), Co1–F1^{i} 2.326(2), Co1–N2 1.950(2), Co1–N3 1.977(2), Co1–N4 1.966(2), Co1–N5 1.968(2), N1–O1 1.143(1), N1A–O1A 1.131(1), H742–F2^{i} 2.37, Co1–N1–O1 121.6(8), Co1–N1A–O1A 121.5(9), N1–Co1–F1^{i} 171.7(5), N2–Co1–N5 170.4(1), N3–Co1–N4 168.3(1), N2–Co1–N3 85.04(8), N4–Co1–N5 85.28(8), N2–Co1–N4 92.57(8), N3–Co1–N5 95.18(8), N1–Co1–N2 100.2(5), N1–Co1–N3 100.2(3), N1–Co1–N4 91.5(3), N1–Co1–N5 89.2(5), F1^{i}–Co1–N2 88.0(1), F1^{i}–Co1–N3 79.59(8), F1^{i}–Co1–N4 88.88(9), F1^{i}–Co1–N5 82.6(1). Symmetry code: ^{i} −1+*x*, *y*, *z*.

Table 2.10: Distances and angles of classical hydrogen bonds in crystals of **4e**. The standard deviation of the last decimal digit is given in parentheses. Values without a standard deviation refer to hydrogen atoms calculated on idealized positions, riding on their parent atoms.

D–H···A	*d*(D–H)/Å	*d*(H···A)/Å	*d*(D···A)/Å	∢(D–H···A)/°
N2–H721···F7^{i}	0.91	2.09	2.977(3)	166
N2–H722···F2^{i}	0.91	2.26	3.026(3)	141
N2–H722···F4^{i}	0.91	2.37	3.002(3)	126
N3–H731···F3^{ii}	0.91	2.26	2.754(3)	113
N3–H731···F5^{iii}	0.91	2.25	3.017(3)	142
N3–H732···F8^{ii}	0.91	2.21	3.085(3)	161

Symmetry codes: ^{i} 1−*x*, 1−*y*, 1−*z*; ^{ii} −½+*x*, ½−*y*, ½+*z*; ^{iii} *x*, *y*, 1+*z*; ^{iv} −1+*x*, *y*, *z*.

Table 2.10, continued.

D–H···A	*d*(D–H)/Å	*d*(H···A)/Å	*d*(D···A)/Å	∢(D–H···A)/°
N4–H741···F6^{i}	0.91	2.11	3.010(3)	171
N4–H742···F2^{iv}	0.91	2.37	3.154(3)	144
N4–H742···F4^{i}	0.91	2.38	2.989(3)	124
N5–H751···F2^{ii}	0.91	2.53	3.302(3)	143
N5–H752···F7^{ii}	0.91	2.07	2.978(3)	173

Symmetry codes: ^{i} 1−*x*, 1−*y*, 1−*z*; ^{ii} −½+*x*, ½−*y*, ½+*z*; ^{iii} *x*, *y*, 1+*z*; ^{iv} −1+*x*, *y*, *z*.

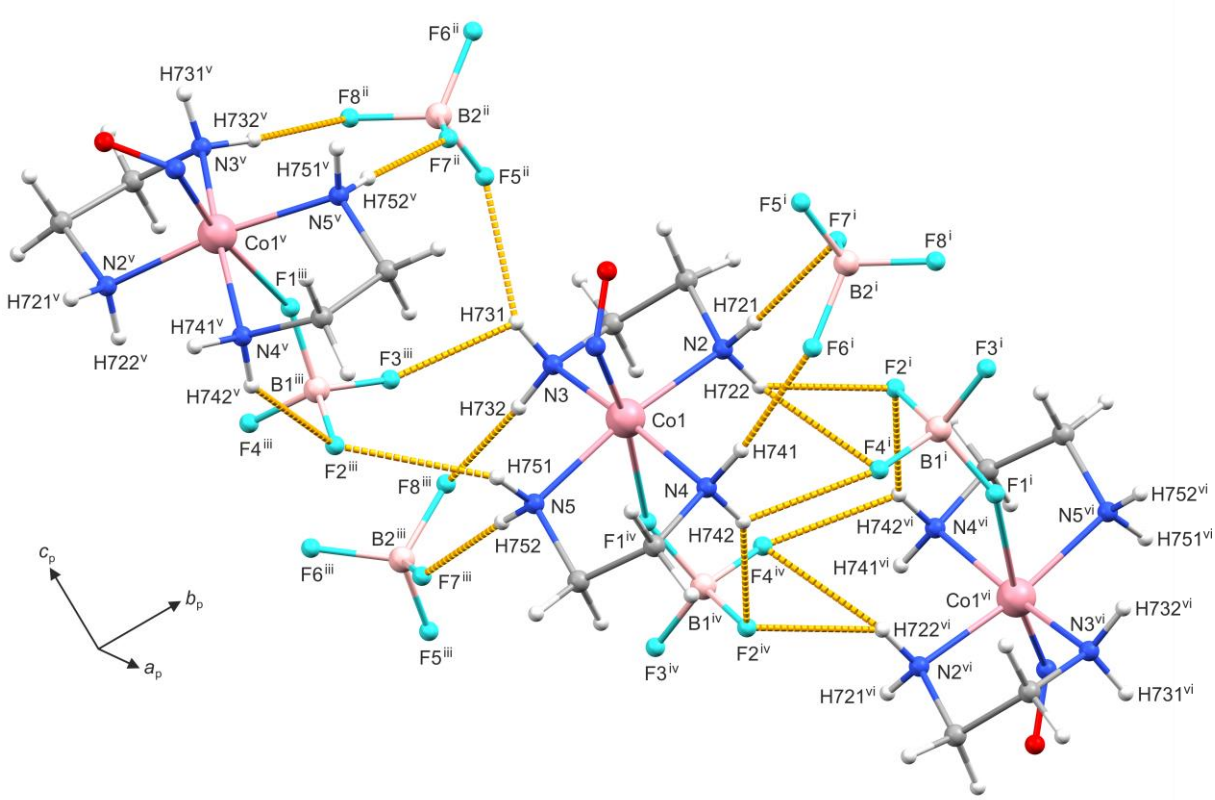

Figure 2.35: Plot of the pattern of classical hydrogen bonds (dashed yellow lines) in crystals of **4e**. For clarity, only the nitrosyl moieties of the major disorder form (52 %) are depicted. Symmetry codes: ^{i} 1−*x*, 1−*y*, 1−*z*; ^{ii} −½+*x*, ½−*y*, ½+*z*; ^{iii} *x*, *y*, 1+*z*; ^{iv} −1+*x*, *y*, *z*; ^{v} ½+*x*, ½−*y*, ½+*z*; ^{vi} −*x*, 1−*y*, 1−*z*.

Isothermal diffusion of an acetonitrilic solution of **4a** into DMSO gave single crystals of the compound *trans*-[Co(dmso-κ*O*)(en)$_2$(NO)](ClO$_4$)$_2$·DMSO (**4f**·DMSO), proving that the position *trans* to NO can also be occupied by an uncharged co-ligand. The crystal structure (Figure 2.36) features disordered nitric oxide with N–O distances of 1.161 Å and 1.178 Å and Co–N bond lengths of 1.819 Å and 1.826 Å. For the bent CoNO moiety, angles of 121.9° and 120.8° are found. The N–O stretching band is located at 1638 cm^{-1}. As for the dmso ligand, κ*O*-coordination is observed. The Co–O bond is 2.234 Å long, thus slightly shorter than the corresponding bonds in the perchlorato and nitrato analogs.

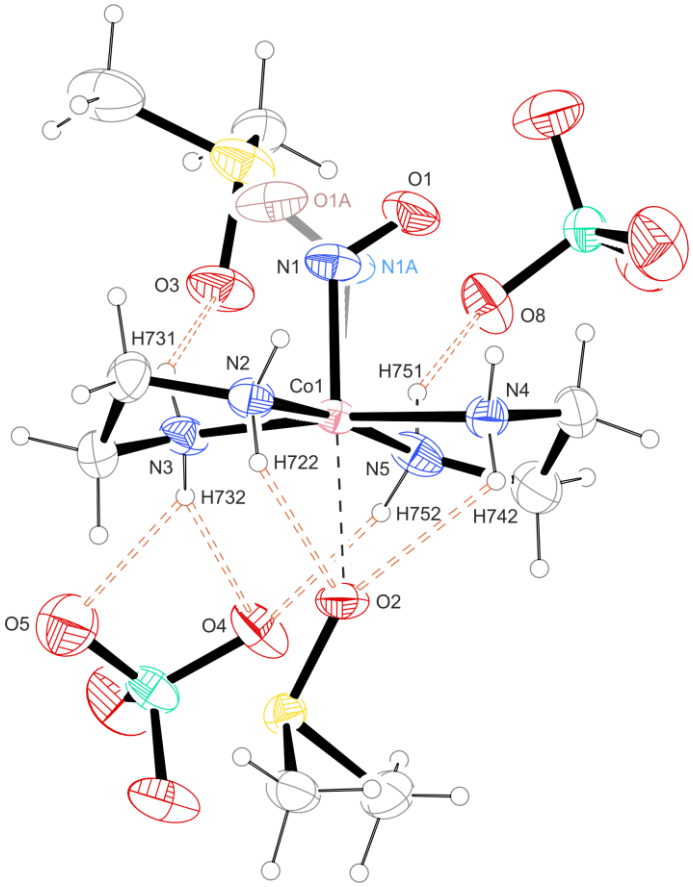

Figure 2.36: ORTEP plot of *tr.*-[Co(dmso-κ*O*)(en)$_2$(NO)](ClO$_4$)$_2$·DMSO in crystals of **4f**·DMSO. The nitrosyl moiety of the minor disorder form (33 %) is depicted in light colors. Thermal ellipsoids drawn at 50 % probability level at 173 K. Interatomic distances (Å) and bond angles (°) with the standard deviation of the last decimal digit given in parentheses: Co1–N1 1.819(6), Co1–N1A 1.826(1), Co1–O2 2.234(1), Co1–N2 1.972(2), Co1–N3 1.969(2), Co1–N4 1.961(2), Co1–N5 1.967(2), N1–O1 1.161(2), N1A–O1A 1.178(3), H722–O2 2.52, H731–O3 2.21, H732–O4 2.49, H732–O5 2.34, H742–O2 2.42, H751–O8 2.22, H752–O4 2.23, Co1–N1–O1 121.9(1), Co1–N1A–O1A 120.8(3), N1–Co1–O2 173.0(7), N2–Co1–N5 173.2(1), N3–Co1–N4 173.5(1), N2–Co1–N3 85.48(8), N4–Co1–N5 85.55(9), N2–Co1–N4 95.03(8), N3–Co1–N5 93.19(9), N1–Co1–N2 89.8(7), N1–Co1–N3 92.7(8), N1–Co1–N4 93.8(8), N1–Co1–N5 96.9(7), O2–Co1–N2 84.96(8), O2–Co1–N3 91.41(8), O2–Co1–N4 82.13(8), O2–Co1–N5 88.44(8).

A plot of the pattern of classical hydrogen bonds is given in Figure 2.37. Both the coordinating and non-binding DMSO molecules are involved in the network, with the former creating cyclic motifs such as $S_2^1(6)$ (–N2–H722···O2···H742–N4–Co1– in the binary graph set). Furthermore, both counterions serve as acceptors for classical interactions, as listed in Table 2.11. Regarding non-classical hydrogen bonds, both DMSO molecules and perchlorate ions contribute to the network. The sulfoxide's methyl groups act as donors, forming hydrogen bonds to the perchlorate ions and nitrosyl-oxygen atoms. For a complete overview of the non-classical interactions, see Table 7.19.

Table 2.11: Distances and angles of classical hydrogen bonds in crystals of **4f**·DMSO. The standard deviation of the last decimal digit is given in parentheses. Values without a standard deviation refer to hydrogen atoms calculated on idealized positions, riding on their parent atoms.

D–H···A	*d*(D–H)/Å	*d*(H···A)/Å	*d*(D···A)/Å	∢(D–H···A)/°
N2–H721···O8^{i}	0.91	2.32	3.181(3)	157
N2–H722···O2	0.91	2.52	2.846(2)	102
N2–H722···O4^{i}	0.91	2.42	3.201(3)	144
N3–H731···O3	0.91	2.21	2.946(3)	138
N3–H732···O4	0.91	2.49	3.354(3)	158
N3–H732···O5	0.91	2.34	3.113(3)	143
N4–H741···O8^{i}	0.91	2.55	3.369(3)	150
N4–H741···O11^{i}	0.91	2.23	3.061(3)	152
N4–H742···O2	0.91	2.42	2.762(3)	103
N4–H742···O9^{ii}	0.91	2.21	3.028(3)	150
N5–H751···O8	0.91	2.22	3.039(3)	150
N5–H752···O4	0.91	2.23	3.128(3)	167

Symmetry codes: ^{i} −1+*x*, *y*, *z*; ^{ii} −1+*x*, ½−*y*, −½+*z*.

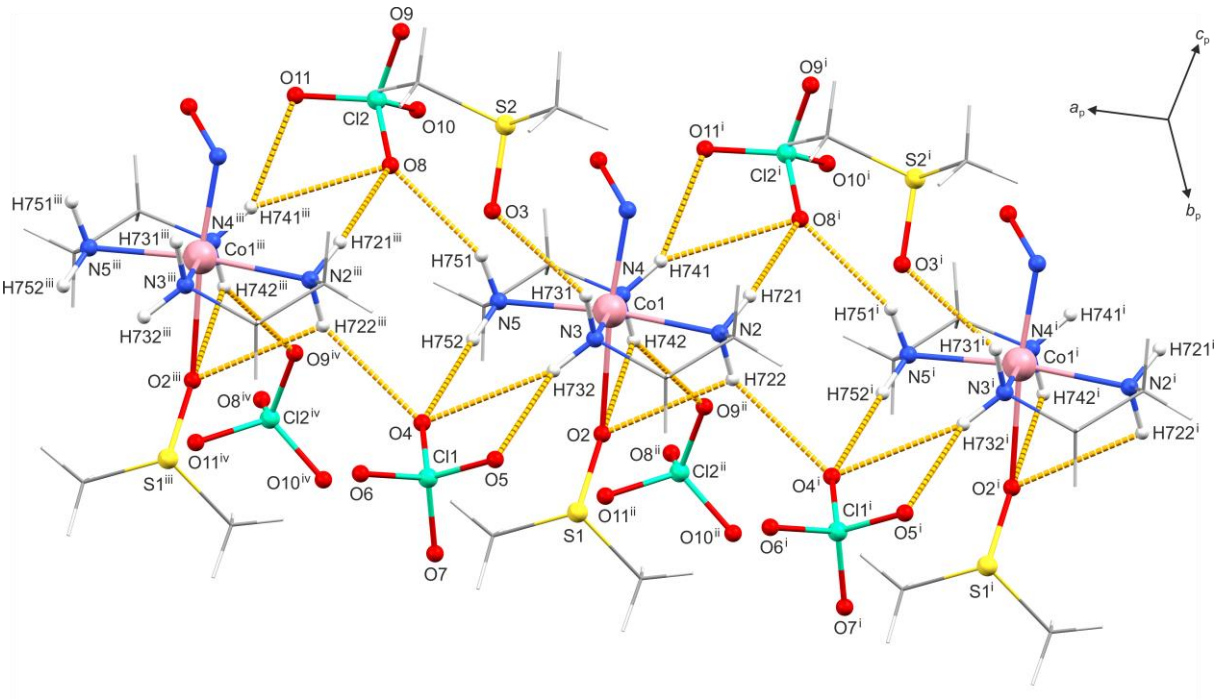

Figure 2.37: Plot of the pattern of classical H-bonds (dashed yellow lines) in crystals of **4f**·DMSO. For clarity, only the nitrosyl moieties of the major disorder form (67 %) are shown. Furthermore, all organic residues are depicted as wireframe. Symmetry codes: [i] −1+*x*, *y*, *z*; [ii] −1+*x*, ½−*y*, −½+*z*; [iii] 1+*x*, *y*, *z*; [iv] *x*, ½−*y*, −½+*z*.

In addition to varying the *trans* co-ligand, further hexacoordinated nitrosyls were synthesized using *N*-substituted derivatives of ethylenediamine. Via the general procedure, the methylated derivative *trans*-[Co(ClO_4)(men)$_2$(NO)]ClO_4 (**4g**) was obtained directly from methanol. Crystallization was achieved by storing the reaction mixture at −25 °C under NO. In constrast to the unsubstituted perchlorato analog (**4a**), the nitrosyl ligand in the crystal structure of **4g** is well ordered (see Figure 2.38). Concerning the structural parameters of the CoNO moiety, the compound lies in the same range as the unsubstituted complexes, showing an N–O distance of 1.138 Å, a Co–N bond length of 1.815 Å and a Co–N–O angle of 124.0°. The Co–O bond is 2.363 Å long, similar to the other derivatives with *O*-coordinating ligands. The N–O stretch is at 1653 cm^{-1}. This species represents the second cobalt nitrosyl with *N*-methylethylenediamine (men) to be characterized structurally by X-ray diffraction, the other being Riggenmann's *trans*-[Co(H_2O)(men)$_2$(NO)](NO_3)$_2$, which he synthesized from methanol using cobalt(II) nitrate hexahydrate. Although the respective hexahydrate was also used in the synthesis of **4g**, the coordination site *trans* to NO is instead entirely occupied by perchlorate. Regarding the first coordination sphere, the aqua complex shows no significant deviations from the other class members, exhibiting N–O and Co–N bond lengths of 1.158 Å and 1.807 Å, respectively. The CoNO moiety is bent at an angle of 124.3° and the Co–O bond is 2.336 Å long. For the nitrosyl stretch, a split absorption band at 1640 cm^{-1} has been reported.[94,95]

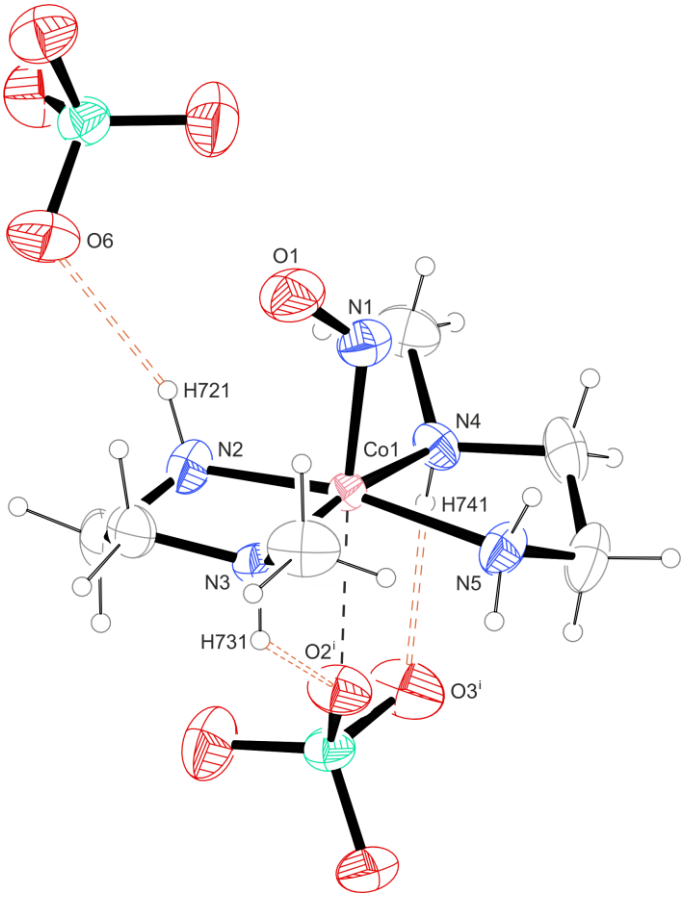

Figure 2.38: ORTEP plot of *trans*-[Co(ClO_4)(men)$_2$(NO)]ClO_4 in crystals of **4g**. Thermal ellipsoids drawn at 50 % probability level at 173 K. Due to the chosen perspective, the hydrogen atom H722 is covered in the plot by its parent atom N2. Interatomic distances (Å) and bond angles (°) with the standard deviation of the last decimal digit given in parentheses: Co1–N1 1.815(3), Co1–O2^{i} 2.363(2), Co1–N2 1.965(3), Co1–N3 1.966(3), Co1–N4 1.992(3), Co1–N5 1.982(3), N1–O1 1.138(4), H721–O6 2.23(5), H731–O2^{i} 2.37(3), H741–O3^{i} 2.25(5), Co1–N1–O1 124.0(2), N1–Co1–O2^{i} 174.8(1), N2–Co1–N5 168.7(1), N3–Co1–N4 170.2(1), N2–Co1–N3 85.9(1), N4–Co1–N5 85.5(1), N2–Co1–N4 94.2(1), N3–Co1–N5 92.6(1), N1–Co1–N2 97.1(1), N1–Co1–N3 98.2(1), N1–Co1–N4 91.5(1), N1–Co1–N5 94.2(1), O2^{i}–Co1–N2 87.9(1), O2^{i}–Co1–N3 81.05(9), O2^{i}–Co1–N4 89.19(9), O2^{i}–Co1–N5 80.8(1). Symmetry code: ^{i} 1−*x*, ½+*y*, ½−*z*.

As can be seen from the pattern of classical hydrogen bonds given in Figure 2.39, the monomethylated compound exhibits fewer of these interactions compared to the unsubstituted derivatives. Two intramolecular rings occur, involving the hydrogen atoms of the substituted amino groups. A detailed overview of all classical H-bonds is given in Table 2.12. However, methylation does not increase the number of non-classical hydrogen bonds (see Table 7.19). Attempts to synthesize further derivative complexes with *N*-methylethylenediamine analogous to **4b–f** were unsuccessful.

Table 2.12: Distances and angles of classical hydrogen bonds in crystals of **4g**. The standard deviation of the last decimal digit is given in parentheses. Values without a standard deviation refer to hydrogen atoms calculated on idealized positions, riding on their parent atoms.

D–H···A	*d*(D–H)/Å	*d*(H···A)/Å	*d*(D···A)/Å	∢(D–H···A)/°
N2–H721···O6	0.89(5)	2.23(5)	3.062(4)	157(4)
N2–H722···O4	0.88(4)	2.33(4)	3.074(4)	142(3)
N3–H731···O2^{i}	0.87(4)	2.37(3)	2.830(3)	113(2)
N3–H731···O5^{ii}	0.87(4)	2.43(3)	3.202(4)	148(3)
N4–H741···O3^{i}	0.86(5)	2.25(5)	3.069(4)	158(4)
N5–H751···O7^{iii}	0.91	2.19	3.072(4)	164
N5–H752···O8^{iv}	0.91	2.32	2.999(4)	132

Symmetry codes: ^{i} 1−*x*, ½+*y*, ½−*z*; ^{ii} *x*, 1+*y*, *z*; ^{iii} −*x*, ½+*y*, ½−*z*; ^{iv} *x*, ³⁄₂−*y*, −½+*z*.

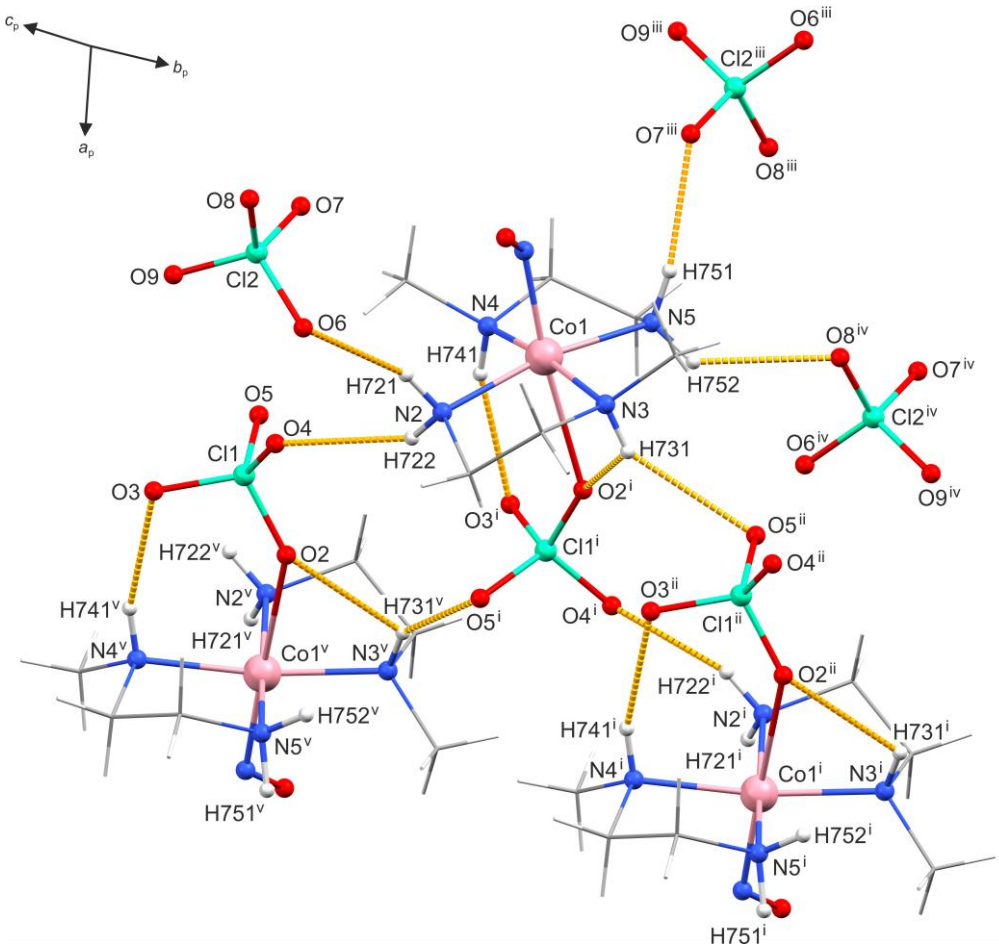

Figure 2.39: Plot of the pattern of classical hydrogen bonds (dashed yellow lines) in crystals of **4g**. For clarity, the organic ligand residues are depicted as wireframe. Symmetry codes: ^{i} 1−*x*, ½+*y*, ½−*z*; ^{ii} *x*, 1+*y*, *z*; ^{iii} −*x*, ½+*y*, ½−*z*; ^{iv} *x*, ³⁄₂−*y*, −½+*z*; ^{v} 1−*x*, −½+*y*, ½−*z*.

Using *N*,*N*-dimethylethylenediamine and the aforementioned DMSO crystallization method, the complex species *trans*-[Co(ClO_4)(*N*,*N*-dmen)$_2$(NO)]ClO_4 (**4h**) was synthesized directly from acetone. When methanol is used as solvent, the compound can be obtained in larger quantitites as a microcrystalline solid. As for the crystal structure (Figure 2.40), the N–O and Co–N distances are 1.165 Å and 1.809 Å, respectively. The CoNO moiety is bent at a bond angle of 123.6°. With a length of 2.394 Å, the Co–O bond to the coordinating perchlorate ion is slightly longer than in the monomethylated derivative (**4g**: 2.363 Å) and even longer than in the unsubstituted analog (**4a**: 2.331 Å). The nitrosyl stretch was measured at 1655 cm^{-1}. Compared to **4g**, it can be seen that the additional substitution of the diamine ligands did not lead to a further decrease in classical hydrogen bonds (Figure 2.41, Table 2.13), but to a higher number of non-classical interactions, as listed in Table 7.19. Contrary to the unsubstituted analog (**4a**), it was not possible to obtain derivatives of **4g** by replacing the *trans* co-ligand.

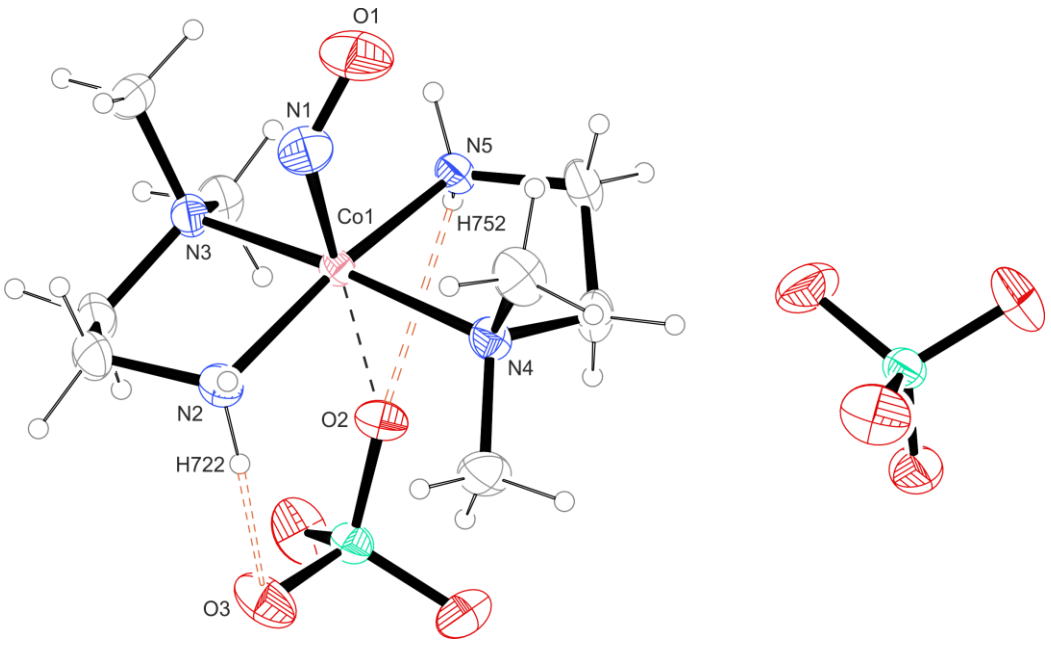

Figure 2.40: ORTEP plot of *trans*-[Co(ClO_4)(*N*,*N*-dmen)$_2$(NO)]ClO_4 in crystals of **4h**. Thermal ellipsoids are drawn at 50% probability level at 173 K. Interatomic distances (Å) and bond angles (°) with the standard deviation of the last decimal digit given in parentheses: Co1–N1 1.809(2), Co1–O2 2.394(1), Co1–N2 1.968(2), Co1–N3 2.065(2), Co1–N4 2.058(2), Co1–N5 1.949(2), N1–O1 1.165(2), H722–O3 2.37, H752–O2 2.51, Co1–N1–O1 123.6(2), N1–Co1–O2 178.91(7), N2–Co1–N5 169.90(6), N3–Co1–N4 171.06(6), N2–Co1–N3 85.81(7), N4–Co1–N5 85.24(6), N2–Co1–N4 94.65(7), N3–Co1–N5 92.74(6), N1–Co1–N2 92.47(7), N1–Co1–N3 93.45(7), N1–Co1–N4 95.45(7), N1–Co1–N5 97.60(7), O2–Co1–N2 88.65(6), O2–Co1–N3 86.58(6), O2–Co1–N4 84.50(6), O2–Co1–N5 81.29(6).

Table 2.13: Distances and angles of classical hydrogen bonds in crystals of **4h**. The standard deviation of the last decimal digit is given in parentheses. Values without a standard deviation refer to hydrogen atoms calculated on idealized positions, riding on their parent atoms.

D–H···A	*d*(D–H)/Å	*d*(H···A)/Å	*d*(D···A)/Å	∢(D–H···A)/°
N2–H721···O4^{i}	0.91	2.09	3.002(2)	176
N2–H722···O3	0.91	2.37	3.167(2)	146
N2–H722···O6^{ii}	0.91	2.51	3.031(2)	117
N5–H751···O7^{iii}	0.91	2.46	3.095(2)	127
N5–H751···O8^{iii}	0.91	2.35	3.215(2)	159
N5–H752···O2	0.91	2.51	2.849(2)	102
N5–H752···O5^{iv}	0.91	2.21	2.944(2)	138

Symmetry codes: ^{i} −½+*x*, ½−*y*, −½+*z*; ^{ii} ½+*x*, ½−*y*, −½+*z*; ^{iii} −*x*, 1−*y*, 1−*z*; ^{iv} 1−*x*, 1−*y*, 1−*z*.

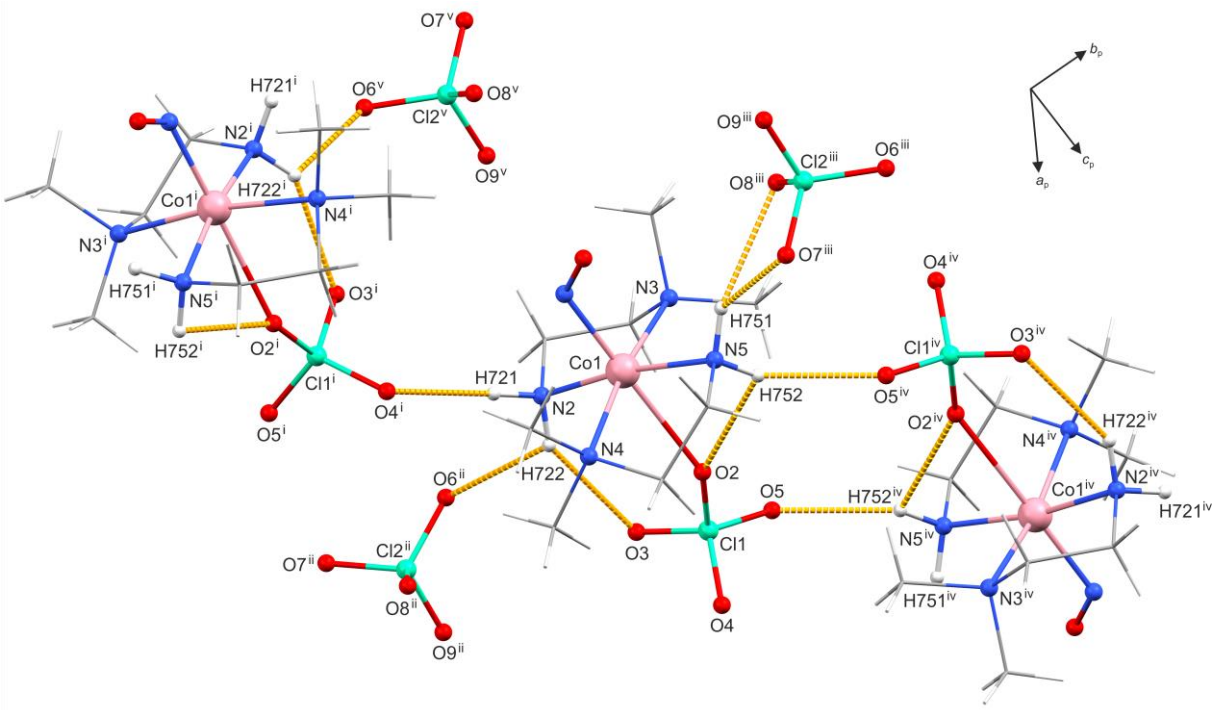

Figure 2.41: Plot of the pattern of classical H-bonds (dashed yellow lines) in crystals of **4h**. For clarity, the organic ligand residues are depicted as wireframe. Symm. codes: ^{i} −½+*x*, ½−*y*, −½+*z*; ^{ii} ½+*x*, ½−*y*, −½+*z*; ^{iii} −*x*, 1−*y*, 1−*z*; ^{iv} 1−*x*, 1−*y*, 1−*z*; ^{v} *x*, *y*, −1+*z*.

Using the direct route, crystalline *trans*-[Co(BF_4)(*N*,*N*-dmen)$_2$(NO)]BF_4 (**4i**) was synthesized in the same way as the previously mentioned perchlorato analog. As in **4h**, the nitrosyl ligand is well ordered in the tetrafluoroborate compound (see Figure 2.42). Regarding the CoNO moiety, the compound has structural parameters similar to **4h**, with an N–O bond length of 1.156 Å, a Co–N distance of 1.806 Å and a Co–N–O angle of 124.3°. Featuring a Co–F bond length of 2.375 Å, this distance is slightly longer than in the unsubstituted analog (**4e**: 2.326 Å), a pattern that was already observed for the perchlorato compounds. The N–O stretch was located at 1656 cm^{-1}. As can be seen from the crystal structure, both tetrafluoroborate ions and methyl groups are oriented in the way as the ions and residues in the analogous perchlorato species. This similarity was also observed for the unsubstituted nitrosyls (**4a+e**). The pattern of classical hydrogen bonds in **4i** (Figure 2.43) thus strongly resembles the one of **4h**. The same applies for the non-classical interactions. A detailed overview of all occurring classical and non-classical H-bonds is given in Tables 2.14 and 7.19, respectively. Another similarity to the unsubstituted derivatives is the isotypism of **4h** and **4i**, crystallizing both in the space group $P2_1/n$ with similar lattice parameters (e.g. **4h:** a = 8.4241 Å, β = 108.195° vs. **4i:** a = 8.3111 Å, β = 107.946°). Further, two similar nitrosyls with symmetrically methylated diamines where prepared using the same procedure, but could only be obtained as microcrystalline solids. For bulk *trans*-[Co(ClO_4)(*N*,*N*'-dmen)$_2$(NO)]ClO_4 (**4j**) and *trans*-[Co(BF_4)(*N*,*N*'-dmen)$_2$(NO)]BF_4 (**4k**), N–O stretches were found at 1651 cm^{-1} and 1652 cm^{-1}, respectively. The composition of the compounds was confirmed by CHN elemental analysis.

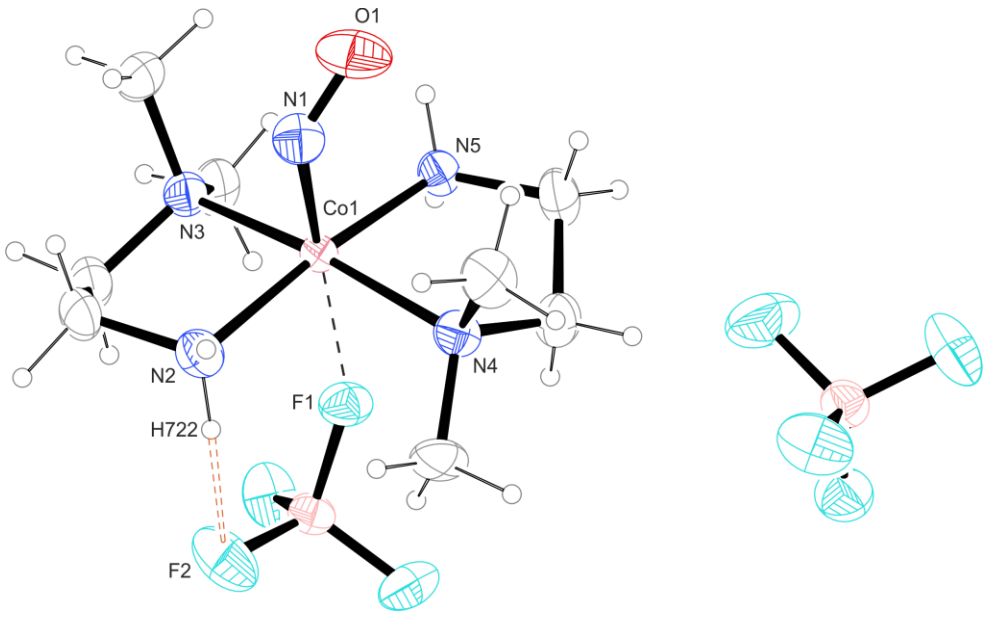

Figure 2.42: ORTEP plot of *trans*-[Co(BF_4)(*N*,*N*-dmen)$_2$(NO)]BF_4 in crystals of **4i**. Thermal ellipsoids drawn at 50 % probability level at 173 K. Interatomic distances (Å) and bond angles (°) with the standard deviation of the last decimal digit given in parentheses: Co1–N1 1.806(3), Co1–F1 2.375(2), Co1–N2 1.961(3), Co1–N3 2.063(3), Co1–N4 2.054(3), Co1–N5 1.961(3), N1–O1 1.156(5), H722–F2 2.42, Co1–N1–O1 124.3(3), N1–Co1–F1 179.7(1), N2–Co1–N5 170.5(1), N3–Co1–N4 169.6(1), N2–Co1–N3 86.1(1), N4–Co1–N5 85.4(1), N2–Co1–N4 94.5(1), N3–Co1–N5 92.2(1), N1–Co1–N2 92.3(1), N1–Co1–N3 94.3(1), N1–Co1–N4 96.0(1), N1–Co1–N5 97.2(1), F1–Co1–N2 87.57(9), F1–Co1–N3 85.89(8), F1–Co1–N4 83.81(8), F1–Co1–N5 83.00(9).

Table 2.14: Distances and angles of classical hydrogen bonds in crystals of **4i**. The standard deviation of the last decimal digit is given in parentheses. Values without a standard deviation refer to hydrogen atoms calculated on idealized positions, riding on their parent atoms.

D–H···A	*d*(D–H)/Å	*d*(H···A)/Å	*d*(D···A)/Å	∢(D–H···A)/°
N2–H721···F3^{i}	0.91	2.06	2.968(4)	177
N2–H722···F2	0.91	2.42	3.199(4)	144
N2–H722···F5^{ii}	0.91	2.43	2.979(4)	119
N5–H751···F6^{iii}	0.91	2.37	3.014(4)	128
N5–H751···F7^{iii}	0.91	2.30	3.165(4)	160
N5–H752···F4^{iv}	0.91	2.13	2.890(3)	140

Symmetry codes: ^{i} −½+*x*, ½−*y*, −½+*z*; ^{ii} ½+*x*, ½−*y*, −½+*z*; ^{iii} −*x*, 1−*y*, 1−*z*; ^{iv} 1−*x*, 1−*y*, 1−*z*.

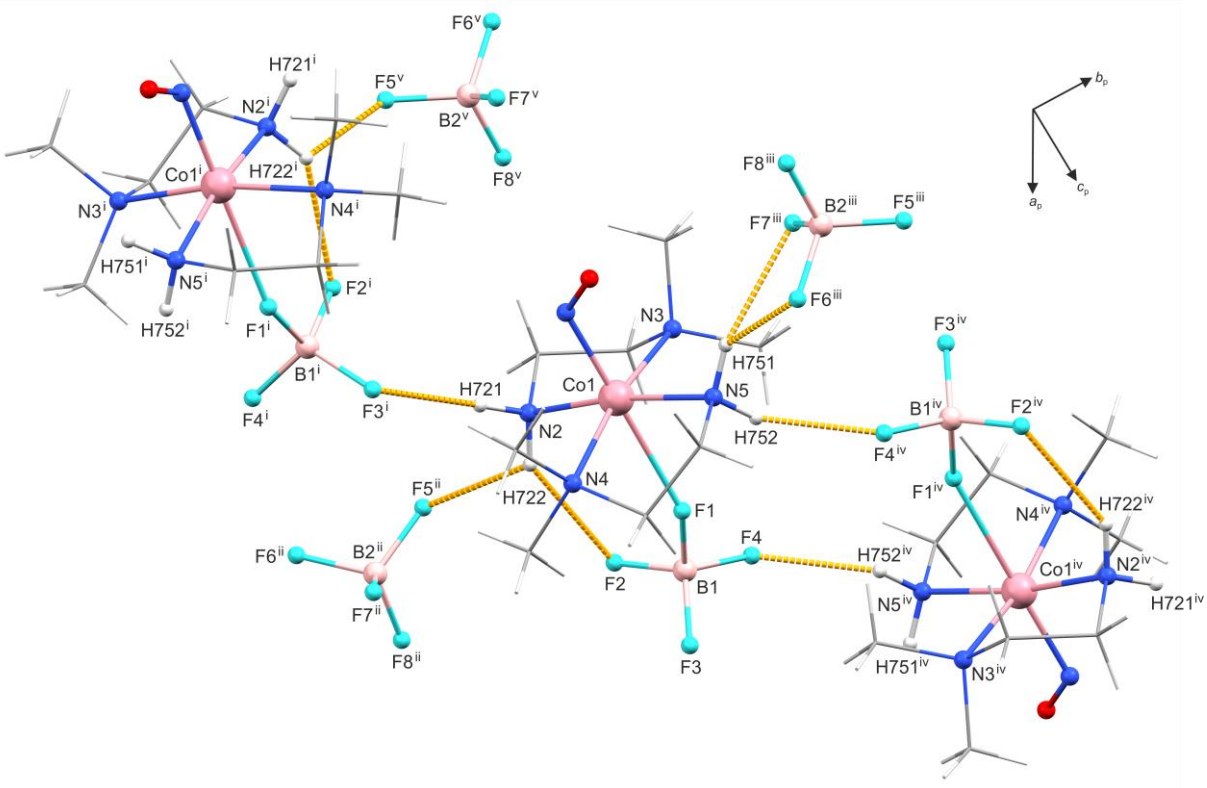

Figure 2.43: Plot of the pattern of classical hydrogen bonds (dashed yellow lines) in crystals of **4i**. For clarity, the organic ligand residues are depicted as wireframe. Symmetry codes: ^{i} −½+*x*, ½−*y*, −½+*z*; ^{ii} ½+*x*, ½−*y*, −½+*z*; ^{iii} −*x*, 1−*y*, 1−*z*; ^{iv} 1−*x*, 1−*y*, 1−*z*; ^{v} *x*, *y*, −1+*z*.

Attempts to synthesize further halogenido and nitrato complexes analogous to **4b–d** using the above-mentioned ethylenediamine derivatives were unsuccessful. However, a novel nitrato nitrosyl complex was obtained with the monobenzylated diamine via the direct route. In contrast to the unsubstituted analog **4d**, the nitrosyl ligand in *trans*-[Co(bnen)$_2$(NO)(NO$_3$)]NO$_3$·MeOH (**4l**·MeOH) is disordered in the crystal structure (see Figure 2.44). The N–O bonds have a length of 1.169 Å and 1.172 Å. For the Co–N bonds, distances of 1.818 Å and 1.821 Å are found. The CoNO moiety is bent within the usual range, with angles of 121.9° and 120.6°. Compared to **4d**, the Co–O bond is slightly longer in the benzylated derivative (**4l**: 2.348 Å vs. **4d**: 2.304 Å). In this context, the nitrato species are similar to the perchlorato and tetrafluoroborato compounds. The infrared stretching vibration of the nitrosyl ligand was measured at 1650 cm^{-1}. Attempts to synthesize further complexes with *N*-benzylethylenediamine analogous to **4a–f** proved to be unsuccessful.

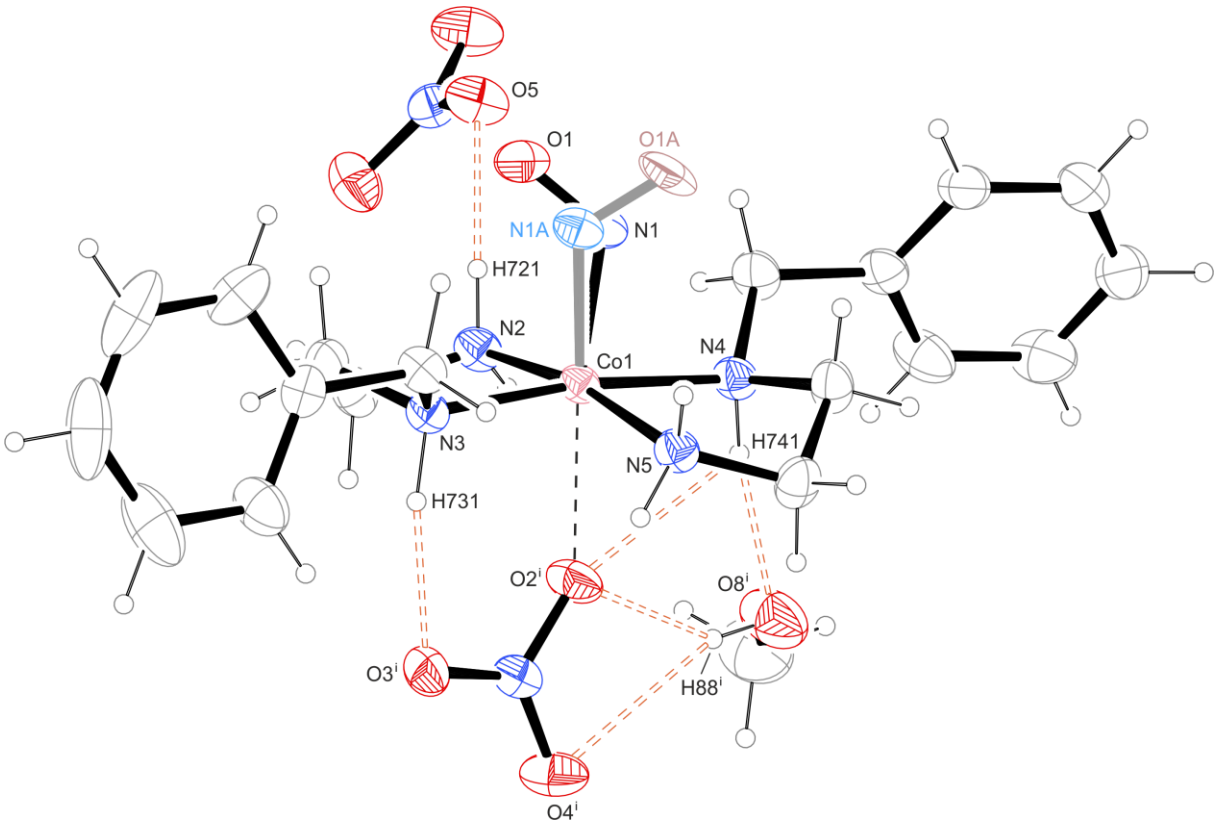

Figure 2.44: ORTEP plot of *trans*-[Co(bnen)$_2$(NO)(NO$_3$)]NO$_3$·MeOH in crystals of **4l**·MeOH. The nitrosyl moiety of the minor disorder form (10 %) is depicted in light colors. Thermal ellipsoids are drawn at 50 % probability level at 173 K. Interatomic distances (Å) and bond angles (°) with the standard deviation of the last decimal digit given in parentheses: Co1–N1 1.818(2), Co1–N1A 1.821(2), Co1–O2^{i} 2.348(1), Co1–N2 1.959(1), Co1–N3 1.993(1), Co1–N4 2.017(1), Co1–N5 1.973(1), N1–O1 1.169(3), N1A–O1A 1.172(2), H721–O5 2.03, H731–O3^{i} 2.08, H741–O2^{i} 2.44, H741–O8^{i} 2.07, H88^{i}–O2^{i} 2.07(3), H88^{i}–O4^{i} 2.55(3), Co1–N1–O1 121.9(2), Co1–N1A–O1A 120.6(2), N1–Co1–O2^{i} 171.12(7), N2–Co1–N5 169.22(5), N3–Co1–N4 172.71(5), N2–Co1–N3 86.48(5), N4–Co1–N5 85.64(5), N2–Co1–N4 94.88(5), N3–Co1–N5 91.69(5), N1–Co1–N2 95.2(1), N1–Co1–N3 98.20(8), N1–Co1–N4 88.82(8), N1–Co1–N5 95.5(1), O2^{i}–Co1–N2 83.68(4), O2^{i}–Co1–N3 90.54(4), O2^{i}–Co1–N4 82.50(4), O2^{i}–Co1–N5 85.72(4). Symmetry code: ^{i} ½−*x*, −½+*y*, ½−*z*.

Concerning the hydrogen bonds in **4l**, almost as many classical interactions are observed as in the unsubstituted analog, despite partial substitution of the diamine. The co-crystallized methanol molecules are non-bridging, binding exclusively to the complex entities and forming intramolecular ring motifs such as $S_1^2(4)$ (···H88^{ii}···O2^{ii}–N6^{ii}–O4^{ii}···) and $S_2^2(4)$ (···O8^{ii}–H88^{ii}···O2^{ii}···H741··· both in the binary graph set). A plot of the pattern of classical hydrogen bonds is shown below in Figure 2.45. Contrary to the unsubstituted compound, the benzylated derivative features far more non-classical interactions, with most of them involving the hydrogen atoms at the benzylic positions. The methanol molecules are not involved in these interactions. A complete overview of all occurring classical and non-classical hydrogen bonds is given in Tables 2.15 and 7.19.

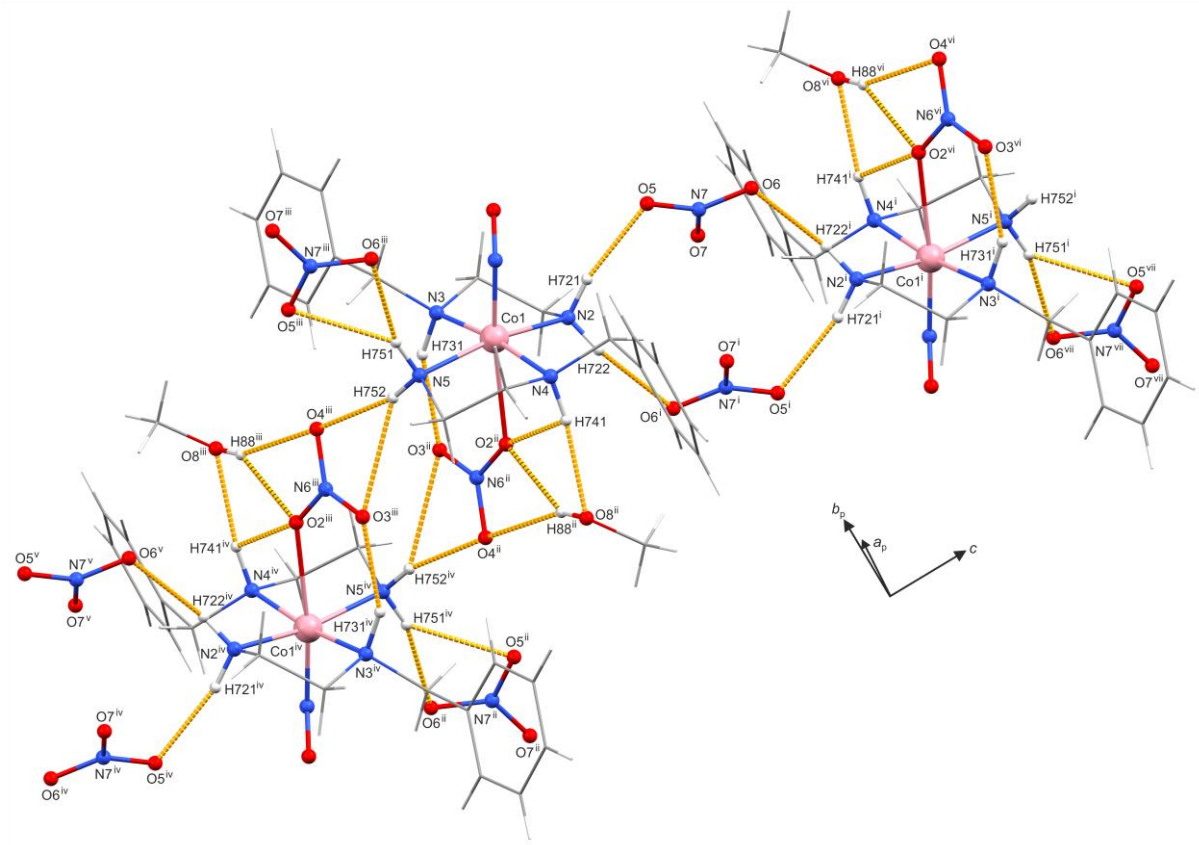

Figure 2.45: Plot of the pattern of classical H-bonds (dashed yellow lines) in crystals of **4l**·MeOH. For clarity, only the nitrosyl moieties of the major disorder form (90 %) are shown. Furthermore, all organic ligand residues are depicted as wireframe. Symmetry codes: [i] ½–*x*, ½–*y*, 1–*z*; [ii] ½–*x*, –½+*y*, ½–*z*; [iii] *x*, 1–*y*, –½+*z*; [iv] ½–*x*, ½–*y*, –*z*; [v] *x*, *y*, –1+*z*; [vi] *x*, 1–*y*, ½+*z*; [vii] ½–*x*, –½+*y*, ¾–*z*.

Table 2.15: Distances and angles of classical hydrogen bonds in crystals of **4l**·MeOH. The standard deviation of the last decimal digit is given in parentheses. Values without a standard deviation refer to hydrogen atoms calculated on idealized positions, riding on their parent atoms.

D–H···A	*d*(D–H)/Å	*d*(H···A)/Å	*d*(D···A)/Å	∢(D–H···A)/°
N2–H721···O5	0.91	2.03	2.925(2)	168
N2–H722···O6^{i}	0.91	2.16	2.977(2)	150
N3–H731···O3^{ii}	1.00	2.08	2.996(2)	152
N4–H741···O2^{ii}	1.00	2.44	2.889(2)	107
N4–H741···O8^{ii}	1.00	2.07	3.061(2)	169
N5–H751···O5^{iii}	0.91	2.33	3.094(2)	142
N5–H751···O6^{iii}	0.91	2.17	3.044(2)	160
N5–H752···O3^{iii}	0.91	2.58	3.332(2)	140
N5–H752···O4^{iii}	0.91	2.18	3.071(2)	166
O8–H88···O2	0.83(3)	2.07(3)	2.786(2)	145(3)
O8–H88···O4	0.83(3)	2.55(3)	3.344(2)	160(3)

Symmetry codes: ^{i} ½–*x*, ½–*y*, 1–*z*; ^{ii} ½–*x*, –½+*y*, ½–*z*; ^{iii} *x*, 1–*y*, –½+*z*.

In summary, it can be stated that the structures of compound class **4** are very similar to the perfluoropinacolato nitrosyls (classes **1–3**) with regard to the CoNO moiety, which is bent at an angle ranging from 121.3° (**4d**) to 124.3° (**4i**). The Co–N bond is ranging from 1.806 Å (**4i**) to 1.832 Å (**4c**), similar to those species of class **1** bearing aromatic *N*-heterocyclic co-ligands. For the N–O bond, distances between 1.138 Å (**4g**) and 1.173 Å (**4d**) are found. Half of the structures exhibit a disordered nitrosyl moiety with only one complex molecule in the asymmetric unit, these being mostly the complexes with unsubstituted ethylenediamine (**4a**, **c**, **e**, **f** and **l**). The infrared stretch of the NO ligand is observed within a range from 1629 cm^{-1} (**4b**) to 1659 cm^{-1} (**4e**). Concerning their stability in solution, none of the newly synthesized compounds showed signs of nitric oxide loss upon purging with argon. For the co-ligand *trans* to nitric oxide, the distance to the metal center was found to depend on the atom that binds to it. The shortest Co–L$_{trans}$ distances were found in the nitrosyls bearing *O*-coordinating ligands, with lengths mostly around 2.3 Å. Furthermore, it is noticeable that in the case of compounds with the same diamine, replacing the perchlorate with tetrafluoroborate leads to identical crystal structures (**4a** vs. **e** and **4h** vs. **i**). Although some interchangeability of the *trans* co-ligand was observed, it was not possible to synthesize a nitrosyl complex with every combination of diamine and co-ligand. A complete overview of the structural and vibrational data of the class **4** nitrosyls is given in Table 2.16.

Table 2.16: X-ray and IR data of the crystalline {CoNO}^{8} compounds **4a–l** related to the CoNO moiety and loss of NO upon argon bubbling in solution. Decomposition of the nitrosyl species was rated as not occurring (–). Distances from cobalt to the co-ligand *trans* to NO ($L_{tr.}$) are listed in the third column.

4		N–O/Å	Co–N/Å	Co–$L_{tr.}$/Å	∢Co–N–O/°	$\tilde{\nu}$/cm^{-1}	NO loss
a	$[Co(ClO_4)(en)_2(NO)]ClO_4$ [a]	1.160	1.817	2.331	122.0	1657	–
b	$[CoCl(en)_2(NO)]Cl{\cdot}S^1$	1.154	1.830	2.6135	123.5	1629	–
c	$[Co(en)_2I(NO)](ClO_4)_{0.6}I_{0.4}$ [a]	1.152	1.832	3.0477	121.9	1632	–
d	$[Co(en)_2(NO)(NO_3)]NO_3$ [b]	1.173	1.820	2.304	121.3	1636	–
e	$[Co(BF_4)(en)_2(NO)]BF_4$ [a]	1.143	1.824	2.326	121.6	1659	–
f	$[Co(dmso\text{-}\kappa O)(en)_2(NO)](ClO_4)_2{\cdot}S^2$ [a]	1.161	1.819	2.234	121.9	1638	–
g	$[Co(ClO_4)(men)_2(NO)]ClO_4$	1.138	1.815	2.363	124.0	1653	–
h	$[Co(ClO_4)(N,N\text{-dmen})_2(NO)]ClO_4$	1.165	1.809	2.394	123.6	1655	–
i	$[Co(BF_4)(N,N\text{-dmen})_2(NO)]BF_4$	1.156	1.806	2.375	124.3	1656	–
j	$[Co(ClO_4)(N,N'\text{-dmen})_2(NO)]ClO_4$ [c]	—	—	—	—	1651	–
k	$[Co(BF_4)(N,N'\text{-dmen})_2(NO)]BF_4$ [c]	—	—	—	—	1652	–
l	$[Co(bnen)_2(NO)(NO_3)_2]{\cdot}S^3$ [a]	1.169	1.818	2.348	121.9	1650	–

[a] Disorder of the nitrosyl ligand. The given structural data refer to the major disorder form.
[b] Structural data from Ref.[94].
[c] Product only obtained as microcrystalline solid unsuitable for single-crystal X-ray diffraction.
Co-crystallized solvents: S^1: H_2O, S^2: DMSO, S^3: MeOH.

With regard to the CoN_5 moiety, all class **4** structures exhibit a coordination geometry that can be best described as a distorted vacant octahedron (*vOC*-5) according to CShM calculations (see Figure 2.46). They differ from a regular square pyramid in that the central cobalt atom is shifted toward the basal plane formed by the four diamine-nitrogen atoms (shown as pyramidalization path in the plot). The quantified shifts are listed in Table 2.17. Concerning the degree of distortion, the halogenido and DMSO derivatives (**4b**, **c**, **f**) come very close to the ideal *vOC*-5 shape, while others (mostly those with substituted ethylenediamine co-ligands) are shifted toward a square pyramid (e.g. **4g+i**). All perchlorato and most tetrafluoroborato species deviate from the pyramidalization path, indicating further distortion of the coordination geometry.

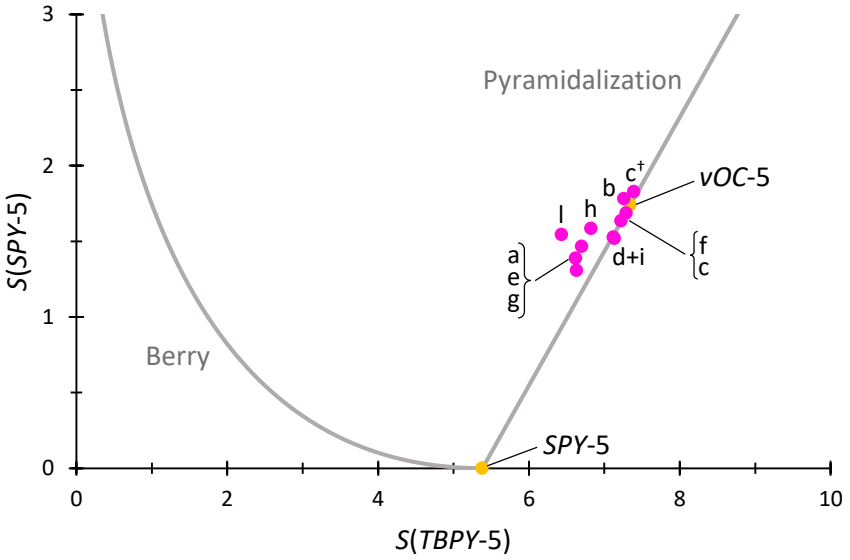

Figure 2.46: CShM map of compounds **4a–i+l** (pink data points) for fivefold-coordinated species, based on the X-ray structural data of the CoN_5 moieties in the crystalline products. Ideal, undistorted polyhedra (yellow data points) as reference. The solid gray lines mark the Berry- and the pyramidalization path, respectively. For most of the disordered structures, only the major form is plotted, since their CShM values do not differ significantly from those of the respective minor form. For compound **4c**, the separate calculations for both disorder forms are shown (major: **4c**, minor: **4c**†, see Figure 2.30). A complete overview of all CShM values is given in Table 7.23 in the appendix. The calculation for **4d** is based on structural data from Ref.[94].

Table 2.17: Distance from the central cobalt atom above the N_4 plane spanned by the diamine ligands in crystal structures of **4a–i+l**. The standard deviation of the last decimal digit is given in parentheses. The calculation for species **4d** is based on structural data from Ref.[94].

4		Co···N_4/Å
a	$[Co(ClO_4)(en)_2(NO)]ClO_4$	0.163(1)
b	$[CoCl(en)_2(NO)]Cl{\cdot}S^1$	0.093(1)
c	$[Co(en)_2I(NO)](ClO_4)_{0.6}I_{0.4}$	0.114(1)
d	$[Co(en)_2(NO)(NO_3)]NO_3$	0.134(1)
e	$[Co(BF_4)(en)_2(NO)]BF_4$	0.181(1)
f	$[Co(dmso\text{-}\kappa O)(en)_2(NO)](ClO_4)_2{\cdot}S^2$	0.113(1)
g	$[Co(ClO_4)(men)_2(NO)]ClO_4$	0.181(1)
h	$[Co(ClO_4)(N,N\text{-dmen})_2(NO)]ClO_4$	0.166(1)
i	$[Co(BF_4)(N,N\text{-dmen})_2(NO)]BF_4$	0.173(1)
l	$[Co(bnen)_2(NO)(NO_3)_2]{\cdot}S^3$	0.153(1)

Co-crystallized solvents: S^1: H_2O, S^2: DMSO, S^3: MeOH.

2.5 Bis(diphosphane)cobalt nitrosyls

In addition to the nitrosyls presented so far, all of which exhibiting a clearly bent CoNO moiety, it was also possible to synthesize {CoNO}^{8} complexes with a linearly bonded nitrosyl ligand. Compounds of the type $[Co(L)_2(NO)]X_2$ (**5a–d**) were obtained in bulk quantity by treating a 1:2 solution of cobalt(II) perchlorate or tetrafluoroborate and a diphosphane with gaseous NO. Recrystallization from acetone via the DMSO method yielded crystals suitable for X-ray diffraction. Cobalt nitrosyls of this composition were already synthesized in a similar manner by Del Zotto *et al.*, using the tetrafluoroborate and various alkylated and aromatically substituted diphosphanes as co-ligands.[109] However, no crystal structures of these compounds have been published. In accordance with the literature-known species, the N–O stretch of the newly synthesized products (see Table 2.18) is found at higher wavenumbers compared to the bent complexes, ranging from 1812 cm^{-1} (**5b**) to 1833 cm^{-1} (**5d**). For the already known dppe, dppv and dppbz bulk derivatives, nitrosyl bands were reported at 1807 cm^{-1}, 1824 cm^{-1} and 1808 cm^{-1}, respectively.[109] With the exception of **5b**, all novel compounds of this class show no signs of nitric oxide loss upon argon purging in solution. Concerning the newly gained structural data, the Co–N–O angle in the compounds is ranging from 170.0° (**5d**) to 180.0° (**5b**). The Co–N bond is slightly shorter than in the bent species, with bond lengths between 1.645 Å (**5b**) and 1.666 Å (**5d**). The N–O bond ranges from 1.148 Å (**5c**) to 1.161 Å (**5c'**). For nearly all crystalline compounds, only non-classical hydrogen bonds are found, occurring mainly between the C–H groups and the counterions (see Table 7.20). Details on the sole classical interaction, which is found in the dppa species (**5b**), are listed in Table 2.19.

Table 2.18: X-ray and IR data of the crystalline {CoNO}^{8} compounds **5a–d** related to the CoNO moiety and loss of NO upon argon bubbling in solution. Decomposition of the nitrosyl species was rated as not occurring (–) or moderate (••).

5		N–O/Å	Co–N/Å	∡Co–N–O/°	$\tilde{\nu}$/cm^{-1}	NO loss
a	$[Co(dppe)_2(NO)](ClO_4)_2 \cdot 2.7S^1 \cdot 0.3S^2$	1.157	1.658	173.8	1813	–
a'	$[Co(dppe)_2(NO)](BF_4)_2 \cdot 2S^1$	1.157	1.662	173.7	1814	–
b	$[Co(dppa)_2(NO)](ClO_4)_2 \cdot 2S^1$	1.152	1.645	180.0	1812	••
c	$[Co(dppv)_2(NO)](ClO_4)_2 \cdot 1.5S^{1\,[a]}$	1.148	1.665	172.4	1818	–
c'	$[Co(dppv)_2(NO)](BF_4)_2 \cdot 1.8S^1 \cdot 0.2S^{2\,[a]}$	1.161	1.662	171.5	1819	–
d	$[Co(dppbz)_2(NO)](ClO_4)_2 \cdot S^{1\,[a]}$	1.149	1.666	170.0	1833	–

[a] Mean structural data of the two entities in the asymmetric unit.
Co-crystallized solvents: S^1: Me_2CO, S^2: DMSO.

With regard to the coordination geometry of the $CoNP_4$ moiety, all structures are best described as a distorted trigonal bipyramid (*TBPY*-5) according to CShM calculations (see Figure 2.47). In the case of the nitrosyls with dppe and dppv (**5a+c** and **5a'+c'**), variation of the counterion has very little to no influence on the distortion of the complex. Only the two entities in each asymmetric unit differ slightly from each other. For the CShM values of the dppbz derivative (**5d**), a greater divergence between the two entities is found. As depicted in the plot, complex **5b** shows the largest deviation from the ideal trigonal bipyramid. Since the corresponding data point is located on the umbrella path, the geometry of this compound can be derived from an ideal polyhedron by shifting the three equatorial atoms along the pyramid's unique axis, creating an edge-capped tetrahedron.[113] All other data points are not on a specific path, indicating multiple types of distortion in the crystal structures.

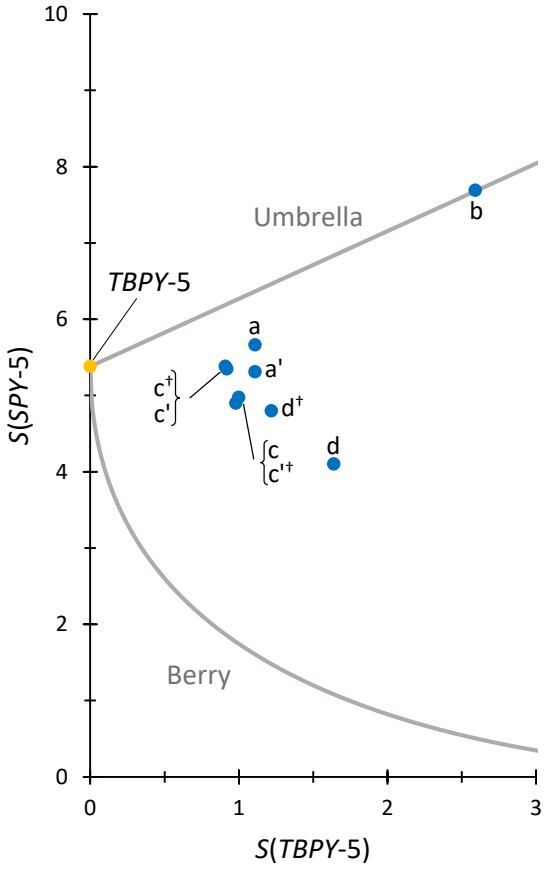

Figure 2.47: CShM map of compounds **5a–d** (dark blue data points) for fivefold-coordinated species, based on the X-ray structural data of the crystalline products. Ideal, undistorted trigonal bipyramid (yellow data point) as reference. The solid gray lines mark the Berry path and the umbrella distortion, respectively. For **5c–d**, the CShM values of both entities in the asymmetric unit (e.g. **5c** and **5c**†, see Figures 2.51 + 7.51) are plotted.

Table 2.19: Distances and angles of classical hydrogen bonds in crystals of **5b**·2Me_2CO. The standard deviation of the last decimal digit is given in parentheses. Due to H721 being calculated on an idealized position riding on its parent atom N2, values based on the position of this hydrogen atom do not possess a standard deviation.

D–H···A	*d*(D–H)/Å	*d*(H···A)/Å	*d*(D···A)/Å	∢(D–H···A)/°
N2–H721···O6	0.88	1.89	2.735(11)	162

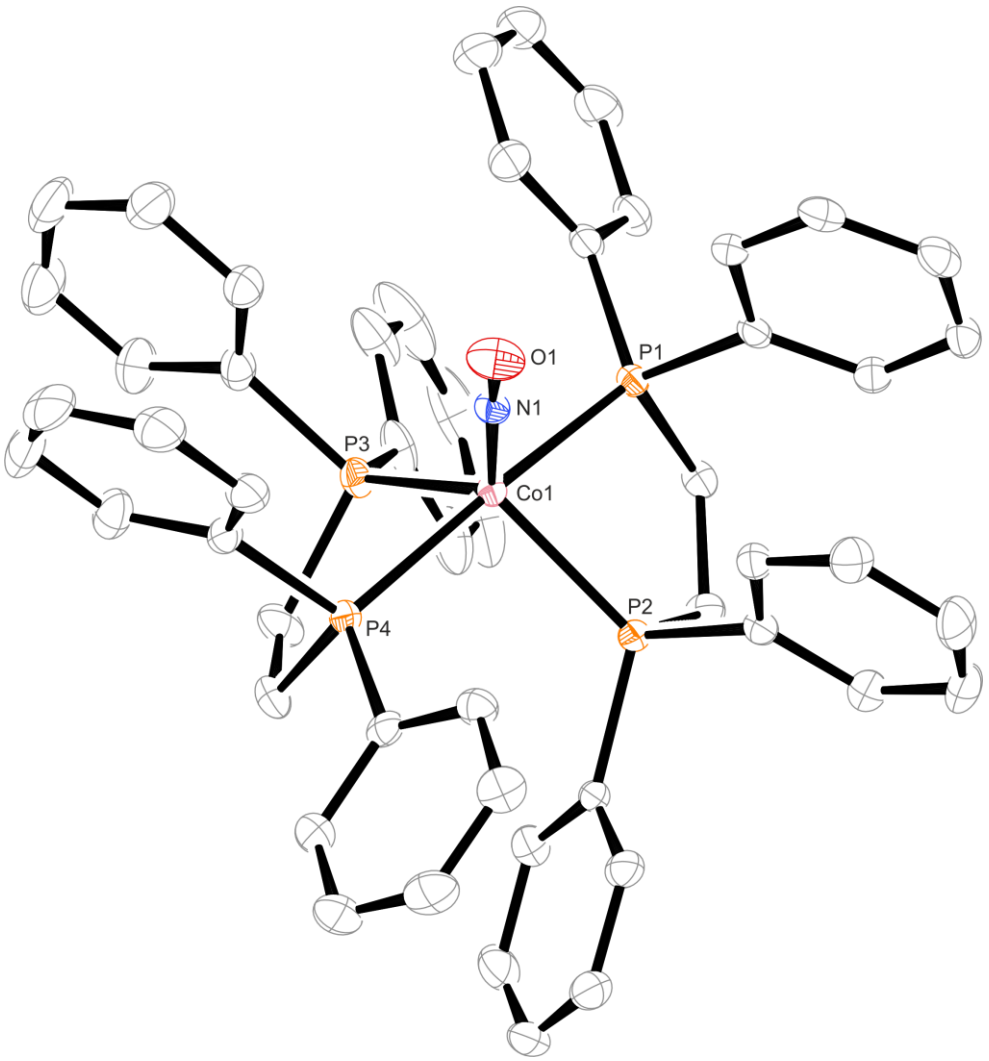

Figure 2.48: ORTEP plot of the cationic complex entity of [Co(dppe)$_2$(NO)](ClO$_4$)$_2$·2.7Me_2CO·0.3DMSO in crystals of **5a**·2.7Me_2CO·0.3DMSO. For clarity, hydrogen atoms are not depicted. Furthermore, all counterions and co-crystallized solvent molecules are omitted. Thermal ellipsoids drawn at 50 % probability level at 102 K. Interatomic distances (Å) and bond angles (°) with the standard deviation of the last decimal digit given in parentheses: Co1–N1 1.658(2), Co1–P1 2.2766(8), Co1–P2 2.2634(8), Co1–P3 2.2833(8), Co1–P4 2.2806(8), N1–O1 1.157(3), Co1–N1–O1 173.8(2), P1–Co1–P4 170.40(3), P2–Co1–P3 113.82(3), P1–Co1–P2 80.84(3), P3–Co1–P4 80.80(3), P1–Co1–P3 92.17(3), P2–Co1–P4 95.94(3), N1–Co1–P1 96.54(8), N1–Co1–P2 119.51(8), N1–Co1–P3 126.67(8), N1–Co1–P4 92.92(8). A plot of the complete asymmetric unit is given in Figure 7.48 in the appendix.

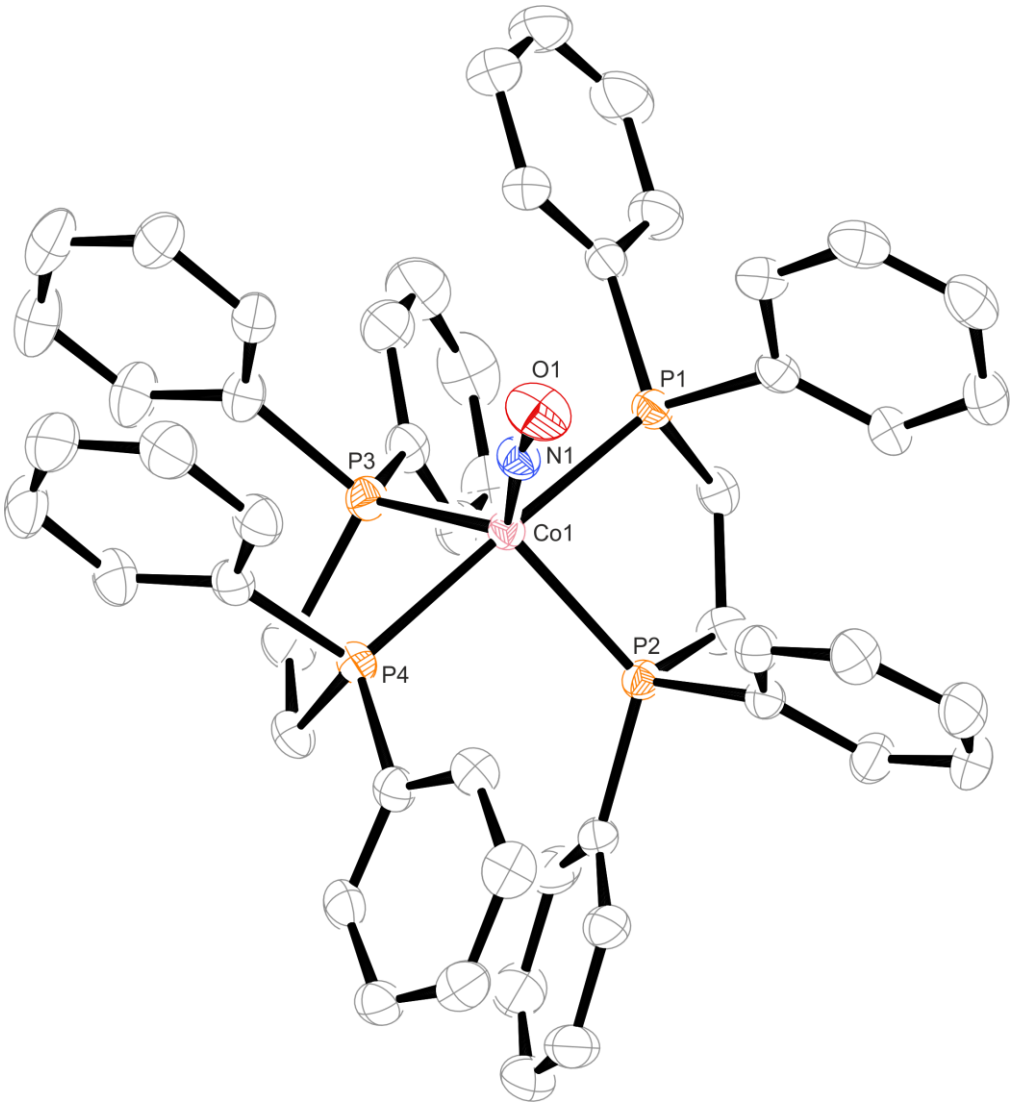

Figure 2.49: ORTEP plot of cationic complex entity of $[Co(dppe)_2(NO)](BF_4)_2 \cdot 2Me_2CO$ in crystals of **5a'**$\cdot 2Me_2CO$. For clarity, hydrogen atoms are not depicted. Furthermore, all counterions and co-crystallized solvent molecules are omitted. Thermal ellipsoids drawn at 50 % probability level at 173 K. Interatomic distances (Å) and bond angles (°) with the standard deviation of the last decimal digit given in parentheses: Co1–N1 1.662(2), Co1–P1 2.2783(8), Co1–P2 2.2812(8), Co1–P3 2.2997(9), Co1–P4 2.2854(8), N1–O1 1.157(3), Co1–N1–O1 173.7(2), P1–Co1–P4 172.43(3), P2–Co1–P3 110.48(3), P1–Co1–P2 81.72(3), P3–Co1–P4 80.59(3), P1–Co1–P3 94.16(3), P2–Co1–P4 94.95(3), N1–Co1–P1 91.6(1), N1–Co1–P2 120.8(1), N1–Co1–P3 128.7(1), N1–Co1–P4 95.9(1). A plot of the complete asymmetric unit is given in Figure 7.49 in the appendix.

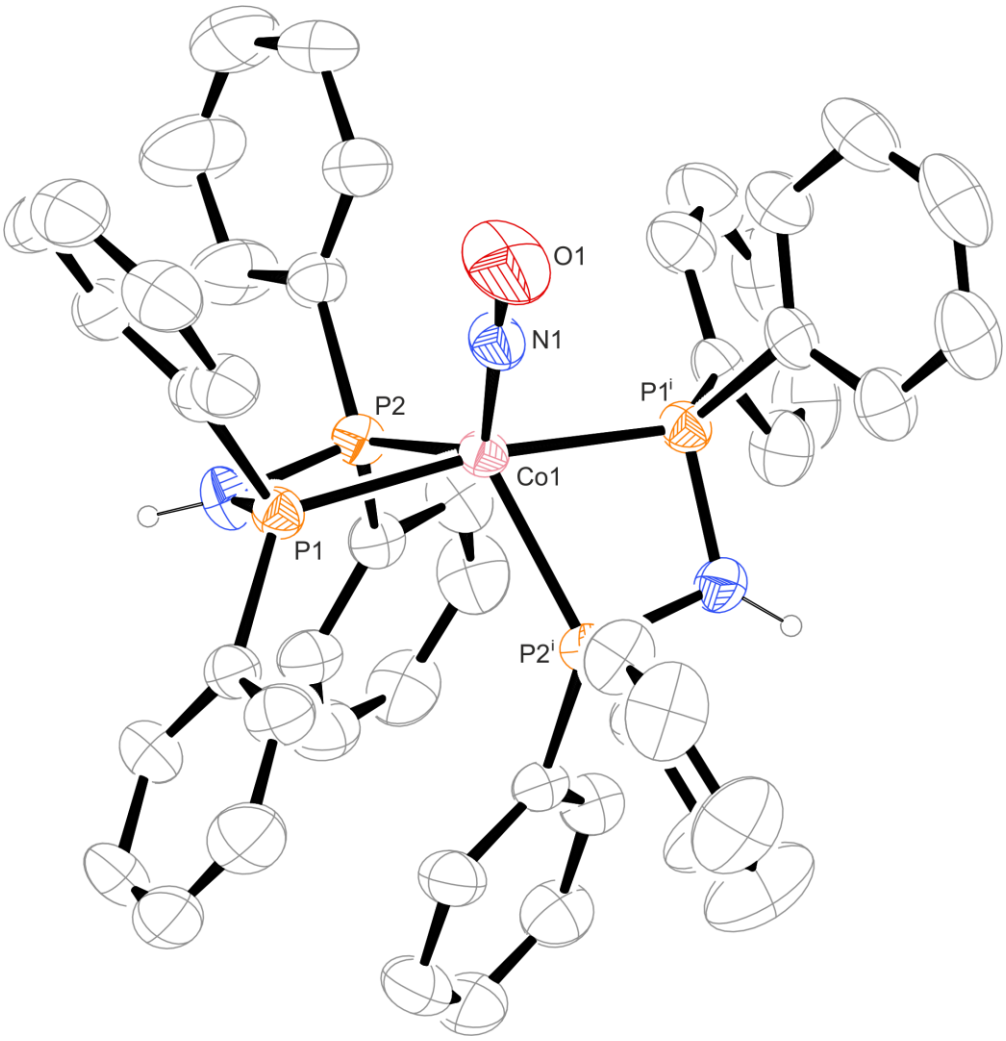

Figure 2.50: ORTEP plot of cationic complex entity of $[Co(dppa)_2(NO)](ClO_4)_2 \cdot 2Me_2CO$ in crystals of **5b**$\cdot 2Me_2CO$. For clarity, carbon-bound hydrogen atoms are not depicted. Furthermore, all counterions and co-crystallized solvent molecules are omitted. Thermal ellipsoids are drawn at 50 % probability level at 173 K. Interatomic distances (Å) and bond angles (°) with the standard deviation of the last decimal digit given in parentheses: Co1–N1 1.645(5), Co1–P1 2.243(2), Co1–P2 2.252(1), N1–O1 1.152(7), Co1–N1–O1 180.00(1), P1–Co1–P1^{i} 167.74(5), P2–Co1–P2^{i} 108.09(5), P1–Co1–P2 70.73(5), P1–Co1–P2^{i} 101.81(5), N1–Co1–P1 96.13(3), N1–Co1–P2 125.96(3). Symmetry code: ^{i} 1–*x*, *y*, ½–*z*. A plot of the complete asymmetric unit is given in Figure 7.50 in the appendix.

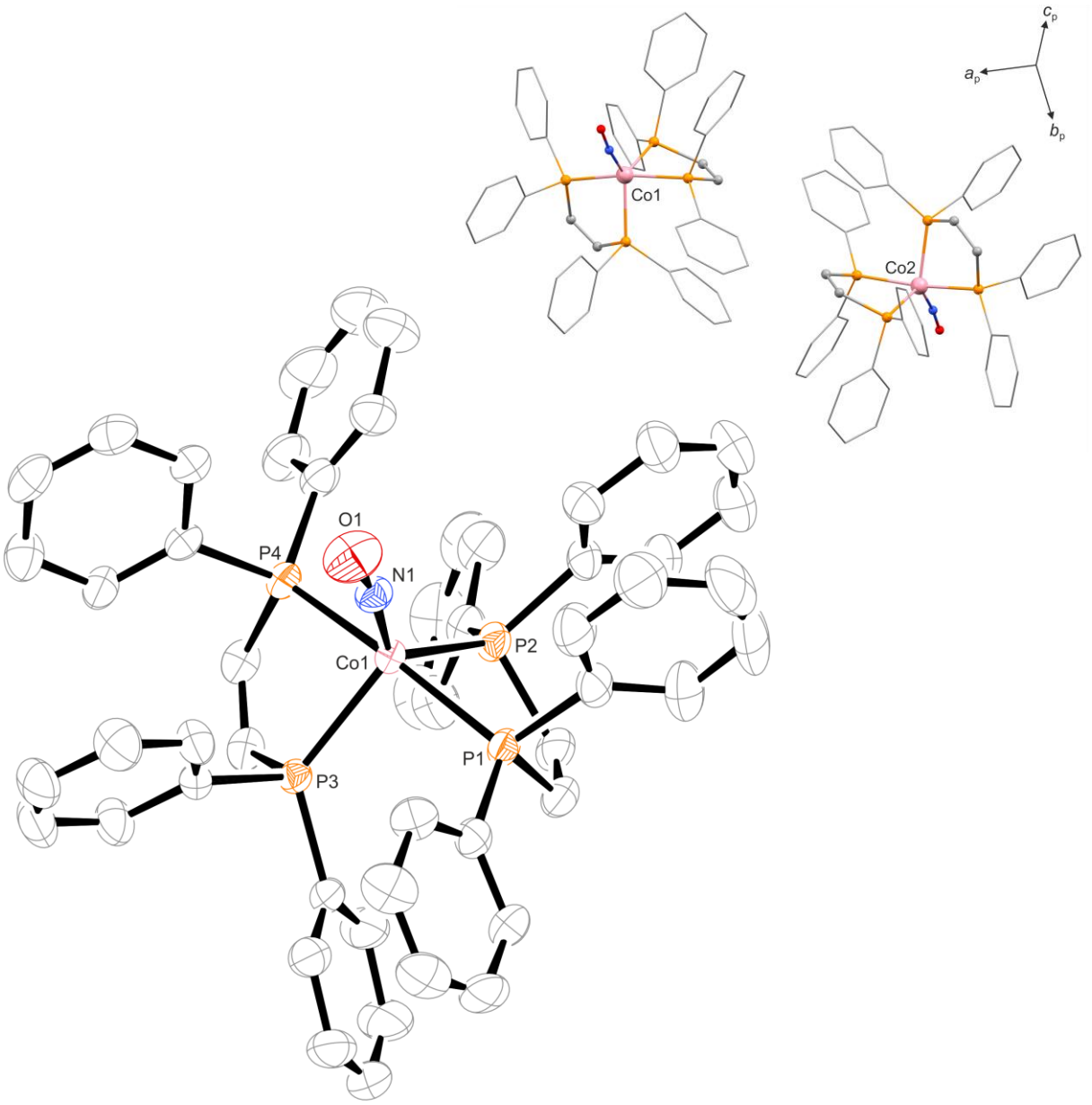

Figure 2.51: Left: ORTEP plot of the cationic complex entity of $[Co(dppv)_2(NO)](ClO_4)_2 \cdot 1.5 Me_2CO$ in crystals of **5c**·1.5 Me_2CO. For clarity, only one entity in the asymmetric unit is depicted. Furthermore, hydrogen atoms as well as all counterions and co-crystallized solvent molecules are omitted. Thermal ellipsoids are drawn at 50 % probability level at 173 K. Interatomic distances (Å) and bond angles (°) with the standard deviation of the last decimal digit given in parentheses: **First molecule (5c, pictured):** Co1–N1 1.663(4), Co1–P1 2.273(2), Co1–P2 2.307(1), Co1–P3 2.282(1), Co1–P4 2.264(1), N1–O1 1.147(6), Co1–N1–O1 172.0(4), P1–Co1–P4 168.37(5), P2–Co1–P3 109.06(5), P1–Co1–P2 81.09(5), P3–Co1–P4 81.60(5), P1–Co1–P3 93.76(5), P2–Co1–P4 90.31(5), N1–Co1–P1 97.7(1), N1–Co1–P2 131.6(1), N1–Co1–P3 119.3(1), N1–Co1–P4 93.9(1); **Second molecule (5c$^+$, not shown):** Co2–N2 1.666(4), Co2–P5 2.278(1), Co2–P6 2.296(1), Co2–P7 2.282(1), Co2–P8 2.269(1), N2–O2 1.149(6), Co2–N2–O2 172.8(4), P5–Co2–P8 168.82(5), P6–Co2–P7 110.05(5), P5–Co2–P6 80.39(5), P7–Co2–P8 82.18(5), P5–Co2–P7 92.63(5), P6–Co2–P8 92.05(5), N2–Co2–P5 97.1(1), N2–Co2–P6 129.1(1), N2–Co2–P7 120.9(1), N2–Co2–P8 94.1(1). The ORTEP plot of the second entity is given in the appendix (Figure 7.51). **Right:** Plot of the asymmetric unit in **5c**. For clarity, hydrogen atoms as well as all counterions and co-crystallized solvent molecules are omitted. Furthermore, all phenyl groups are depicted as wireframe. A plot of the complete asymmetric unit is given in Figure 7.52.

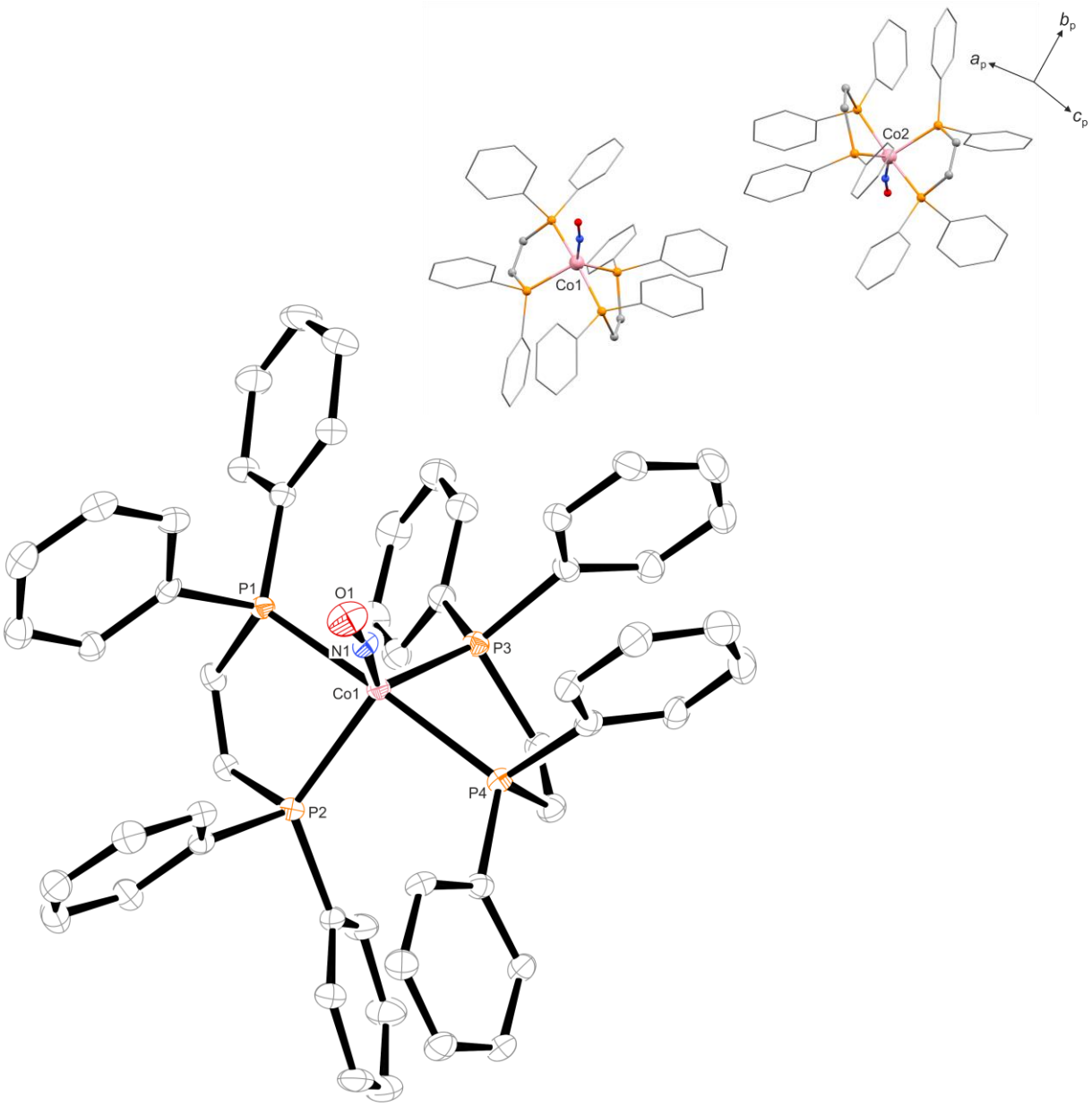

Figure 2.52: Left: ORTEP plot of the complex entity of $[Co(dppv)_2(NO)](BF_4)_2 \cdot 1.8 Me_2CO \cdot 0.2 DMSO$ in crystals of **5c'**$\cdot 1.8 Me_2CO \cdot 0.2 DMSO$. For clarity, only one entity in the asymmetric unit is depicted. Furthermore, hydrogen atoms as well as all counterions and co-crystallized solvent molecules are omitted. Thermal ellipsoids are drawn at 50 % probability level at 100 K. Interatomic distances (Å) and bond angles (°) with the standard deviation of the last decimal digit given in parentheses: **First molecule (5c', pictured):** Co1–N1 1.663(2), Co1–P1 2.263(1), Co1–P2 2.281(1), Co1–P3 2.292(1), Co1–P4 2.273(1), N1–O1 1.159(3), Co1–N1–O1 172.9(3), P1–Co1–P4 168.17(4), P2–Co1–P3 110.71(4), P1–Co1–P2 82.28(3), P3–Co1–P4 80.29(3), P1–Co1–P3 91.70(4), P2–Co1–P4 92.36(4), N1–Co1–P1 94.0(1), N1–Co1–P2 120.2(1), N1–Co1–P3 129.1(1), N1–Co1–P4 97.8(1); **Second molecule (5c'$^+$, not shown):** Co2–N2 1.661(2), Co2–P5 2.257(1), Co2–P6 2.274(1), Co2–P7 2.303(1), Co2–P8 2.266(1), N2–O2 1.162(3), Co2–N2–O2 170.0(3), P5–Co2–P8 167.56(4), P6–Co2–P7 110.41(4), P5–Co2–P6 81.44(4), P7–Co2–P8 81.01(3), P5–Co2–P7 89.87(4), P6–Co2–P8 93.77(4), N2–Co2–P5 93.8(1), N2–Co2–P6 117.8(1), N2–Co2–P7 131.7(1), N2–Co2–P8 98.6(1). The ORTEP plot of the second entity is given in the appendix (Figure 7.53). **Right:** Plot of the asymmetric unit in **5c'**. For clarity, hydrogen atoms as well as all counterions and co-crystallized solvent molecules are omitted. Furthermore, all phenyl groups are depicted as wireframe. A plot of the complete asymmetric unit is given in Figure 7.54.

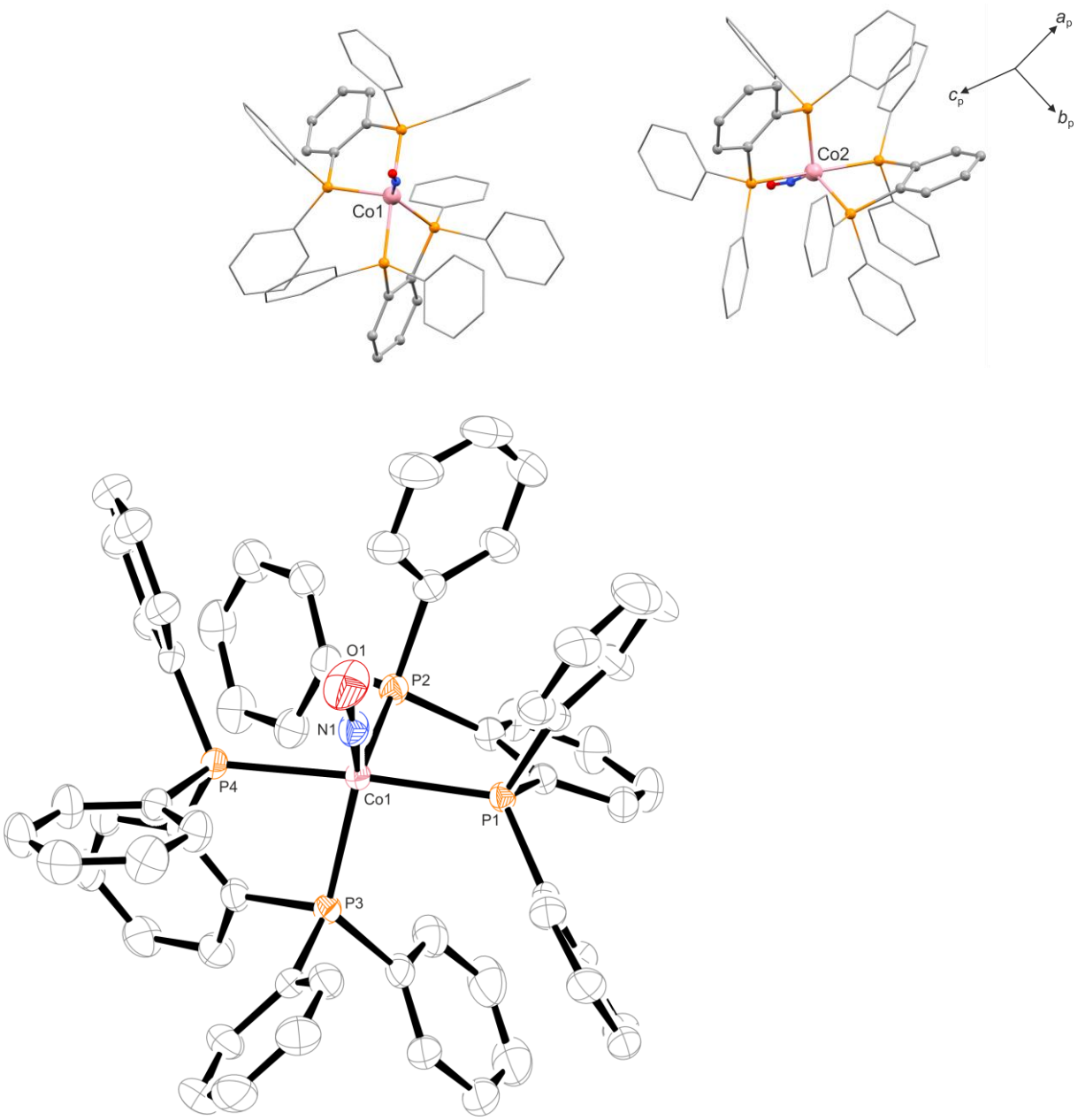

Figure 2.53: Left: ORTEP plot of the cationic complex entity of $[Co(dppbz)_2(NO)](ClO_4)_2 \cdot Me_2CO$ in crystals of **5d**·Me_2CO. For clarity, only one entity in the asymmetric unit is depicted. Furthermore, hydrogen atoms as well as all counterions and co-crystallized solvent molecules are omitted. Thermal ellipsoids are drawn at 50 % probability level at 173 K. Interatomic distances (Å) and bond angles (°) with the standard deviation of the last decimal digit given in parentheses: **First molecule (5d, pictured):** Co1–N1 1.664(2), Co1–P1 2.2998(9), Co1–P2 2.271(1), Co1–P3 2.296(1), Co1–P4 2.276(1), N1–O1 1.152(4), Co1–N1–O1 169.3(3), P1–Co1–P4 175.90(4), P2–Co1–P3 109.36(4), P1–Co1–P2 82.30(3), P3–Co1–P4 80.97(4), P1–Co1–P3 95.15(4), P2–Co1–P4 97.69(4), N1–Co1–P1 94.2(1), N1–Co1–P2 114.8(1), N1–Co1–P3 135.7(1), N1–Co1–P4 89.6(1); **Second molecule (5d†, not shown):** Co2–N2 1.667(2), Co2–P5 2.295(1), Co2–P6 2.258(1), Co2–P7 2.286(1), Co2–P8 2.297(1), N2–O2 1.146(3), Co2–N2–O2 170.6(3), P5–Co2–P8 174.33(4), P6–Co2–P7 108.98(4), P5–Co2–P6 82.88(4), P7–Co2–P8 81.15(4), P5–Co2–P7 94.41(4), P6–Co2–P8 95.18(4), N2–Co2–P5 89.6(1), N2–Co2–P6 119.8(1), N2–Co2–P7 131.1(1), N2–Co2–P8 96.0(1). The ORTEP plot of the second entity is given in the appendix (Figure 7.55). **Right:** Plot of the asymmetric unit in **5d**. For clarity, hydrogen atoms as well as all counterions and co-crystallized solvent molecules are omitted. Furthermore, the terminal phenyl groups are depicted as wireframe. A plot of the complete asymmetric unit is given in Figure 7.56.

2.6 Dichlorido- and dibromidocobalt nitrosyls with diphosphanes as co-ligands

Similar to the class **3** perfluoropinacolato compounds, another series of electroneutral $\{CoNO\}^8$ complexes was synthesized via direct reaction of the respective cobalt(II) halogenide and diphosphane with nitric oxide. Seven novel pentacoordinated species of the type $[Co(L)(NO)(X)_2]$ (**6a–d**) were obtained as single crystals. Using the usual DMSO method, they were grown from either an acetonic reaction mixture or a solution of the bulk product in chloroform. All crystal structures feature a well-ordered bent CoNO moiety with bond angles ranging from 137.6° (**6d**) to 141.2° (**6a'**), thus being more obtuse than classes **1–3**. Within the class, this angle is slightly more acute in the chlorido complexes compared to their respective bromido derivatives. The nitrosyl ligand points away from both the halogenido ligands and the phenyl groups of the phosphane. For the Co–N bond, distances between 1.736 Å (**6a'**) and 1.751 Å (**6d**) are found, the N–O bond is ranging from 1.160 Å (**6a'**) to 1.178 Å (**6d'**). The N–O stretching vibration ranges from 1616 cm^{-1} (**6b**) to 1693 cm^{-1} (**6a'**), with some of the products exhibiting band splitting in the solid state (**6a–b**). A complete overview of the structural and vibrational data is given in Table 2.20. The crystalline compounds are held together solely by dispersive forces and non-classical hydrogen bonds, the latter mostly occurring between the halogenido ligands and C–H moieties. All occurring H-bonds are listed in the appendix (see Table 7.21). In solution, the complexes remain stable when purged with argon.

Table 2.20: X-ray and IR data of the crystalline $\{CoNO\}^8$ compounds **6a–d** related to the CoNO moiety and loss of NO upon argon bubbling in solution. Decomposition of the nitrosyl species was rated as not occurring (–).

6		N–O/Å	Co–N/Å	∡Co–N–O/°	$\tilde{\nu}$/cm^{-1}	NO loss
a	$[CoCl_2(dppe)(NO)]\cdot S^1$ [a]	1.173	1.750	137.9	1661, 1682	–
a'	$[CoBr_2(dppe)(NO)]$ [a, b]	1.160	1.736	141.2	1667, 1693	–
b	$[CoCl_2(dppp)(NO)]$ [a, b]	1.165	1.746	138.1	1616, 1627	–
c	$[CoCl_2(dppv)(NO)]$	1.164	1.749	138.8	1686	–
c'	$[CoBr_2(dppv)(NO)]\cdot S^2$	1.169	1.737	140.9	1680	–
d	$[CoCl_2(dppbz)(NO)]$	1.166	1.751	137.6	1638	–
d'	$[CoBr_2(dppbz)(NO)]$	1.178	1.738	139.5	1644	–

[a] Split band of the NO vibration in the IR spectrum. The band with the higher relative intensity is listed first.
[b] Mean structural data of the two entities in the asymmetric unit.
Co-crystallized solvents: S^1: Me_2CO, S^2: $CHCl_3$.

Looking at the CShM map shown in Figure 2.54, this product class appears to be more heterogenous than the other two classes of diphosphane-bearing nitrosyls (**3+5**). While both entities of **6b** and **6c'** have a distorted square pyramidal coordination geometry similar to the fpin analogs, the species **6a** and **6d+d'** are more similar in shape to the bis(diamine) nitrosyls (**4**), where the CoN_5 moiety resembles a vacant octahedron, rather than a square pyramid. In the case of [$CoBr_2$(dppe)(NO)], the first coordination sphere of one entity in the asymmetric unit is very close to ideal *vOC*-5 geometry (**6a'$^{+}$**), while the other is strongly distorted toward a trigonal bipyramid. An outlier in its own compound class, the shape of entity **6a'** also differs greatly from the linear bis(diphosphane) complexes (**5**). One reason for this is the larger angular deviation of the equatorial Br–Co–P moiety from 120° in the ideal trigonal bipyramid (**6a'**: 18.29° vs. **5a**: −6.18° and **5a'**: −9.52°). Secondly, the equatorial Co–P and Co–Br bond lengths differ by 0.2177 Å, which is far larger than the difference between the two related Co–P distances in the bis(dppe) nitrosyls (**5a:** 0.0199 Å, **5a':** 0.0185 Å).

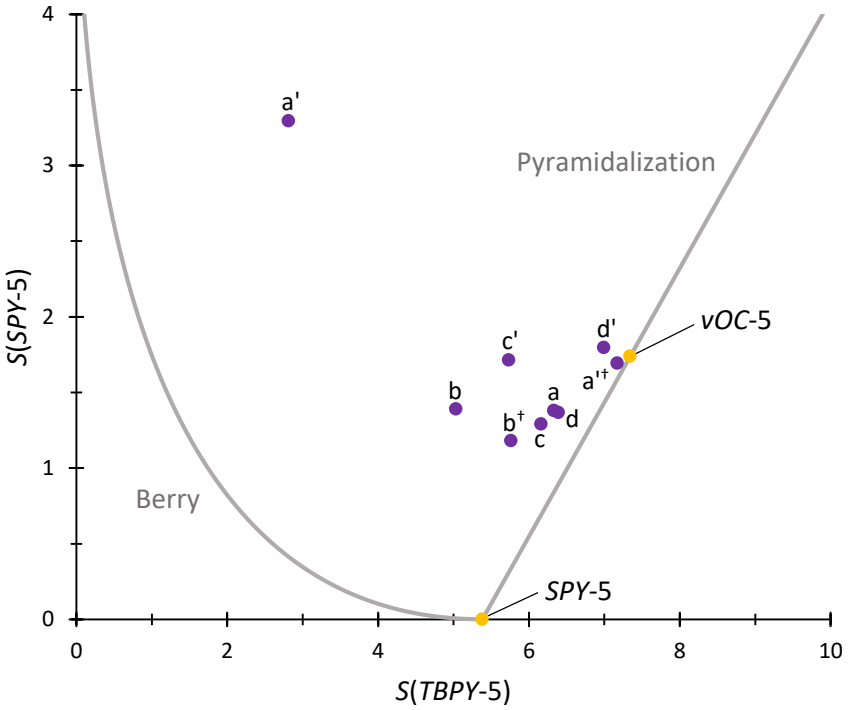

Figure 2.54: CShM map of compounds **6a–d** (purple data points) for fivefold-coordinated species, based on the X-ray structural data of the crystalline products. Ideal, undistorted polyhedra (yellow data points) as reference. The solid gray lines mark the Berry- and the pyramidalization path, respectively. For compounds **6a'+b**, the CShM values of both entities in the asymmetric unit (e.g. **6a'** and **6a'$^{+}$**, see Figures 2.56 + 7.57) are plotted.

The crystal structures on the following pages represent the first crystallographic data provided on this class of compounds. Only $[CoCl_2(dppe)(NO)]$ (**6a**) was already synthesized. In this procedure, the complex was obtained by treating the dinitrosyl $[Co(dppe)(NO)_2]Cl$ with excess dppe, resulting in the formation of **6a** and $[Co_2(dppe)_3(NO)_2]$ as by-product.[114] The authors reported a nitrosyl stretching band at 1676 cm^{-1}, which is close to the value of 1661 cm^{-1} measured for the newly synthesized compound **6a**·Me_2CO. Furthermore, crystal structures of the PMe_3-[81] and $PMePh_2$ [83] analogs with chloride, bromide and iodide are reported as well. They are readily obtained by treating the precursor species $[Co(L)_2(X)_2]$ with nitric oxide. In contrast to the square pyramidal diphosphane derivatives, they exhibit a trigonal bipyramidal geometry instead. With regard to the nitrosyl IR stretch, the bis(monophosphane) complexes often show a second absorption band in the NO region at higher wavenumbers, e.g. for $[CoCl_2(NO)(PMe_3)_2]$, bands at 1637 cm^{-1} and 1725 cm^{-1} are found.[81] While the existence of a second, linear isomer could not be proven crystallographically, it is assumed that the two nitrosyl vibrations occurring in these compounds result from singlet / triplet equilibria. Splitting of the N–O band is observed not only in the solids, but also in solution.[83] Further halogenido and also nitrito nitrosyls with various alkylated and aromatic monophosphanes have been synthesized in bulk. For some of these compounds, the split N–O stretch was confirmed by ^{15}N isotopic shifts.[81, 115–118] In contrast, the class **6** diphosphane analogs show either a single (**6c+d**) or a narrowly split (**6a+b**) nitrosyl band in the solid state. For the latter, a much smaller energy difference between the two bands is found compared to the monophosphane derivatives (**6a:** 21 cm^{-1}, **6a':** 26 cm^{-1}, **6b:** 11 cm^{-1}).

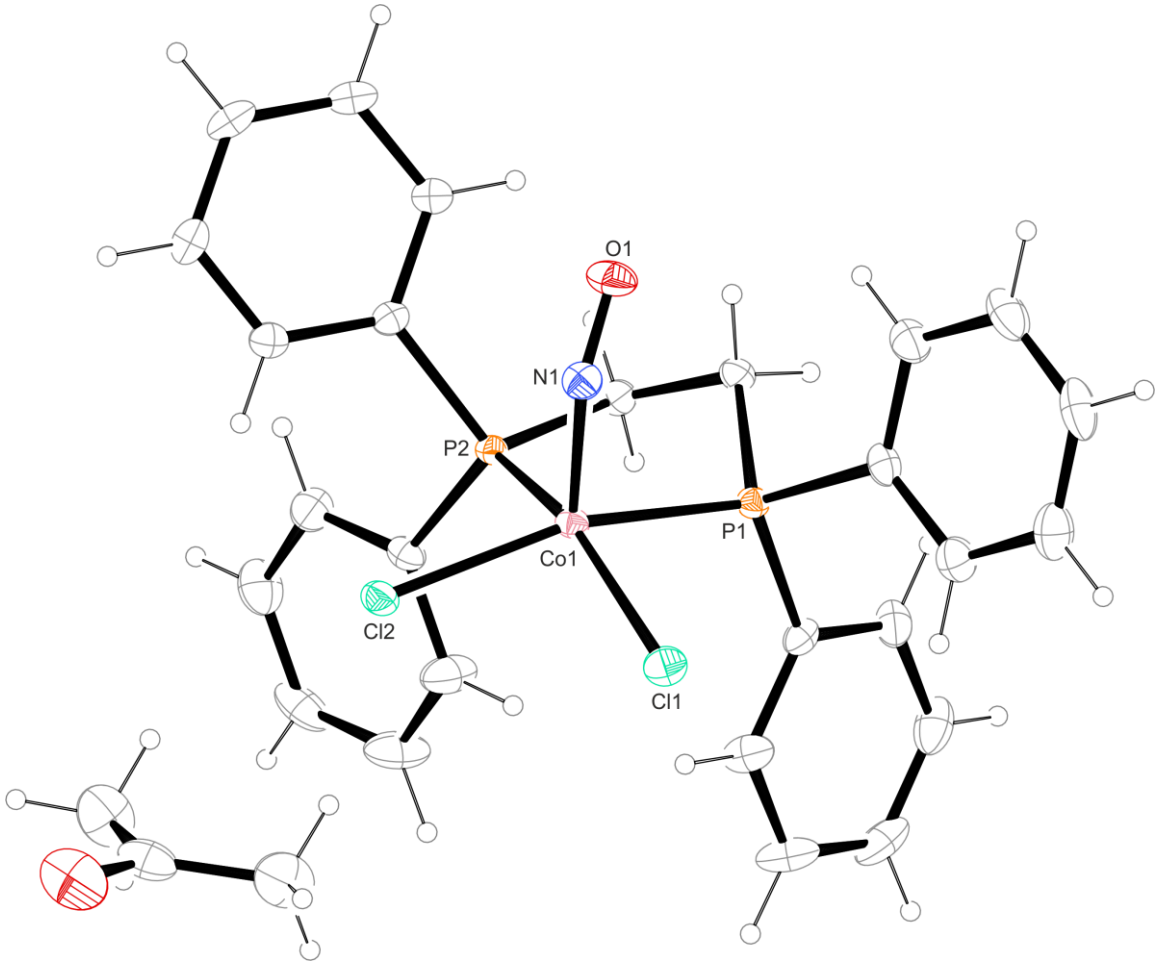

Figure 2.55: ORTEP plot of $[CoCl_2(dppe)(NO)]\cdot Me_2CO$ in crystals of **6a**·Me_2CO. Thermal ellipsoids drawn at 50 % probability level at 106 K. Interatomic distances (Å) and bond angles (°) with the standard deviation of the last decimal digit given in parentheses: Co1–N1 1.750(1), Co1–P1 2.1949(5), Co1–P2 2.2132(5), Co1–Cl1 2.2714(5), Co1–Cl2 2.2728(5), N1–O1 1.173(2), Co1–N1–O1 137.9(1), P1–Co1–Cl2 159.63(2), P2–Co1–Cl1 155.82(2), P1–Co1–P2 85.60(2), Cl1–Co1–Cl2 91.96(2), P1–Co1–Cl1 86.89(2), P2–Co1–Cl2 87.24(2), N1–Co1–P1 94.51(4), N1–Co1–P2 97.14(5), N1–Co1–Cl1 106.36(5), N1–Co1–Cl2 105.29(4).

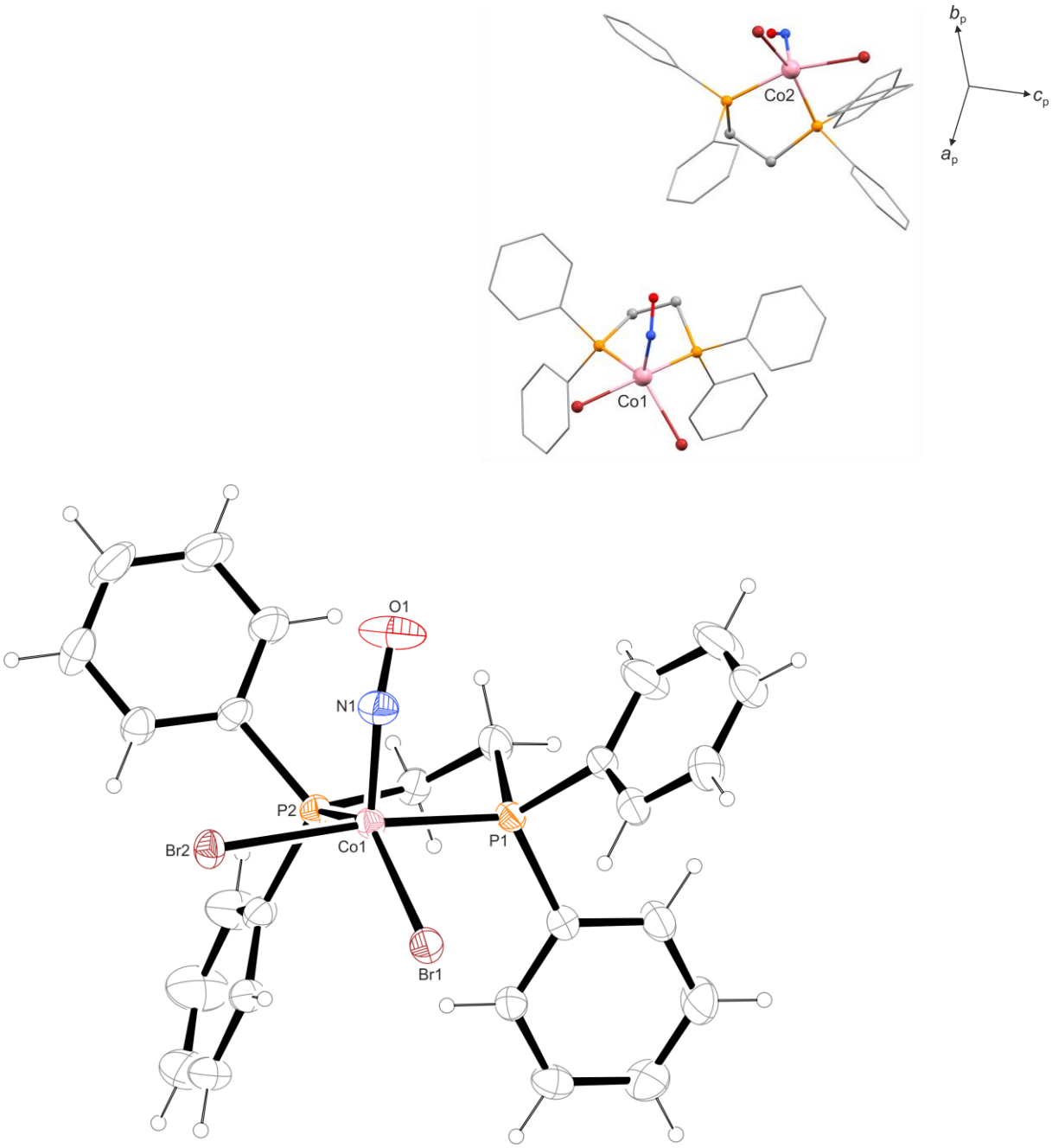

Figure 2.56: Left: ORTEP plot of [$CoBr_2$(dppe)(NO)] in crystals of **6a'**. For clarity, only one entity in the asymmetric unit is depicted. Thermal ellipsoids drawn at 50 % probability level at 173 K. Interatomic distances (Å) and bond angles (°) with the standard deviation of the last decimal digit given in parentheses: **First molecule (6a', pictured):** Co1–N1 1.729(2), Co1–P1 2.2110(6), Co1–P2 2.1986(6), Co1–Br1 2.4163(5), Co1–Br2 2.4225(6), N1–O1 1.153(3), Co1–N1–O1 142.7(2), P1–Co1–Br2 169.79(2), P2–Co1–Br1 138.29(2), P1–Co1–P2 85.45(2), Br1–Co1–Br2 91.59(2), P1–Co1–Br1 89.49(2), P2–Co1–Br2 86.99(2), N1–Co1–P1 91.61(6), N1–Co1–P2 103.13(5), N1–Co1–Br1 118.40(5), N1–Co1–Br2 96.80(6); **Second molecule (6a'^{t}, not shown):** Co2–N2 1.742(1), Co2–P3 2.2240(6), Co2–P4 2.2016(6), Co2–Br3 2.4213(6), Co2–Br4 2.4058(6), N2–O2 1.166(2), Co2–N2–O2 139.6(2), P3–Co2–Br4 156.33(2), P4– Co2–Br3 157.59(2), P3–Co2–P4 85.61(2), Br3–Co2–Br4 92.07(2), P3–Co2–Br3 88.15(2), P4–Co2–Br4 85.23(2), N2–Co2–P3 97.57(6), N2–Co2–P4 96.60(6), N2–Co2–Br3 105.57(6), N2–Co2–Br4 105.14(6). The ORTEP plot of the second entity is given in the appendix (Figure 7.57). **Right:** Plot of the asymm. unit in **6a'**. For clarity, hydrogen atoms are omitted. Furthermore, all phenyl groups are depicted as wireframe.

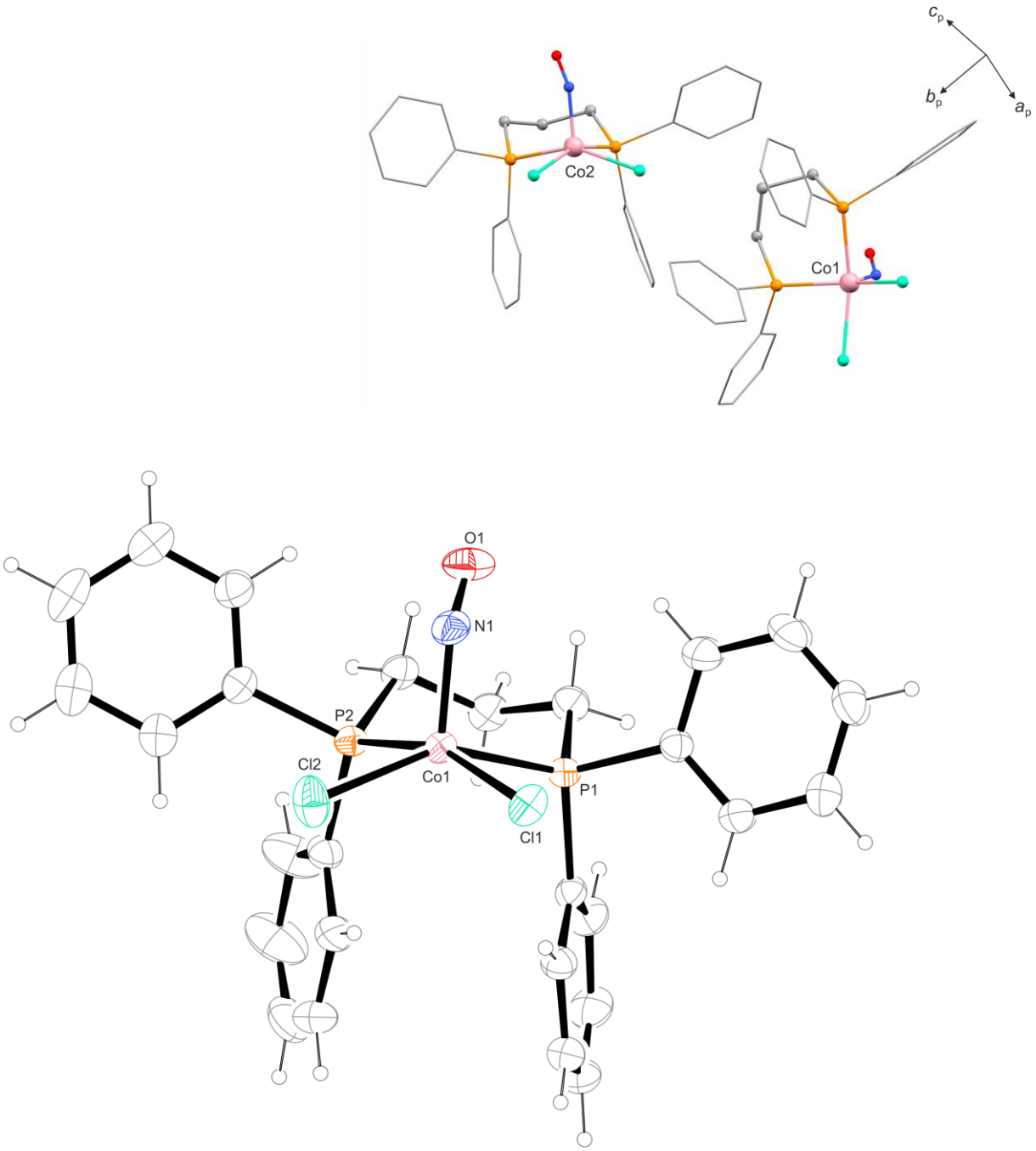

Figure 2.57: Left: ORTEP plot of [$CoCl_2$(dppp)(NO)] in crystals of **6b**. For clarity, only one entity in the asymmetric unit is depicted. Thermal ellipsoids drawn at 50 % probability level at 173 K. Interatomic distances (Å) and bond angles (°) with the standard deviation of the last decimal digit given in parentheses: **First molecule (6b, pictured):** Co1–N1 1.748(3), Co1–P1 2.2259(9), Co1–P2 2.2247(9), Co1–Cl1 2.2658(9), Co1–Cl2 2.2726(9), N1–O1 1.164(4), Co1–N1–O1 138.0(2), P1–Co1–Cl2 149.82(4), P2–Co1–Cl1 160.61(3), P1–Co1–P2 90.69(3), Cl1–Co1–Cl2 89.82(4), P1–Co1–Cl1 84.96(3), P2–Co1–Cl2 84.48(3), N1–Co1–P1 98.5(1), N1–Co1–P2 95.22(9), N1–Co1–Cl1 104.11(9), N1–Co1–Cl2 111.6(1); **Second molecule (6b$^+$, not shown):** Co2–N2 1.744(3), Co2–P3 2.2356(8), Co2–P4 2.2105(8), Co2–Cl3 2.2635(8), Co2–Cl4 2.2516(8), N2–O2 1.165(4), Co2–N2–O2 138.1(2), P3–Co2–Cl4 158.41(3), P4– Co2–Cl3 152.74(3), P3–Co2–P4 89.43(3), Cl3–Co2–Cl4 88.29(4), P3–Co2–Cl3 86.47(3), P4–Co2–Cl4 85.69(3), N2–Co2–P3 97.07(9), N2–Co2–P4 98.08(9), N2–Co2–Cl3 109.17(9), N2–Co2–Cl4 104.44(9). The ORTEP plot of the second entity is given in the appendix (Figure 7.58). **Right:** Plot of the asymmetric unit in **6b**. For clarity, hydrogen atoms are omitted. Furthermore, all phenyl groups are depicted as wireframe.

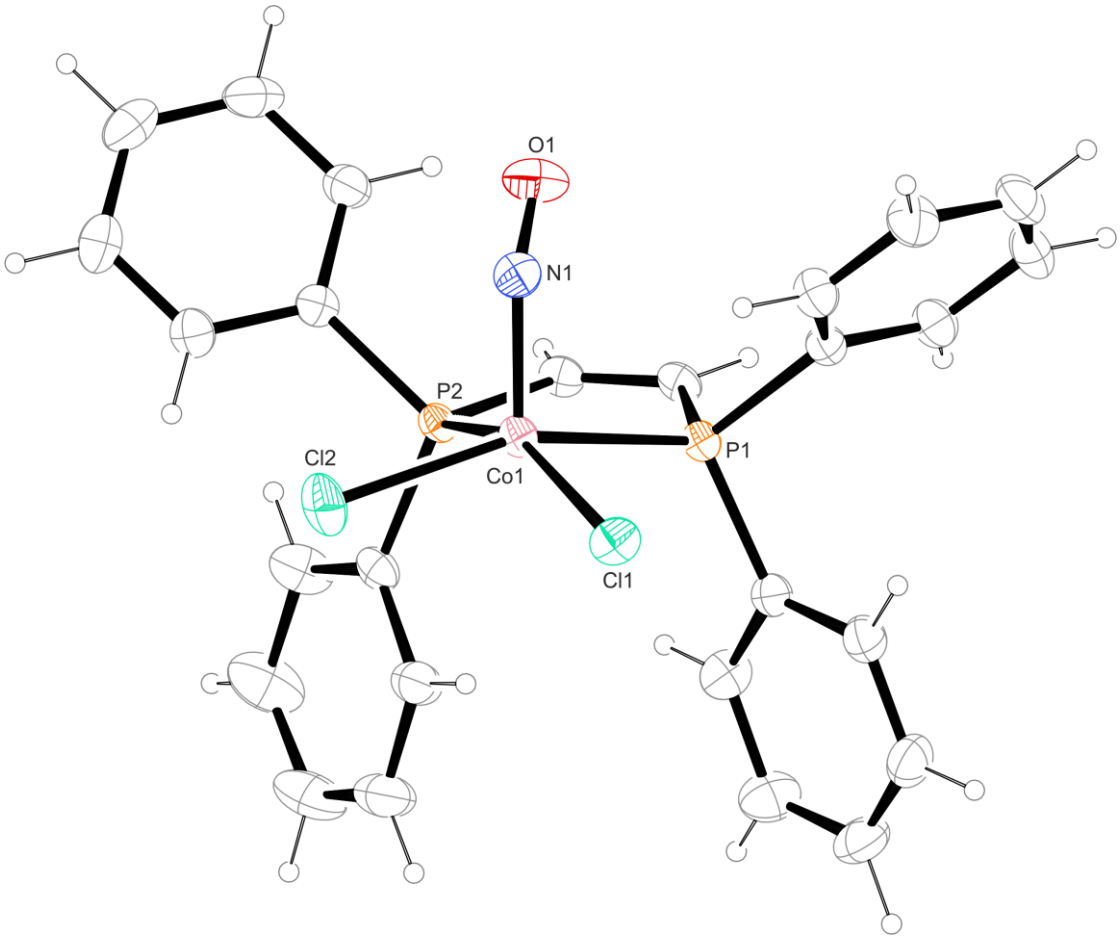

Figure 2.58: ORTEP plot of [$CoCl_2$(dppv)(NO)] in crystals of **6c**. Thermal ellipsoids drawn at 50 % probability level at 173 K. Interatomic distances (Å) and bond angles (°) with the standard deviation of the last decimal digit given in parentheses: Co1–N1 1.749(2), Co1–P1 2.1952(6), Co1–P2 2.1798(5), Co1–Cl1 2.2820(5), Co1–Cl2 2.2648(6), N1–O1 1.164(2), Co1–N1–O1 138.8(2), P1–Co1–Cl2 157.09(2), P2–Co1–Cl1 153.55(2), P1–Co1–P2 85.84(2), Cl1–Co1–Cl2 93.44(2), P1–Co1–Cl1 86.30(2), P2–Co1–Cl2 84.28(2), N1–Co1–P1 96.73(6), N1–Co1–P2 96.37(7), N1–Co1–Cl1 109.63(7), N1–Co1–Cl2 104.87(6).

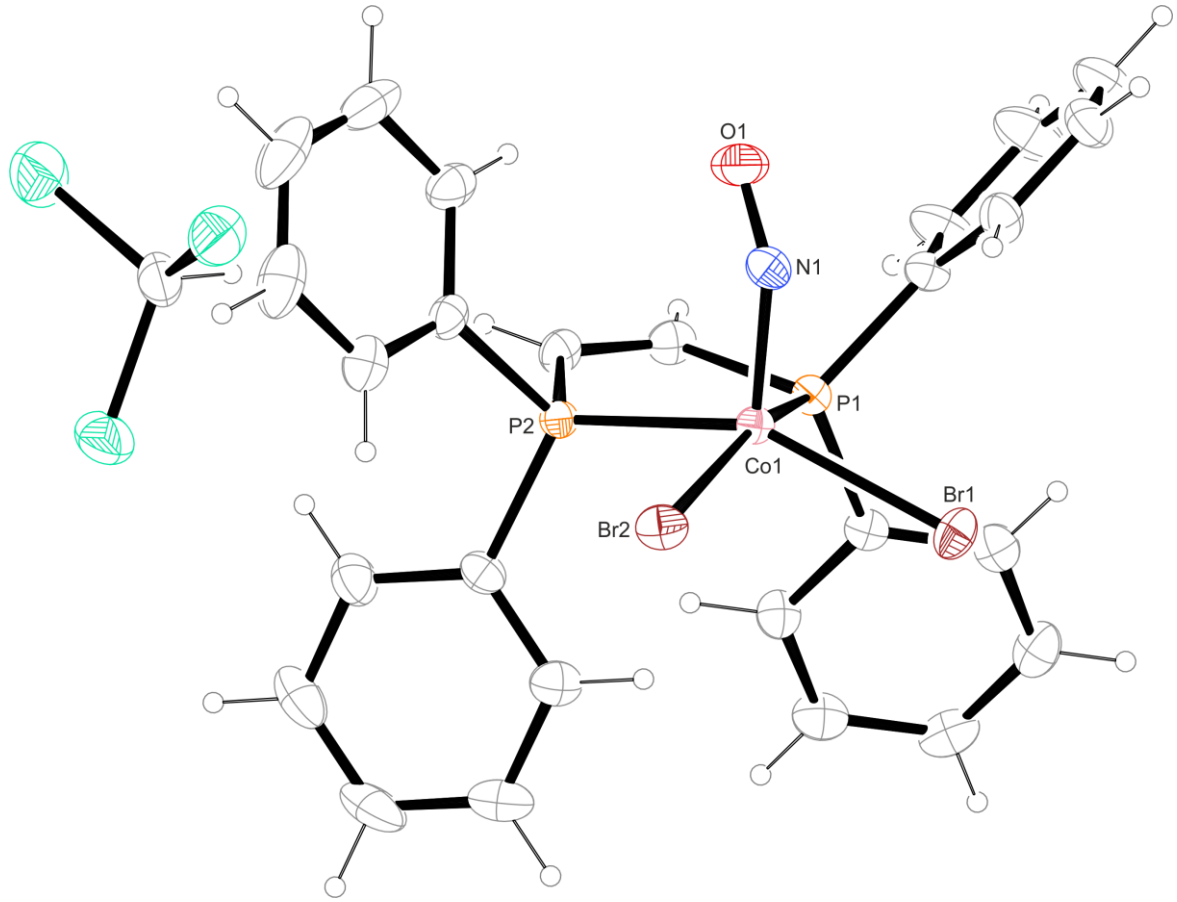

Figure 2.59: ORTEP plot of $[CoBr_2(dppv)(NO)]\cdot CHCl_3$ in crystals of **6c'**$\cdot CHCl_3$. Thermal are ellipsoids drawn at 50 % probability level at 173 K. Interatomic distances (Å) and bond angles (°) with the standard deviation of the last decimal digit given in parentheses: Co1–N1 1.737(1), Co1–P1 2.2082(7), Co1–P2 2.1893(7), Co1–Br1 2.4099(7), Co1–Br2 2.4203(6), N1–O1 1.169(2), Co1–N1–O1 140.9(1), P1–Co1–Br2 159.03(2), P2–Co1–Br1 151.07(2), P1–Co1–P2 85.60(2), Br1–Co1–Br2 92.66(2), P1–Co1–Br1 87.14(2), P2–Co1–Br2 84.50(2), N1–Co1–P1 97.41(5), N1–Co1–P2 98.70(5), N1–Co1–Br1 110.00(5), N1–Co1–Br2 102.33(5).

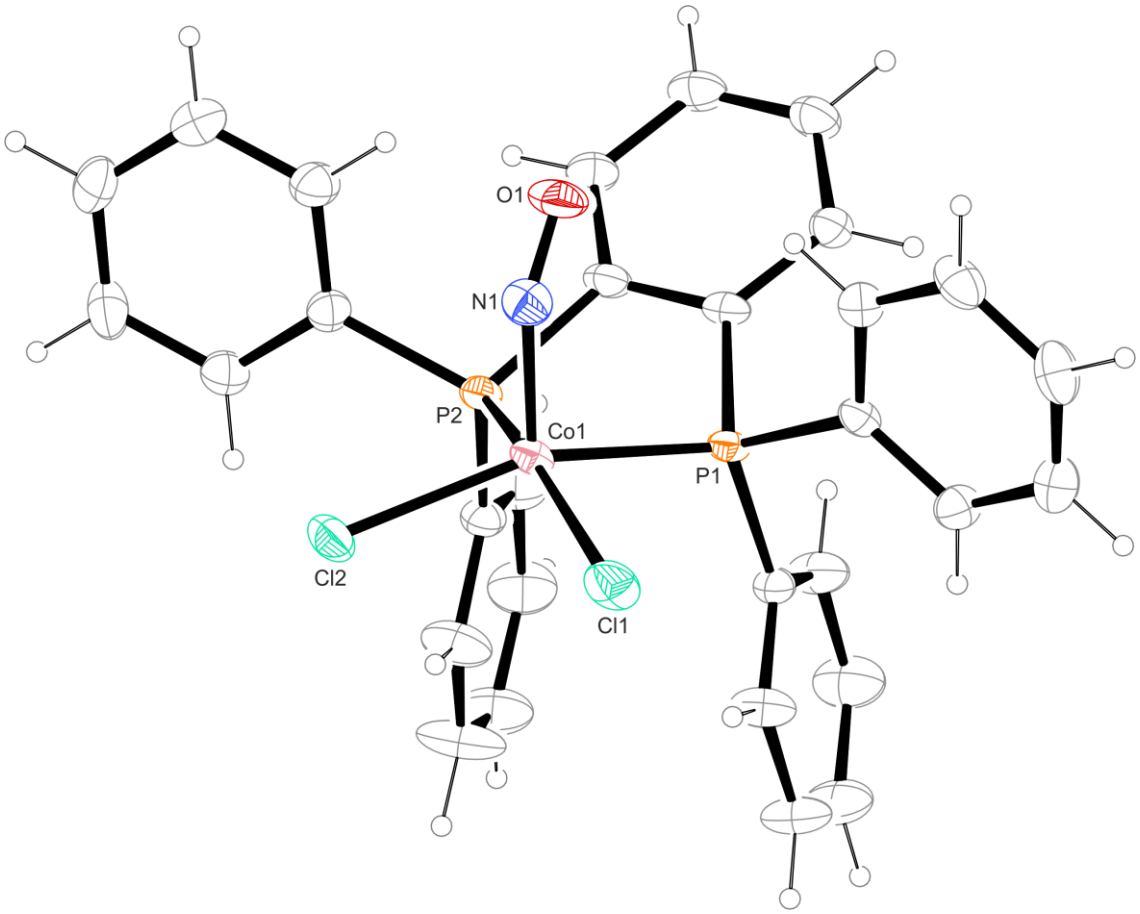

Figure 2.60: ORTEP plot of [$CoCl_2$(dppbz)(NO)] in crystals of **6d**. Thermal ellipsoids drawn at 50 % probability level at 173 K. Interatomic distances (Å) and bond angles (°) with the standard deviation of the last decimal digit given in parentheses: Co1–N1 1.751(3), Co1–P1 2.198(1), Co1–P2 2.203(1), Co1–Cl1 2.263(1), Co1–Cl2 2.265(1), N1–O1 1.166(4), Co1–N1–O1 137.6(3), P1–Co1–Cl2 155.40(5), P2–Co1–Cl1 158.33(5), P1–Co1–P2 82.79(4), Cl1–Co1–Cl2 93.14(4), P1–Co1–Cl1 87.10(4), P2–Co1–Cl2 88.29(4), N1–Co1–P1 97.3(1), N1–Co1–P2 94.8(1), N1–Co1–Cl1 105.5(1), N1–Co1–Cl2 106.3(1).

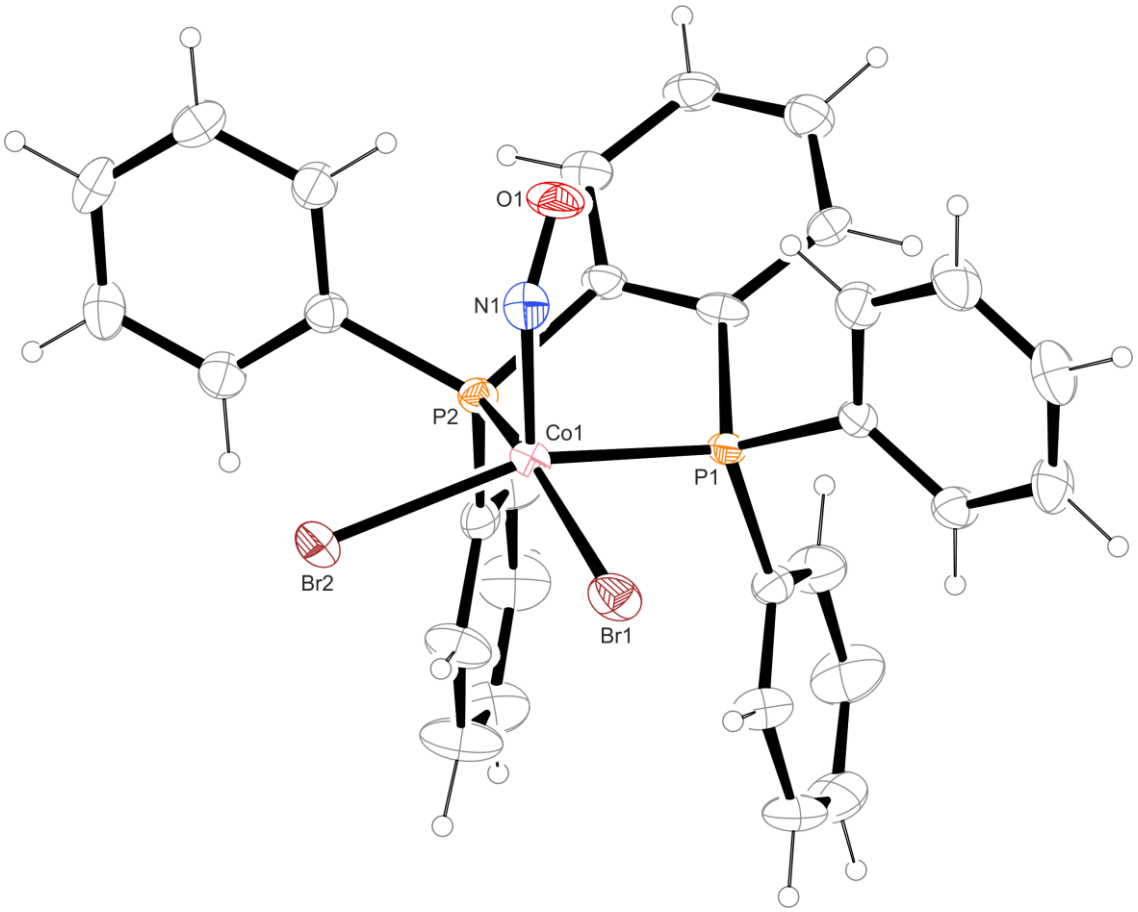

Figure 2.61: ORTEP plot of [$CoBr_2$(dppbz)(NO)] in crystals of **6d'**. Thermal ellipsoids drawn at 50 % probability level at 173 K. Interatomic distances (Å) and bond angles (°) with the standard deviation of the last decimal digit given in parentheses: Co1–N1 1.738(5), Co1–P1 2.204(1), Co1–P2 2.202(2), Co1–Br1 2.4047(9), Co1–Br2 2.4051(9), N1–O1 1.178(6), Co1–N1–O1 139.5(4), P1–Co1–Br2 155.88(6), P2–Co1–Br1 157.89(7), P1–Co1–P2 82.82(6), Br1–Co1–Br2 92.36(3), P1–Co1–Br1 87.46(5), P2–Co1–Br2 88.60(5), N1–Co1–P1 97.3(1), N1–Co1–P2 95.1(1), N1–Co1–Br1 105.8(1), N1–Co1–Br2 105.9(1).

2.7 Further cobalt nitrosyls and hyponitrite complexes

2.7.1 *rac-cis*-[Co(NO)(NO_2-κ*N*)(phen)$_2$]ClO_4 (7a)

To expand the structure class of hexacoordinated cobalt nitrosyls (**4**), further experiments were carried out using aromatic *N*,*N*'-co-ligands instead of diamines. Complexes $[Co(L)_2(NO)(X)]Y$ with L = phenanthroline or 2,2'-bipyridine and X = Cl, I, NO_2 were already described by Vlček *et al*.[119] The compounds were obtained in bulk as perchlorate or hexafluorophosphate salts via the direct reaction with gaseous nitric oxide in ethanol, using stoichiometric amounts of cobalt(II) halogenide, co-ligand and counterion salt. For the nitrito species, cobalt(II) nitrate and sodium nitrite were used. While they failed to obtain the solids in a crystallinity suitable for X-ray diffraction, it was now possible to prepare single crystals of *rac-cis*-[Co(NO)(NO_2-κ*N*)(phen)$_2$]ClO_4 (**7a**) by diffusion of an acetonitrilic bulk solution into DMSO. The crystal structure is depicted in Figure 2.62. Contrary to the bis(diamine) nitrosyls (**4**), the anionic ligand in **7a** is arranged *cis* to NO. The nitrosyl ligand is disordered with the nitrite, with N–O distances of 1.156 Å and 1.196 Å and Co–N bond lengths of 1.890 Å and 1.886 Å. The structure shows a rotational 180°-disorder around the C_2 axis of the Co(phen)$_2$ fragment, involving the metal center as well. For the *N*-bonded nitrito ligand, Co–N distances of 1.924 Å and 1.921 Å are found, which is in agreement with the literature values reported for nitrito-κ*N* complexes of cobalt.[120,121] For the CoNO moiety, bond angles of 119.9° and 117.5° are observed. Overall, the structural parameters of this unit differ from the class **4** nitrosyl species only by a slightly longer Co–N bond and a more acute Co–N–O angle. The N–O stretch of species **7a** consists of a split band with peaks at 1649 cm^{-1} and 1658 cm^{-1}, which is in the same range as the bipyridine analog, for which an absorption band at 1642 cm^{-1} has been reported (however, no spectroscopic data were provided on the phenanthroline complex).[119] In contrast to its solution-stable *trans* analogs, **7a** shows moderately rapid decomposition upon argon purging. Concerning the coordination geometry, both disorder forms of the nitrito nitrosyl are best described as a slightly distorted octahedron (see Table 7.23 for CShM values). With regard to H-bonds, only non-classical interactions are found, occurring mainly between the C–H groups and the nitrosyl and nitrito ligands. A complete list is given in Table 7.22 in the appendix. The other nitrosyl complexes described by Vlček were also crystallized using the DMSO method. However, the solids obtained were unsuitable for X-ray analysis. In the recorded structure of *rac-cis*-$[Co(bpy)_2Cl(NO)]ClO_4$, for example, almost all atoms meet the crystallographic standards except for the nitrosyl nitrogen, which shows a reproducible disorder that could not be resolved (failed Hirshfeld test for atom N1, see Figure 7.61 in the appendix). Also, CHN analysis of the crystals and bulk indicated the presence of impurities in both solids. Since it was not possible to determine its exact composition, this compound was therefore excluded from the structural discussion presented in this work. Contrary to **7a**, the bipyridine complex crystallizes in the space group $P2_12_12_1$ and was obtained as a 1:1 mixture of the enantiopure crystals. Their nitrosyl stretch was measured at 1643 cm^{-1}, which is in good agreement with the literature value of 1642 cm^{-1}.[119] In solution, it was found to decompose at a rate similar to **7a** when purged with argon.

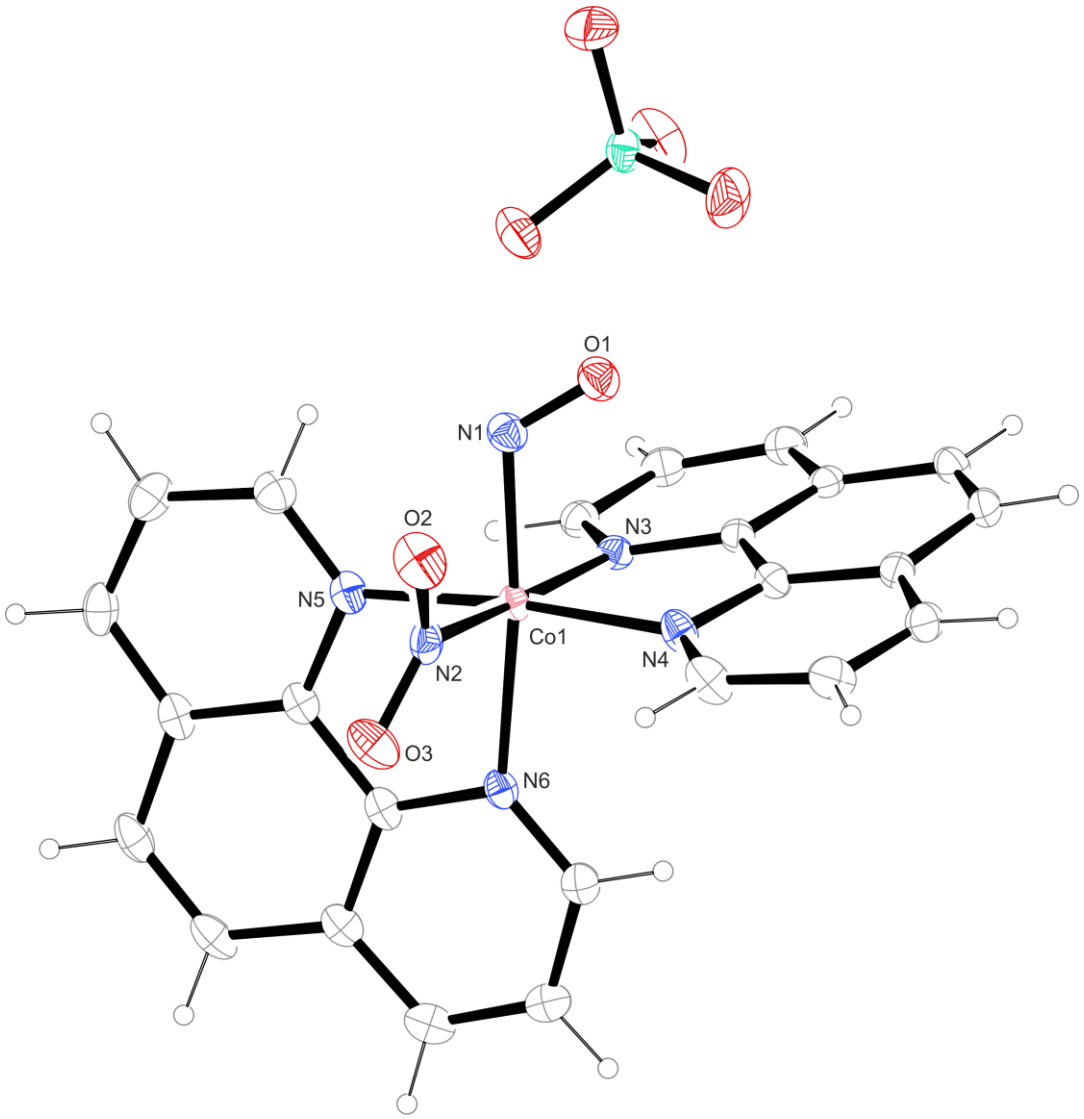

Figure 2.62: ORTEP plot of *rac-cis*-[Co(NO)(NO_2-κ*N*)(phen)$_2$]ClO_4 in crystals of **7a**. For clarity, only the major disorder (80 %) form is shown. Furthermore, only the Δ enantiomer is depicted. Thermal ellipsoids drawn at 50 % probability level at 101 K. Interatomic distances (Å) and bond angles (°) with the standard deviation of the last decimal digit given in parentheses: **Major disorder form (7a, pictured):** Co1–N1 1.890(4), Co1–N2 1.924(5), Co1–N3 1.965(4), Co1–N4 1.967(3), Co1–N5 1.953(3), Co1–N6 2.138(4), N1–O1 1.156(1), N2–O2 1.245(5), N2–O3 1.241(1), Co1–N1–O1 119.9(6), N1–Co1–N6 171.5(2), Co1–N2–O2 119.1(3), Co1–N2–O3 121.2(5), O2–N2–O3 119.7(5), N2–Co1–N3 174.4(2), N4–Co1–N5 174.3(2), N2–Co1–N5 85.2(2), N3–Co1–N4 83.5(1), N2–Co1–N4 92.8(2), N3–Co1–N5 98.9(1), N1–Co1–N2 87.7(2), N1–Co1–N3 88.3(2), N1–Co1–N4 94.2(2), N1–Co1–N5 91.0(2), N6–Co1–N2 94.1(2), N6–Co1–N3 90.4(2), N6–Co1–N4 93.9(2), N6–Co1–N5 80.9(1); **Minor disorder form (7a†, not shown):** Co1A–N1A 1.886(2), Co1A–N2A 1.921(2), Co1A– N3 2.119(1), Co1A–N4 1.879(1), Co1A–N5 2.058(1), Co1A–N6 1.894(1), N1A–O1A 1.196(4), N2A–O2A 1.240(5), N2A–O3A 1.252(2), Co1A–N1A–O1A 117.5(2), N1A–Co1A–N6 90.8(6), Co1A–N2A–O2A 127.2(3), Co1A–N2A–O3A 118.2(1), O2A–N2A–O3A 114.1(3), N2A–Co1A–N3 90.9(7), N4–Co1A–N5 167.6(7), N2A–Co1A–N5 90.5(7), N3–Co1A–N4 81.6(5), N2A–Co1A–N4 80.1(7), N3–Co1A–N5 90.6(5), N1A–Co1A–N2A 85.9(9), N1A–Co1A–N3 172.6(9), N1A–Co1A–N4 91.2(8), N1A–Co1A–N5 96.2(8), N6–Co1A–N2A 173.7(1), N6–Co1A–N3 92.8(6), N6–Co1A–N4 105.6(7), N6–Co1A–N5 84.2(5). The ORTEP plot of the minor disorder form is shown in the appendix (Figure 7.59). A plot of the complete asymmetric unit is given in Figure 7.60.

2.7.2 $(ppzH_2)_{0.5}[Co(fpin)(NO)_2]$ (7b)

During the search for new class **1** nitrosyls, the potential use of piperazine as a co-ligand was investigated as well. The intended goal was to crystallize a compound such as [Co(fpin)(NO)(ppz)], in which the cyclic diamine would act as a chelator. Only a few examples of complexes with chelating piperazine are known to literature. These species have platinum(II)-, palladium(II)-[122] or nickel(II)[123] centers. In the square planar compounds, the ligand adopts a distorted boat conformation. With cobalt(II), however, a dinitrosyl has now been obtained using the usual route for class **1** nitrosyl complexes. Treatment of a methanolic solution containing stoichiometric amounts of cobalt(II) triflate, piperazine and $(NBnMe_3)_2$(fpin) with nitric oxide gas resulted in the formation of $(ppzH_2)_{0.5}[Co(fpin)(NO)_2]$ (**7b**). Brown single crystals of the compound were grown via the DMSO method. Upon solving the recorded crystal structure (Figure 2.63), it became clear that both amino groups of the diamine were protonated and that the resulting piperazinium ions occupy positions with inversion symmetry. Therefore, half a counterion can be assigned to a dinitrosyl complex in the asymmetric unit.

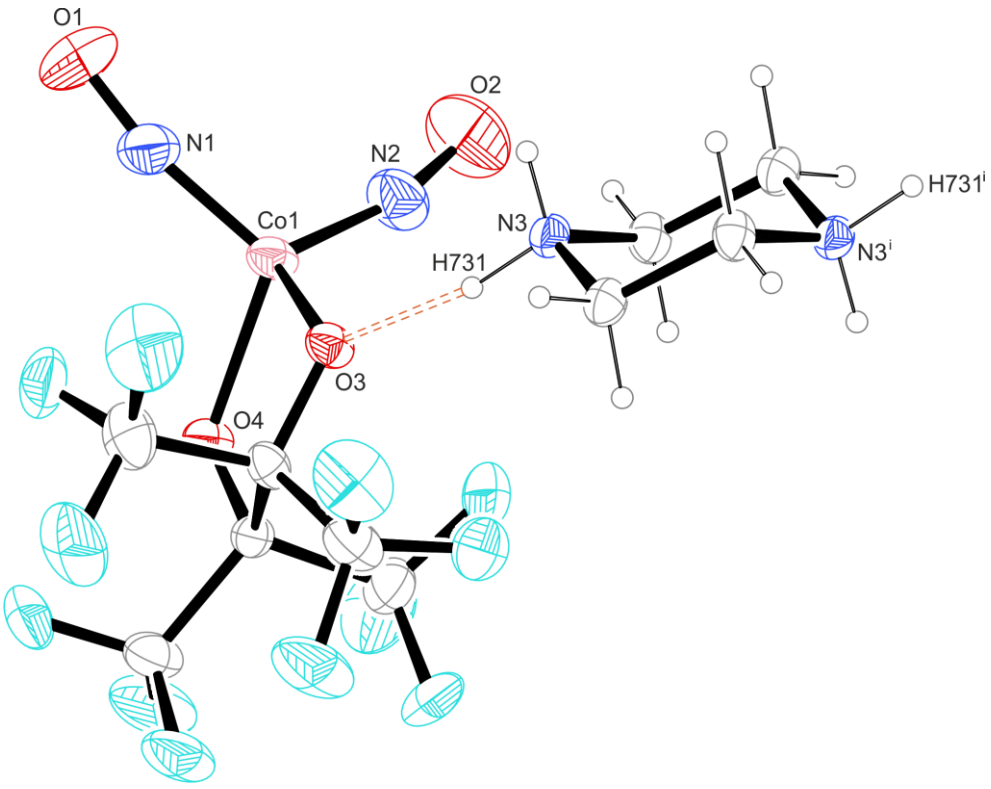

Figure 2.63: ORTEP plot of $(ppzH_2)_{0.5}[Co(fpin)(NO)_2]$ in crystals of **7b**. For clarity, the entire piperazinium ion is shown, including the symmetry-generated half. Thermal ellipsoids are drawn at 50% probability level at 173 K. Interatomic distances (Å) and bond angles (°) with the standard deviation of the last decimal digit given in parentheses: Co1–N1 1.658(3), Co1–N2 1.662(3), Co1–O3 1.973(2), Co1–O4 1.978(2), N1–O1 1.153(4), N2–O2 1.148(4), H731–O3 1.80(4), Co1–N1–O1 166.2(3), Co1–N2–O2 165.8(3), N1–Co1–N2 112.0(1), N1–Co1–O3 116.5(1), N1–Co1–O4 112.2(1), N2–Co1–O3 113.8(1), N2–Co1–O4 116.8(1), O3–Co1–O4 82.7(1). Symmetry code: ^{i} 1−*x*, 1−*y*, 1−*z*.

Consequently, the product is best described as a $\{Co(NO)_2\}^{10}$ compound. This dinitrosyl complex was already synthesized by Neumann with $NBnMe_3^+$ as counterion, but could not be crystallized reproducibly. In the recorded structure, N–O distances of 1.161 Å and 1.172 Å are found. The Co–N bonds are 1.662 Å and 1.670 Å long, with the CoNO moieties being slightly bent at angles of 161.4° and 163.9°.[124] In comparison, the two nitrosyl ligands of **7b** exhibit slightly shorter N–O bond lengths of 1.153 Å and 1.148 Å and Co–N distances of 1.658 Å and 1.662 Å. With angles of 166.2° and 165.8°, the CoNO moieties in **7b** are more obtuse. Like Neumann's product, the complex exhibits a slightly distorted tetrahedral coordination geometry (see Table 7.23 for CShM values), typical for $\{Co(NO)_2\}^{10}$ dinitrosyls.[125–129] In the infrared spectrum of **7b**, symmetric and asymmetric N–O stretching vibrations were found at 1855 cm^{-1} and 1766 cm^{-1}, respectively. For the ammonium salt, these bands were found at slightly lower wavenumbers of 1830 cm^{-1} and 1750 cm^{-1}. There are two classical hydrogen bonds in the structure of **7b**, with the piperazinium ion linking four complex entities via chain motifs of the $C_2^2(6)$-type (–O3···H731–N3–H732···O4^{i}–Co1^{i}– in the binary graph set). For a complete overview, see Table 2.21. A single non-classical interaction occurs between a C–H group of the counterion and the perfluoropinacolato ligand. Details on this bond are listed in Table 7.22 in the appendix.

Table 2.21: Distances and angles of classical hydrogen bonds in crystals of **7b**. The standard deviation of the last decimal digit is given in parentheses.

D–H···A	*d*(D–H)/Å	*d*(H···A)/Å	*d*(D···A)/Å	∢(D–H···A)/°
N3–H731···O3	0.97(4)	1.80(4)	2.740(3)	162(3)
N3–H732···O4^{i}	0.91(4)	1.83(4)	2.713(3)	164(3)

Symmetry code: ^{i} 1–*x*, ½+*y*, ½–*z*.

2.7.3 *rac*-[Co(en)$_2$(*cis*-N_2O_2-κ^2*O*,*O*′)]ClO_4 (7c)

In search for further class **4** compounds, experiments to obtain bis(diamine) nitrosyls with nitrite as anionic co-ligand were conducted. For the attempted synthesis of the respective ethylenediamine derivative, Feltham's ligand-replacement approach using the precursor *trans*-[Co(ClO_4)(en)$_2$(NO)]ClO_4 (**4a**) was chosen.[85] Sodium nitrite, added to an aqueous bulk solution of the complex, was used as the co-ligand source. Therefore, this procedure combines the routes of Feltham and Vlček (the latter being used for the synthesis of *cis* nitrosyl **7a**).[119] For crystallization, the regular DMSO method was applied. However, this approach did not lead to a mononitrosyl complex. Instead, the new hyponitrito compound *rac*-[Co(en)$_2$(*cis*-N_2O_2-κ^2*O*,*O*′)]ClO_4 (**7c**) was obtained.

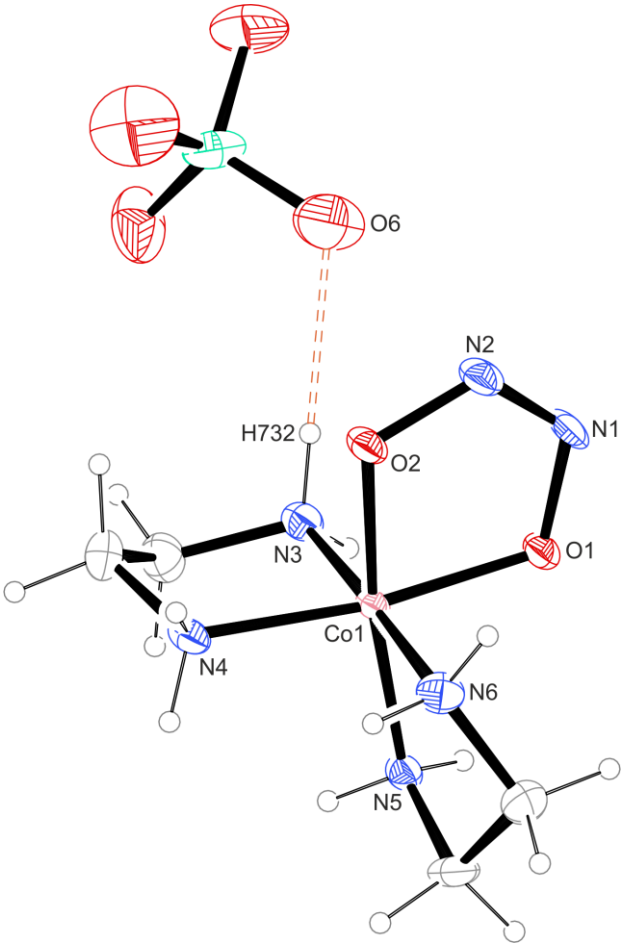

Figure 2.64: ORTEP plot of *rac*-[Co(en)$_2$(*cis*-N_2O_2-κ^2*O*,*O*′)]ClO_4 in crystals of **7c**. For clarity, only the Δ enantiomer is depicted. Thermal ellipsoids are drawn at 50% probability level at 173 K. Interatomic distances (Å) and bond angles (°) with the standard deviation of the last decimal digit given in parentheses: Co1–O1 1.872(2), Co1–O2 1.864(2), Co1–N3 1.956(3), Co1–N4 1.972(3), Co1–N5 1.973(3), Co1–N6 1.957(3), O1–N1 1.377(4), O2–N2 1.376(4), N1–N2 1.247(5), H732–O6 2.17, Co1–O1–N1 110.8(2), Co1–O2–N2 110.8(2), O1–N1–N2 116.9(3), O2–N2–N1 117.4(3), O1–Co1–N4 172.2(1), O2–Co1–N5 172.6(1), N3–Co1–N6 178.1(1), O1–Co1–N3 90.3(1), O1–Co1–N6 91.0(1), N3–Co1–N4 85.8(1), N4–Co1–N6 93.1(1), O2–Co1–O1 84.1(1), O2–Co1–N3 90.4(1), O2–Co1–N4 89.2(1), O2–Co1–N6 91.2(1), N5–Co1–O1 89.3(1), N5–Co1–N3 93.1(1), N5–Co1–N4 97.6(1), N5–Co1–N6 85.5(1).

As can be seen from the crystal structure in Figure 2.64, the complex features a chelating hyponitrite, making **7c** the first-ever reported cobalt compound in which the ligand adapts this binding mode. So far, only a few complexes with chelating *cis*-hyponitrite have been characterized by X-ray diffraction, including two square planar nickel(II) species with 2,2'-bipyridine[130] and 1,1'-bis(diphenylphosphino)-ferrocene[131] and a tetrahedral platinum(II) complex with triphenylphosphane.[132,133] For the hyponitrito ligand in **7c**, an N–N distance of 1.247 Å and N–O bond lengths of 1.377 Å and 1.376 Å are found, which is in good agreement with the structures known from literature. The Co–O distances of 1.872 Å and 1.864 Å are slightly longer (about 0.06 Å) than the analogous Ni–O bonds and about 0.15 Å shorter compared to the platinum(II) species. The N–N–O bond angles of 116.9° and 117.4° deviate from those of the group-10 derivatives by about 1.5°, with the angles being more acute than in the Ni(II) analogs, but more obtuse compared to the Pt(II) derivative. Only a few very small, reddish-orange crystals were obtained, therefore it was not possible to characterize this compound by IR spectroscopy. The product was reproducibly crystallized in racemic form. Regarding the coordination geometry, the complex entity in **7c** exhibits a slightly distorted octahedral shape (see Table 7.23 for CShM values). From the classical hydrogen-bonding pattern shown in Figure 2.65, it can be seen that all hyponitrite atoms act as acceptors. Neighboring complexes are linked by the perchlorate ions and form cyclic motifs such as $R_2^2(7)$ (–N4–H742···N2^{iii}–N1^{iii}···H751–N5–Co1–) and $R_2^2(8)$ (–N5–H752···O2^{iv}–Co1^{iv}–N4^{iv}–H741^{iv}···O1–Co1– both in the binary graph set). An overview of all classical hydrogen bonds is given in Table 2.22. Only one non-classical interaction is found, occurring between the organic backbone of an ethylenediamine ligand and the counterion. Details on this bond are listed in Table 7.22. Attempts to synthesize derivatives of **7c** with *N*-methylated en ligands were unsuccessful.

Table 2.22: Distances and angles of classical hydrogen bonds in crystals of **7c**. The standard deviation of the last decimal digit is given in parentheses. Values without a standard deviation refer to hydrogen atoms calculated on idealized positions, riding on their parent atoms.

D–H···A	*d*(D–H)/Å	*d*(H···A)/Å	*d*(D···A)/Å	∢(D–H···A)/°
N3–H731···O3^{i}	0.91	2.09	2.926(5)	153
N3–H732···O6	0.91	2.17	3.077(5)	175
N4–H741···O1^{ii}	0.91	2.14	3.024(4)	162
N4–H742···N2^{iii}	0.91	2.21	3.067(4)	157
N5–H751···N1^{iii}	0.91	2.30	3.090(4)	145
N5–H752···O2^{iv}	0.91	2.14	2.961(4)	150
N6–H761···O3^{v}	0.91	2.20	3.006(5)	147
N6–H762···O5^{vi}	0.91	2.19	3.064(5)	160

Symm. codes: ^{i} 1−*x*, 1−*y*, 1−*z*; ^{ii} 1−*x*, −½+*y*, ½−*z*; ^{iii} −1+*x*, *y*, *z*; ^{iv} 1−*x*, ½+*y*, ½−*z*; ^{v} *x*, ½−*y*, −½+*z*; ^{vi} −1+*x*, ½−*y*, −½+*z*.

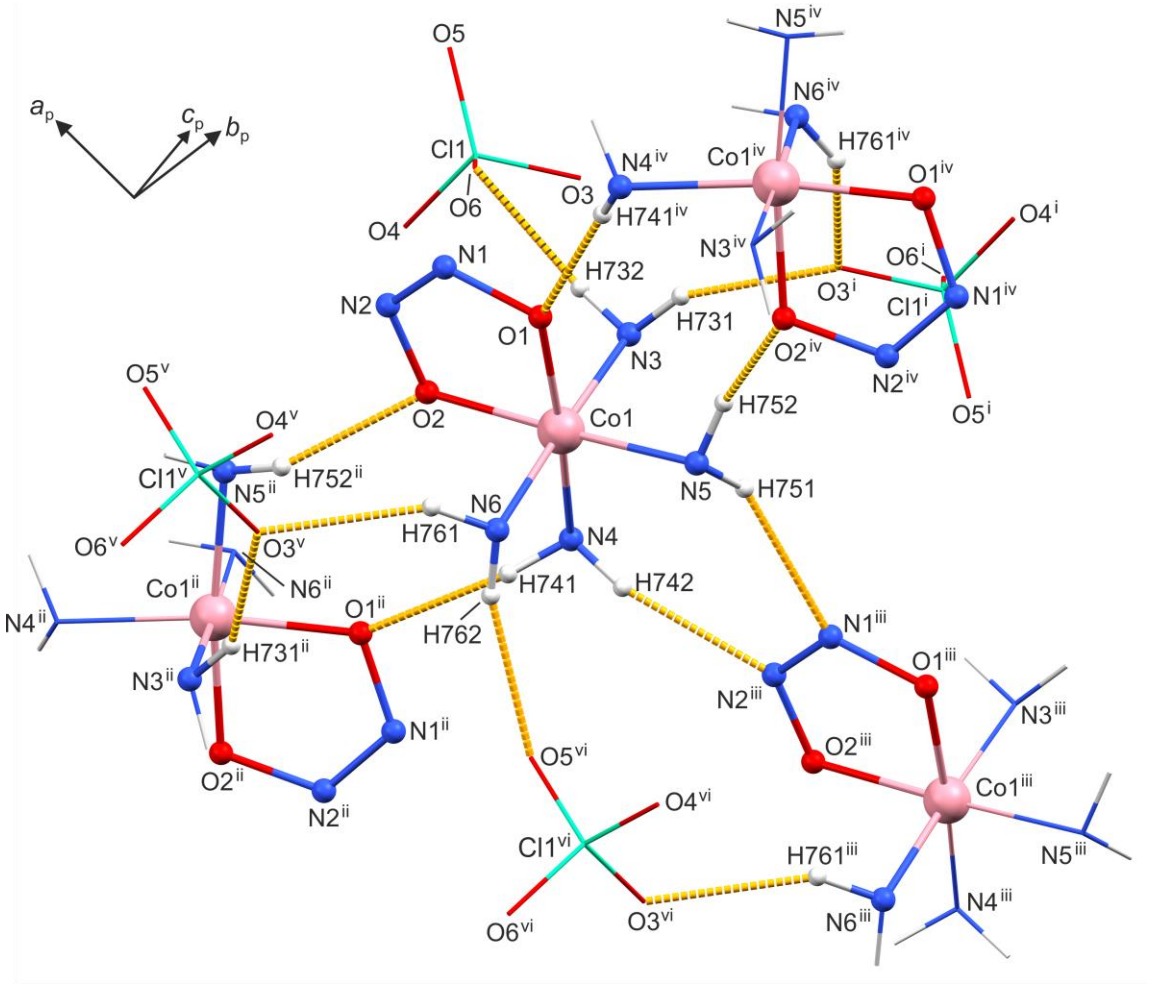

Figure 2.65: Plot of the pattern of classical hydrogen bonds (dashed yellow lines) in crystals of **7c**. For clarity, the organic ligand residues are omitted. Furthermore, the perchlorate ions and parts of the co-ligand's amino groups are depicted as wireframe. Symm. codes: [i] 1−*x*, 1−*y*, 1−*z*; [ii] 1−*x*, −½+*y*, ½−*z*; [iii] −1+*x*, *y*, *z*; [iv] 1−*x*, ½+*y*, ½−*z*; [v] *x*, ½−*y*, −½+*z*; [vi] −1+*x*, ½−*y*, −½+*z*.

2.8 Quantum-chemical calculations

To gain a better understanding of their electronic properties, quantum-chemical DFT calculations were performed on the novel mononitrosyl complexes by Daniel Schröder, M.Sc. and Prof. Dr. Peter Klüfers (LMU München). The computational studies focused on the structural parameters of the CoNO moiety and the nitrosyl ligand's IR stretching frequency. In order to assign oxidation states in the $\{CoNO\}^8$ entity, charge- and oxidation-state analyses were conducted as well.

2.8.1 Structural optimization and calculated IR frequencies

Starting geometries for the structural optimizations were derived from the respective crystallographic data. The optimization results were intended to reproduce the experimental values as accurately as possible. The $\{CoNO\}^8$ structures were optimized using the def2-TZVP basis set,[134] its auxiliary basis def2/J[135] and the density functional BP86. Van-der-Waals interactions were taken into account by Grimme's D3- and D4 dispersion corrections.[136–138] CPCM(∞)[139] was utilized to simulate the crystal environment, taking electrostatic interactions and hydrogen bonds into account. For integration acceleration, the RIJCOSX method was applied.[140] In the case of **4c**, ZORA[141,142] was used together with a SARC-[143] TZVPP basis set[134] for the iodido ligand to account for possible relativistic effects caused by this heavy atom.

As can be seen from Table 2.23, the values obtained with the abovementioned methods are in good agreement with the experimentally determined parameters. While the N–O distance was slightly overestimated for all species, marginally shorter Co–N bonds were calculated for every complex except **5b**. Concerning these parameters, the linear class **5** nitrosyls show the smallest deviation from the measured values. In contrast, the results for the Co–N–O angle vary to a greater extent, being either slightly more acute or obtuse than in the crystal structures. Nevertheless, most bond angles were reproduced within a range of ±2°. The highest deviation was found for complex **5c** with a bond angle 7.7° greater than in the experiment. Among the different classes, reproduction of the bent fpin and bis(diamine) nitrosyls **1+4** was the most accurate. Regarding the nitrosyl stretch, the measured values were sufficiently reproduced as well, most accurately for the species of classes **5+6**. With the exception of a few dihalogenido nitrosyls (**6**), the energy of the stretching vibration was underestimated for most compounds. In the case of complexes **2b** and **4l**, the calculations yielded two stretches for each species due to symmetric and antisymmetric coupling of this vibration with the H–N–H deformation of the coligand's amino group. Two wavenumbers were also obtained for **7a** due to coupling with vibrations of the phenanthroline ligands.

Table 2.23: Differences between the experimental X-ray / IR data and calculated values of the singlet BP86 / def2-TZVP-optimized {CoNO}^{8} structures, given as $\Delta = x_{calc.} - x_{obs.}$. Computations were done with D3 / D4 dispersion- and CPCM(∞) solvent corrections. For the compounds with two complex entities in the asymmetric unit, $x_{obs.}$ is defined as the mean of the two molecules. For disordered structures, the computed values were compared to the respective major form. In the case of species with an experimentally observed split nitrosyl stretch, $\Delta\tilde{\nu}$ refers to the band with the higher relative intensity. Calculations for **4d** are based on structural data from Ref.[94].

	ΔN–O /Å	ΔCo–N /Å	ΔCo–N–O /°	$\Delta\tilde{\nu}$ / cm^{-1}		ΔN–O /Å	ΔCo–N /Å	ΔCo–N–O /°	$\Delta\tilde{\nu}$ / cm^{-1}
1 a	0.014	−0.035	−0.6	−46	**4 a**	0.027	−0.038	0.2	−42
b	0.019	−0.042	−0.5	−48	**b**	0.046	−0.041	−3.2	−67
c	0.022	−0.036	−2.0	−58	**c**[b]	0.042	−0.061	0.5	−49
d	0.017	−0.044	1.5	−69	**d**	0.022	−0.042	0.3	−45
e	0.016	−0.047	−0.2	−46	**e**	0.043	−0.052	0.9	−35
f	0.027	−0.046	0.6	−43	**f**	0.034	−0.035	0.0	−45
g	0.015	−0.040	−0.6	−71	**g**	0.051	−0.043	−1.5	−44
h	0.031	−0.038	1.2	−48	**h**	0.020	−0.030	−0.7	−18
i	0.014	−0.043	0.7	−62	**i**	0.029	−0.039	−0.7	−27
j	0.018	−0.060	5.6	−40	**l**[a]	0.026	−0.042	−0.1	−79, −62
k	0.020	−0.046	0.3	−67					
l	0.010	−0.037	−1.4	−51					
m	0.009	−0.028	0.7	−43	**5 a**	0.008	−0.001	5.6	−27
n	0.019	−0.045	0.8	−54	**b**	0.010	0.015	0.0	−5
					c	0.010	−0.005	7.7	−19
2 a	0.014	−0.040	2.3	−51	**d**	0.011	−0.016	4.0	−34
b[a]	0.055	−0.043	−1.8	−77, −62					
					6 a	0.004	−0.031	3.0	−1
					a'	0.021	−0.029	2.7	21
3 a	0.016	−0.040	2.3	−17	**b**	0.018	−0.037	2.9	25
b	0.035	−0.040	1.2	−45	**c**	0.014	−0.039	2.5	−20
c	0.025	−0.042	1.0	−52	**c'**	0.007	−0.031	1.9	−4
d	0.031	−0.045	3.7	−26	**d**	0.014	−0.040	2.7	13
					d'	0.001	−0.031	1.8	13
					7 a[c]	0.032	−0.055	0.6	−53, −39

[a] N–O stretch symm. and antisymm. coupled to the H–N–H deformation of the co-ligand's amino function.

[b] Relativistic approach with ZORA-def2-TZVP basis set for all non-iodine atoms. For the *trans* iodide, SARC-ZORA-TZVPP was used. Co–I bond lengths: experimental: 3.048 Å, calculated: 3.036 Å.

[c] Coupling of the N–O stretch with vibrations of the phenanthroline ligands.

2.8.2 Charge analysis and calculation of oxidation states

For the newly synthesized $\{CoNO\}^8$ compounds, the charge of the nitrosyl ligand was calculated using the quantum theory of atoms in molecules (QTAIM).[144] For compound **5d**, also an alternative partitioning approach involving topological fuzzy Voronoi cells (TFVC)[145] was tested. The computations were based on the def2-TZVP-optimized structures, again using BP86 as the density functional. As a result, the nitrosyl charge was determined to be around −0.30 *e* for all species (see Table 2.24). Within class **1**, a slightly less negative charge was found for the complexes with a coordinating *N*-heterocyclic system. Minimally lower charges were also observed for the perchlorate and tetrafluoroborate derivatives of class **4** and the related *cis* complex **7a**, as well as for the linear species (**5**).

Oxidation states of the cobalt center and the nitrosyl ligand in the optimized structures were calculated using Salvador's effective oxidation-state (EOS) analysis.[146] The method uses effective fragment orbitals (EFOs),[147] extracted from the respective wave functions, and the EFO's occupation numbers. Both are obtained independently for each atom / ligand and each spin case. These spin-resolved EFOs are then sorted by their occupation number in descending order. Integer electrons are assigned to the orbitals until the total number of electrons is reached. This is done separately for alpha and beta electrons. The result is an effective electron configuration for each entity. The EOS of each atom or ligand is then calculated by subtracting the total number of assigned electrons of both spin cases from its atomic number. The frontier EFOs can be used to assess how closely the obtained electron distribution is related to the actual distribution in the investigated system. Using the occupation numbers of the last occupied (λ^{σ}_{LO}) and the first unoccupied EFO (λ^{σ}_{FU}), a reliability index *R* can be calculated for each spin case:

$$R_{\sigma}(\%) = 100 \times \min[1, \max(0, \lambda^{\sigma}_{LO} - \lambda^{\sigma}_{FU} + ½)] \qquad (2.1)$$

The overall-reliability index can then be defined as the minimum value obtained for either the alpha or beta electrons: $R = \min(R_{\alpha}, R_{\beta})$ (2.2). Since integer electrons are used to calculate the EOS, the assignment is considered indisputable if the occupation of the frontier EFOs differs by more than half an electron. The larger this difference, the better the electronic distribution can be represented as a discrete ionic model.[148]

As can be seen from Table 2.24, almost all $\{CoNO\}^8$ species were assigned as Co^{I}–NO^{+} pairs, with the exceptions of **5d** and **6a'**, for which EOS analysis resulted in Co^{-I}–NO^{+} and Co^{0}–NO^{+}, respectively. It is striking that, with the exception of the latter compound, the assignment for the class **6** nitrosyls has significantly lower reliability indices, well below 60%. Particularly low *R* values near the 50.0%-threshold were observed for the linear complexes (class **5**), with the exception of **5d**. Within the group of the perfluoropinacolato species (**1–3**), a trend toward lower reliability indices is noticeable for the phosphorus-containing nitrosyls of classes **2+3**. In class **1**, the compounds with an *N*-heterocyclic co-

ligand reached slightly higher *R* values compared to those bearing ethylenediamine derivatives. Comparatively high assignment indices were observed for class **4** species with coordinating *trans* perchlorate or tetrafluoroborate, while the other members of this product group remained below 60 %.

Table 2.24: Assignment of effective oxidation states (EOS) for Co and NO moieties in the singlet BP86 / def2-TZVP-optimized $\{CoNO\}^8$ structures, computed with D3 / D4 dispersion- and CPCM(∞) solvent corrections. For each assignment, the reliability index *R* (see Equations 2.1+2.2) and QTAIM charge of the nitrosyl ligand are listed. Calculations for compound **4d** are based on structural data from Ref.[94].

	EOS_{Co}	EOS_{NO}	*R* / %	Q_{NO}/e		EOS_{Co}	EOS_{NO}	*R* / %	Q_{NO}/e
1 a	+1	+1	65.6	−0.32	**4 a**	+1	+1	60.5	−0.29
b	+1	+1	65.5	−0.32	**b**	+1	+1	53.0	−0.38
c	+1	+1	65.9	−0.32	**c**[a]	+1	+1	58.5	−0.33
d	+1	+1	67.1	−0.34	**d**	+1	+1	59.3	−0.31
e	+1	+1	68.1	−0.32	**e**	+1	+1	62.5	−0.28
f	+1	+1	67.7	−0.32	**f**	+1	+1	56.3	−0.34
g	+1	+1	67.2	−0.30	**g**	+1	+1	60.6	−0.30
h	+1	+1	67.8	−0.28	**h**	+1	+1	61.7	−0.27
i	+1	+1	70.0	−0.22	**i**	+1	+1	64.0	−0.27
j	+1	+1	72.7	−0.21	**l**	+1	+1	56.5	−0.35
k	+1	+1	69.9	−0.26					
l	+1	+1	67.5	−0.25	**5 a**	+1	+1	50.3	−0.30
m	+1	+1	69.6	−0.20	**b**	+1	+1	51.9	−0.25
n	+1	+1	68.1	−0.29	**c**	+1	+1	50.8	−0.28
					d[b]	−1	+1	62.8	−0.26
2 a	+1	+1	64.5	−0.33					
b	+1	+1	63.6	−0.36	**6 a**	+1	+1	53.1	−0.28
					a'	0	+1	64.7	−0.28
3 a	+1	+1	59.0	−0.31	**b**	+1	+1	53.2	−0.32
b	+1	+1	64.2	−0.31	**c**	+1	+1	51.9	−0.29
c	+1	+1	66.9	−0.32	**c'**	+1	+1	50.9	−0.29
d	+1	+1	53.3	−0.34	**d**	+1	+1	51.9	−0.31
					d'	+1	+1	51.1	−0.30
					7 a	+1	+1	54.2	−0.28

[a] Relativistic approach with ZORA-def2-TZVP basis set for all non-iodine atoms. For the *trans* iodide, SARC-ZORA-TZVPP was used. Co–I bond lengths: experimental: 3.048 Å, calculated: 3.043 Å.

[b] Results for alternative TFVC approach: EOS_{Co} = −1, EOS_{NO} = +1, *R* = 62.6 %, Q_{NO} = −0.28 *e*.

3 Discussion

3.1 Perfluoropinacolatocobalt nitrosyls

In the course of this work, twenty new $\{CoNO\}^8$ compounds with perfluoropinacolate and either one bidentate or two monodentate co-ligands were synthesized and characterized by X-ray crystallography and infrared spectroscopy. All of the pentacoordinated, uncharged mononitrosyl complexes of classes **1–3** possess a bent CoNO moiety with structural parameters matching Riggenmann's related cobalt nitrosyls with perfluoropinacolate and *N*,*N*'-ligands.[94,95] It was now possible to show that the synthetic one-pot concept of directly reacting gaseous nitric oxide with stoichiometric amounts of a non-coordinating cobalt(II) salt, perfluoropinacol and a sterically hindered base for its deprotonation can be applied to a wider range of co-ligands from ethylenediamine-like building blocks to *P*,*N*-ligands and common mono- and diphosphanes.

Although all newly synthesized products of classes **1–3** show a high degree of similarity, some differences in specific properties were identified. This concerns, for example, the stability of the complexes in solution. Some of the compounds lose the nitrosyl ligand upon purging with argon, which is expressed by a decoloration visible to the naked eye and was also monitored by in-situ infrared spectroscopy. The species with aromatic, *N*-heterocyclic co-ligands (**1i–n**) are particularly unstable in solution and could only be crystallized under an atmosphere of nitric oxide because they readily decompose when left under argon. Since this reaction can be reversed when NO is applied again, the formation of the perfluoropinacolatonitrosyls can be formulated by the equation given in Scheme 3.1.

$$Co(OTf)_2 + (NBnMe_3)_2(fpin) + L/2L + NO \rightleftharpoons [Co(fpin)(L/L_2)(NO)] + 2(NBnMe_3)(OTf)$$

Scheme 3.1: Equilibrium of formation and decomposition of unstable class **1** perfluoropinacolatocobalt nitrosyls in solution with L = aromatic *N*-heterocyclic co-ligand.

Also, when compared to the solution-stable diamine species of class **1**, the structures of the aromatic heterocycle-bearing complexes tend to show slightly shorter N–O bonds, slightly longer Co–N bonds and nitrosyl stretches at higher wavenumbers. This effect appears to be weaker if only one of the two coordinating nitrogen atoms is part of an aromatic system, as in the 2-aepy product (**1g**). Substitution of a nitrogen atom with an electron-donating group, as in **1h** with the *N*-methylated ligand, seems to have the opposite effect and, thus, stabilizes the species in solution. On the other hand, not all non-aromatic class **1** nitrosyls remain completely stable in their mother liquor. For the compounds **1c–f**, purging with argon results in partial decomposition, recognizable by a slowly proceeding, slight brightening of the solution. Since the co-ligands in **1d–f** are rather bulky – and so is fpin – the stability of the nitrosyl species in solution could also be related to the steric demand of the ligands to some extent.

As for **1c**, the slight instability can be explained by the presence of the electron-withdrawing oxygen atom in the morpholinyl group, especially when compared to **1b**, the solution-stable analog in which the six-membered ring is not substituted at that position. However, it should be noted that no ideal correlation between the complex stability in solution and the parameters of the CoNO moiety can be drawn since the position of the equlibrium is also determined by the stability of the respective educt species.

While the fpin nitrosyls bearing *P*,*N*-ligands (**2**) and phosphanes (**3**) remain stable in solution and show structural bonding parameters similar to the stable analogs of class **1**, they differ from the diamine and heterocycle species by a wider Co–N–O angle. For class **2**, it is about 8° more obtuse and for compound class **3** about 10°. However, the more upright position of the nitrosyl ligand should not be correlated with the substitution of the coordinating phosphorus atoms with sterically demanding phenyl and isopropyl groups. Calculations by Klüfers on the supposedly less bulkier $[Co(dmpe)_2(NO)]^{2+}$ resulted in the same linear *TBPY*-5 geometry as the related class **5** nitrosyls (see Section 3.3 for details).

The newly obtained dinitrosyl $(ppzH_2)_{0.5}[Co(fpin)(NO)_2]$ (**7b**) represents an exception to the straightforward synthesis of the class **1** mononitrosyls. This complex was previously reported by Neumann with $NBnMe_3^+$ as counterion, the latter originating from the corresponding methoxide, which was used in excess in the synthesis.[124] It is likely that in both cases the dinitrosyl was formed by reductive nitrosylation (see Scheme 3.2). In this type of reaction, nitric oxide reduces the metal center to Co(I) and the resulting NO^+ reacts with the solvent (in this case methanol) to form methyl nitrite. The process is accelerated in the presence of a base, which binds the protons that are released upon MeONO formation.[149–151] In the case of **7b**, the non-coordinating piperazine would undertake this task. The synthesis of $\{Co(NO)_2\}^{10}$ compounds in the presence of gaseous NO and an amine base has been reported for several dinitrosyls such as $[Co(NO)_2(tmen)]^+$ and $[Co(NO)_2(p\text{-toluidine})_2]^+$, using either an excess of the basic amine ligand or another amine base such as triethylamine.[149,152] The same route can also be applied to phosphanes to form complexes such as $[Co(NO)_2(PPh_3)_2]^+$ and $[Co(dppe)(NO)_2]^+$.[152,153] The formation of methyl nitrite via NO^+ is also known for playing a role in the synthesis of dinitrosyl iron complexes (DNICs)[151] and is not limited to methanol as a solvent, since it is also observed in acetonitrile.[154,155] As for the fpin dinitrosyl complex with cobalt, Riggenmann detected the formation of MeONO after nitric oxide exposure by monitoring a 1:1:2 solution of cobalt(II) nitrate, perfluoropinacol and $(NBnMe_3)(OMe)$ via in-situ IR- and UV/Vis spectroscopy. He found that a $\{CoNO\}^8$ species is formed first, indicated by an absorption band at 1643 cm^{-1}. In the further course of the reaction, this band vanished completely and new absorption bands at 1740 cm^{-1} and 1820 cm^{-1}, characteristic for $\{Co(NO)_2\}^{10}$ complexes, arose. The isosbestic points observed in the corresponding UV/Vis spectrum confirm that consecutive reactions are taking place.[95] Hence, it can be concluded that if a ligand of significant basicity (such as diamines and aromatic *N*-heterocycles) does not coordinate in the above-

mentioned system or the initially formed mononitrosyl complex does not crystallize in a reasonable amount of time, a consecutive reaction to a dinitrosyl species will occur.

$$Co^{II} + NO \longrightarrow Co^{I} + NO^{+}$$

$$NO^{+} + MeOH \longrightarrow MeONO + H^{+}$$

$$Co^{II} + NO + MeOH \longrightarrow Co^{I} + MeONO + H^{+}$$

$$Co(OTf)_2 + (NBnMe_3)_2(fpin) + 0.5\,ppz + 3\,NO + MeOH \longrightarrow \mathbf{7b} + 2\,(NBnMe_3)(OTf) + MeONO$$

Scheme 3.2: Top: Reductive nitrosylation of cobalt(II) with methanol. **Bottom:** Proposed reaction for the formation of $(ppzH_2)_{0.5}[Co(fpin)(NO)_2]$ (**7b**) via reductive nitrosylation.

3.2 Hexacoordinated cobalt nitrosyls with *trans*- and *cis* co-ligands

Ten novel hexacoordinated $\{CoNO\}^8$ compounds were synthesized and characterized by X-ray diffraction and IR spectroscopy. For another three already known compounds, more convenient syntheses, respectively crystallization methods, were developed in order to obtain this products reproducibly in a single-crystalline form. Of these thirteen nitrosyls in total, all but one are bis(diamine) complexes bearing an anionic or uncharged co-ligand at the position *trans* to NO. Consisting of two equatorial ethylenediamine ligands (or mono- and dimethylated derivatives thereof), a nitrosyl ligand in the apical position and a *trans* ligand (which is either chloride, iodide, nitrate, perchlorate, tetrafluoroborate or dimethyl sulfoxide), they show a high degree of similarity regarding the CoNO moiety and the nitrosyl stretching band. Nitric oxide is bound to cobalt at angles between 121.3° and 124.3° with a Co–N distance ranging from 1.806 Å to 1.832 Å and the N–O bond ranging from 1.138 Å to 1.173 Å. The infrared band for the nitrosyl stretch is between 1629 cm^{-1} and 1659 cm^{-1}. In this respect, the products of class **4** are thus very similar to the previously described perfluoropinacolato nitrosyls.

When comparing the hexacoordinated compounds with each other, it can further be seen that the distance from the *trans* ligand to cobalt is similar for all *O*- and *F*-binding co-ligands with about 2.3 Å for the anionic ligands and about 2.2 Å for the DMSO derivative. This is in accordance with Riggenmann's *trans*-$[Co(H_2O)(men)_2(NO)]^{2+}$, which shows a distance of the aqua ligand of about 2.3 Å.[94,95] Only for the chlorido and iodido complexes (**4b+c**), longer distances of about 2.6 Å and 3.0 Å are found, respectively. The original procedure for these compounds was developed by Feltham *et al*. and is based on a one-pot synthesis of the precursor *trans*-$[Co(ClO_4)(en)_2(NO)]ClO_4$.[85] Although they were of good quality, half of the structures of this product class exhibit a reproducible disorder of the nitrosyl

ligand, affecting almost exclusively complexes that bear unsubstituted ethylenediamine. Then again, it cannot be concluded that substitution of the diamine necessarily prevents said disorder since two of the ethylenediamine complexes are well ordered (namely the chlorido and nitrato derivatives **4b+d**), while the benzyl-substituted product (**4l**) features a disordered nitrosyl ligand. Concerning the coordination geometry of the CoN_5 fragment, the class **4** complexes resemble a vacant octahedron rather than the square pyramidal shape found for the perfluoropinacolato nitrosyls. Within the bis(diamine) nitrosyl class, it is noticeable that the halogenido and DMSO derivatives (**4b**, **c**, **f**) show the lowest degree of distortion while for the nitrato, tetrafluoroborato and perchlorato entities, a shift toward the square pyramidal geometry is observed. All of the latter, as well as one tetrafluoroborate (**4e**) and the bnen product (**4l**), deviate from the pyramidalization path, thus indicating the involvement of additional types of distortion. For the two *N*,*N*'-dmen compounds **4j+k**, it was not possible to obtain single crystals suitable for X-ray diffraction. Riggenmann made the same observations for his class **1** nitrosyl [Co(*N*,*N*'-dmen)(fpin)(NO)], which he could only synthesize as bulk.[95] He assumed that the symmetric methylation of the diamine would lead to more possible orientations of said groups and thus to a variety of possible overall conformations of the complex, preventing it from crystallizing. Bearing two of these co-ligands, an even higher degree of distortion can be expected for the class **4** products.

Finally, the question arises as to how the bonding of the *trans* co-ligand can be assessed. Klüfers and Schröder[94] reproduced the *trans* distances for the well-ordered nitrosyls **4b+d** via BP86/def2-TZVP structure optimization and used QTAIM analyses in order to compare them with the corresponding $[Co(NH_3)_5(Cl/NO_3)]^{2+}$ species, Co(III) entities in which chloride or nitrate acts as a normal, datively bonded ligand. They found that for both compounds, the electron density at the Co–L_{trans} bond critical point (BCP) was about half of the value that was obtained for the corresponding ammine species (**4b**: 0.034 e a_0^{-3} vs. 0.070 e a_0^{-3} and **4d**: 0.037 e a_0^{-3} vs. 0.084 e a_0^{-3}). For a bond with a purely ionic character, this value would approximate to zero. Furthermore, the charge of the *trans* nitrato ligand in **4d** is closer to −1 than in the ammine complex (−0.88 *e* vs. −0.73 *e*) and the total energy density at the BCP (H_b) for the Co–O bond is closer to zero (−0.003 $E_h a_0^{-3}$ vs. −0.015 $E_h a_0^{-3}$). With H_b being less than 0, the Cremer–Kraka criterion for an electrostatic interaction is fulfilled (the opposite case would mark a covalent bond).[156] Thus, evidence has been provided that the bond of the *trans* co-ligand to the cobalt center in the class **4** nitrosyls is best described as a weak electrostatic interaction.

The compound *rac*-*cis*-$[Co(NO)(NO_2\text{-}\kappa N)(phen)_2]ClO_4$ (**7a**) stands out from the group of hexacoordinated cobalt nitrosyls presented in this work. Regarding the question as to why the nitrito ligand does not bind *trans* to NO, the sterical demand of the phenanthroline ligands seems to be the most obvious reason. However, examples of complexes with two phenanthroline or bipyridine ligands and derivatives thereof occupying all four equatorial coordination sites have been reported, but only with palladium and platinum.[157–160] In these square planar compounds, the ligand's aromatic groups are either

twisted against each other or bent out of the equatorial plane so that the opposing hydrogen atoms in *ortho* position avoid contact while maintaining the planarity of the CoN_4 moiety (so-called bow-incline distortion).[161] The assumption that the *cis* configuration in **7a** is caused by the heterocycle's sterical demands is supported by the crystal structure of *rac-cis*-$[Co(bpy)_2Cl(NO)]ClO_4$, which was also recorded during the course of this thesis. Synthesized by Vlček's procedure [119] and crystallized in the same manner as **7a**, the structure unfortunately exhibits a reproducible disorder at the nitrosyl ligand (atom N1, see Figure 7.61) that could not be solved sufficiently, although all other thermal ellipsoids appear to be neat. Again, the anionic co-ligand – with chloride being more compact than nitrite – binds *cis* to nitric oxide. It can therefore be concluded that the coordination of the monodentate co-ligand relative to NO is determined by the sterics of the heterocycle rather than the anionic ligand itself. As previously observed for the aromatic *N*-heterocyclic class **1** products, both the phenanthroline and the bipyridine *cis* complex rapidly lose nitric oxide when purged with argon in solution.

For the compound *trans*-$[Co(ClO_4)(en)_2(NO)]ClO_4$ (**4a**), a remarkable reactivity toward a novel hyponitrito complex was discovered. Reaction of the cobalt nitrosyl with sodium nitrite in aqueous solution yielded *rac*-$[Co(en)_2(cis\text{-}N_2O_2\text{-}\kappa^2O,O')]ClO_4$ (**7c**). The recorded crystal structure represents the first reported specimen of a mononuclear cobalt complex bearing a chelating *cis*-hyponitrite. Although fewer than thirty structures of transition metal complexes with hyponitrite are known to date, it was already shown that this ligand can exist in a wide variety of binding modes, including chelating modes (known for the *cis* and the *trans* form) as well as bridging arrangements, where the ion can coordinate up to four metal centers.[162, 163] Since no general synthetic approaches to hyponitrito complexes exist and most of the known compounds were serendipitous discoveries, there is only limited understanding on the formation of these complexes.[162] The product **7c** is no exception to this. While it was not possible to extend the procedure to other diamines (and therefore, no general route could be developed), attempts to determine the colorless microcrystalline by-product that occurred upon crystallization were unsuccessful as well. Made with the original intention of replacing the co-ordinating perchlorate in **4a**, the hyponitrito complex was generated by accident, but could be crystallized reproducibly. While solving the crystal structure (Figure 2.64), it became clear that the hyponitrito ligand should be considered fully deprotonated, since on the one hand, no significant residual electron density was observed on any of the ligand's two oxygen atoms. Secondly, the very low electron densities that were indeed found at one oxygen atom (O2) pointed toward the hydrogen atom of an amino group. Thus, the assignment of these residual densities would not fit into the crystal's network of hydrogen bonds. Also, the distances of the two densities (0.24 e $Å^{-3}$ and 0.26 e $Å^{-3}$) from atom O2 were measured at 1.245 Å and 0.647 Å, respectively. In both cases, this is too far off to be considered an O–H bond. In structures of hydrogenhyponitrito complexes, the bond length for this entity is usually around 0.95 Å.[163] Instead, the residual density at 1.245 Å is likely to be an artifact and the closer one can be assigned to an electron pair of the oxygen atom.[164] Hence, when a fully deprotonated hyponitrito ligand is assumed, the oxidation state of the cobalt metal center would have changed during

the course of the reaction from Co(I) in **4a** to Co(III) in **7c**, with NO^+ being reduced to $\frac{1}{2}N_2O_2^{2-}$. Regarding its formation, several mechanisms are conceivable. One explanation involves the coupling of two nitrosyl complexes (see Scheme 3.3). Such a reaction mechanism was already postulated for the compound $[(NH_3)_5Co(cis\text{-}\mu\text{-}N_2O_2\text{-}\kappa^2O,N)\text{-}Co(NH_3)_5]^{4+}$, which is described as the red, dimeric form of the black nitrosyl species $[Co(NH_3)_5(NO)]^{2+}$.[162,165,166] The coupling of two (formally) NO^- entities is also believed for the formation of $[Ni(bpy)(cis\text{-}N_2O_2\text{-}\kappa^2O,O')]$ from $[Ni(bpy)_2(NO)]PF_6$. In this case, the hyponitrite and the by-product $[Ni(bpy)_3](PF_6)_2$ are yielded from an acetonitrilic solution of the nitrosyl upon standing at room temperature.[130,167] The formation of another species besides **7c** is conceivable as well, possibly a hexacoordinated cobalt(III) complex such as $[Co(ClO_4)_2(en)_2]^+$ or a species with aqua ligands replacing one or both perchlorate ions. However, unlike the nickel compound, nitrosyl **4a** has proven to be stable in solution and transforms to **7c** only after the addition of nitrite and treatment with DMSO. No other compound was observed when crystallizing an aqueous solution of pure **4a**. This brings up a more plausible mechanism in which a nitrite ion couples to the nitrosyl ligand in the first step (Scheme 3.3). DMSO diffused into the complex solution can then abstract one oxygen atom from the intermediate species, yielding the hyponitrito ligand and dimethyl sulfone as a by-product. With regard to the question of why no derivatives of **7c** with alkylated diamines were obtained by the same procedure, hydrogen bonding seems to play a crucial role in the stabilization of the complex, presumably not only in terms of crystallization, but also for the formation of the product in solution. Since half of the amino groups are involved in classical interactions with all four atoms of the hyponitrito ligand and the other two groups are binding to the counterion, any substitution of an NH_2 group would apparently greatly reduce the ability to form a stable network of hydrogen bonds.

$$2[Co^{I}(ClO_4)(en)_2(NO^+)]ClO_4 \longrightarrow rac\text{-}[Co^{III}(en)_2(cis\text{-}N_2O_2^{2-})]ClO_4 + [Co^{III}(ClO_4)_2(en)_2]ClO_4$$

$$[Co^{I}(ClO_4)(en)_2(NO^+)]ClO_4 + NaNO_2 + DMSO \longrightarrow rac\text{-}[Co^{III}(en)_2(cis\text{-}N_2O_2^{2-})]ClO_4 + NaClO_4 + DMSO_2$$

Scheme 3.3: Proposed reactions for the formation of *rac*-$[Co(en)_2(cis\text{-}N_2O_2\text{-}\kappa^2O,O')]ClO_4$ (**7c**) from the precursor compound *trans*-$[Co(ClO_4)(en)_2(NO)]ClO_4$ (**4a**). For the sake of clarity, the postulated oxidation states of the metal center and the charges of the nitrosyl and hyponitrito ligands are depicted. **Top:** Coupling of two mononitrosyls. **Bottom:** Reaction with sodium nitrite and dimethyl sulfoxide.

3.3 Bis(diphosphane)cobalt nitrosyls, charge analysis and oxidation-state assignment of {CoNO}^{8} complexes

Four new trigonal bipyramidal, dicationic {CoNO}^{8} nitrosyls were obtained, which, in contrast to all other products presented in this work, feature a linear CoNO moiety. Only one crystal structure of a similarly shaped cobalt compound is known to literature, namely $[Co(diars)_2(NO)](ClO_4)_2$, synthesized by Enemark and Feltham with 1,2-bis(dimethylarsino)benzene (diars, also called 'das' in the literature) as co-ligand.[82, 85, 168] For this complex, bond lengths of 1.68 Å for the Co–N distance and 1.16 Å for the N–O bond were published, both being slightly longer (about 0.015 Å) than in the class **5** diphosphane analogs. As Co–N–O bond angle, a value of 178° was reported, matching the newly obtained compounds (see Table 2.18). The nitrosyl stretch at 1852 cm^{-1} is in compliance as well.[82, 168]

The blueshift of this absorption band in the linear complexes by more than 100 cm^{-1} marks the second striking difference from the bent products. According to a common consensus within the coordination chemistry community that remains widespread to this day, a linearly bonded nitrosyl ligand is always assigned a positive charge. Conversely, a bent NO ligand is assumed to have a negative charge which occupies an antibonding π^* orbital, thus weakening the N–O bond and decreasing the force constant and therefore redshifting the corresponding infrared stretch.[101–104] However, the QTAIM charge analysis and calculation of EOS values presented in this work (Table 2.24) result in a Co^{I}–NO^{+} pair for almost every synthesized {CoNO}^{8} nitrosyl, regardless of the Co–N–O angle and the overall charge of the complex entity. Concerning the reliabilty index *R* for the EOS assignment, large values are found for most of the bent species, while for the class **5** compounds, values just above 50 % were calculated, making the assignment for the linear complexes appear more doubtful at first glance. However, the reason for this lies in the strong σ-donating capabilites of the diphosphane ligands, putting a non-negligible charge on a d(x^2-y^2) EFO of the cobalt atom and depopulating the σ bonds at the phosphorus atoms.[94] The nitrosyl ligand's QTAIM charge appears to be almost a constant with a mean value of around −0.30 *e*. At first glance, this seems to contradict the EOS results, which postulate an NO^{+} ligand for every product. Nevertheless, this can be clarified: Using product **1a** as an example, QTAIM charges of +1.10 *e* for the cobalt center and −0.32 *e* for the nitrosyl ligand were calculated. In the context of the two-bond scenario implied with this method, this means a charge flow of less than one electron from Co^{I} (the donor) to NO^{+} (the acceptor) via the σ bond and a flow of less than one electron via the π backbond in the same direction. Hence, a flow of about 1.3 electrons in total, which is enough to induce an overall charge −0.32 *e* of for the nitrosyl ligand, but not enough in terms of EOS analysis to assign an NO^{-}, since at least one full electron in one of the two bonds is required to shift the entire electron pair of said bond to the ligand. For the chosen example of **1a**, occupation numbers of 0.434 for the σ EFO and 0.246 for the π EFO were calculated.[94] In conclusion, the negative (QTAIM) charge of a formally (according to EOS) NO^{+} ligand depicts the situation that two metal-centered bonds put a negative charge on the nitrosyl ligand but do not transfer more than one electron into either bond,

and thus not meet the requirement for an oxidation-state change. Hence, the bonding situation results from the partial occupation of the N–O π^* orbitals. Even in rare cases such as **2a**, for which an occupation value of 0.518 for the σ EFO was computed, the EOS calculation results in a Co^{I}–NO^{+} pair since, on the cobalt center, the occupation numbers of the complementary d-type frontier EFOs are slightly higher with values of 0.548 and 0.537.[94] Furthermore, it should be noted that in the case of class **5** nitrosyls, the two EFOs considered for the EOS assignment correlate to two nonequivalent π bonds with the cobalt center. Reliability indices close to 50% indicating a higher Co–NO covalency were also observed for the class **6** products, which constitutes a striking difference from their fpin analogs of class **3**. A possible explanation for this could be that the halogenido ligands are able to provide slightly more electron density to the cobalt center compared to the alkoxido functions of perfluoropinacolate with its electron-withdrawing CF_3 groups. In the case of **6a'**, the combination of one strongly σ-donating dppe and two bromido ligands (the latter can be regarded as soft Lewis base according to HSAB theory) seems to provide enough electron density at the metal to result in a homolytical cleavage of the Co–P bond, upon which one electron falls to cobalt, generating a Co^{0}–NO^{+} assignment and a positively charged diphosphane. The same applies for **5d**, where one electron of each of the two diphosphanes falls to the metal, thus reducing it even further and assigning Co^{-I}–NO^{+}. An alternative TFVC approach to this compound yielded similar results. Hence, the EOS algorithm postulates perfect covalency for these borderline cases. This, however, does not invalidate the results for the other species of this thesis, since the oxidation state in general is defined as a winner-take-all principle. This means that one full electron is shifted to the metal as soon as the threshold of R = 0.5 is undercut. Furthermore, one should keep in mind that this value was set arbitrarily. In summary, the consensus that a linearly bonded nitrosyl ligand should generally be addressed as NO^{+} and a bent ligand as NO^{-} should be dismissed as obsolete. Apart from these results, Enemark and Feltham had already warned about this in their 1974 review on nitrosyls.[38] Moreover, a recent publication on Riggenmann's $[Co(fpin)_2(NO)]^{2-}$ complex (Co–N–O angle of 120.6°) showed that the bent compound is, in fact, a Co^{I}–NO^{+} species by using the same methodology as in this work, therefore providing the first evidence for the inaccuracy of this still widely accepted claim.[99] As it was demonstrated by Klüfers and Schröder, in electron-rich $\{MNO\}^n$ complexes with $n \geq 7$, the M–N–O angle can be viewed as a measure of Pauli repulsion occurring between the 3σ electron pair of the nitrosyl ligand and the metal's occupied orbitals.[94]

While it has now been proven that neither the Co–N–O angle nor the related infrared nitrosyl stretch can be used to determine the charge of the NO ligand, the question remains as to why the transition from a linear to a bent moiety causes a redshift of said IR stretching vibration. As recently shown by Klüfers *et al.*, the previously mentioned consensus is based on conclusions derived from the Dewar–Chatt–Duncanson (DCD) model which cannot be extrapolated to nitrosyl complexes.[169] The DCD model is a concept used to assess the synergetic bonding of a donor/acceptor ligand to a metal center.[170,171] One typical application for the model are carbonyl complexes.[172,173] In this context, it can be used to explain, for example, the redshift of the C–O stretch in the series $[Fe(CO)_6]^{2+}$, $[Fe(CO)_5]$,

$[Fe(CO)_4]^{2-}$ by arguing that the increasing capability of the metal center to form Fe–CO backbonds goes along with an increasing occupation of the two antibonding C–O π^* orbitals. In return, this decreases said bond's order, therefore elongating the C–O distance and shifting the respective infrared stretching vibration to lower wavenumbers. Hence, in this case, the DCD concept correlates the shift from an electron-poor d^6-iron(II) to an electron-rich d^{10}-iron(−II) species with the redshift of the carbonyl stretch. Because negative charge is drained from the carbonyl ligands through the CO–Fe donor bonds, the increasing backbonding in the series is accompanied by an increasing charge on the carbonyl moiety. However, contrary to these findings, the negative charge of the nitrosyl ligand (as determined by QTAIM) in the $\{CoNO\}^8$ species presented in this thesis is not correlated with the redshifting of the N–O stretch in the same way. As previously mentioned, it is almost constant instead. Further computations [169] based on structures of **4h** and **5a'** showed that even when straightening a class **4** nitrosyl or bending a class **5** compound, neither the nitrosyl charge nor the ligand's antibond occupation change significantly compared to the respective ground-state structures, making the linear-to-bent transition a non-DCD event for these NO complexes. By including product **6a** in the calculations, it was furthermore shown that the redshift of the nitrosyl stretch (expressed as the local force constant [174] of the N–O vibration, decoupled from that of the Co–N bond) is correlated to a shift from a trigonal bipyramidal geometry to a square pyramidal shape. This means that for **5a'**, a redshift for the computed bent species (*SPY*-5) compared to the ground-state structure (*TBPY*-5) is noticed while for **4h** and **6a** (both *SPY*-5 ground state concerning the CoN_5 / $CoCl_2N_3$ moiety), a blueshift for the calculated linear structures (*TBPY*-5) is observed. In addition, the computed *TBPY*-5 structures have a slightly shorter N–O bond compared to their related *SPY*-5 ground-state counterparts and vice versa, which is consistent with the crystallographic results. An explanation for these findings can be given if the interaction of a lateral positive unit charge Q^+ with the nitrosyl ligand is taken into account. Angle scans for the Q···N–O moiety showed that the relative energy of the calculated nitrosyl stretching vibration (computed on the BP86/def2-TZVP level) becomes minimal around 120°, a value similar to the Co–N–O bond angles that are found in the crystal structures of the bent $\{CoNO\}^8$ compounds. Moreover, the decrease of the Q···N–O angle from 180° to 120° resulted in a redshift of the infrared nitrosyl stretch by about 600 cm^{-1} to 700 cm^{-1}, independently of the electronic state of the ligand (scanning was done for NO, $^1NO^-$ and $^3NO^-$). Since Q^+ is replaceable by a real metal fragment in this context, [175–177] it can be concluded that the nitrosyl stretch cannot be used to assess the charge or antibond occupation of the nitrosyl ligand in $\{MNO\}^8$ complexes, because the correlation between the M–N–O angle and the N–O stretching vibration and bond length cannot be rationalized with the DCD model. In summary, the energy of this vibration is defined by the angle at which the metal *orbitals* interact with the nitrosyl ligand, rather than the just angle at which the metal's *center of charge* is oriented to it.

As the diphosphane ligands in the class **5** complexes are rather bulky, one might wonder if the linear binding of the nitrosyl moiety and the *TBPY*-5 coordination geometry are due only to the high sterical

demand of these ligands. To answer this question, a structure optimization based on **5a'** was carried out where the phenyl groups of dppe were replaced by methyl functions, resulting in the 1,2-bis(dimethylphosphino)ethane species $[Co(dmpe)_2(NO)]^{2+}$. As a result, the trigonal bipyramidal geometry was maintained, with a Co–N distance of 1.657 Å, an N–O bond length of 1.164 Å and a Co–N–O bond angle of 180.0°, all values that are similar to the experimentally determined structures.[169] Furthermore, the nitrosyl stretch was calculated to be at 1786 cm^{-1}, which matches the 1785 cm^{-1} stretch of bulk $[Co(dmpe)_2(NO)]BF_4$ reported by Del Zotto *et al*.[109] This indicates that for the $\{CoNO\}^8$ bis(diphosphane) nitrosyls, a linear *TBPY*-5 structure is obtained even with less sterically demanding co-ligands and that the ligand's sterics have no significant influence on their coordination geometry.

3.4 Dihalogenidocobalt nitrosyls, structure- and spin-state assignment of $\{CoNO\}^8$ complexes

Seven novel square pyramidal, uncharged $\{CoNO\}^8$ nitrosyl complexes, each bearing two halogenido ligands (chloride or bromide) and a diphosphane, were synthesized and analyzed during the course of this work. With two *cis*-standing anionic ligands and an uncharged bidentate chelate, the constitution of the class **6** compounds strongly resembles that of the fpin nitrosyls (**1–3**) at first glance. However, the dihalogenido products depict a Co–N bond that is slightly shorter (about 0.05 Å) and a more obtuse Co–N–O angle compared to the fpin complexes. As mentioned before, since this angle is not correlated with the energy of the nitrosyl stretch, the wider angles in class **6** nitrosyls are not reflected in a blue-shift of said vibration. Rather, they are an example for the well-known variability of the M–N–O bond angle in nitrosyl complexes. This becomes even clearer when comparing the abovementioned ground-state (GS) structures of **4h**, **5a'** and **6a** with their linear/bent counterparts: While the GS of **6a** shows a Co–N–O angle of 141° (138° in the crystal structure), which is more obtuse than in GS-**4h** (123°, crystal: 124°) and the calculated chloride adduct of **5a'** (126°, *SPY*-5+1 geometry like the full GS-**4h** entity), the computation of a *TBPY*-5 isomer of **6a** resulted in a 165° angle, being more acute than the values found for the GS of **5a'** (180°, crystal: 174°) and the *TBPY*-5 structure of **4h** (177°). The calculation for a (supposedly bent) *SPY*-5 isomer of **5a'** gave an angle of 157°, which is in the same range as the 'linear' *TBPY*-5 structure of **6a** (165°). Furthermore, very similar nitrosyl stretches were computed for both isomers (*SPY*-5–**5a'**: 1759 cm^{-1}, *TBPY*-5–**6a**: 1751 cm^{-1}).[169] This illustrates that the categorization of nitrosyl complexes into 'linear' and 'bent' cannot be applied unreservedly, but only for cases in which a clear distinction is possible, such as for class **4** and **5** compounds. Species such as the class **6** nitrosyls are unsuitable for such labels. According to EOS analysis, all isomers calculated are best described as Co^{I}–NO^{+} pairs.

Besides their structural peculiarities, the research on the new dihalogenido complexes also revealed a different reactivity of the bis(diphosphane) nitrosyls (**5**) compared to their literature-known diars relative. Attempts to synthesize a chlorido adduct of $[Co(dppe)_2(NO)]^{2+}$ by adding LiCl to an acetonic solution of **5a** resulted in the substitution of one diphosphane with two chlorido ligands instead, which was confirmed by IR- and CHN analysis of the product. Hence, another route to $[CoCl_2(dppe)(NO)]$ (**6a**) was found. In this context, compound **5a** stands in contrast to the related $[Co(diars)_2(NO)](ClO_4)_2$, which has been reported by Enemark and Feltham to react to $[Co(diars)_2(NO)(X)]X$ upon addition of halogenide (with X = chloride, bromide or iodide). For these complexes, split absorption bands were recorded for the nitrosyl stretch, with peaks in the range of 1548 cm^{-1} to 1576 cm^{-1}, indicating the formation of species that are structurally similar to the class **4** *trans*-bis(diamine) nitrosyls.[82,85] While it was not possible to obtain a crystal structure of these compounds, the characterization succeeded for *trans*-$[Co(diars)_2(NO)(SCN\text{-}\kappa N)]SCN$. For this complex, the authors reported a Co–N bond length of 1.87 Å, an N–O distance of 1.18 Å and a Co–N–O angle of 132.3°. The *trans* thiocyanate binds at a distance of 2.13 Å to the metal center, which gives the complex a *SPY*-5+1 geometry.[82] Peaks for the split nitrosyl stretch were observed at 1587 cm^{-1} and 1561 cm^{-1}. Since these absorption bands are in the infrared region where vibrations of N=O double bonds are found, they concluded that nitric oxide was coordinated as $N{=}O^-$ in this compound and in the related halogenido adducts of the linear diars nitrosyl. Enemark and Feltham called this novel reactivity 'stereochemical control of valence', meaning that the valence of the complex is controlled by its overall stereochemistry and can be switched from $Co^{I}–NO^+$ in the linear nitrosyl (*TBPY*-5 geometry) to $Co^{III}–NO^-$ (*SPY*-5+1) in the bent (pseudo)halogenido adducts via addition of a sixth ligand.[38,82,167,178–180] However, given the new results of this work, it is questionable whether a negatively charged nitrosyl ligand can be assigned for the bent species. The computed chloride adduct of **5a'** mentioned above can be viewed as a structure that resembles the bent diars nitrosyls. For this isomer (*SPY*-5+1, Co–N–O angle of 126°, QTAIM charge of −0.38 *e* for NO), an infrared stretching vibration at 1558 cm^{-1} was calculated for the nitrosyl ligand.[169] Since the nitrosyl stretches reported for the diars species are in the same range, it can be argued that the *trans*-$[Co(diars)_2(NO)(X)]^+$ complexes can be described as $Co^{I}–NO^+$ as well. Hence, the reactivity of the diars nitrosyls should rather be termed 'stereochemical control of the nitrosyl stretching vibration'.

While the class **6** nitrosyls synthesized in this work exhibit a square pyramidal structure, the literature-known monophosphane derivatives possess a trigonal bipyramidal geometry, with the halogenido and nitrosyl ligands occupying the equatorial positions. In addition, the Co–N–O angles of these species differ from those of the diphosphane complexes as well and, to some extent, also the N–O stretches. While for the well-ordered $[CoI_2(NO)(PMe_3)_2]$,[81] values of 179.6° and 1753 cm^{-1} were reported for the nitrosyl moiety, a disorder of the NO ligand was discovered for the structures of $[Co(NO)(PMePh_2)_2(X)_2]$ (for X = Cl: 173.2° and 156.9°, 1655 cm^{-1} and 1771 cm^{-1}; X = Br: 171.9° and 152.9°, 1664 cm^{-1} and 1771 cm^{-1}).[83] In $[CoCl_2(NO)(PMe_3)_2]$, nitric oxide is disordered with one of the chlorido ligands, showing two N–O stretches as well (1637 cm^{-1} and 1725 cm^{-1}), but only one Co–N–O angle (129.0°)

could be determined due to said disorder.[81] Since the occurrence of two nitrosyl bands in solution and bulk is also observed for other related $[Co(NO)(PR_3)_2(X)_2]$ compounds,[81,115,117,118] the question arises as to what causes the presence of two infrared stretches. In a recent publication, the crystallographic and spectroscopic results of the previously mentioned $PMePh_2$ species were interpreted as equilibria between a linear singlet species (*TBPY*-5, $Co^{I}–NO^{+}$) and a bent triplet form (*SPY*-5, $Co^{III}–NO^{-}$), caused by ultrafast, reversible intersystem crossing.[83] The authors concluded that this spin crossover can occur at room temperature since they found that the energy change between the triplet and singlet isomers is very small, with about 0.7 kJ mol^{-1} for the chlorido nitrosyl complex and −2.1 kJ mol^{-1} for the bromido derivative. These results were derived from the solution equilibrium constants determined by infrared spectroscopy, which were in quantitative agreement with those calculated from the occupancy numbers of the disordered nitrosyl site in the crystal structures. Since the population of triplet states for $\{CoNO\}^8$ compounds is rare but has been suggested not only for the abovementioned cases, but also for some tropocoronand nitrosyls (as opposed to the usual assignment as singlets), it is worth considering such a spin state for the complexes presented in this work as well. Using the pentacoordinated tropocoronand nitrosyls as test systems for their DFT study, Ghosh *et al*. reported two thermally accessible triplet states for these compounds, depending on the starting point of the search on the hypersurface.[181] This could be confirmed for $[Co(NH_3)_4(NO)]^{2+}$: A linear isomer was found at about 70 kJ mol^{-1} above the singlet ground state, resembling a metal-based $d(z^2)^1d(x^2-y^2)^1$ exitation. The second triplet state at about 100 kJ mol^{-1} above GS results from a metal-to-ligand charge transfer exciting one electron from the $d(z^2)$ orbital to an empty orbital of the Co–NO π antibonds, yielding a slightly bent nitrosyl moiety. In terms of EOS, the first triplet state corresponds to a $Co^{I}–NO^{+}$ pair and the second, less stable one, to a $Co^{II}–NO^{\bullet}$ species.[94] Concerning the newly synthesized $\{CoNO\}^8$ complexes, Klüfers and Schröder computed singlet states and triplets based on the cobalt-centered $d(z^2)^1d(x^2-y^2)^1$ excitation for **1a**, **3a** and **5a** and compared the BP86/def2-TZVP-derived X-ray and IR parameters of the NO moiety with the experimental data.[94] They found that only the values calculated for the singlets matched those determined experimentally. In the case of the triplets, a particularly strong deviation was observed for the calculated Co–N–O angles. Also the nitrosyl stretch was way off the mark for the triplets of **1a** and **5a**. Further, it was shown that the computed singlet of **6a** also reproduced the experimental values well.[169] Based on a CASSCF(8,7) calculation of the hypothetical $[Co(NH_3)_4(NO)]^{2+}$ species in the triplet state, showing a linearly bonded NO and *SPY*-5 overall structure, a correlation between the spin state and the two possible geometries can be established: As a first option, the NO ligand rotates upon relaxation to the singlet GS in such a way that the metal's $d(z^2)$ electron pair can bind in a lobe of an empty N–O π^* antibond, resulting in a bent $d(z^2)^2d(x^2-y^2)^0$ configuration with the CoN_4 plane mostly untouched. Alternatively, the $d(z^2)$ pair can make way for the NO ligand's lone pair, cancelling the metal–ligand σ bonds in the CoN_4 square basal plane so that this moiety has to re-adjust to *TBPY*-5 in order to avoid increased repulsion. This leads to retention of the linear Co–N–O angle in the resulting $d(z^2)^0d(x^2-y^2)^2$ configuration.[94] In conclusion, all new $\{CoNO\}^8$ nitrosyls in this work are best described as singlet species, regardless of their Co–N–O angle.

4 Summary

This thesis focuses on the synthesis, crystallographic and spectroscopic characterization as well as the quantum-chemical analysis of $\{CoNO\}^8$ compounds. Based on the work of Riggenmann,[94, 95] it was possible to extend the family of electroneutral, pentacoordinated perfluoropinacolatocobalt nitrosyls [Co(fpin)(L/L_2)(NO)] (**1–3**) by twenty new species, including complexes with *P*,*N*-ligands (**2**) and diphosphanes (**3**) as well as monodentate amine and phosphane co-ligands (**1l–n**, **3d**). Applying the direct one-pot route by treating cobalt(II) triflate, co-ligand, perfluoropinacol and base with gaseous nitric oxide, the subsequent concentration of the complex solutions using DMSO has proven to be particularly suitable for the crystallization of these compounds. In this context, two-chambered Schlenk tubes were superior to the original crystallization method, in which a glass vial of the complex solution was placed in a regular Schlenk tube filled with the sulfoxide. Within the group of fpin nitrosyls, the Co–N–O angle was found to be wider in the phosphane-bearing products compared to the complexes with *P*,*N*-ligands and even more obtuse compared to those with nitrogen donor ligands. This indicates that the structure of the bent CoNO moiety might be influenced to some extent by the elements that bind to cobalt. In addition to the variance of the Co–N–O angle, those class **1** nitrosyls with a coordinating aromatic system show a rapid loss of nitric oxide in solution when purged with argon. This reaction was found to be reversible upon re-introduction of gaseous NO. Besides the $\{CoNO\}^8$-mononitrosyls **1–3**, the dinitrosyl $(ppzH_2)_{0.5}$[Co(fpin)$(NO)_2$] (**7b**) was obtained, proving that the abovementioned system can also be used to generate $\{Co(NO)_2\}^{10}$ compounds.

Hexacoordinated bis(diamine) complexes with a weakly coordinating co-ligand mark the second class of bent nitrosyls obtained in the course of this work. From these eleven new compounds in total, ten feature an anionic or neutral ligand occupying the sixth position *trans* to NO. The synthesis of these class **4** species is based on the procedure from Feltham *et al*. in which the perchlorate precursor *trans*-[Co$(ClO_4)(en)_2(NO)]ClO_4$ (**4a**, obtained in a one-pot route from cobalt(II) perchlorate, diamine and NO gas) is reacted with lithium halogenide or nitrate in order to replace both anions.[85] Further pro-ducts with tetrafluoroborate were synthesized in a similar manner to **4a**. In all species with *O*- and *F*-bound co-ligands, a *trans* distance of about 2.3 Å was found. Only the chlorido and iodido derivatives (**4b+c**) had longer distances of about 2.6 Å and 3.0 Å, respectively. The perchlorato products **4a+h** were found to crystallize isotypically to their tetrafluoroborato analogs (**4e+i**). In addition, a remarkable reactivity for the parent precursor compound was found: recrystallization of **4a** in acetonitrile via the DMSO method led to the replacement of the coordinating perchlorate ion with a molecule of the sulfoxide, binding via oxygen. Moreover, in an attempt to exchange the perchlorate for nitrite, treatment of the **4a** with $NaNO_2$ gave the new hyponitrito compound *rac*-[Co$(en)_2$(*cis*-N_2O_2-κ^2*O*,*O*′)]ClO_4 (**7c**), a rare example of a complex with chelating *cis*-$N_2O_2^{2-}$. Since this product was observed only in DMSO crystallization batches, it is very likely that the sulfoxide is also involved in its formation. By using said method, it was furthermore possible to record crystal structures of **4a+b** with better quality and to

obtain the nitrate derivative (**4d**) in a reproducible manner. Quantum-chemical calculations done by Schröder and Klüfers [94] reproduced the *trans* distances in **4b+d** and by comparing them with Co(III) ammine species, it was found that they fulfill the Cremer–Kraka criterion, [156] therefore the binding of the *trans* co-ligand should be assessed as a weak electrostatic interaction. In addition to the class **4** compounds, also one hexacoordinated *cis*-{CoNO}^{8} nitrosyl, *rac*-*cis*-[Co(NO)(NO_2-κ*N*)(phen)$_2$]ClO_4 (**7a**) was successfully crystallized and characterized. The same configuration was found in the recorded crystal structure of *rac*-*cis*-[Co(bpy)$_2$Cl(NO)]ClO_4 which, however, could not be analyzed further due to an unsolvable disorder of the nitrosyl moiety. Both compounds have been known in the literature for a long time, but have not been crystallized before.[119] Again, treatment with DMSO provided the final key to elucidating the structure of these compounds. Derived from the bis(perchlorate) product **4a**, the compound *rac*-[Co(en)$_2$(*cis*-N_2O_2-κ^2*O*,*O*')]ClO_4 (**7c**) was discovered, being the first reported mononuclear cobalt complex with chelating *cis*-hyponitrite to be structurally characterized.

The synthesis and structural elucidation of a new series of four linear {CoNO}^{8} complexes (class **5**) provided the basis to refute the general consensus that the Co–N–O angle is related to the charge of the nitrosyl ligand. The products were obtained from 1:2 solutions of cobalt(II) perchlorate or tetrafluoroborate and diphosphane treated with gaseous NO. Calculation of the effective oxidation states (EOS) [146] by Schröder and Klüfers [94] revealed that not only the linear bis(diphosphane) nitrosyls are best decribed as Co^{I}–NO^{+} pairs, but also all the bent species synthesized in this work, therefore contradicting the common belief that the NO ligand should possess a negative charge in bent complexes. This was further supported by their QTAIM charge analyses of the nitrosyl ligand that resulted in a mean charge of about −0.30 *e* for all {CoNO}^{8} species, which is not enough to assign an NO^{-} in the concept of EOS analysis.[94] Moreover, it was shown that the energy of the infrared nitrosyl stretching vibration depends on the interaction angle of the cobalt orbitals with NO rather than just the angle of the metal's center of charge relative to the ligand. By comparing the nitrosyl charge as well as the structural and spectroscopic parameters of the ground-state structures of **4h**, **5a'** and **6a** with their respective theoretical *SPY*-5 / *TBPY*-5 isomers, Schröder and Klüfers illustrated that the transition from linear to bent cannot be explained by the Dewar–Chatt–Duncanson (DCD) model.[169] This further debunks the consensus mentioned above, as it is based on the assumption that the bending of the CoNO moiety can be viewed as a DCD event. Computation of the literature-known complex [Co(dmpe)$_2$(NO)]$^{2+}$ proved that the trigonal bipyramidal structure in the class **5** species is not caused by the sterics of the diphosphane ligands since the *TBPY*-5 geometry was maintained and the derived nitrosyl stretch closely matched the experimental value.[169]

The compound [Co(dppe)$_2$(NO)]$(ClO_4)_2$ (**5a**) was found to react with lithium chloride to give the nitrosyl [$CoCl_2$(dppe)(NO)] (**6a**), which was also obtained successfully via the one-pot reaction of cobalt(II) chloride and diphosphane with nitric oxide gas. These findings formed the basis for the development of a series of seven new pentacoordinated, uncharged nitrosyls [Co(L)(NO)$(X)_2$] (class **6**) bearing a diphos-

phane and two chlorido or bromido ligands. These species exhibit slightly wider Co–N–O angles than the class **3** fpin analogs. The bond angles in the bromido nitrosyls were found to be about 2° more obtuse compared to their related chlorido derivatives. A comparison by Klüfers and Schröder of the theoretical *TBPY*-5 isomer of **6a** with the computed *SPY*-5 isomer of **5a'** showed that both structures have similar nitrosyl bond angles (165° vs. 157°), demonstrating that mononitrosyl complexes cannot be categorized universally into 'linear' and 'bent' due to the variability of said angle, a phenomenon inherent to this class of compounds.[169] With their square pyramidal geometry, the class **6** diphosphane nitrosyls differ significantly from their *TBPY*-5-shaped bis(monophosphane) analogs.[81,83] While the latter exhibit two nitrosyl stretches and disorder of the NO ligand in some cases, both of which being attributed to room-temperature spin crossover,[83] calculation of the singlet and triplet states of **1a**, **3a**, **5a** and **6a** revealed that only the structural and spectroscopic parameters derived from the singlets match the experimental values.[94,169] Klüfers and Schröder provided a rationale for these findings by computing the relaxation of the hypothetical, linear triplet species $[Co(NH_3)_4(NO)]^{2+}$ with *SPY*-5 geometry. They found that the complex could either transform into a bent $d(z^2)^2d(x^2-y^2)^0$ ground state via the binding of the metal's $d(z^2)$ electron pair with an empty N–O π^* antibond, or by cancelling the metal–ligand σ bonds in the CoN_4 square basal plane, with the $d(z^2)$ pair giving way to the nitrosyl ligand's lone pair, resulting in re-adjustment of the coordination geometry to *TBPY*-5 and a linear $d(z^2)^0d(x^2-y^2)^2$ ground state.[94] Hence, it can be conlcuded that all novel $\{CoNO\}^8$ compounds synthesized in this work should be considered as singlet species, irrespectively of their nitrosyl angle.

In summary, this work showed that the charge of the nitrosyl ligand in $\{CoNO\}^8$ complexes cannot be derived from the energy of its infrared stretching vibration. Furthermore, it was demonstrated that bent and linearly bonded nitric oxide cannot be unquestioningly assigned to NO^- or, respectively, NO^+. The further development of the DMSO crystallization method laid the groundwork for the quantum-chemical calculations which led to these findings. In some cases, such as the bis(diamine) nitrosyls of class **4**, isothermal diffusion of the reaction solvent into DMSO was not just the only way to crystallize the compound, but also proved to be more reliable than classical methods such as cooling down of the mother liquor. Due to their small size and relatively simple structure, the novel complexes presented in this work were particularly suitable for the abovementioned computations to address the questions dealt with in this thesis.

5 Outlook

Since the procedure for class **1–3** nitrosyls has proven to be suitable for the crystallization of many novel $\{CoNO\}^8$ compounds, it is worth testing a variety of other ligands with this system. While the class of group-15 ligands has so far been limited mainly to *N*- and *P*-donors (which is especially true for chelators), recent advances in organoarsenic synthesis have made a new series of diarsane compounds available, many of which being analogs of common diphosphanes.[182–185] Also electron-poor phosphanes with perfluorinated residues, such as $P(C_6F_5)_3$ and $(F_5C_2)_2P–C_2H_4–P(C_2F_5)_2$, can be considered candidates for further complexes with similar structure.[186] In addition, other perfluorinated alcohols with an acidity similar to fpin, such as perfluoro-*tert*-butanol or perfluorophenol, can be tested to obtain analogous species. They might also be suitable for synthesizing new derivatives of dinitrosyl **7b**.[187] Some of the class **1** species exhibited NO loss in solution. Since the speed of nitrosyl decomposition depended on the argon flow rate (vigorous purging resulted in a much faster decay than gentle bubbling), the loss could only be rated qualitatively. In order to determine the exact kinetics, efforts need to be made to react the cobalt nitrosyls with a trapping complex or other scavengers to which nitric oxide can be transferred. This would allow for time-resolved in-situ UV/Vis monitoring of the reaction. To ensure that NO exchange proceeds exclusively in solution and not via the gas phase in the flask's headspace, stopped-flow techniques should be used. Early studies on several $\{CoNO\}^8$ species have already shown the feasibility of such a transfer in solution. The complex $[Co(dmgH)_2(NO)]$, for example, reacts with some coordinatively unsaturated, phosphane-bearing chlorido complexes of Fe, Co, Ni and Ru to give the respective mono- and dinitrosyls.[188] Further, several cobalt compounds were found to be capable of NO transfer to Fe^{II}-heme proteins such as hemoglobin and myoglobin.[189,190] Since the use of such proteins for measurements is limited to water-soluble $\{CoNO\}^8$ complexes and physiological conditions, they are unsuitable as NO-trapping agents for the class **1** nitrosyls. Instead, the scavengers should rather be based on trapping species used for the abovementioned $[Co(dmgH)_2(NO)]$. Besides these studies, only one other example of nitrosyl transfer from a $\{CoNO\}^8$ species is known, involving cobalt complexes with cyclam ligands of different ring sizes.[191]

Although the class of bis(diamine) $\{CoNO\}^8$ nitrosyls seems to be sufficiently studied now, there are still many starting points for the discovery of further compounds of this type. Starting with the *trans* co-ligand, further anions such as F^- or pseudohalogenides can be tested, as well as weakly coordinating anions such as PF_6^- or AsF_6^-. Moreover, other amines need to be screened as well. Literature-known compounds such as $[Co(aziridine)_4(NO)](NO_3)_2$ show, for example, that also monoamines can act as ligands for such nitrosyls. Since this and similar complexes with pyridine and *o*-phenylenediamine have been obtained only as bulk products, application of the DMSO crystallization method may help to elucidate the structure of these species.[152] Furthermore, they can be used as possible precursors to replace the *trans* ligand. Similar to the class **4** derivatives, further *N*-heterocycles and anions need to be tested in order to expand the library of *cis*-$\{CoNO\}^8$ nitrosyls.

With the long-known compound $[Co(diars)_2(NO)](ClO_4)_2$ as the first and, to date, only arsenic representative of this class,[82, 85, 168] the abovementioned diarsane ligands are expected to be promising candidates for the synthesis of further linear $\{CoNO\}^8$ nitrosyls, which would allow for a characterization and computational analysis as it was done for the phosphorus analogs. In addition, the diars species was found to react with (pseudo)halogenides to give the class **4**-type compounds $[Co(diars)_2(NO)(X)]X$.[82, 85] Hence, if the development of new bis(diarsane) nitrosyls succeeds, they could pave the way to a new series of bent $\{CoNO\}^8$ complexes when treated in a similar manner. Regarding the dihalogenidocobalt nitrosyls (**6**), analogous bis(monophosphane) species with other anionic ligands are known,[81] hence testing of other ligands can be considered a promising route to expand this library and, possibly, also the range of the nitrosyl angle. Suitable anions include F^-, I^-, pseudohalogenides and NO_2^-.

Although there is a risk that the sulfoxide might react with the target complex in some way, the DMSO method should be considered a potential option for the crystallization of room-temperature-stable compounds. Other low-volatile solvents such as dimethylformamide or chloro- and bromobenzene should also be checked for their suitability as crystallization agents. Concerning a practical application of the new products, the complexes can be tested for their potential as homogenous catalysts in organic reactions. In this context, the hydrogenation of alkenes would be a suitable example of a reaction to study. A few cobalt-containing catalysts for this reaction type were already reported, but none of them bears a nitrosyl ligand.[192, 193] However, there are also examples of NO complexes that are known to act as hydrogenation catalysts for alkenes. Among those is *trans*-$[Re(H_2O)I_2(NO)(PR_3)_2]$ with R = ^{i}Pr, Cy, which has been shown to significantly increase the reaction efficiency when combined with a Lewis acid such as $SiEt_3^+$. In this system, the silyl cation binds to the complex's nitrosyl moiety and enhances its electrophilicity.[194] Since these compounds are quite similar in composition to some of the species in this work, particularly the class **6** nitrosyls, they might be worth testing. Another potential application for the new products would be their use as donors for NO^- / HNO. Nitroxyl (HNO) is of pharmaceutical interest as a potential agent for treating heart failure and ischemia, exhibiting a biochemical behavior different from the uncharged radical nitric oxide.[195–197] Hence, compounds that release NO^- under physiological conditions to form nitroxyl represent possible drugs for the treatment of such diseases. In fact, the ability to release NO^- was already reported for one $\{CoNO\}^8$ compound. An electroneutral, square pyramidal cobalt nitrosyl bearing a diimine-dipyrrolide ligand was found to react with the heme model complex $[Fe^{III}Cl(tpp)]$ to give [Fe(tpp)(NO)]. Furthermore, reaction with two equivalents of PPh_3 resulted in the formation of $Ph_3P{=}O$ and $Ph_3P{=}NH$.[198] Both findings indicate the cleavage of NO^- from the cobalt nitrosyl. Since many of the novel $\{CoNO\}^8$ species synthesized in this work are structurally similar to this complex, they may provide a basis for future research in this field. Furthermore, the new compounds could prove to be suitable candidates for photoinduced linkage isomerism. In recent measurements on Riggenmann's complex [Co(fpin)(NO)(phen)], a shift of the nitrosyl IR stretch upon irradiation with laser light was observed, making it the first – and so far only – known $\{CoNO\}^8$ species to exhibit such behavior.[199]

6 Experimental part

6.1 Common working techniques

All reactions, as far as not explicitly described otherwise, were carried out at room temperature under an atmosphere of argon using standard Schlenk techniques. Syringes and cannulas used for the dosage and transfer of liquids were flushed with argon at least three times prior to use. Solvents were degassed by purging them with argon for at least ten minutes before usage. All reactions were carried out in Schlenk tubes rather than round-bottom flasks.

For the introduction of gaseous nitric oxide, a custom-made Schlenk line was used. This apparatus featured a four-way cross piece with the ports being connected to the reaction vessel, the NO cylinder, the argon cylinder and the vacuum pump, respectively. Each port was equipped with a stop cock. This setup allowed for the quick change of the gas atmosphere inside the Schlenk tube by applying a slight vacuum prior to the introduction of nitric oxide, thereby facilitating its diffusion into the reaction solution. After the reaction had been carried out, the reaction vessel was removed and the respective port connected to a row of gas washing bottles filled with an aqueous 2 M solution of amidosulfonic acid in order to destroy excess NO. It was driven out of the apparatus via argon stream. Gaseous nitric oxide was obtained from a compressed gas cylinder, depressurized to ca. 0.3 bar positive pressure and passed over Ascarite II® prior to use in order to exclude other NO_x species (with the exception of N_2O due to its neutral, i.e. non-acidic character).

Perfluoropinacolate was introduced using a 0.1 M methanolic $(NBnMe_3)_2$(fpin) stock solution made from neat perfluoropinacol, benzyltrimethylammonium methoxide (40 wt. % in MeOH) and methanol. For the preparation procedure, see Section 6.4.2.

Crystallization of the product compounds was almost exclusively achieved by isothermal diffusion of the solvent into DMSO, resulting in a slow concentration of the reaction mixture. For this purpose, custom-made two-chambered Schlenk tubes were used. They consisted of a regular Schlenk tube with NS 29/32 joint and an overall length of 13–16 cm (depending on the size of the batch), into which a glass partition was melted that reached from the bottom to about half the length of the tube, dividing the lower half into two equally sized compartments. One chamber was filled with the reaction mixture and the other with DMSO. The batch was then stored at room temperature under argon or NO atmosphere. Other crystallization methods used include storing the reaction mixture under argon or NO atmosphere at low temperatures (4 °C and −25 °C) and solvent evaporation in air at room temperature.

Prior to further analysis (IR, CHN), the crystalline product compounds were washed three times each with isopropanol and diethyl ether, subsequently air-dried for ten minutes in order to gently remove residual solvent (avoiding the use of high vacuum) and then stored under argon.

6.2 Analytical methods

6.2.1 Elemental analysis

CHN analyses were performed on *elementar vario EL* and *vario micro cube* analyzers. Interpretation of the data was done with the web application *JASPER*.[200] In case of phosphorus- and / or fluorine-containing compounds, significant deviations from the calculated values were observed due to the systematic error caused by the presence of these elements. This applies in particular to the measured carbon mass fraction.[201, 202]

6.2.2 IR spectroscopy

IR spectra of the solid samples were recorded on a *JASCO FT/IR-4600* spectrometer equipped with a *PIKE MIRacle Single Reflection* ATR unit that was used with a diamond crystal plate. The spectra were interpreted with *JASCO*'s *Spectra Manager (Version 2.07.00)* software.[203]

In-situ IR spectra of reaction mixtures were recorded on a *Mettler-Toledo ReactIR 15* using an ATR probe equipped with a diamond crystal plate. Three-dimensional plotting of time-dependent IR spectra was done with the *iC IR (Version 7.0.297)* program from *Mettler-Toledo*.[204]

Solid samples were recorded from 650 to 4000 cm^{-1}, solutions from 650 to 2000 cm^{-1}. The relative intensities of the vibration bands are given in parentheses behind the wavenumber and are designated as very strong (vs), strong (s), medium (m), weak (w) or very weak (vw).

6.2.3 Single-crystal X-ray diffraction

Crystals suitable for X-ray diffraction were selected using a *Leica MZ12* microscope equipped with polarization filters. The measurements were performed at temperatures around 100 K or 170 K on a *Bruker D8Venture* diffractometer equipped with a *Bruker AXS* area detector using molybdenum-K_α radiation (λ = 0.71073 Å) from a *Bruker TXS* rotating anode. Multiscan absorption was applied using *SADABS (Version 2014)*.[205] The raw data were processed with *Bruker*'s *APEX3 (Version 2016)* software.[206] Structures were solved by direct methods using *SHELXT (Version 2014/5)*[207] and refined by full-matrix least-squares calculations on F^2 with *ShelXle (SHELXL Version 2016/6)*.[208] The validation of space groups and calculation of distances and angles was done with *PLATON (Version 230418)*.[209, 210] In the case of twinned crystals, twin laws were identified with *CELL_NOW (Version 2008/4)*.[211] Molecular structures were visualized using *ORTEP-3 (Version 2.0)*.[212] Packing diagrams were created with *Mercury (Version 3.0)*[213] and visualized with *POV-Ray (Version 3.6.2)*.[214] Further information on the measurement experiments is given in Section 7.2.

6.2.4 Stability testing of products for NO loss in solution

A freshly prepared solution (1.5 mL) of the respective nitrosyl complex with the same composition as used for crystallization (see Sections 6.5–6.11) was quickly transferred to an argon-filled Schlenk tube via syringe. Then, argon was bubbled at room temperature through a cannula (0.80 mm ⌀) for 10 minutes at a rate of 220 mL/min while stirring at a rate of 500 rpm. Occurring NO loss was rated qualitatively as slow (only slight brightening of the typical dark brown/dark red color), medium (considerable brightening within 5–8 minutes) and rapid (complete color change to pale red/yellow within 3 minutes).

6.2.5 Monitoring of NO binding via in-situ IR spectroscopy

For the monitoring experiments, 10.0 mL of the reaction mixture were placed in a three-necked round-bottom flask (total volume: 25.0 mL) equipped with a magnetic stirring bar. The ports of the flask were equipped with the IR sample probe, a septum with two cannulas (0.80 mm ⌀, one for nitrogen purging, immersing into the solution and the other one for venting) and a tube connection to the NO apparatus, respectively. To induce nitrosyl formation, stirring was shortly stopped and the gas atmosphere inside the Schlenk flask quickly changed by applying a slight vacuum prior to the introduction of nitric oxide. Stirring was then continued at a rate of 375 rpm. After the absorption band of the N–O stretch had reached its maximum, nitrogen was bubbled through the cannula under continued stirring to monitor the decay of the previously formed nitrosyl species.

6.3 Computational methods

Structural optimizations and IR frequency analyses were performed by Daniel Schröder, M.Sc. and Prof. Dr. Peter Klüfers (LMU München) with *ORCA (Versions 4.2.1 + 5.0.4)*[215,216] using the def2-TZVP basis set,[134] the auxiliary basis def2/J[135] and the functional BP86 as well as D3- and D4 dispersion correction[136–138] and CPCM(∞) solvent correction.[139] Integration acceleration was done using the RIJCOSX method.[140] In the case of the iodine-containing species **4c**, relativistic effects were taken into account by using ZORA[141,142] and a SARC-[143] TZVPP basis set[134] for the iodido ligand. With the exception of **4d**,[94] the initial geometries for all optimizations were taken from the respective crystal structures recorded in this work. For charge analyses of the nitrosyl ligand, quantum theory of atoms in molecules (QTAIM)[144] calculations were carried out with the program *Multiwfn (Version 3.8)*.[217] Oxidation states of the cobalt center and nitrosyl ligand were calculated using Salvador's effective oxidation-state (EOS) analysis[146,148] with the optimized structures as input. For evaluating the distortion of the coordination geometries, continous-shape measurements (CShM) were performed with the program *SHAPE (Version 2.1)*.[110]

6.4 Reagents and solvents

6.4.1 Commercially available chemicals

Table 6.1: List of purchased chemicals used in experiments with their respective purities and manufacturers.

chemical	purity	manufacturer
metal salts		
cobalt(II) bromide	99 %	Sigma-Aldrich
cobalt(II) chloride hexahydrate	98 %	Acros Organics
cobalt(II) nitrate hexahydrate	98 %	Sigma-Aldrich
cobalt(II) perchlorate hexahydrate	98 %	Sigma-Aldrich
cobalt(II) tetrafluoroborate hexahydrate	99 %	fluorochem
cobalt(II) triflate	98 %	abcr
lithium bromide	≥ 99 %	Sigma-Aldrich
lithium chloride	≥ 99 %	Fluka
lithium iodide	99.9 %	Sigma-Aldrich
lithium nitrate	≥ 99.9 %	Acros Organics
lithium perchlorate	≥ 99 %	Acros Organics
potassium carbonate	≥ 99.5 %	AppliChem
potassium hydroxide (powdered)	≥ 85 %	Sigma-Aldrich
sodium nitrite	≥ 98 %	VWR
ligands		
(2-aminoethyl)diisopropylphosphane (in THF)	10 wt. %	abcr
N-(2-aminoethyl)morpholine	99 %	Sigma-Aldrich
N-(2-aminoethyl)piperidine	98 %	abcr
2-(2′-aminoethyl)pyridine	96 %	Sigma-Aldrich
N-(2-aminoethyl)pyrrolidine	98 %	Sigma-Aldrich
N-benzylethylenediamine	97 %	Sigma-Aldrich
2,2′-bipyridine	≥ 98 %	Fluka
2,2′-bipyrimidine	95 %	abcr
bis(1-pyrazolyl)methane	97 %	[a]
bis(diphenylphosphino)amine	98 %	abcr
1,2-bis(diphenylphosphino)benzene	98 %	abcr
1,4-bis(diphenylphosphino)butane	98 %	abcr
1,2-bis(diphenylphosphino)ethane	97 %	abcr
cis-1,2-bis(diphenylphosphino)ethene	97 %	abcr
1,3-bis(diphenylphosphino)propane	98 %	abcr
2,9-dimethyl-4,7-diphenyl-1,10-phenanthroline	98 %	abcr
N,*N*-dimethylethylenediamine	≥ 98 %	Sigma-Aldrich
N,*N*′-dimethylethylenediamine	98 %	Sigma-Aldrich

[a] Synthesized according to Ref. [218].

Table 6.1, continued.

chemical	purity	manufacturer
ligands		
2-(diphenylphosphino)ethanaminium tetrafluoroborate	96 %	Sigma-Aldrich
1,2-dipiperidinoethane	98 %	Acros Organics
ethylenediamine	≥ 99.5 %	Sigma-Aldrich
N-methyl-2-(aminomethyl)pyridine	97 %	Sigma-Aldrich
methyldiphenylphosphane	≥ 97 %	TCI
N-methylethylenediamine	95 %	Alfa Aesar
N-methylimidazole	99 %	Sigma-Aldrich
nitric oxide	≥ 99.5 %	Air Liquide
perfluoropinacol	97 %	fluorochem
1,10-phenanthroline	≥ 99 %	Aldrich
pyridazine	98 %	Sigma-Aldrich
pyridine	99.5 %	Acros Organics
N,*N*,*N*′,*N*′-tetraethylethylenediamine	98 %	Sigma-Aldrich
solvents		
acetone	≥ 99.5 %	Bernd Kraft
acetonitrile	≥ 99.5 %	VWR
chloroform	≥ 99.8 %	Fisher Chemical
dichloromethane	99.8 %	Acros Organics
diethyl ether	≥ 99.5 %	Fisher Chemical
dimethyl sulfoxide	≥ 99.9 %	Fisher Chemical
ethanol	99.8 %	Acros Organics
n-heptane	≥ 99 %	Acros Organics
isopropanol	≥ 99.8 %	Merck
methanol	99.9 %	Acros Organics
tetrahydrofuran	99.5 %	Acros Organics
water	deionized	house installation
other educts and compounds		
amidosulfonic acid	99.5 %	Grüssing
argon	≥ 99.9 %	Air Liquide
Ascarite II® (8–20 mesh)	–	Acros Organics
benzyltrimethylammonium methoxide (in MeOH)	40 wt. %	Santa Cruz Biotech
4,4′-bipyridine	≥ 99 %	Fluka
piperazine hexahydrate	≥ 97 %	TCI
pyrazole	≥ 98 %	TCI
tetrabutylammonium hydrogen sulfate	97 %	Sigma-Aldrich
triethylamine	≥ 99 %	Riedel-de Haën

6.4.2 Preparation of a methanolic 0.1 M $(NBnMe_3)_2$(fpin) stock solution

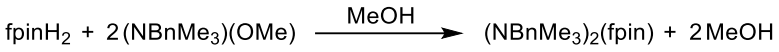

Starting materials:

(NBnMe)(OMe) solution (40 wt. % in MeOH), perfluoropinacol, methanol.

Procedure:

A solution of benzyltrimethylammonium methoxide in methanol (40 wt. %, 4.000 mL, 8.000 mmol, 1.0 equiv.) was diluted with further MeOH (35.285 mL) followed by the addition of perfluoropinacol (0.715 mL, 4.000 mmol, 0.5 equiv.) to give a methanolic $(NBnMe_3)_2$(fpin) stock solution (c = 0.1 M, 40.000 mL). Prior to experimental use, the solution was purged with argon for 5 minutes and then stored under this inert gas.

6.5 Synthesis of perfluoropinacolatocobalt nitrosyls with diamines and aromatic *N*-heterocycles as co-ligands

6.5.1 [Co(2-aepyrr)(fpin)(NO)] (1a)

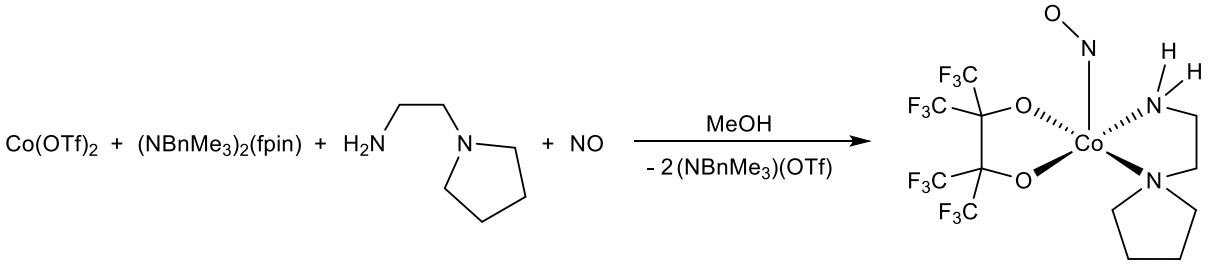

1a

Starting materials:

N-(2-Aminoethyl)pyrrolidine (2-aepyrr), $(NBnMe_3)_2$(fpin) solution (0.1 M in MeOH), cobalt(II) triflate, nitric oxide, methanol, dimethyl sulfoxide.

Procedure:

Cobalt(II) triflate (0.018 g, 0.050 mmol, 1 equiv.) was added to a solution of $(NBnMe_3)_2$(fpin) in methanol (0.1 M, 0.5 mL, 0.050 mmol, 1 equiv.) followed by the addition of *N*-(2-aminoethyl)pyrrolidine (6.0 µL, 0.050 mmol, 1 equiv.). Then, additional MeOH (0.5 mL) was added in order to dissolve all educts completely. The argon atmosphere was then replaced with nitric oxide and the resulting dark brown solution was stirred for 15 minutes. The batch was then transferred to a two-chambered Schlenk tube filled with DMSO (3.0 mL) in the second chamber. After four days, brown single crystals of **1a** suitable for X-ray diffraction were collected.

Yield: 0.011 g (0.021 mmol, 41 %).

Empirical formula: $C_{12}H_{14}CoF_{12}N_3O_3$ (535.18 g mol^{-1}).

Elemental analysis: found (calcd.): C 26.79 % (26.93 %), H 2.25 % (2.64 %), N 7.80 % (7.85 %).

IR (solid, ATR): $\tilde{\nu}$ = 3326 (vw), 3213 (vw), 3139 (vw), 2991 (vw), 2156 (vw), 2033 (vw), 1643 (s, NO), 1597 (m), 1464 (vw), 1455 (vw), 1319 (vw), 1261 (m), 1220 (vs), 1200 (vs), 1181 (vs), 1155 (vs), 1139 (vs), 1109 (vs), 1054 (w), 1042 (w), 1013 (w), 983 (w), 943 (s), 900 (vw), 865 (s), 779 (w), 758 (w), 741 (m), 730 (w), 713 (s), 684 (w), 657 (w) cm^{-1}.

6.5.2 [Co(2-aepip)(fpin)(NO)] (1b)

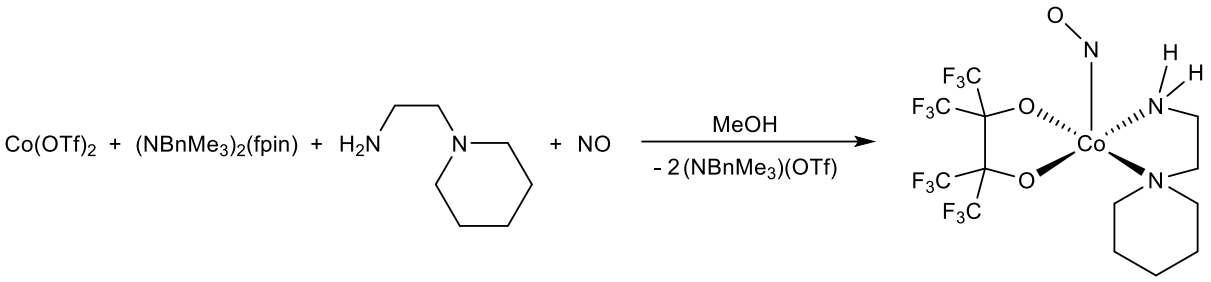

1b

Starting materials:

N-(2-Aminoethyl)piperidine (2-aepip), $(NBnMe_3)_2$(fpin) solution (0.1 M in MeOH), cobalt(II) triflate, nitric oxide, methanol.

Procedure:

Cobalt(II) triflate (0.018 g, 0.050 mmol, 1 equiv.) was added to a solution of $(NBnMe_3)_2$(fpin) in methanol (0.1 M, 0.5 mL, 0.050 mmol, 1 equiv.) followed by the addition of *N*-(2-aminoethyl)piperidine (7.0 µL, 0.050 mmol, 1 equiv.). Then, additional MeOH (1.0 mL) was added in order to dissolve all educts completely. The argon atmosphere was then replaced with nitric oxide and the resulting dark brown solution was stirred for 15 minutes. The batch was then stored under NO atmosphere at 4 °C. After four days, brown single crystals of **1b** suitable for X-ray diffraction were collected.

Yield: 0.007 g (0.013 mmol, 25 %).

Empirical formula: $C_{13}H_{16}CoF_{12}N_3O_3$ (549.20 g mol^{-1}).

Elemental analysis: found (calcd.): C 28.23 % (28.43 %), H 2.93 % (2.94 %), N 7.62 % (7.65 %).

IR (solid, ATR): $\tilde{\nu}$ = 3330 (vw), 3213 (vw), 3131 (vw), 2964 (vw), 2875 (vw), 2155 (vw), 2014 (vw), 1968 (vw), 1644 (m, NO), 1599 (m), 1455 (vw), 1390 (w), 1362 (w), 1348 (w), 1316 (vw), 1292 (vs), 1260 (m), 1217 (vs), 1183 (vs), 1174 (vs), 1151 (vs), 1139 (vs), 1108 (vs), 1050 (w), 1033 (w), 992 (s), 981 (w), 943 (s), 902 (vw), 862 (s), 757 (vw), 742 (s), 730 (w), 713 (m), 684 (w), 657 (w) cm^{-1}.

6.5.3 [Co(2-aemor)(fpin)(NO)] (1c)

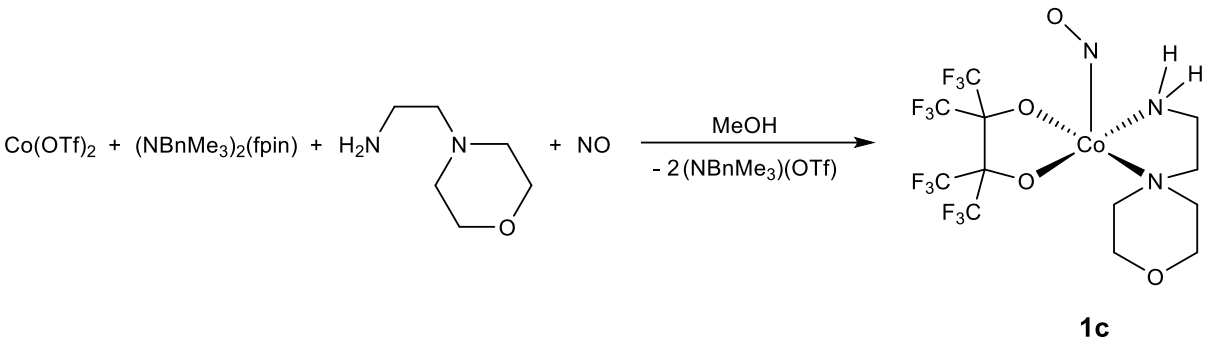

1c

Starting materials:

N-(2-Aminoethyl)morpholine (2-aemor), $(NBnMe_3)_2$(fpin) solution (0.1 M in MeOH), cobalt(II) triflate, nitric oxide, methanol, dimethyl sulfoxide.

Procedure:

Cobalt(II) triflate (0.018 g, 0.050 mmol, 1 equiv.) was added to a solution of $(NBnMe_3)_2$(fpin) in methanol (0.1 M, 0.5 mL, 0.050 mmol, 1 equiv.) followed by the addition of *N*-(2-aminoethyl)morpholine (7.0 µL, 0.050 mmol, 1 equiv.). Then, additional MeOH (0.8 mL) was added in order to dissolve all educts completely. The argon atmosphere was then replaced with nitric oxide and the resulting dark brown solution was stirred for 15 minutes. The batch was then transferred to a two-chambered Schlenk tube filled with DMSO (6.0 mL) in the second chamber. After four days, brown single crystals of **1c** suitable for X-ray diffraction were collected.

Yield: 0.018 g (0.033 mmol, 65 %).

Empirical formula: $C_{12}H_{14}CoF_{12}N_3O_4$ (551.18 g mol^{-1}).

Elemental analysis: found (calcd.): C 26.13 % (26.15 %), H 2.14 % (2.56 %), N 7.64 % (7.62 %).

IR (solid, ATR): $\tilde{\nu}$ = 3330 (vw), 3220 (vw), 3123 (vw), 2984 (vw), 2875 (vw), 2159 (vw), 2028 (vw), 1962 (vw), 1658 (m, NO), 1606 (m), 1471 (vw), 1455 (vw), 1394 (vw), 1321 (vw), 1257 (m), 1217 (vs), 1175 (vs), 1142 (s), 1112 (vs), 1051 (w), 1041 (w), 1015 (vw), 993 (w), 982 (w), 943 (s), 904 (vw), 894 (vw), 867 (s), 848 (w), 943 (m), 756 (vw), 741 (m), 730 (w), 713 (m), 683 (w), 662 (w) cm^{-1}.

6.5.4 [Co(bnen)(fpin)(NO)]·DMSO (1d·DMSO)

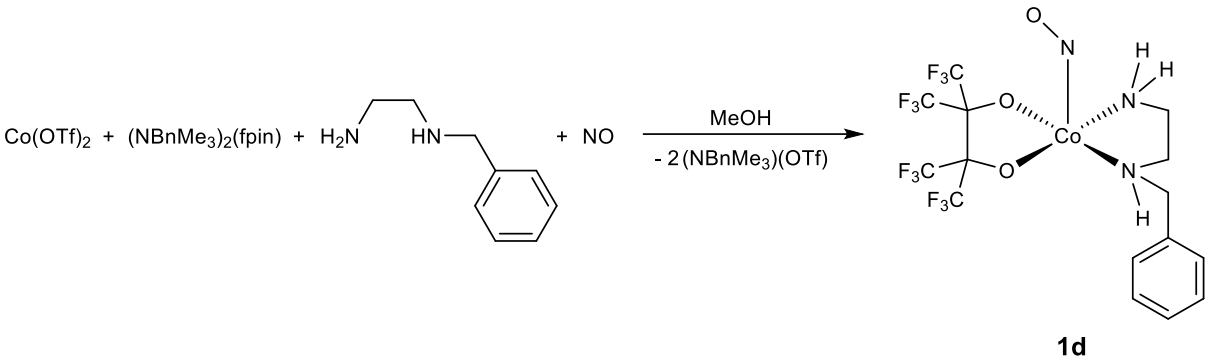

1d

Starting materials:

N-Benzylethylenediamine (bnen), $(NBnMe_3)_2$(fpin) solution (0.1 M in MeOH), cobalt(II) triflate, nitric oxide, methanol, dimethyl sulfoxide.

Procedure:

Cobalt(II) triflate (0.018 g, 0.050 mmol, 1 equiv.) was added to a solution of $(NBnMe_3)_2$(fpin) in methanol (0.1 M, 0.5 mL, 0.050 mmol, 1 equiv.) followed by the addition of *N*-benzylethylenediamine (8.0 µL, 0.050 mmol, 1 equiv.). Then, additional MeOH (0.8 mL) was added in order to dissolve all educts completely. The argon atmosphere was then replaced with nitric oxide and the resulting dark brown solution was stirred for 15 minutes. The batch was then transferred to a two-chambered Schlenk tube filled with DMSO (6.0 mL) in the second chamber. After four days, brown single crystals of **1d**·DMSO suitable for X-ray diffraction were collected.

Yield: 0.005 g (0.008 mmol, 15 %).

Empirical formula: $C_{17}H_{20}CoF_{12}N_3O_4S$ (649.34 g mol^{-1}).

Elemental analysis: found (calcd.): C 30.76 % (31.45 %), H 3.58 % (3.10 %), N 5.61 % (6.47 %).

IR (solid, ATR): $\tilde{\nu}$ = 3312 (vw), 3217 (vw), 3104 (vw), 2162 (vw), 1975 (vw), 1659 (m, NO), 1607 (w), 1497 (vw), 1458 (vw), 1436 (vw), 1417 (vw), 1404 (vw), 1365 (vw), 1311 (vw), 1259 (m), 1227 (vs), 1211 (vs), 1180 (vs), 1155 (m), 1130 (s), 1109 (s), 1061 (m), 1047 (m), 1012 (s), 980 (m), 940 (s), 895 (vw), 866 (s), 843 (w), 758 (m), 742 (m), 730 (w), 713 (m), 702 (s), 680 (w), 656 (w) cm^{-1}.

6.5.5 [Co(dpipe)(fpin)(NO)] (1e)

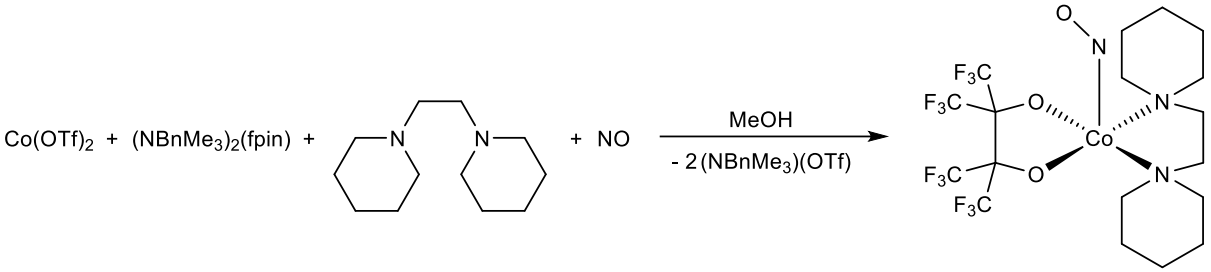

1e

Starting materials:

1,2-Dipiperidinoethane (dpipe), $(NBnMe_3)_2$(fpin) solution (0.1 M in MeOH), cobalt(II) triflate, nitric oxide, methanol, dimethyl sulfoxide.

Procedure:

Cobalt(II) triflate (0.018 g, 0.050 mmol, 1 equiv.) was added to a solution of $(NBnMe_3)_2$(fpin) in methanol (0.1 M, 0.5 mL, 0.050 mmol, 1 equiv.) followed by the addition of 1,2-dipiperidinoethane (11.0 µL, 0.050 mmol, 1 equiv.). Then, additional MeOH (1.0 mL) was added in order to dissolve all educts completely. The argon atmosphere was then replaced with nitric oxide and the resulting dark brown solution was stirred for 15 minutes. The batch was then transferred to a two-chambered Schlenk tube filled with DMSO (6.0 mL) in the second chamber. After four days, brown single crystals of **1e** suitable for X-ray diffraction were collected.

Yield: 0.009 g (0.015 mmol, 30 %).

Empirical formula: $C_{18}H_{24}CoF_{12}N_3O_3$ (617.32 g mol^{-1}).

Elemental analysis: found (calcd.): C 34.40 % (35.02 %), H 3.78 % (3.92 %), N 6.31 % (6.81 %).

IR (solid, ATR): $\tilde{\nu}$ = 2988 (vw), 2948 (vw), 2933 (vw), 2867 (vw), 1866 (vw), 1793 (vw), 1660 (m, NO), 1483 (vw), 1452 (vw), 1389 (vw), 1360 (vw), 1304 (vw), 1256 (s), 1224 (vs), 1203 (vs), 1181 (s), 1151 (s), 1140 (vs), 1109 (s), 1059 (w), 1041 (w), 1029 (m), 997 (w), 982 (w), 940 (s), 892 (vw), 864 (s), 797 (vw), 775 (w), 756 (w), 742 (m), 729 (w), 710 (m), 678 (w), 658 (vw) cm^{-1}.

6.5.6 [Co(fpin)(NO)(teen)] (1f)

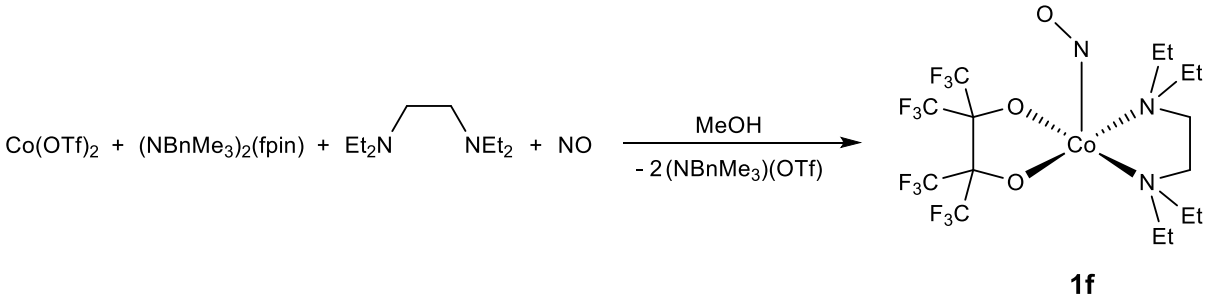

1f

Starting materials:

N,*N*,*N*′,*N*′-Tetraethylethylenediamine (teen), $(NBnMe_3)_2$(fpin) stock solution (0.1 M in MeOH), cobalt(II) triflate, nitric oxide, methanol, dimethyl sulfoxide.

Procedure:

Cobalt(II) triflate (0.018 g, 0.050 mmol, 1 equiv.) was added to a solution of $(NBnMe_3)_2$(fpin) in methanol (0.1 M, 0.5 mL, 0.050 mmol, 1 equiv.) followed by the addition of *N*,*N*,*N*′,*N*′-tetraethylethylenediamine (11.0 µL, 0.050 mmol, 1 equiv.). Then, additional MeOH (1.0 mL) was added in order to dissolve all educts completely. The argon atmosphere was then replaced with nitric oxide and the resulting dark brown solution was stirred for 15 minutes. The batch was then transferred to a two-chambered Schlenk tube filled with DMSO (6.0 mL) in the second chamber. After two days, brown single crystals of **1f** suitable for X-ray diffraction were collected.

Yield: 0.004 g (0.007 mmol, 14 %).

Empirical formula: $C_{16}H_{24}CoF_{12}N_3O_3$ (593.30 g mol^{-1}).

Elemental analysis: found (calcd.): C 32.05 % (32.39 %), H 4.03 % (4.08 %), N 6.67 % (7.08 %).

IR (solid, ATR): $\tilde{\nu}$ = 3010 (vw), 2973 (vw), 2953 (vw), 2899 (vw), 2169 (vw), 1986 (vw), 1655 (m, NO), 1469 (vw), 1445 (vw), 1397 (vw), 1353 (vw), 1253 (m), 1211 (vs), 1191 (m), 1176 (s), 1145 (m), 1132 (s), 1102 (s), 1051 (w), 1036 (w), 1019 (w), 982 (w), 938 (m), 862 (w), 802 (vw), 754 (w), 742 (m), 729 (w), 712 (m), 679 (vw), 667 (vw), 658 (vw) cm^{-1}.

6.5.7 [Co(2-aepy)(fpin)(NO)] (1g)

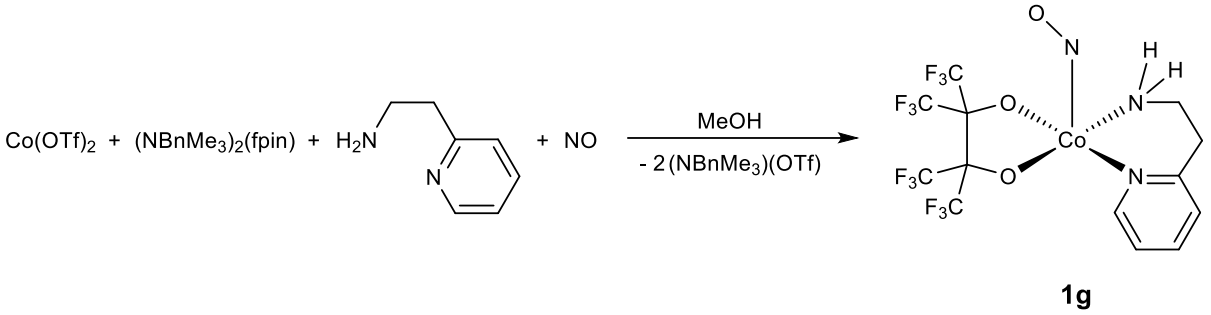

1g

Starting materials:

2-(2'-Aminoethyl)pyridine (2-aepy), $(NBnMe_3)_2$(fpin) stock solution (0.1 M in MeOH), cobalt(II) triflate, nitric oxide, methanol, dimethyl sulfoxide.

Procedure:

Cobalt(II) triflate (0.018 g, 0.050 mmol, 1 equiv.) was added to a solution of $(NBnMe_3)_2$(fpin) in methanol (0.1 M, 0.5 mL, 0.050 mmol, 1 equiv.) followed by the addition of 2-(2'-aminoethyl)pyridine (6.0 µL, 0.050 mmol, 1 equiv.). Then, additional MeOH (0.5 mL) was added in order to dissolve all educts completely. The argon atmosphere was then replaced with nitric oxide and the resulting dark brown solution was stirred for 15 minutes. The batch was then transferred to a two-chambered Schlenk tube filled with DMSO (3.0 mL) in the second chamber. After four days, brown single crystals of **1g** suitable for X-ray diffraction were collected.

Yield: 0.007 g (0.013 mmol, 26 %).

Empirical formula: $C_{13}H_{10}CoF_{12}N_3O_3$ (543.16 g mol^{-1}).

Elemental analysis: found (calcd.): C 28.55 % (28.75 %), H 1.48 % (1.86 %), N 7.58 % (7.74 %).

IR (solid, ATR): $\tilde{\nu}$ = 3298 (vw), 3220 (vw), 3147 (vw), 2158 (vw), 1993 (vw), 1683 (m, NO), 1598 (m), 1487 (vw), 1465 (vw), 1453 (vw), 1444 (vw), 1393 (vw), 1319 (vw), 1259 (m), 1218 (vs), 1179 (vs), 1150 (vs), 1137 (vs), 1105 (s), 1067 (w), 1032 (vw), 996 (vw), 983 (w), 961 (vw), 942 (s), 866 (s), 792 (vw), 783 (vw), 765 (m), 740 (m), 730 (w), 711 (m), 682 (w), 659 (vw), 653 (vw) cm^{-1}.

6.5.8 [Co(fpin)(mampy)(NO)]·DMSO (1h·DMSO)

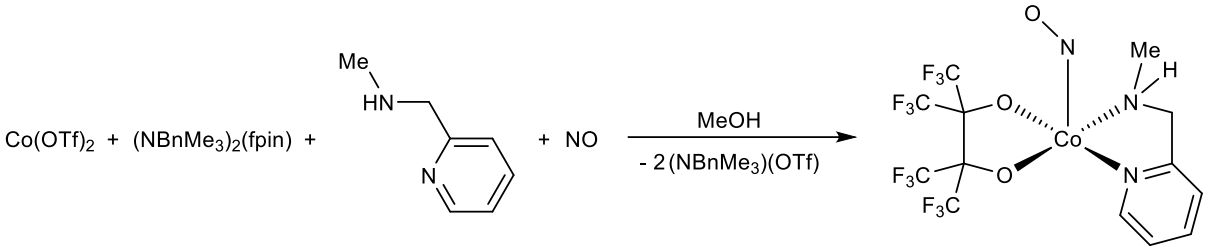

1h

Starting materials:

N-Methyl-2-(aminomethyl)pyridine (mampy), $(NBnMe_3)_2$(fpin) stock sol. (0.1 M in MeOH), cobalt(II) triflate, nitric oxide, methanol, dimethyl sulfoxide.

Procedure:

Cobalt(II) triflate (0.018 g, 0.050 mmol, 1 equiv.) was added to a solution of $(NBnMe_3)_2$(fpin) in methanol (0.1 M, 0.5 mL, 0.050 mmol, 1 equiv.) followed by the addition of *N*-methyl-2-(aminomethyl)pyridine (6.0 µL, 0.050 mmol, 1 equiv.). Then, additional MeOH (1.0 mL) was added in order to dissolve all educts completely. The argon atmosphere was then replaced with nitric oxide and the resulting dark brown solution was stirred for 15 minutes. The batch was then transferred to a two-chambered Schlenk tube filled with DMSO (6.0 mL) in the second chamber. After four days, brown single crystals of **1h**·DMSO suitable for X-ray diffraction were collected.

Yield: 0.003 g (0.005 mmol, 10 %).

Empirical formula: $C_{15}H_{16}CoF_{12}N_3O_4S$ (621.28 g mol^{-1}).

Elemental analysis: found (calcd.): C 30.91 % (29.00 %), H 3.04 % (2.60 %), N 5.92 % (6.76 %).

IR (solid, ATR): $\tilde{\nu}$ = 3085 (vw), 3041 (vw), 2892 (vw), 2156 (vw), 1986 (vw), 1673 (w, NO), 1653 (w, NO), 1613 (vw), 1482 (w), 1455 (vw), 1438 (vw), 1415 (vw), 1373 (vw), 1319 (vw), 1256 (vs), 1226 (vs), 1204 (s), 1165 (vs), 1151 (vs), 1136 (s), 1108 (m), 1089 (w), 1052 (w), 1030 (vs), 990 (w), 979 (w), 955 (w), 939 (m), 920 (w), 891 (w), 862 (m), 778 (m), 757 (w), 742 (w), 727 (m), 711 (m), 703 (m), 683 (vw), 664 (vw) cm^{-1}.

6.5.9 [Co(bpm)(fpin)(NO)] (1i)

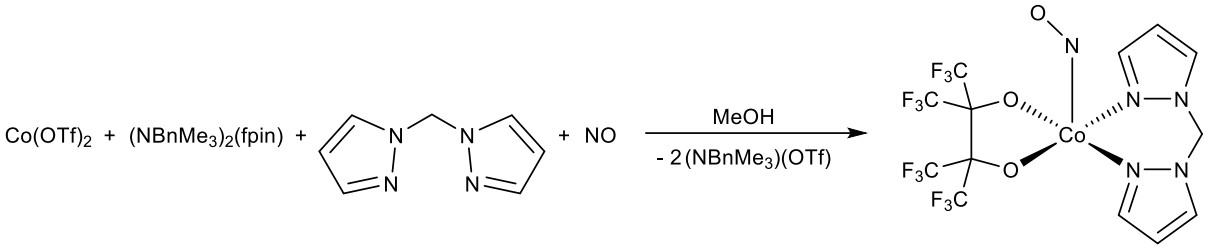

1i

Starting materials:

Bis(1-pyrazolyl)methane (bpm),[218] $(NBnMe_3)_2$(fpin) stock solution (0.1 M in MeOH), cobalt(II) triflate, nitric oxide, methanol, dimethyl sulfoxide.

Procedure:

One compartment of a two-chambered Schlenk tube was loaded with cobalt(II) triflate (0.018 g, 0.050 mmol, 1 equiv.) and bis(1-pyrazolyl)methane (0.007 g, 0.050 mmol, 1 equiv.) followed by the addition of a methanolic $(NBnMe_3)_2$(fpin) solution (0.1 M, 0.5 mL, 0.050 mmol, 1 equiv.). Then, additional MeOH (0.8 mL) was added to dissolve all educts completely. The second chamber was filled with DMSO (6.0 mL). The argon atmosphere was then replaced with nitric oxide. Stirring of the resulting dark brown reaction mixture was discontinued after 15 minutes and the batch was left under NO for crystallization. After four days, brown single crystals of **1i** suitable for X-ray diffraction were collected.

Yield: 0.005 g (0.009 mmol, 18 %).

Empirical formula: $C_{13}H_8CoF_{12}N_5O_3$ (569.15 g mol^{-1}).

Elemental analysis: found (calcd.): C 27.40 % (27.43 %), H 1.09 % (1.42 %), N 12.35 % (12.31 %).

IR (solid, ATR): $\tilde{\nu}$ = 3148 (vw), 3125 (vw), 3101 (vw), 1704 (m, NO), 1518 (vw), 1461 (vw), 1447 (vw), 1411 (w), 1401 (w), 1346 (vw), 1339 (vw), 1287 (w), 1277 (m), 1258 (m), 1208 (vs), 1180 (vs), 1148 (s), 1132 (vs), 1107 (s), 1071 (m), 1030 (w), 995 (m), 982 (m), 939 (vs), 915 (w), 864 (s), 783 (m), 767 (s), 759 (m), 742 (s), 730 (m), 712 (s), 681 (w), 660 (w) cm^{-1}.

6.5.10 [Co(bpym)(fpin)(NO)]·MeOH (1j·MeOH)

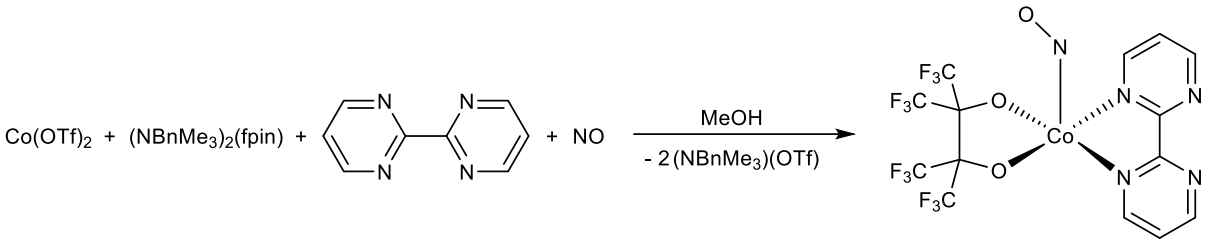

1j

Starting materials:

2,2'-Bipyrimidine (bpym), $(NBnMe_3)_2$(fpin) stock solution (0.1 M in MeOH), cobalt(II) triflate, nitric oxide, methanol, dimethyl sulfoxide.

Procedure:

One compartment of a two-chambered Schlenk tube was loaded with cobalt(II) triflate (0.018 g, 0.050 mmol, 1 equiv.) and 2,2'-bipyrimidine (0.008 g, 0.050 mmol, 1 equiv.) followed by the addition of a methanolic $(NBnMe_3)_2$(fpin) solution (0.1 M, 0.5 mL, 0.050 mmol, 1 equiv.). Then, additional MeOH (0.8 mL) was added to dissolve all educts completely. The second chamber was filled with DMSO (6.0 mL). The argon atmosphere was then replaced with nitric oxide. Stirring of the resulting dark brown reaction mixture was discontinued after 15 minutes and the batch was left under NO for crystallization. After four days, brown single crystals of **1j**·MeOH suitable for X-ray diffraction were collected.

Yield: 0.022 g (0.036 mmol, 72 %).

Empirical formula: $C_{15}H_{10}CoF_{12}N_5O_4$ (611.19 g mol^{-1}).

Elemental analysis: found (calcd.): C 29.46 % (29.48 %), H 1.23 % (1.65 %), N 11.47 % (11.46 %).

IR (solid, ATR): $\tilde{\nu}$ = 3489 (vw), 3112 (vw), 3083 (vw), 2961 (vw), 2156 (vw), 1986 (vw), 1692 (m, NO), 1600 (vw), 1583 (w), 1556 (vw), 1458 (vw), 1409 (m), 1255 (m), 1231 (vs), 1212 (vs), 1181 (vs), 1149 (s), 1136 (s), 1107 (s), 1021 (m), 1001 (vw), 981 (w), 942 (s), 863 (s), 817 (m), 793 (vw), 753 (m), 744 (m), 730 (w), 713 (m), 700 (w), 685 (w), 675 (m) cm^{-1}.

6.5.11 [Co(dmdpphen)(fpin)(NO)] (1k)

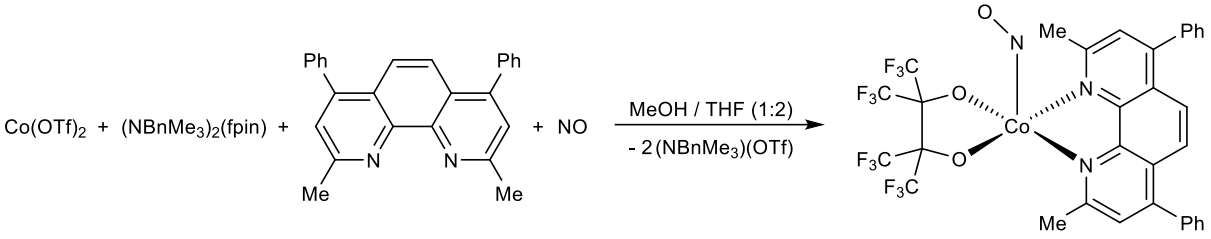

1k

Starting materials:

2,9-Dimethyl-4,7-diphenyl-1,10-phenanthroline (dmdpphen), $(NBnMe_3)_2$(fpin) sol. (0.1 M in MeOH), cobalt(II) triflate, nitric oxide, methanol, tetrahydrofuran, dimethyl sulfoxide.

Procedure:

One compartment of a two-chambered Schlenk tube was loaded with cobalt(II) triflate (0.018 g, 0.050 mmol, 1 equiv.) and 2,9-dimethyl-4,7-diphenyl-1,10-phenanthroline (0.018 g, 0.050 mmol, 1 equiv.) followed by the addition of a methanolic $(NBnMe_3)_2$(fpin) solution (0.1 M, 0.5 mL, 0.050 mmol, 1 equiv.). Then, THF (1.0 mL) was added to dissolve all educts completely. The second chamber was filled with DMSO (6.0 mL). The argon atmosphere was then replaced with nitric oxide. Stirring of the resulting dark brown reaction mixture was discontinued after 15 minutes and the batch was left under NO for crystallization. After four days, brown single crystals of **1k** suitable for X-ray diffraction were collected.

Yield: 0.025 g (0.032 mmol, 64 %).

Empirical formula: $C_{32}H_{20}CoF_{12}N_3O_3$ (781.44 g mol^{-1}).

Elemental analysis: found (calcd.): C 50.63 % (49.18 %), H 2.32 % (2.58 %), N 5.42 % (5.38 %).

IR (solid, ATR): $\tilde{\nu}$ = 3382 (vw), 3058 (vw), 2938 (vw), 1701 (s, NO), 1622 (vw), 1602 (vw), 1583 (vw), 1571 (w), 1550 (w), 1511 (vw), 1485 (w), 1443 (vw), 1396 (w), 1380 (w), 1317 (vw), 1257 (m), 1225 (vs), 1207 (vs), 1177 (vs), 1152 (s), 1136 (vs), 1107 (s), 1081 (w), 1029 (w), 1020 (w), 1000 (w), 981 (w), 942 (m), 927 (w), 889 (m), 863 (s), 831 (w), 782 (w), 772 (w), 760 (m), 742 (m), 730 (m), 704 (vs), 678 (m), 666 (w), 656 (w) cm^{-1}.

6.5.12 [Co(fpin)(NO)(py)$_2$] (1l)

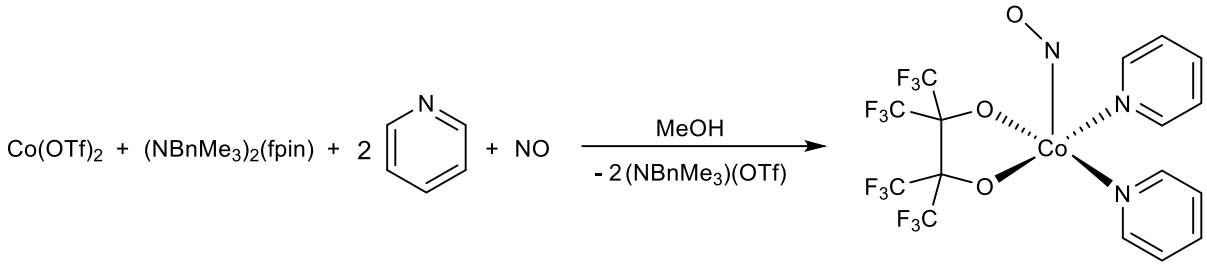

1l

Starting materials:

Pyridine (py), $(NBnMe_3)_2$(fpin) stock solution (0.1 M in MeOH), cobalt(II) triflate, nitric oxide, methanol, dimethyl sulfoxide.

Procedure:

One compartment of a two-chambered Schlenk tube was loaded with cobalt(II) triflate (0.018 g, 0.050 mmol, 1 equiv.) and methanolic $(NBnMe_3)_2$(fpin) stock solution (0.1 M, 0.5 mL, 0.050 mmol, 1 equiv.) followed by the addition of pyridine (8.0 µL, 0.100 mmol, 2 equiv.). Then, additional MeOH (1.0 mL) was added to dissolve all educts completely. The second chamber was filled with DMSO (6.0 mL). The argon atmosphere was then replaced with nitric oxide. Stirring of the resulting dark brown reaction mixture was discontinued after 15 minutes and the batch was left under NO for crystallization. After two days, brown single crystals of **1l** suitable for X-ray diffraction were collected.

Yield: 0.010 g (0.017 mmol, 34 %).

Empirical formula: $C_{16}H_{10}CoF_{12}N_3O_3$ (579.19 g mol^{-1}).

Elemental analysis: found (calcd.): C 30.25 % (33.18 %), H 2.27 % (1.74 %), N 6.74 % (7.26 %).

IR (solid, ATR): $\tilde{\nu}$ = 3118 (vw), 3083 (vw), 2156 (vw), 2014 (vw), 1849 (vw), 1682 (m, NO), 1640 (vw), 1609 (vw), 1546 (vw), 1489 (vw), 1452 (w), 1393 (w), 1361 (w), 1326 (w), 1253 (m), 1221 (vs), 1206 (vs), 1177 (s), 1160 (s), 1140 (vs), 1116 (m), 1108 (s), 1071 (m), 1049 (w), 1030 (m), 1019 (w), 1005 (w), 983 (w), 940 (m), 889 (vw), 864 (s), 827 (vw), 781 (vw), 758 (s), 740 (m), 729 (m), 710 (s), 688 (s), 681 (s), 661 (m) cm^{-1}.

6.5.13 [Co(fpin)(NO)(pydz)$_2$] (1m)

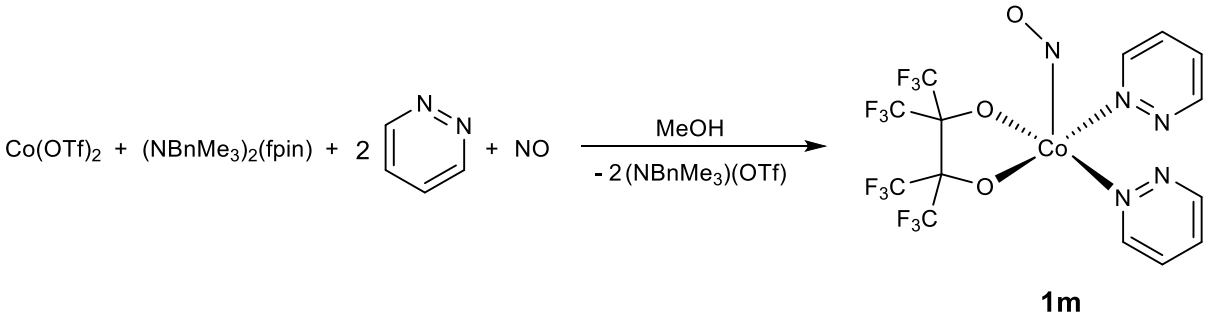

1m

Starting materials:

Pyridazine (pydz), $(NBnMe_3)_2$(fpin) solution (0.1 M in MeOH), cobalt(II) triflate, nitric oxide, methanol, dimethyl sulfoxide.

Procedure:

One compartment of a two-chambered Schlenk tube was loaded with cobalt(II) triflate (0.018 g, 0.050 mmol, 1 equiv.) and methanolic $(NBnMe_3)_2$(fpin) stock solution (0.1 M, 0.5 mL, 0.050 mmol, 1 equiv.) followed by the addition of pyridazine (7.0 µL, 0.100 mmol, 2 equiv.). Then, additional MeOH (1.0 mL) was added to dissolve all educts completely. The second chamber was filled with DMSO (5.5 mL). The argon atmosphere was then replaced with nitric oxide. Stirring of the resulting dark brown reaction mixture was discontinued after 15 minutes and the batch was left under NO for crystallization. After two days, brown single crystals of **1m** suitable for X-ray diffraction were collected.

Yield: 0.003 g (0.005 mmol, 10 %).

Empirical formula: $C_{14}H_8CoF_{12}N_5O_3$ (581.16 g mol^{-1}).

Elemental analysis: found (calcd.): C 28.49 % (28.93 %), H 2.08 % (1.39 %), N 11.23 % (12.05 %).

IR (solid, ATR): $\tilde{\nu}$ = 3097 (vw), 3074 (vw), 2177 (vw), 2028 (vw), 1693 (w, NO), 1582 (vw), 1572 (vw), 1489 (vw), 1478 (vw), 1454 (vw), 1422 (vw), 1339 (vw), 1298 (w), 1256 (m), 1225 (vs), 1206 (s), 1181 (vs), 1166 (s), 1132 (vs), 1105 (s), 1076 (m), 1067 (w), 1030 (w), 977 (s), 941 (m), 887 (vw), 864 (m), 808 (vw), 776 (m), 758 (w), 741 (m), 728 (w), 711 (m), 685 (w), 675 (w), 656 (w) cm^{-1}.

6.5.14 [Co(fpin)(mim)$_2$(NO)] (1n)

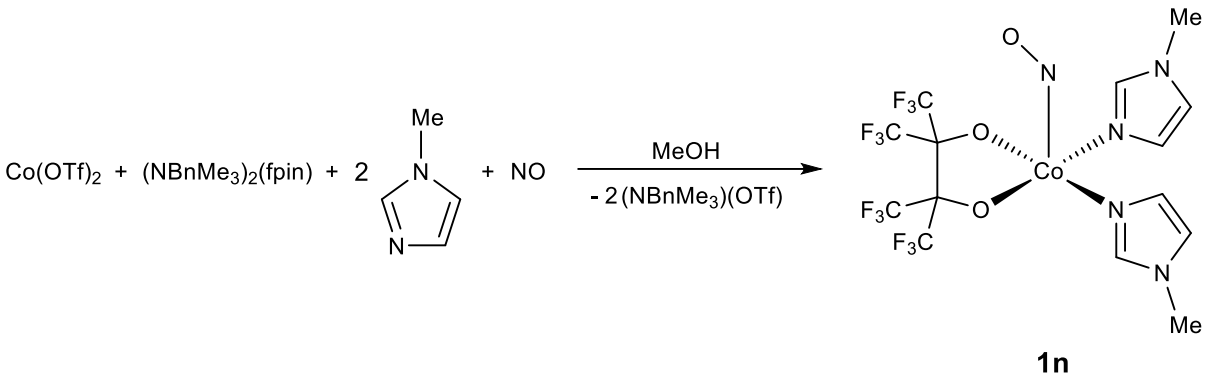

1n

Starting materials:

1-Methylimidazole (mim), (NBnMe$_3$)$_2$(fpin) solution (0.1 M in MeOH), cobalt(II) triflate, nitric oxide, methanol, dimethyl sulfoxide.

Procedure:

One compartment of a two-chambered Schlenk tube was loaded with cobalt(II) triflate (0.018 g, 0.050 mmol, 1 equiv.) and methanolic (NBnMe$_3$)$_2$(fpin) stock solution (0.1 M, 0.5 mL, 0.050 mmol, 1 equiv.) followed by the addition of 1-methylimidazole (8.0 µL, 0.100 mmol, 2 equiv.). Then, additional MeOH (1.0 mL) was added to dissolve all educts completely. The second chamber was filled with DMSO (6.0 mL). The argon atmosphere was then replaced with nitric oxide. Stirring of the resulting dark brown reaction mixture was discontinued after 15 minutes and the batch was left under NO for crystallization. After two days, brown single crystals of **1n** suitable for X-ray diffraction were collected.

Yield: 0.008 g (0.014 mmol, 28 %).

Empirical formula: $C_{14}H_{12}CoF_{12}N_5O_3$ (585.20 g mol^{-1}).

Elemental analysis: found (calcd.): C 26.24 % (28.73 %), H 1.83 % (2.07 %), N 10.92 % (11.97 %).

IR (solid, ATR): $\tilde{\nu}$ = 3160 (vw), 3148 (vw), 2169 (vw), 1996 (vw), 1671 (s, NO), 1589 (vw), 1540 (w), 1524 (vw), 1479 (vw), 1453 (vw), 1430 (vw), 1287 (vw), 1258 (m), 1241 (m), 1222 (vs), 1210 (vs), 1171 (vs), 1156 (s), 1139 (vs), 1105 (s), 1091 (vs), 1025 (w), 1015 (vw), 981 (w), 960 (w), 941 (s), 864 (s), 829 (m), 749 (m), 740 (s), 728 (w), 713 (s), 681 (vw), 660 (m), 653 (w) cm^{-1}.

6.6 Synthesis of perfluoropinacolatocobalt nitrosyls with aminoethyl-substituted phosphanes as co-ligands

6.6.1 [Co(2-aedpp)(fpin)(NO)]·0.5 MeOH (2a·0.5 MeOH)

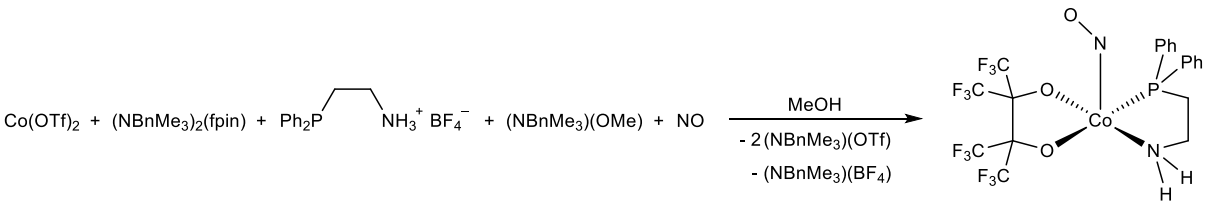

2a

Starting materials:

2-(Diphenylphosphino)ethanaminium tetrafluoroborate (2-aedpp·HBF_4), ($NBnMe_3$)(OMe) solution (40 wt. % in MeOH), $(NBnMe_3)_2$(fpin) stock solution (0.1 M in MeOH), cobalt(II) triflate, nitric oxide, methanol.

Procedure:

Cobalt(II) triflate (0.018 g, 0.050 mmol, 1 equiv.) was added to a solution of $(NBnMe_3)_2$(fpin) in methanol (0.1 M, 0.5 mL, 0.050 mmol, 1 equiv.) followed by the addition of 2-(diphenylphosphino)-ethanaminium tetrafluoroborate (0.016 g, 0.050 mmol, 1 equiv.). Then, a solution of ($NBnMe_3$)(OMe) in methanol (40 wt. %, 25.0 µL, 0.050 mmol, 1 equiv.) and additional MeOH (1.0 mL) was added in order to dissolve all educts completely. The argon atmosphere was then replaced with nitric oxide and the resulting dark brown solution was stirred for 15 minutes. The reaction mixture was then concentrated in vacuo to approximately half of its original volume and stored under argon at −25 °C. After seven days, a few brown single crystals of **2a**·0.5 MeOH suitable for X-ray diffraction were collected along with precipitated *P*,*N*-ligand.

Yield: n.a., few brown crystals.

Empirical formula: $C_{20}H_{16}CoF_{12}N_2O_3P$ (650.25 g mol^{-1}).

IR (solid, ATR): $\tilde{\nu}$ = 3062 (vw), 3044 (vw), 1860 (vw), 1795 (vw), 1653 (w, NO), 1591 (vw), 1493 (w), 1483 (w), 1459 (vw), 1437 (vw), 1422 (vw), 1380 (vw), 1287 (w), 1256 (m), 1220 (m), 1182 (w), 1163 (w), 1130 (w), 1104 (m), 1050 (s), 1028 (vs), 991 (m), 940 (w), 922 (vw), 889 (m), 867 (w), 838 (vw), 779 (w), 756 (vw), 741 (vw), 721 (s), 699 (m), 657 (vw) cm^{-1}.

6.6.2 [Co(2-aedip)(fpin)(NO)] (2b)

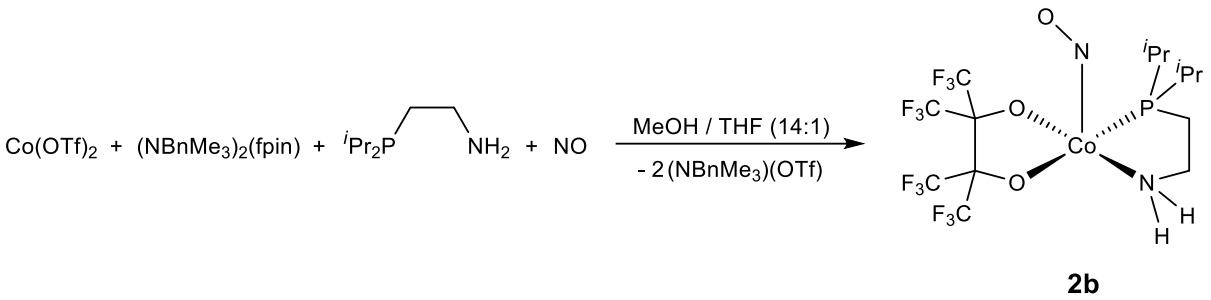

2b

Starting materials:

(2-Aminoethyl)diisopropylphosphane (2-aedip, 10 wt. % in THF), $(NBnMe_3)_2$(fpin) stock sol. (0.1 M in MeOH), cobalt(II) triflate, nitric oxide, methanol, dimethyl sulfoxide.

Procedure:

Cobalt(II) triflate (0.018 g, 0.050 mmol, 1 equiv.) was added to a solution of $(NBnMe_3)_2$(fpin) in methanol (0.1 M, 0.5 mL, 0.050 mmol, 1 equiv.) followed by the addition of a stock solution of (2-aminoethyl)-diisopropylphosphane in THF (10 wt. %, 93.0 µL, 0.050 mmol, 1 equiv.). Then, additional methanol (0.9 mL) was added in order to dissolve all educts completely. The argon atmosphere was then replaced with nitric oxide and the resulting dark brown solution was stirred for 15 minutes. The batch was then transferred to a two-chambered Schlenk tube filled with DMSO (6.0 mL) in the second chamber. After four days, brown single crystals of **2b** suitable for X-ray diffraction were collected.

Yield: 0.006 g (0.010 mmol, 20 %).

Empirical formula: $C_{14}H_{20}CoF_{12}N_2O_3P$ (582.21 g mol^{-1}).

Elemental analysis: found (calcd.): C 28.09 % (28.88 %), H 2.98 % (3.46 %), N 4.67 % (4.81 %).

IR (solid, ATR): $\tilde{\nu}$ = 3301 (vw), 3207 (vw), 3065 (vw), 2994 (vw), 2972 (vw), 2936 (vw), 2903 (vw), 2881 (vw), 1649 (m, NO), 1602 (w), 1474 (vw), 1461 (vw), 1418 (vw), 1395 (vw), 1373 (vw), 1315 (vw), 1256 (m), 1217 (vs), 1202 (s), 1175 (vs), 1139 (s), 1132 (s), 1115 (w), 1103 (s), 1063 (m), 1031 (w), 1016 (vw), 978 (w), 970 (vw), 939 (s), 919 (w), 887 (w), 863 (m), 833 (w), 756 (w), 739 (m), 730 (w), 711 (m), 693 (vw), 672 (w), 666 (w) cm^{-1}.

6.7 Synthesis of perfluoropinacolatocobalt nitrosyls with mono- and diphosphanes as co-ligands

6.7.1 [Co(dppe)(fpin)(NO)] (3a)

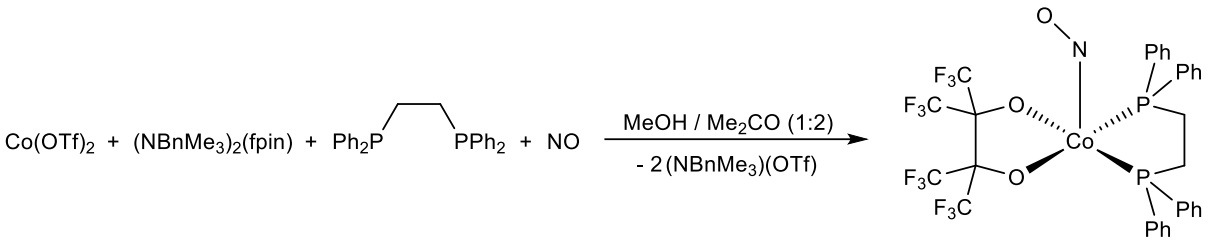

3a

Starting materials:

1,2-Bis(diphenylphosphino)ethane (dppe), $(NBnMe_3)_2$(fpin) stock solution (0.1 M in MeOH), cobalt(II) triflate, nitric oxide, acetone, methanol, dimethyl sulfoxide.

Procedure:

Cobalt(II) triflate (0.018 g, 0.050 mmol, 1 equiv.) was added to a solution of $(NBnMe_3)_2$(fpin) in methanol (0.1 M, 0.5 mL, 0.050 mmol, 1 equiv.) followed by the addition of 1,2-bis(diphenylphosphino)-ethane (0.020 g, 0.050 mmol, 1 equiv.). Then, acetone (1.0 mL) was added in order to dissolve all educts completely. The argon atmosphere was then replaced with nitric oxide and the resulting dark brown solution was stirred for 15 minutes. The batch was then transferred to a two-chambered Schlenk tube filled with DMSO (6.0 mL) in the second chamber. After four days, brown single crystals of **3a** suitable for X-ray diffraction were collected.

Yield: 0.030 g (0.037 mmol, 73 %).

Empirical formula: $C_{32}H_{24}CoF_{12}NO_3P_2$ (819.41 g mol^{-1}).

Elemental analysis: found (calcd.): C 46.81 % (46.91 %), H 2.85 % (2.95 %), N 1.77 % (1.71 %).

IR (solid, ATR): $\tilde{\nu}$ = 3062 (vw), 2363 (vw), 2334 (vw), 2318 (vw), 2158 (vw), 1972 (vw), 1824 (vw), 1645 (s, NO), 1588 (vw), 1573 (vw), 1485 (vw), 1437 (w), 1421 (vw), 1410 (vw), 1340 (vw), 1312 (vw), 1255 (m), 1235 (m), 1221 (vs), 1203 (s), 1182 (vs), 1163 (m), 1152 (m), 1135 (vs), 1114 (m), 1099 (vs), 1074 (w), 1028 (vw), 997 (vw), 978 (vw), 934 (s), 864 (m), 839 (vw), 820 (vw), 804 (vw), 779 (vw), 757 (w), 740 (s), 710 (s), 702 (s), 690 (vs), 676 (s), 662 (w) cm^{-1}.

6.7.2 [Co(dppp)(fpin)(NO)] (3b)

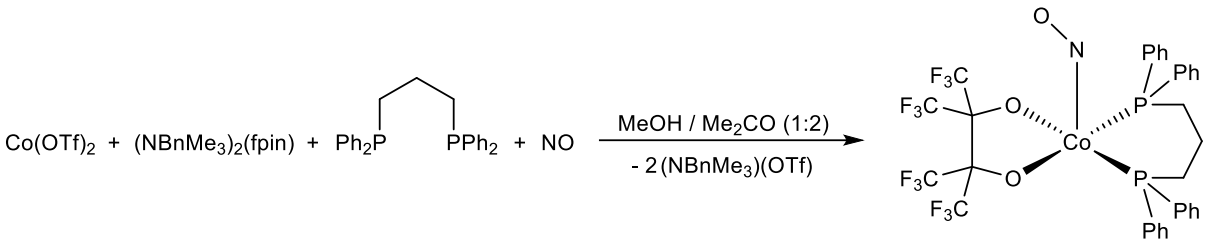

3b

Starting materials:

1,3-Bis(diphenylphosphino)propane (dppp), $(NBnMe_3)_2$(fpin) stock solution (0.1 M in MeOH), cobalt(II) triflate, nitric oxide, acetone, methanol, dimethyl sulfoxide.

Procedure:

Cobalt(II) triflate (0.018 g, 0.050 mmol, 1 equiv.) was added to a solution of $(NBnMe_3)_2$(fpin) in methanol (0.1 M, 0.5 mL, 0.050 mmol, 1 equiv.) followed by the addition of 1,3-bis(diphenylphosphino)-propane (0.021 g, 0.050 mmol, 1 equiv.). Then, acetone (1.0 mL) was added in order to dissolve all educts completely. The argon atmosphere was then replaced with nitric oxide and the resulting dark brown solution was stirred for 15 minutes. The batch was then transferred to a two-chambered Schlenk tube filled with DMSO (6.0 mL) in the second chamber. After four days, brown single crystals of **3b** suitable for X-ray diffraction were collected.

Yield: 0.010 g (0.012 mmol, 24 %).

Empirical formula: $C_{33}H_{26}CoF_{12}NO_3P_2$ (833.44 g mol^{-1}).

Elemental analysis: found (calcd.): C 47.15 % (47.56 %), H 2.81 % (3.14 %), N 1.75 % (1.68 %).

IR (solid, ATR): $\tilde{\nu}$ = 3083 (vw), 3058 (vw), 2941 (vw), 2878 (vw), 2162 (vw), 2024 (vw), 1968 (vw), 1803 (vw), 1652 (m, NO), 1589 (vw), 1574 (vw), 1486 (vw), 1457 (vw), 1436 (w), 1427 (vw), 1410 (vw), 1337 (vw), 1310 (vw), 1249 (m), 1226 (s), 1206 (vs), 1180 (s), 1162 (m), 1150 (m), 1130 (vs), 1109 (s), 1099 (s), 1050 (vw), 1027 (vw), 1001 (vw), 971 (w), 931 (m), 922 (vw), 863 (m), 834 (w), 813 (vw), 795 (vw), 754 (vw), 746 (w), 739 (s), 730 (vw), 711 (m), 705 (w), 688 (s), 670 (m), 656 (w) cm^{-1}.

6.7.3 [Co(dppb)(fpin)(NO)] (3c)

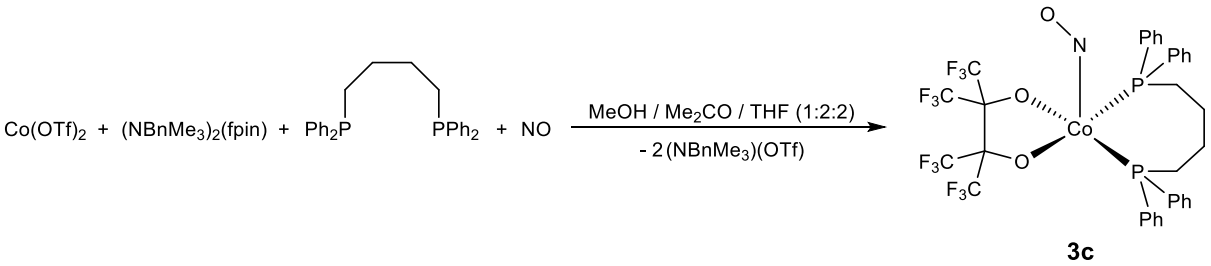

3c

Starting materials:

1,4-Bis(diphenylphosphino)butane (dppb), $(NBnMe_3)_2$(fpin) stock solution (0.1 M in MeOH), cobalt(II) triflate, nitric oxide, acetone, methanol, tetrahydrofuran, dimethyl sulfoxide.

Procedure:

Cobalt(II) triflate (0.018 g, 0.050 mmol, 1 equiv.) was added to a solution of $(NBnMe_3)_2$(fpin) in methanol (0.1 M, 0.5 mL, 0.050 mmol, 1 equiv.) followed by the addition of 1,4-bis(diphenylphosphino)-butane (0.021 g, 0.050 mmol, 1 equiv.). Then, acetone (1.0 mL) and THF (1.0 mL) were added in order to dissolve all educts completely. The argon atmosphere was then replaced with nitric oxide and the resulting dark brown solution was stirred for 15 minutes. The batch was then transferred to a two-chambered Schlenk tube filled with DMSO (1.6 mL) in the second chamber. After four days, a few brown single crystals of **3c** suitable for X-ray diffraction were collected along with precipitated diphosphane.

Yield: n.a., few brown crystals.

Empirical formula: $C_{34}H_{28}CoF_{12}NO_3P_2$ (847.46 g mol^{-1}).

IR (solid, ATR): $\tilde{\nu}$ = 3073 (vw), 3051 (vw), 2931 (vw), 2864 (vw), 2152 (vw), 2099 (vw), 2018 (vw), 1958 (vw), 1905 (vw), 1849 (vw), 1798 (vw), 1654 (m, NO), 1588 (vw), 1574 (vw), 1485 (vw), 1462 (vw), 1449 (vw), 1435 (w), 1416 (vw), 1335 (vw), 1309 (vw), 1248 (m), 1234 (m) 1226 (s), 1208 (vs), 1179 (vs), 1160 (m), 1149 (w), 1128 (s), 1106 (s), 1100 (s), 1075 (w), 1028 (w), 999 (w), 977 (w), 969 (vw), 955 (vw), 930 (m), 898 (w), 881 (w), 864 (m), 843 (w), 826 (vw), 798 (vw), 791 (vw), 758 (w), 740 (s), 729 (w), 712 (m), 691 (vs), 672 (m), 654 (w) cm^{-1}.

6.7.4 [Co(fpin)(NO)(PMePh$_2$)$_2$] (3d)

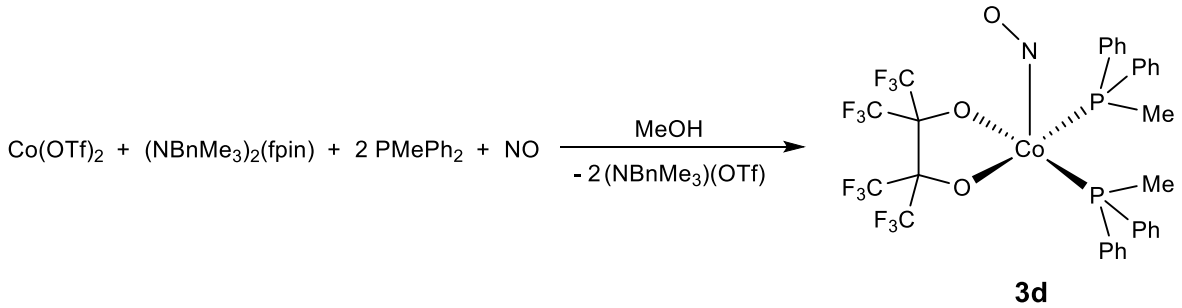

3d

Starting materials:

Methyldiphenylphosphane (PMePh$_2$), (NBnMe$_3$)$_2$(fpin) solution (0.1 M in MeOH), cobalt(II) triflate, nitric oxide, methanol, dimethyl sulfoxide.

Procedure:

One compartment of a two-chambered Schlenk tube was loaded with cobalt(II) triflate (0.018 g, 0.050 mmol, 1 equiv.) and a stock solution of (NBnMe$_3$)$_2$(fpin) in methanol (0.1 M, 0.5 mL, 0.050 mmol, 1 equiv.) followed by the addition of methyldiphenylphosphane (19.0 µL, 0.100 mmol, 2 equiv.). Then, additional MeOH (1.0 mL) was added to dissolve all educts completely. The second chamber was filled with DMSO (6.0 mL). The argon atmosphere was then replaced with nitric oxide. Stirring of the resulting dark brown reaction mixture was quickly discontinued just after 15 seconds and the gas atmosphere was changed back to argon for crystallization. After two days, brown single crystals of **3d** suitable for X-ray diffraction were collected.

Yield: 0.005 g (0.006 mmol, 12 %).

Empirical formula: $C_{32}H_{26}CoF_{12}NO_3P_2$ (821.43 g mol^{-1}).

Elemental analysis: found (calcd.): C 46.58 % (46.79 %), H 2.95 % (3.19 %), N 1.76 % (1.71 %).

IR (solid, ATR): $\tilde{\nu}$ = 3079 (vw), 3054 (vw), 2928 (vw), 2892 (vw), 2156 (vw), 1993 (vw), 1644 (s, NO), 1587 (vw), 1571 (vw), 1485 (vw), 1474 (vw), 1435 (w), 1411 (vw), 1338 (vw), 1315 (vw), 1287 (vw), 1246 (w), 1226 (vs), 1213 (s), 1180 (s), 1174 (s), 1164 (m), 1144 (m), 1132 (s), 1102 (vs), 1028 (w), 1015 (vw), 998 (vw), 980 (w), 972 (vw), 931 (m), 910 (vw), 882 (m), 863 (m), 791 (vw), 779 (vw), 751 (vw), 738 (s), 711 (m), 690 (s), 675 (m), 662 (vw), 654 (vw) cm^{-1}.

6.8 Synthesis of bis(diamine)cobalt nitrosyls with anionic and neutral co-ligands in *trans* position

6.8.1 *trans*-$[Co(ClO_4)(en)_2(NO)]ClO_4$ (4a)

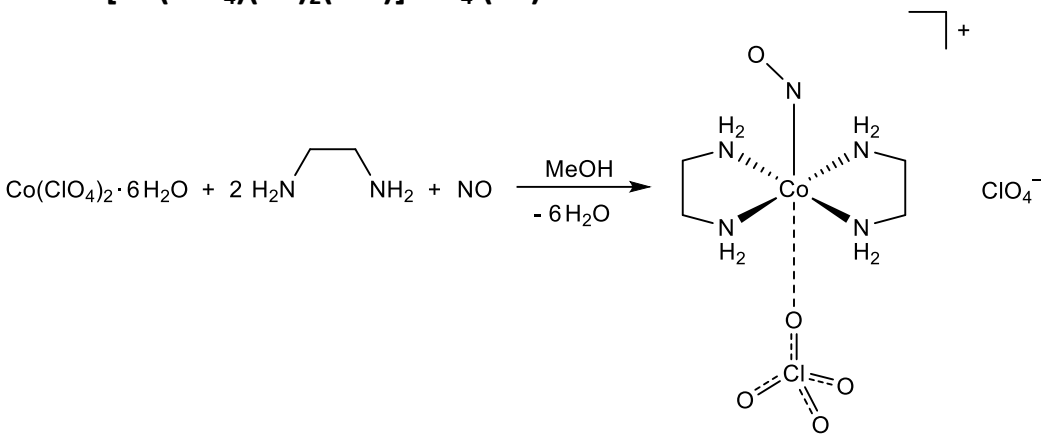

4a

According to:

R. D. Feltham, R. S. Nyholm, *Inorg. Chem.* **1965**, *4*, 1334–1339.

Starting materials:

Ethylenediamine (en), cobalt(II) perchlorate hexahydrate, nitric oxide, methanol, diethyl ether, water, dimethyl sulfoxide.

Procedure:

To a solution of cobalt(II) perchlorate hexahydrate (0.110 g, 0.300 mmol, 1 equiv.) in MeOH (1.2 mL), ethylenediamine (40.0 µL, 0.600 mmol, 2 equiv.) was added. The argon atmosphere was then replaced with nitric oxide, resulting in the formation of **4a** as a dark red precipitate. The solid was filtered off, washed with diethyl ether (3×5.0 mL) and air-dried for 15 minutes. For crystallization, one compartment of a two-chambered Schlenk tube was loaded with a solution of the bulk product (0.025 g) in water (0.5 mL), while the second chamber was filled with DMSO (6.0 mL). After five days, brown single crystals of **4a** suitable for X-ray diffraction were collected.

Yield (crystals)**:** 0.074 g (0.181 mmol, 60 %).

Empirical formula: $C_4H_{16}Cl_2CoN_5O_9$ (408.03 g mol^{-1}).

Elemental analysis: found (calcd.): C 11.90 % (11.77 %), H 3.87 % (3.95 %), N 17.10 % (17.16 %).

IR (solid, ATR): $\tilde{\nu}$ = 3306 (vw), 3256 (w), 3150 (vw), 2963 (vw), 2896 (vw), 1657 (w, NO), 1606 (vw), 1590 (m), 1462 (vw), 1397 (vw), 1370 (vw), 1322 (vw), 1288 (vw), 1225 (vw), 1170 (vw), 1129 (m), 1087 (s), 1063 (vs), 1049 (vs), 997 (m), 936 (w), 890 (vw), 870 (vw), 775 (w), 698 (vw), 683 (vw), 661 (vw) cm^{-1}.

6.8.2 *trans*-[CoCl(en)$_2$(NO)]Cl·H$_2$O (4b·H$_2$O)

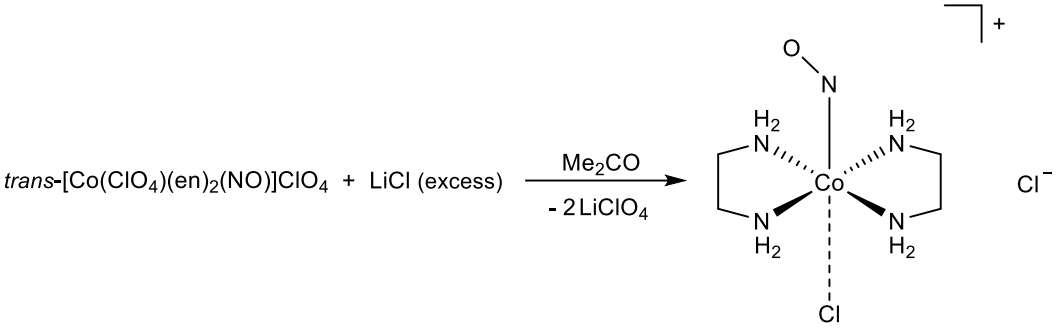

4b

According to:

R. D. Feltham, R. S. Nyholm, *Inorg. Chem.* **1965**, *4*, 1334–1339.

Starting materials:

tr.-[Co(ClO$_4$)(en)$_2$(NO)]ClO$_4$ (**4a**),[85] lithium chloride, acetone, diethyl ether, water, dimethyl sulfoxide.

Procedure:

To a solution of *trans*-[Co(ClO$_4$)(en)$_2$(NO)]ClO$_4$ (**4a**) (0.082 g, 0.200 mmol, 1 equiv.) in Me$_2$CO (15.0 mL), lithium chloride (0.051 g, 1.200 mmol, 6 equiv.) was added in small portions under vigorous stirring, resulting in the formation of **4b** as a brown precipitate. After further 20 minutes of strirring, the solid was collected, washed with acetone (3×25.0 mL) and diethyl ether (3×15.0 mL) and air-dried for 15 minutes. For crystallization, one compartment of a two-chambered Schlenk tube was loaded with a solution of the bulk product (0.025 g) in water (0.5 mL), while the second chamber was filled with DMSO (8.0 mL). After six days, brown single crystals of **4b**·H$_2$O suitable for X-ray diffraction were collected.

Yield (crystals)**:** 0.021 g (0.070 mmol, 35 %).

Empirical formula: $C_4H_{18}Cl_2CoN_5O_2$ (298.05 g mol^{-1}).

Elemental analysis: found (calcd.): C 15.63 % (16.12 %), H 5.84 % (6.09 %), N 17.76 % (23.50 %).

IR (solid, ATR): $\tilde{\nu}$ = 3385 (m), 3343 (m), 3305 (m), 3266 (m), 3230 (s), 3195 (s), 3130 (m), 3100 (s), 2959 (w), 2877 (vw), 2351 (vw), 2114 (vw), 1629 (vs, NO), 1595 (vs), 1578 (vs), 1457 (w), 1450 (m), 1418 (w), 1386 (w), 1364 (w), 1341 (w), 1317 (w), 1296 (w), 1281 (m), 1227 (w), 1178 (w), 1156 (w), 1118 (s), 1052 (vs), 1012 (vs), 990 (s), 951 (m), 888 (w), 854 (w), 827 (w), 786 (m), 742 (m), 713 (m), 683 (m), 670 (s), 658 (s) cm^{-1}.

6.8.3 *trans*-$[Co(en)_2I(NO)](ClO_4)_{0.6}I_{0.4}$ (4c)

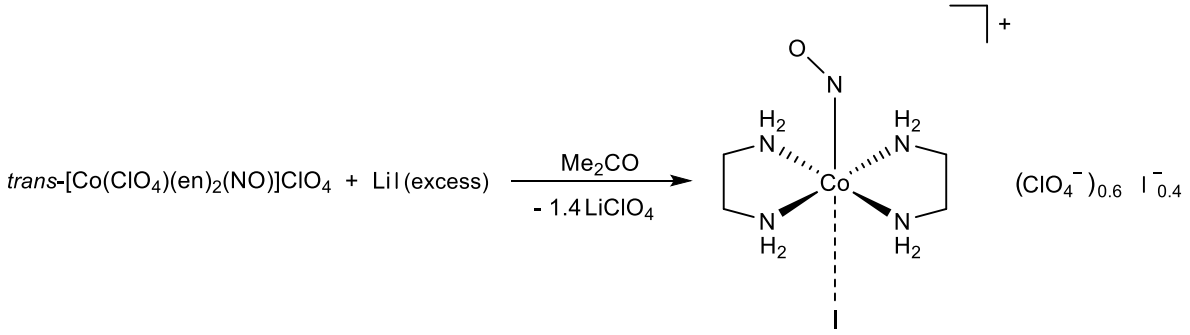

4c

According to:

R. D. Feltham, R. S. Nyholm, *Inorg. Chem.* **1965**, *4*, 1334–1339.

Starting materials:

trans-$[Co(ClO_4)(en)_2(NO)]ClO_4$ (**4a**),[85] lithium iodide, acetone, diethyl ether, water, dimethyl sulfoxide.

Procedure:

To a solution of *trans*-$[Co(ClO_4)(en)_2(NO)]ClO_4$ (**4a**) (0.082 g, 0.200 mmol, 1 equiv.) in Me_2CO (15.0 mL), lithium iodide (0.161 g, 1.200 mmol, 6 equiv.) was added in small portions under vigorous stirring, resulting in the formation of **4c** as a brown precipitate. After further 20 minutes of strirring, the solid was collected, washed with acetone (3×25.0 mL) and diethyl ether (3×15.0 mL) and air-dried for 15 minutes. For crystallization, one compartment of a two-chambered Schlenk tube was loaded with a solution of the bulk product (0.042 g) in water (0.5 mL), while the second chamber was filled with DMSO (8.0 mL). After six days, brown single crystals of **4c** suitable for X-ray diffraction were collected.

Yield (crystals)**:** 0.029 g (0.065 mmol, 33 %).

Empirical formula: $C_4H_{16}Cl_{0.6}CoI_{1.4}N_5O_{3.4}$ (446.47 g mol^{-1}).

Elemental analysis: found (calcd.): C 11.06 % (10.76 %), H 3.58 % (3.61 %), N 14.25 % (15.69 %).

IR (solid, ATR): $\tilde{\nu}$ = 3286 (vw), 3252 (vw), 3179 (w), 3157 (w), 3101 (w), 2985 (vw), 2945 (vw), 2873 (vw), 2353 (vw), 2116 (vw), 1880 (vw), 1632 (s, NO), 1593 (w), 1565 (vs), 1462 (w), 1446 (m), 1394 (w), 1360 (vw), 1316 (vw), 1279 (w), 1264 (vw), 1205 (vw), 1141 (vw), 1109 (m), 1100 (s), 1096 (s), 1074 (s), 1049 (vs), 1030 (m), 1007 (m), 997 (m), 984 (s), 954 (w), 936 (w), 880 (w), 769 (m), 719 (vw), 684 (w), 667 (vw), 654 (vw) cm^{-1}.

6.8.4 *trans*-$[Co(en)_2(NO)(NO_3)]NO_3$ (4d)

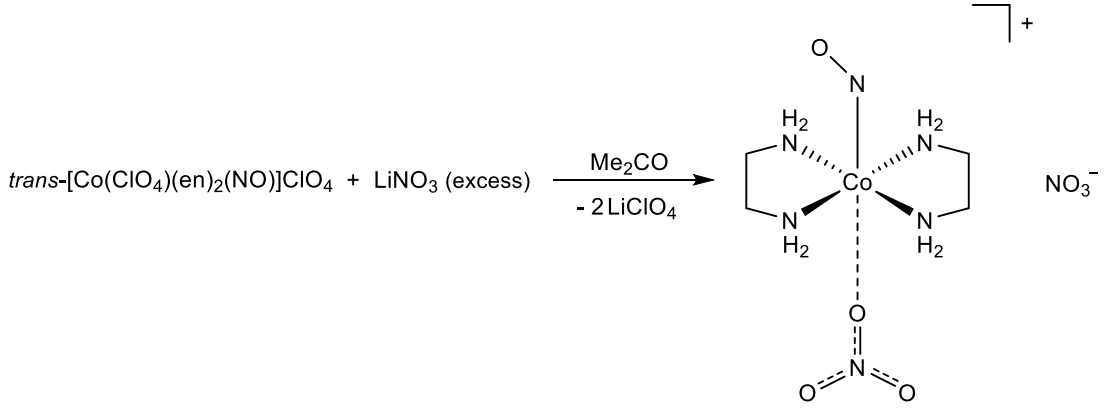

4d

According to:

R. D. Feltham, R. S. Nyholm, *Inorg. Chem.* **1965**, *4*, 1334–1339.

Starting materials:

tr.-$[Co(ClO_4)(en)_2(NO)]ClO_4$ (**4a**),[85] lithium nitrate, acetone, diethyl ether, water, dimethyl sulfoxide.

Procedure:

To a solution of *trans*-$[Co(ClO_4)(en)_2(NO)]ClO_4$ (**4a**) (0.082 g, 0.200 mmol, 1 equiv.) in Me_2CO (15.0 mL), lithium nitrate (0.083 g, 1.200 mmol, 6 equiv.) was added in small portions under vigorous stirring, resulting in the formation of **4d** as a brown precipitate. After further 20 minutes of strirring, the solid was collected, washed with acetone (3×25.0 mL) and diethyl ether (3×15.0 mL) and air-dried for 15 minutes. For crystallization, one compartment of a two-chambered Schlenk tube was loaded with a solution of the bulk product (0.044 g) in water (0.5 mL), while the second chamber was filled with DMSO (8.0 mL). After six days, brown single crystals of **4d** suitable for X-ray diffraction were collected.

Yield (crystals)**:** 0.018 g (0.054 mmol, 27 %).

Empirical formula: $C_4H_{16}CoN_7O_7$ (333.15 g mol^{-1}).

Elemental analysis: found (calcd.): C 14.35 % (14.42 %), H 4.64 % (4.84 %), N 29.35 % (29.43 %).

IR (solid, ATR): $\tilde{\nu}$ = 3383 (vw), 3315 (w), 3292 (w), 3285 (w), 3257 (w), 3233 (w), 3223 (w), 3148 (w), 2994 (vw), 2977 (vw), 2959 (vw), 2913 (vw), 2347 (vw), 1753 (vw), 1636 (s, NO), 1598 (s), 1466 (vw), 1456 (vw), 1435 (vw), 1398 (m), 1373 (s), 1343 (vs), 1317 (vs), 1308 (vs), 1266 (s), 1159 (w), 1101 (s), 1055 (s), 1043 (s), 1015 (s), 988 (s), 952 (m), 896 (w), 889 (w), 865 (w), 825 (m), 786 (m), 748 (m), 711 (m), 696 (m), 660 (w) cm^{-1}.

6.8.5 *trans*-[Co(BF$_4$)(en)$_2$(NO)]BF$_4$ (4e)

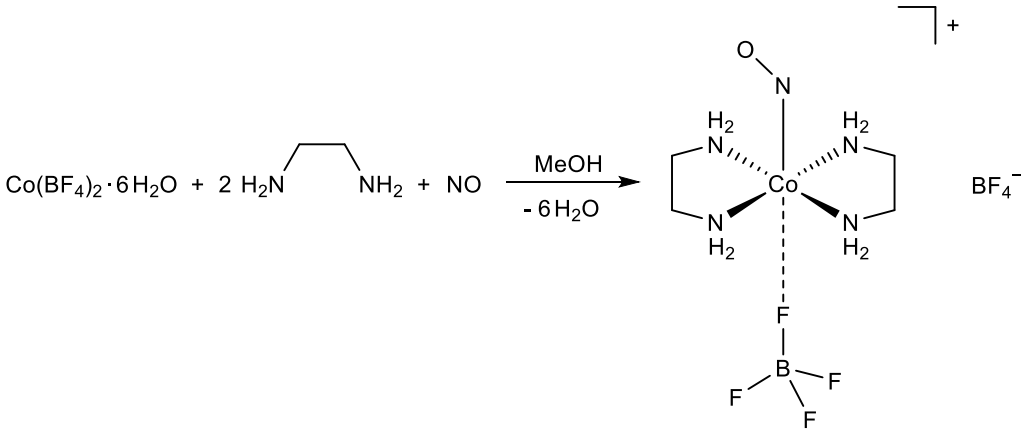

4e

Starting materials:

Ethylenediamine (en), cobalt(II) tetrafluoroborate hexahydrate, nitric oxide, methanol, dimethyl sulfoxide.

Procedure:

One compartment of a two-chambered Schlenk tube was loaded with cobalt(II) tetrafluoroborate hexahydrate (0.102 g, 0.300 mmol, 1 equiv.) and MeOH (1.2 mL) followed by the addition of ethylenediamine (40.0 µL, 0.600 mmol, 2 equiv.). The second chamber was filled with DMSO (6.0 mL). The argon atmosphere was then replaced with nitric oxide. Stirring of the resulting dark red reaction mixture was discontinued after 5 minutes and the gas atmosphere was changed back to argon for crystallization. After two days, brown single crystals of **4e** suitable for X-ray diffraction were collected.

Yield: 0.017 g (0.044 mmol, 15 %).

Empirical formula: $C_4H_{16}B_2CoF_8N_5O$ (382.75 g mol^{-1}).

Elemental analysis: found (calcd.): C 12.52 % (12.55 %), H 3.98 % (4.21 %), N 18.07 % (18.30 %).

IR (solid, ATR): $\tilde{\nu}$ = 3605 (vw), 3324 (w), 3283 (w), 3213 (vw), 3167 (vw), 2972 (vw), 2903 (vw), 1792 (vw), 1704 (vw), 1659 (m, NO), 1613 (vw), 1598 (w), 1464 (vw), 1439 (vw), 1417 (vw), 1402 (vw), 1377 (vw), 1325 (vw), 1289 (vw), 1227 (vw), 1163 (vw), 1134 (w), 1110 (w), 1046 (vs), 1008 (vs), 993 (vs), 961 (s), 895 (w), 872 (vw), 772 (w), 728 (vw), 700 (vw), 673 (vw), 661 (vw) cm^{-1}.

6.8.6 *trans*-[Co(dmso-κ*O*)(en)$_2$(NO)](ClO$_4$)$_2$·DMSO (4f·DMSO)

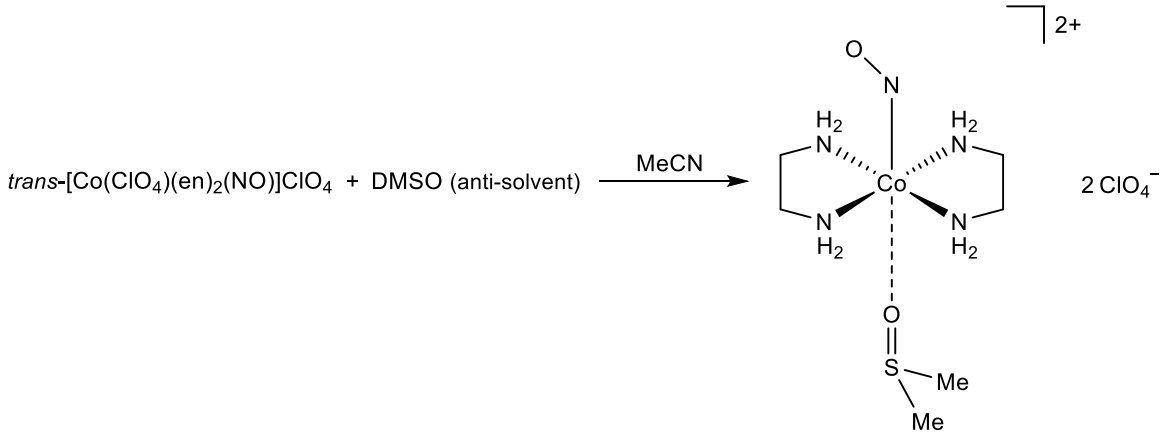

4f

Starting materials:

trans-[Co(ClO$_4$)(en)$_2$(NO)]ClO$_4$ (**4a**),[85] acetonitrile, dimethyl sulfoxide.

Procedure:

One compartment of a two-chambered Schlenk tube was loaded with a solution of the precursor *trans*-[Co(ClO$_4$)(en)$_2$(NO)]ClO$_4$ (**4a**) (0.041 g, 0.100 mmol, 1 equiv.) in acetonitrile (3.0 mL). The second chamber was filled with DMSO (6.0 mL). The tube was then sealed and the batch was left under argon atmosphere for crystallization. After four days, brown single crystals of **4f**·DMSO suitable for X-ray diffraction were collected.

Yield: 0.009 g (0.016 mmol, 16 %).

Empirical formula: $C_8H_{28}Cl_2CoN_5O_{11}S_2$ (564.29 g mol^{-1}).

Elemental analysis: found (calcd.): C 16.72 % (17.03 %), H 4.55 % (5.00 %), N 11.91 % (12.41 %).

IR (solid, ATR): $\tilde{\nu}$ = 3534 (vw), 3316 (w), 3261 (w), 3156 (vw), 3111 (vw), 3011 (vw), 2966 (vw), 2911 (vw), 2901 (vw), 2322 (vw), 1982 (vw), 1638 (m, NO), 1601 (w), 1592 (w), 1467 (vw), 1457 (vw), 1439 (vw), 1406 (vw), 1369 (vw), 1338 (vw), 1316 (vw), 1294 (vw), 1281 (vw), 1211 (vw), 1154 (vw), 1084 (vs), 1050 (vs), 1022 (vs), 1009 (vs), 988 (s), 961 (s), 953 (s), 932 (m), 901 (w), 884 (w), 862 (vw), 813 (vw), 774 (w), 702 (w), 688 (vw), 671 (vw), 657 (vw) cm^{-1}.

6.8.7 *trans*-[Co(ClO$_4$)(men)$_2$(NO)]ClO$_4$ (4g)

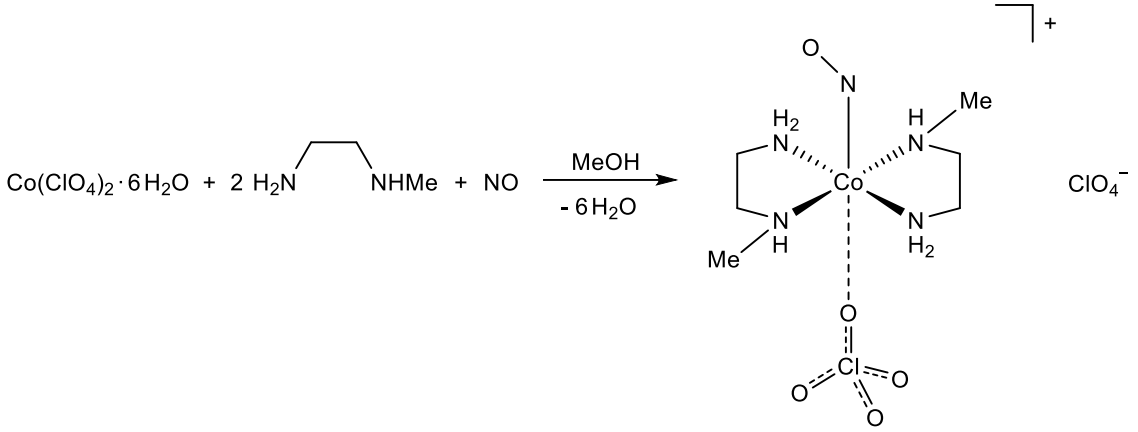

4g

Starting materials:

N-Methylethylenediamine (men), cobalt(II) perchlorate hexahydrate, nitric oxide, methanol.

Procedure:

To a solution of cobalt(II) perchlorate hexahydrate (0.110 g, 0.300 mmol, 1 equiv.) in MeOH (1.2 mL), *N*-methylethylenediamine (52.0 µL, 0.600 mmol, 2 equiv.) was added. The argon atmosphere was then replaced with nitric oxide and the resulting dark red solution was stirred for 15 minutes. The batch was then stored under NO atmosphere at −25 °C. After four days, brown single crystals of **4g** suitable for X-ray diffraction were collected.

Yield: 0.030 g (0.069 mmol, 23 %).

Empirical formula: $C_6H_{20}Cl_2CoN_5O_9$ (436.09 g mol^{-1}).

Elemental analysis: found (calcd.): C 16.87 % (16.53 %), H 4.55 % (4.62 %), N 14.72 % (16.06 %).

IR (solid, ATR): $\tilde{\nu}$ = 3545 (vw), 3297 (vw), 3234 (w), 3159 (vw), 2991 (vw), 2956 (vw), 2888 (vw), 2829 (vw), 2166 (vw), 2007 (vw), 1653 (m, NO), 1593 (w), 1467 (vw), 1455 (w), 1424 (vw), 1396 (vw), 1348 (vw), 1315 (vw), 1289 (vw), 1261 (vw), 1196 (vw), 1157 (vw), 1087 (s), 1061 (vs), 1051 (vs), 1032 (vs), 1019 (vs), 996 (vs), 973 (m), 931 (w), 904 (w), 840 (w), 827 (vw), 707 (vw), 673 (vw) cm^{-1}.

6.8.8 *trans*-[Co(ClO$_4$)(*N*,*N*-dmen)$_2$(NO)]ClO$_4$ (4h)

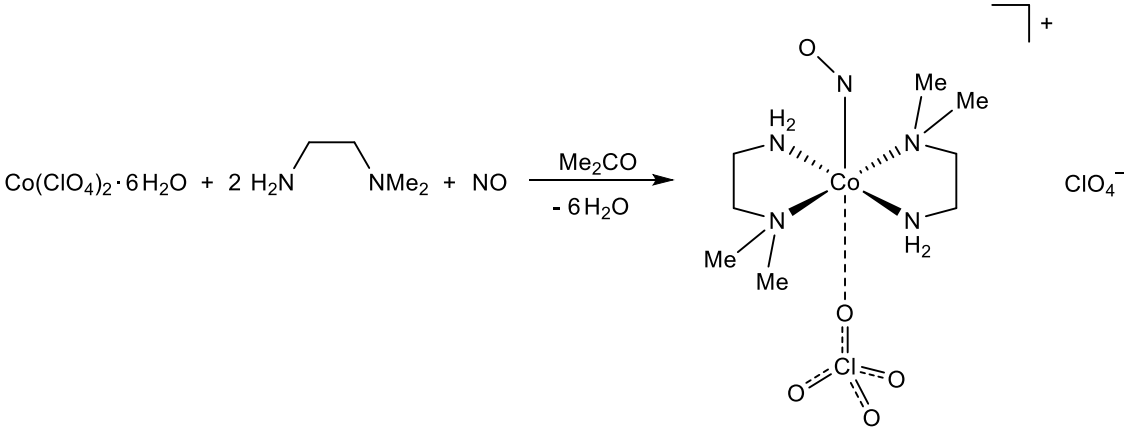

4h

Starting materials:

N,*N*-Dimethylethylenediamine (*N*,*N*-dmen), cobalt(II) perchlorate hexahydrate, nitric oxide, acetone, dimethyl sulfoxide.

Procedure:

To a solution of cobalt(II) perchlorate hexahydrate (0.110 g, 0.300 mmol, 1 equiv.) in acetone (1.2 mL), *N*,*N*-dimethylethylenediamine (66.0 µL, 0.600 mmol, 2 equiv.) was added. The argon atmosphere was then replaced with nitric oxide and the resulting dark red solution was stirred for 15 minutes. After that, the batch was transferred to a two-chambered Schlenk tube filled with DMSO (6.0 mL) in the second chamber. After three days, brown single crystals of **4h** suitable for X-ray diffraction were collected.

Yield: 0.013 g (0.028 mmol, 9 %).

Empirical formula: $C_8H_{24}Cl_2CoN_5O_9$ (464.14 g mol^{-1}).

Elemental analysis: found (calcd.): C 20.41 % (20.70 %), H 5.07 % (5.21 %), N 14.99 % (15.09 %).

IR (solid, ATR): $\tilde{\nu}$ = 3520 (vw), 3337 (vw), 3299 (vw), 3257 (vw), 3166 (vw), 2977 (vw), 2939 (vw), 2890 (vw), 2851 (vw), 2162 (vw), 2011 (vw), 1869 (vw), 1793 (vw), 1700 (vw), 1655 (w, NO), 1596 (vw), 1476 (w), 1464 (w), 1437 (vw), 1415 (vw), 1397 (vw), 1370 (vw), 1317 (vw), 1289 (vw), 1237 (vw), 1201 (vw), 1168 (vw), 1077 (vs), 1049 (vs), 997 (m), 984 (s), 931 (m), 903 (w), 884 (w), 834 (vw), 826 (vw), 780 (m), 726 (vw), 698 (vw), 669 (vw), 652 (vw) cm^{-1}.

6.8.9 *trans*-[Co(BF$_4$)(*N*,*N*-dmen)$_2$(NO)]BF$_4$ (4i)

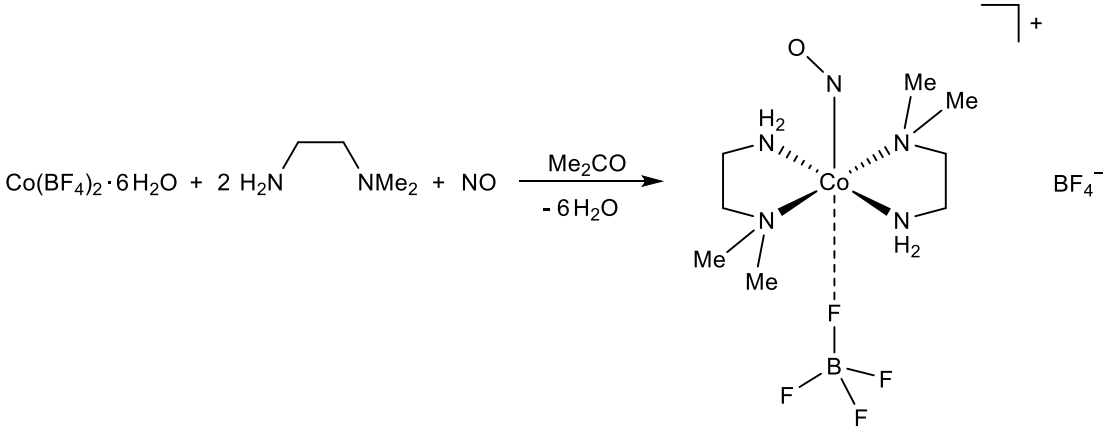

4i

Starting materials:

N,*N*-Dimethylethylenediamine (*N*,*N*-dmen), cobalt(II) tetrafluoroborate hexahydrate, nitric oxide, acetone, dimethyl sulfoxide.

Procedure:

To a solution of cobalt(II) tetrafluoroborate hexahydrate (0.102 g, 0.300 mmol, 1 equiv.) in acetone (1.2 mL), *N*,*N*-dimethylethylenediamine (66.0 µL, 0.600 mmol, 2 equiv.) was added. The argon atmosphere was then replaced with nitric oxide and the resulting dark red solution was stirred for 15 minutes. After that, the batch was transferred to a two-chambered Schlenk tube filled with DMSO (5.5 mL) in the second chamber. After two days, brown single crystals of **4i** suitable for X-ray diffraction were collected.

Yield: 0.016 g (0.036 mmol, 12 %).

Empirical formula: $C_8H_{24}B_2CoF_8N_5O$ (438.85 g mol^{-1}).

Elemental analysis: found (calcd.): C 21.62 % (21.90 %), H 5.53 % (5.51 %), N 15.71 % (15.96 %).

IR (solid, ATR): $\tilde{\nu}$ = 3558 (vw), 3320 (vw), 3277 (vw), 3181 (vw), 2941 (vw), 2913 (vw), 2158 (vw), 1993 (vw), 1656 (m, NO), 1602 (w), 1479 (w), 1468 (w), 1438 (vw), 1416 (vw), 1401 (vw), 1361 (vw), 1318 (vw), 1290 (vw), 1237 (vw), 1203 (w), 1171 (vw), 1143 (vw), 1120 (w), 1073 (s), 1049 (vs), 1036 (vs), 1022 (vs), 1000 (s), 981 (vs), 972 (vs), 935 (s), 906 (w), 900 (w), 825 (vw), 811 (vw), 781 (m), 767 (w), 725 (vw), 712 (vw), 699 (vw), 691 (vw), 677 (vw), 665 (vw) cm^{-1}.

6.8.10 *trans*-[Co(ClO$_4$)(*N*,*N*'-dmen)$_2$(NO)]ClO$_4$ (4j)

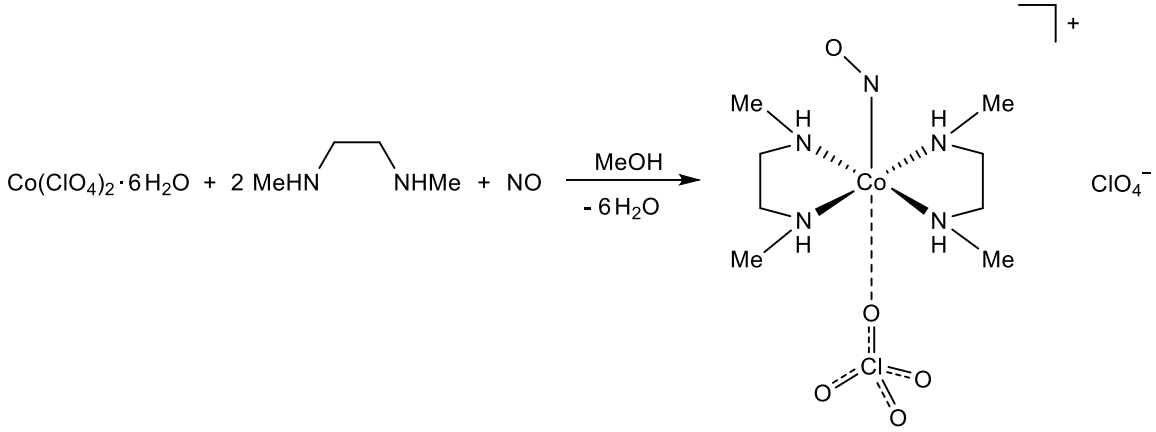

4j

Starting materials:

N,*N*'-Dimethylethylenediamine (*N*,*N*'-dmen), cobalt(II) perchlorate hexahydrate, nitric oxide, methanol, diethyl ether.

Procedure:

To a solution of cobalt(II) perchlorate hexahydrate (0.110 g, 0.300 mmol, 1 equiv.) in MeOH (1.2 mL), *N*,*N*'-dimethylethylenediamine (65.0 µL, 0.600 mmol, 2 equiv.) was added. The argon atmosphere was then replaced with nitric oxide oxide, resulting in the formation of **4j** as a dark red precipitate. The microcrystalline product was filtered off, washed with diethyl ether (3×5.0 mL) and then air-dried for 15 minutes.

Yield: 0.020 g (0.043 mmol, 14 %).

Empirical formula: $C_8H_{24}Cl_2CoN_5O_9$ (464.14 g mol^{-1}).

Elemental analysis: found (calcd.): C 20.55 % (20.70 %), H 5.18 % (5.21 %), N 15.21 % (15.09 %).

IR (solid, ATR): $\tilde{\nu}$ = 3284 (vw), 3238 (vw), 2956 (vw), 2194 (vw), 1979 (vw), 1651 (w, NO), 1485 (vw), 1456 (vw), 1417 (vw), 1375 (vw), 1343 (vw), 1295 (vw), 1276 (vw), 1232 (vw), 1187 (vw), 1167 (vw), 1133 (w), 1101 (s), 1064 (vs), 1037 (vs), 988 (m), 976 (m), 968 (w), 932 (w), 862 (w), 822 (w), 794 (vw), 732 (vw), 720 (vw), 690 (vw), 670 (vw), 661 (vw) cm^{-1}.

6.8.11 *trans*-[Co(BF$_4$)(*N*,*N*'-dmen)$_2$(NO)]BF$_4$ (4k)

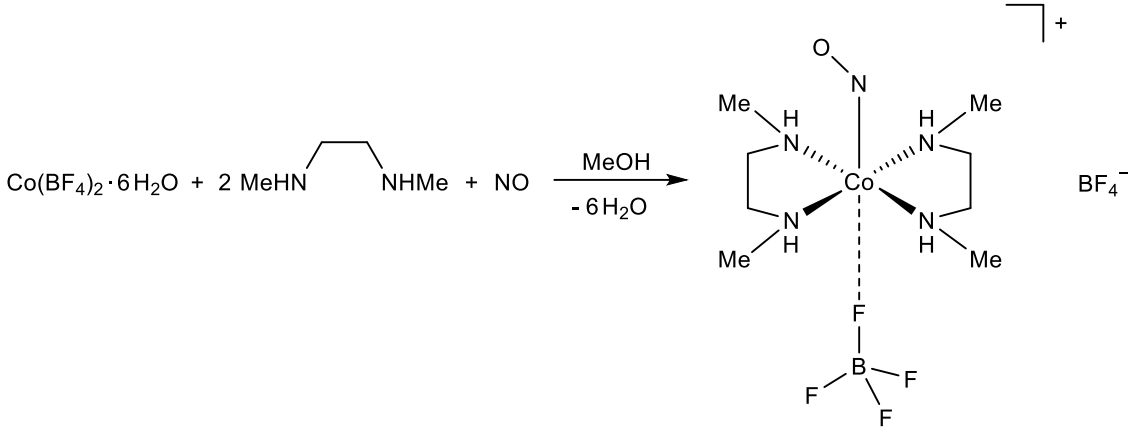

4k

Starting materials:

N,*N*'-Dimethylethylenediamine (*N*,*N*'-dmen), cobalt(II) tetrafluoroborate hexahydrate, nitric oxide, methanol, diethyl ether.

Procedure:

To a solution of cobalt(II) tetrafluoroborate hexahydrate (0.102 g, 0.300 mmol, 1 equiv.) in methanol (1.2 mL), *N*,*N*'-dimethylethylenediamine (65.0 µL, 0.600 mmol, 2 equiv.) was added. The argon atmosphere was then replaced with nitric oxide oxide, resulting in the formation of **4k** as a dark red precipitate. The microcrystalline product was filtered off, washed with diethyl ether (3×5.0 mL) and air-dried for 15 minutes.

Yield: 0.057 g (0.130 mmol, 43 %).

Empirical formula: $C_8H_{24}B_2CoF_8N_5O$ (438.85 g mol^{-1}).

Elemental analysis: found (calcd.): C 21.61 % (21.90 %), H 5.45 % (5.51 %), N 15.87 % (15.96 %).

IR (solid, ATR): $\tilde{\nu}$ = 3305 (vw), 3256 (vw), 3044 (vw), 2994 (vw), 2960 (vw), 2183 (vw), 1652 (w, NO), 1482 (vw), 1461 (vw), 1420 (vw), 1375 (vw), 1345 (vw), 1295 (vw), 1232 (vw), 1191 (vw), 1165 (vw), 1139 (w), 1083 (s), 1062 (s), 1051 (s), 1025 (vs), 1014 (vs), 1000 (vs), 987 (vs), 974 (vs), 862 (w), 823 (vw), 800 (vw), 769 (vw), 748 (vw), 702 (vw), 695 (vw), 678 (vw), 663 (vw) cm^{-1}.

6.8.12 *trans*-[Co(bnen)$_2$(NO)(NO$_3$)]NO$_3$·MeOH (4l·MeOH)

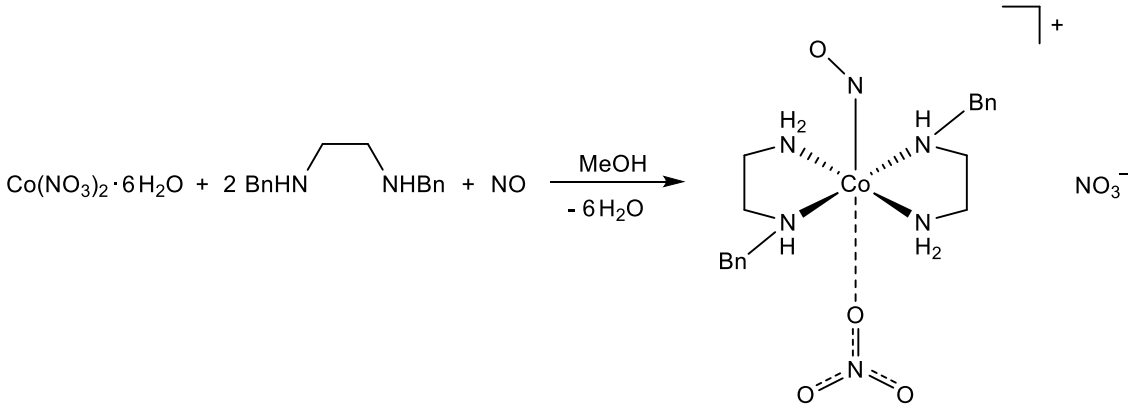

4l

Starting materials:

N-Benzylethylenediamine (bnen), cobalt(II) nitrate hexahydrate, nitric oxide, methanol, dimethyl sulfoxide.

Procedure:

To a solution of cobalt(II) nitrate hexahydrate (0.029 g, 0.100 mmol, 1 equiv.) in methanol (1.5 mL), *N*-benzylethylenediamine (30.0 µL, 0.200 mmol, 2 equiv.) was added. The argon atmosphere was then replaced with nitric oxide and the resulting dark red solution was stirred for 15 minutes. After that, the batch was transferred to a two-chambered Schlenk tube filled with DMSO (7.0 mL) in the second chamber. After two days, brown single crystals of **4l**·MeOH suitable for X-ray diffraction were collected.

Yield: 0.019 g (0.035 mmol, 35 %).

Empirical formula: $C_{19}H_{32}CoN_7O_8$ (545.44 g mol^{-1}).

Elemental analysis: found (calcd.): C 40.98 % (41.84 %), H 5.51 % (5.91 %), N 18.47 % (17.98 %).

IR (solid, ATR): $\tilde{\nu}$ = 3474 (vw), 3273 (vw), 3217 (w), 3133 (w), 2956 (vw), 2892 (vw), 2356 (vw), 1785 (vw), 1753 (vw), 1665 (w), 1650 (m, NO), 1603 (w), 1496 (vw), 1455 (w), 1389 (vs), 1359 (vs), 1325 (vs), 1307 (vs), 1283 (vs), 1203 (w), 1168 (m), 1109 (w), 1071 (w), 1038 (m), 1007 (m), 949 (w), 923 (vw), 907 (vw), 835 (vw), 823 (w), 754 (m), 723 (vw), 701 (vs), 670 (vw) cm^{-1}.

6.9 Synthesis of bis(diphosphane)cobalt nitrosyls

6.9.1 $[Co(dppe)_2(NO)](ClO_4)_2 \cdot 2.7\,Me_2CO \cdot 0.3\,DMSO$ (5a·2.7 Me_2CO · 0.3 DMSO)

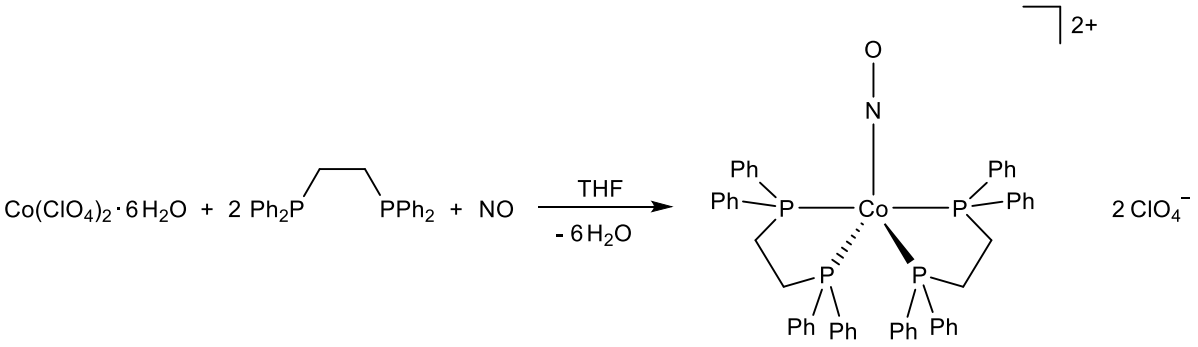

5a

Starting materials:

1,2-Bis(diphenylphosphino)ethane (dppe), cobalt(II) perchlorate hexahydrate, nitric oxide, tetrahydrofuran, acetone, dimethyl sulfoxide.

Procedure:

To a solution of cobalt(II) perchlorate hexahydrate (0.037 g, 0.100 mmol, 1 equiv.) in THF (3.0 mL), 1,2-bis(diphenylphosphino)ethane (0.080 g, 0.200 mmol, 2 equiv.) was added. The argon atmosphere was then replaced with nitric oxide and the reaction mixture stirred overnight, during which time the initially yellow precipitate that had formed upon addition of the diphosphane turned brown. For crystallization, the solvent was removed in vacuo and acetone was added until the bulk product was completely dissolved. This solution (2.0 mL) was then transferred to one compartment of a two-chambered Schlenk tube with the second chamber being filled with DMSO (6.0 mL). After three days, brown single crystals of **5a**·2.7 Me_2CO · 0.3 DMSO suitable for X-ray diffraction were collected.

Yield (bulk)**:** 0.033 g (0.030 mmol, 30 %).

Empirical formula: $C_{52}H_{48}Cl_2CoNO_9P_4$ (1084.68 g mol^{-1}).

Elemental analysis: found (calcd.): C 57.76 % (57.58 %), H 4.81 % (4.46 %), N 1.14 % (1.29 %).

IR (solid, ATR): $\tilde{\nu}$ = 3495 (vw), 3086 (vw), 3058 (vw), 2968 (vw), 2941 (vw), 2195 (vw), 1986 (vw), 1909 (vw), 1852 (vw), 1813 (w, NO), 1705 (vw), 1584 (vw), 1574 (vw), 1481 (vw), 1434 (m), 1418 (vw), 1358 (vw), 1337 (vw), 1313 (vw), 1281 (vw), 1251 (vw), 1221 (vw), 1184 (vw), 1167 (vw), 1115 (w), 1079 (vs), 1025 (w), 997 (m), 951 (w), 911 (vw), 875 (vw), 840 (vw), 815 (vw), 801 (vw), 765 (vw), 752 (w), 739 (m), 723 (m), 715 (m), 692 (vs), 669 (w) cm^{-1}.

6.9.2 $[Co(dppe)_2(NO)](BF_4)_2 \cdot 2\,Me_2CO$ (5a'·2 Me_2CO)

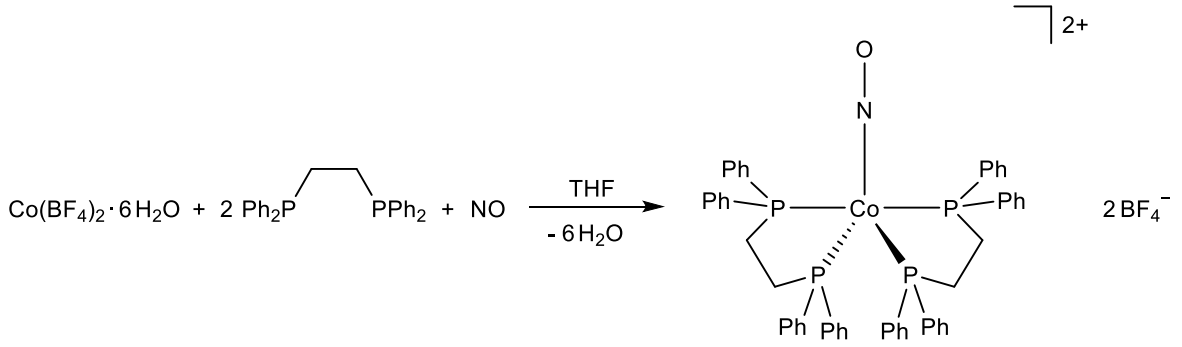

5a'

Starting materials:

1,2-Bis(diphenylphosphino)ethane (dppe), cobalt(II) tetrafluoroborate hexahydrate, nitric oxide, tetrahydrofuran, diethyl ether, acetone, dimethyl sulfoxide.

Procedure:

To a solution of cobalt(II) tetrafluoroborate hexahydrate (0.034 g, 0.100 mmol, 1 equiv.) in THF (3.0 mL), 1,2-bis(diphenylphosphino)ethane (0.080 g, 0.200 mmol, 2 equiv.) was added. The argon atmosphere was then replaced with nitric oxide and the reaction mixture stirred for 1.5 hours, during which time the initially yellow precipitate that had formed upon addition of the diphosphane turned brown. The solid was filtered off, washed with diethyl ether (3 × 15.0 mL) and air-dried for 5 minutes. For crystallization, the bulk product was filled in a Schlenk tube and acetone was added until it was completely dissolved. This solution (2.0 mL) was then transferred to one compartment of a two-chambered Schlenk tube with the second chamber being filled with DMSO (6.0 mL). After three days, brown single crystals of **5a'**·2 Me_2CO suitable for X-ray diffraction were collected.

Yield (bulk)**:** 0.036 g (0.034 mmol, 34 %).

Empirical formula: $C_{52}H_{48}B_2CoF_8NOP_4$ (1059.40 g mol^{-1}).

Elemental analysis: found (calcd.): C 57.39 % (58.96 %), H 4.55 % (4.57 %), N 1.51 % (1.32 %).

IR (solid, ATR): $\tilde{\nu}$ = 3060 (vw), 2991 (vw), 2941 (vw), 2920 (vw), 1851 (vw), 1814 (m, NO), 1705 (w), 1670 (vw), 1614 (vw), 1582 (vw), 1573 (vw), 1481 (vw), 1434 (m), 1418 (vw), 1406 (vw), 1358 (vw), 1336 (vw), 1312 (vw), 1283 (vw), 1256 (vw), 1221 (vw), 1193 (vw), 1183 (vw), 1168 (vw), 1115 (vw), 1086 (m), 1046 (vs), 1033 (vs), 996 (s), 972 (w), 953 (w), 927 (vw), 900 (vw), 841 (vw), 765 (vw), 754 (w), 739 (m), 716 (m), 693 (vs), 667 (m) cm^{-1}.

6.9.3 $[Co(dppa)_2(NO)](ClO_4)_2 \cdot 2\,Me_2CO$ (5b·2 Me_2CO)

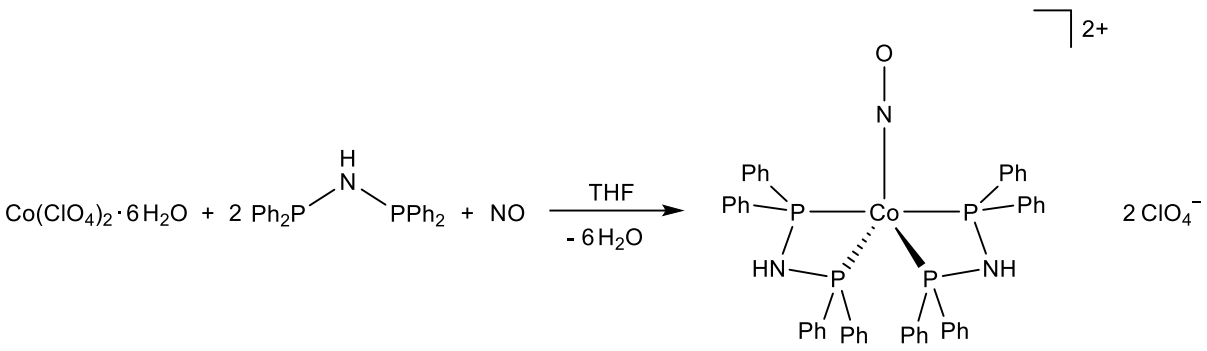

5b

Starting materials:

Bis(diphenylphosphino)amine (dppa), cobalt(II) perchlorate hexahydrate, nitric oxide, tetrahydrofuran, acetone.

Procedure:

To a solution of cobalt(II) perchlorate hexahydrate (0.037 g, 0.100 mmol, 1 equiv.) in THF (3.0 mL), bis(diphenylphosphino)amine (0.077 g, 0.200 mmol, 2 equiv.) was added. The argon atmosphere was then replaced with nitric oxide and the reaction mixture stirred overnight, resulting in the formation of a brown precipitate. For crystallization, the solvent was removed in vacuo and acetone was added until the bulk product was completely dissolved. This solution (2.0 mL) was transferred to a 10.0 mL glass vial left open for slow evaporation in air at room temperature. After three hours, brown single crystals of **5b**·2 Me_2CO suitable for X-ray diffraction were collected.

Yield (bulk)**:** 0.023 g (0.022 mmol, 22 %).

Empirical formula: $C_{48}H_{42}Cl_2CoN_3O_9P_4$ (1058.60 g mol^{-1}).

Elemental analysis: found (calcd.): C 54.98 % (54.46 %), H 4.77 % (4.00 %), N 3.40 % (3.97 %).

IR (solid, ATR): $\tilde{\nu}$ = 2938 (vw), 2543 (vw), 2173 (vw), 2007 (vw), 1968 (vw), 1812 (m, NO), 1785 (vw), 1692 (m), 1664 (vw), 1654 (vw), 1585 (vw), 1572 (vw), 1482 (vw), 1435 (m), 1423 (vw), 1368 (vw), 1355 (vw), 1336 (vw), 1292 (vw), 1236 (vw), 1189 (vw), 1166 (vw), 1128 (vw), 1078 (vs), 1027 (vw), 996 (w), 976 (vw), 923 (vw), 911 (vw), 854 (m), 834 (vw), 814 (vw), 759 (vw), 742 (m), 718 (w), 691 (s), 677 (m), 661 (vw) cm^{-1}.

6.9.4 $[Co(dppv)_2(NO)](ClO_4)_2 \cdot 1.5\,Me_2CO$ (5c·1.5 Me_2CO)

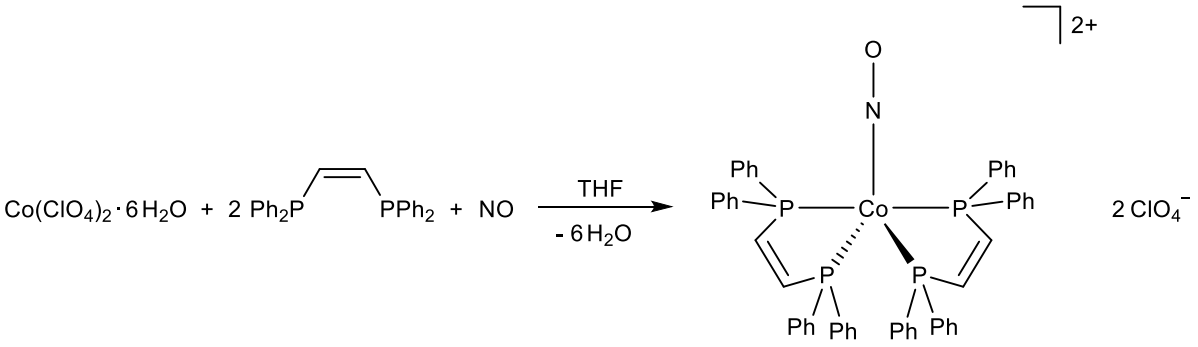

5c

Starting materials:

cis-1,2-Bis(diphenylphosphino)ethene (dppv), cobalt(II) perchlorate hexahydrate, nitric oxide, tetrahydrofuran, acetone, dimethyl sulfoxide.

Procedure:

To a solution of cobalt(II) perchlorate hexahydrate (0.037 g, 0.100 mmol, 1 equiv.) in THF (3.0 mL), *cis*-1,2-bis(diphenylphosphino)ethene (0.079 g, 0.200 mmol, 2 equiv.) was added. The argon atmosphere was then replaced with nitric oxide and the reaction mixture stirred overnight, during which time the initially orange precipitate that had formed upon addition of the diphosphane turned brown. For crystallization, the solvent was removed in vacuo and acetone was added until the bulk product was completely dissolved. This solution (2.0 mL) was then transferred to one compartment of a two-chambered Schlenk tube with the second chamber being filled with DMSO (6.0 mL). After three days, brown single crystals of **5c**·1.5 Me_2CO suitable for X-ray diffraction were collected.

Yield (bulk)**:** 0.022 g (0.020 mmol, 20 %).

Empirical formula: $C_{52}H_{44}Cl_2CoNO_9P_4$ (1080.65 g mol^{-1}).

Elemental analysis: found (calcd.): C 57.04 % (57.80 %), H 4.59 % (4.10 %), N 1.15 % (1.30 %).

IR (solid, ATR): $\tilde{\nu}$ = 3059 (vw), 3026 (vw), 3002 (vw), 2953 (vw), 2923 (vw), 2868 (vw), 2855 (vw), 1990 (vw), 1860 (vw), 1818 (m, NO), 1799 (vw), 1580 (vw), 1572 (vw), 1547 (vw), 1481 (vw), 1460 (vw), 1434 (w), 1366 (vw), 1334 (vw), 1310 (vw), 1281 (vw), 1247 (vw), 1187 (vw), 1164 (vw), 1081 (vs), 1069 (vs), 1051 (s), 1029 (w), 997 (w), 970 (vw), 916 (vw), 892 (vw), 850 (vw), 833 (vw), 796 (vw), 751 (m), 739 (m), 727 (m), 708 (m), 687 (s) cm^{-1}.

6.9.5 $[Co(dppv)_2(NO)](BF_4)_2 \cdot 1.8\,Me_2CO \cdot 0.2\,DMSO$ (5c'·1.8 Me_2CO · 0.2 DMSO)

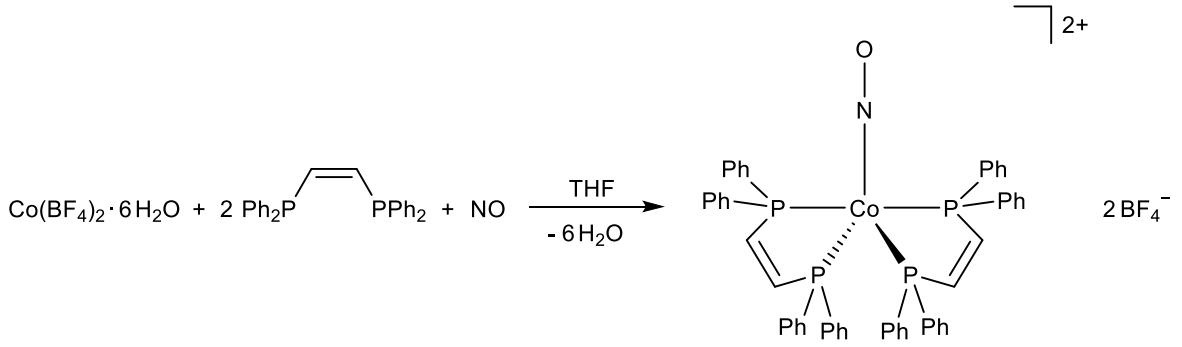

5c'

Starting materials:

cis-1,2-Bis(diphenylphosphino)ethene (dppv), cobalt(II) tetrafluoroborate hexahydrate, nitric oxide, tetrahydrofuran, diethyl ether, acetone, dimethyl sulfoxide.

Procedure:

To a solution of cobalt(II) tetrafluoroborate hexahydrate (0.034 g, 0.100 mmol, 1 equiv.) in THF (3.0 mL), *cis*-1,2-bis(diphenylphosphino)ethene (0.079 g, 0.200 mmol, 2 equiv.) was added. The argon atmosphere was then replaced with nitric oxide and the reaction mixture stirred overnight, during which time the initially orange precipitate that had formed upon addition of the diphosphane turned brown. The solid was filtered off, washed with diethyl ether (3 × 15.0 mL) and air-dried for 5 minutes. For crystallization, the bulk product was filled in a Schlenk tube and acetone was added until it was completely dissolved. This solution (2.0 mL) was then transferred to one compartment of a two-chambered Schlenk tube with the second chamber being filled with DMSO (6.0 mL). After three days, brown single crystals of **5c'**·1.8 Me_2CO · 0.2 DMSO suitable for X-ray diffraction were collected.

Yield (bulk)**:** 0.037 g (0.035 mmol, 35 %).

Empirical formula: $C_{52}H_{44}B_2CoF_8NOP_4$ (1055.37 g mol^{-1}).

Elemental analysis: found (calcd.): C 59.25 % (59.18 %), H 4.69 % (4.20 %), N 1.38 % (1.33 %).

IR (solid, ATR): $\tilde{\nu}$ = 3059 (vw), 3003 (vw), 2980 (vw), 2867 (vw), 2367 (vw), 2332 (vw), 2102 (vw), 1862 (vw), 1819 (w, NO), 1797 (vw), 1581 (vw), 1570 (vw), 1482 (vw), 1460 (vw), 1435 (w), 1335 (vw), 1312 (vw), 1282 (vw), 1247 (vw), 1224 (vw), 1186 (vw), 1165 (vw), 1143 (w), 1117 (vw), 1098 (w), 1088 (w), 1047 (vs), 1035 (vs), 1025 (s), 997 (w), 975 (vw), 918 (vw), 894 (vw), 819 (vw), 793 (vw), 752 (m), 740 (m), 727 (m), 707 (w), 689 (s), 671 (vw), 659 (vw) cm^{-1}.

6.9.6 $[Co(dppbz)_2(NO)](ClO_4)_2 \cdot Me_2CO$ (5d·Me_2CO)

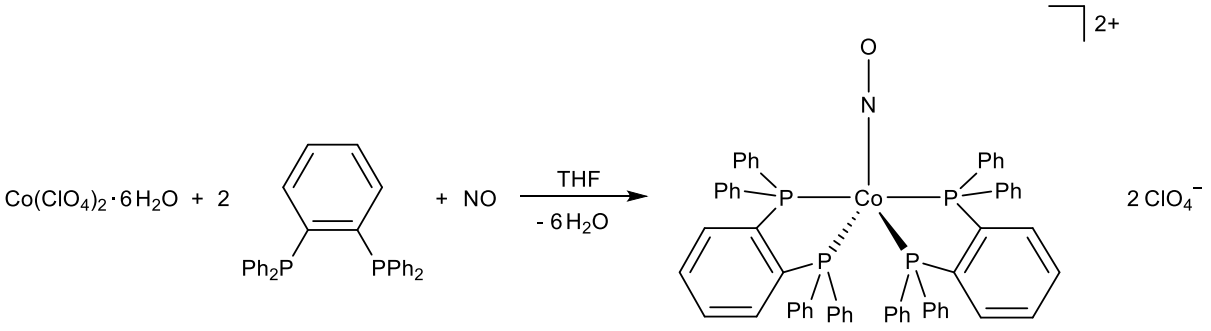

5d

Starting materials:

1,2-Bis(diphenylphosphino)benzene (dppbz), cobalt(II) perchlorate hexahydrate, nitric oxide, tetrahydrofuran, acetone, dimethyl sulfoxide.

Procedure:

To a solution of cobalt(II) perchlorate hexahydrate (0.037 g, 0.100 mmol, 1 equiv.) in THF (3.0 mL), 1,2-bis(diphenylphosphino)benzene (0.089 g, 0.200 mmol, 2 equiv.) was added. Then, the argon atmosphere was replaced with nitric oxide and the reaction mixture stirred overnight, resulting in the formation of a brown precipitate. For crystallization, the solvent was removed in vacuo and acetone was added until the bulk product was completely dissolved. This solution (2.0 mL) was then transferred to one compartment of a two-chambered Schlenk tube with the second chamber being filled with DMSO (6.0 mL). After three days, brown single crystals of **5d**·Me_2CO suitable for X-ray diffraction were collected.

Yield (bulk)**:** 0.029 g (0.025 mmol, 25 %).

Empirical formula: $C_{60}H_{48}Cl_2CoNO_9P_4$ (1180.77 g mol^{-1}).

Elemental analysis: found (calcd.): C 61.74 % (61.03 %), H 5.24 % (4.10 %), N 1.02 % (1.19 %).

IR (solid, ATR): $\tilde{\nu}$ = 3060 (vw), 2963 (vw), 2924 (vw), 2850 (vw), 2096 (vw), 1996 (vw), 1912 (vw), 1851 (vw), 1833 (w, NO), 1806 (vw), 1713 (vw), 1582 (vw), 1572 (vw), 1443 (vw), 1434 (w), 1416 (vw), 1360 (vw), 1333 (vw), 1313 (vw), 1278 (vw), 1256 (vw), 1220 (vw), 1186 (vw), 1160 (vw), 1111 (w), 1082 (vs), 1075 (vs), 1025 (w), 997 (w), 968 (vw), 955 (vw), 931 (vw), 895 (vw), 873 (vw), 859 (vw), 845 (vw), 814 (vw), 796 (vw), 783 (vw), 772 (vw), 740 (m), 726 (m), 700 (m), 690 (s), 669 (w), 658 (vw) cm^{-1}.

6.10 Synthesis of dichlorido- and dibromidocobalt nitrosyls with diphosphanes as co-ligands

6.10.1 $[CoCl_2(dppe)(NO)]\cdot Me_2CO$ (6a·Me_2CO)

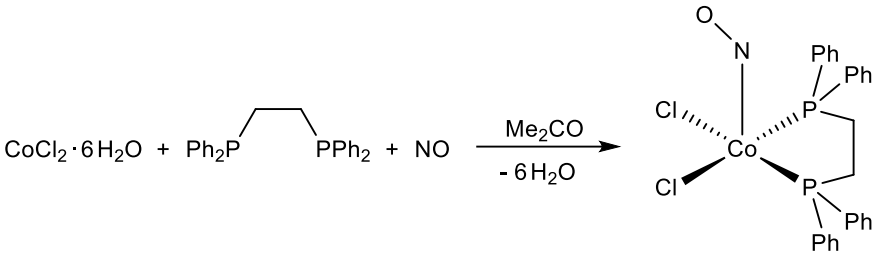

6a

Starting materials:

1,2-Bis(diphenylphosphino)ethane (dppe), cobalt(II) chloride hexahydrate, nitric oxide, acetone, diethyl ether, dimethyl sulfoxide.

Procedure:

To a solution of cobalt(II) chloride hexahydrate (0.012 g, 0.050 mmol, 1 equiv.) in acetone (1.5 mL), 1,2-bis(diphenylphosphino)ethane (0.020 g, 0.050 mmol, 1 equiv.) was added. The argon atmosphere was then replaced with nitric oxide, resulting in the formation of **6a** as a dark brown precipitate after 30 minutes. Then, the solid was filtered off, washed with diethyl ether (3×15.0 mL) and air-dried for 5 minutes. For crystallization instead, stirring was discontinued just 5 minutes after NO introduction and the resulting dark red solution was quickly transferred to a two-chambered Schlenk tube filled with DMSO (5.5 mL) in the second chamber. After two days, brown single crystals of **6a**·Me_2CO suitable for X-ray diffraction were collected.

Yield (bulk)**:** 0.018 g (0.032 mmol, 64 %).

Empirical formula: $C_{26}H_{24}Cl_2CoNOP_2$ (558.26 g mol^{-1}).

Elemental analysis: found (calcd.): C 55.11 % (55.94 %), H 4.13 % (4.33 %), N 2.42 % (2.51 %).

IR (solid, ATR): $\tilde{\nu}$ = 3073 (vw), 3055 (vw), 2993 (vw), 2952 (vw), 2913 (vw), 2681 (vw), 2360 (vw), 2328 (vw), 2099 (vw), 1894 (vw), 1845 (vw), 1797 (vw), 1706 (vw), 1682 (m, NO), 1661 (s, NO), 1585 (vw), 1570 (vw), 1482 (w), 1433 (m), 1411 (w), 1386 (vw), 1362 (vw), 1336 (vw), 1310 (vw), 1275 (vw), 1240 (vw), 1231 (vw), 1186 (vw), 1162 (vw), 1157 (vw), 1127 (vw), 1098 (m), 1071 (vw), 1060 (vw), 1027 (vw), 1011 (vw), 997 (w), 953 (vw), 916 (vw), 902 (vw), 877 (vw), 865 (vw), 844 (vw), 812 (w), 762 (vw), 743 (m), 715 (s), 701 (m), 686 (vs), 654 (m) cm^{-1}.

6.10.2 [$CoBr_2$(dppe)(NO)] (6a')

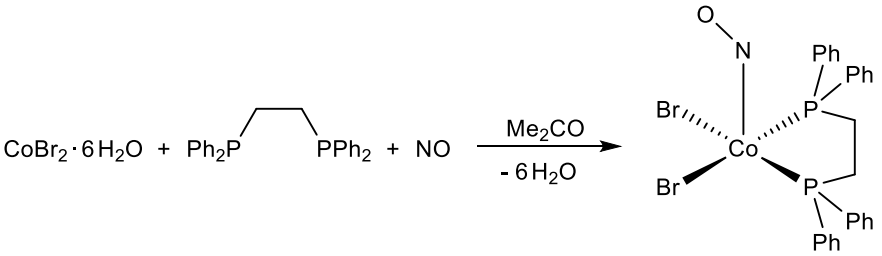

6a'

Starting materials:

1,2-Bis(diphenylphosphino)ethane (dppe), cobalt(II) bromide, water, nitric oxide, acetone, diethyl ether, chloroform, dimethyl sulfoxide.

Procedure:

To a solution of cobalt(II) bromide (0.022 g, 0.100 mmol, 1 equiv.) in acetone (4.0 mL), water (11.0 µL, 0.600 mmol, 6 equiv.) and 1,2-bis(diphenylphosphino)ethane (0.040 g, 0.100 mmol, 1 equiv.) were added. The argon atmosphere was then replaced with nitric oxide, resulting in the formation of **6a'** as a dark brown precipitate after 15 minutes. The solid was filtered off, washed with diethyl ether (3×15.0 mL) and air-dried for 5 minutes. For crystallization, one compartment of a two-chambered Schlenk tube was loaded with a solution of the bulk product (0.006 g) in chloroform (1.5 mL), while the second chamber was filled with DMSO (5.5 mL). After two days, brown single crystals of **6a'** suitable for X-ray diffraction were collected.

Yield (bulk)**:** 0.012 g (0.019 mmol, 19 %).

Empirical formula: $C_{26}H_{24}Br_2CoNOP_2$ (647.17 g mol^{-1}).

Elemental analysis: found (calcd.): C 46.63 % (48.25 %), H 3.62 % (3.74 %), N 1.90 % (2.16 %).

IR (solid, ATR): $\tilde{\nu}$ = 3075 (vw), 3051 (vw), 2949 (vw), 2917 (vw), 2677 (vw), 2353 (vw), 2328 (vw), 2106 (vw), 1894 (vw), 1849 (vw), 1796 (vw), 1750 (vw), 1693 (m, NO), 1667 (s, NO), 1585 (vw), 1570 (vw), 1482 (vw), 1467 (vw), 1433 (m), 1417 (vw), 1407 (w), 1334 (vw), 1309 (vw), 1274 (vw), 1256 (vw), 1230 (vw), 1186 (vw), 1176 (vw), 1158 (vw), 1127 (vw), 1097 (m), 1076 (vw), 1069 (vw), 1051 (vw), 1026 (vw), 1012 (vw), 997 (w), 946 (vw), 928 (vw), 918 (vw), 900 (vw), 877 (vw), 857 (vw), 844 (vw), 813 (w), 777 (vw), 760 (w), 741 (m), 713 (s), 701 (m), 686 (vs), 681 (vs), 652 (m) cm^{-1}.

6.10.3 [$CoCl_2$(dppp)(NO)] (6b)

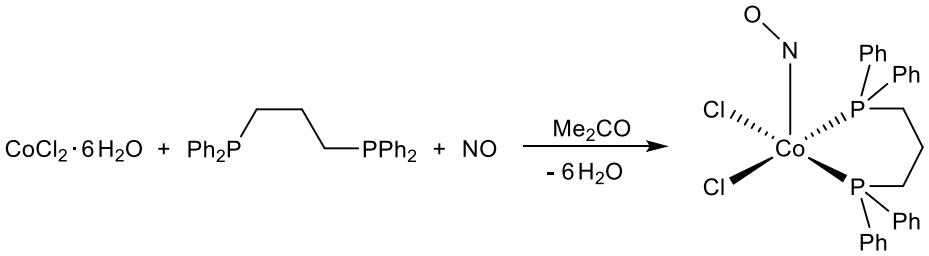

6b

Starting materials:

1,3-Bis(diphenylphosphino)propane (dppp), cobalt(II) chloride hexahydrate, nitric oxide, acetone, diethyl ether, chloroform, dimethyl sulfoxide.

Procedure:

To a solution of cobalt(II) chloride hexahydrate (0.024 g, 0.100 mmol, 1 equiv.) in acetone (4.0 mL), 1,3-bis(diphenylphosphino)propane (0.041 g, 0.100 mmol, 1 equiv.) was added. Then, the argon atmosphere was replaced with nitric oxide, resulting in the formation of **6b** as a dark brown precipitate after 5 minutes. The solid was then filtered off, washed with Et_2O (3 × 15.0 mL) and air-dried for 5 minutes. For crystallization, one compartment of a two-chambered Schlenk tube was loaded with a solution of the bulk product (0.004 g) in chloroform (2.0 mL), while the second chamber was filled with DMSO (5.5 mL). After two days, brown single crystals of **6b** suitable for X-ray diffraction were collected.

Yield (bulk)**:** 0.010 g (0.017 mmol, 17 %).

Empirical formula: $C_{27}H_{26}Cl_2CoNOP_2$ (572.29 g mol^{-1}).

Elemental analysis: found (calcd.): C 55.56 % (56.67 %), H 4.24 % (4.58 %), N 2.24 % (2.45 %).

IR (solid, ATR): $\tilde{\nu}$ = 3055 (vw), 2984 (vw), 2952 (vw), 2910 (vw), 2363 (vw), 2324 (vw), 2215 (vw), 2096 (vw), 1845 (vw), 1788 (vw), 1756 (vw), 1627 (s, NO), 1616 (s, NO), 1591 (w), 1573 (w), 1507 (vw), 1483 (w), 1443 (vw), 1433 (m), 1413 (w), 1402 (w), 1335 (vw), 1316 (vw), 1309 (vw), 1270 (vw), 1190 (vw), 1155 (w), 1122 (vw), 1097 (m), 1072 (vw), 1053 (vw), 1026 (w), 1018 (vw), 997 (w), 967 (w), 961 (w), 911 (vw), 853 (vw), 832 (vw), 827 (vw), 814 (vw), 780 (w), 742 (s), 722 (vw), 710 (w), 690 (vs), 670 (w), 655 (m) cm^{-1}.

6.10.4 [$CoCl_2$(dppv)(NO)] (6c)

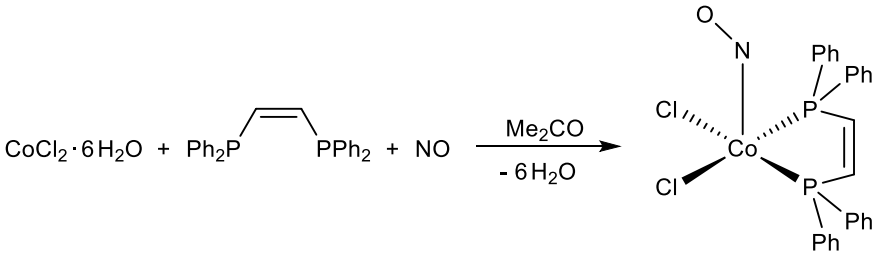

6c

Starting materials:

cis-1,2-Bis(diphenylphosphino)ethene (dppv), cobalt(II) chloride hexahydrate, nitric oxide, acetone, diethyl ether, $[Co(dppv)_2(NO)](ClO_4)_2$ (**5c**), lithium chloride.

Procedure:

To a solution of cobalt(II) chloride hexahydrate (0.024 g, 0.100 mmol, 1 equiv.) in acetone (4.0 mL), *cis*-1,2-bis(diphenylphosphino)ethene (0.040 g, 0.100 mmol, 1 equiv.) was added. Then, the argon atmosphere was replaced with nitric oxide, resulting in the formation of **6c** as a dark brown precipitate after 5 minutes. The solid was filtered off, washed with Et_2O (3×15.0 mL) and air-dried for 5 minutes.

To obtain the product in a single-crystalline form, a different route was applied: To a solution of $[Co(dppv)_2(NO)](ClO_4)_2$ (**5c**) (0.027 g, 0.025 mmol, 1.0 equiv.) in acetone (6.0 mL), lithium chloride (0.006 g, 0.140 mmol, 5.6 equiv.) was added in small portions under vigorous stirring. After 15 minutes, the resulting dark red solution was concentrated in vacuo to a volume of approximately 1.0 mL and stored under argon at −25 °C. After six days, brown single crystals of **6c** suitable for X-ray diffraction were collected.

Yield (bulk)**:** 0.020 g (0.036 mmol, 36 %).

Empirical formula: $C_{26}H_{22}Cl_2CoNOP_2$ (556.25 g mol^{-1}).

Elemental analysis: found (calcd.): C 55.23 % (56.14 %), H 3.94 % (3.99 %), N 2.52 % (2.52 %).

IR (solid, ATR): $\tilde{\nu}$ = 3373 (vw), 3079 (vw), 3051 (vw), 3001 (vw), 2974 (vw), 2328 (vw), 2096 (vw), 1788 (vw), 1686 (w, NO), 1647 (vw), 1584 (vw), 1570 (vw), 1558 (vw), 1541 (vw), 1482 (vw), 1460 (vw), 1433 (w), 1333 (vw), 1304 (m), 1265 (m), 1228 (vs), 1265 (s), 1181 (s), 1147 (s), 1121 (vs), 1099 (vs), 1025 (vw), 997 (m), 979 (s), 849 (vw), 839 (vw), 807 (w), 775 (w), 752 (w), 743 (m), 724 (m), 695 (m), 683 (s), 657 (m) cm^{-1}.

6.10.5 $[CoBr_2(dppv)(NO)]\cdot CHCl_3$ (6c'·$CHCl_3$)

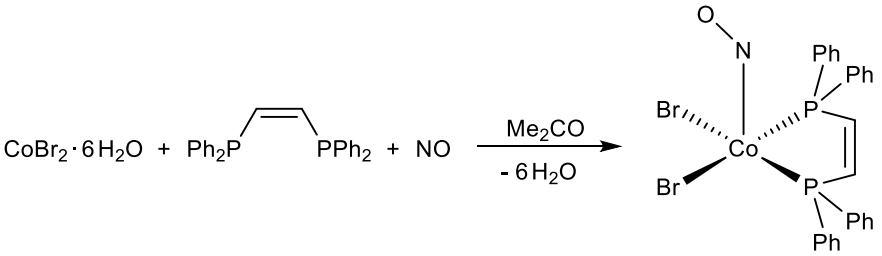

6c'

Starting materials:

cis-1,2-Bis(diphenylphosphino)ethene (dppv), cobalt(II) bromide, water, nitric oxide, acetone, diethyl ether, chloroform, dimethyl sulfoxide.

Procedure:

To a solution of cobalt(II) bromide (0.022 g, 0.100 mmol, 1 equiv.) in acetone (4.0 mL), water (11.0 µL, 0.600 mmol, 6 equiv.) was added followed by *cis*-1,2-bis(diphenylphosphino)ethene (0.040 g, 0.100 mmol, 1 equiv.). The argon atmosphere was then replaced with nitric oxide, resulting in the formation of **6c'** as a dark brown precipitate after 2 minutes. For crystallization, one compartment of a two-chambered Schlenk tube was loaded with a solution of the bulk product (0.014 g) in chloroform (4.0 mL), while the second chamber was filled with DMSO (6.5 mL). After two days, brown single crystals of **6c'**·$CHCl_3$ suitable for X-ray diffraction were collected.

Yield (bulk)**:** 0.028 g (0.043 mmol, 43 %).

Empirical formula: $C_{26}H_{22}Br_2CoNOP_2$ (645.16 g mol^{-1}).

Elemental analysis: found (calcd.): C 47.88 % (48.40 %), H 3.46 % (3.44 %), N 1.87 % (2.17 %).

IR (solid, ATR): $\tilde{\nu}$ = 3071 (vw), 3050 (vw), 3019 (vw), 2992 (vw), 2324 (vw), 2086 (vw), 1992 (vw), 1890 (vw), 1792 (vw), 1680 (s, NO), 1584 (vw), 1571 (vw), 1519 (vw), 1482 (w), 1433 (m), 1397 (vw), 1391 (vw), 1338 (vw), 1311 (vw), 1275 (vw), 1269 (vw), 1221 (vw), 1212 (vw), 1187 (vw), 1159 (vw), 1147 (vw), 1098 (m), 1071 (w), 1024 (w), 997 (w), 973 (vw), 957 (vw), 923 (vw), 909 (vw), 888 (vw), 870 (vw), 851 (vw), 844 (vw), 821 (vw), 785 (vw), 758 (m), 740 (vs), 727 (vs), 701 (m), 687 (vs), 665 (m), 654 (w) cm^{-1}.

6.10.6 [$CoCl_2$(dppbz)(NO)] (6d)

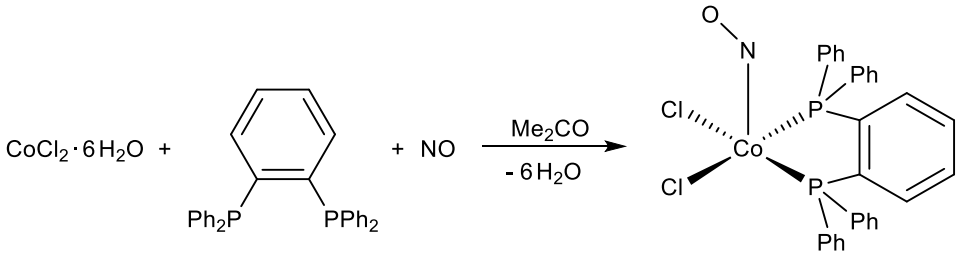

6d

Starting materials:

1,2-Bis(diphenylphosphino)benzene (dppbz), cobalt(II) chloride hexahydrate, nitric oxide, acetone, dimethyl sulfoxide.

Procedure:

To a solution of cobalt(II) chloride hexahydrate (0.024 g, 0.100 mmol, 1 equiv.) in acetone (4.0 mL), 1,2-bis(diphenylphosphino)benzene (0.045 g, 0.100 mmol, 1 equiv.) was added. Then, the argon atmosphere was replaced with nitric oxide, resulting in the formation of a small amount of green precipitate after 5 minutes. The dark red supernatant solution (1.5 mL) was then transferred to a two-chambered Schlenk tube filled with DMSO (6.0 mL) in the second chamber. After two days, brown single crystals of **6d** suitable for X-ray diffraction were collected.

Yield: 0.013 g (0.021 mmol, 21 %).

Empirical formula: $C_{30}H_{24}Cl_2CoNOP_2$ (606.31 g mol^{-1}).

Elemental analysis: found (calcd.): C 58.11 % (59.43 %), H 3.69 % (3.99 %), N 2.36 % (2.31 %).

IR (solid, ATR): $\tilde{\nu}$ = 3393 (vw), 3252 (vw), 3057 (vw), 3041 (vw), 2988 (vw), 2913 (vw), 2677 (vw), 2360 (vw), 2096 (vw), 1986 (vw), 1937 (vw), 1894 (vw), 1859 (vw), 1806 (w), 1671 (vw), 1638 (s, NO), 1586 (vw), 1571 (w), 1558 (vw), 1481 (w), 1434 (s), 1394 (vw), 1332 (vw), 1310 (vw), 1290 (vw), 1255 (vw), 1186 (vw), 1166 (vw), 1159 (vw), 1115 (w), 1096 (s), 1075 (w), 1046 (vw), 1026 (w), 997 (w), 988 (vw), 949 (vw), 933 (vw), 921 (vw), 845 (vw), 782 (w), 753 (s), 743 (w), 729 (m), 714 (w), 706 (m), 687 (vs), 672 (s), 663 (w) cm^{-1}.

6.10.7 [$CoBr_2$(dppbz)(NO)] (6d')

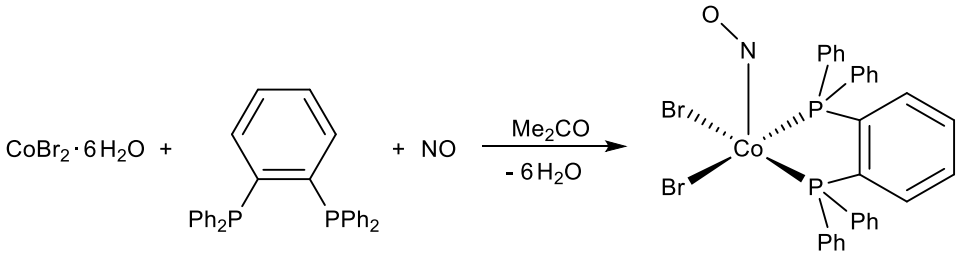

6d'

Starting materials:

1,2-Bis(diphenylphosphino)benzene (dppbz), cobalt(II) bromide, water, nitric oxide, acetone, dimethyl sulfoxide.

Procedure:

To a solution of cobalt(II) bromide (0.022 g, 0.100 mmol, 1 equiv.) in acetone (4.0 mL), water (11.0 µL, 0.600 mmol, 6 equiv.) was added, followed by the addition of 1,2-bis(diphenylphosphino)benzene (0.045 g, 0.100 mmol, 1 equiv.). The argon atmosphere was replaced with nitric oxide, resulting in the formation of a yellow precipitate. Additional acetone (2.0 mL) was added. After stirring for 1.5 hours, during which time most of the solid dissolved, the dark red supernatant solution (3.0 mL) was transferred to a two-chambered Schlenk tube filled with DMSO (6.5 mL) in the second chamber. After two days, brown single crystals of **6d'** suitable for X-ray diffraction were collected.

Yield: 0.008 g (0.012 mmol, 12 %).

Empirical formula: $C_{30}H_{24}Br_2CoNOP_2$ (695.22 g mol^{-1}).

Elemental analysis: found (calcd.): C 49.01 % (51.83 %), H 3.42 % (3.48 %), N 2.00 % (2.01 %).

IR (solid, ATR): $\tilde{\nu}$ = 3361 (vw), 3075 (vw), 3054 (vw), 2984 (vw), 2910 (vw), 2864 (vw), 2324 (vw), 2106 (vw), 1852 (w), 1796 (m), 1735 (vw), 1644 (m, NO), 1600 (vw), 1586 (vw), 1571 (vw), 1496 (vw), 1481 (w), 1434 (m), 1392 (vw), 1332 (vw), 1309 (vw), 1289 (vw), 1255 (vw), 1223 (vw), 1184 (w), 1164 (w), 1115 (m), 1094 (m), 1071 (w), 1052 (w), 1046 (w), 1025 (m), 997 (m), 950 (w), 921 (w), 846 (vw), 817 (vw), 781 (w), 768 (vw), 749 (s), 727 (s), 712 (m), 701 (m), 689 (vs), 670 (s), 655 (m) cm^{-1}.

6.11 Synthesis of further cobalt nitrosyls and hyponitrite complexes

6.11.1 *rac-cis*-[Co(NO)(NO_2-κ*N*)(phen)$_2$]ClO_4 (7a)

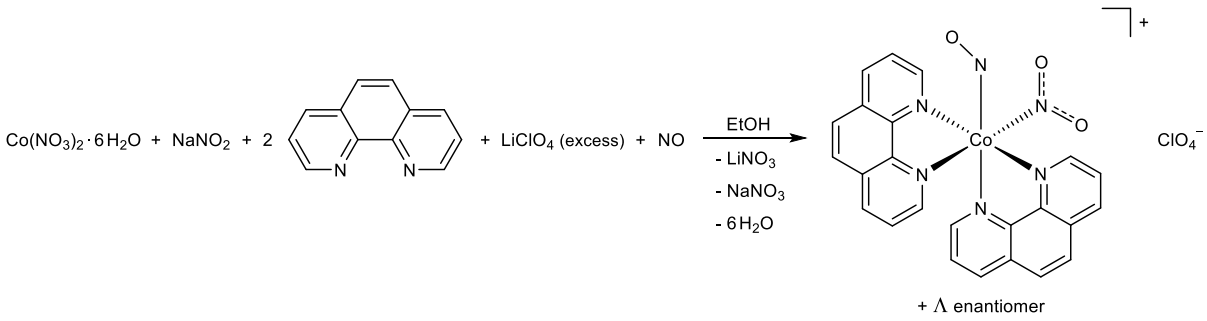

7a

According to:

A. Vlček Jr., A. A. Vlček, *Inorg. Chim. Acta* **1974**, *9*, 165–170.

Starting materials:

1,10-Phenanthroline (phen), cobalt(II) nitrate hexahydrate, sodium nitrite, lithium perchlorate, nitric oxide, ethanol, diethyl ether, acetonitrile, dimethyl sulfoxide.

Procedure:

To a solution of $Co(NO_3)_2{\cdot}6H_2O$ (0.029 g, 0.100 mmol, 1 equiv.) in ethanol (3.0 mL), 1,10-phenanthroline (0.036 g, 0.200 mmol, 2 equiv.) was added. Then, lithium perchlorate (0.021 g, 0.200 mmol, 2 equiv.) and sodium nitrite (0.007 g, 0.100 mmol, 1 equiv.) were added under vigorous stirring. The argon atmosphere was changed to nitric oxide and the batch stirred for 1 hour, yielding a brown precipitate. The solid was filtered off, washed with ethanol (3×25.0 mL) and diethyl ether (3×5.0 mL) and air-dried for 15 minutes. Acetonitrile was added to the bulk product until it was completely dissolved. This solution (3.0 mL) was then transferred to one compartment of a two-chambered Schlenk tube with DMSO (7.5 mL) in the second chamber. The atmosphere was then changed to nitric oxide. After three days, brown single crystals of **7a** suitable for X-ray diffraction were collected.

Yield (crystals)**:** 0.010 g (0.017 mmol, 17 %).

Empirical formula: $C_{24}H_{16}ClCoN_6O_7$ (594.81 g mol^{-1}).

Elemental analysis: found (calcd.): C 47.09 % (48.46 %), H 3.06 % (2.71 %), N 14.64 % (14.13 %).

IR (solid, ATR): $\tilde{\nu}$ = 3097 (vw), 3063 (vw), 2998 (vw), 2928 (vw), 2628 (vw), 2247 (vw), 2102 (vw), 1996 (vw), 1658 (w, NO), 1649 (w, NO), 1633 (w), 1607 (w), 1584 (w), 1519 (m), 1495 (w), 1457 (w), 1443 (m), 1422 (s), 1413 (s), 1397 (m), 1377 (w), 1335 (m), 1321 (m), 1300 (s), 1278 (m), 1261 (w), 1226 (w), 1215 (w), 1204 (w), 1149 (w), 1108 (m), 1099 (s), 1078 (vs), 1038 (s), 1000 (m), 992 (m), 953 (m), 932 (w), 918 (m), 893 (w), 879 (w), 871 (w), 848 (vs), 816 (vs), 800 (m), 779 (m), 745 (m), 717 (vs), 692 (w), 671 (w), 652 (m) cm^{-1}.

6.11.2 $(ppzH_2)_{0.5}[Co(fpin)(NO)_2]$ (7b)

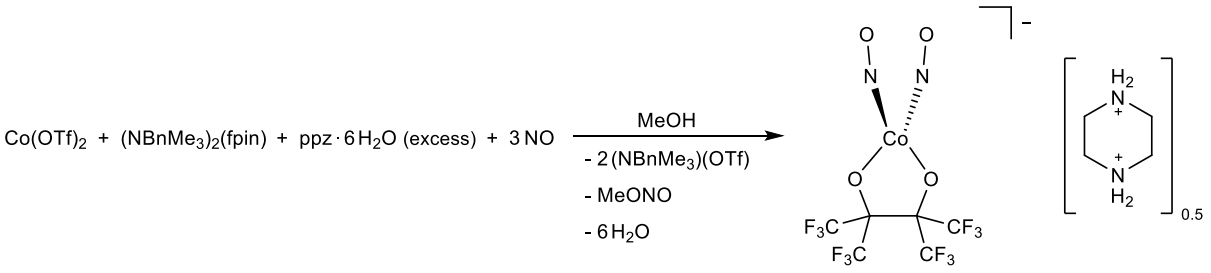

7b

Starting materials:

Piperazine hexahydrate (ppz·6H_2O), $(NBnMe_3)_2$(fpin) stock solution (0.1 M in MeOH), cobalt(II) triflate, nitric oxide, methanol, dimethyl sulfoxide.

Procedure:

Cobalt(II) triflate (0.018 g, 0.050 mmol, 1 equiv.) was added to a solution of $(NBnMe_3)_2$(fpin) in methanol (0.1 M, 0.5 mL, 0.050 mmol, 1 equiv.) followed by the addition of piperazine hexahydrate (0.010 g, 0.050 mmol, 1 equiv.). Then, additional MeOH (1.0 mL) was added in order to dissolve all educts completely. The argon atmosphere was then replaced with nitric oxide and the resulting dark brown solution was stirred overnight. The batch was then transferred to a two-chambered Schlenk tube filled with DMSO (6.0 mL) in the second chamber. After four days, brown single crystals of **7b** suitable for X-ray diffraction were collected.

Yield: 0.003 g (0.006 mmol, 12 %).

Empirical formula: $C_8H_6CoF_{12}N_3O_4$ (495.07 g mol^{-1}).

Elemental analysis: found (calcd.): C 19.43 % (19.41 %), H 1.44 % (1.22 %), N 8.28 % (8.49 %).

IR (solid, ATR): $\tilde{\nu}$ = 3005 (vw), 2839 (vw), 2737 (vw), 2631 (vw), 2589 (vw), 2392 (vw), 2219 (vw), 2022 (vw), 1968 (vw), 1855 (w, NO, sym.), 1766 (m, NO, asym.), 1624 (vw), 1538 (vw), 1497 (vw), 1478 (vw), 1457 (vw), 1422 (vw), 1385 (vw), 1361 (vw), 1350 (vw), 1326 (vw), 1259 (s), 1239 (s), 1222 (vs), 1211 (vs), 1177 (vs), 1169 (vs), 1136 (vs), 1104 (s), 1084 (m), 1029 (s), 981 (m), 941 (vs), 914 (w), 889 (w), 867 (s), 805 (vw), 781 (vw), 758 (w), 740 (m), 729 (w), 713 (s), 701 (w), 683 (vw), 673 (vw), 665 (vw), 660 (vw) cm^{-1}.

6.11.3 *rac*-[Co(en)$_2$(*cis*-N_2O_2-κ^2*O*,*O*′)]ClO_4 (7c)

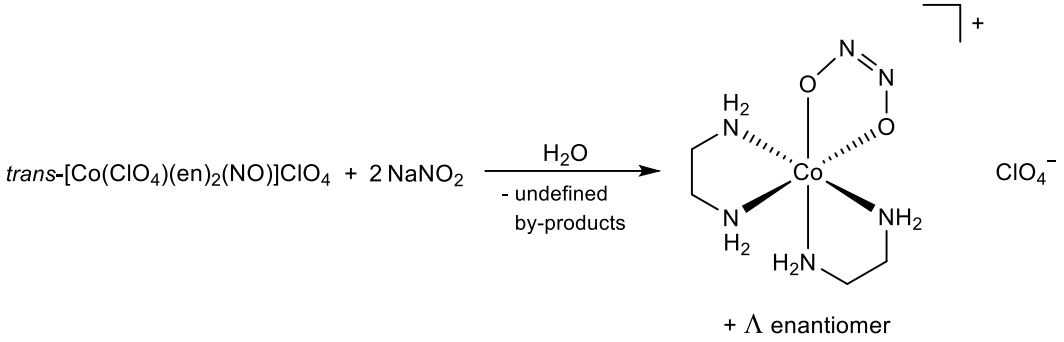

7c

Starting materials:

trans-[Co(ClO_4)(en)$_2$(NO)]ClO_4 (**4a**),[85] sodium nitrite, water, dimethyl sulfoxide.

Procedure:

In one compartment of a two-chambered Schlenk tube, a solution of sodium nitrite (0.028 g, 0.400 mmol, 2 equiv.) and *trans*-[Co(ClO_4)(en)$_2$(NO)]ClO_4 (**4a**) (0.082 g, 0.200 mmol, 1 equiv.) in water (0.8 mL) was prepared. The second chamber was filled with DMSO (7.0 mL). The tube was then sealed and the batch was left under argon atmosphere for crystallization. After two days, a few small reddish-orange single crystals of **7c** suitable for X-ray diffraction were collected along with a colourless micro-crystalline precipitate.

Yield: n.a., few small reddish-orange crystals.

Empirical formula: $C_4H_{16}ClCoN_5O_6$ (324.58 g mol^{-1}).

7 Appendix

7.1 Packing diagrams of the crystal structures

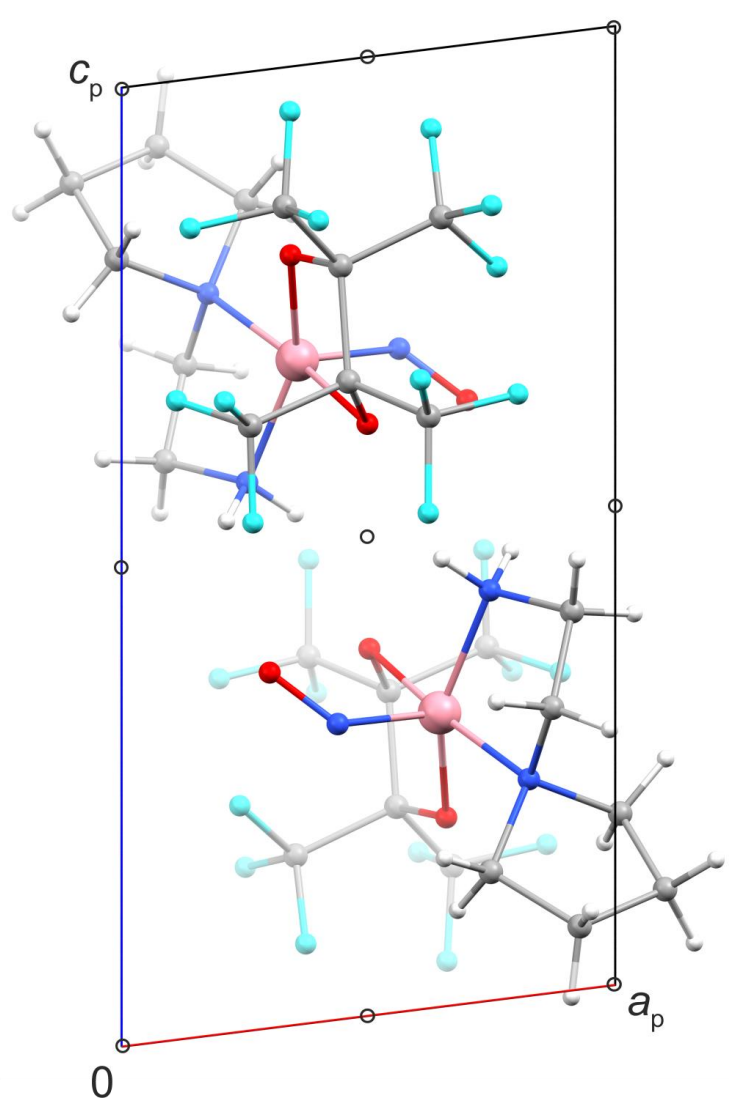

Figure 7.1: Packing diagram of [Co(2-aepyrr)(fpin)(NO)] (**1a**) in the triclinic space group $P\bar{1}$ with view along [010]. The symmetry elements of the space group $P\bar{1}$ are overlaid. Atoms: carbon (gray), hydrogen (white), cobalt (pink), fluorine (turquoise), nitrogen (blue), oxygen (red).

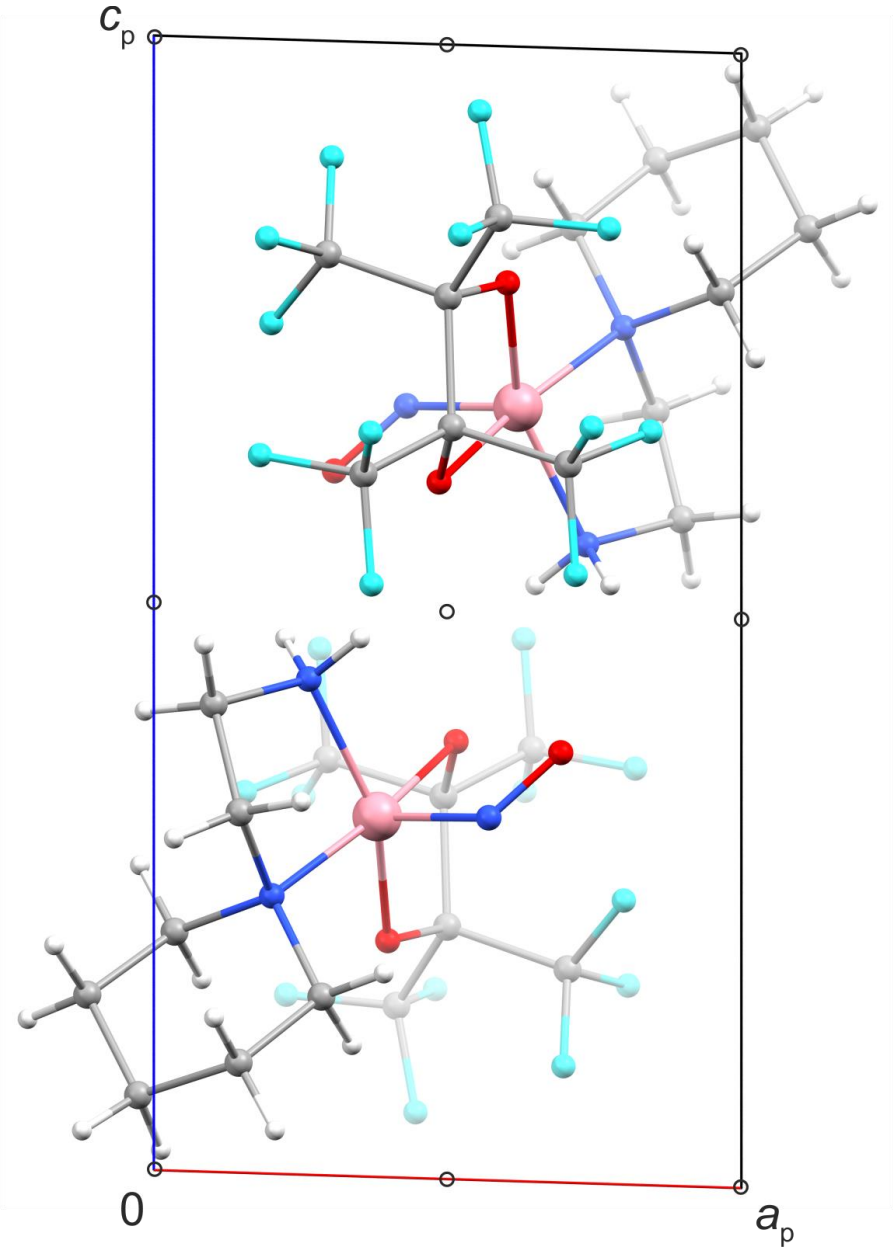

Figure 7.2: Packing diagram of [Co(2-aepip)(fpin)(NO)] (**1b**) in the triclinic space group $P\bar{1}$ with view along [010]. The symmetry elements of the space group $P\bar{1}$ are overlaid. Atoms: carbon (gray), hydrogen (white), cobalt (pink), fluorine (turquoise), nitrogen (blue), oxygen (red).

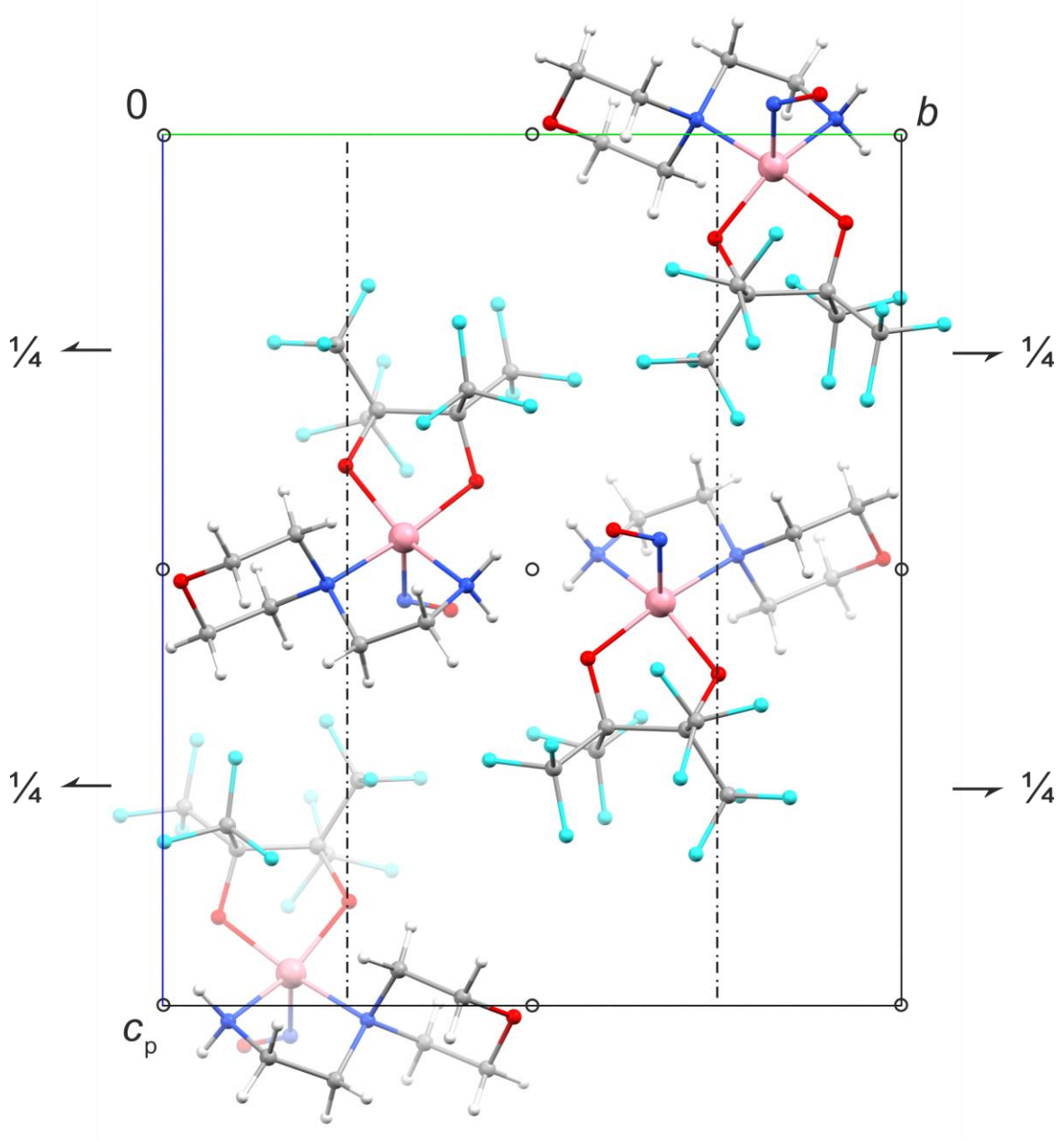

Figure 7.3: Packing diagram of [Co(2-aemor)(fpin)(NO)] (**1c**) in the monoclinic space group $P2_1/n$ with view along [100]. The symmetry elements of the space group $P2_1/n$ are overlaid. Atoms: carbon (gray), hydrogen (white), cobalt (pink), fluorine (turquoise), nitrogen (blue), oxygen (red).

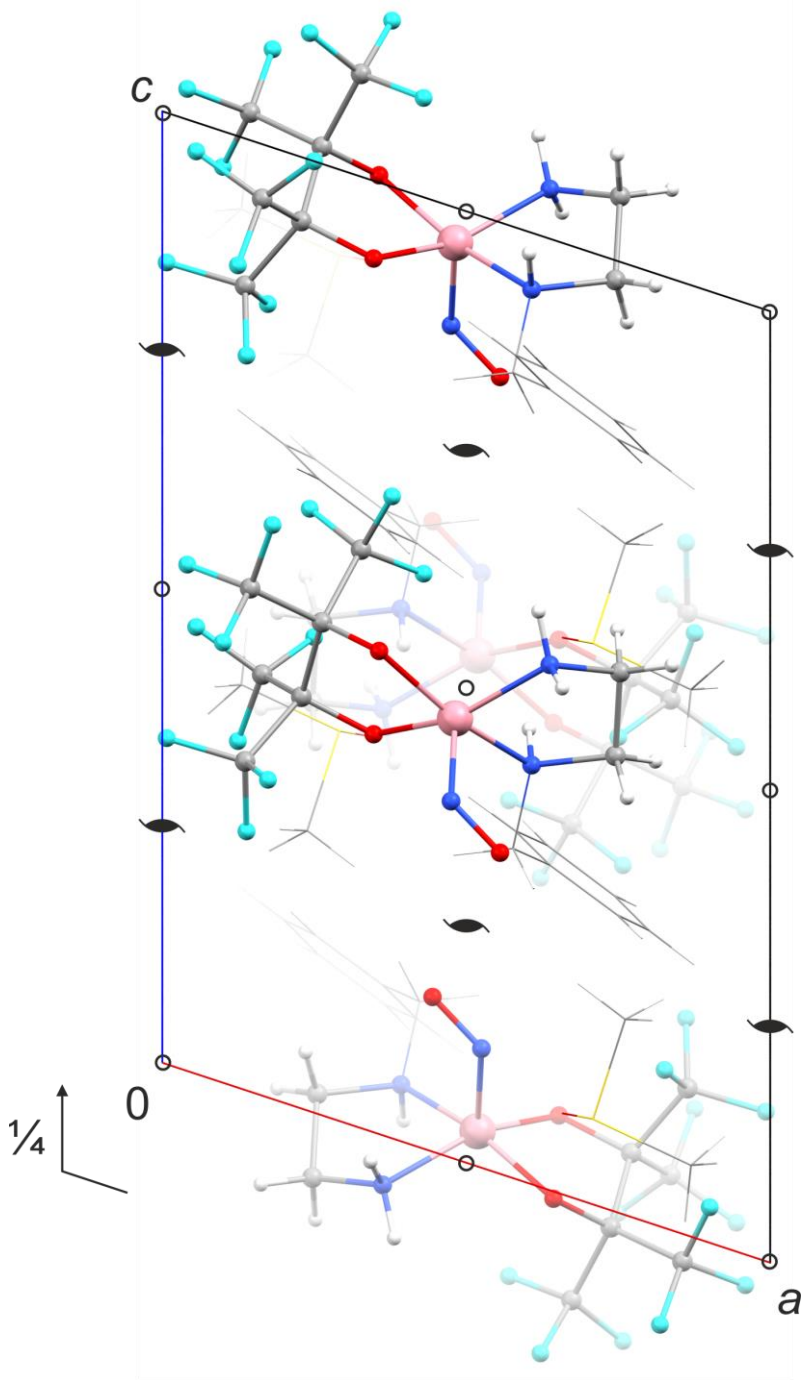

Figure 7.4: Packing diagram of [Co(bnen)(fpin)(NO)]·DMSO (**1d**·DMSO) in the monoclinic space group $P2_1/c$ with view along [010]. The symmetry elements of the space group $P2_1/c$ are overlaid. Atoms: carbon (gray), hydrogen (white), cobalt (pink), fluorine (turquoise), nitrogen (blue), oxygen (red), sulfur (yellow). The benzyl groups and the co-crystallized DMSO molecules are depicted as wireframe.

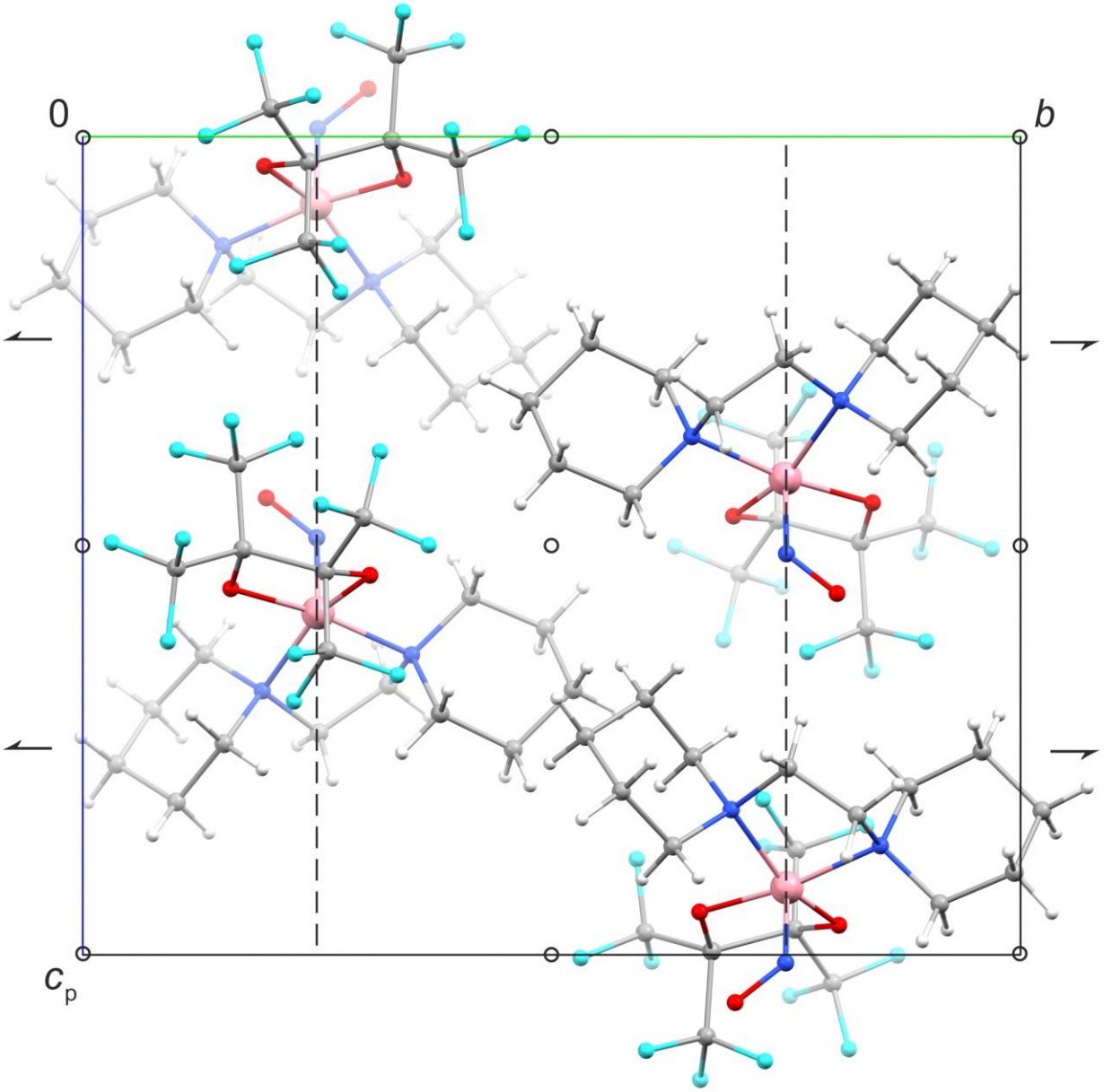

Figure 7.5: Packing diagr. of [Co(dpipe)(fpin)(NO)] (**1e**) in the monoclinic space group $P2_1/c$ with view along [100]. The symmetry elements of the space group $P2_1/c$ are overlaid. Atoms: carbon (gray), hydrogen (white), cobalt (pink), fluorine (turquoise), nitrogen (blue), oxygen (red).

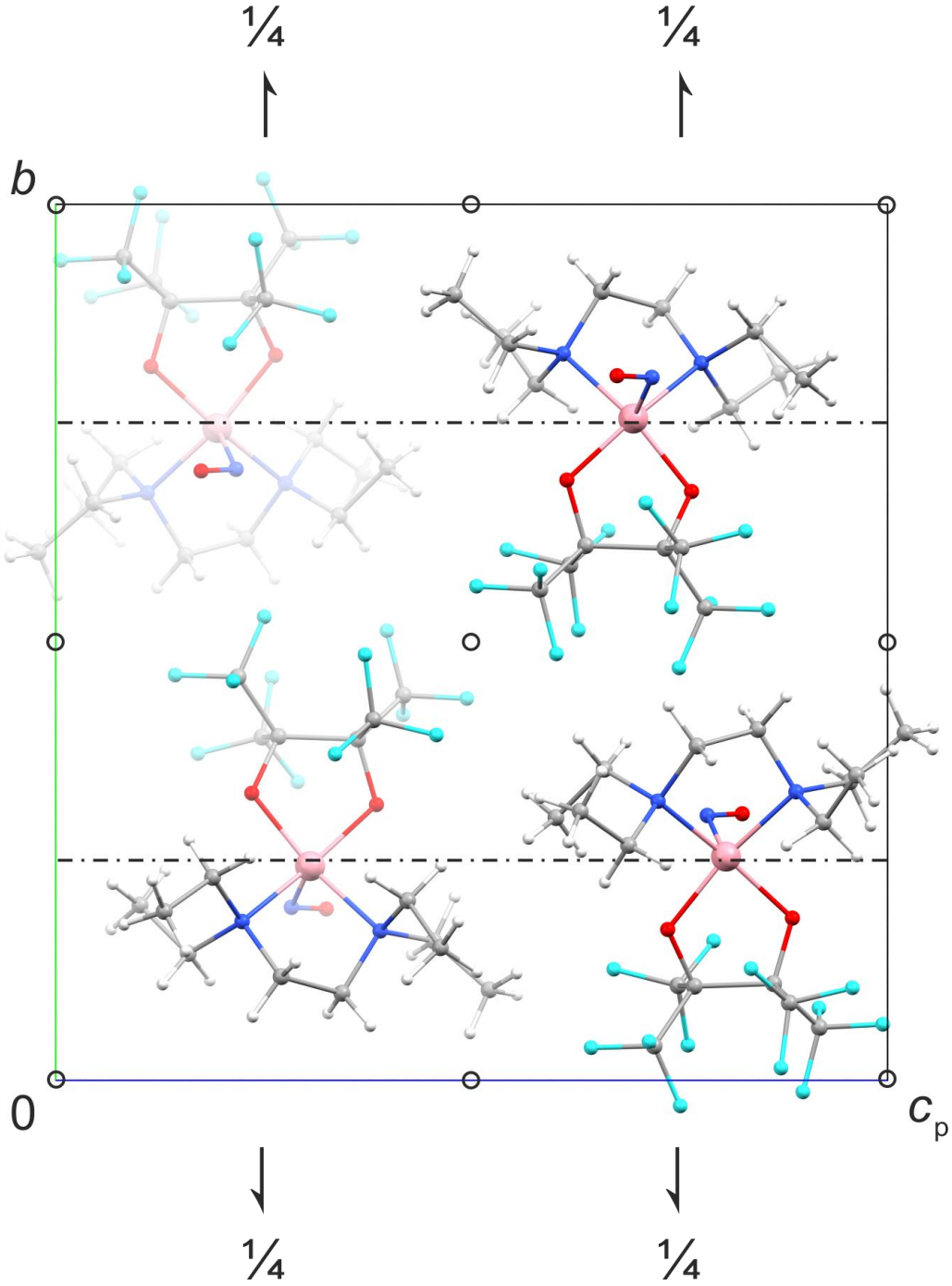

Figure 7.6: Packing diagr. of [Co(fpin)(NO)(teen)] (**1f**) in the monoclinic space group $P2_1/n$ with view along [100]. The symmetry elements of the space group $P2_1/n$ are overlaid. Atoms: carbon (gray), hydrogen (white), cobalt (pink), fluorine (turquoise), nitrogen (blue), oxygen (red). The nitrosyl moieties of the minor disorder form are omitted for clarity.

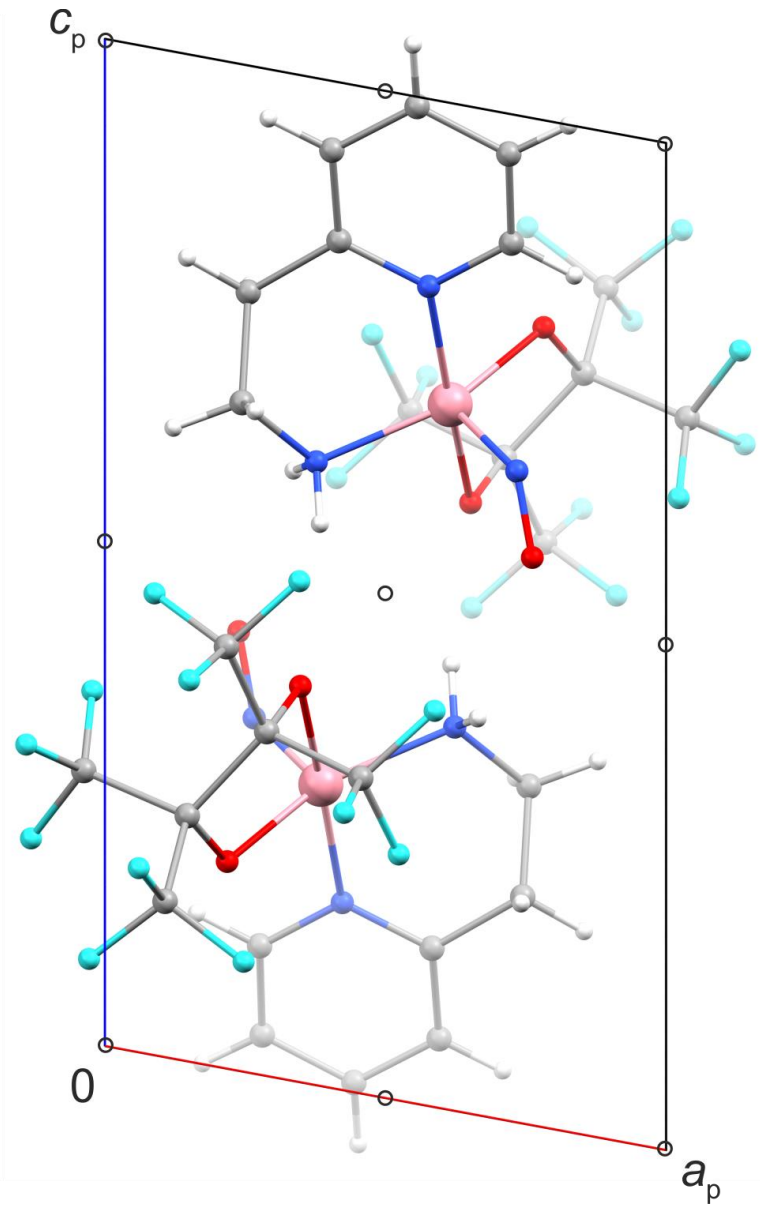

Figure 7.7: Packing diagram of [Co(2-aepy)(fpin)(NO)] (**1g**) in the triclinic space group $P\bar{1}$ with view along [010]. The symmetry elements of the space group $P\bar{1}$ are overlaid. Atoms: carbon (gray), hydrogen (white), cobalt (pink), fluorine (turquoise), nitrogen (blue), oxygen (red).

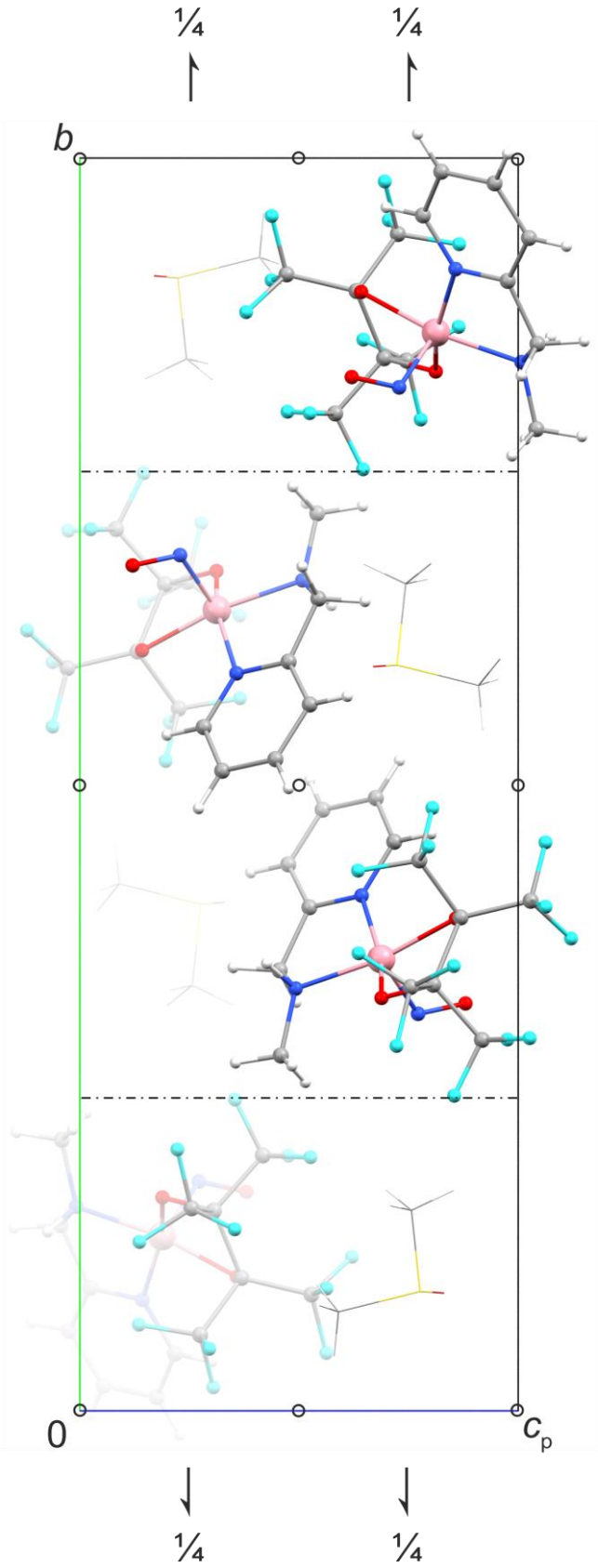

Figure 7.8: Packing diagram of [Co(fpin)(mampy)(NO)]·DMSO (**1h**·DMSO) in the monoclinic space group $P2_1/n$ with view along [100]. The symmetry elements of the space group $P2_1/n$ are overlaid. Atoms: carbon (gray), hydrogen (white), cobalt (pink), fluorine (turquoise), nitrogen (blue), oxygen (red), sulfur (yellow). The co-crystallized DMSO molecules are depicted as wireframe.

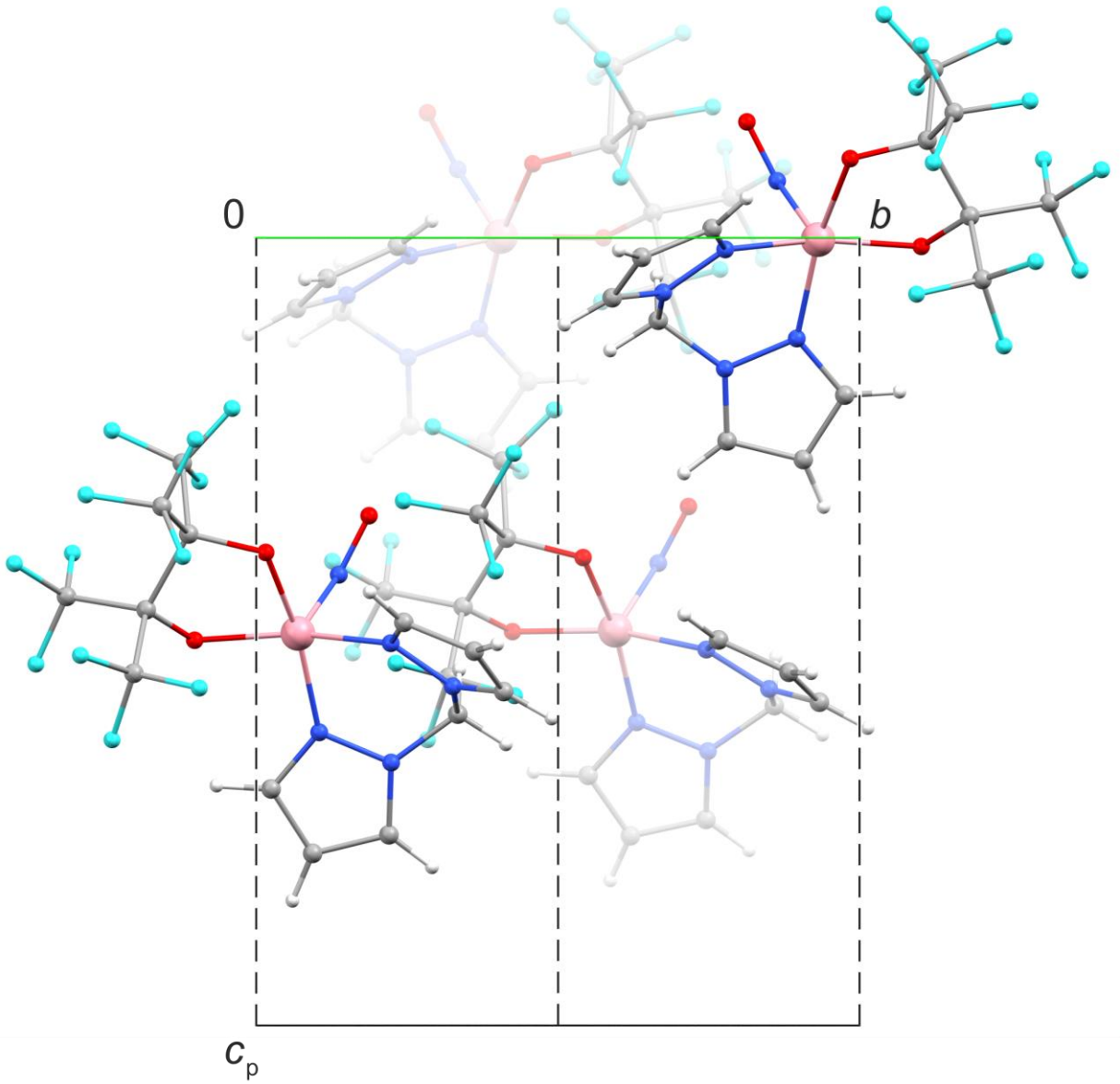

Figure 7.9: Packing diagram of [Co(bpm)(fpin)(NO)] (**1i**) in the monoclinic space group *Pc* with view along [100]. The symmetry elements of the space group *Pc* are overlaid. Atoms: carbon (gray), hydrogen (white), cobalt (pink), fluorine (turquoise), nitrogen (blue), oxygen (red).

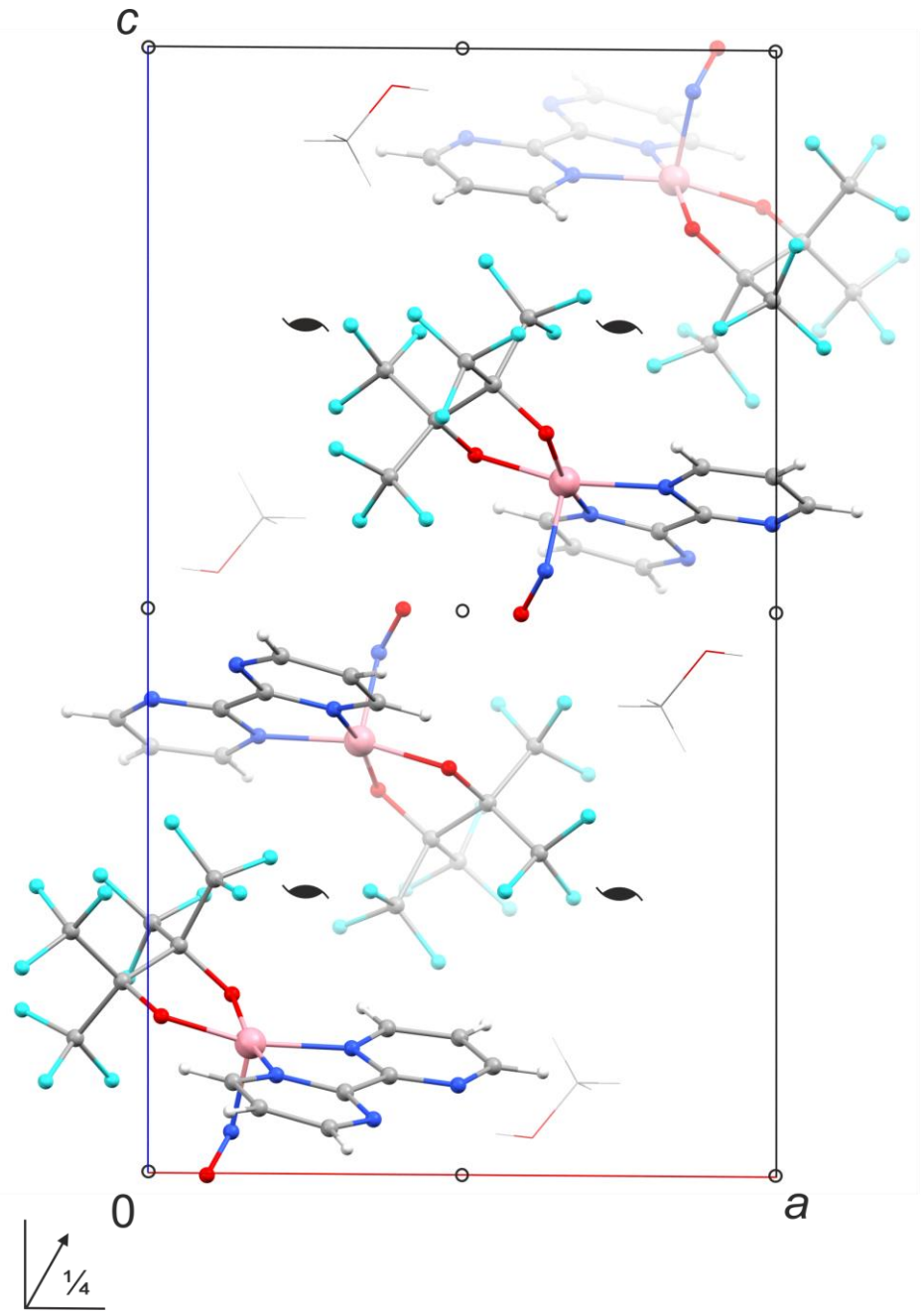

Figure 7.10: Packing diagram of [Co(bpym)(fpin)(NO)]·MeOH (**1j**·MeOH) in the monoclinic space group $P2_1/n$ with view along [010]. The symmetry elements of the space group $P2_1/n$ are overlaid. Atoms: carbon (gray), hydrogen (white), cobalt (pink), fluorine (turquoise), nitrogen (blue), oxygen (red). The co-crystallized MeOH molecules are depicted as wireframe.

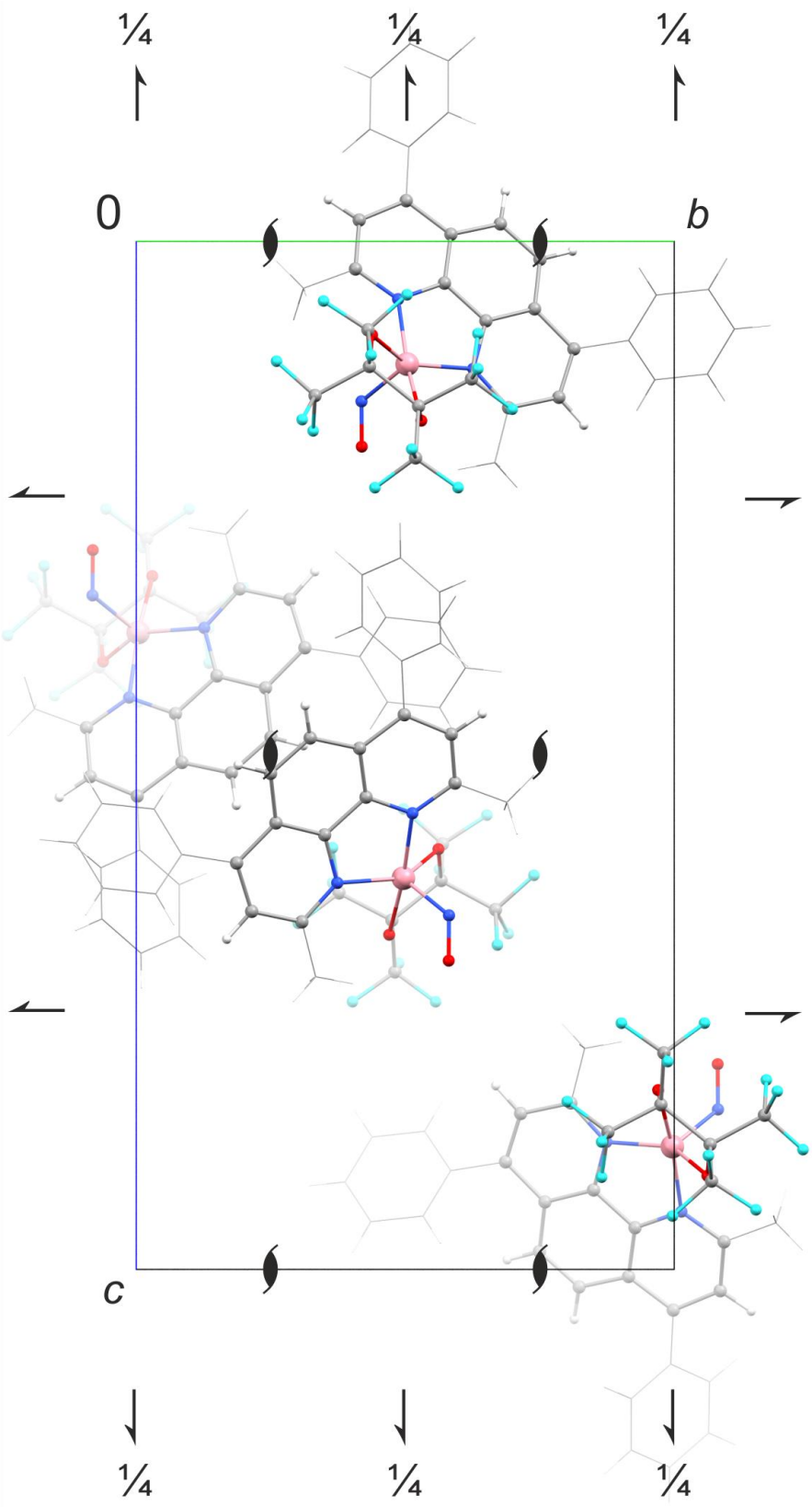

Figure 7.11: Packing diagr. of [Co(dmdpphen)(fpin)(NO)] (**1k**) in the orthorhombic space group $P2_12_12_1$ with view along [100]. The symmetry elements of the space group $P2_12_12_1$ are overlaid. Atoms: carbon (gray), hydrogen (white), cobalt (pink), fluorine (turquoise), nitrogen (blue), oxygen (red). The methyl and phenyl groups are depicted as wireframe.

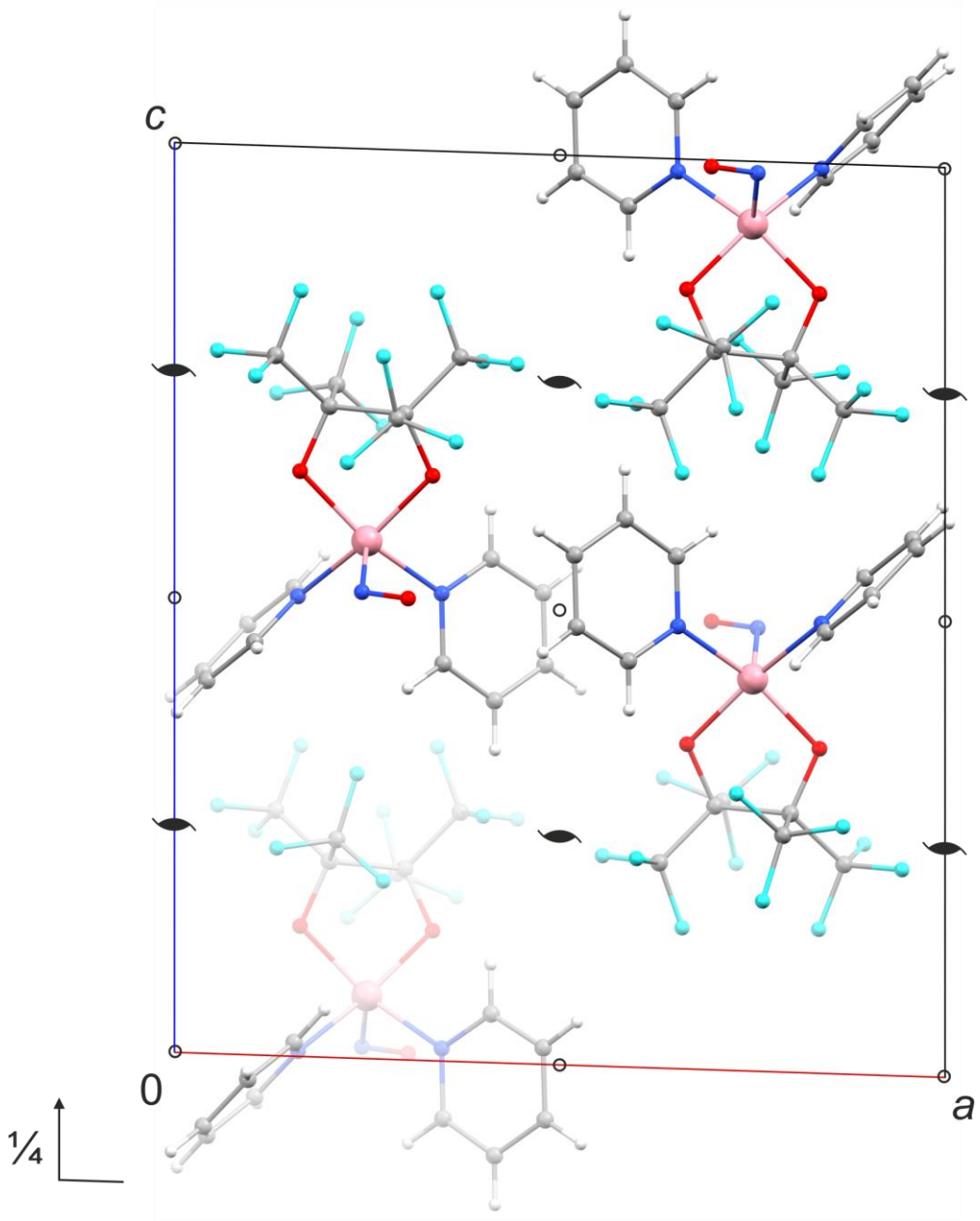

Figure 7.12: Packing diagr. of [Co(fpin)(NO)(py)$_2$] (**1l**) in the monoclinic space group $P2_1/c$ with view along [010]. The symmetry elements of the space group $P2_1/c$ are overlaid. Atoms: carbon (gray), hydrogen (white), cobalt (pink), fluorine (turquoise), nitrogen (blue), oxygen (red).

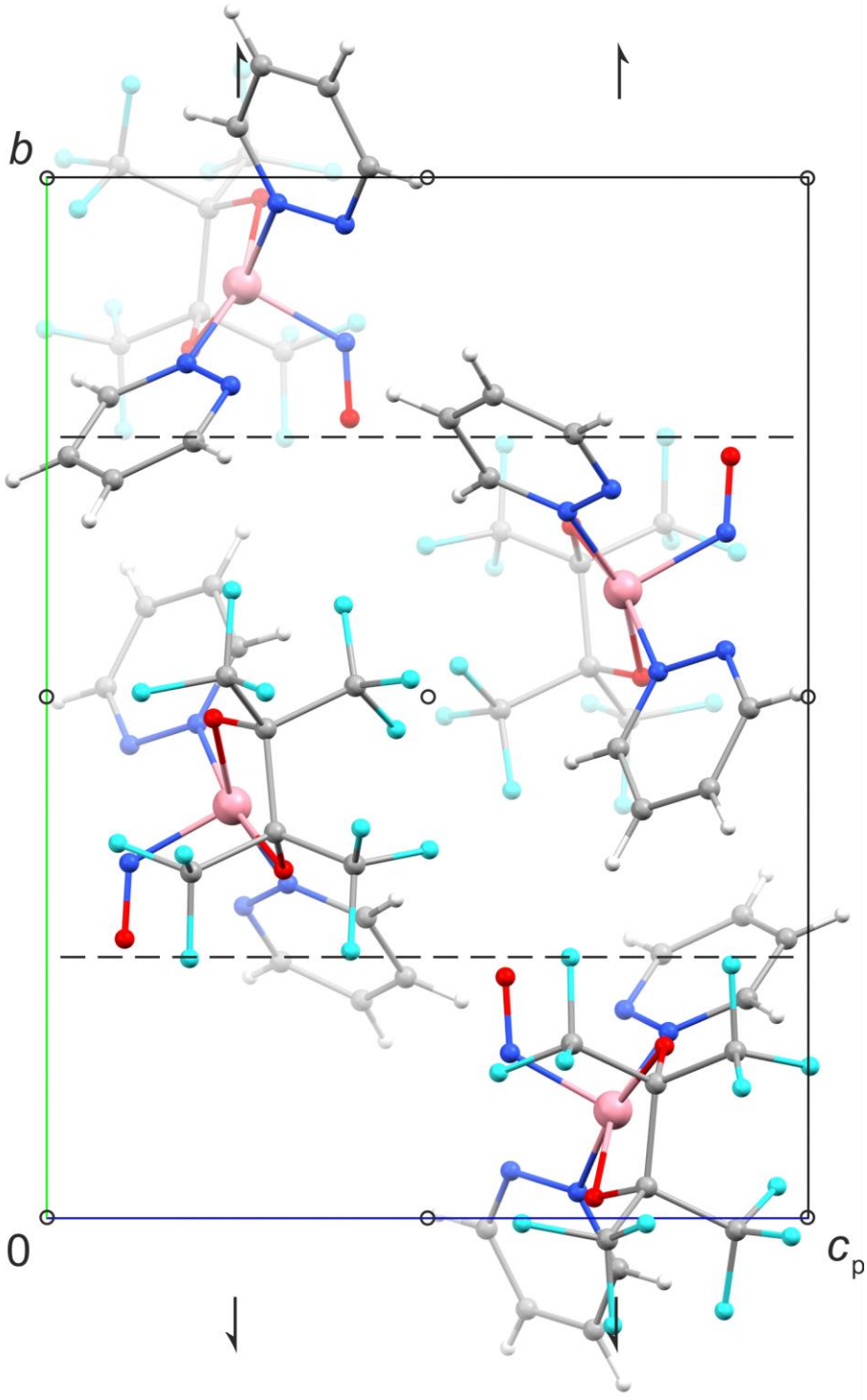

Figure 7.13: Packing diagram of [Co(fpin)(NO)(pydz)$_2$] (**1m**) in the monoclinic space group $P2_1/c$ with view along [100]. The symmetry elements of the space group $P2_1/c$ are overlaid. Atoms: carbon (gray), hydrogen (white), cobalt (pink), fluorine (turquoise), nitrogen (blue), oxygen (red).

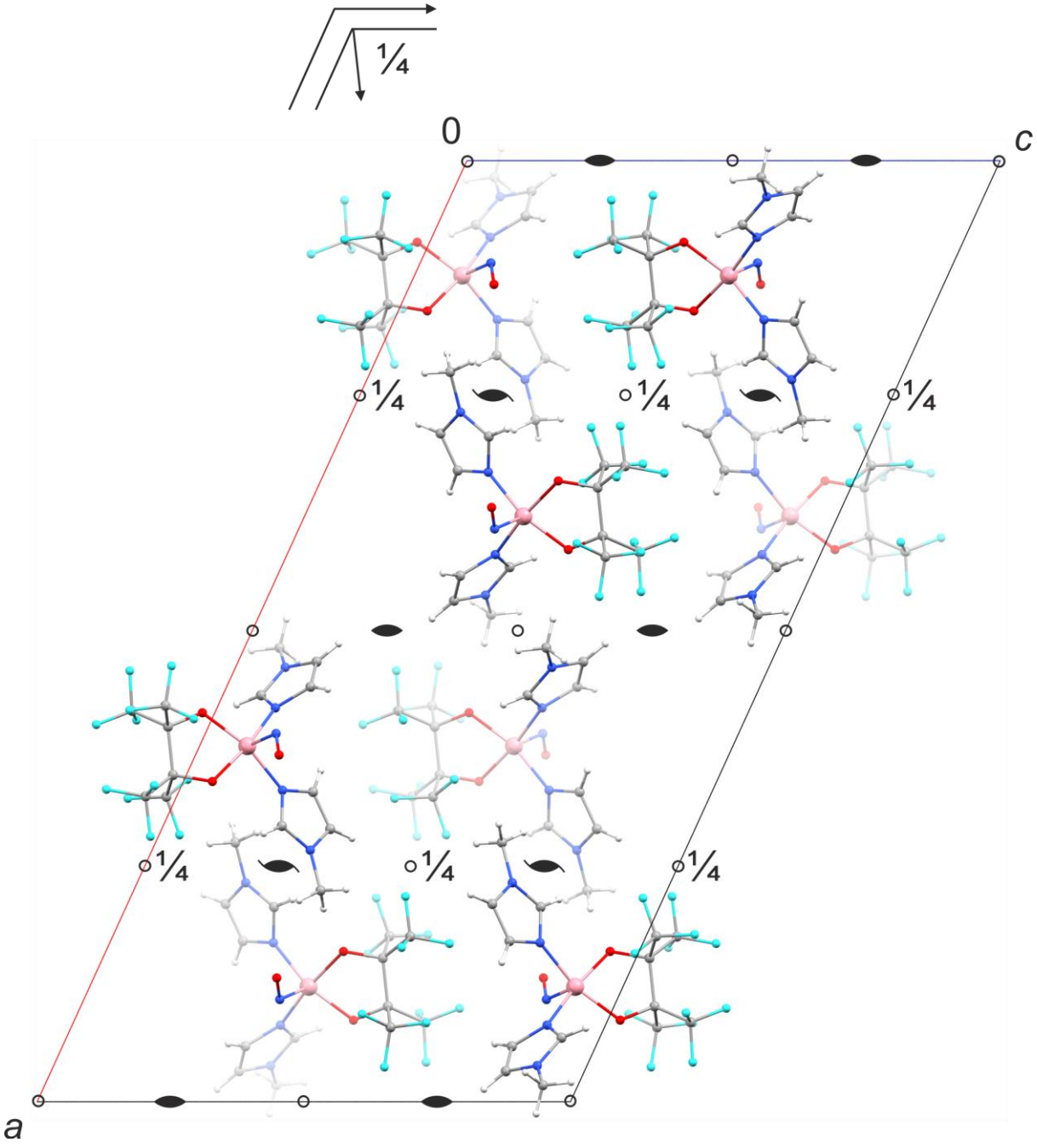

Figure 7.14: Packing diagr. of [Co(fpin)(mim)$_2$(NO)] (**1n**) in the monoclinic space group *C*2/*c* with view along [010]. The symmetry elements of the space group *C*2/*c* are overlaid. Atoms: carbon (gray), hydrogen (white), cobalt (pink), fluorine (turquoise), nitrogen (blue), oxygen (red).

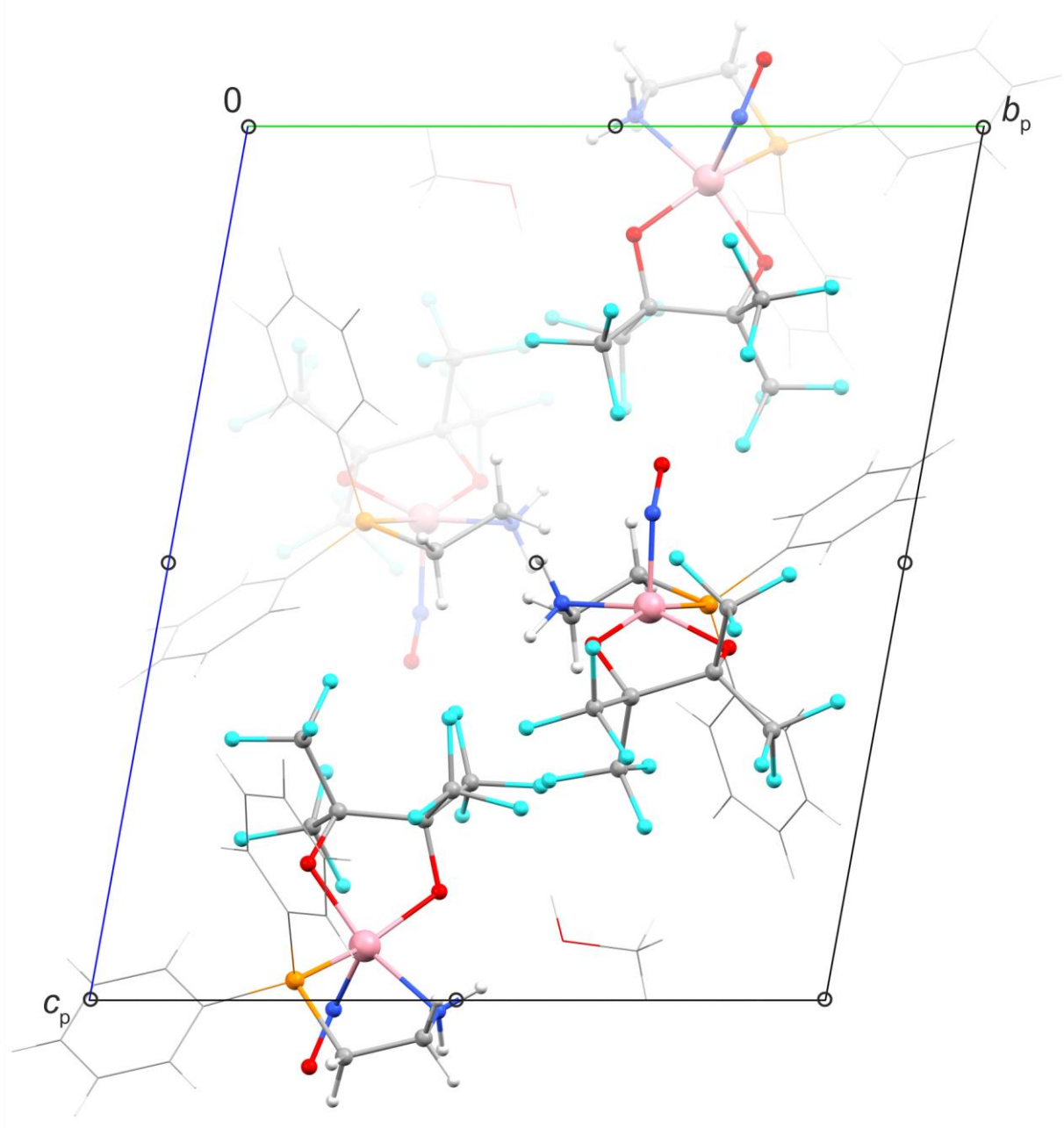

Figure 7.15: Packing diagram of [Co(2-aedpp)(fpin)(NO)]·0.5MeOH (**2a**·0.5MeOH) in the triclinic space group $P\bar{1}$ with view along [100]. The symmetry elements of the space group $P\bar{1}$ are overlaid. Atoms: carbon (gray), hydrogen (white), cobalt (pink), fluorine (turquoise), nitrogen (blue), oxygen (red), phosphorus (orange). The phenyl groups and the co-crystallized MeOH are depicted as wireframe.

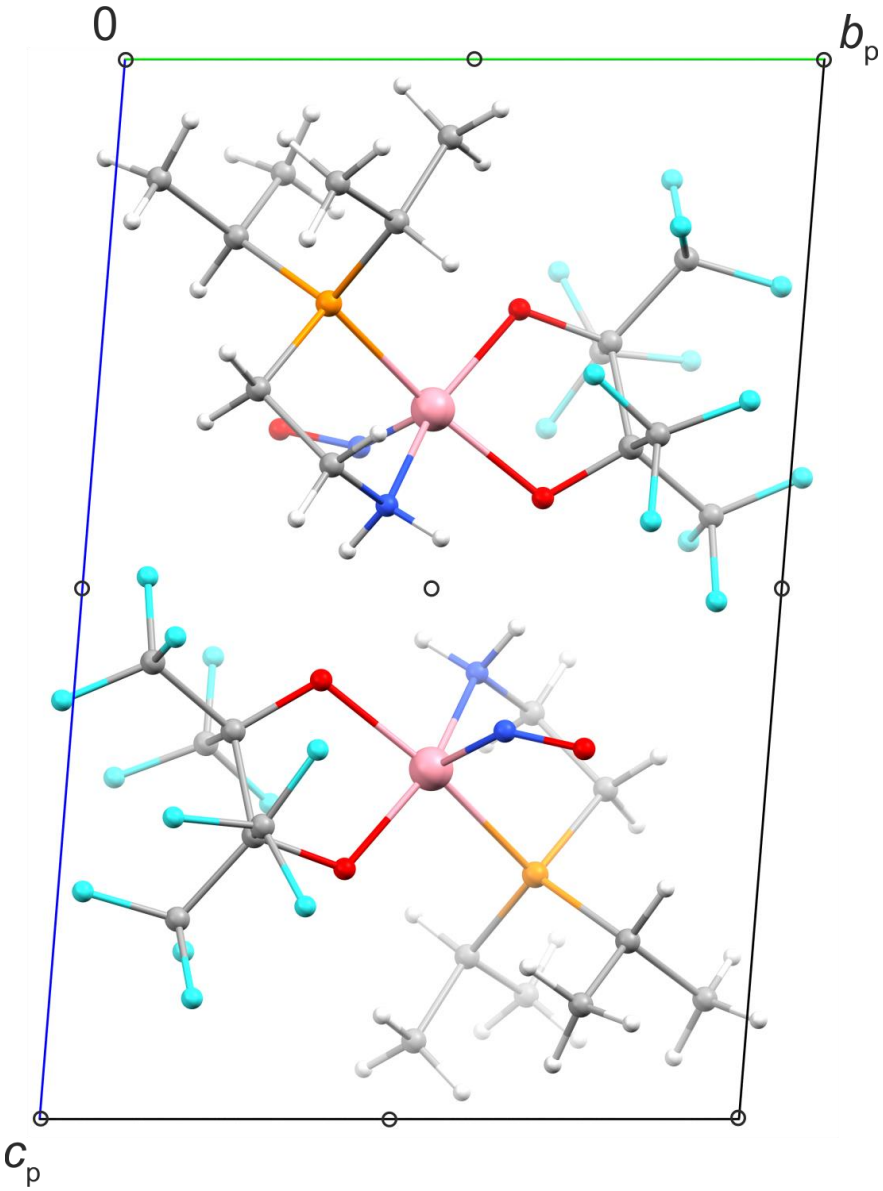

Figure 7.16: Packing diagram of [Co(2-aedip)(fpin)(NO)] (**2b**) in the triclinic space group $P\bar{1}$ with view along [100]. The symmetry elements of the space group $P\bar{1}$ are overlaid. Atoms: carbon (gray), hydrogen (white), cobalt (pink), fluorine (turquoise), nitrogen (blue), oxygen (red), phosphorus (orange).

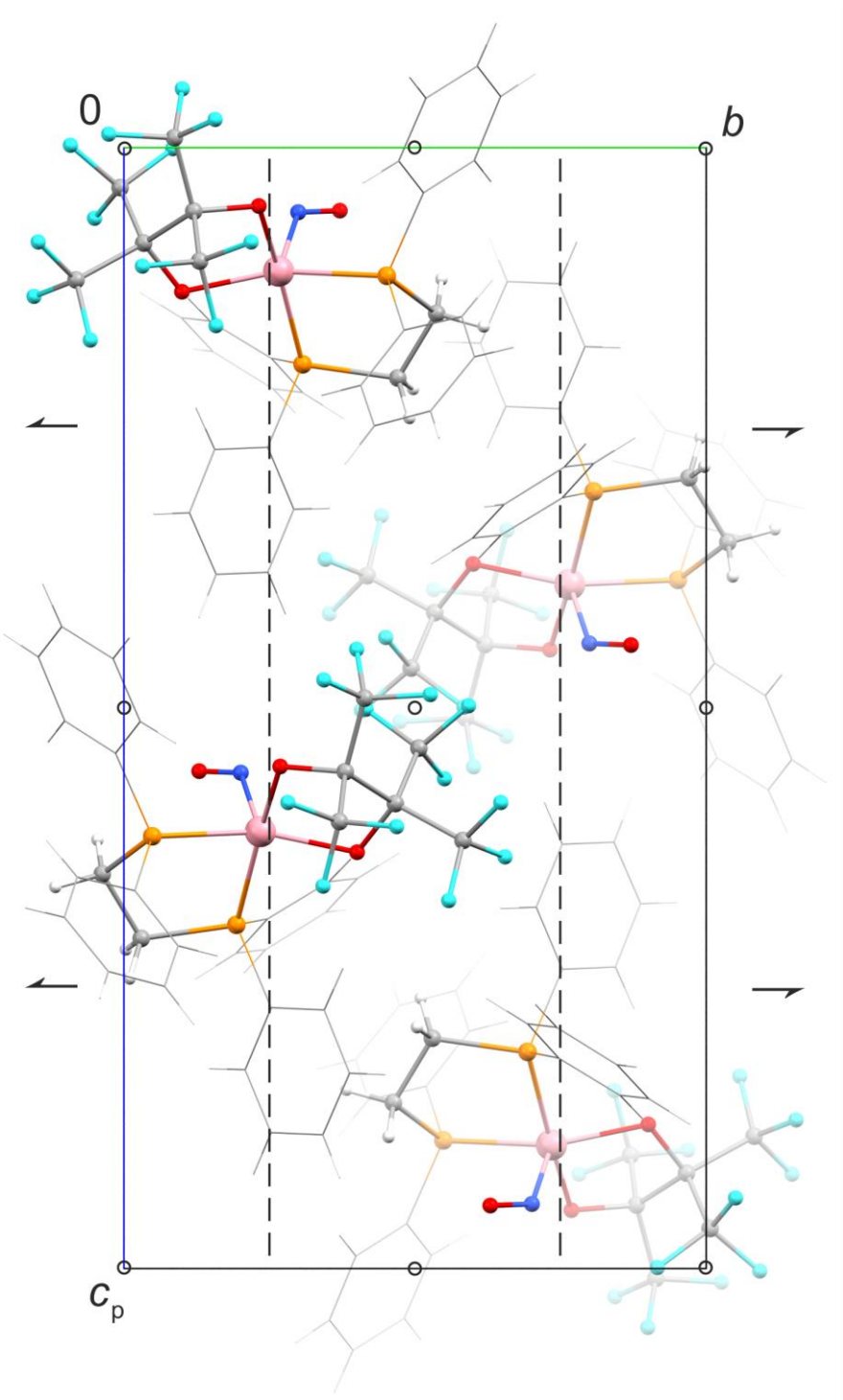

Figure 7.17: Packing diagram of [Co(dppe)(fpin)(NO)] (**3a**) in the monoclinic space group $P2_1/c$ with view along [100]. The symmetry elements of the space group $P2_1/c$ are overlaid. Atoms: carbon (gray), hydrogen (white), cobalt (pink), fluorine (turquoise), nitrogen (blue), oxygen (red), phosphorus (orange). The phenyl groups are depicted as wireframe.

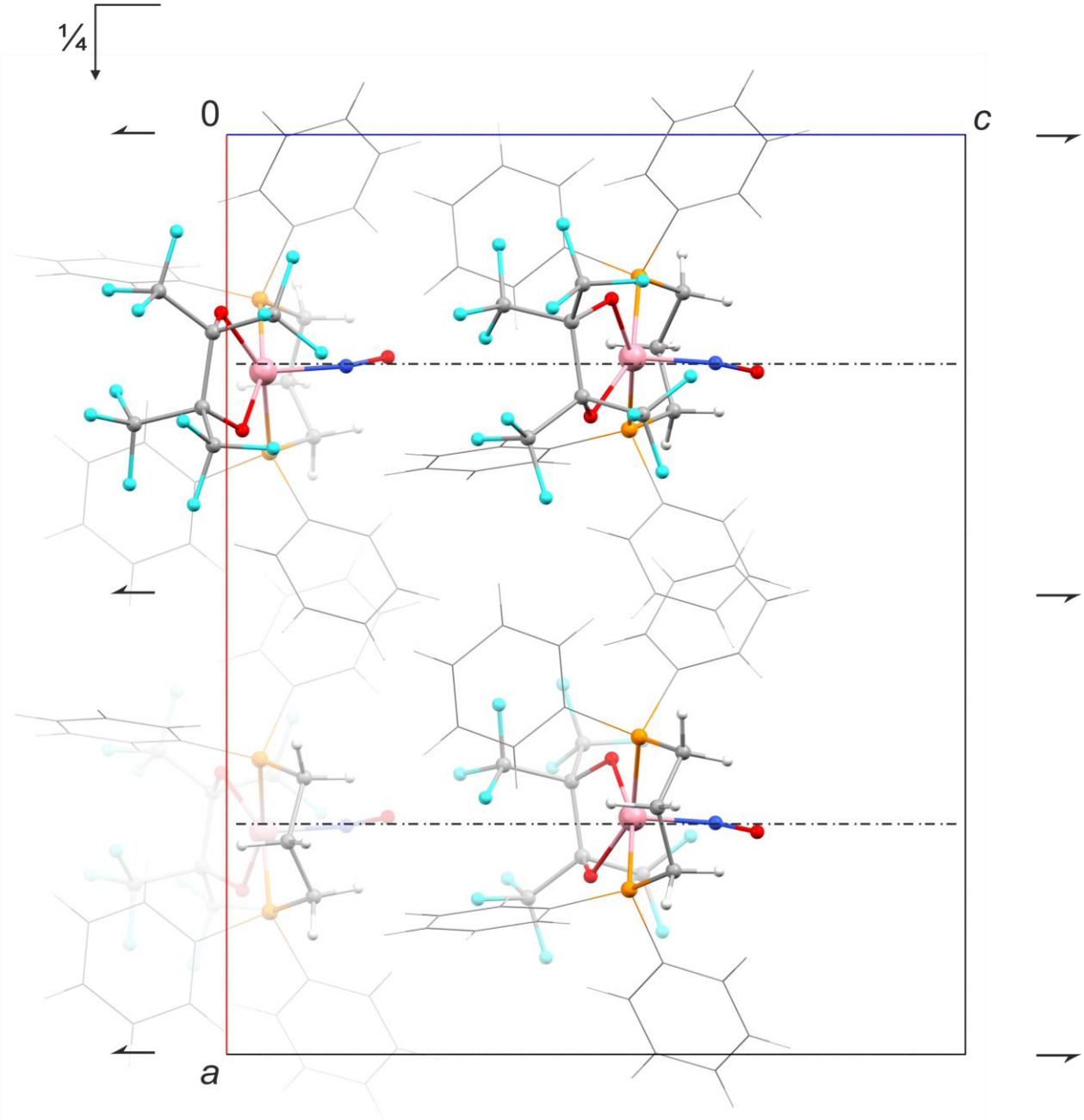

Figure 7.18: Packing diagram of [Co(dppp)(fpin)(NO)] (**3b**) in the orthorhombic space group *Pna*2_1 with view along [010]. The symmetry elements of the space group *Pna*2_1 are overlaid. Atoms: carbon (gray), hydrogen (white), cobalt (pink), fluorine (turquoise), nitrogen (blue), oxygen (red), phosphorus (orange). The phenyl groups are depicted as wireframe.

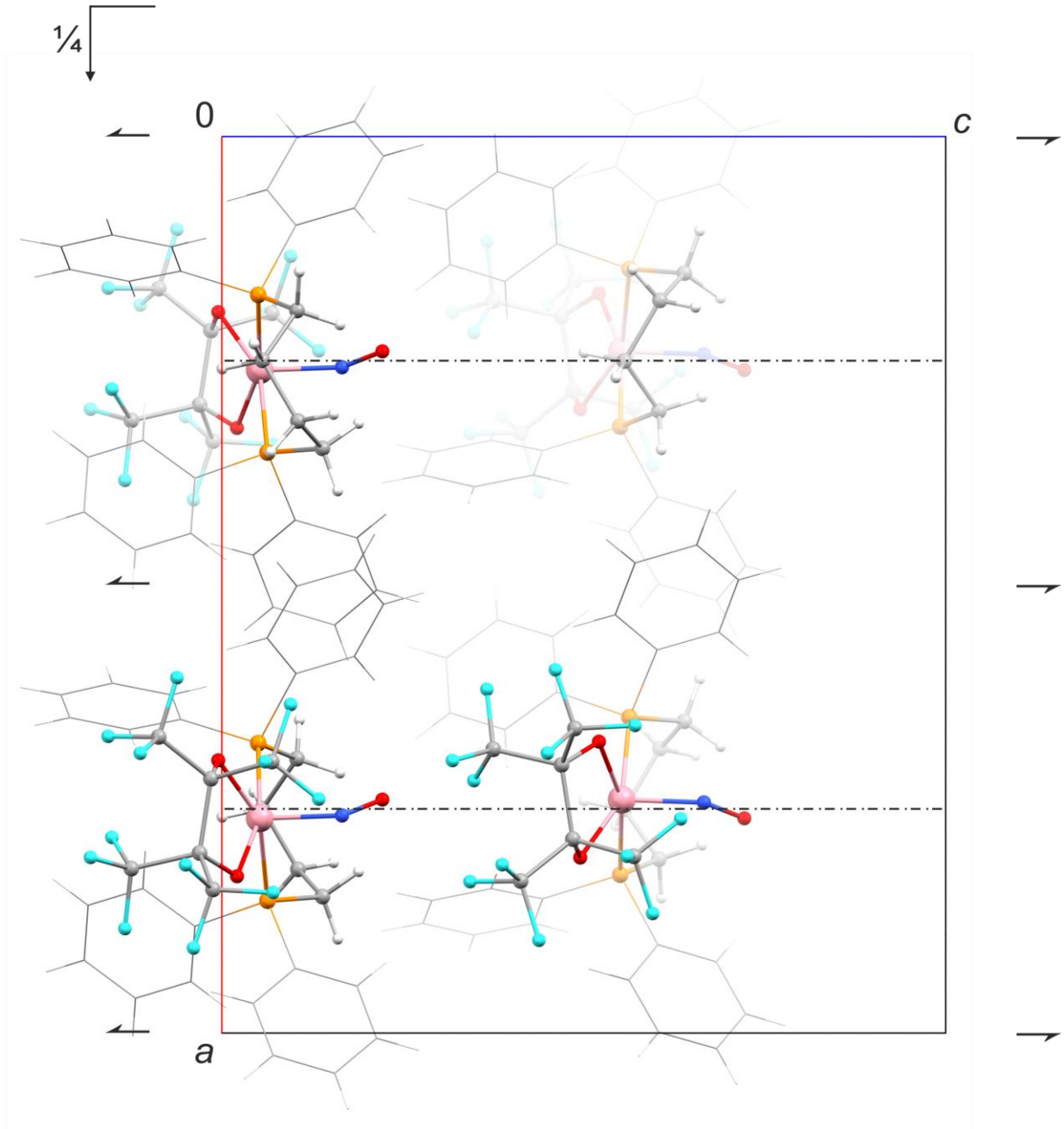

Figure 7.19: Packing diagram of [Co(dppb)(fpin)(NO)] (**3c**) in the orthorhombic space group *Pna*2_1 with view along [010]. The symmetry elements of the space group *Pna*2_1 are overlaid. Atoms: carbon (gray), hydrogen (white), cobalt (pink), fluorine (turquoise), nitrogen (blue), oxygen (red), phosphorus (orange). The phenyl groups are depicted as wireframe.

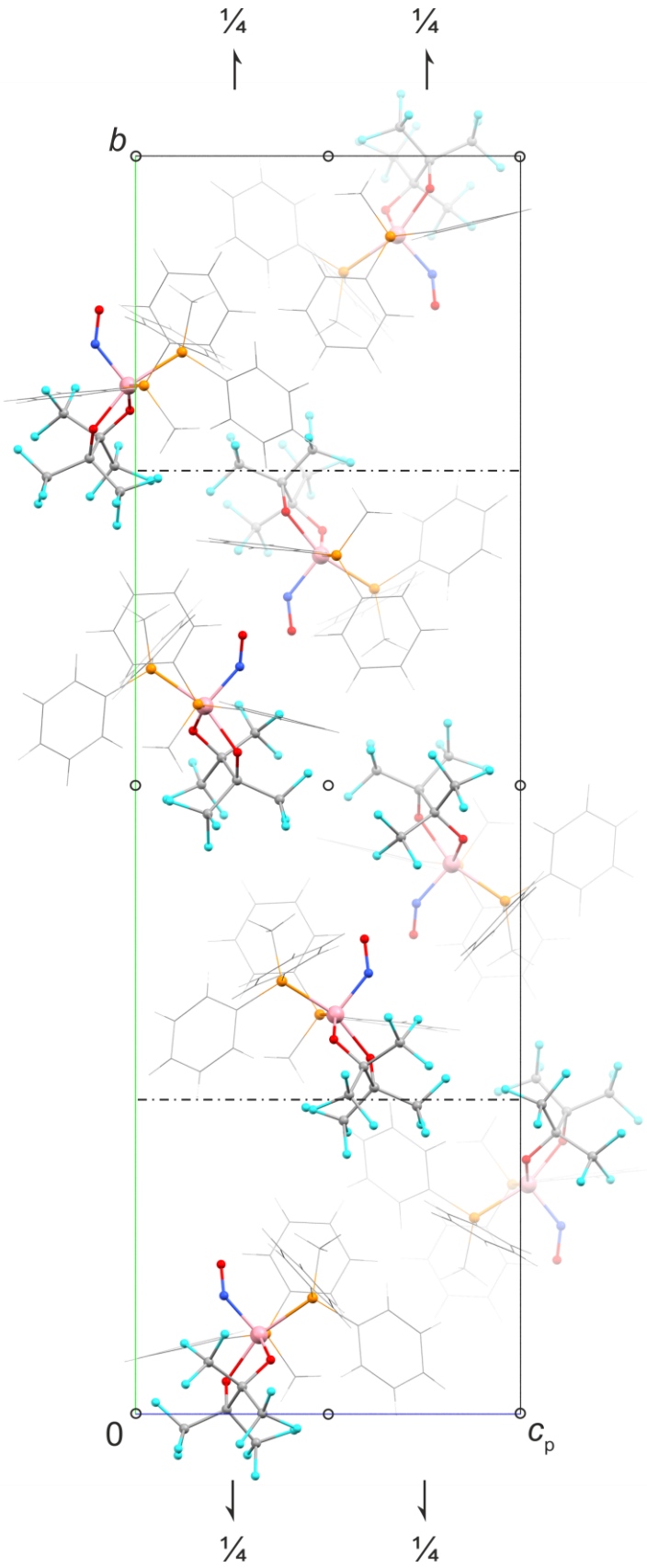

Figure 7.20: Packing diagram of [Co(fpin)(NO)($PMePh_2$)$_2$] (**3d**) in the monoclinic space group $P2_1/n$ with view along [100]. The symmetry elements of the space group $P2_1/n$ are overlaid. Atoms: carbon (gray), hydrogen (white), cobalt (pink), fluorine (turquoise), nitrogen (blue), oxygen (red), phosphorus (orange). The methyl and phenyl groups are depicted as wireframe.

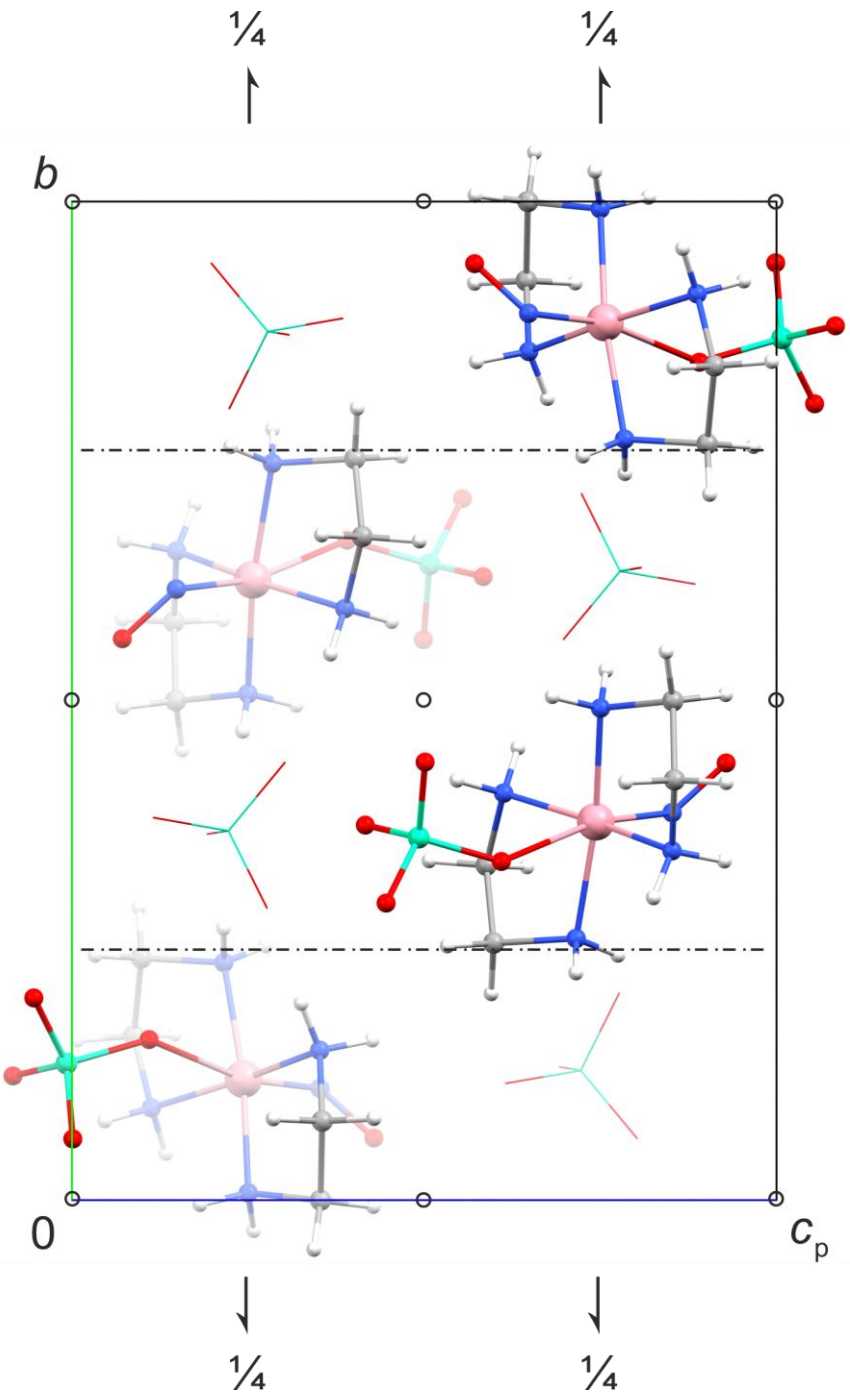

Figure 7.21: Packing diagram of *trans*-[Co(ClO_4)$(en)_2$(NO)]ClO_4 (**4a**) in the monoclinic space group $P2_1/n$ with view along [100]. The symmetry elements of the space group $P2_1/n$ are overlaid. Atoms: carbon (gray), hydrogen (white), chlorine (green), cobalt (pink), nitrogen (blue), oxygen (red). The non-coordinating perchlorate ions are depicted as wireframe. The nitrosyl moieties of the minor disorder form are omitted for clarity.

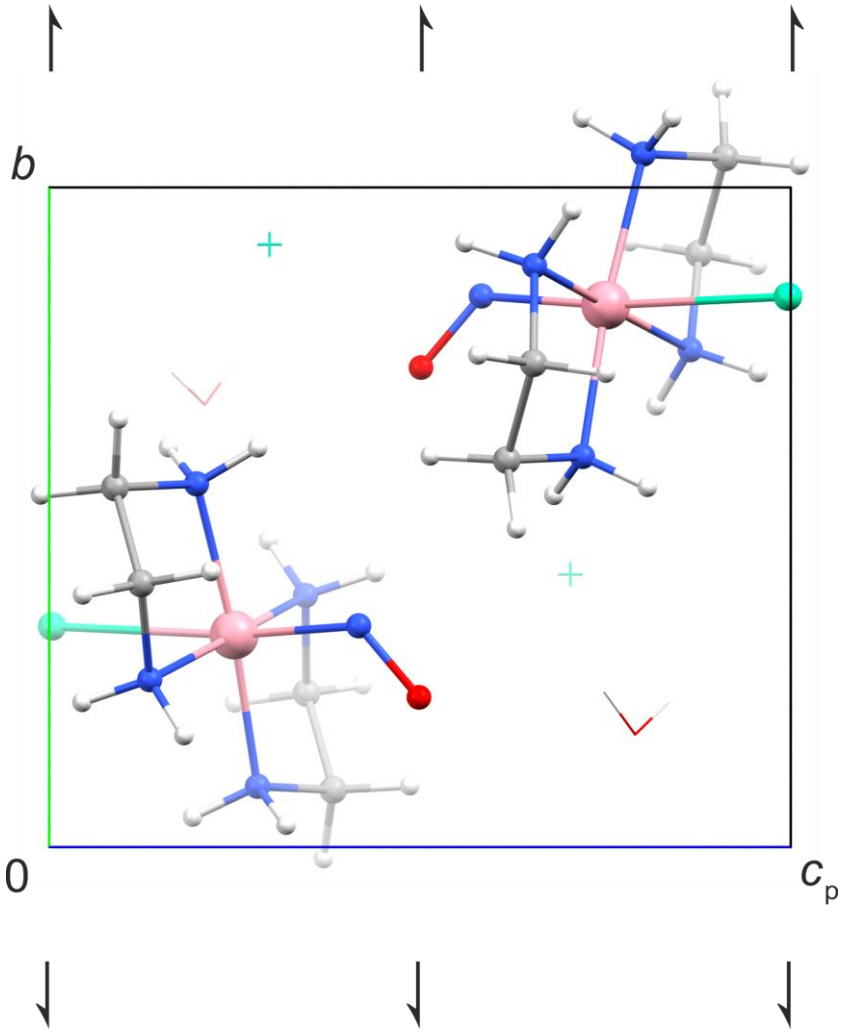

Figure 7.22: Packing diagram of *trans*-[CoCl(en)$_2$(NO)]Cl·H$_2$O (**4b**·H$_2$O) in the monoclinic space group $P2_1$ with view along [100]. The symmetry elements of the space group $P2_1$ are overlaid. Atoms: carbon (gray), hydrogen (white), chlorine (green), cobalt (pink), nitrogen (blue), oxygen (red). The non-coordinating chloride ions and co-crystallized water molecules are depicted as wireframe.

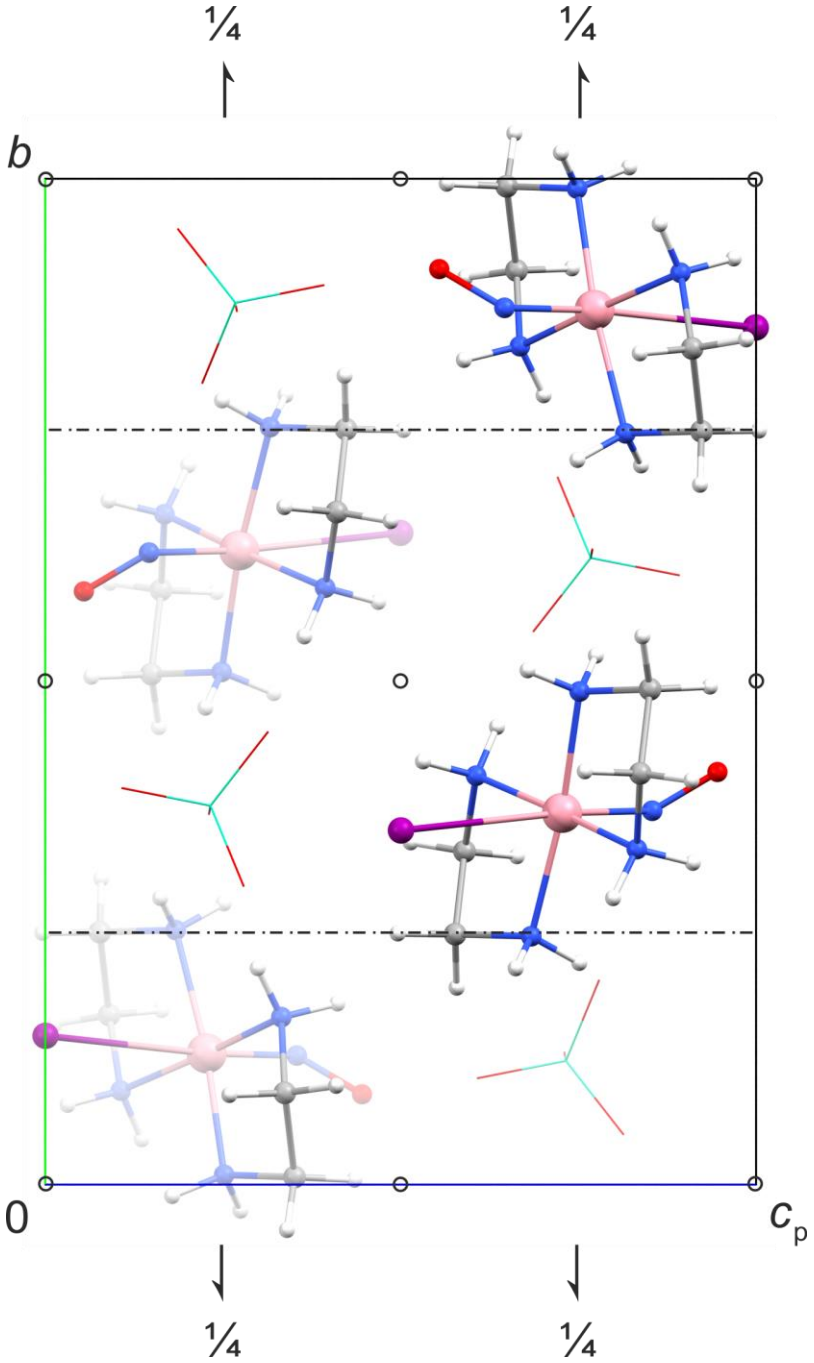

Figure 7.23: Packing diagram of *trans*-$[Co(en)_2I(NO)](ClO_4)_{0.6}I_{0.4}$ (**4c**) in the monoclinic space group $P2_1/n$ with view along [100]. The symmetry elements of the space group $P2_1/n$ are overlaid. Atoms: carbon (gray), hydrogen (white), chlorine (green), cobalt (pink), iodine (purple), nitrogen (blue), oxygen (red). The perchlorate ions of the major disorder form are depicted as wireframe. The non-coordinating iodide ions and the nitrosyl moieties of the minor disorder form are omitted for clarity.

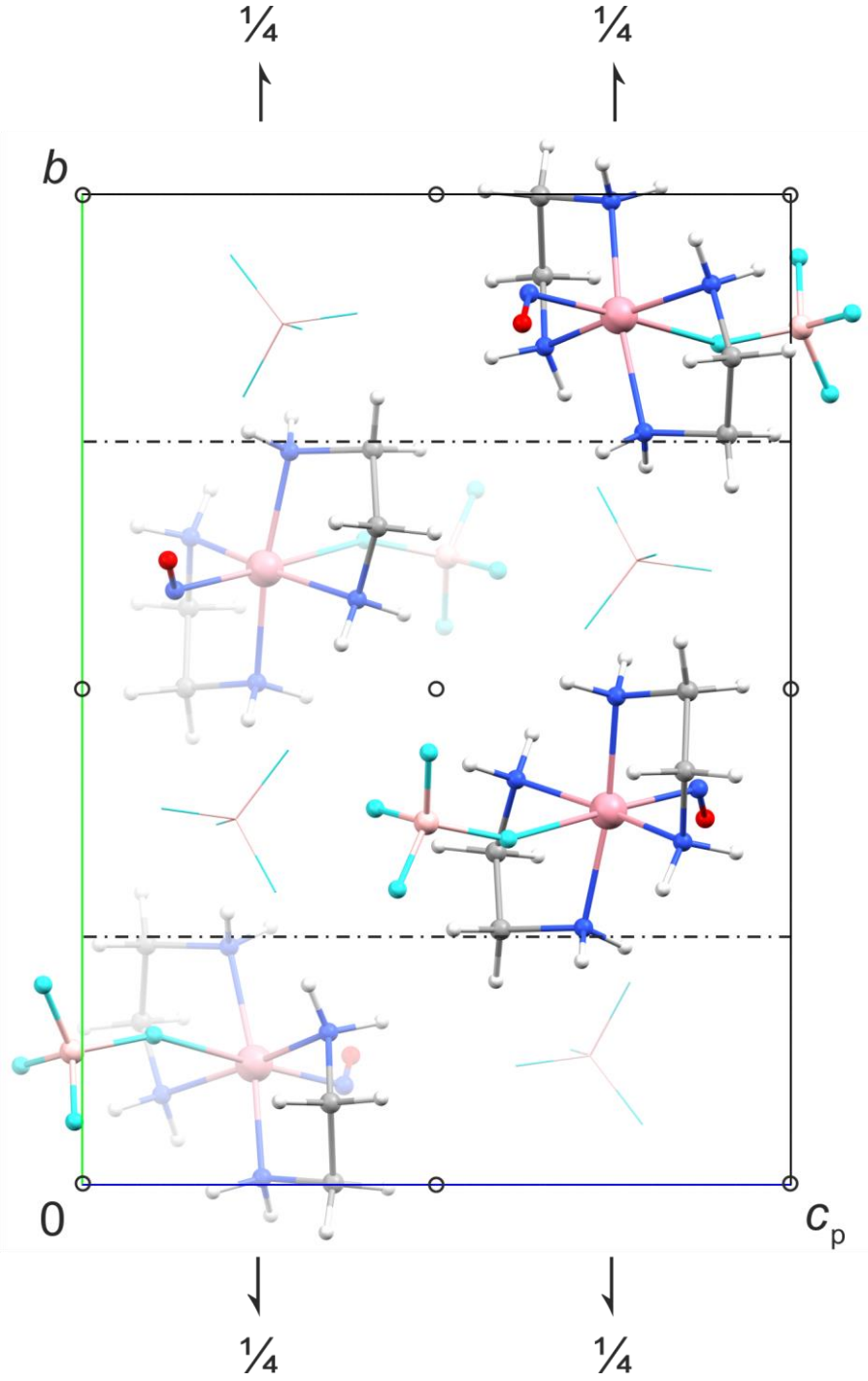

Figure 7.24: Packing diagram of *trans*-[Co(BF_4)$(en)_2$(NO)]BF_4 (**4e**) in the monoclinic space group $P2_1/n$ with view along [100]. The symmetry elements of the space group $P2_1/n$ are overlaid. Atoms: carbon (gray), hydrogen (white), boron (pearl), cobalt (pink), fluorine (turquoise), nitrogen (blue), oxygen (red). The non-coordinating tetrafluoroborate ions are depicted as wireframe. The nitrosyl moieties of the minor disorder form are omitted for clarity.

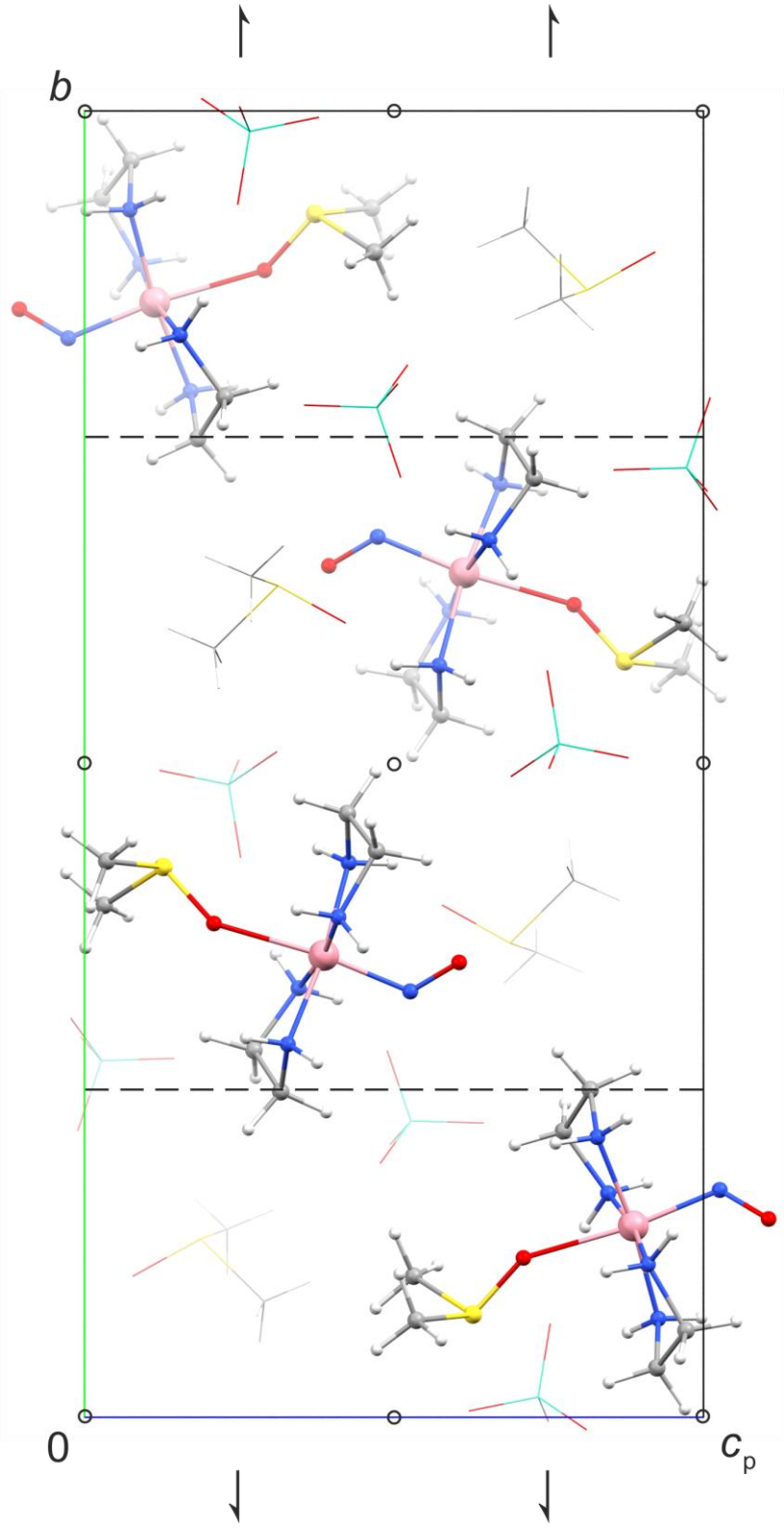

Figure 7.25: Packing diagram of *trans*-[Co(dmso-κ*O*)(en)$_2$(NO)](ClO$_4$)$_2$·DMSO (**4f**·DMSO) in the monoclinic space group *P*2$_1$/*c* with view along [100]. The symmetry elements of the space group *P*2$_1$/*c* are overlaid. Atoms: carbon (gray), hydrogen (white), chlorine (green), cobalt (pink), nitrogen (blue), oxygen (red), sulfur (yellow). The non-coordinating DMSO molecules and the perchlorate ions are depicted as wireframe. The nitrosyl moieties of the minor disorder form are omitted for clarity.

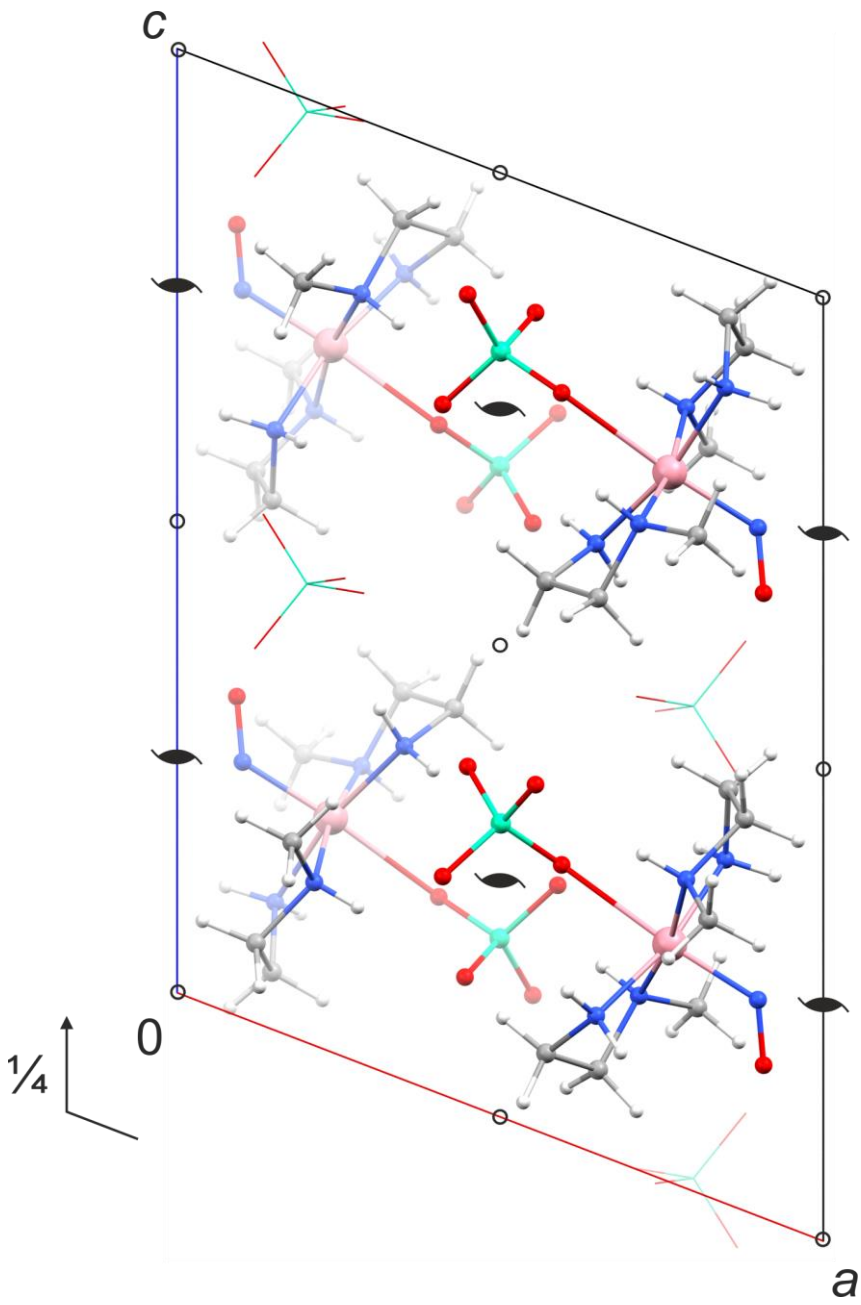

Figure 7.26: Packing diagram of *trans*-[Co(ClO_4)(men)$_2$(NO)]ClO_4 (**4g**) in the monoclinic space group $P2_1/c$ with view along [010]. The symmetry elements of the space group $P2_1/c$ are overlaid. Atoms: carbon (gray), hydrogen (white), chlorine (green), cobalt (pink), nitrogen (blue), oxygen (red). The non-coordinating perchlorate ions are depicted as wireframe.

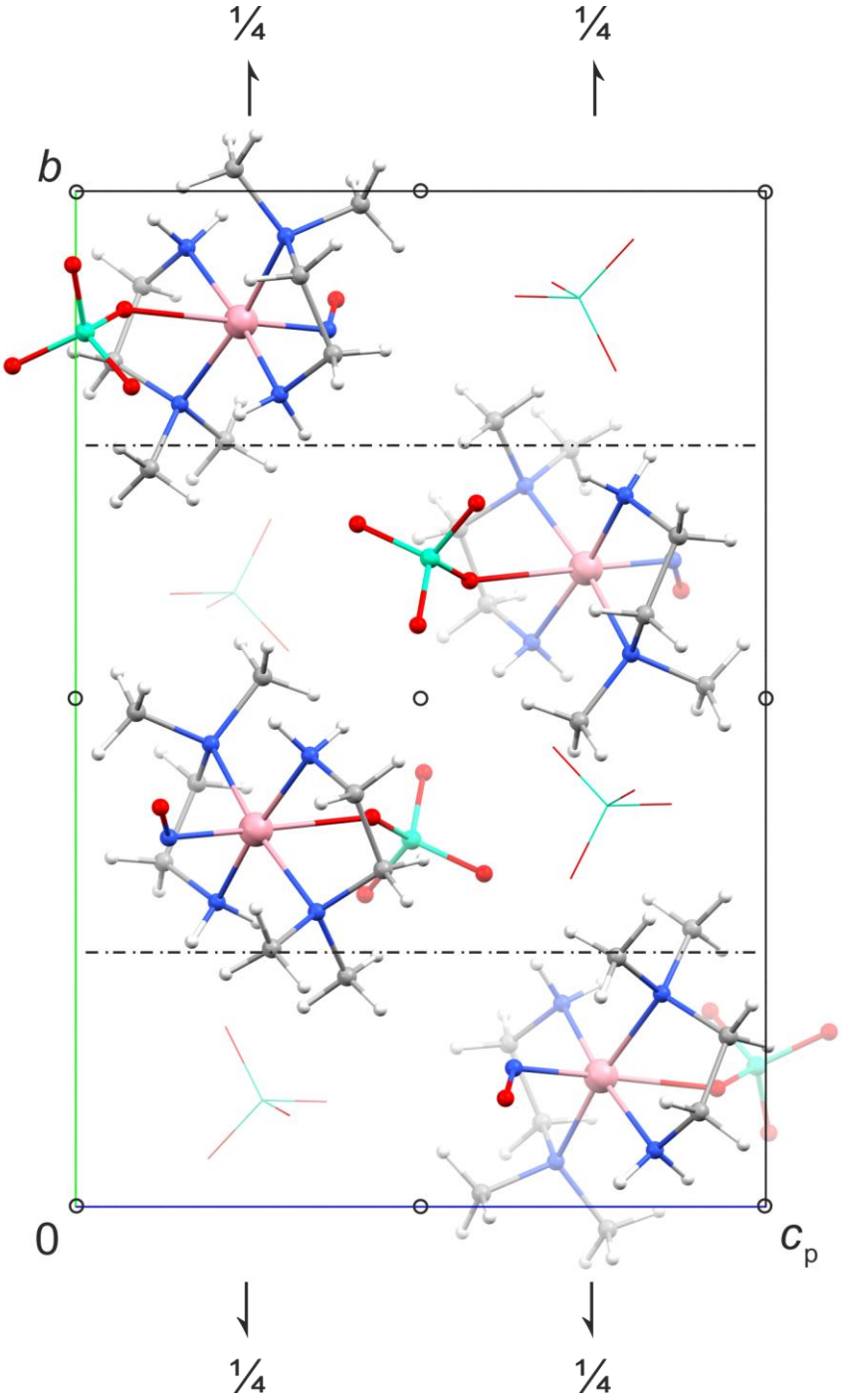

Figure 7.27: Packing diagram of *trans*-[Co(ClO_4)(*N*,*N*-dmen)$_2$(NO)]ClO_4 (**4h**) in the monoclinic space group $P2_1/n$ with view along [100]. The symmetry elements of the space group $P2_1/n$ are overlaid. Atoms: carbon (gray), hydrogen (white), chlorine (green), cobalt (pink), nitrogen (blue), oxygen (red). The non-coordinating perchlorate ions are depicted as wireframe.

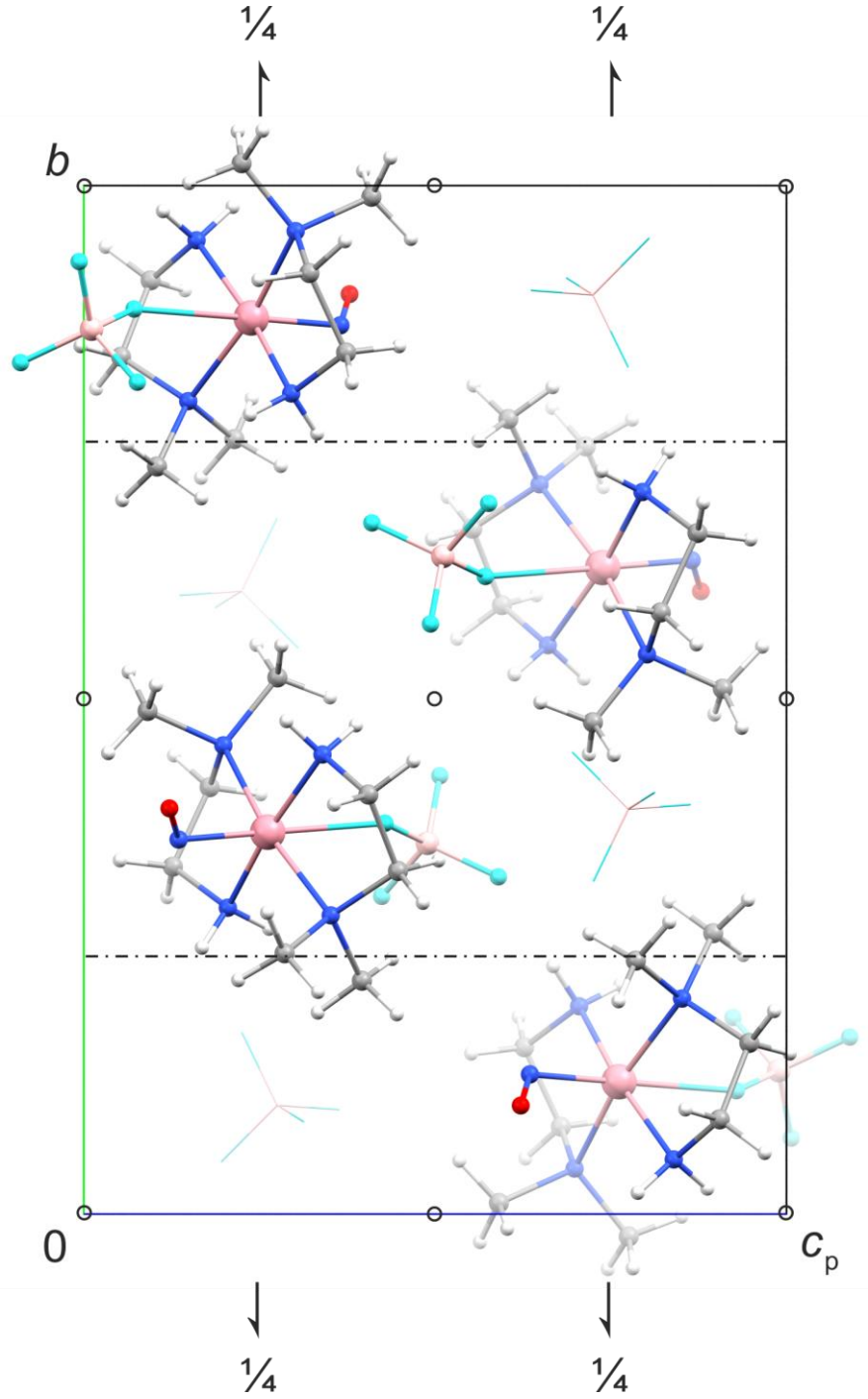

Figure 7.28: Packing diagram of *trans*-[Co(BF_4)(*N*,*N*-dmen)$_2$(NO)]BF_4 (**4i**) in the monoclinic space group $P2_1/n$ with view along [100]. The symmetry elements of the space group $P2_1/n$ are overlaid. Atoms: carbon (gray), hydrogen (white), boron (pearl), cobalt (pink), fluorine (turquoise), nitrogen (blue), oxygen (red). The non-coordinating tetrafluoroborate ions are depicted as wireframe.

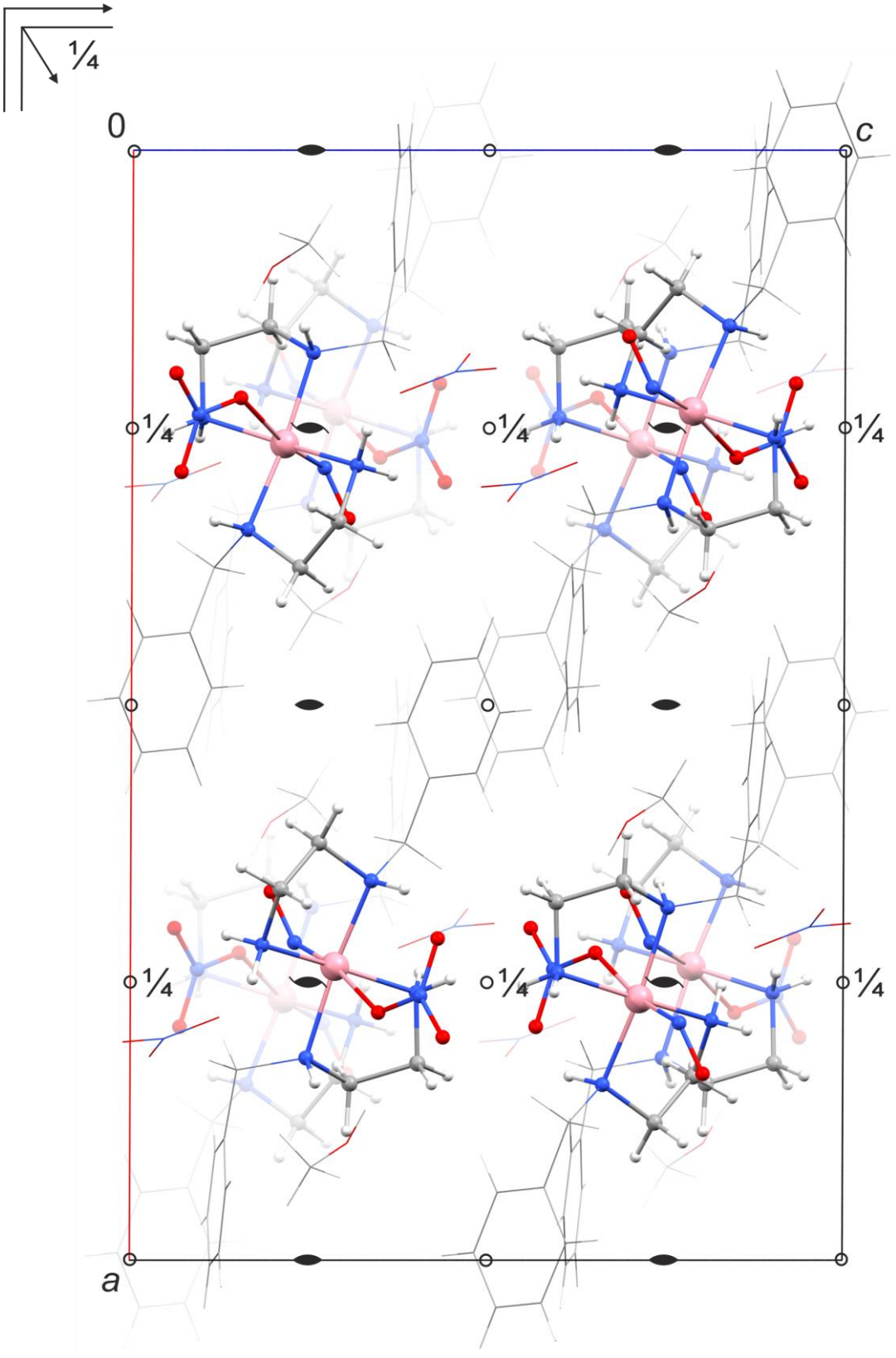

Figure 7.29: Packing diagram of *trans*-[Co(bnen)$_2$(NO)(NO$_3$)]NO$_3$·MeOH (**4l**·MeOH) in the monoclinic space group *C*2/*c* with view along [010]. The symmetry elements of the space group *C*2/*c* are overlaid. Atoms: carbon (gray), hydrogen (white), cobalt (pink), nitrogen (blue), oxygen (red). The benzyl groups and non-coordinating nitrate ions as well as the co-crystallized MeOH molecules are depicted as wireframe. The nitrosyl moieties of the minor disorder form are omitted for clarity.

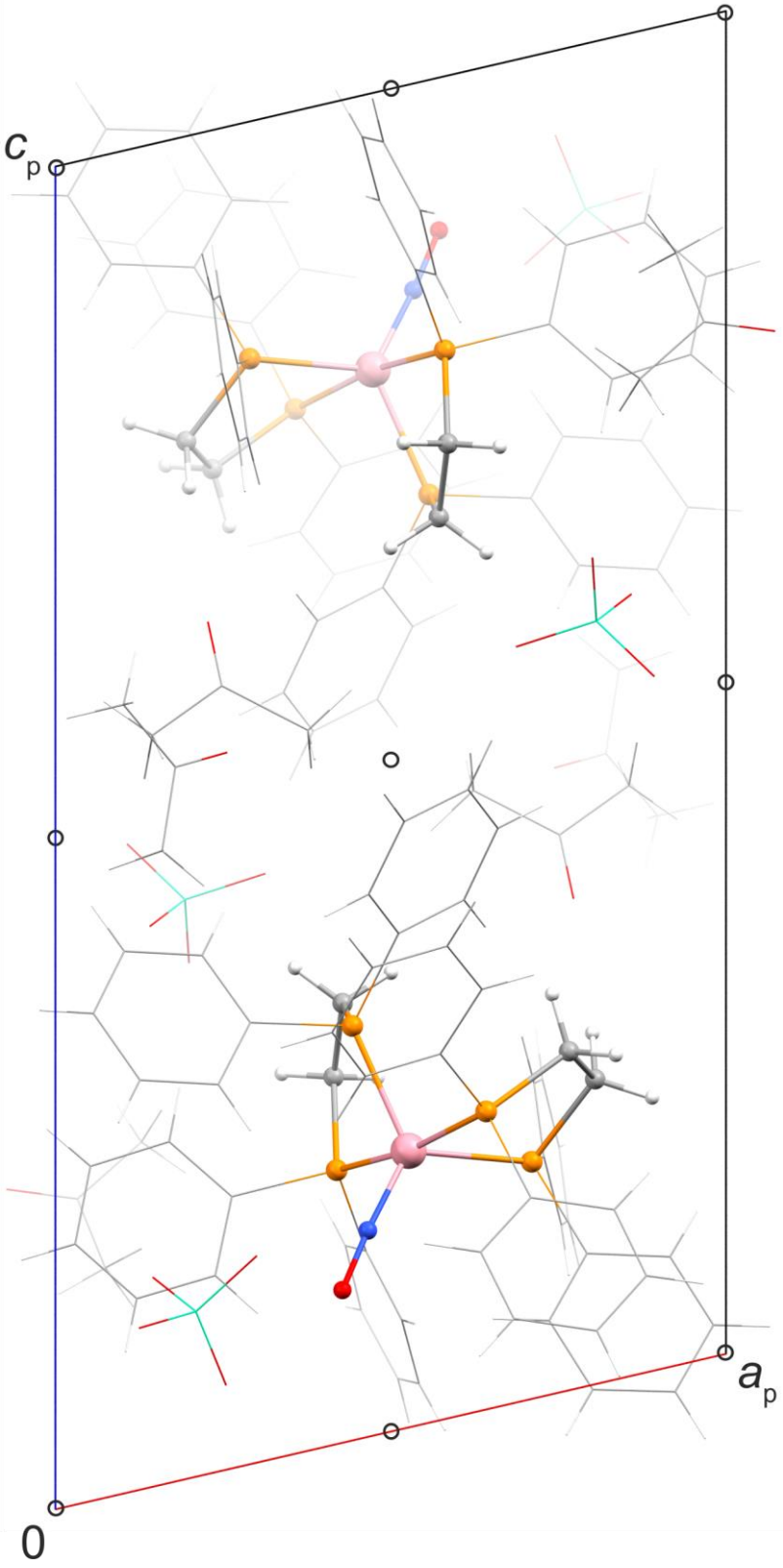

Figure 7.30: Packing diagram of $[Co(dppe)_2(NO)](ClO_4)_2 \cdot 2.7 Me_2CO \cdot 0.3 DMSO$ (**5a**$\cdot 2.7 Me_2CO \cdot 0.3 DMSO$) in the triclinic space group $P\bar{1}$ with view along [010]. The symmetry elements of the space group $P\bar{1}$ are overlaid. Atoms: carbon (gray), hydrogen (white), chlorine (green), cobalt (pink), nitrogen (blue), oxygen (red), phosphorus (orange). The phenyl groups and perchlorate ions as well as the co-crystallized Me_2CO molecules are depicted as wireframe. The perchlorate ions and co-crystallized DMSO molecules of the minor disorder form are omitted for clarity.

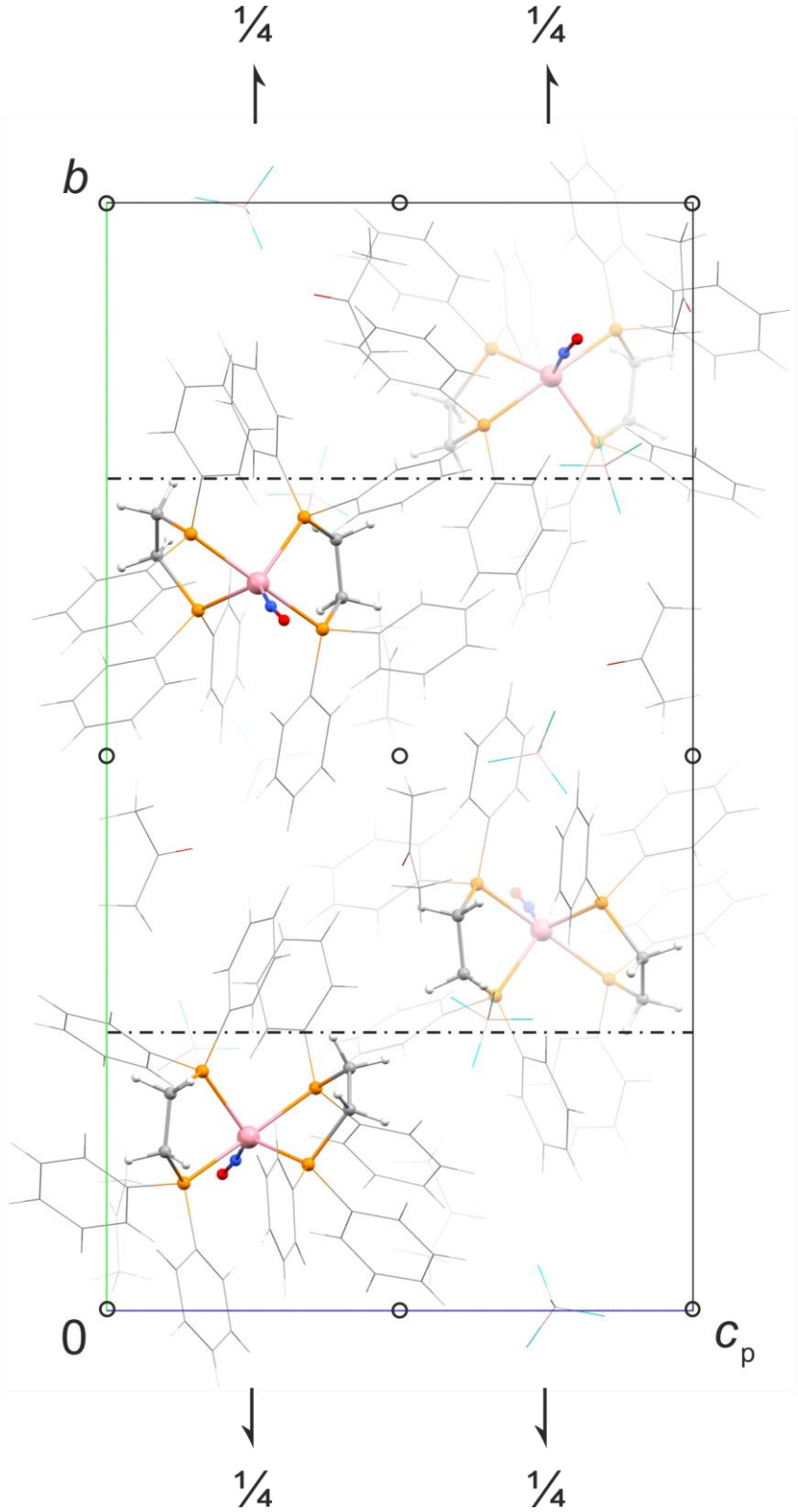

Figure 7.31: Packing diagr. of $[Co(dppe)_2(NO)](BF_4)_2 \cdot 2Me_2CO$ (**5a'**$\cdot 2Me_2CO$) in the monoclinic space group $P2_1/n$ with view along [100]. The symmetry elements of the space group $P2_1/n$ are overlaid. Atoms: carbon (gray), hydrogen (white), boron (pearl), cobalt (pink), fluorine (turquoise), nitrogen (blue), oxygen (red), phosphorus (orange). The phenyl groups and tetrafluoroborate ions as well as the co-crystallized Me_2CO molecules are depicted as wireframe.

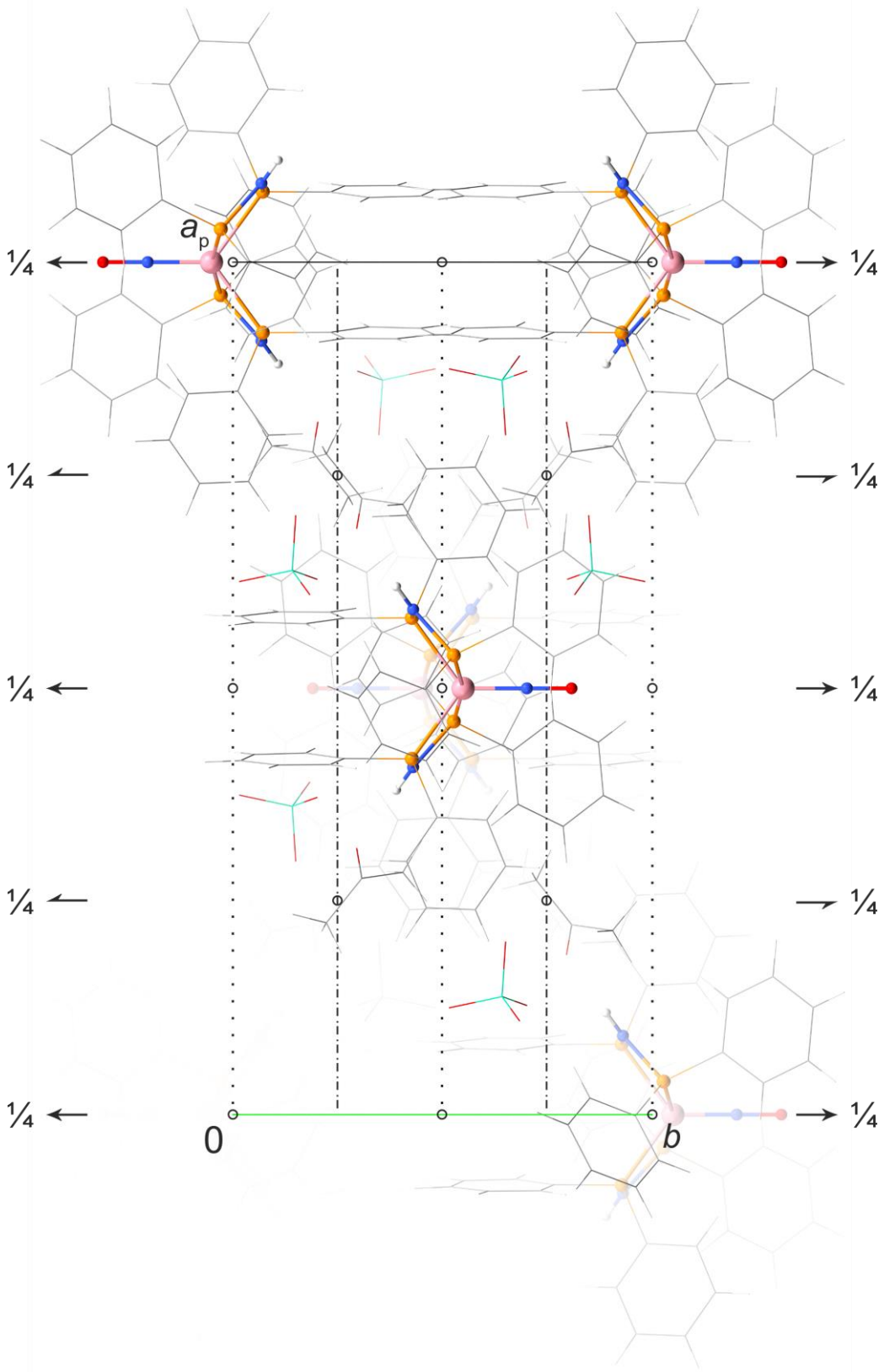

Figure 7.32: Packing diagr. of $[Co(dppa)_2(NO)](ClO_4)_2 \cdot 2Me_2CO$ (**5b**·2Me_2CO) in the monoclinic space group *C*2/*c* with view along [001]. The symmetry elements of the space group *C*2/*c* are overlaid. Atoms: carbon (gray), hydrogen (white), chlorine (green), cobalt (pink), nitrogen (blue), oxygen (red), phosphorus (orange). The phenyl groups and perchlorate ions as well as the co-crystallized Me_2CO molecules are depicted as wireframe. The perchlorate ions of the minor disorder form are omitted for clarity.

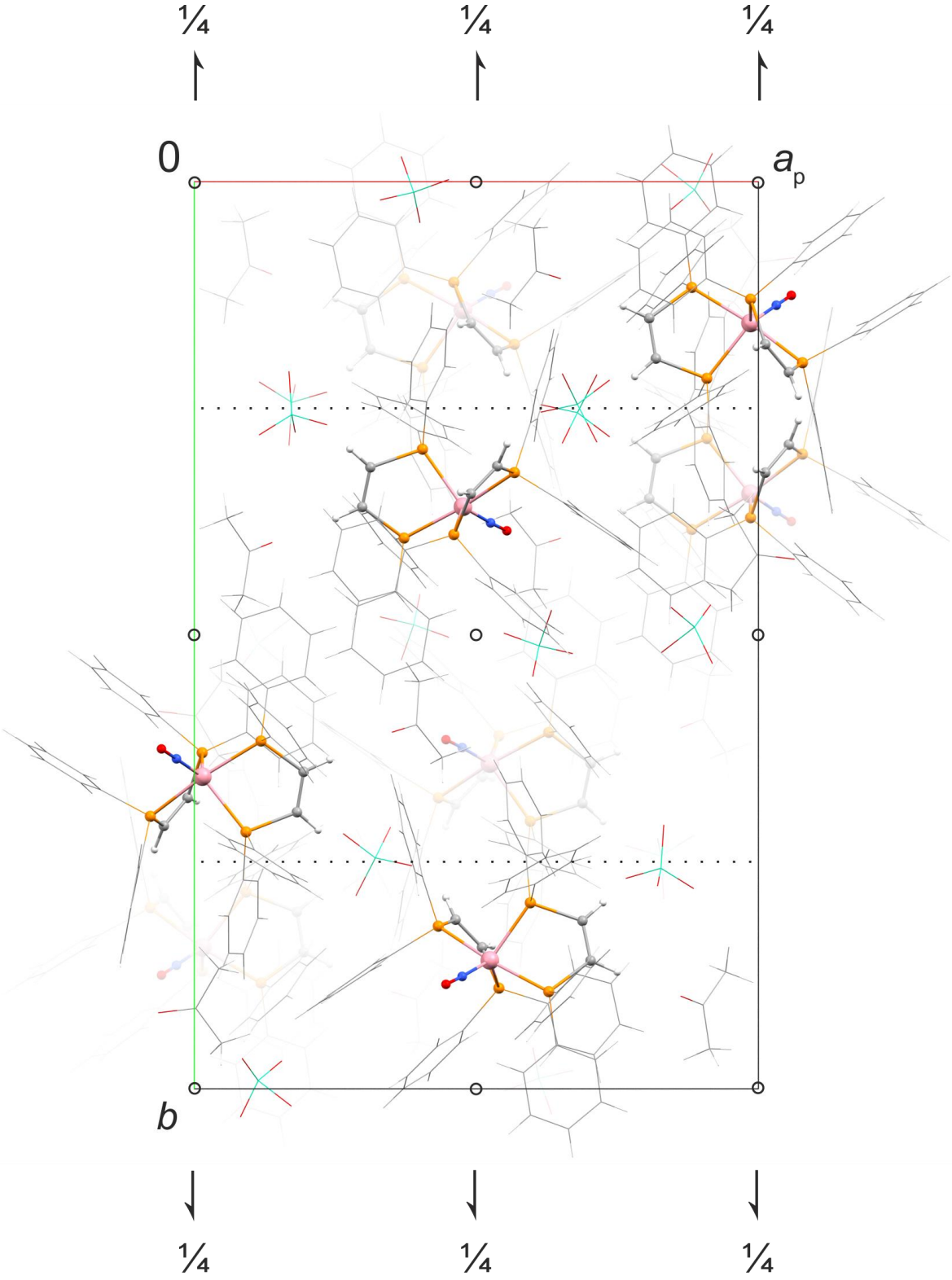

Figure 7.33: Packing diagram of $[Co(dppv)_2(NO)](ClO_4)_2 \cdot 1.5 Me_2CO$ (**5c**$\cdot 1.5 Me_2CO$) in the monoclinic space group $P2_1/c$ with view along [001]. The symmetry elements of the space group $P2_1/c$ are overlaid. Atoms: carbon (gray), hydrogen (white), chlorine (green), cobalt (pink), nitrogen (blue), oxygen (red), phosphorus (orange). The phenyl groups and perchlorate ions as well as the co-crystallized Me_2CO molecules are depicted as wireframe.

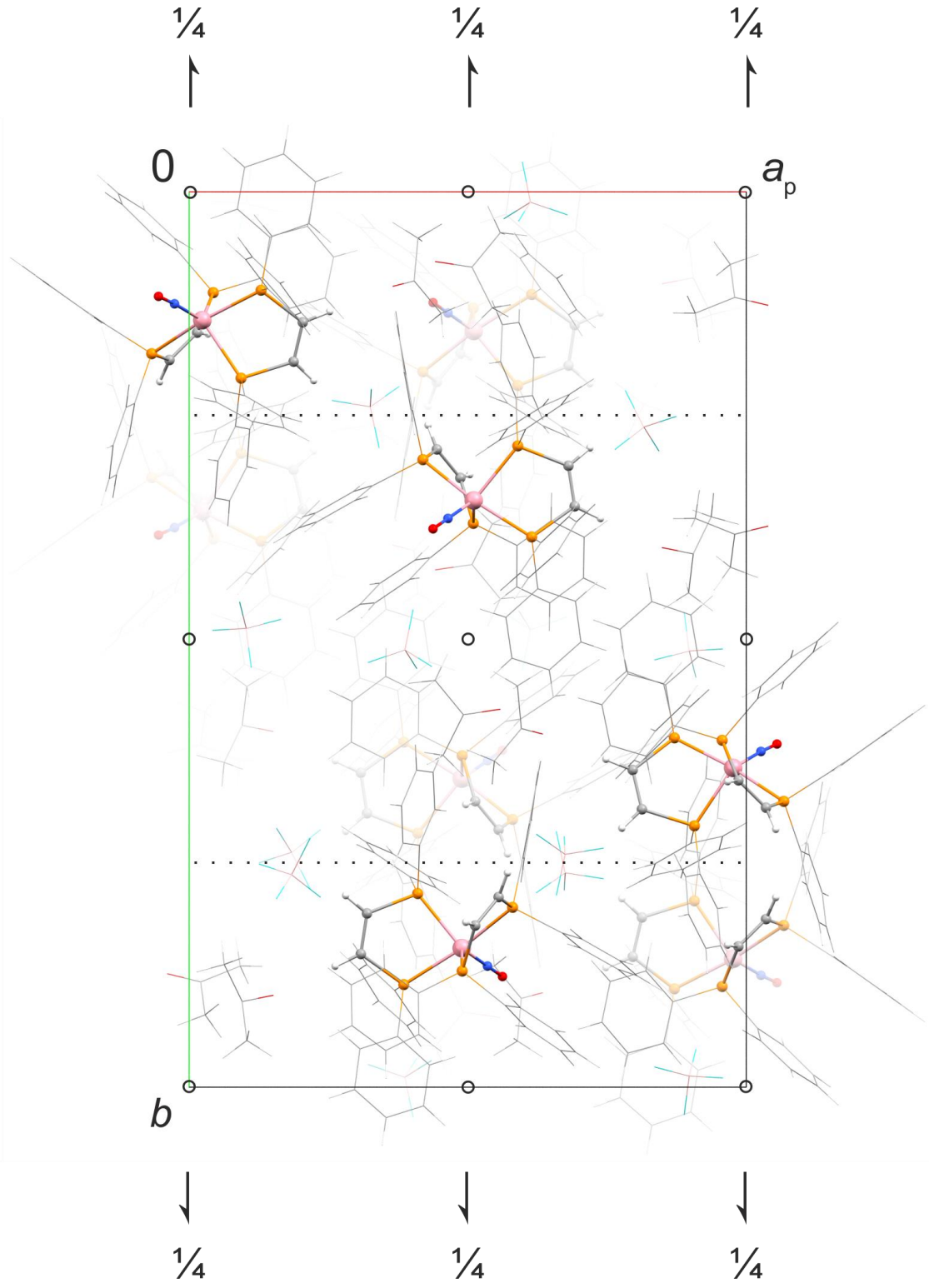

Figure 7.34: Packing diagram of $[Co(dppv)_2(NO)](BF_4)_2 \cdot 1.8Me_2CO \cdot 0.2DMSO$ (**5c'**$\cdot 1.8Me_2CO \cdot 0.2DMSO$) in the monoclinic space group $P2_1/c$ with view along [001]. The symmetry elements of the space group $P2_1/c$ are overlaid. Atoms: carbon (gray), hydrogen (white), boron (pearl), cobalt (pink), fluorine (turquoise), nitrogen (blue), oxygen (red), phosphorus (orange). The phenyl groups and tetrafluoroborate ions as well as the co-crystallized Me_2CO molecules are depicted as wireframe. The sulfur atoms of the co-crystallized DMSO molecules of the minor disorder form are omitted for clarity.

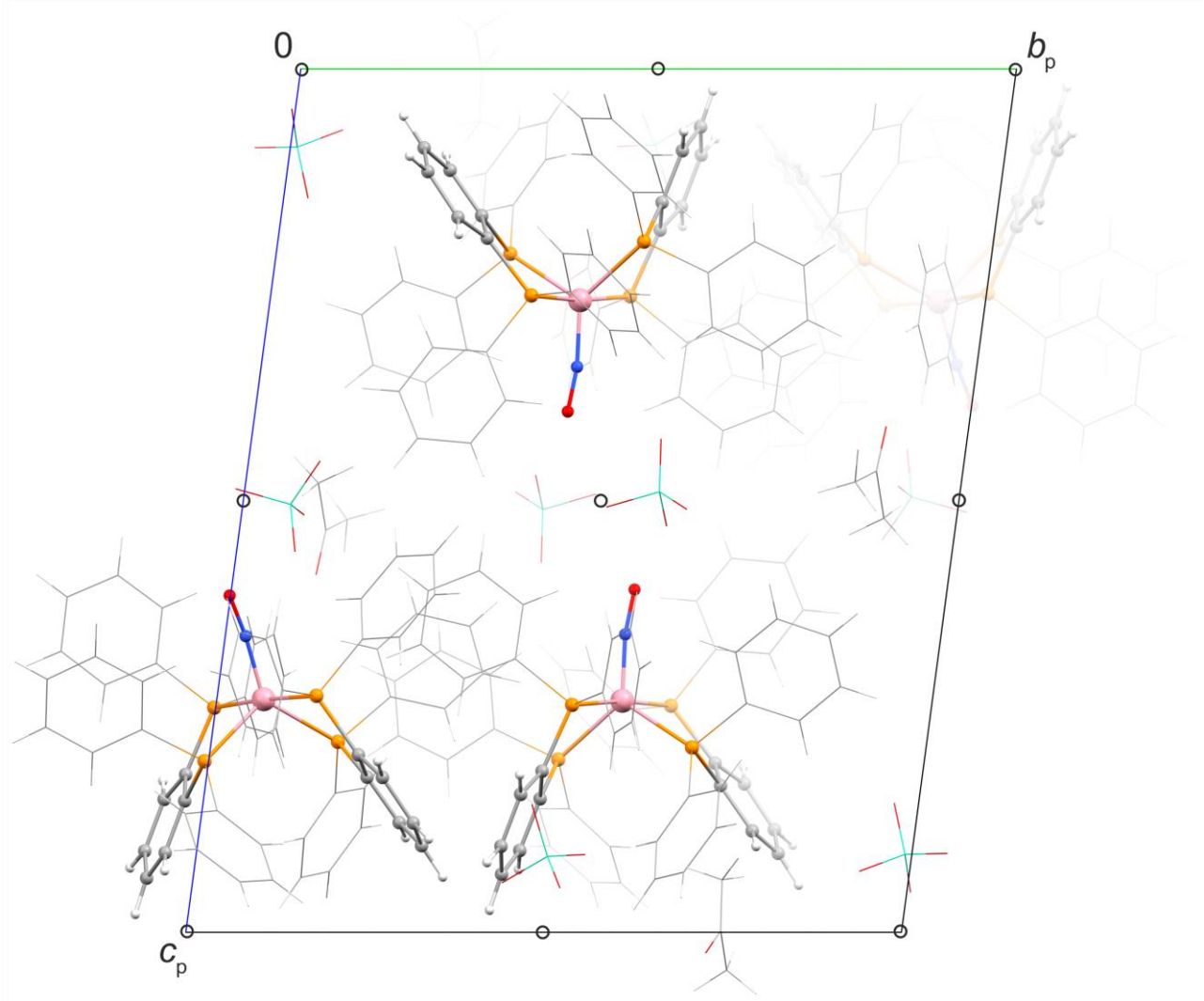

Figure 7.35: Packing diagram of $[Co(dppbz)_2(NO)](ClO_4)_2 \cdot Me_2CO$ (**5d**$\cdot Me_2CO$) in the triclinic space group $P\bar{1}$ with view along [100]. The symmetry elements of the space group $P\bar{1}$ are overlaid. Atoms: carbon (gray), hydrogen (white), chlorine (green), cobalt (pink), nitrogen (blue), oxygen (red), phosphorus (orange). The phenyl groups and perchlorate ions as well as the co-crystallized Me_2CO molecules are depicted as wireframe.

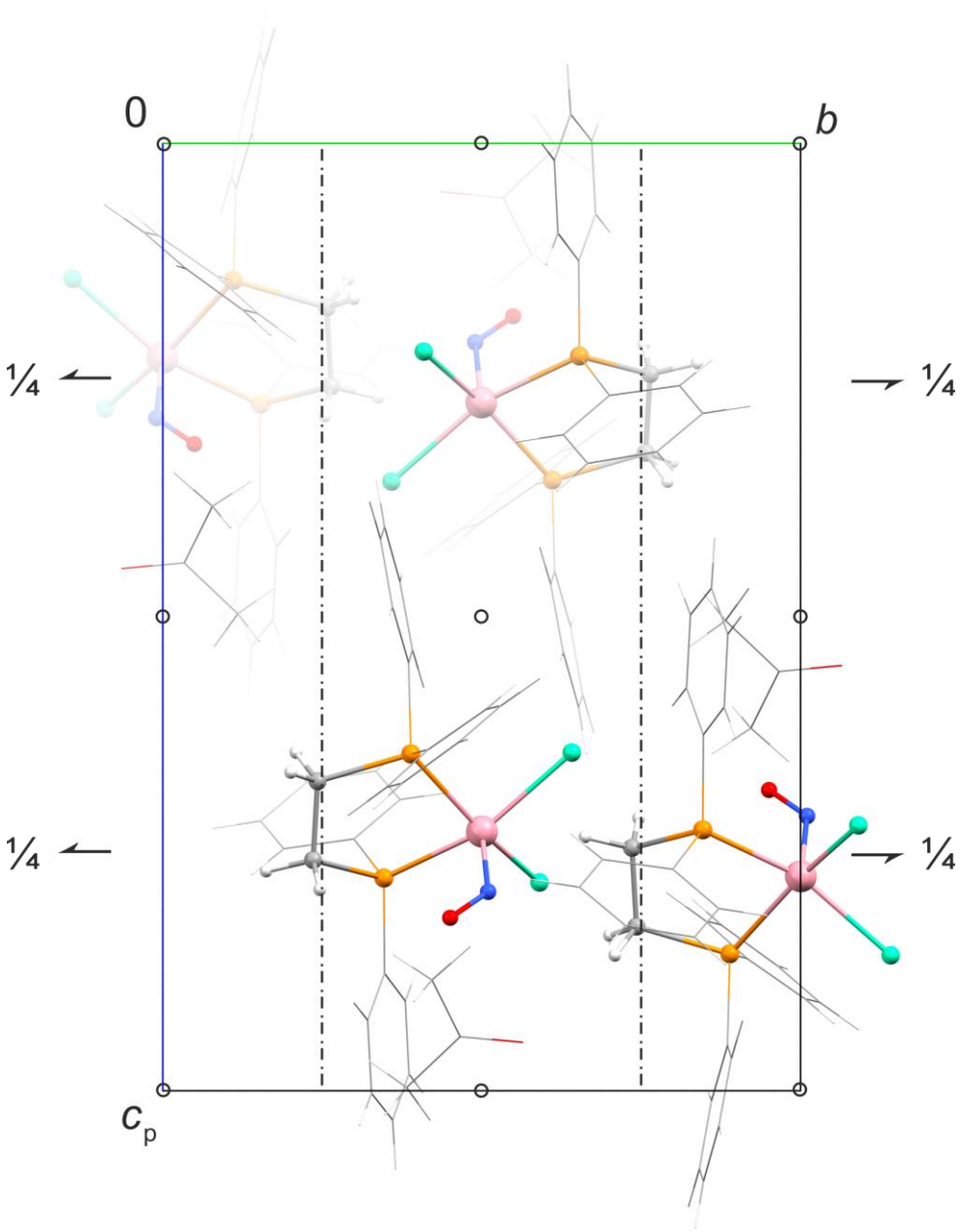

Figure 7.36: Packing diagram of $[CoCl_2(dppe)(NO)]\cdot Me_2CO$ (**6a**·Me_2CO) in the monoclinic space group $P2_1/n$ with view along [100]. The symmetry elements of the space group $P2_1/n$ are overlaid. Atoms: carbon (gray), hydrogen (white), chlorine (green), cobalt (pink), nitrogen (blue), oxygen (red), phosphorus (orange). The phenyl groups and the co-crystallized Me_2CO molecules are depicted as wireframe.

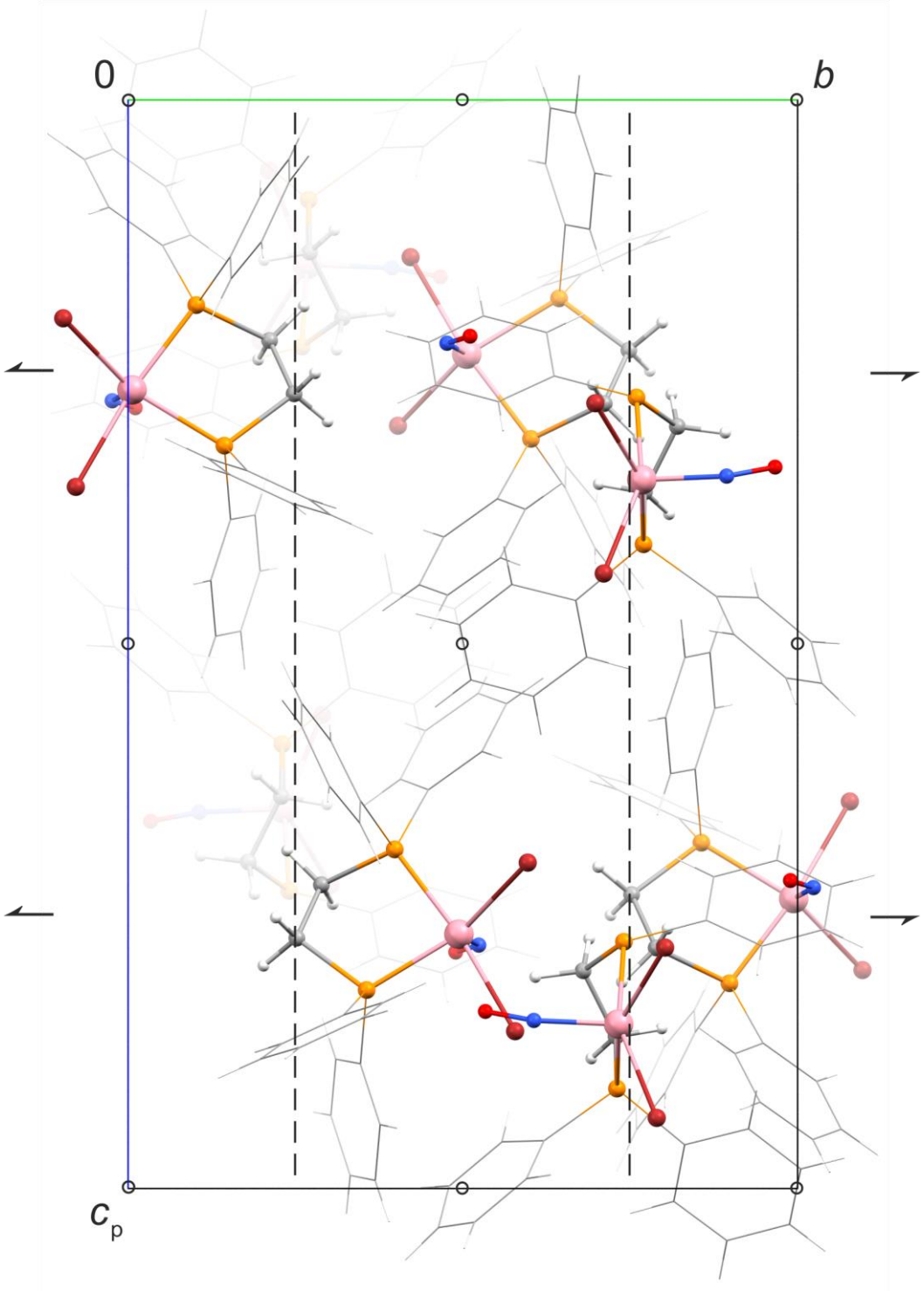

Figure 7.37: Packing diagr. of [$CoBr_2$(dppe)(NO)] (**6a'**) in the monoclinic space group $P2_1/c$ with view along [100]. The symmetry elements of the space group $P2_1/c$ are overlaid. Atoms: carbon (gray), hydrogen (white), bromine (maroon), cobalt (pink), nitrogen (blue), oxygen (red), phosphorus (orange). The phenyl groups and the co-crystallized Me_2CO molecules are depicted as wireframe. The disordered phenyl groups of the minor disorder form are omitted for clarity.

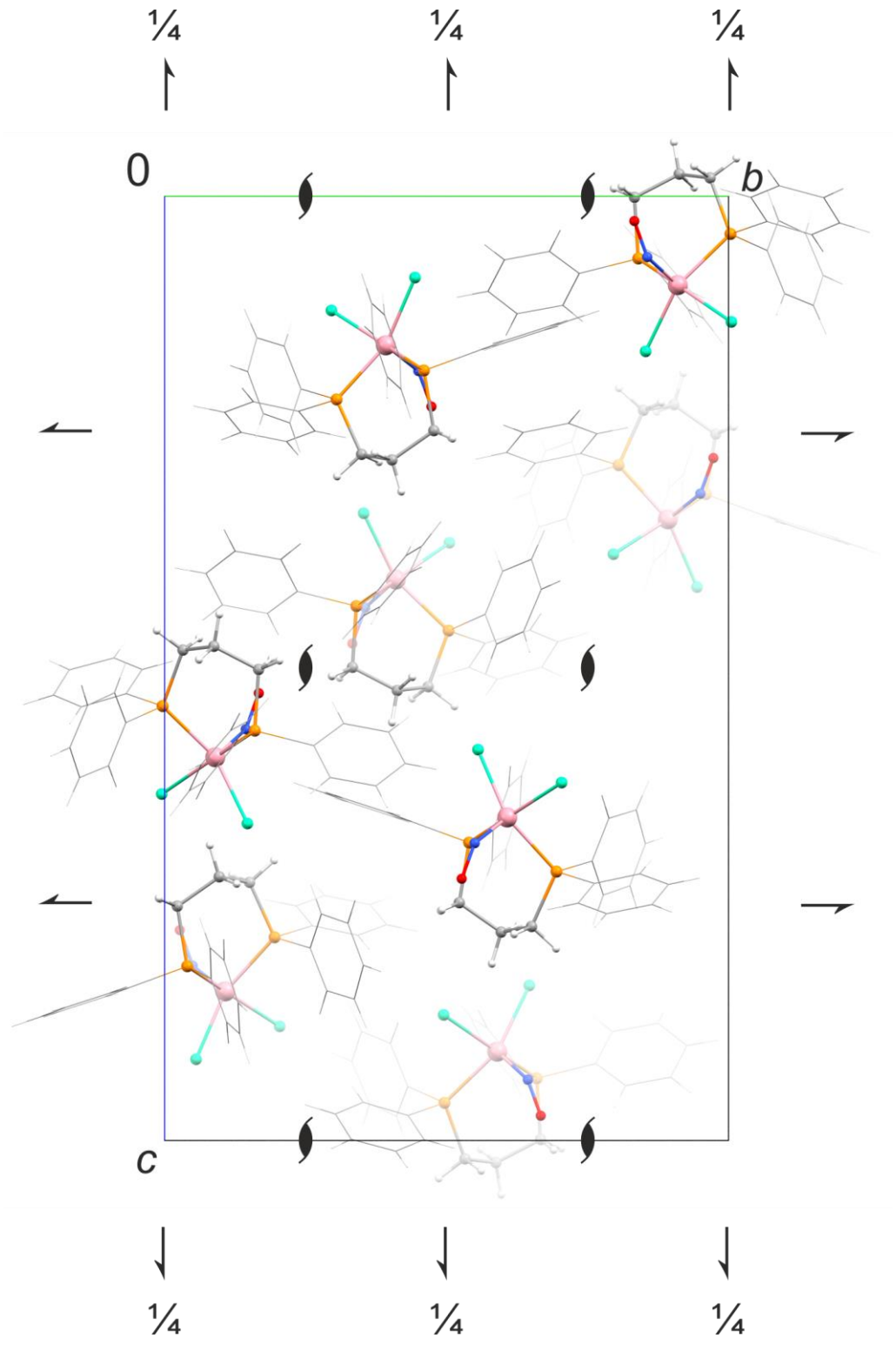

Figure 7.38: Packing diagram of [$CoCl_2$(dppp)(NO)] (**6b**) in the orthorhombic space group $P2_12_12_1$ with view along [100]. The symmetry elements of the space group $P2_12_12_1$ are overlaid. Atoms: carbon (gray), hydrogen (white), chlorine (green), cobalt (pink), nitrogen (blue), oxygen (red), phosphorus (orange). The phenyl groups are depicted as wireframe.

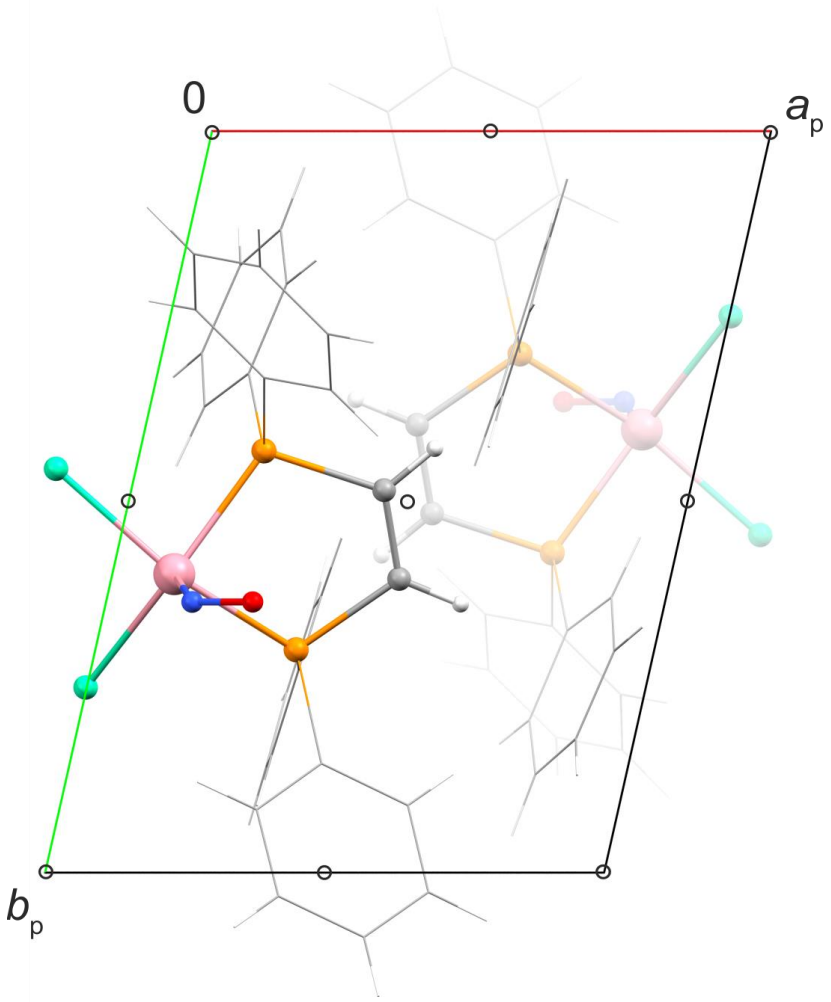

Figure 7.39: Packing diagram of [$CoCl_2$(dppv)(NO)] (**6c**) in the triclinic space group $P\bar{1}$ with view along [001]. The symmetry elements of the space group $P\bar{1}$ are overlaid. Atoms: carbon (gray), hydrogen (white), chlorine (green), cobalt (pink), nitrogen (blue), oxygen (red), phosphorus (orange). The phenyl groups are depicted as wireframe.

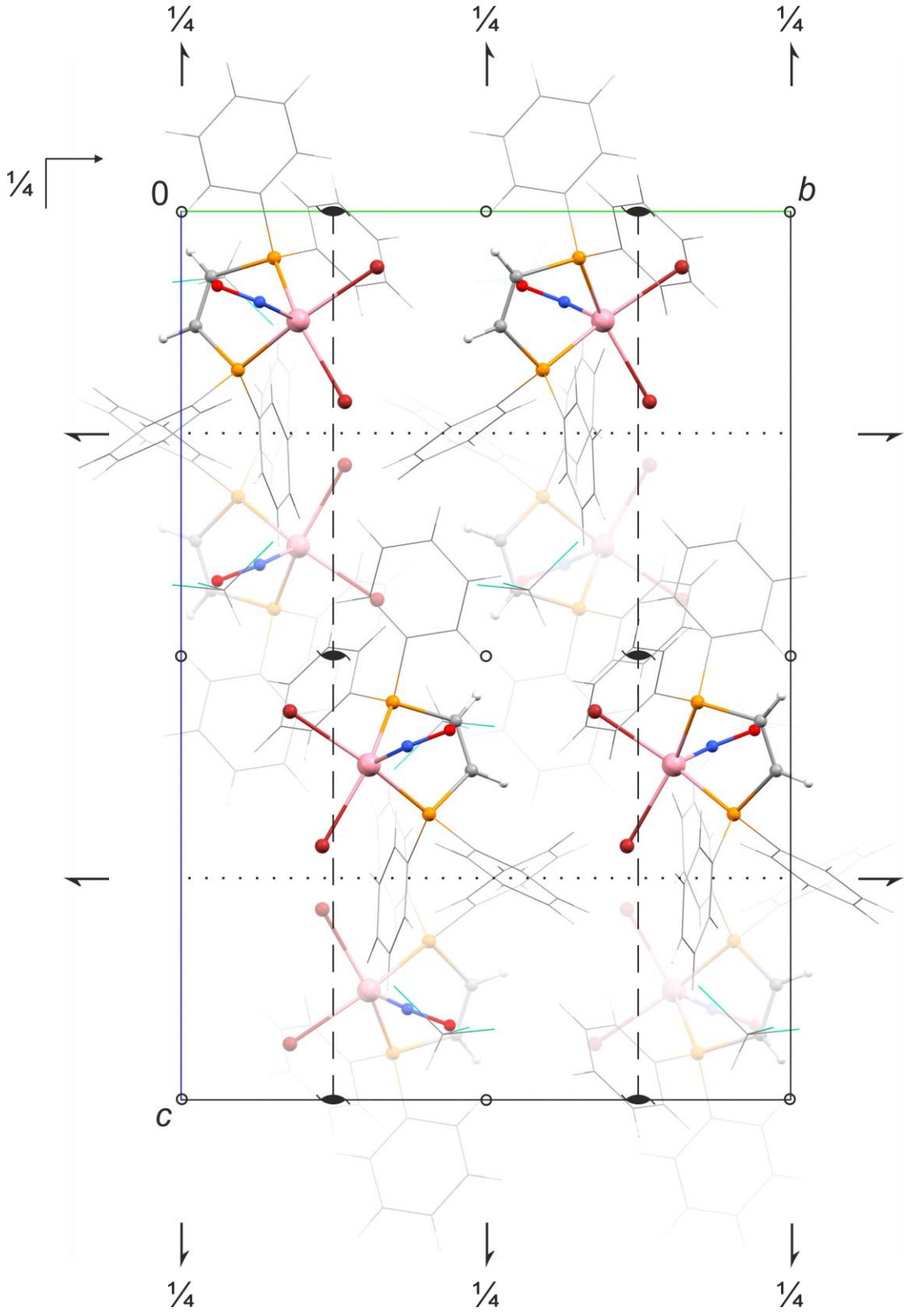

Figure 7.40: Packing diagram of $[CoBr_2(dppv)(NO)]\cdot CHCl_3$ (**6c'**·$CHCl_3$) in the orthorhombic space group *Pbca* with view along [100]. The symmetry elements of the space group *Pbca* are overlaid. Atoms: carbon (gray), hydrogen (white), bromine (maroon), cobalt (pink), nitrogen (blue), oxygen (red), phosphorus (orange). The phenyl groups and the co-crystallized $CHCl_3$ molecules are depicted as wireframe.

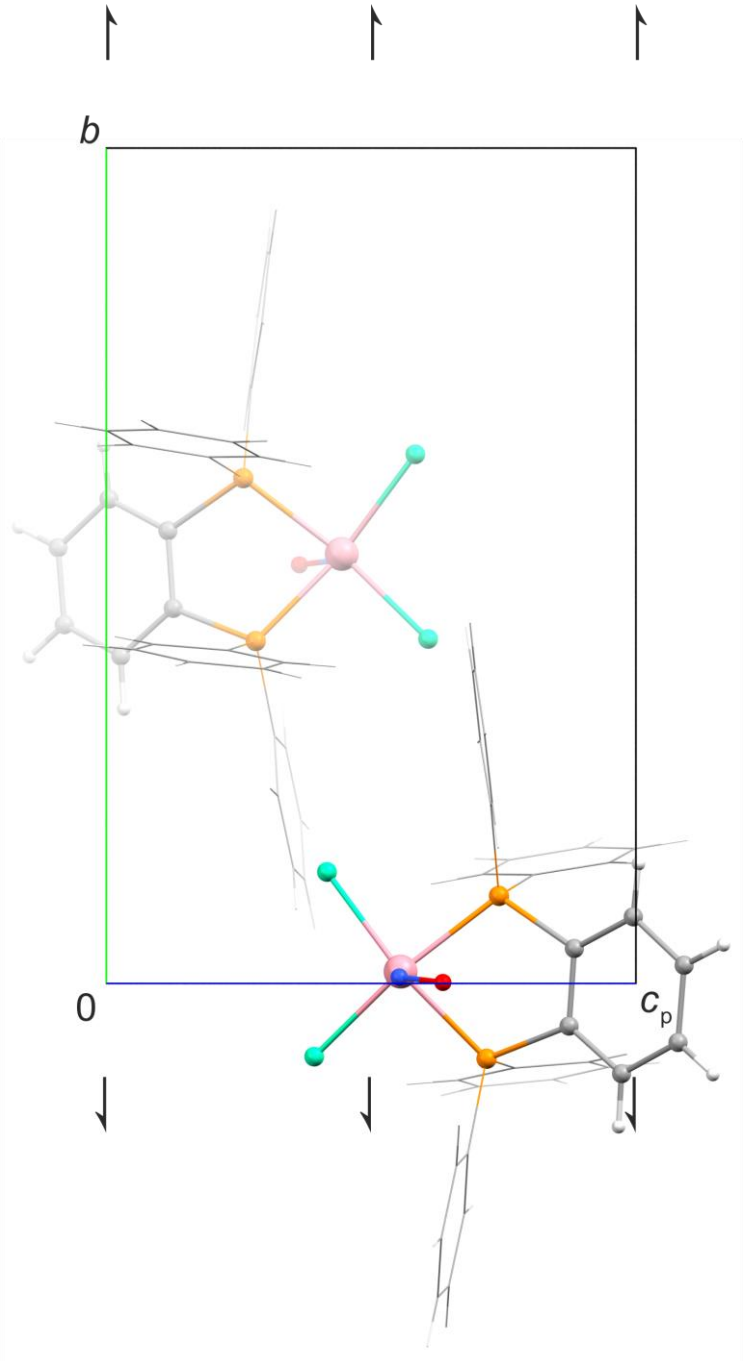

Figure 7.41: Packing diagram of [$CoCl_2$(dppbz)(NO)] (**6d**) in the monoclinic space group $P2_1$ with view along [100]. The symmetry elements of the space group $P2_1$ are overlaid. Atoms: carbon (gray), hydrogen (white), chlorine (green), cobalt (pink), nitrogen (blue), oxygen (red), phosphorus (orange). The phenyl groups are depicted as wireframe.

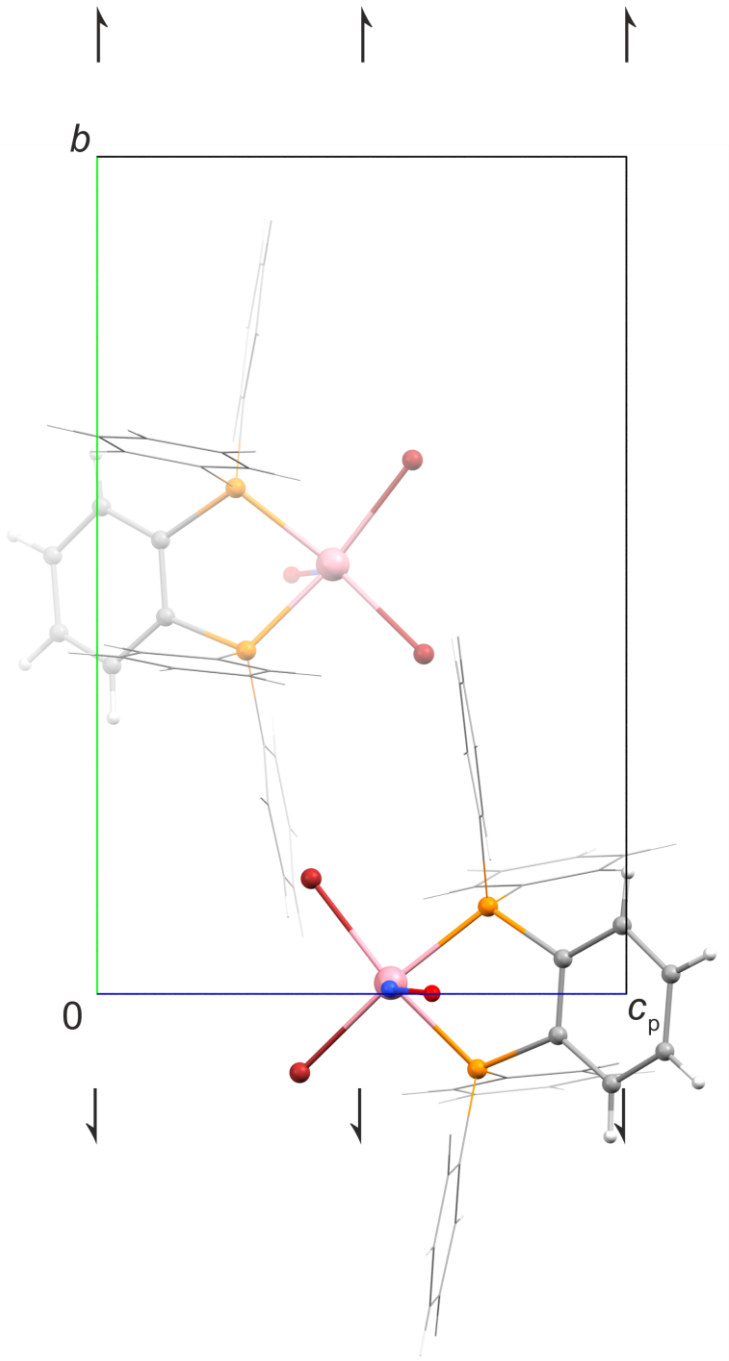

Figure 7.42: Packing diagr. of [$CoBr_2$(dppbz)(NO)] (**6d'**) in the monoclinic space group $P2_1$ with view along [100]. The symmetry elements of the space group $P2_1$ are overlaid. Atoms: carbon (gray), hydrogen (white), bromine (maroon), cobalt (pink), nitrogen (blue), oxygen (red), phosphorus (orange). The phenyl groups are depicted as wireframe.

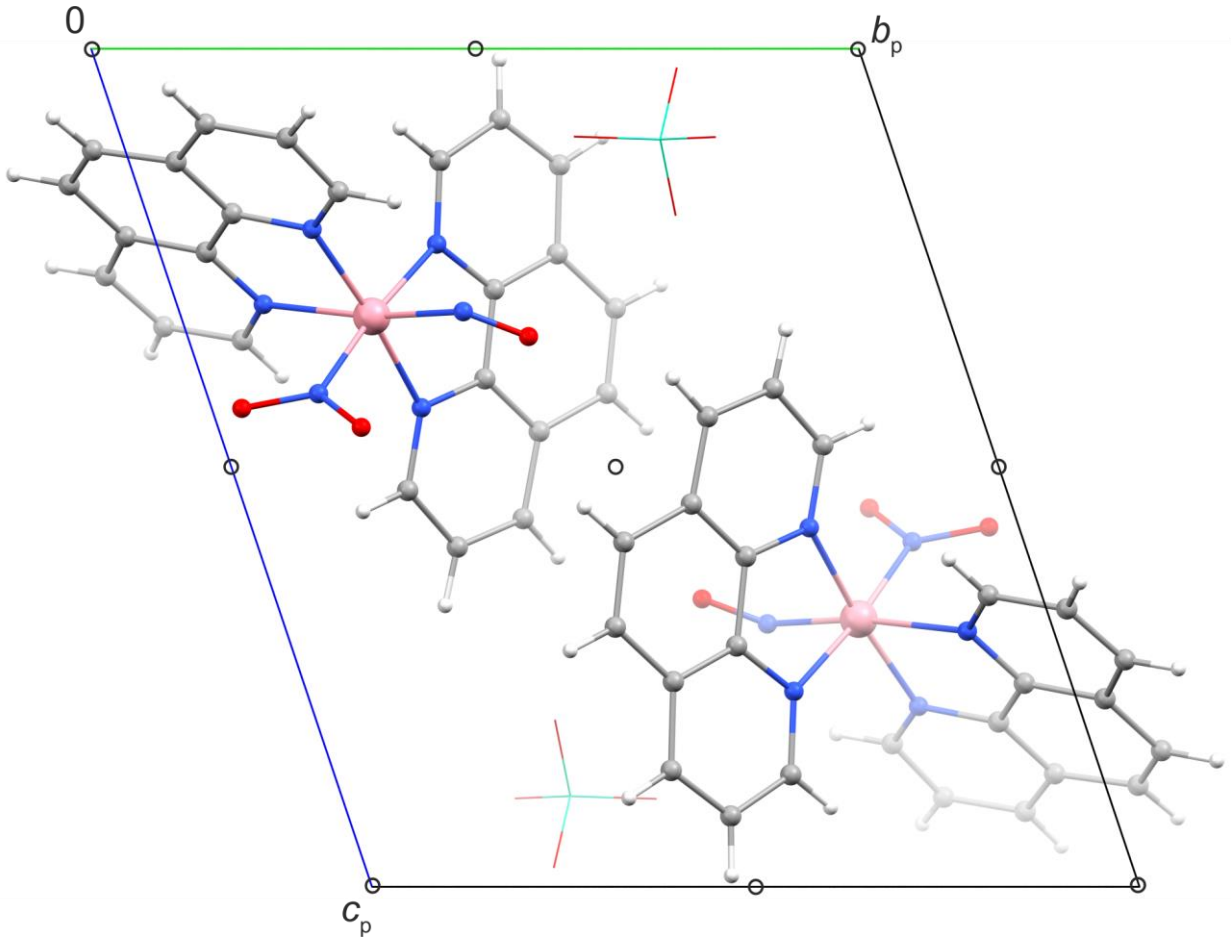

Figure 7.43: Packing diagram of *rac*-*cis*-[Co(NO)(NO_2-κ*N*)(phen)$_2$]ClO_4 (**7a**) in the triclinic space group $P\bar{1}$ with view along [100]. The symmetry elements of the space group $P\bar{1}$ are overlaid. Atoms: carbon (gray), hydrogen (white), chlorine (green), cobalt (pink), nitrogen (blue), oxygen (red). The perchlorate ions are depicted as wire-frame. The nitrito and nitrosyl moieties of the minor disorder form are omitted for clarity.

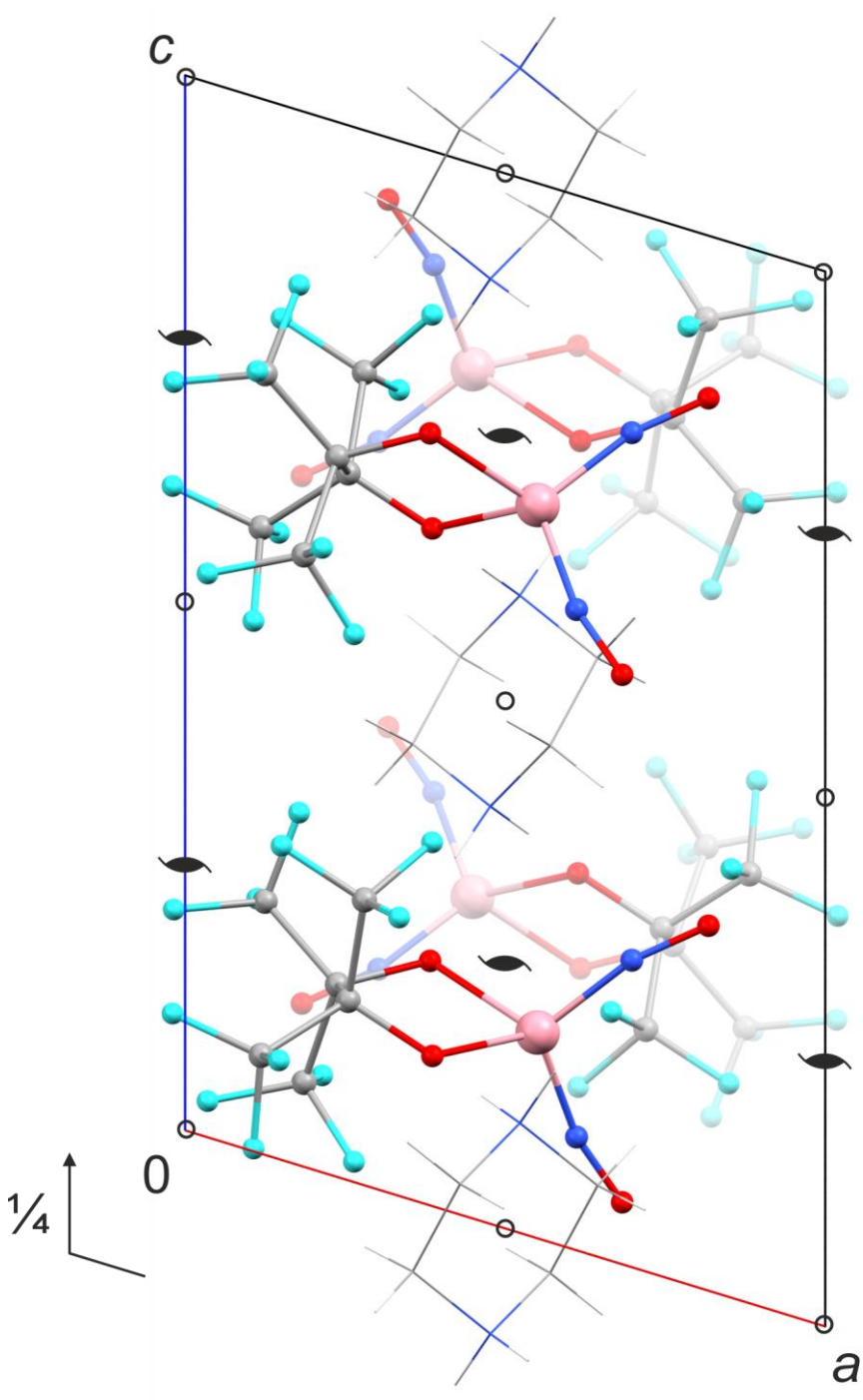

Figure 7.44: Packing diagram of $(ppzH_2)_{0.5}[Co(fpin)(NO)_2]$ (**7b**) in the monoclinic space group $P2_1/c$ with view along [010]. The symmetry elements of the space group $P2_1/c$ are overlaid. Atoms: carbon (gray), hydrogen (white), cobalt (pink), fluorine (turquoise), nitrogen (blue), oxygen (red). The piperazinium ions are depicted as wireframe.

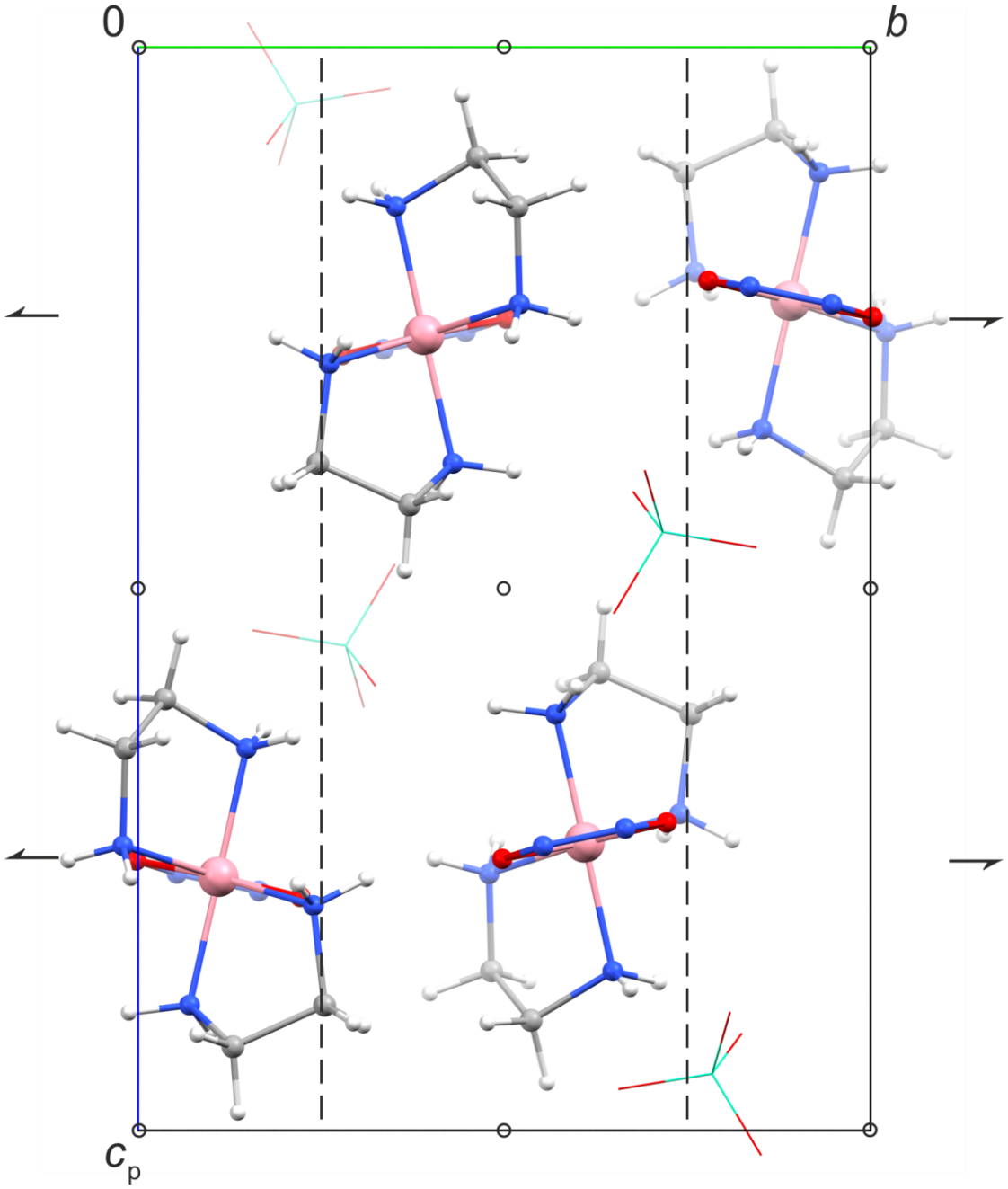

Figure 7.45: Packing diagram of *rac*-[Co(en)$_2$(*cis*-N_2O_2-κ^2*O,O'*)]ClO_4 (**7c**) in the monoclinic space group $P2_1/c$ with view along [100]. The symmetry elements of the space group $P2_1/c$ are overlaid. Atoms: carbon (gray), hydrogen (white), chlorine (green), cobalt (pink), nitrogen (blue), oxygen (red). The perchlorate ions are depicted as wireframe.

7.2 Crystallographic tables

Table 7.1: Crystallographic data of compounds [Co(2-aepyrr)(fpin)(NO)] (**1a**), [Co(2-aepip)(fpin)(NO)] (**1b**) and [Co(2-aemor)(fpin)(NO)] (**1c**).

	1a	**1b**	**1c**
empirical formula	$C_{12}H_{14}CoF_{12}N_3O_3$	$C_{13}H_{16}CoF_{12}N_3O_3$	$C_{12}H_{14}CoF_{12}N_3O_4$
M_r/g mol^{-1}	535.19	549.22	551.19
crystal system	triclinic	triclinic	monoclinic
space group	$P\bar{1}$	$P\bar{1}$	$P2_1/n$
a/Å	7.1186(3)	7.2942(10)	7.6413(6)
b/Å	9.7755(4)	9.6583(12)	14.3149(9)
c/Å	13.4183(5)	13.7021(18)	17.2503(13)
α/°	80.3330(10)	91.364(4)	90
β/°	80.5850(10)	91.391(4)	101.597(3)
γ/°	74.1500(10)	103.475(4)	90
V/Å^3	878.65(6)	938.0(2)	1848.4(2)
Z	2	2	4
ρ_{calcd}/g cm^{-3}	2.023	1.945	1.981
μ/mm^{-1}	1.122	1.054	1.074
crystal size/mm	0.040 × 0.040 × 0.010	0.050 × 0.040 × 0.010	0.040 × 0.030 × 0.020
temperature/K	102(2)	102(2)	105(2)
rated input/kW	2.5	2.5	2.5
θ-range/°	2.998–27.08	3.170–25.45	3.091–27.13
reflections for metric	5733	4174	7230
absorption correction	multi-scan	multi-scan	multi-scan
transmission factors	0.6729–0.7455	0.7228–0.8620	0.6913–0.7455
reflections measured	16018	14853	34729
independent reflections	3834	3454	4063
R_{int}	0.0320	0.0736	0.0644
mean σ(I)/I	0.086	0.084	0.082
reflections with $I \geq 2\sigma(I)$	3117	2645	3126
x, y (weighting scheme)	0.0000, 1.2671	0.0000, 2.0783	0.0193, 1.3476
hydrogen refinement	[a]	[a]	[a]
Flack parameter	–	–	–
parameters	280	289	289
restraints	0	0	0
$R(F_{obs})$	0.0346	0.0462	0.0350
$R_w(F^2)$	0.0698	0.0913	0.0774
S	1.086	1.075	1.070
shift/error$_{max}$	0.001	0.001	0.001
max. electron density/e Å^{-3}	0.438	0.667	0.405
min. electron density/e Å^{-3}	−0.457	−0.527	−0.403
measurement code	yv359	yv403	yv374
CCDC number	2074574	2074578	2074576

[a] All hydrogen atoms were calculated in idealized positions, riding on their parent atoms. U_{iso} was always coupled to the parent atom.

Table 7.2: Crystallogr. data of compounds [Co(bnen)(fpin)(NO)]·DMSO (**1d**·DMSO), [Co(dpipe)(fpin)(NO)] (**1e**) and [Co(fpin)(NO)(teen)] (**1f**).

	1d·DMSO	**1e**	**1f**
empirical formula	$C_{17}H_{20}CoF_{12}N_3O_4S$	$C_{18}H_{24}CoF_{12}N_3O_3$	$C_{16}H_{24}CoF_{12}N_3O_3$
M_r/g mol^{-1}	649.35	617.33	593.31
crystal system	monoclinic	monoclinic	monoclinic
space group	$P2_1/c$	$P2_1/c$	$P2_1/n$
a/Å	10.5414(4)	9.2286(5)	7.4430(4)
b/Å	15.4146(7)	16.7790(9)	17.5598(10)
c/Å	15.6955(7)	15.0244(9)	16.8282(11)
α/°	90	90	90
β/°	108.2290(10)	102.917(2)	98.184(2)
γ/°	90	90	90
V/Å^3	2422.39(18)	2267.6(2)	2177.0(2)
Z	4	4	4
ρ_{calcd}/g cm^{-3}	1.781	1.808	1.810
μ/mm^{-1}	0.918	0.883	0.916
crystal size/mm	0.050 × 0.040 × 0.040	0.040 × 0.040 × 0.030	0.090 × 0.070 × 0.050
temperature/K	103(2)	102(2)	173(2)
rated input/kW	2.5	2.5	2.5
θ-range/°	2.975–26.40	2.670–27.12	3.384–28.28
reflections for metric	9964	9968	9781
absorption correction	multi-scan	multi-scan	multi-scan
transmission factors	0.6490–0.7454	0.7032–0.7455	0.7020–0.7457
reflections measured	42757	42697	55145
independent reflections	4950	5008	5392
R_{int}	0.0491	0.0552	0.0534
mean σ(I)/I	0.077	0.058	0.062
reflections with $I \geq 2\sigma(I)$	3944	4330	4853
x, y (weighting scheme)	0.0052, 4.5358	0.0240, 1.3527	0.0245, 2.0805
hydrogen refinement	[a]	[a]	[a]
Flack parameter	–	–	–
parameters	345	334	333
restraints	0	0	9
$R(F_{obs})$	0.0351	0.0297	0.0323
$R_w(F^2)$	0.0825	0.0740	0.0804
S	1.088	1.042	1.030
shift/error$_{max}$	0.001	0.002	0.001
max. electron density/e Å^{-3}	0.449	0.561	0.601
min. electron density/e Å^{-3}	−0.439	−0.348	−0.561
measurement code	yv397	yv604	zv304
CCDC number	2074577	–	–

[a] All hydrogen atoms were calculated in idealized positions, riding on their parent atoms. U_{iso} was always coupled to the parent atom.

Table 7.3: Crystallogr. data of compounds [Co(2-aepy)(fpin)(NO)] (**1g**), [Co(fpin)(mampy)(NO)]·DMSO (**1h**·DMSO) and [Co(bpm)(fpin)(NO)] (**1i**).

	1g	**1h**·DMSO [a,b]	**1i**
empirical formula	$C_{13}H_{10}CoF_{12}N_3O_3$	$C_{15}H_{16}CoF_{12}N_3O_4S$	$C_{13}H_8CoF_{12}N_5O_3$
M_r/g mol^{-1}	543.17	621.30	569.17
crystal system	triclinic	monoclinic	monoclinic
space group	$P\bar{1}$	$P2_1/n$	Pc
a/Å	7.7668(3)	9.1777(11)	13.0841(7)
b/Å	8.8923(3)	26.498(3)	10.4697(5)
c/Å	13.4540(5)	10.3210(13)	14.9108(7)
α/°	95.0380(10)	90	90
β/°	99.1630(10)	116.368(4)	113.664(2)
γ/°	102.0600(10)	90	90
V/Å^3	890.01(6)	2248.8(5)	1870.83(16)
Z	2	4	4
ρ_{calcd}/g cm^{-3}	2.027	1.835	2.021
μ/mm^{-1}	1.110	0.984	1.064
crystal size/mm	0.040 × 0.030 × 0.030	0.130 × 0.100 × 0.070	0.080 × 0.070 × 0.070
temperature/K	102(2)	173(2)	102(2)
rated input/kW	2.5	2.5	2.5
θ-range/°	3.372–27.16	2.333–27.49	3.307–27.13
reflections for metric	7412	9856	9947
absorption correction	multi-scan	multi-scan	multi-scan
transmission factors	0.6698–0.7455	0.6984–0.7456	0.6852–0.7455
reflections measured	16561	55253	33080
independent reflections	3891	5152	6682
R_{int}	0.0264	0.0332	0.0373
mean σ(I)/I	0.063	0.220	0.085
reflections with $I \geq 2\sigma(I)$	3360	4849	6123
x, y (weighting scheme)	0.0155, 0.7432	0.0898, 2.2177	0.0374, 3.4739
hydrogen refinement	[c]	[d]	[d]
Flack parameter	–	–	0.019(8)
parameters	297	329	613
restraints	0	6	2
$R(F_{obs})$	0.0290	0.0715	0.0405
$R_w(F^2)$	0.0620	0.1797	0.1037
S	1.026	1.336	1.046
shift/error$_{max}$	0.001	0.001	0.001
max. electron density/e Å^{-3}	0.408	0.773	0.960
min. electron density/e Å^{-3}	−0.351	−0.882	−0.346
measurement code	yv360	zv450	yv433
CCDC number	2074575	–	2074580

[a] Due to strong diffraction of the measured crystal, an extinction correction was carried out using an extinction parameter of 0.160(7).

[b] One C atom of the co-crystallized DMSO was restrained in a way that its U_{ij} component approximates to isotropic behavior, using the ''ISOR'' command in *SHELXL*.

[c] C-bonded hydrogen atoms were calculated in idealized positions, riding on their parent atoms. The coordinates of N-bonded hydrogen atoms were refined freely.

[d] All hydrogen atoms were calculated in idealized positions, riding on their parent atoms. U_{iso} was always coupled to the parent atom.

Table 7.4: Crystallographic data of [Co(bpym)(fpin)(NO)]·MeOH (**1j**·MeOH), [Co(dmdpphen)(fpin)(NO)] (**1k**) and [Co(fpin)(NO)(py)$_2$] (**1l**).

	1j·MeOH	**1k**	**1l**
empirical formula	$C_{15}H_{10}CoF_{12}N_5O_4$	$C_{32}H_{20}CoF_{12}N_3O_3$	$C_{16}H_{10}CoF_{12}N_3O_3$
M_r/g mol^{-1}	611.21	781.44	579.20
crystal system	monoclinic	orthorhombic	monoclinic
space group	$P2_1/n$	$P2_12_12_1$	$P2_1/c$
a/Å	11.8847(3)	8.5184(2)	14.838(4)
b/Å	7.9569(2)	13.6823(4)	7.5415(18)
c/Å	21.3078(4)	26.1759(9)	17.531(4)
α/°	90	90	90
β/°	90.4110(10)	90	91.863(8)
γ/°	90	90	90
V/Å^3	2014.93(8)	3050.84(16)	1960.7(8)
Z	4	4	4
ρ_{calcd}/g cm^{-3}	2.015	1.701	1.962
μ/mm^{-1}	0.999	0.677	1.015
crystal size/mm	0.080 × 0.080 × 0.040	0.050 × 0.040 × 0.030	0.050 × 0.040 × 0.040
temperature/K	103(2)	102(2)	100(2)
rated input/kW	2.5	2.5	2.5
θ-range/°	3.081–27.12	3.078–27.11	3.230–27.15
reflections for metric	9853	9970	9870
absorption correction	multi-scan	multi-scan	multi-scan
transmission factors	0.6989–0.7455	0.6923–0.7455	0.6650–0.7455
reflections measured	38111	63864	36255
independent reflections	4450	6733	4294
R_{int}	0.0334	0.0701	0.0643
mean σ(I)/I	0.058	0.062	0.094
reflections with $I \geq 2\sigma(I)$	3850	5786	3699
x, y (weighting scheme)	0.0156, 1.8365	0.0216, 1.1178	0.0538, 0.4112
hydrogen refinement	[a]	[b]	[b]
Flack parameter	–	−0.001(8)	–
parameters	339	462	316
restraints	0	0	0
$R(F_{obs})$	0.0271	0.0320	0.0358
$R_w(F^2)$	0.0600	0.0721	0.0996
S	1.077	1.079	1.048
shift/error$_{max}$	0.001	0.001	0.001
max. electron density/e Å^{-3}	0.409	0.411	0.396
min. electron density/e Å^{-3}	−0.327	−0.400	−0.460
measurement code	yv399	yv435	zv358
CCDC number	2074579	2074581	–

[a] C-bonded hydrogen atoms were calculated in idealized positions, riding on their parent atoms. The coordinates of the O-bonded hydrogen atom were refined freely.

[b] All hydrogen atoms were calculated in idealized positions, riding on their parent atoms. U_{iso} was always coupled to the parent atom.

Table 7.5: Crystallographic data of compounds [Co(fpin)(NO)(pydz)$_2$] (**1m**), [Co(fpin)(mim)$_2$(NO)] (**1n**) and [Co(2-aedpp)(fpin)(NO)]·0.5MeOH (**2a**·0.5MeOH).

	1m	**1n**	**2a**·0.5MeOH
empirical formula	$C_{14}H_8CoF_{12}N_5O_3$	$C_{14}H_{12}CoF_{12}N_5O_3$	$C_{20.5}H_{18}CoF_{12}N_2O_{3.5}P$
M_r/g mol^{-1}	581.18	585.22	666.27
crystal system	monoclinic	monoclinic	triclinic
space group	$P2_1/c$	$C2/c$	$P\bar{1}$
a/Å	10.1239(19)	34.352(3)	11.1949(5)
b/Å	15.968(3)	7.3076(5)	14.0452(6)
c/Å	11.908(2)	17.7089(14)	16.7175(7)
α/°	90	90	97.9060(10)
β/°	101.327(6)	114.545(2)	98.680(2)
γ/°	90	90	103.064(2)
V/Å^3	1887.5(6)	4043.8(5)	2490.67(19)
Z	4	8	2
ρ_{calcd}/g cm^{-3}	2.045	1.923	1.777
μ/mm^{-1}	1.057	0.988	0.873
crystal size/mm	0.050 × 0.050 × 0.020	0.140 × 0.110 × 0.060	0.080 × 0.080 × 0.070
temperature/K	100(2)	173(2)	102(2)
rated input/kW	2.5	2.5	2.5
θ-range/°	2.052–27.19	3.237–28.30	2.505–27.12
reflections for metric	8067	9846	9488
absorption correction	multi-scan	multi-scan	multi-scan
transmission factors	0.6756–0.7455	0.6895–0.7457	0.7018–0.7455
reflections measured	45424	55331	46745
independent reflections	4161	5013	10898
R_{int}	0.0827	0.0329	0.0365
mean σ(I)/I	0.087	0.050	0.059
reflections with $I \geq 2\sigma(I)$	3053	4599	9396
x, y (weighting scheme)	0.0230, 2.0687	0.0238, 5.6748	0.0164, 1.7148
hydrogen refinement	[a]	[a]	[b]
Flack parameter	–	–	–
parameters	316	318	726
restraints	0	0	0
$R(F_{obs})$	0.0375	0.0255	0.0312
$R_w(F^2)$	0.0825	0.0651	0.0737
S	1.064	1.051	1.036
shift/error$_{max}$	0.001	0.001	0.001
max. electron density/e Å^{-3}	0.406	0.409	0.390
min. electron density/e Å^{-3}	−0.470	−0.317	−0.311
measurement code	zv369	zv441	yv639
CCDC number	–	–	–

[a] All hydrogen atoms were calculated in idealized positions, riding on their parent atoms. U_{iso} was always coupled to the parent atom.

[b] C- and N-bonded hydrogen atoms were calculated in idealized positions, riding on their parent atoms. The coordinates of the O-bonded hydrogen atom were refined freely.

Table 7.6: Crystallographic data of compounds [Co(2-aedip)(fpin)(NO)] (**2b**), [Co(dppe)(fpin)(NO)] (**3a**) and [Co(dppp)(fpin)(NO)] (**3b**).

	2b	**3a**	**3b**
empirical formula	$C_{14}H_{20}CoF_{12}N_2O_3P$	$C_{32}H_{24}CoF_{12}NO_3P_2$	$C_{33}H_{26}CoF_{12}NO_3P_2$
M_r/g mol^{-1}	582.22	819.39	833.42
crystal system	triclinic	monoclinic	orthorhombic
space group	$P\bar{1}$	$P2_1/c$	$Pna2_1$
a/Å	7.8456(10)	13.2871(4)	19.6029(7)
b/Å	9.7935(14)	11.2207(4)	11.0991(3)
c/Å	14.366(2)	21.6466(7)	15.7402(5)
α/°	94.291(5)	90	90
β/°	90.538(5)	92.4190(10)	90
γ/°	105.479(4)	90	90
V/Å^3	1060.3(3)	3224.43(18)	3424.67(19)
Z	2	4	4
ρ_{calcd}/g cm^{-3}	1.824	1.688	1.616
μ/mm^{-1}	1.009	0.738	0.696
crystal size/mm	0.050 × 0.050 × 0.020	0.090 × 0.030 × 0.020	0.070 × 0.060 × 0.020
temperature/K	173(2)	102(2)	102(2)
rated input/kW	2.5	2.5	2.5
θ-range/°	3.009–27.11	2.992–27.50	2.772–26.752
reflections for metric	8355	9860	9918
absorption correction	multi-scan	multi-scan	multi-scan
transmission factors	0.6327–0.7455	0.6871–0.7456	0.7087–0.7452
reflections measured	19090	59290	37286
independent reflections	4621	7408	7247
R_{int}	0.0222	0.0488	0.0342
mean σ(I)/I	0.053	0.071	0.037
reflections with $I \geq 2\sigma(I)$	4009	5915	7036
x, y (weighting scheme)	0.0293, 0.6306	0.0337, 2.6546	0.0191, 0.6583
hydrogen refinement	[a]	[a]	[a]
Flack parameter	–	–	0.007(4)
parameters	302	460	469
restraints	0	0	1
$R(F_{obs})$	0.0309	0.0381	0.0210
$R_w(F^2)$	0.0744	0.0846	0.0495
S	1.042	1.017	1.055
shift/error$_{max}$	0.001	0.001	0.002
max. electron density/e Å^{-3}	0.471	0.707	0.224
min. electron density/e Å^{-3}	−0.357	−0.396	−0.198
measurement code	yv700	yv198	yv202
CCDC number	–	2074569	2074571

[a] All hydrogen atoms were calculated in idealized positions, riding on their parent atoms. U_{iso} was always coupled to the parent atom.

Table 7.7: Crystallographic data of compounds [Co(dppb)(fpin)(NO)] (**3c**), [Co(fpin)(NO)($PMePh_2$)$_2$] (**3d**) and *trans*-[Co(ClO_4)(en)$_2$(NO)]ClO_4 (**4a**).

	3c	**3d** [a]	**4a**
empirical formula	$C_{34}H_{28}CoF_{12}NO_3P_2$	$C_{32}H_{26}CoF_{12}NO_3P_2$	$C_4H_{16}Cl_2CoN_5O_9$
M_r/g mol^{-1}	847.44	821.41	408.05
crystal system	orthorhombic	monoclinic	monoclinic
space group	*Pna*2$_1$	*P*2$_1$/*n*	*P*2$_1$/*n*
a/Å	19.3437(7)	12.3683(9)	7.7695(5)
b/Å	11.6252(4)	41.975(3)	15.9639(10)
c/Å	15.6224(6)	13.0009(10)	11.6108(7)
α/°	90	90	90
β/°	90	99.189(3)	104.291(2)
γ/°	90	90	90
V/Å^3	3513.1(2)	6662.9(8)	1395.54(15)
Z	4	8	4
ρ_{calcd}/g cm^{-3}	1.602	1.638	1.942
μ/mm^{-1}	0.680	0.714	1.666
crystal size/mm	0.100 × 0.030 × 0.030	0.030 × 0.030 × 0.016	0.040 × 0.030 × 0.010
temperature/K	102(2)	173(2)	101(2)
rated input/kW	2.5	2.5	2.5
θ-range/°	2.740–28.30	3.149–26.39	2.991–27.12
reflections for metric	9669	9877	7376
absorption correction	multi-scan	multi-scan	multi-scan
transmission factors	0.7181–0.7457	0.7002–0.7454	0.6707–0.7455
reflections measured	65076	169728	26194
independent reflections	8665	13648	3078
R_{int}	0.0431	0.0807	0.0498
mean σ(*I*)/*I*	0.042	0.073	0.084
reflections with $I \geq 2\sigma(I)$	8070	10628	2513
x, *y* (weighting scheme)	0.0229, 0.8435	0.0097, 14.2213	0.0214, 2.1738
hydrogen refinement	[b]	[b]	[b]
Flack parameter	0.010(5)	–	–
parameters	478	923	203
restraints	1	6	9
$R(F_{obs})$	0.0247	0.0533	0.0304
$R_w(F^2)$	0.0564	0.0954	0.0758
S	1.028	1.106	1.055
shift/error$_{max}$	0.001	0.001	0.001
max. electron density/e Å^{-3}	0.258	0.878	0.702
min. electron density/e Å^{-3}	−0.254	−0.486	−0.529
measurement code	yv201	zv443	yv493
CCDC number	2074570	–	–

[a] One F atom of a perfluoropinacolato ligand was restrained in a way that its U_{ij} component approximates to isotropic behavior, using the ''ISOR'' command in *SHELXL*.

[b] All hydrogen atoms were calculated in idealized positions, riding on their parent atoms. U_{iso} was always coupled to the parent atom.

Table 7.8: Crystallogr. data of *trans*-[Co(Cl)(en)$_2$(NO)]Cl·H$_2$O (**4b**·H$_2$O), *trans*-[Co(en)$_2$I(NO)](ClO$_4$)$_{0.6}$I$_{0.4}$ (**4c**) and *trans*-[Co(BF$_4$)(en)$_2$(NO)]BF$_4$ (**4e**).

	4b·H$_2$O	**4c**	**4e**
empirical formula	$C_4H_{18}Cl_2CoN_5O_2$	$C_4H_{16}Cl_{0.6}CoI_{1.4}N_5O_{3.4}$	$C_4H_{16}B_2CoF_8N_5O$
M_r/g mol^{-1}	298.06	446.46	382.77
crystal system	monoclinic	monoclinic	monoclinic
space group	$P2_1$	$P2_1/n$	$P2_1/n$
a/Å	7.8573(4)	7.9698(4)	7.6626(8)
b/Å	8.0884(4)	15.0852(8)	15.6875(15)
c/Å	9.7370(5)	11.2581(6)	11.5798(11)
α/°	90	90	90
β/°	110.997(2)	108.850(2)	104.552(4)
γ/°	90	90	90
V/Å^3	577.73(5)	1280.92(12)	1347.3(2)
Z	2	4	4
ρ_{calcd}/g cm^{-3}	1.713	2.315	1.887
μ/mm^{-1}	1.934	4.840	1.372
crystal size/mm	0.050 × 0.050 × 0.010	0.030 × 0.030 × 0.010	0.070 × 0.060 × 0.040
temperature/K	102(2)	103(2)	173(2)
rated input/kW	2.5	2.5	2.5
θ-range/°	3.371–29.57	3.020–27.11	2.597–27.12
reflections for metric	8420	9996	6400
absorption correction	multi-scan	multi-scan	multi-scan
transmission factors	0.6719–0.7459	0.6549–0.7455	0.6746–0.7455
reflections measured	14604	29579	25354
independent reflections	3227	2836	2978
R_{int}	0.0356	0.0336	0.0665
mean σ(I)/I	0.064	0.075	0.074
reflections with $I \geq 2\sigma(I)$	3038	2629	2408
x, y (weighting scheme)	0.0187, 0.0016	0.0044, 1.0977	0.0274, 1.3964
hydrogen refinement	[a, b]	[c]	[c]
Flack parameter	[d]	–	–
parameters	135	178	203
restraints	4	9	9
$R(F_{obs})$	0.0240	0.0163	0.0363
$R_w(F^2)$	0.0526	0.0343	0.0920
S	1.045	1.107	1.036
shift/error$_{max}$	0.001	0.002	0.001
max. electron density/e Å^{-3}	0.341	0.489	0.641
min. electron density/e Å^{-3}	−0.344	−0.389	−0.488
measurement code	yv444	yv476	zv252
CCDC number	2074566	–	–

[a] C- and N-bonded hydrogen atoms were calculated in idealized positions, riding on their parent atoms. The coordinates of O-bonded hydrogen atoms were refined freely.

[b] O-bonded hydrogen atoms: O-H fixed to 0.83 Å, H...H fixed to 1.31 Å.

[c] All hydrogen atoms were calculated in idealized positions, riding on their parent atoms. U_{iso} was always coupled to the parent atom.

[d] Structure was refined as a two-component inversion twin. Volume fraction of the twin component from refinement (BASF): 0.044(15). Twin law: −1 0 0 0 −1 0 0 0 −1.

Table 7.9: Crystallographic data of the compounds *trans*-[Co(dmso-κ*O*)(en)$_2$(NO)](ClO$_4$)$_2$·DMSO (**4f**·DMSO), *trans*-[Co(ClO$_4$)(men)$_2$(NO)]ClO$_4$ (**4g**) and *trans*-[Co(ClO$_4$)(*N*,*N*-dmen)$_2$(NO)]ClO$_4$ (**4h**).

	4f·DMSO	**4g**	**4h**
empirical formula	$C_8H_{28}Cl_2CoN_5O_{11}S_2$	$C_6H_{20}Cl_2CoN_5O_9$	$C_8H_{24}Cl_2CoN_5O_9$
M_r/g mol^{-1}	564.30	436.10	464.15
crystal system	monoclinic	monoclinic	monoclinic
space group	$P2_1/c$	$P2_1/c$	$P2_1/n$
a/Å	7.3869(6)	11.8484(14)	8.4241(5)
b/Å	25.306(2)	8.9135(10)	17.5988(9)
c/Å	12.0474(11)	16.1727(17)	12.5786(7)
α/°	90	90	90
β/°	95.999(3)	111.040(4)	108.195(2)
γ/°	90	90	90
V/Å^3	2239.8(3)	1594.1(3)	1771.59(17)
Z	4	4	4
ρ_{calcd}/g cm^{-3}	1.673	1.817	1.740
μ/mm^{-1}	1.249	1.465	1.324
crystal size/mm	0.100 × 0.080 × 0.080	0.040 × 0.030 × 0.020	0.040 × 0.040 × 0.030
temperature/K	173(2)	173(2)	173(2)
rated input/kW	2.5	2.5	2.5
θ-range/°	2.773–27.11	2.666–27.16	3.410–27.50
reflections for metric	9904	8794	9988
absorption correction	multi-scan	multi-scan	multi-scan
transmission factors	0.6905–0.7455	0.6746–0.7455	0.6926–0.7456
reflections measured	42127	29765	37457
independent reflections	4946	3520	4058
R_{int}	0.0506	0.0514	0.0463
mean σ(I)/I	0.066	0.075	0.063
reflections with $I \geq 2\sigma(I)$	4285	2985	3479
x, y (weighting scheme)	0.0340, 1.9007	0.0261, 2.2987	0.0230, 1.2431
hydrogen refinement	[a]	[b]	[a]
Flack parameter	–	–	–
parameters	285	226	230
restraints	9	0	0
$R(F_{obs})$	0.0341	0.0378	0.0292
$R_w(F^2)$	0.0866	0.0890	0.0681
S	1.042	1.049	1.045
shift/error$_{max}$	0.001	0.001	0.001
max. electron density/e Å^{-3}	1.117	0.801	0.476
min. electron density/e Å^{-3}	−1.036	−0.351	−0.390
measurement code	zv276	zv255	zv167
CCDC number	–	–	2129960

[a] All hydrogen atoms were calculated in idealized positions, riding on their parent atoms. U_{iso} was always coupled to the parent atom.

[b] C- and N2-bonded hydrogen atoms were calculated in idealized positions, riding on their parent atoms. The coordinates of all other N-bonded hydrogen atoms were refined freely.

Table 7.10: Crystallogr. data of *trans*-[Co(BF_4)(*N*,*N*-dmen)$_2$(NO)]BF_4 (**4i**), *trans*-[Co(bnen)$_2$(NO)(NO_3)]NO_3·MeOH (**4l**·MeOH) and [Co(dppe)$_2$(NO)](ClO_4)$_2$·2.7Me_2CO·0.3DMSO (**5a**·2.7Me_2CO·0.3DMSO).

	4i	**4l**·MeOH	**5a**·2.7Me_2CO·0.3DMSO[a]
empirical formula	$C_8H_{24}B_2CoF_8N_5O$	$C_{19}H_{32}CoN_7O_8$	$C_{60.7}H_{66}Cl_2CoNO_{12}P_4S_{0.3}$
M_r/g mol^{-1}	438.87	545.44	1264.61
crystal system	monoclinic	monoclinic	triclinic
space group	$P2_1/n$	$C2/c$	$P\bar{1}$
a/Å	8.3111(10)	23.0103(13)	11.6596(2)
b/Å	17.390(2)	14.6614(8)	11.9495(3)
c/Å	12.4746(16)	14.7724(8)	22.3802(5)
α/°	90	90	85.1890(10)
β/°	107.946(4)	90.221(2)	76.2380(10)
γ/°	90	90	78.1490(10)
V/Å^3	1715.3(4)	4983.6(5)	2962.07(11)
Z	4	8	2
ρ_{calcd}/g cm^{-3}	1.699	1.454	1.418
μ/mm^{-1}	1.090	0.746	0.561
crystal size/mm	0.050 × 0.040 × 0.030	0.160 × 0.140 × 0.050	0.050 × 0.050 × 0.020
temperature/K	173(2)	173(2)	102(2)
rated input/kW	2.5	2.5	2.5
θ-range/°	2.342–27.14	2.997–28.39	2.239–27.12
reflections for metric	4923	9882	9940
absorption correction	multi-scan	multi-scan	multi-scan
transmission factors	0.7046–0.7455	0.7001–0.7457	0.7079–0.7455
reflections measured	32229	78354	55662
independent reflections	3789	6248	12982
R_{int}	0.0718	0.0383	0.0408
mean σ(I)/I	0.088	0.050	0.078
reflections with $I \geq 2\sigma(I)$	2852	5450	10428
x, y (weighting scheme)	0.0427, 2.5560	0.0319, 4.0117	0.0501, 5.5097
hydrogen refinement	[b]	[c]	[b]
Flack parameter	–	–	–
parameters	230	337	867
restraints	0	9	60
$R(F_{obs})$	0.0471	0.0279	0.0511
$R_w(F^2)$	0.1212	0.0725	0.1302
S	1.051	1.044	1.017
shift/error$_{max}$	0.001	0.001	0.001
max. electron density/e Å^{-3}	0.699	0.304	1.186
min. electron density/e Å^{-3}	−0.475	−0.281	−0.791
measurement code	zv273	zv442	yv586
CCDC number	–	–	2074572

[a] Some O atoms of the perchlorate ions were restrained in a way that their U_{ij} components approximate to isotropic behavior, using the ''ISOR'' command in *SHELXL*.

[b] All hydrogen atoms were calculated in idealized positions, riding on their parent atoms. U_{iso} was always coupled to the parent atom.

[c] C- and N-bonded hydrogen atoms were calculated in idealized positions, riding on their parent atoms. The coordinates of O-bonded hydrogen atoms were refined freely.

Table 7.11: Crystallogr. data of $[Co(dppe)_2(NO)](BF_4)_2 \cdot 2Me_2CO$ (**5a'**·$2Me_2CO$), $[Co(dppa)_2(NO)](ClO_4)_2 \cdot 2Me_2CO$ (**5b**·$2Me_2CO$) and $[Co(dppv)_2(NO)](ClO_4)_2 \cdot 1.5Me_2CO$ (**5c**·$1.5Me_2CO$).

	5a'·$2Me_2CO$ [a]	**5b**·$2Me_2CO$ [b]	**5c**·$1.5Me_2CO$ [c]
empirical formula	$C_{58}H_{60}B_2CoF_8NO_3P_4$	$C_{54}H_{54}Cl_2CoN_3O_{11}P_4$	$C_{56.5}H_{53}Cl_2CoNO_{10.5}P_4$
M_r/g mol^{-1}	1175.50	1174.71	1167.71
crystal system	monoclinic	monoclinic	monoclinic
space group	$P2_1/n$	$C2/c$	$P2_1/c$
a/Å	12.4082(5)	30.305(2)	18.698(2)
b/Å	29.1382(14)	10.8197(7)	29.284(4)
c/Å	15.4884(7)	23.8123(17)	21.157(2)
α/°	90	90	90
β/°	96.756(2)	133.394(2)	103.287(4)
γ/°	90	90	90
V/Å^3	5561.0(4)	5673.6(7)	11275(2)
Z	4	4	4
ρ_{calcd}/g cm^{-3}	1.404	1.375	1.376
μ/mm^{-1}	0.496	0.569	0.571
crystal size/mm	0.080 × 0.050 × 0.040	0.040 × 0.040 × 0.010	0.110 × 0.090 × 0.080
temperature/K	173(2)	173(2)	173(2)
rated input/kW	2.5	2.5	2.5
θ-range/°	2.112–26.39	3.202–27.11	2.037–26.38
reflections for metric	9839	6085	9965
absorption correction	multi-scan	multi-scan	multi-scan
transmission factors	0.7215–0.7454	0.6546–0.7455	0.6956–0.7454
reflections measured	127642	53328	133709
independent reflections	11389	6265	23037
R_{int}	0.0785	0.0816	0.0613
mean σ(I)/I	0.068	0.091	0.280
reflections with $I \geq 2\sigma(I)$	8882	4404	17470
x, y (weighting scheme)	0.0399, 8.6717	0.0935, 29.4615	0.1681, 32.8274
hydrogen refinement	[d]	[d]	[d]
Flack parameter	–	–	–
parameters	698	341	1357
restraints	6	46	84
$R(F_{obs})$	0.0475	0.0693	0.0919
$R_w(F^2)$	0.1196	0.2091	0.2837
S	1.039	1.014	1.067
shift/error$_{max}$	0.002	0.001	0.001
max. electron density/e Å^{-3}	1.298	1.127	1.912
min. electron density/e Å^{-3}	−0.915	−0.784	−2.392
measurement code	zv344	yv678	yv735
CCDC number	2129959	2074573	2074584

[a] One F atom of a tetrafluoroborate ion was restrained in a way that its U_{ij} component approximates to isotropic behavior, using the ''ISOR'' command in *SHELXL*.

[b] All perchlorate O atoms were refined isotropically with the same temperature factor. Furthermore, a C atom of acetone was restrained so that U_{ij} approximates to isotropic behavior, using the ''ISOR'' command in *SHELXL*.

[c] Some perchlorate O- and acetone C atoms were restrained in a way that their U_{ij} components approximate to isotropic behavior, using the ''ISOR'' command in *SHELXL*.

[d] All hydrogen atoms were calculated in idealized positions, riding on their parent atoms. U_{iso} was always coupled to the parent atom.

Table 7.12: Crystallographic data of $[Co(dppv)_2(NO)](BF_4)_2 \cdot 1.8Me_2CO \cdot 0.2DMSO$ (**5c'**·$1.8Me_2CO \cdot 0.2DMSO$), $[Co(dppbz)_2(NO)](ClO_4)_2 \cdot Me_2CO$ (**5d**·Me_2CO) and $[CoCl_2(dppe)(NO)] \cdot Me_2CO$ (**6a**·Me_2CO).

	5c'·$1.8Me_2CO \cdot 0.2DMSO$ [a]	**5d**·Me_2CO [b]	**6a**·Me_2CO
empirical formula	$C_{57.8}H_{56}B_2CoF_8NO_3P_4S_{0.2}$	$C_{63}H_{54}Cl_2CoNO_{10}P_4$	$C_{29}H_{30}Cl_2CoNO_2P_2$
M_r/g mol^{-1}	1174.82	1238.78	616.31
crystal system	monoclinic	triclinic	monoclinic
space group	$P2_1/c$	$P\bar{1}$	$P2_1/n$
a/Å	18.569(2)	15.3496(7)	13.4019(3)
b/Å	28.998(3)	17.9117(8)	11.9820(3)
c/Å	20.733(3)	22.9304(11)	17.9727(4)
α/°	90	97.188(2)	90
β/°	103.917(4)	108.143(2)	97.6220(10)
γ/°	90	90.074(2)	90
V/Å^3	10837(2)	5938.5(5)	2860.58(12)
Z	4	4	4
ρ_{calcd}/g cm^{-3}	1.440	1.386	1.431
μ/mm^{-1}	0.515	0.546	0.926
crystal size/mm	0.050 × 0.060 × 0.070	0.090 × 0.070 × 0.040	0.050 × 0.040 × 0.040
temperature/K	100(2)	173(2)	106(2)
rated input/kW	2.5	2.5	2.5
θ-range/°	2.183–27.14	1.963–27.13	2.850–27.10
reflections for metric	9854	9940	9964
absorption correction	multi-scan	multi-scan	multi-scan
transmission factors	0.6809–0.7455	0.8345–0.8620	0.6984–0.7455
reflections measured	294209	148117	53896
independent reflections	23974	26168	6302
R_{int}	0.1028	0.0559	0.0394
mean $\sigma(I)/I$	0.097	0.085	0.054
reflections with $I \geq 2\sigma(I)$	18000	19246	5522
x, y (weighting scheme)	0.0620, 35.3878	0.0785, 10.1215	0.0198, 1.8716
hydrogen refinement	[c]	[c]	[c]
Flack parameter	–	–	–
parameters	1417	1463	336
restraints	36	67	0
$R(F_{obs})$	0.0591	0.0603	0.0268
$R_w(F^2)$	0.1618	0.1725	0.0619
S	1.022	1.033	1.041
shift/error$_{max}$	0.001	0.001	0.001
max. electron density/e Å^{-3}	2.656	1.506	0.393
min. electron density/e Å^{-3}	−1.278	−0.991	−0.250
measurement code	zv368	yv693	yv572
CCDC number	–	–	2129961

[a] Some F atoms of the tetrafluoroborate ions and some C atoms of the co-crystallized acetone as well as one S atom of DMSO were restrained in a way that their U_{ij} components approximate to isotropic behavior, using the ''ISOR'' command in *SHELXL*.

[b] Some perchlorate O atoms as well as the O- and C atoms of a co-crystallized acetone molecule were restrained in a way that their U_{ij} components approximate to isotropic behavior, using the ''ISOR'' command in *SHELXL*.

[c] All hydrogen atoms were calculated in idealized positions, riding on their parent atoms. U_{iso} was always coupled to the parent atom.

Table 7.13: Crystallogr. data of [$CoBr_2$(dppe)(NO)] (**6a'**), [$CoCl_2$(dppp)(NO)] (**6b**) and [$CoCl_2$(dppv)(NO)] (**6c**).

	6a'	**6b**	**6c**
empirical formula	$C_{26}H_{24}Br_2CoNOP_2$	$C_{27}H_{26}Cl_2CoNOP_2$	$C_{26}H_{22}Cl_2CoNOP_2$
M_r/g mol^{-1}	647.15	572.26	556.21
crystal system	monoclinic	orthorhombic	triclinic
space group	$P2_1/c$	$P2_12_12_1$	$P\bar{1}$
a/Å	17.4717(9)	10.6309(6)	7.9968(6)
b/Å	13.5782(7)	16.8779(9)	10.8721(8)
c/Å	22.1221(11)	28.2980(16)	14.3556(11)
α/°	90	90	90.513(2)
β/°	92.329(2)	90	92.781(2)
γ/°	90	90	102.636(2)
V/Å^3	5243.8(5)	5077.4(5)	1216.20(16)
Z	8	8	2
ρ_{calcd}/g cm^{-3}	1.639	1.497	1.519
μ/mm^{-1}	3.844	1.034	1.077
crystal size/mm	0.170 × 0.130 × 0.090	0.160 × 0.140 × 0.120	0.130 × 0.030 × 0.020
temperature/K	173(2)	173(2)	173(2)
rated input/kW	2.5	2.5	2.5
θ-range/°	2.914–28.31	3.129–27.50	3.172–26.40
reflections for metric	9613	9499	9924
absorption correction	multi-scan	multi-scan	multi-scan
transmission factors	0.6420–0.7457	0.6979–0.7456	0.6913–0.7454
reflections measured	166867	126572	28001
independent reflections	13021	11639	4957
R_{int}	0.0441	0.0371	0.0254
mean $\sigma(I)/I$	0.068	0.052	0.053
reflections with $I \geq 2\sigma(I)$	11020	11151	4392
x, y (weighting scheme)	0.0231, 3.7209	0.0323, 2.1520	0.0286, 0.7662
hydrogen refinement	[a]	[a]	[a]
Flack parameter	–	[b]	–
parameters	632	614	298
restraints	12	0	0
$R(F_{obs})$	0.0245	0.0264	0.0273
$R_w(F^2)$	0.0588	0.0675	0.0663
S	1.056	1.068	1.052
$shift/error_{max}$	0.002	0.002	0.001
max. electron density/e Å^{-3}	0.398	0.338	0.449
min. electron density/e Å^{-3}	−0.524	−0.310	−0.266
measurement code	zv428	zv415	zv416
CCDC number	–	–	–

[a] All hydrogen atoms were calculated in idealized positions, riding on their parent atoms. U_{iso} was always coupled to the parent atom.

[b] Structure was refined as a two-component inversion twin. Volume fraction of the twin component from refinement (BASF): 0.049(10). Twin law: −1 0 0 0 −1 0 0 0 −1.

Table 7.14: Crystallographic data of compounds $[CoBr_2(dppv)(NO)]\cdot CHCl_3$ (**6c'**·$CHCl_3$), $[CoCl_2(dppbz)(NO)]$ (**6d**) and $[CoBr_2(dppbz)(NO)]$ (**6d'**).

	6c'·$CHCl_3$	**6d**	**6d'**
empirical formula	$C_{27}H_{23}Br_2Cl_3CoNOP_2$	$C_{30}H_{24}Cl_2CoNOP_2$	$C_{30}H_{24}Br_2CoNOP_2$
M_r/g mol^{-1}	764.50	606.27	695.19
crystal system	orthorhombic	monoclinic	monoclinic
space group	*Pbca*	$P2_1$	$P2_1$
a/Å	17.1223(17)	9.7583(7)	9.8559(6)
b/Å	15.3527(17)	14.8231(10)	14.9205(9)
c/Å	22.395(3)	10.3867(7)	10.5789(6)
α/°	90	90	90
β/°	90	115.411(2)	117.081(2)
γ/°	90	90	90
V/Å^3	5887.1(11)	1357.06(16)	1385.12(14)
Z	8	2	2
ρ_{calcd}/g cm^{-3}	1.725	1.484	1.667
μ/mm^{-1}	3.702	0.972	3.645
crystal size/mm	0.120 × 0.060 × 0.030	0.800 × 0.060 × 0.040	0.120 × 0.090 × 0.020
temperature/K	173(2)	173(2)	173(2)
rated input/kW	2.5	2.5	2.5
θ-range/°	2.995–28.31	3.503–26.55	3.484–27.50
reflections for metric	9733	9854	9946
absorption correction	multi-scan	multi-scan	multi-scan
transmission factors	0.6508–0.7457	0.6297–0.7454	0.6496–0.7456
reflections measured	162158	31144	34146
independent reflections	7301	5540	6336
R_{int}	0.0553	0.0404	0.0450
mean σ(*I*)/*I*	0.063	0.055	0.081
reflections with $I \geq 2\sigma(I)$	6134	5330	5677
x, *y* (weighting scheme)	0.0175, 4.3720	0.0232, 0.7829	0.0251, 1.0173
hydrogen refinement	[a]	[a]	[a]
Flack parameter	–	[b]	[c]
parameters	335	335	335
restraints	0	1	1
$R(F_{obs})$	0.0232	0.0289	0.0338
$R_w(F^2)$	0.0504	0.0674	0.0689
S	1.028	1.094	1.056
shift/error$_{max}$	0.002	0.001	0.001
max. electron density/e Å^{-3}	0.462	0.536	1.063
min. electron density/e Å^{-3}	−0.393	−0.328	−0.489
measurement code	zv425	zv417	zv426
CCDC number	–	–	–

[a] All hydrogen atoms were calculated in idealized positions, riding on their parent atoms. U_{iso} was always coupled to the parent atom.

[b] Structure was refined as a two-component inversion twin. Volume fraction of the twin component from refinement (BASF): 0.465(16). Twin law: −1 0 0 0 −1 0 0 0 −1.

[c] Refined as a two-component inversion twin with a volume fraction of the twin component from refinement (BASF) of 0.462(10). Twin law: −1 0 0 0 −1 0 0 0 −1.

Table 7.15: Crystal. data of compounds *rac-cis*-[Co(NO)(NO_2-κ*N*)(phen)$_2$]ClO_4 (**7a**), ($ppzH_2$)$_{0.5}$[Co(fpin)$(NO)_2$] (**7b**) and *rac*-[Co(en)$_2$(*cis*-N_2O_2-κ^2*O*,*O*′)]ClO_4 (**7c**).

	7a[a]	**7b**[b]	**7c**[c]
empirical formula	$C_{24}H_{16}ClCoN_6O_7$	$C_8H_6CoF_{12}N_3O_4$	$C_4H_{16}ClCoN_6O_6$
M_r/g mol^{-1}	594.81	495.09	338.61
crystal system	triclinic	monoclinic	monoclinic
space group	$P\bar{1}$	$P2_1/c$	$P2_1/c$
a/Å	6.9579(2)	9.0050(5)	6.8633(6)
b/Å	12.3661(3)	12.2648(7)	10.8839(10)
c/Å	14.1769(3)	14.2036(9)	16.2480(14)
α/°	70.5260(10)	90	90
β/°	82.1110(10)	107.045(2)	97.362(3)
γ/°	80.0630(10)	90	90
V/Å^3	1128.59(5)	1499.80(15)	1203.71(18)
Z	2	4	4
ρ_{calcd}/g cm^{-3}	1.750	2.193	1.868
μ/mm^{-1}	0.943	1.310	1.680
crystal size/mm	0.040 × 0.030 × 0.030	0.060 × 0.050 × 0.030	0.090 × 0.060 × 0.040
temperature/K	101(2)	173.(2)	173.(2)
rated input/kW	2.5	2.5	2.5
θ-range/°	3.229–27.15	3.000–27.098	3.146–26.370
reflections for metric	8056	9959	7948
absorption correction	multi-scan	multi-scan	multi-scan
transmission factors	0.6821–0.7455	0.6970–0.7455	0.6707–0.7456
reflections measured	19605	3310	2682
independent reflections	4958	3310	2682
R_{int}	0.0279	0.0539	0.0378
mean σ(I)/I	0.064	0.082	0.091
reflections with $I \geq 2\sigma(I)$	4247	2982	2569
x, y (weighting scheme)	0.0190, 1.2960	0.0390, 1.3413	0.0360, 3.7188
hydrogen refinement	[d]	[e]	[d]
Flack parameter	–	–	–
parameters	407	262	164
restraints	18	0	6
$R(F_{obs})$	0.0379	0.0355	0.0387
$R_w(F^2)$	0.0822	0.0936	0.0949
S	1.098	1.109	1.072
shift/error$_{max}$	0.001	0.001	0.001
max. electron density/e Å^{-3}	0.464	0.413	1.600
min. electron density/e Å^{-3}	−0.531	−0.309	−0.926
measurement code	yv487	yv725	zv490
CCDC number	–	–	–

[a] The nitrosyl and nitrito O atoms of the minor disorder form were restrained in a way that their U_{ij} components approximate to isotropic behavior, using the ''ISOR'' command in *SHELXL*.

[b] The structure was refined as a non-merohedral two-component twin. Volume fraction of the twin component from refinement (BASF): 0.4566(14). Twin law: 1 0 0.372 0 −1 0 0 0 −1.

[c] One perchlorate O atom was restrained in a way that U_{ij} approximates to isotropic behavior using ISOR. Refined as a non-merohedral two-component twin with a BASF of 0.153(10). Twin law: 1 0 0 0 −1 0 −0.585 0 −1.

[d] All H atoms calculated in idealized positions, riding on their parent atoms with U_{iso} always coupled to them.

[e] C- and N-bonded H atoms calcd. in idealized riding positions. Coordinates of O-bonded H atoms refined freely.

7.3 Non-classical hydrogen bonds in the crystalline compounds

Table 7.16: Distances and angles of non-classical hydrogen bonds in crystalline compounds of class **1**. The standard deviation of the last decimal digit is given in parentheses. Values without a standard deviation refer to hydrogen atoms calculated on idealized positions, riding on their parent atoms.

1	D–H···A	*d*(D–H)/Å	*d*(H···A)/Å	*d*(D···A)/Å	∢(D–H···A)/°
a	N2–H722···O1^{i}	0.91	2.42	3.169(3)	140
	C8–H81···F3^{ii}	0.99	2.54	3.211(3)	125
	C12–H122···O3	0.99	2.36	2.941(3)	117
b	N2–H722···O1^{i}	0.91	2.39	3.134(4)	138
	C7–H72···O1^{iii}	0.99	2.58	3.568(5)	176
	C8–H81···F1^{ii}	0.99	2.43	3.174(4)	131
	C9–H91···O1^{iii}	0.99	2.60	3.507(5)	153
	C9–H92···O3	0.99	2.40	2.948(5)	115
	C13–H131···N1	0.99	2.58	3.025(6)	107
	C13–H132···O3	0.99	2.58	3.096(5)	113
c	N2–H722···O1^{i}	0.91	2.33	3.085(3)	140
	C7–H71···F6^{i}	0.99	2.52	3.416(3)	150
	C8–H82···F11^{iv}	0.99	2.52	3.358(3)	143
	C9–H91···F3^{v}	0.99	2.48	3.193(3)	129
	C9–H91···N1	0.99	2.54	2.945(3)	104
	C12–H122···O3	0.99	2.35	2.936(3)	117
d	N2–H722···N1^{vi}	0.91	2.59	3.115(3)	117
	C7–H72···O4^{i}	0.99	2.53	3.263(3)	130
	C9–H91···O1	0.99	2.51	3.027(3)	112
	C9–H92···O3	0.99	2.45	3.009(4)	115
	C16–H161···F9^{vii}	0.98	2.49	3.459(4)	169
	C16–H163···O1^{viii}	0.98	2.57	3.474(4)	153
e	C7–H71···F3^{ix}	0.99	2.52	3.185(2)	125
	C8–H81···F3^{ix}	0.99	2.55	3.198(2)	123
	C9–H91···N1	0.99	2.51	2.964(2)	108
	C9–H92···O2	0.99	2.50	3.056(2)	115
	C13–H132···F2	0.99	2.55	3.417(2)	147
	C13–H132···O2	0.99	2.53	3.076(2)	114
	C14–H141···F3^{ix}	0.99	2.49	3.238(2)	132
	C14–H141···N1	0.99	2.61	3.001(2)	103

Symmetry codes: ^{i} 1−*x*, 1−*y*, 1−*z*; ^{ii} *x*, −1+*y*, *z*; ^{iii} −1+*x*, *y*, *z*; ^{iv} −½+*x*, ½−*y*, ½+*z*; ^{v} ½+*x*, ½−*y*, ½+*z*; ^{vi} 1−*x*, −*y*, 1−*z*; ^{vii} −*x*, ½+*y*, ½−*z*; ^{viii} 1−*x*, ½+*y*, ½−*z*; ^{ix} 1+*x*, *y*, *z*; ^{x} ³⁄₂−*x*, −½+*y*, ½−*z*; ^{xi} −½+*x*, ½−*y*, −½+*z*; ^{xii} 1+*x*, 1+*y*, *z*; ^{xiii} *x*, *y*, −1+*z*; ^{xiv} 2−*x*, 1−*y*, 1−*z*; ^{xv} *x*, 1−*y*, ½+*z*; ^{xvi} *x*, −*y*, ½+*z*; ^{xvii} 1+*x*, 1−*y*, ½+*z*; ^{xviii} 1+*x*, −*y*, ½+*z*; ^{xix} *x*, 1+*y*, *z*; ^{xx} −½+*x*, ³⁄₂−*y*, 1−*z*; ^{xxi} −*x*, 1−*y*, 1−*z*; ^{xxii} *x*, ½−*y*, −½+*z*; ^{xxiii} *x*, ½−*y*, ½+*z*; ^{xxiv} 1−*x*, −½+*y*, ½−*z*; ^{xxv} *x*, −*y*, −½+*z*; ^{xxvi} *x*, 1−*y*, −½+*z*; ^{xxvii} ½−*x*, ½+*y*, ½−*z*.

Table 7.16, continued.

1	D–H···A	*d*(D–H)/Å	*d*(H···A)/Å	*d*(D···A)/Å	∢(D–H···A)/°
	C14–H142···F12^{vi}	0.99	2.55	3.286(2)	131
	C16–H162···F8^{vi}	0.99	2.51	3.453(2)	160
	C18–H181···F1	0.99	2.49	3.016(2)	113
	C18–H182···O3	0.99	2.41	2.985(2)	116
f	C7–H71···F8^{x}	0.99	2.52	3.163(2)	123
	C7–H71···N1A	0.99	2.60	3.009(18)	105
	C9–H91···N1	0.99	2.61	3.154(4)	114
	C9–H91···O1	0.99	2.31	3.069(3)	133
	C9–H92···O2	0.99	2.43	2.967(2)	114
	C13–H131···O3	0.99	2.36	2.890(2)	112
	C14–H142···O1A^{iii}	0.98	2.48	2.872(7)	103
	C15–H151···F6^{x}	0.99	2.54	3.129(2)	118
	C15–H151···N1	0.99	2.44	2.881(4)	106
	C15–H151···N1A	0.99	2.59	3.063(18)	109
	C15–H152···F4^{xi}	0.99	2.52	3.409(2)	149
	C16–H161···O1A	0.98	2.58	3.186(7)	120
	C16–H161···O3	0.98	2.47	3.186(2)	130
g	N2–H722···O1^{i}	0.90(3)	2.58(2)	3.235(3)	131(2)
	C8–H81···F12^{xii}	0.99	2.55	3.429(2)	148
	C8–H82···F8^{ix}	0.99	2.51	3.432(2)	155
h	C7–H711···F12^{xiii}	0.99	2.46	3.392(5)	156
	C11–H11···O4^{xiv}	0.95	2.54	3.221(5)	128
	C12–H12···O3	0.95	2.44	2.951(5)	114
	C13–H132···O2	0.98	2.53	3.043(6)	112
	C14–H142···O3^{xiii}	0.98	2.56	3.501(5)	160
i	C7–H72···F21^{xv}	0.99	2.45	3.191(8)	131
	C7–H72···F24^{xv}	0.99	2.46	3.411(7)	160
	C9–H9···F18^{xvi}	0.95	2.42	3.221(8)	142
	C10–H10···O6^{xv}	0.95	2.39	3.332(8)	173
	C12–H12···O5^{iii}	0.95	2.35	3.266(8)	162
	C20–H201···F10^{xii}	0.99	2.53	3.492(7)	165
	C20–H201···N6	0.99	2.62	3.204(8)	118
	C20–H202···F12^{xvii}	0.99	2.43	3.367(7)	159
	C22–H22···F5^{xviii}	0.95	2.42	3.258(8)	147

Symmetry codes: ^{i} 1−*x*, 1−*y*, 1−*z*; ^{ii} *x*, −1+*y*, *z*; ^{iii} −1+*x*, *y*, *z*; ^{iv} −½+*x*, ½−*y*, ½+*z*; ^{v} ½+*x*, ½−*y*, ½+*z*; ^{vi} 1−*x*, −*y*, 1−*z*; ^{vii} −*x*, ½+*y*, ½−*z*; ^{viii} 1−*x*, ½+*y*, ½−*z*; ^{ix} 1+*x*, *y*, *z*; ^{x} ³⁄₂−*x*, −½+*y*, ½−*z*; ^{xi} −½+*x*, ½−*y*, −½+*z*; ^{xii} 1+*x*, 1+*y*, *z*; ^{xiii} *x*, *y*, −1+*z*; ^{xiv} 2−*x*, 1−*y*, 1−*z*; ^{xv} *x*, 1−*y*, ½+*z*; ^{xvi} *x*, −*y*, ½+*z*; ^{xvii} 1+*x*, 1−*y*, ½+*z*; ^{xviii} 1+*x*, −*y*, ½+*z*; ^{xix} *x*, 1+*y*, *z*; ^{xx} −½+*x*, ³⁄₂−*y*, 1−*z*; ^{xxi} −*x*, 1−*y*, 1−*z*; ^{xxii} *x*, ½−*y*, −½+*z*; ^{xxiii} *x*, ½−*y*, ½+*z*; ^{xxiv} 1−*x*, −½+*y*, ½−*z*; ^{xxv} *x*, −*y*, −½+*z*; ^{xxvi} *x*, 1−*y*, −½+*z*; ^{xxvii} ½−*x*, ½+*y*, ½−*z*.

Table 7.16, continued.

1	D–H···A	*d*(D–H)/Å	*d*(H···A)/Å	*d*(D···A)/Å	∢(D–H···A)/°
	C23–H23···O3^{xvii}	0.95	2.44	3.375(8)	169
	C25–H25···O2^{xix}	0.95	2.51	3.349(9)	148
	C26–H26···F6^{xix}	0.95	2.46	3.269(8)	143
j	C9–H9···O2	0.95	2.54	3.011(2)	111
	C11–H11···F9^{iii}	0.95	2.50	3.447(2)	175
	C12–H12···O4^{ix}	0.95	2.32	3.267(2)	173
	C13–H13···N1^{ii}	0.95	2.59	3.399(2)	143
	C14–H14···O3	0.95	2.44	2.917(2)	111
k	C19–H191···O2	0.98	2.51	2.876(5)	102
	C19–H193···O1	0.98	2.52	3.431(5)	155
	C20–H201···F12^{xx}	0.98	2.54	3.485(4)	161
	C20–H202···O3	0.98	2.28	3.003(4)	130
l	C10–H10···O2^{xxi}	0.95	2.50	3.154(3)	127
	C11–H11···F5^{xxii}	0.95	2.52	3.249(3)	133
	C11–H11···N1	0.95	2.49	2.978(3)	112
	C12–H12···F8^{xxii}	0.95	2.44	3.169(3)	134
	C16–H16···O3	0.95	2.47	2.879(3)	106
m	C8–H8···O1^{vii}	0.95	2.56	3.422(3)	151
	C9–H9···F12^{vii}	0.95	2.51	3.408(3)	157
	C11–H11···O1^{xxiii}	0.95	2.46	3.161(3)	130
	C11–H11···O3	0.95	2.40	2.806(3)	105
	C12–H12···N5^{xxiii}	0.95	2.55	3.455(3)	160
	C14–H14···F4^{xxiv}	0.95	2.31	2.994(4)	128
n	C7–H7···F6^{xix}	0.95	2.45	3.318(2)	152
	C8–H8···F5^{xxv}	0.95	2.43	3.202(2)	138
	C10–H101···O2^{i}	0.98	2.39	3.350(2)	168
	C11–H11···O3	0.95	2.43	2.872(2)	108
	C13–H13···F7^{xxvi}	0.95	2.41	3.074(2)	127
	C14–H141···O3^{xxvii}	0.98	2.53	3.505(2)	170

Symmetry codes: ^{i} 1−*x*, 1−*y*, 1−*z*; ^{ii} *x*, −1+*y*, *z*; ^{iii} −1+*x*, *y*, *z*; ^{iv} −½+*x*, ½−*y*, ½+*z*; ^{v} ½+*x*, ½−*y*, ½+*z*; ^{vi} 1−*x*, −*y*, 1−*z*; ^{vii} −*x*, ½+*y*, ½−*z*; ^{viii} 1−*x*, ½+*y*, ½−*z*; ^{ix} 1+*x*, *y*, *z*; ^{x} ³⁄₂−*x*, −½+*y*, ½−*z*; ^{xi} −½+*x*, ½−*y*, −½+*z*; ^{xii} 1+*x*, 1+*y*, *z*; ^{xiii} *x*, *y*, −1+*z*; ^{xiv} 2−*x*, 1−*y*, 1−*z*; ^{xv} *x*, 1−*y*, ½+*z*; ^{xvi} *x*, −*y*, ½+*z*; ^{xvii} 1+*x*, 1−*y*, ½+*z*; ^{xviii} 1+*x*, −*y*, ½+*z*; ^{xix} *x*, 1+*y*, *z*; ^{xx} −½+*x*, ³⁄₂−*y*, 1−*z*; ^{xxi} −*x*, 1−*y*, 1−*z*; ^{xxii} *x*, ½−*y*, −½+*z*; ^{xxiii} *x*, ½−*y*, ½+*z*; ^{xxiv} 1−*x*, −½+*y*, ½−*z*; ^{xxv} *x*, −*y*, −½+*z*; ^{xxvi} *x*, 1−*y*, −½+*z*; ^{xxvii} ½−*x*, ½+*y*, ½−*z*.

Table 7.17: Distances and angles of non-classical hydrogen bonds in crystalline compounds of class **2**. The standard deviation of the last decimal digit is given in parentheses. Values without a standard deviation refer to hydrogen atoms calculated on idealized positions, riding on their parent atoms.

2	D–H···A	*d*(D–H)/Å	*d*(H···A)/Å	*d*(D···A)/Å	∢(D–H···A)/°
a	N4–H742···F3	0.91	2.41	3.098(2)	132
	O7–H87···F1	0.88(5)	2.36(6)	3.014(2)	131(6)
	O7–H87···F14	0.88(5)	2.54(5)	3.328(2)	150(6)
	C7–H71···F5^{i}	0.99	2.46	3.095(2)	122
	C13–H13···F12^{ii}	0.95	2.48	3.297(3)	144
	C16–H16···O3	0.95	2.56	3.328(2)	139
	C27–H271···F16^{iii}	0.99	2.40	3.091(2)	126
	C34–H34···O6	0.95	2.51	3.306(2)	141
	C36–H36···O6	0.95	2.51	3.138(3)	124
b	C7–H71···F5^{iv}	0.99	2.54	3.204(3)	124
	C9–H9···O1	1.00	2.47	3.129(3)	123
	C12–H12···F2	1.00	2.54	3.381(3)	141
	C14–H142···O3	0.98	2.36	3.194(3)	143

Symmetry codes: ^{i} 1−*x*, 1−*y*, −*z*; ^{ii} 1+*x*, *y*, *z*; ^{iii} 2−*x*, 1−*y*, 1−*z*; ^{iv} 1−*x*, 1−*y*, 1−*z*.

Table 7.18: Distances and angles of non-classical hydrogen bonds in crystalline compounds of class **3**. The standard deviation of the last decimal digit is given in parentheses. Values without a standard deviation refer to hydrogen atoms calculated on idealized positions, riding on their parent atoms.

3	D–H···A	*d*(D–H)/Å	*d*(H···A)/Å	*d*(D···A)/Å	∢(D–H···A)/°
a	C7–H71···O1	0.99	2.47	3.088(3)	120
	C12–H12···F1^{i}	0.95	2.53	3.395(3)	151
	C20–H20···O2	0.95	2.51	2.978(3)	111
	C22–H22···O3	0.95	2.48	3.292(3)	144
	C29–H29···F7^{ii}	0.95	2.54	3.285(3)	136
	C32–H32···O3	0.95	2.33	3.116(3)	140
b	C7–H71···F8^{iii}	0.99	2.36	3.343(3)	171
	C15–H15···O2	0.95	2.55	2.995(3)	109
	C17–H17···F7	0.95	2.48	3.120(3)	124
	C17–H17···O2	0.95	2.33	3.129(3)	141
	C24–H24···F3^{iv}	0.95	2.51	3.444(3)	166
	C33–H33···O3	0.95	2.57	2.967(3)	105
c	C7–H71···O1	0.99	2.59	3.365(3)	135
	C9–H91···F9^{v}	0.99	2.37	3.332(2)	163

Symm. codes: ^{i} −*x*, −½+*y*, ³⁄₂−*z*; ^{ii} *x*, ½−*y*, ½+*z*; ^{iii} ³⁄₂−*x*, −½+*y*, ½+*z*; ^{iv} ³⁄₂−*x*, −½+*y*, −½+*z*; ^{v} *x*, 1+*y*, *z*; ^{vi} ³⁄₂−*x*, ½+*y*, ½+*z*; ^{vii} ³⁄₂−*x*, ½+*y*, −½+*z*; ^{viii} 1+*x*, *y*, *z*; ^{ix} 2−*x*, 1−*y*, 1−*z*; ^{x} 1−*x*, 1−*y*, 2−*z*.

Table 7.18, continued.

3	D–H···A	*d*(D–H)/Å	*d*(H···A)/Å	*d*(D···A)/Å	∢(D–H···A)/°
	C10–H101···F3^{vi}	0.99	2.45	3.366(3)	154
	C21–H21···F7^{vii}	0.95	2.48	3.408(3)	166
	C22–H22···F2	0.95	2.52	3.164(3)	125
	C28–H28···F2	0.95	2.42	3.196(3)	139
	C28–H28···O3	0.95	2.35	3.114(3)	137
	C34–H34···O3	0.95	2.51	3.023(3)	114
d	C14–H14···O2	0.95	2.26	2.855(4)	120
	C17–H17···F8^{viii}	0.95	2.43	3.353(4)	163
	C19–H193···F2	0.98	2.52	3.461(4)	161
	C32–H323···O1	0.98	2.52	3.127(5)	120
	C40–H40···O5	0.95	2.22	2.869(5)	125
	C42–H42···F18^{ix}	0.95	2.35	3.213(8)	151
	C53–H53···O6	0.95	2.47	3.213(4)	135
	C60–H60···F13^{x}	0.95	2.51	3.413(4)	159
	C62–H62···F9	0.95	2.49	3.401(5)	162

Symm. codes: ^{i} $-x, -½+y, ¾-z$; ^{ii} $x, ½-y, ½+z$; ^{iii} $¾-x, -½+y, ½+z$; ^{iv} $¾-x, -½+y, -½+z$; ^{v} $x, 1+y, z$; ^{vi} $¾-x, ½+y, ½+z$; ^{vii} $¾-x, ½+y, -½+z$; ^{viii} $1+x, y, z$; ^{ix} $2-x, 1-y, 1-z$; ^{x} $1-x, 1-y, 2-z$.

Table 7.19: Distances and angles of non-classical hydrogen bonds in crystalline compounds of class **4**. The standard deviation of the last decimal digit is given in parentheses. Values without a standard deviation refer to hydrogen atoms calculated on idealized positions, riding on their parent atoms. Values for **4d** refer to Ref.[94].

4	D–H···A	*d*(D–H)/Å	*d*(H···A)/Å	*d*(D···A)/Å	∢(D–H···A)/°
a	N5–H751···O1	0.91	2.53	2.971(4)	110
	C1–H11···O1A^{i}	0.99	2.55	3.494(9)	159
	C1–H12···O6^{ii}	0.99	2.50	3.386(4)	148
	C3–H32···O4	0.99	2.54	3.222(3)	126
	C4–H41···O6^{iii}	0.99	2.54	3.477(4)	159
b	N2–H721···O1	0.91	2.47	2.824(3)	103
	N5–H751···O1^{iv}	0.91	2.37	3.141(3)	143
c	C1–H11···O1A	0.99	2.56	3.156(12)	118
	C1–H11···O3^{iii}	0.99	2.45	3.231(4)	135
	C2–H21···O5^{iii}	0.99	2.41	3.359(4)	160
	C2–H22···O3	0.99	2.54	3.264(4)	130
	C3–H31···O5^{v}	0.99	2.43	3.112(3)	125

Symmetry codes: ^{i} $1-x, 1-y, 2-z$; ^{ii} $-x, 1-y, 1-z$; ^{iii} $½+x, ½-y, ½+z$; ^{iv} $1-x, ½+y, 1-z$; ^{v} $x, y, 1+z$; ^{vi} $½-x, -½+y, -½+z$; ^{vii} $-1+x, y, z$; ^{viii} $x, ½-y, -½+z$; ^{ix} $1-x, 1-y, -z$; ^{x} $-1+x, ½-y, -½+z$; ^{xi} $1-x, 1-y, 1-z$; ^{xii} $1+x, y, z$; ^{xiii} $-x, ½+y, ½-z$; ^{xiv} $x, y, -1+z$; ^{xv} $-½+x, ½-y, -½+z$; ^{xvi} $½-x, ½-y, 1-z$.

Table 7.19, continued.

4	D–H···A	*d*(D–H)/Å	*d*(H···A)/Å	*d*(D···A)/Å	∢(D–H···A)/°
	C3–H32···O5^{ii}	0.99	2.57	3.407(4)	142
	C4–H41···O5^{v}	0.99	2.51	2.985(3)	109
d	C1–H11···O4^{vi}	0.99	2.53	3.065(4)	113
e	N5–H751···O1A	0.91	2.60	3.010(6)	108
	C1–H11···O1^{i}	0.99	2.52	3.437(7)	153
	C1–H12···F5^{ii}	0.99	2.50	3.387(4)	149
	C4–H41···F5^{iii}	0.99	2.49	3.414(3)	154
f	C1–H11···O1A	0.99	2.49	3.069(7)	117
	C2–H22···O6^{vii}	0.99	2.49	3.249(4)	133
	C3–H31···O1	0.99	2.48	3.053(3)	117
	C3–H32···O1A^{viii}	0.99	2.58	3.540(7)	163
	C5–H51···O7^{ix}	0.98	2.60	3.449(3)	145
	C5–H53···O11^{x}	0.98	2.54	3.448(3)	155
	C6–H63···O7^{ix}	0.98	2.57	3.424(3)	146
	C7–H73···O5^{xi}	0.98	2.51	3.344(4)	143
	C8–H81···O1A^{xii}	0.98	2.42	3.087(7)	125
g	C1–H11···O4^{xi}	0.99	2.52	3.470(4)	161
	C4–H41···O8^{xiii}	0.99	2.57	3.376(4)	139
	C6–H61···O8^{viii}	0.98	2.54	3.514(4)	173
	C6–H62···N1	0.98	2.60	3.017(4)	106
	C6–H63···O4	0.98	2.49	3.380(4)	151
h	N5–H751···O1	0.91	2.52	2.879(2)	104
	C1–H11···O9^{xiv}	0.99	2.45	3.318(3)	146
	C3–H32···O2	0.99	2.51	3.070(3)	115
	C5–H52···O8^{ii}	0.98	2.49	3.413(3)	158
	C6–H62···O2	0.98	2.39	3.092(2)	128
	C7–H71···O9^{xv}	0.98	2.50	3.411(3)	154
	C7–H72···O4^{xv}	0.98	2.46	3.396(3)	159
	C7–H73···O1	0.98	2.53	3.116(3)	118
	C8–H82···O2	0.98	2.52	3.172(3)	124
i	N5–H751···O1	0.91	2.52	2.880(4)	104
	C1–H11···F8^{xiv}	0.99	2.43	3.306(4)	147
	C3–H32···F1	0.99	2.51	3.064(5)	115
	C5–H52···F7^{ii}	0.98	2.43	3.371(5)	161
	C5–H53···N1	0.98	2.51	2.844(5)	100

Symmetry codes: ^{i} 1−*x*, 1−*y*, 2−*z*; ^{ii} −*x*, 1−*y*, 1−*z*; ^{iii} ½+*x*, ½−*y*, ½+*z*; ^{iv} 1−*x*, ½+*y*, 1−*z*; ^{v} *x*, *y*, 1+*z*; ^{vi} ½−*x*, −½+*y*, −½+*z*; ^{vii} −1+*x*, *y*, *z*; ^{viii} *x*, ½−*y*, −½+*z*; ^{ix} 1−*x*, 1−*y*, −*z*; ^{x} −1+*x*, ½−*y*, −½+*z*; ^{xi} 1−*x*, 1−*y*, 1−*z*; ^{xii} 1+*x*, *y*, *z*; ^{xiii} −*x*, ½+*y*, ½−*z*; ^{xiv} *x*, *y*, −1+*z*; ^{xv} −½+*x*, ½−*y*, −½+*z*; ^{xvi} ½−*x*, ½−*y*, 1−*z*.

Table 7.19, continued.

4	D–H···A	*d*(D–H)/Å	*d*(H···A)/Å	*d*(D···A)/Å	∢(D–H···A)/°
	C6–H61···F8^{xi}	0.98	2.55	3.502(5)	164
	C6–H62···F1	0.98	2.36	3.067(4)	128
	C7–H71···F8^{xv}	0.98	2.46	3.361(5)	153
	C7–H72···F3^{xv}	0.98	2.44	3.382(5)	161
	C7–H73···O1	0.98	2.54	3.131(5)	119
	C8–H82···F1	0.98	2.42	3.093(4)	125
I	C3–H31···O1A	0.99	2.45	3.064(11)	119
	C5–H51···N1A	0.99	2.50	2.99(4)	110
	C5–H51···O1	0.99	2.45	3.148(2)	127
	C5–H52···N5	0.99	2.62	3.120(2)	111
	C12–H121···N1	0.99	2.50	3.019(3)	113
	C12–H121···O1A	0.99	2.31	3.020(1)	128
	C12–H122···O7^{xvi}	0.99	2.43	3.403(2)	169
	C13–H13···O3	0.95	2.43	3.350(2)	163

Symmetry codes: [i] 1−*x*, 1−*y*, 2−*z*; [ii] −*x*, 1−*y*, 1−*z*; [iii] ½+*x*, ½−*y*, ½+*z*; [iv] 1−*x*, ½+*y*, 1−*z*; [v] *x*, *y*, 1+*z*; [vi] ½−*x*, −½+*y*, −½+*z*; [vii] −1+*x*, *y*, *z*; [viii] *x*, ½−*y*, −½+*z*; [ix] 1−*x*, 1−*y*, −*z*; [x] −1+*x*, ½−*y*, −½+*z*; [xi] 1−*x*, 1−*y*, 1−*z*; [xii] 1+*x*, *y*, *z*; [xiii] −*x*, ½+*y*, ½−*z*; [xiv] *x*, *y*, −1+*z*; [xv] −½+*x*, ½−*y*, −½+*z*; [xvi] ½−*x*, ½−*y*, 1−*z*.

Table 7.20: Distances and angles of non-classical hydrogen bonds in crystalline compounds of class **5**. The standard deviation of the last decimal digit is given in parentheses. Values without a standard deviation refer to hydrogen atoms calculated on idealized positions, riding on their parent atoms.

5	D–H···A	*d*(D–H)/Å	*d*(H···A)/Å	*d*(D···A)/Å	∢(D–H···A)/°
a	C1–H11···O11^{i}	0.99	2.36	3.261(3)	152
	C2–H21···O3A^{ii}	0.99	2.60	3.491(12)	150
	C3–H31···O7	0.99	2.42	3.152(7)	130
	C3–H31···O9	0.99	2.59	3.534(11)	158
	C3–H31···O9A	0.99	2.37	3.298(9)	157
	C7–H7···O5A^{iii}	0.95	2.39	3.091(16)	131
	C10–H10···O2A	0.95	2.52	3.411(14)	156
	C14–H14···O8A^{iv}	0.95	2.32	3.097(12)	139
	C17–H17···N1	0.95	2.59	3.432(3)	147
	C24–H24···O12^{v}	0.95	2.44	3.174(13)	134
	C24–H24···O12A^{v}	0.95	2.18	2.94(4)	136
	C29–H29···O2A	0.95	2.57	3.290(13)	133

Symmetry codes: [i] 1+*x*, −1+*y*, *z*; [ii] 1+*x*, *y*, *z*; [iii] 1−*x*, −*y*, −*z*; [iv] *x*, −1+*y*, *z*; [v] 1−*x*, 1−*y*, 1−*z*; [vi] 1−*x*, 1−*y*, −*z*; [vii] −*x*, 1−*y*, 1−*z*; [viii] *x*, 1+*y*, *z*; [ix] ½+*x*, ½−*y*, ½+*z*; [x] ½+*x*, ½−*y*, −½+*z*; [xi] ½−*x*, ½+*y*, ½−*z*; [xii] *x*, −*y*, −½+*z*; [xiii] *x*, ½−*y*, −½+*z*; [xiv] −*x*, ½+*y*, ½−*z*; [xv] −1+*x*, *y*, *z*; [xvi] 1−*x*, ½+*y*, ½−*z*; [xvii] 1−*x*, −½+*y*, ½−*z*; [xviii] *x*, ³⁄₂−*y*, −½+*z*; [xix] 1−*x*, −*y*, 1−*z*; [xx] *x*, *y*, 1+*z*; [xxi] −*x*, −*y*, 1−*z*.

Table 7.20, continued.

5	D–H···A	*d*(D–H)/Å	*d*(H···A)/Å	*d*(D···A)/Å	∢(D–H···A)/°
	C40–H40···O12^{v}	0.95	2.46	3.235(13)	139
	C40–H40···O12A^{v}	0.95	2.35	3.17(4)	144
	C46–H46···O1^{vi}	0.95	2.56	3.229(4)	128
	C52–H52···O7A	0.95	2.43	3.293(9)	151
	C55–H551···O6A^{iv}	0.98	2.52	3.473(19)	164
	C55–H553···O6A^{vii}	0.98	2.53	3.40(2)	148
	C56–H561···O2^{viii}	0.98	2.59	3.505(7)	155
	C56–H562···O8	0.98	2.50	3.250(10)	133
	C58–H581···O3^{viii}	0.98	2.39	3.145(6)	134
	C61–H611···O10	0.98	2.60	3.491(14)	152
a'	C1–H11···O3	0.99	2.58	3.163(4)	117
	C2–H22···F6	0.99	2.49	3.185(3)	127
	C4–H41···F6^{ix}	0.99	2.42	3.316(4)	150
	C4–H41···F7^{ix}	0.99	2.41	3.266(4)	144
	C5–H5···F2^{v}	0.95	2.45	3.289(4)	147
	C16–H16···O3	0.95	2.54	3.480(4)	173
	C17–H17···N1	0.95	2.56	3.367(4)	144
	C19–H19···F8^{x}	0.95	2.46	3.126(4)	127
	C24–H24···F8	0.95	2.47	3.257(5)	140
	C29–H29···F1^{v}	0.95	2.48	3.178(4)	130
	C38–H38···F3^{vii}	0.95	2.50	3.321(5)	145
	C44–H44···O3^{ix}	0.95	2.46	3.322(4)	150
	C46–H46···F7^{ii}	0.95	2.36	3.286(4)	166
	C47–H47···F5^{ii}	0.95	2.52	3.191(4)	127
	C58–H583···F6	0.98	2.51	3.444(6)	160
b	C2–H2···N2	0.95	2.62	3.063(6)	109
	C8–H8···O2^{v}	0.95	2.47	3.349(17)	154
	C8–H8···O4A^{v}	0.95	2.40	3.19(2)	140
	C10–H10···O3A^{viii}	0.95	2.36	3.21(2)	149
	C11–H11···O5^{xi}	0.95	2.56	3.326(19)	137
	C15–H15···O3^{xii}	0.95	2.45	3.372(16)	163
	C18–H18···N2	0.95	2.59	3.022(6)	108
	C27–H271···O5^{xi}	0.98	2.54	3.406(17)	148
	C27–H271···O5A^{xi}	0.98	2.49	3.30(2)	140
	C27–H273···O2A	0.98	2.23	3.13(2)	151

Symmetry codes: [i] 1+*x*, −1+*y*, *z*; [ii] 1+*x*, *y*, *z*; [iii] 1−*x*, −*y*, −*z*; [iv] *x*, −1+*y*, *z*; [v] 1−*x*, 1−*y*, 1−*z*; [vi] 1−*x*, 1−*y*, −*z*; [vii] −*x*, 1−*y*, 1−*z*; [viii] *x*, 1+*y*, *z*; [ix] ½+*x*, ½−*y*, ½+*z*; [x] ½+*x*, ½−*y*, −½+*z*; [xi] ½−*x*, ½+*y*, ½−*z*; [xii] *x*, −*y*, −½+*z*; [xiii] *x*, ½−*y*, −½+*z*; [xiv] −*x*, ½+*y*, ½−*z*; [xv] −1+*x*, *y*, *z*; [xvi] 1−*x*, ½+*y*, ½−*z*; [xvii] 1−*x*, −½+*y*, ½−*z*; [xviii] *x*, ³⁄₂−*y*, −½+*z*; [xix] 1−*x*, −*y*, 1−*z*; [xx] *x*, *y*, 1+*z*; [xxi] −*x*, −*y*, 1−*z*.

Table 7.20, continued.

5	D–H···A	*d*(D–H)/Å	*d*(H···A)/Å	*d*(D···A)/Å	∢(D–H···A)/°
c	C1–H1···O11^{xiii}	0.95	2.35	3.247(14)	157
	C3–H3···O5^{xiii}	0.95	2.34	3.221(8)	153
	C4–H4···O19	0.95	2.28	3.223(8)	175
	C5–H5···O5^{vii}	0.95	2.54	3.373(8)	147
	C8–H8···O20^{v}	0.95	2.32	3.262(8)	175
	C17–H17···O20^{xiii}	0.95	2.43	3.364(9)	169
	C19–H19···O12	0.95	2.55	3.438(15)	155
	C20–H20···O14	0.95	2.51	3.136(11)	123
	C26–H26···O7	0.95	2.56	3.260(10)	130
	C46–H46···O19	0.95	2.54	3.487(10)	172
	C65–H65···O19^{xiv}	0.95	2.43	3.281(9)	148
	C67–H67···O4^{xiv}	0.95	2.51	3.399(12)	156
	C73–H73···O16^{xv}	0.95	2.50	3.254(18)	136
	C76–H76···O13^{v}	0.95	2.57	3.193(18)	123
	C94–H94···O20^{v}	0.95	2.44	3.371(8)	167
	C102–H102···O18^{vi}	0.95	2.58	3.284(14)	131
c'	C1–H1···O5^{v}	0.95	2.31	3.256(5)	177
	C2–H2···F11	0.95	2.46	3.058(5)	121
	C4–H4···F3	0.95	2.41	3.251(4)	147
	C5–H5···O6^{xv}	0.95	2.26	3.209(5)	177
	C6–H6···F3^{xiv}	0.95	2.29	3.120(4)	146
	C7–H7···O4^{xvi}	0.95	2.50	3.349(5)	149
	C8–H8···F9^{xvi}	0.95	2.24	3.153(5)	160
	C11–H11···F7	0.95	2.54	3.238(5)	130
	C14–H14···O5^{v}	0.95	2.38	3.308(5)	166
	C17–H17···F6^{vi}	0.95	2.49	3.230(6)	135
	C34–H34···F11	0.95	2.49	3.144(5)	126
	C44–H44···F5	0.95	2.54	3.353(5)	144
	C53–H53···O6^{xvii}	0.95	2.44	3.241(5)	142
	C55–H55···F4^{xiii}	0.95	2.33	3.231(5)	159
	C56–H56···F1^{xiii}	0.95	2.45	3.113(4)	127
	C62–H62···O6^{xv}	0.95	2.47	3.420(5)	174
	C66–H66···F15^{vii}	0.95	2.55	3.151(5)	121
	C92–H92···F16	0.95	2.36	3.123(5)	137
	C96–H96···F7	0.95	2.50	3.335(5)	147

Symmetry codes: [i] 1+*x*, −1+*y*, *z*; [ii] 1+*x*, *y*, *z*; [iii] 1−*x*, −*y*, −*z*; [iv] *x*, −1+*y*, *z*; [v] 1−*x*, 1−*y*, 1−*z*; [vi] 1−*x*, 1−*y*, −*z*; [vii] −*x*, 1−*y*, 1−*z*; [viii] *x*, 1+*y*, *z*; [ix] ½+*x*, ½−*y*, ½+*z*; [x] ½+*x*, ½−*y*, −½+*z*; [xi] ½−*x*, ½+*y*, ½−*z*; [xii] *x*, −*y*, −½+*z*; [xiii] *x*, ½−*y*, −½+*z*; [xiv] −*x*, ½+*y*, ½−*z*; [xv] −1+*x*, *y*, *z*; [xvi] 1−*x*, ½+*y*, ½−*z*; [xvii] 1−*x*, −½+*y*, ½−*z*; [xviii] *x*, ³⁄₂−*y*, −½+*z*; [xix] 1−*x*, −*y*, 1−*z*; [xx] *x*, *y*, 1+*z*; [xxi] −*x*, −*y*, 1−*z*.

Table 7.20, continued.

5	D–H···A	*d*(D–H)/Å	*d*(H···A)/Å	*d*(D···A)/Å	∢(D–H···A)/°
	C101–H101···O5^{xviii}	0.95	2.36	3.303(5)	172
	C103–H103···F12^{v}	0.95	2.39	3.282(5)	157
	C104–H104···F10^{v}	0.95	2.45	3.095(5)	125
	C113–H133···F13^{vii}	0.98	2.48	3.440(7)	166
	C114–H143···F10^{v}	0.98	2.49	3.379(6)	151
	C115–H152···F6	0.98	2.26	3.164(8)	154
	C116–H162···F1^{xvi}	0.98	2.44	3.209(6)	135
d	C10–H10···O8^{xix}	0.95	2.56	3.343(8)	139
	C11–H11···O10^{xx}	0.95	2.47	3.369(6)	158
	C12–H12···O9^{xx}	0.95	2.60	3.268(6)	128
	C22–H22···O14^{vi}	0.95	2.53	3.407(6)	154
	C30–H30···O1	0.95	2.57	3.013(6)	109
	C54–H54···O3	0.95	2.54	3.203(5)	127
	C62–H62···O6^{xxi}	0.95	2.49	3.263(8)	139
	C65–H65···O7^{xxi}	0.95	2.57	3.418(6)	149
	C72–H72···N1	0.95	2.44	3.116(5)	128
	C72–H72···O3	0.95	2.51	3.350(6)	147
	C74–H74···O15	0.95	2.45	3.291(7)	148
	C108–H108···O15	0.95	2.52	3.235(6)	132
	C120–H120···N2	0.95	2.57	3.152(6)	120
	C120–H120···O2	0.95	2.55	3.323(7)	139

Symmetry codes: ^{i} 1+*x*, −1+*y*, *z*; ^{ii} 1+*x*, *y*, *z*; ^{iii} 1−*x*, −*y*, −*z*; ^{iv} *x*, −1+*y*, *z*; ^{v} 1−*x*, 1−*y*, 1−*z*; ^{vi} 1−*x*, 1−*y*, −*z*; ^{vii} −*x*, 1−*y*, 1−*z*; ^{viii} *x*, 1+*y*, *z*; ^{ix} ½+*x*, ½−*y*, ½+*z*; ^{x} ½+*x*, ½−*y*, −½+*z*; ^{xi} ½−*x*, ½+*y*, ½−*z*; ^{xii} *x*, −*y*, −½+*z*; ^{xiii} *x*, ½−*y*, −½+*z*; ^{xiv} −*x*, ½+*y*, ½−*z*; ^{xv} −1+*x*, *y*, *z*; ^{xvi} 1−*x*, ½+*y*, ½−*z*; ^{xvii} 1−*x*, −½+*y*, ½−*z*; ^{xviii} *x*, ³⁄₂−*y*, −½+*z*; ^{xix} 1−*x*, −*y*, 1−*z*; ^{xx} *x*, *y*, 1+*z*; ^{xxi} −*x*, −*y*, 1−*z*.

Table 7.21: Distances and angles of non-classical hydrogen bonds in crystalline compounds of class **6**. The standard deviation of the last decimal digit is given in parentheses. Values without a standard deviation refer to hydrogen atoms calculated on idealized positions, riding on their parent atoms.

6	D–H···A	*d*(D–H)/Å	*d*(H···A)/Å	*d*(D···A)/Å	∢(D–H···A)/°
a	C1–H11···Cl2^{i}	0.99	2.77	3.633(2)	146
	C2–H21···N1^{i}	0.99	2.54	3.276(2)	131
	C2–H22···O2^{ii}	0.99	2.44	3.310(2)	146
	C3–H3···Cl1	0.95	2.68	3.369(2)	130
	C16–H16···Cl2^{iii}	0.95	2.77	3.630(2)	150
a'	C3–H31···Br2^{iv}	0.99	2.88	3.707(2)	142

Symmetry codes: ^{i} ³⁄₂−*x*, ½+*y*, ½−*z*; ^{ii} *x*, 1+*y*, *z*; ^{iii} 1−*x*, 1−*y*, 1−*z*; ^{iv} 1−*x*, ½+*y*, ½−*z*; ^{v} 1+*x*, *y*, *z*; ^{vi} −*x*, ½+*y*, ½−*z*; ^{vii} ³⁄₂−*x*, 1−*y*, ½+*z*; ^{viii} ½−*x*, ½+*y*, *z*; ^{ix} *x*, *y*, −1+*z*.

Table 7.21, continued.

6	D–H···A	*d*(D–H)/Å	*d*(H···A)/Å	*d*(D···A)/Å	∢(D–H···A)/°
	C6–H6···Br4^{v}	0.95	2.87	3.795(2)	164
	C16–H16···Br1	0.95	2.79	3.560(2)	138
	C17–H17···Br2	0.95	2.92	3.490(2)	120
	C40–H40···Br3	0.95	2.74	3.576(11)	147
	C51–H51···Br3^{vi}	0.95	2.93	3.785(3)	151
b	C3–H31···O1	0.99	2.57	3.263(4)	127
	C5–H51···Cl1^{vii}	0.99	2.69	3.478(3)	137
	C6–H61···O2	0.99	2.59	3.242(4)	124
	C7–H7···Cl1	0.95	2.63	3.423(3)	141
	C13–H13···Cl3	0.95	2.64	3.457(3)	145
	C19–H19···Cl2	0.95	2.82	3.482(4)	128
	C33–H33···Cl3	0.95	2.69	3.481(3)	141
	C45–H45···Cl4	0.95	2.76	3.541(3)	140
c	C2–H2···Cl2^{v}	0.95	2.62	3.359(2)	135
c'	C10–H10···N1	0.95	2.58	3.168(3)	120
	C27–H27···Br2^{viii}	1.00	2.89	3.747(2)	145
d	C5–H5···Cl1^{ix}	0.95	2.69	3.436(4)	136
	C8–H8···Cl1	0.95	2.69	3.488(5)	141
	C14–H14···O1	0.95	2.57	3.415(5)	148
	C20–H20···Cl2	0.95	2.82	3.576(5)	138
	C30–H30···O1	0.95	2.58	3.335(5)	137
d'	C5–H5···Br1^{ix}	0.95	2.79	3.569(6)	140
	C8–H8···Br1	0.95	2.79	3.597(7)	143
	C14–H14···O1	0.95	2.56	3.407(8)	149
	C30–H30···O1	0.95	2.60	3.341(7)	135

Symmetry codes: ^{i} ¾−*x*, ½+*y*, ½−*z*; ^{ii} *x*, 1+*y*, *z*; ^{iii} 1−*x*, 1−*y*, 1−*z*; ^{iv} 1−*x*, ½+*y*, ½−*z*; ^{v} 1+*x*, *y*, *z*; ^{vi} −*x*, ½+*y*, ½−*z*; ^{vii} ¾−*x*, 1−*y*, ½+*z*; ^{viii} ½−*x*, ½+*y*, *z*; ^{ix} *x*, *y*, −1+*z*.

Table 7.22: Distances and angles of non-classical hydrogen bonds in crystalline compounds of class **7**. The standard deviation of the last decimal digit is given in parentheses. Values without a standard deviation refer to hydrogen atoms calculated on idealized positions, riding on their parent atoms.

7	D–H···A	*d*(D–H)/Å	*d*(H···A)/Å	*d*(D···A)/Å	∢(D–H···A)/°
a	C5–H5···N1A	0.95	2.26	2.792(17)	114
	C5–H5···O1A^{i}	0.95	2.42	2.93(5)	114
	C5–H5···O3^{i}	0.95	2.56	3.088(11)	115

Symmetry codes: ^{i} 1−*x*, −*y*, 1−*z*; ^{ii} 1−*x*, 1−*y*, 1−*z*; ^{iii} 1−*x*, 1−*y*, −*z*; ^{iv} *x*, −1+*y*, *z*; ^{v} 1+*x*, −1+*y*, *z*; ^{vi} 1+*x*, *y*, *z*; ^{vii} −1+*x*, ½−*y*, −½+*z*.

Table 7.22, continued.

7	D–H···A	*d*(D–H)/Å	*d*(H···A)/Å	*d*(D···A)/Å	∢(D–H···A)/°
	C7–H7···O1^{ii}	0.95	2.46	3.293(12)	147
	C7–H7···O2A^{ii}	0.95	2.51	3.30(5)	141
	C13–H13···O4^{iii}	0.95	2.54	3.212(3)	128
	C14–H14···O5^{iii}	0.95	2.57	3.458(3)	156
	C15–H15···N1	0.95	2.38	2.891(5)	113
	C19–H19···O5^{iv}	0.95	2.51	3.397(3)	156
	C20–H20···O7^{v}	0.95	2.59	3.339(3)	136
	C23–H23···O1A^{vi}	0.95	2.40	3.16(4)	137
	C23–H23···O3^{vi}	0.95	2.60	3.330(11)	134
	C24–H24···O2^{vi}	0.95	2.52	3.390(3)	152
b	C7–H71···F4	0.99	2.47	3.163(3)	127
c	C3–H31···O4^{vii}	0.99	2.42	3.289(6)	146

Symmetry codes: ^{i} 1−*x*, −*y*, 1−*z*; ^{ii} 1−*x*, 1−*y*, 1−*z*; ^{iii} 1−*x*, 1−*y*, −*z*; ^{iv} *x*, −1+*y*, *z*; ^{v} 1+*x*, −1+*y*, *z*; ^{vi} 1+*x*, *y*, *z*; ^{vii} −1+*x*, ½−*y*, −½+*z*.

7.4 CShM values of the complex species

Table 7.23: Calculated CShM values [110,111] of the complex species in the crystalline compounds. Pentacoordinated species (**1–6**) are compared to an ideal, undistorted trigonal bipyramid (*TBPY*-5) and square pyramid (*SPY*-5), four- and sixfold coordinated species (**7**) to an ideal tetrahedron (*T*-4) and vacant trigonal bipyramid (*vTBPY*-4) or ideal octahedron (*OC*-6) and trigonal prism (*TPR*-6), respectively. Values marked with a dagger (†) either refer to the second entity in the asymmetric unit or, in case of class **4** and **7a**, to the minor disorder form of the nitrosyl complex. For a plot of the nitrosyl species **1–6**, see Figure 7.46. Calculation for **4d** based on structural data from Ref. [94].

	S(*TBPY*-5)	*S*(*SPY*-5)
1 a	3.407	1.283
b	3.971	1.043
c	3.695	1.071
d	4.578	0.754
e	4.175	0.981
f	5.969	0.845
g	3.645	1.247
h	4.395	0.949
i	5.368	0.618
i†	5.209	0.661
j	5.621	0.833
k	2.574	1.472
l	5.124	0.720
m	5.412	1.005
n	3.845	1.428
2 a	6.305	0.784
a†	6.001	0.824
b	4.367	1.091
3 a	5.103	1.472
b	5.540	1.722
c	6.138	2.228
d	5.297	1.748
d†	5.257	1.854

	S(*TBPY*-5)	*S*(*SPY*-5)
4 a	6.699	1.467
a†	6.734	1.539
b	7.264	1.783
c	7.220	1.635
c†	7.390	1.828
d	7.133	1.520
e	6.616	1.388
e†	6.725	1.460
f	7.289	1.686
f†	7.252	1.659
g	6.629	1.308
h	6.817	1.586
i	7.124	1.529
l	6.434	1.546
l†	6.446	1.543
5 a	1.106	5.664
a'	1.107	5.310
b	2.588	7.591
c	0.979	4.898
c†	0.920	5.350
c'	0.914	5.383
c'†	1.000	4.975
d	1.644	4.101
d†	1.223	4.799

	S(*TBPY*-5)	*S*(*SPY*-5)
6 a	6.330	1.381
a'	2.811	3.295
a'†	7.168	1.693
b	5.029	1.392
b†	5.762	1.181
c	6.157	1.291
c'	5.732	1.714
d	6.389	1.368
d'	6.991	1.798

	S(*OC*-6)	*S*(*TPR*-6)
7 a	0.656	13.085
a†	0.940	12.392
c	0.392	14.059

	S(*T*-4)	*S*(*vTBPY*-4)
b	1.907	4.118

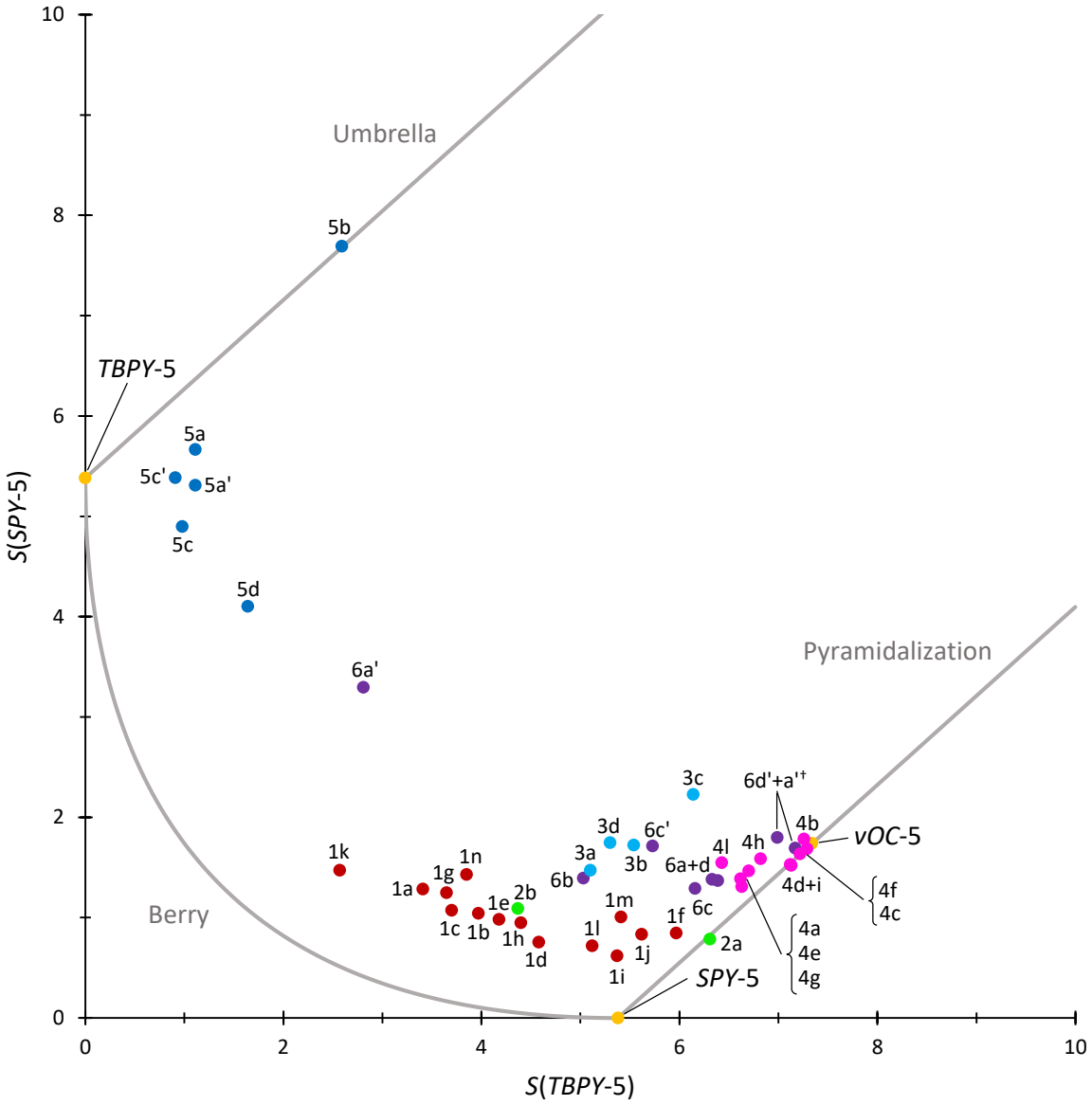

Figure 7.46: CShM map of nitrosyl complexes **1–6** (colored data points) for fivefold-coordinated species, based on the X-ray structural data of the crystalline products. Ideal, undistorted polyhedra (yellow data points): trigonal bipyramid (*TBPY*-5) at (0, 5.382), square pyramid (*SPY*-5) at (5.382, 0) and vacant octahedron (*vOC*-5) at (7.344, 1.740). The solid gray lines mark the Berry path (pseudorotation), the umbrella distortion [112, 113] (''folding'' of the equatorial plane in *TBPY*-5 along the unique axis) and the pyramidalization path (movement of the central metal in *SPY*-5 from the pyramid's center to its basal plane), respectively. For clarity, only the first entity in the asym-metric unit is plotted, with the exception of compound **6a'**. For class **4** species, only the values for the major disorder forms are plotted. Calculation for **4d** based on structural data from Ref. [94]. For a list of all values, see Table 7.23.

7.5 Further plots of the crystal structures

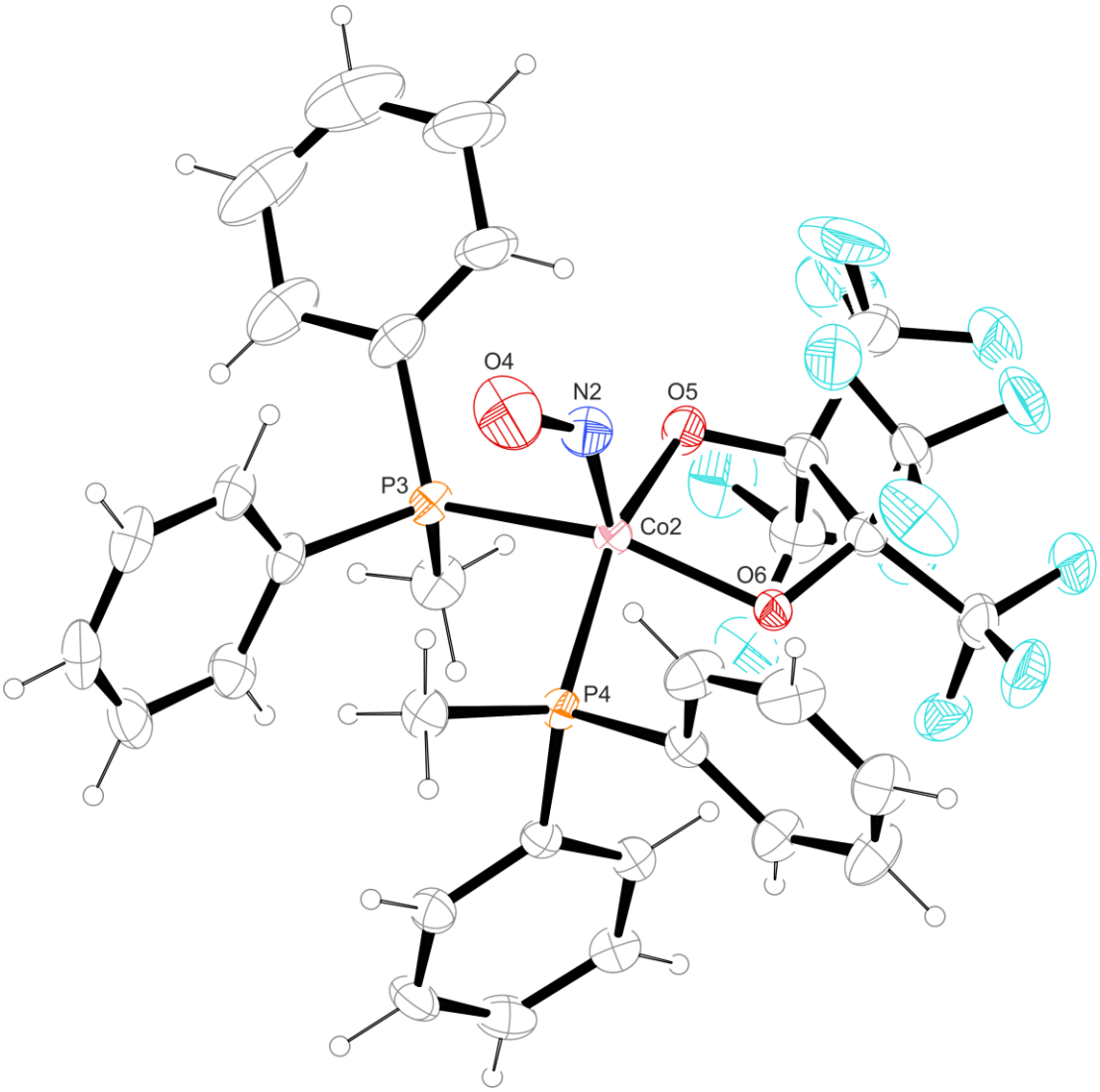

Figure 7.47: ORTEP plot of the second entity in the asymmetric unit of [Co(fpin)(NO)($PMePh_2$)$_2$] in crystals of **3d**. For clarity, only one entity is depicted. For the other one, see Figure 2.22. Thermal ellipsoids drawn at 50 % probability level at 173 K. Interatomic distances (Å) and bond angles (°) with the standard deviation of the last decimal digit given in parentheses: Co2–N2 1.765(3), Co2–P3 2.218(1), Co2–P4 2.231(1), Co2–O5 1.914(2), Co2–O6 1.887(2), N2–O4 1.129(4), Co2–N2–O4 136.2(2), P3–Co2–O6 149.37(8), P4–Co2–O5 159.73(8), P3–Co2–P4 97.91(4), O5–Co2–O6 83.5(1), P3–Co2–O5 86.35(8), P4–Co2–O6 82.93(8), N2–Co2–P3 96.35(9), N2–Co2–P4 96.0(1), N2–Co2–O5 103.3(1), N2–Co2–O6 114.1(1).

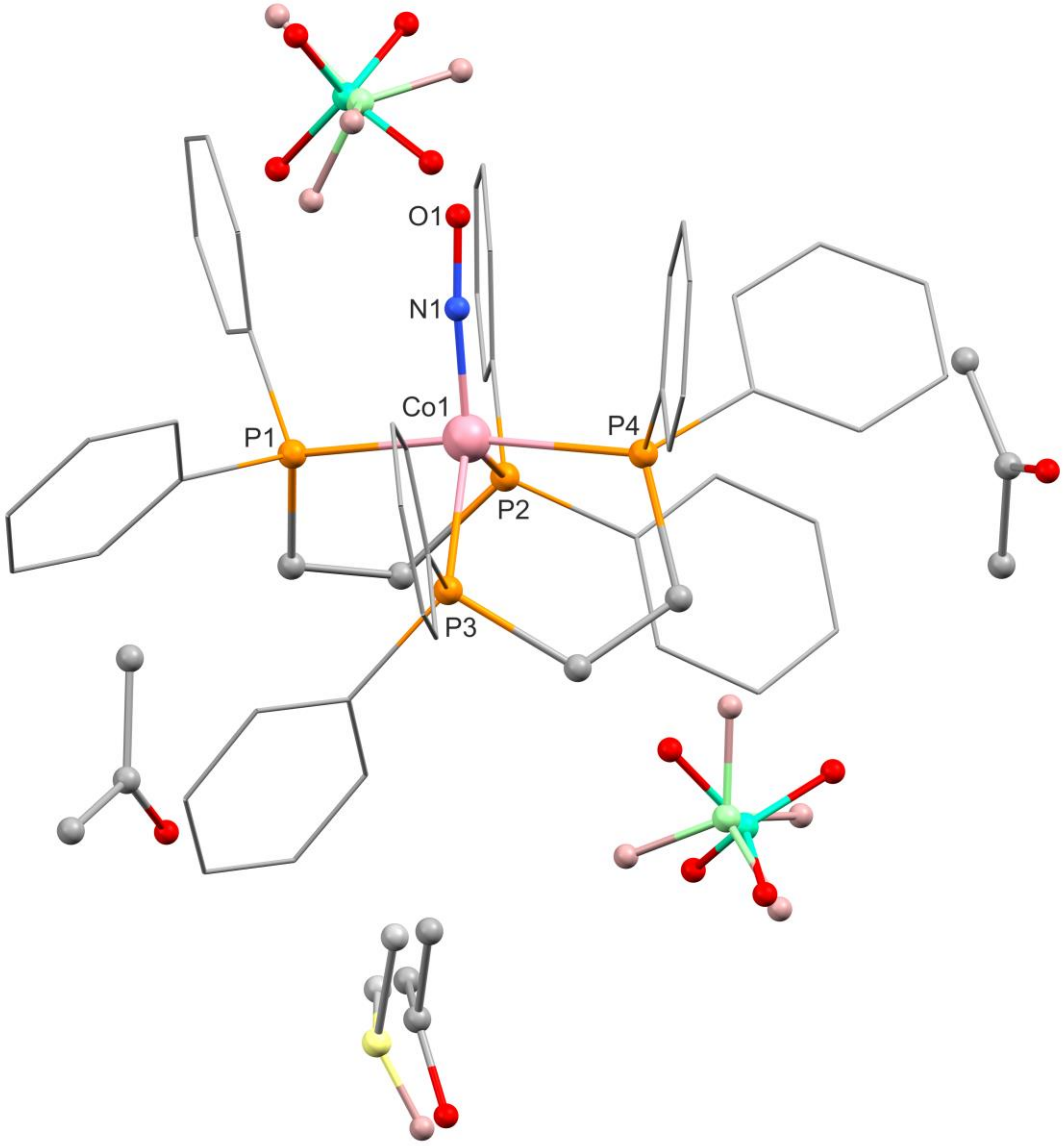

Figure 7.48: Plot of $[Co(dppe)_2(NO)](ClO_4)_2 \cdot 2.7Me_2CO \cdot 0.3DMSO$ in crystals of **5a**$\cdot 2.7Me_2CO \cdot 0.3DMSO$. For clarity, hydrogen atoms are not depicted. Furthermore, the phenyl groups are shown as wireframe. The minor disorder forms of the perchlorate ions (33 % and 43 %) as well as the co-crystallized DMSO molecule (29 %) are depicted in light colors. For a list of the interatomic distances and bond angles in the cationic complex entity, see Figure 2.48.

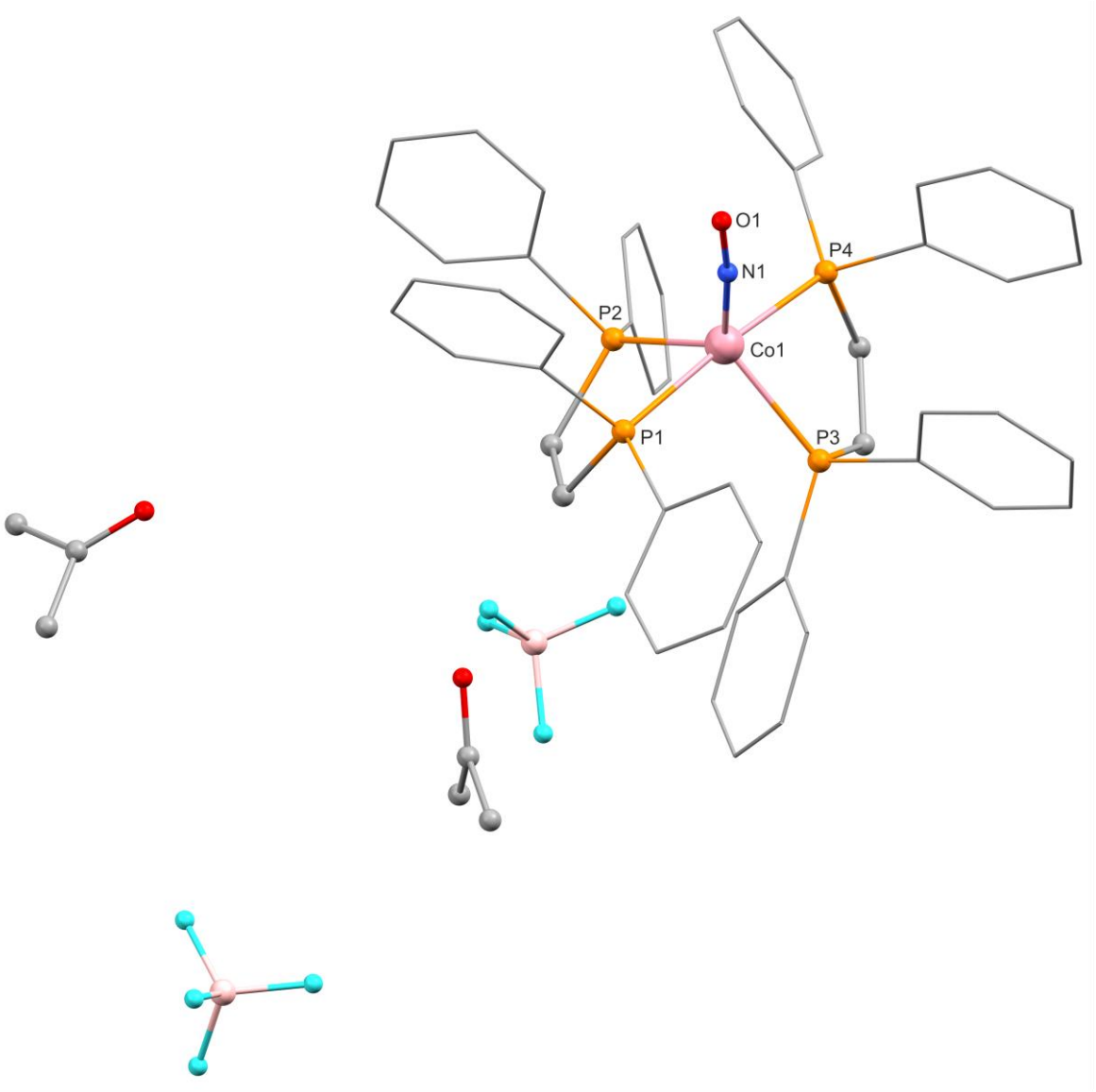

Figure 7.49: Plot of $[Co(dppe)_2(NO)](BF_4)_2 \cdot 2Me_2CO$ in crystals of **5a'**$\cdot 2Me_2CO$. For clarity, hydrogen atoms are not depicted. Furthermore, the phenyl groups are shown as wireframe. For a list of the interatomic distances and bond angles in the cationic complex entity, see Figure 2.49.

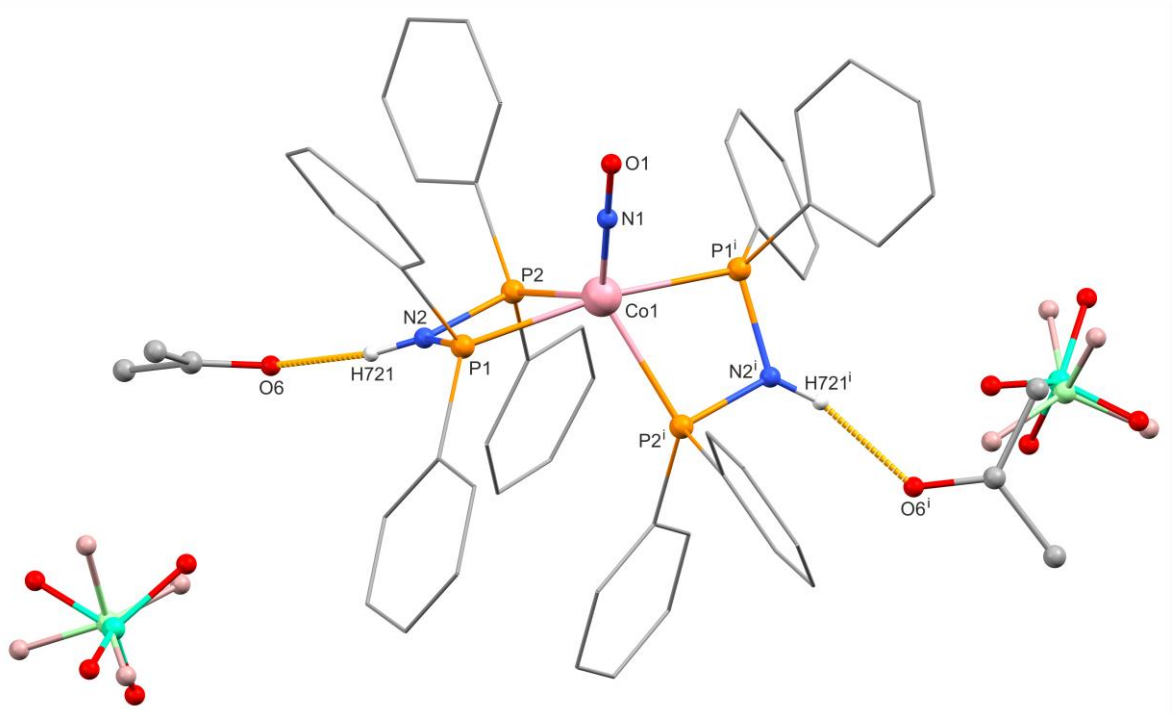

Figure 7.50: Plot of $[Co(dppa)_2(NO)](ClO_4)_2 \cdot 2Me_2CO$ in crystals of **5b**$\cdot 2Me_2CO$. For clarity, carbon-bound hydrogen atoms are not depicted. Furthermore, the phenyl groups are shown as wireframe. The minor disorder form of the perchlorate ion (39 %) is depicted in light colors. Symmetry code: ^{i} 1−*x*, *y*, ½−*z*. For a list of the interatomic distances and bond angles in the cationic complex entity, see Figure 2.50. Details on the classical hydrogen bond (dashed yellow lines) are listed in Table 2.19.

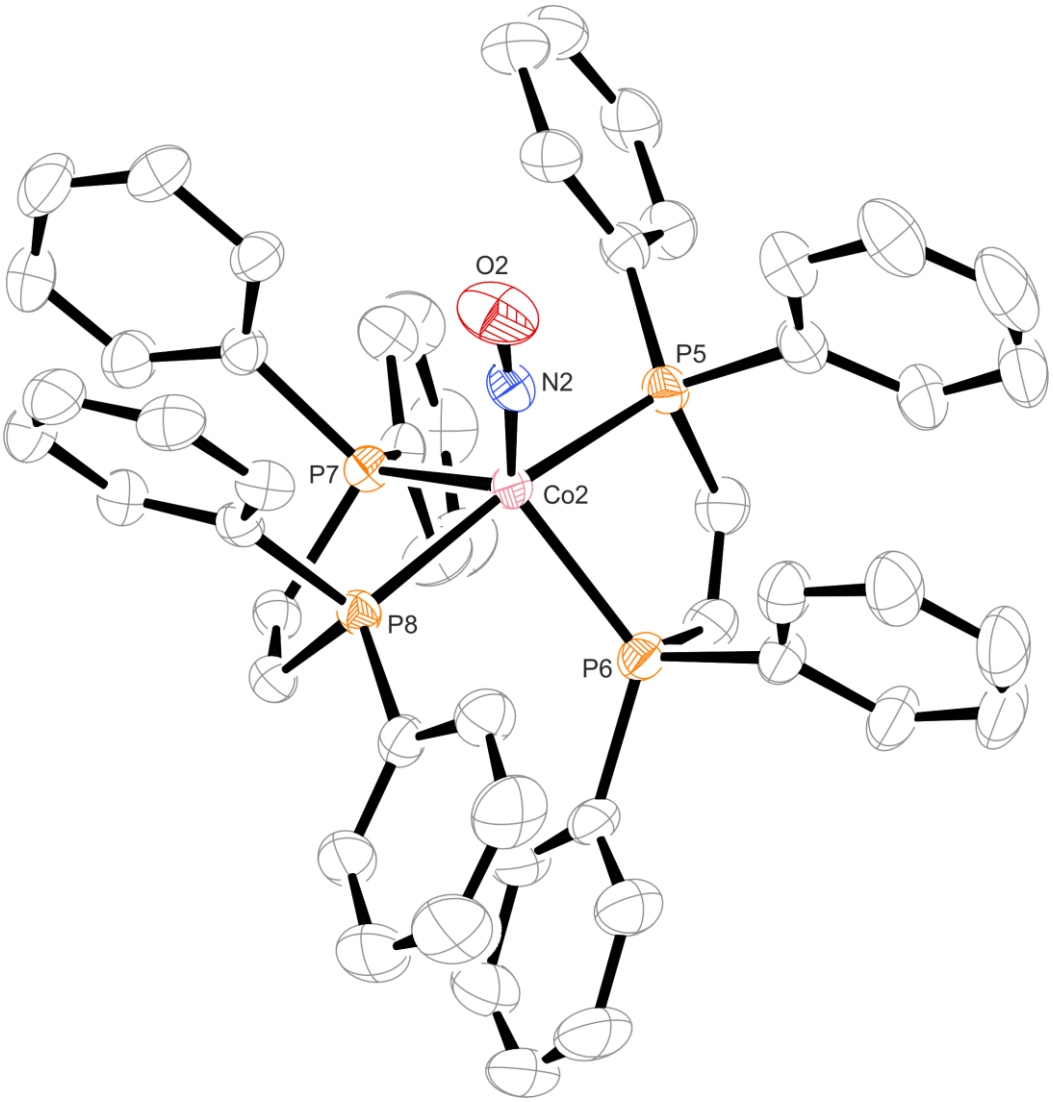

Figure 7.51: ORTEP plot of the second entity in the asymm. unit of $[Co(dppv)_2(NO)](ClO_4)_2 \cdot 1.5 Me_2CO$ in crystals of **5c**$\cdot 1.5 Me_2CO$. For clarity, only one cationic complex entity is depicted. For the other one, see Figure 2.51. Furthermore, hydrogen atoms as well as all counterions and co-crystallized solvent molecules are omitted. Thermal ellipsoids drawn at 50 % probability level at 173 K. Interatomic distances (Å) and bond angles (°) with the standard deviation of the last decimal digit given in parentheses: Co2–N2 1.666(4), Co2–P5 2.278(1), Co2–P6 2.296(1), Co2–P7 2.282(1), Co2–P8 2.269(1), N2–O2 1.149(6), Co2–N2–O2 172.8(4), P5–Co2–P8 168.82(5), P6–Co2–P7 110.05(5), P5–Co2–P6 80.39(5), P7–Co2–P8 82.18(5), P5–Co2–P7 92.63(5), P6–Co2–P8 92.05(5), N2–Co2–P5 97.1(1), N2–Co2–P6 129.1(1), N2–Co2–P7 120.9(1), N2–Co2–P8 94.1(1). A plot of the complete asymmetric unit is given in Figure 7.52.

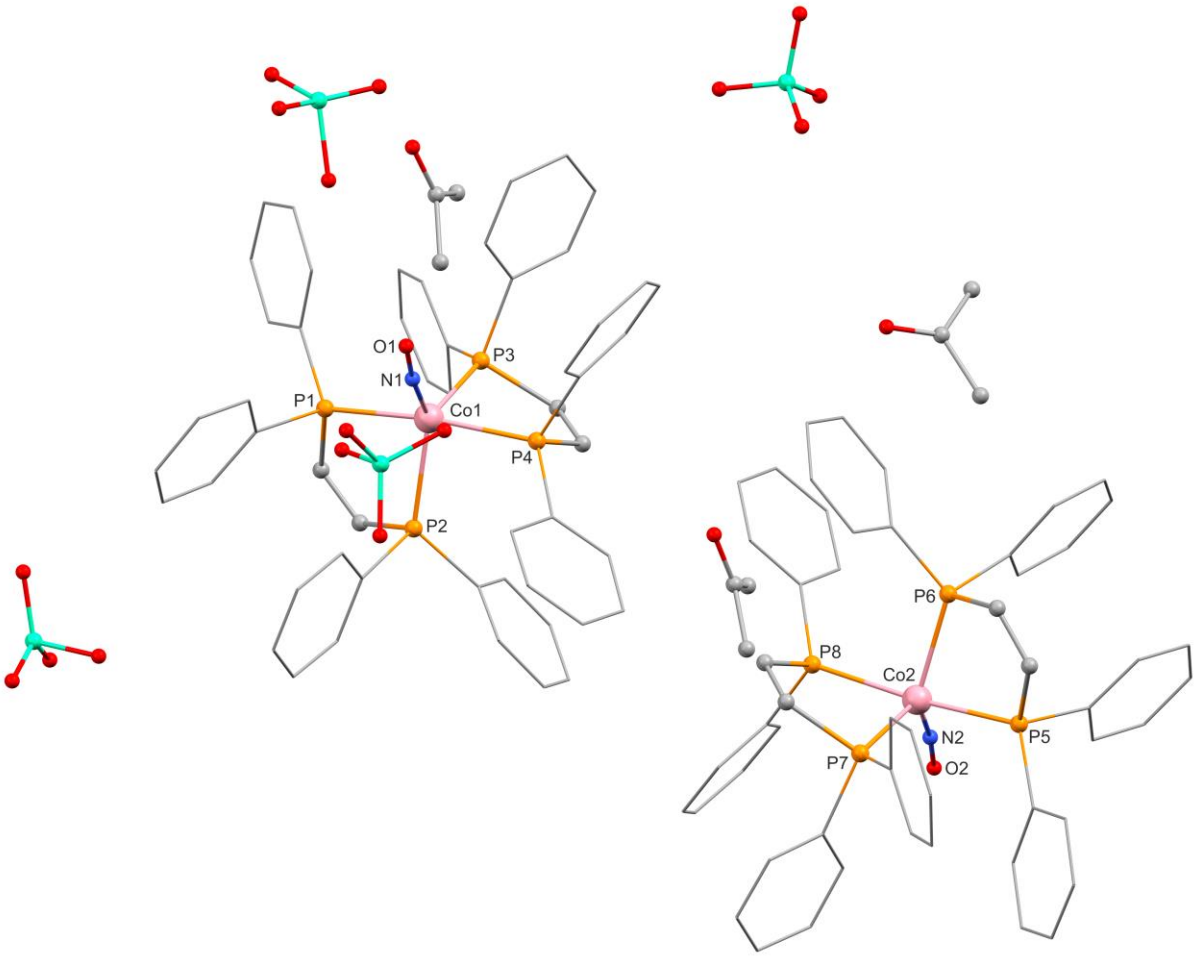

Figure 7.52: Plot of $[Co(dppv)_2(NO)](ClO_4)_2 \cdot 1.5Me_2CO$ in crystals of **5c**$\cdot 1.5Me_2CO$. For clarity, hydrogen atoms are not depicted. Furthermore, the phenyl groups are shown as wireframe. For a list of the interatomic distances and bond angles in the cationic complex entities, see Figure 2.51.

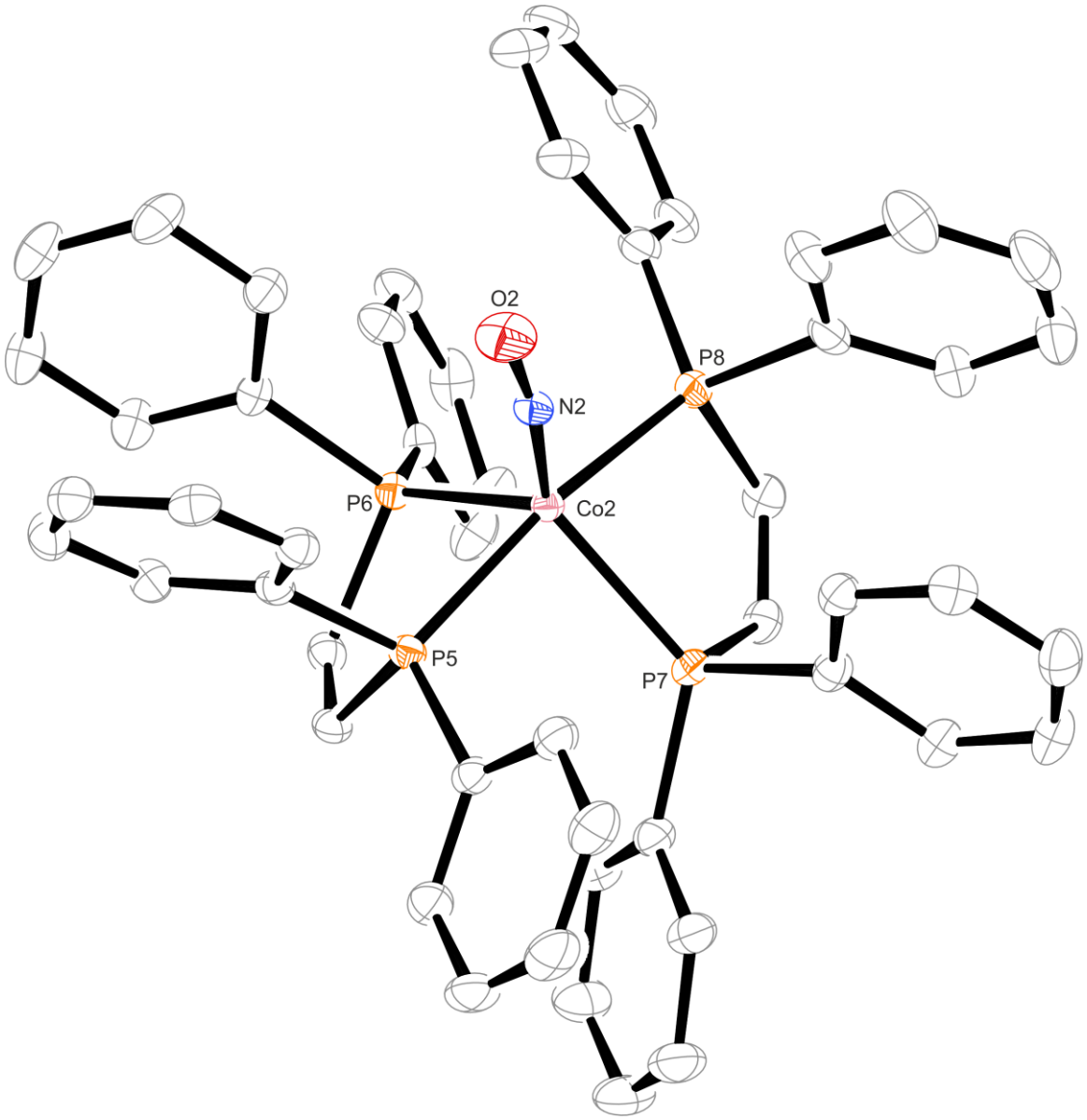

Figure 7.53: ORTEP plot of the second entity of $[Co(dppv)_2(NO)](BF_4)_2 \cdot 1.8Me_2CO \cdot 0.2DMSO$ in the asymmetric unit in crystals of **5c'**$\cdot 1.8Me_2CO \cdot 0.2DMSO$. For clarity, only one cationic complex entity is depicted. For the other one, see Figure 2.52. Furthermore, hydrogen atoms as well as all counterions and co-crystallized solvent molecules are omitted. Thermal ellipsoids drawn at 50 % probability level at 100 K. Interatomic distances (Å) and bond angles (°) with the standard deviation of the last decimal digit given in parentheses: Co2–N2 1.661(2), Co2–P5 2.257(1), Co2–P6 2.274(1), Co2–P7 2.303(1), Co2–P8 2.266(1), N2–O2 1.162(3), Co2–N2–O2 170.0(3), P5–Co2–P8 167.56(4), P6–Co2–P7 110.41(4), P5–Co2–P6 81.44(4), P7–Co2–P8 81.01(3), P5–Co2–P7 89.87(4), P6–Co2–P8 93.77(4), N2–Co2–P5 93.8(1), N2–Co2–P6 117.8(1), N2–Co2–P7 131.7(1), N2–Co2–P8 98.6(1). A plot of the complete asymmetric unit is given in Figure 7.54.

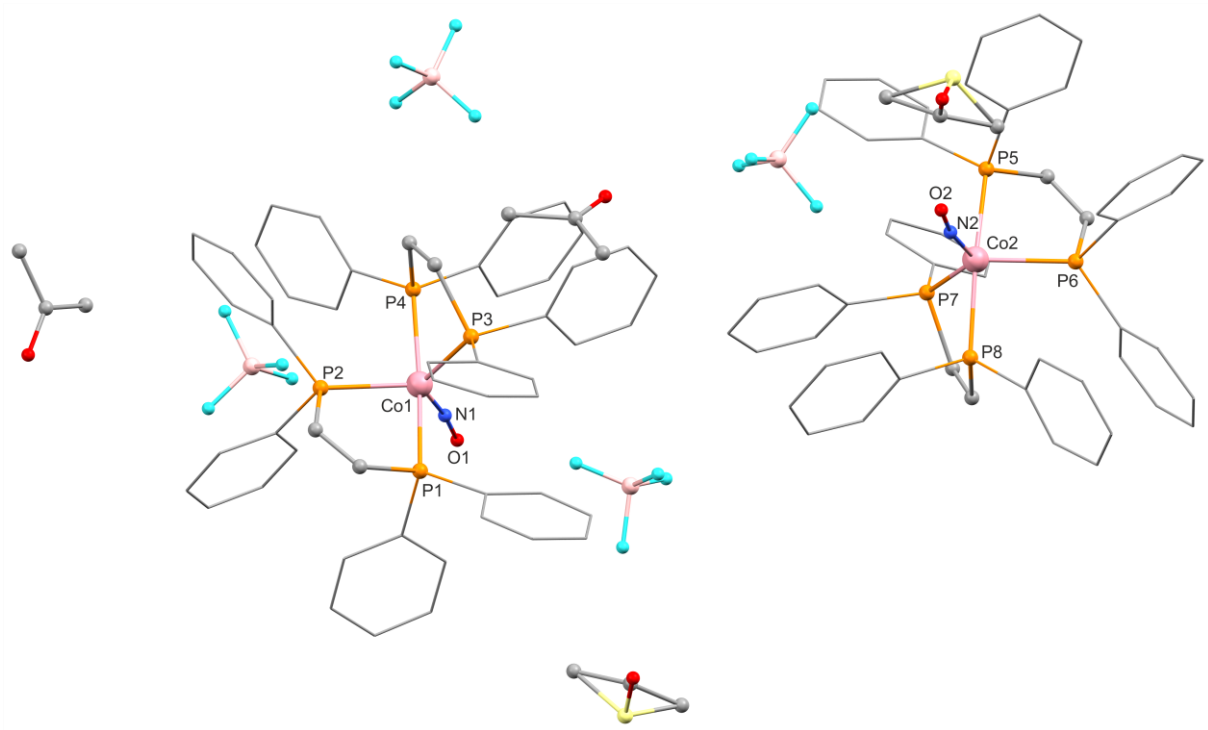

Figure 7.54: Plot of $[Co(dppv)_2(NO)](BF_4)_2 \cdot 1.8Me_2CO \cdot 0.2DMSO$ in crystals of **5c'**$\cdot 1.8Me_2CO \cdot 0.2DMSO$. For clarity, hydrogen atoms are not depicted. Furthermore, the phenyl groups are shown as wireframe. The sulfur atoms of the co-crystallized DMSO molecules (disordered with acetone by 9 % and 25 %, respectively) are depicted in light yellow. For a list of the interatomic distances and bond angles in the cationic complex entities, see Figure 2.52.

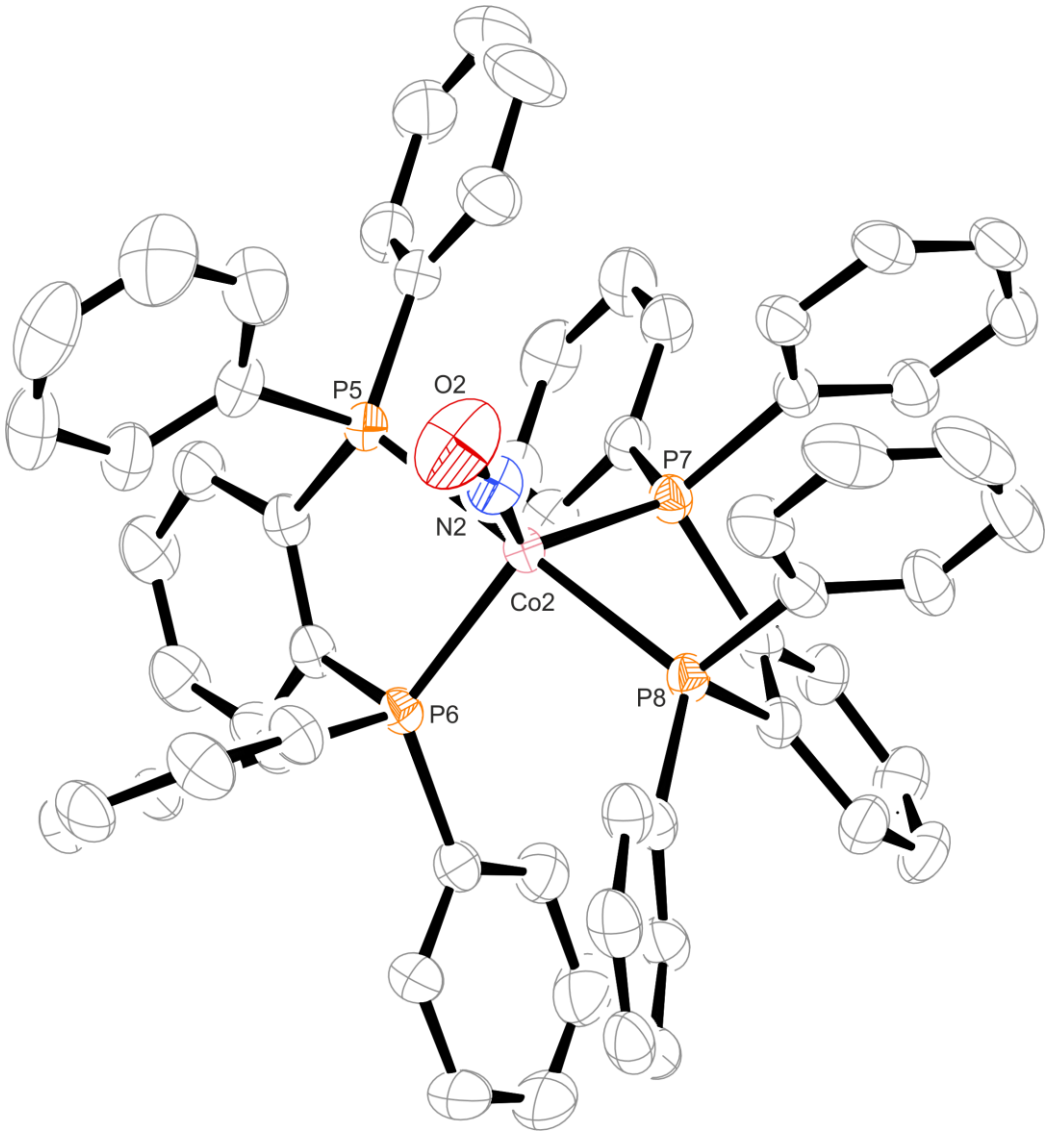

Figure 7.55: ORTEP plot of the second entity in the asymmetric unit of $[Co(dppbz)_2(NO)](ClO_4)_2 \cdot Me_2CO$ in crystals of **5d**·Me_2CO. For clarity, only one cationic complex entity is depicted. For the other one, see Figure 2.53. Furthermore, hydrogen atoms as well as all counterions and co-crystallized solvent molecules are omitted. Thermal ellipsoids drawn at 50 % probability level at 173 K. Interatomic distances (Å) and bond angles (°) with the standard deviation of the last decimal digit given in parentheses: Co2–N2 1.667(2), Co2–P5 2.295(1), Co2–P6 2.258(1), Co2–P7 2.286(1), Co2–P8 2.297(1), N2–O2 1.146(3), Co2–N2–O2 170.6(3), P5–Co2–P8 174.33(4), P6–Co2–P7 108.98(4), P5–Co2–P6 82.88(4), P7–Co2–P8 81.15(4), P5–Co2–P7 94.41(4), P6–Co2–P8 95.18(4), N2–Co2–P5 89.6(1), N2–Co2–P6 119.8(1), N2–Co2–P7 131.1(1), N2–Co2–P8 96.0(1). A plot of the complete asymmetric unit is given in Figure 7.56.

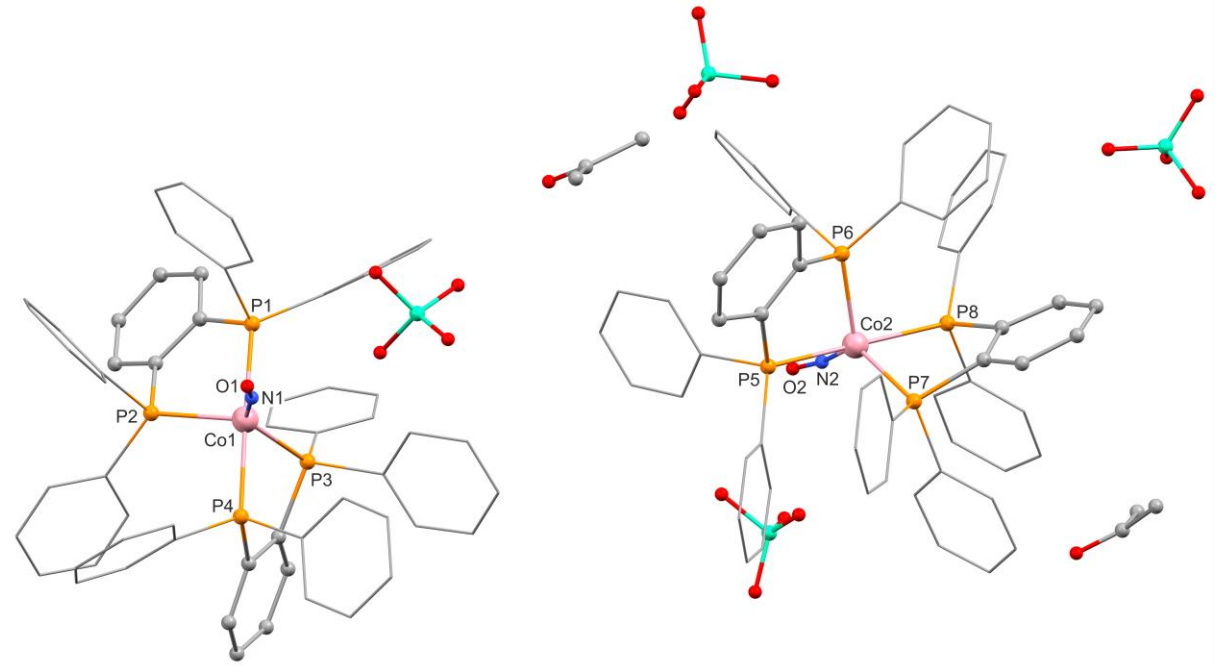

Figure 7.56: Plot of $[Co(dppbz)_2(NO)](ClO_4)_2 \cdot Me_2CO$ in crystals of **5d**$\cdot Me_2CO$. For clarity, hydrogen atoms are not depicted. Furthermore, the terminal phenyl groups are shown as wireframe. For a list of interatomic distances and bond angles in the cationic complex entities, see Figure 2.53.

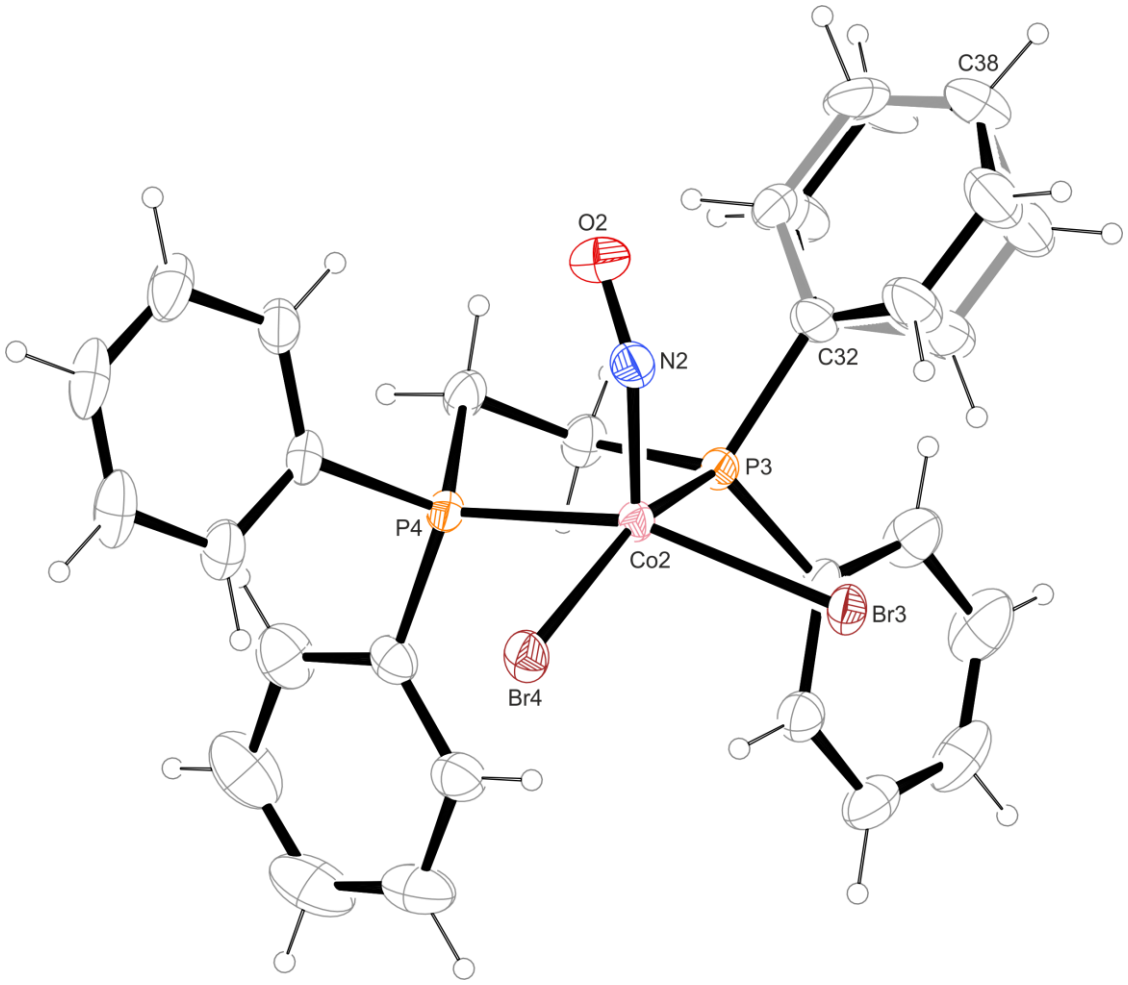

Figure 7.57: ORTEP plot of the second entity in the asymm. unit of [$CoBr_2$(dppe)(NO)] in crystals of **6a'**. For clarity, only one entity is depicted. For the other one, see Figure 2.56. The C–C bonds of the minor disorder form of one of the phenyl groups (45 %, pivoted around the common axis C32···C38) are depicted in gray. Thermal ellipsoids drawn at 50 % probability level at 173 K. Interatomic distances (Å) and bond angles (°) with the standard deviation of the last decimal digit given in parentheses: Co2–N2 1.742(1), Co2–P3 2.2240(6), Co2–P4 2.2016(6), Co2–Br3 2.4213(6), Co2–Br4 2.4058(6), N2–O2 1.166(2), Co2–N2–O2 139.6(2), P3–Co2–Br4 156.33(2), P4– Co2–Br3 157.59(2), P3–Co2–P4 85.61(2), Br3–Co2–Br4 92.07(2), P3–Co2–Br3 88.15(2), P4–Co2–Br4 85.23(2), N2–Co2–P3 97.57(6), N2–Co2–P4 96.60(6), N2–Co2–Br3 105.57(6), N2–Co2–Br4 105.14(6).

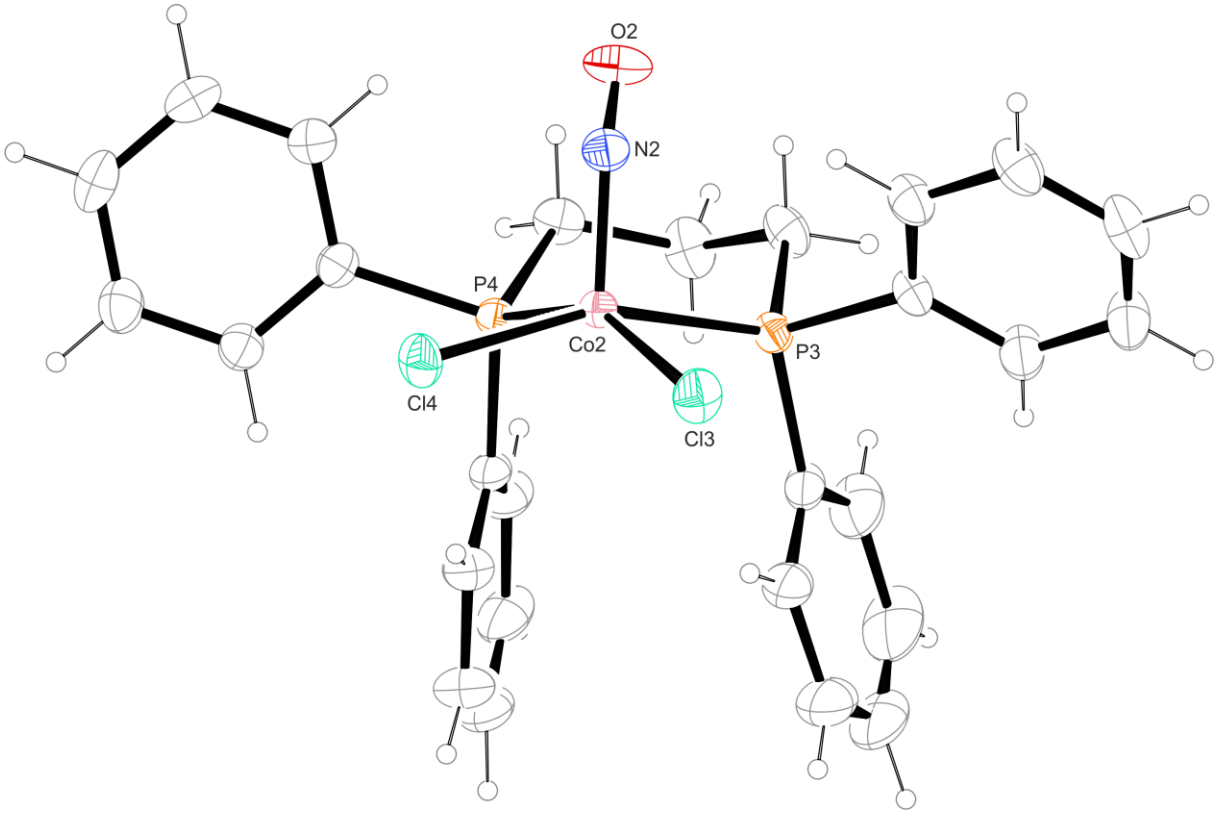

Figure 7.58: ORTEP plot of the second entity in the asymm. unit of [$CoCl_2$(dppp)(NO)] in crystals of **6b**. For clarity, only one entity is depicted. For the other one, see Figure 2.57. Thermal ellipsoids drawn at 50 % probability level at 173 K. Interatomic distances (Å) and bond angles (°) with the standard deviation of the last decimal digit given in parentheses: Co2–N2 1.744(3), Co2–P3 2.2356(8), Co2–P4 2.2105(8), Co2–Cl3 2.2635(8), Co2–Cl4 2.2516(8), N2–O2 1.165(4), Co2–N2–O2 138.1(2), P3–Co2–Cl4 158.41(3), P4– Co2–Cl3 152.74(3), P3–Co2–P4 89.43(3), Cl3–Co2–Cl4 88.29(4), P3–Co2–Cl3 86.47(3), P4–Co2–Cl4 85.69(3), N2–Co2–P3 97.07(9), N2–Co2–P4 98.08(9), N2–Co2–Cl3 109.17(9), N2–Co2–Cl4 104.44(9).

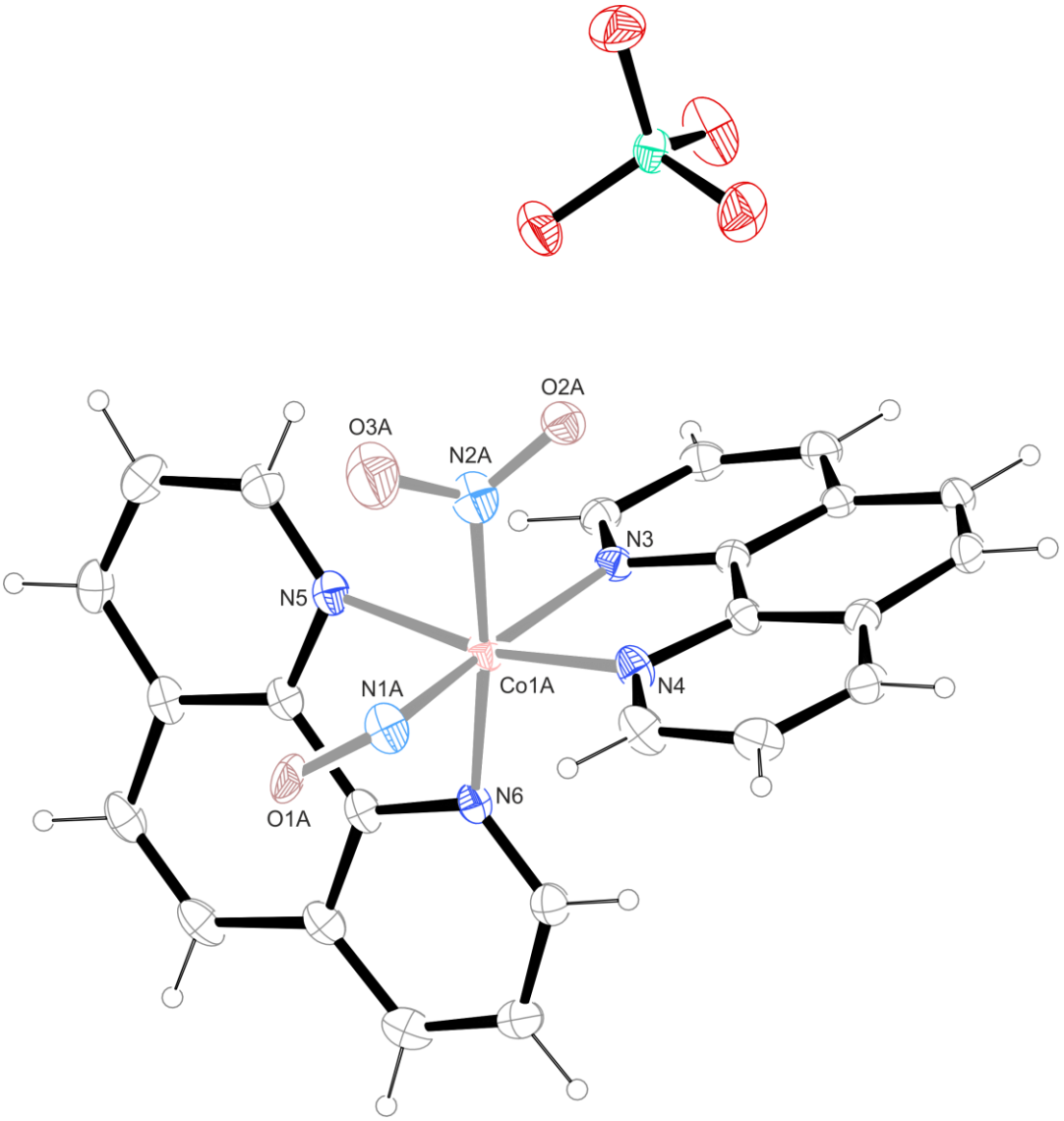

Figure 7.59: ORTEP plot of the minor disorder form (20 %) of *rac-cis*-[Co(NO)(NO_2-κ*N*)(phen)$_2$]ClO_4 in crystals of **7a**. For clarity, only the Δ enantiomer is depicted. Atoms and bonds affected by the disorder are depicted in light colors. For the major form, see Figure 2.62. Thermal ellipsoids drawn at 50 % probability level at 101 K. Interatomic distances (Å) and bond angles (°) with the standard deviation of the last decimal digit given in parentheses: Co1A–N1A 1.886(2), Co1A–N2A 1.921(2), Co1A–N3 2.119(1), Co1A–N4 1.879(1), Co1A–N5 2.058(1), Co1A–N6 1.894(1), N1A–O1A 1.196(4), N2A–O2A 1.240(5), N2A–O3A 1.252(2), Co1A–N1A–O1A 117.5(2), N1A–Co1A–N6 90.8(6), Co1A–N2A–O2A 127.2(3), Co1A–N2A–O3A 118.2(1), O2A–N2A–O3A 114.1(3), N2A–Co1A–N3 90.9(7), N4–Co1A–N5 167.6(7), N2A–Co1A–N5 90.5(7), N3–Co1A–N4 81.6(5), N2A–Co1A–N4 80.1(7), N3–Co1A–N5 90.6(5), N1A–Co1A–N2A 85.9(9), N1A–Co1A–N3 172.6(9), N1A–Co1A–N4 91.2(8), N1A–Co1A–N5 96.2(8), N6–Co1A–N2A 173.7(1), N6–Co1A–N3 92.8(6), N6–Co1A–N4 105.6(7), N6–Co1A–N5 84.2(5). A plot of the complete asymmetric unit is given in Figure 7.60.

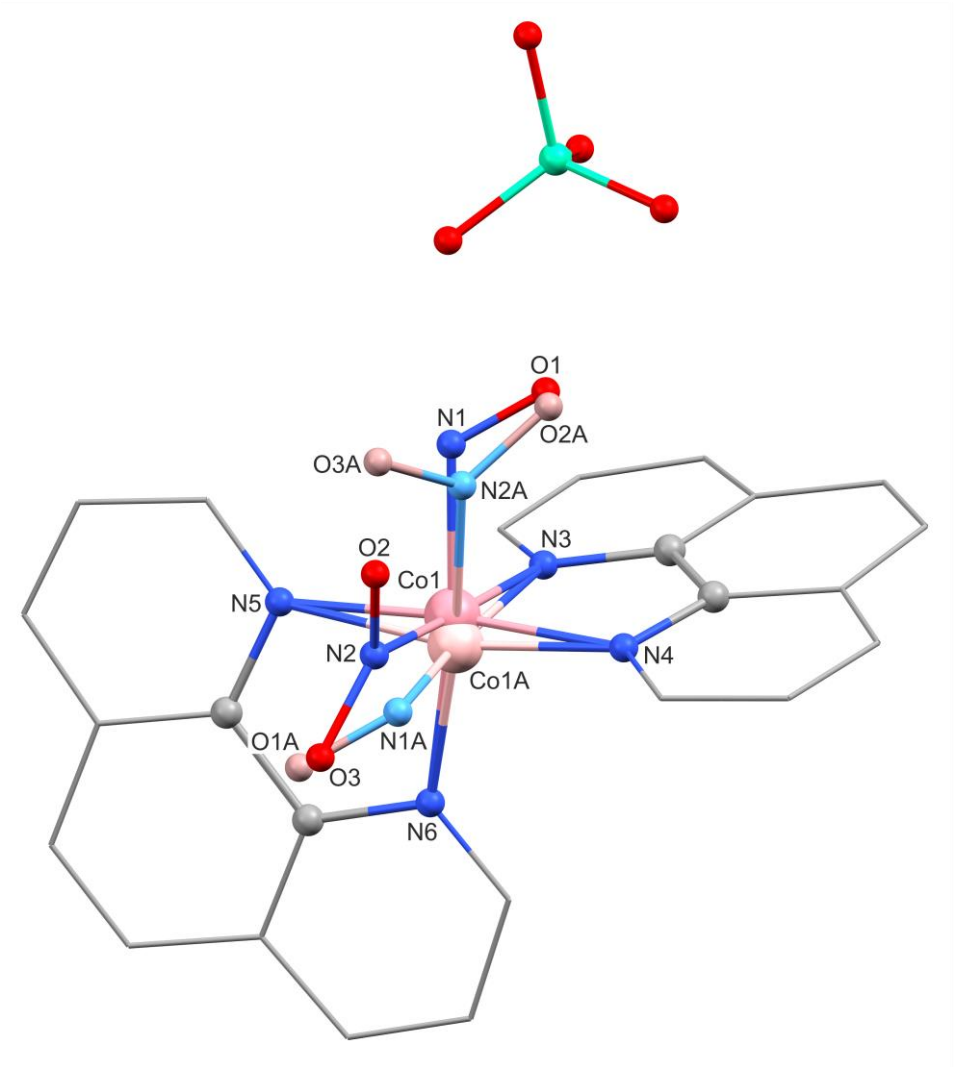

Figure 7.60: Plot of *rac-cis*-[Co(NO)(NO_2-κ*N*)(phen)$_2$]ClO_4 in crystals of **7a**. For clarity, hydrogen atoms are not depicted. Furthermore, only the Δ enantiomer is depicted and the outer backbone of the phenanthroline ligands is shown as wireframe. Disordered atoms and bonds of the minor form (20 %) are depicted in light colors. For a list of the interatomic distances and bond angles in the cationic complex entities, see Figure 2.62.

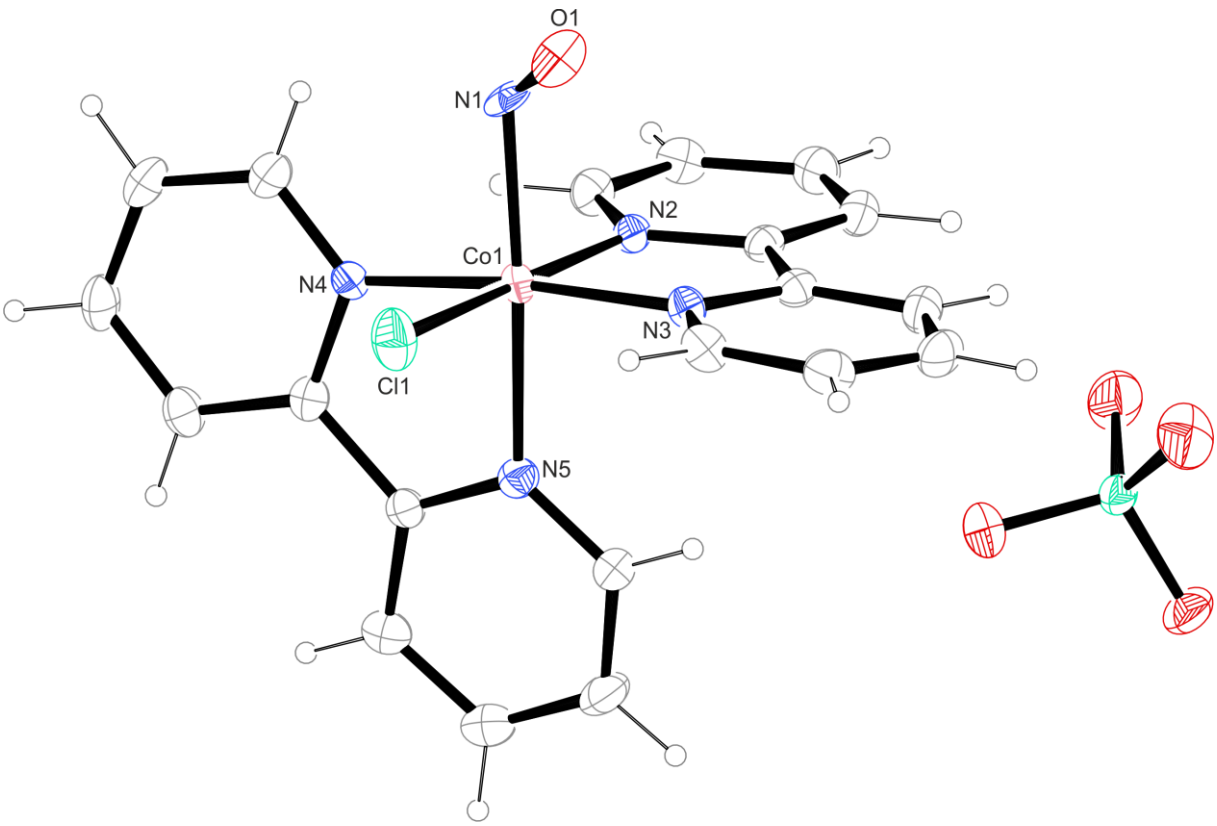

Figure 7.61: ORTEP plot of *rac-cis*-[Co(bpy)$_2$Cl(NO)]ClO$_4$. For the measurement, a crystal of the Δ enantiomer was selected. Thermal ellipsoids are drawn at 50 % probability level at 101 K. Crystallization procedure: A saturated solution (4.0 mL) of the bulk product (synthesized according to Vlček, but at room temperature)[119] in acetonitrile was added to one compartment of a two-chambered Schlenk tube filled with DMSO (7.5 mL) in the second chamber. The atmosphere was then changed to nitric oxide for crystallization. Due to the reproducible disorder of atom N1, causing the structure to fail the Hirshfeld rigid-bond test, [219,220] and the inability to define a precise composition by CHN analysis, this compound was excluded from the structural discussion presented in this thesis.

8 Bibliography

[1] M. W. G. De Bolster, *Pure Appl. Chem.* **1997**, *69*, 1251–1303.

[2] M. C. Etter, J. C. MacDonald, J. Bernstein, *Acta Cryst. B* **1990**, *46*, 256–262.

[3] J. Bernstein, R. E. Davis, *Implications of Molecular and Materials Structure for New Technologies*, Springer Science+Business Media, Dordrecht, **1999**, 275–290.

[4] P. Brimblecombe, D. H. Stedman, *Nature* **1982**, *298*, 460–462.

[5] B. Hileman, *Environ. Sci. Technol.* **1984**, *18*, 8A–10A.

[6] B. Hileman, *Environ. Sci. Technol.* **1984**, *18*, 341A–344A.

[7] P. Grennfelt, A. Engleryd, M. Forsius, Ø. Hov, H. Rodhe, E. Cowling, *Ambio* **2020**, *49*, 849–864.

[8] H. Ohshima, H. Bartsch, *Mutat. Res.* **1994**, *305*, 253–264.

[9] D. A. Wink, Y. Vodovotz, J. Laval, F. Laval, M. W. Dewhirst, J. B. Mitchell, *Carcinogenesis* **1998**, *19*, 711–721.

[10] P. J. Crutzen, *Quart. J. R. Met. Soc.* **1970**, *96*, 320–325.

[11] H. Johnston, *Science* **1971**, *173*, 517–522.

[12] P. J. Crutzen, *Ann. Rev. Earth Planet. Sci.* **1979**, *7*, 443–472.

[13] A. R. Ravishankara, J. S. Daniel, R. W. Portmann, *Science* **2009**, *326*, 123–125.

[14] J. Loscalzo, G. Welch, *Prog. Cardiovasc. Dis.* **1995**, *38*, 87–104.

[15] M. Houston, L. Hays, *J. Clin. Hypertens.* **2014**, *16*, 524–529.

[16] J. F. Kerwin, J. R. Lancaster, P. L. Feldman, *J. Med. Chem.* **1995**, *38*, 4343–4362.

[17] F. Murad, *Rambam Maimonides Med. J.* **2011**, *2*:e0038.

[18] C. Bogdan, *Nat. Immunol.* **2001**, *2*, 907–916.

[19] J. W. Coleman, *Int. Immunopharmacol.* **2001**, *1*, 1397–1406.

[20] Pa. Tripathi, Pr. Tripathi, L. Kashyap, V. Singh, *FEMS Immunol. Med. Microbiol.* **2007**, *51*, 443–452.

[21] R. Farias-Eisner, M. P. Sherman, E. Aeberhard, G. Chaudhuri, *Proc. Natl. Acad. Sci. USA* **1994**, *91*, 9407–9411.

[22] E. C. Brantley, L. Guo, C. Zhang, Q. Lin, K. Yokoi, R. R. Langley, E. Kruzel, M. Maya, S. W. Kim, S.-J. Kim, D. Fan, I. J. Fidler, *Transl. Oncol.* **2010**, *3*, 380–388.

[23] S. Korde Choudhari, M. Chaudhary, S. Bagde, A. R. Gadbail, V. Joshi, *World J. Surg. Oncol.* **2013**, *11*:118.

[24] D. E. Koshland, *Science* **1992**, *258*, 1861.

[25] E. Culotta, D. E. Koshland, *Science* **1992**, *258*, 1862–1865.

[26] https://www.nitricoxidesociety.org (visited on 24.03.2023).

[27] https://www.nobelprize.org/prizes/medicine/1998/summary/ (visited on 24.03.2023).

[28] A. F. Holleman, E. Wiberg, N. Wiberg, *Lehrbuch der Anorganischen Chemie*, 102nd Edition, Walter de Gruyter, Berlin · New York, **2007**, 707–712.

[29] J. R. Hickok, D. Vasudevan, G. R. J. Thatcher, D. D. Thomas, *Antioxid. Redox Signal.* **2012**, *17*, 962–968.

[30] H. L. Wong, S. E. Murphy, M. Wang, S. S. Hecht, *Carcinogenesis* **2003**, *24*, 291–300.

[31] I. G. Zacharia, W. M. Deen, *Ann. Biomed. Eng.* **2005**, *33*, 214–222.

[32] C. P. Smyth, K. B. McAlpine, *J. Chem. Phys.* **1933**, *1*, 60–61.

[33] B. M. Aas, Ph.D. thesis, Ludwig-Maximilians-Universität München, **2018**.

[34] J. A. McCleverty, *Chem. Rev.* **2004**, *104*, 403–418.

[35] C. Klixbüll Jørgensen, *Coord. Chem. Rev.* **1966**, *1*, 164–178.

[36] W. Kaim, B. Schwederski, *Coord. Chem. Rev.* **2010**, *254*, 1580–1588.

[37] S. Ganguly, A. Ghosh, *Acc. Chem. Res.* **2019**, *52*, 2003–2014.

[38] J. H. Enemark, R. D. Feltham, *Coord. Chem. Rev.* **1974**, *13*, 339–406.

[39] F. Roncaroli, M. Videla, L. D. Slep, J. A. Olabe, *Coord. Chem. Rev.* **2007**, *251*, 1903–1930.

[40] T. Mayer, H.-C. Böttcher, *Polyhedron* **2014**, *69*, 240–243.

[41] T. Nakajima, I. Shimizu, K. Kobayashi, Y. Wakatsuki, *Organometallics* **1998**, *17*, 262–269.

[42] H. Zöllner, W. Krasser, T. Woike, S. Haussühl, *Chem. Phys. Lett.* **1989**, *161*, 497–501.

[43] H. Zöllner, T. Woike, W. Krasser, S. Haussühl, *Z. Kristallogr.* **1989**, *188*, 139–153.

[44] D. V. Fomitchev, I. Novozhilova, P. Coppens, *Tetrahedron* **2000**, *56*, 6813–6820.

[45] P. Coppens, I. Novozhilova, A. Kovalevsky, *Chem. Rev.* **2002**, *102*, 861–883.

[46] U. Hauser, V. Oestreich, H. D. Rohrweck, *Z. Physik A* **1977**, *280*, 17–25.

[47] U. Hauser, V. Oestreich, H. D. Rohrweck, *Z. Physik A* **1977**, *280*, 125–130.

[48] D. Schaniel, T. Woike, L. Tsankov, M. Imlau, *Thermochim. Acta* **2005**, *429*, 19–23.

[49] D. Schaniel, T. Woike, B. Delley, D. Biner, K. W. Krämer, H.-U. Güdel, *Phys. Chem. Chem. Phys.* **2007**, *9*, 5149–5157.

[50] I. Stepanenko, M. Zalibera, D. Schaniel, J. Telser, V. B. Arion, *Dalton Trans.* **2022**, *51*, 5367–5393.

[51] F. Murad, *Angew. Chem. Int. Ed.* **1999**, *38*, 1856–1868.

[52] R. F. Furchgott, *Angew. Chem. Int. Ed.* **1999**, *38*, 1870–1880.

[53] L. J. Ignarro, *Angew. Chem. Int. Ed.* **1999**, *38*, 1882–1892.

[54] S. Khatua, A. Majumdar, *J. Inorg. Biochem.* **2015**, *142*, 145–153.

[55] P. Picón-Pagès, J. Garcia-Buendia, F. J. Muñoz, *Biochim. Biophys. Acta Mol. Basis Dis.* **2019**, *1865*, 1949–1967.

[56] V. B. O'Donnell, B. A. Freeman, *Circ. Res.* **2001**, *88*, 12–21.

[57] R. Ahmad, Z. Rasheed, H. Ahsan, *Immunopharmacol. Immunotoxicol.* **2009**, *31*, 388–396.

[58] K. L. Salguero, J. J. Cummings, *Pulm. Pharmacol. Ther.* **2002**, *15*, 1–5.

[59] D. B. Graham, G. J. Jasso, A. Mok, G. Goel, A. C. Y. Ng, R. Kolde, M. Varma, J. G. Doench, D. E. Root, C. B. Clish, S. A. Carr, R. J. Xavier, *Cell Rep.* **2018**, *24*, 838–850.

[60] Y. Kobayashi, *J. Leukoc. Biol.* **2010**, *88*, 1157–1162.

[61] F. H. Khan, E. Dervan, D. D. Bhattacharyya, J. D. McAuliffe, K. M. Miranda, S. A. Glynn, *Int. J. Mol. Sci.* **2020**, *21*:9393.

[62] J. L. Caulfield, J. S. Wishnok, S. R. Tannenbaum, *J. Biol. Chem.* **1998**, *273*, 12689–12695.

[63] V. Labet, A. Grand, C. Morell, J. Cadet, L. A. Eriksson, *Phys. Chem. Chem. Phys.* **2009**, *11*, 2379–2386.

[64] P. Cabrales, J. M. Friedman, *Antioxid. Redox Signal.* **2013**, *18*, 2284–2297.

[65] J. R. Lancaster, *Future Sci. OA* **2015**, *1*:FSO59.

[66] R. Pacelli, D. A. Wink, J. A. Cook, M. C. Krishna, W. DeGraff, N. Friedman, M. Tsokos, A. Samuni, J. B. Mitchell, *J. Exp. Med.* **1995**, *182*, 1469–1479.

[67] J. Jones-Carson, A. Yahashiri, J.-S. Kim, L. Liu, L. F. Fitzsimmons, D. S. Weiss, A. Vázquez-Torres, *Sci. Adv.* **2020**, *6*:eaaz0260.

[68] K. Nakahara, T. Tanimoto, K. Hatano, K. Usuda, H. Shoun, *J. Biol. Chem.* **1993**, *268*, 8350–8355.

[69] D. M. Kurtz, *Dalton Trans.* **2007**, 4115–4121.

[70] P. van der Maas, L. Harmsen, S. Weelink, B. Klapwijk, P. Lens, *J. Chem. Technol. Biotechnol.* **2004**, *79*, 835–841.

[71] C. de Salas, M. R. Heinrich, *Green Chem.* **2014**, *16*, 2982–2987.

[72] Z. Hu, H. J. C. T. Wessels, T. van Alen, M. S. M. Jetten, B. Kartal, *Nat. Commun.* **2019**, *10*:1244.

[73] B. Kartal, N. M. de Almeida, W. J. Maalcke, H. J. M. Op den Camp, M. S. M. Jetten, J. T. Keltjens, *FEMS Microbiol. Rev.* **2013**, *37*, 428–461.

[74] D. E. Canfield, A. N. Glazer, P. G. Falkowski, *Science* **2010**, *330*, 192–196.

[75] N. Verma, S. Tiwari, V. P. Singh, S. M. Prasad, *Plant Growth Regul.* **2020**, *90*, 1–13.

[76] A. Weichsel, J. F. Andersen, D. E. Champagne, F. A. Walker, W. R. Montfort, *Nat. Struct. Biol.* **1998**, *5*, 304–309.

[77] M. A. Rhine Walter, Ph.D. thesis, University of Georgia, **2016**.

[78] C. S. Pratt, B. A. Coyle, J. A. Ibers, *J. Chem. Soc. A* **1971**, 2146–2151.

[79] D. A. Snyder, D. L. Weaver, *Inorg. Chem.* **1970**, *9*, 2760–2767.

[80] P. L. Johnson, J. H. Enemark, R. D. Feltham, K. Bizot Swedo, *Inorg. Chem.* **1976**, *15*, 2989–2993.

[81] O. Alnaji, Y. Peres, M. Dartiguenave, F. Dahan, Y. Dartiguenave, *Inorg. Chim. Acta* **1986**, *114*, 151–158.

[82] J. H. Enemark, R. D. Feltham, J. Riker-Nappier, K. F. Bizot, *Inorg. Chem.* **1975**, *14*, 624–632.

[83] H. J. B. Marroux, B. F. E. Curchod, C. A. Faradji, T. A. Shuttleworth, H. A. Sparkes, P. G. Pringle, A. J. Orr-Ewing, *Angew. Chem. Int. Ed.* **2017**, *56*, 13713–13716.

[84] E. P. Bertin, S. Mizushima, T. J. Lane, J. V. Quagliano, *J. Am. Chem. Soc.* **1959**, *81*, 3821–3823.

[85] R. D. Feltham, R. S. Nyholm, *Inorg. Chem.* **1965**, *4*, 1334–1339.

[86] P. Kumar, Y.-M. Lee, Y. J. Park, M. A. Siegler, K. D. Karlin, W. Nam, *J. Am. Chem. Soc.* **2015**, *137*, 4284–4287.

[87] A. K. Patra, K. S. Dube, B. C. Sanders, G. C. Papaefthymiou, J. Conradie, A. Ghosh, T. C. Harrop, *Chem. Sci.* **2012**, *3*, 364–369.

[88] M. Tamaki, I. Masuda, K. Shinra, *Bull. Chem. Soc. Jpn.* **1972**, *45*, 171–174.

[89] U. Englert, J. Strähle, *Gazz. Chim. Ital.* **1988**, *118*, 845–855.

[90] C. Uyeda, J. C. Peters, *J. Am. Chem. Soc.* **2013**, *135*, 12023–12031.

[91] K. J. Franz, L. H. Doerrer, B. Spingler, S. J. Lippard, *Inorg. Chem.* **2001**, *40*, 3774–3780.

[92] W. R. Scheidt, J. L. Hoard, *J. Am. Chem. Soc.* **1973**, *95*, 8281–8288.

[93] C. J. Groombridge, L. F. Larkworthy, A. Marécaux, D. C. Povey, G. W. Smith, J. Mason, *J. Chem. Soc., Dalton Trans.* **1992**, 3125–3131.

[94] J. Popp, T. Riggenmann, D. Schröder, T. Ampßler, P. Salvador, P. Klüfers, *Inorg. Chem.* **2021**, *60*, 15980–15996.

[95] T. Riggenmann, private communication, Ludwig-Maximilians-Universität München, **2020**.

[96] J. L. Hess, H. L. Conder, K. N. Green, M. Y. Darensbourg, *Inorg. Chem.* **2008**, *47*, 2056–2063.

[97] R. Nast, H. Bier, *Chem. Ber.* **1959**, *92*, 1858–1863.

[98] U. Englert, J. Strähle, *Z. Naturforsch. B* **1987**, *42*, 959–966.

[99] T. Ampßler, G. Monsch, J. Popp, T. Riggenmann, P. Salvador, D. Schröder, P. Klüfers, *Angew. Chem. Int. Ed.* **2020**, *59*, 12381–12386.

[100] J. H. Enemark, R. D. Feltham, *J. Chem. Soc., Dalton Trans.* **1972**, 718–722.

[101] D. J. Hodgson, N. C. Payne, J. A. McGinnety, R. G. Pearson, J. A. Ibers, *J. Am. Chem. Soc.* **1968**, *90*, 4486–4488.

[102] C. G. Pierpont, R. Eisenberg, *Inorg. Chem.* **1972**, *11*, 1088–1094.

[103] P. Karen, P. McArdle, J. Takats, *Pure Appl. Chem.* **2014**, *86*, 1017–1081.

[104] A. C. Cabelof, V. Carta, C.-H. Chen, K. G. Caulton, *Dalton Trans.* **2020**, *49*, 7891–7896.

[105] D. Hall, A. A. Taggart, *J. Chem. Soc.* **1965**, 1359–1363.

[106] D. Dale, D. Crowfoot Hodgkin, *J. Chem. Soc.* **1965**, 1364–1371.

[107] P. Karen, *Angew. Chem. Int. Ed.* **2015**, *54*, 4716–4726.

[108] P. Karen, P. McArdle, J. Takats, *Pure Appl. Chem.* **2016**, *88*, 831–839.

[109] A. Del Zotto, A. Mezzetti, P. Rigo, *Inorg. Chim. Acta* **1990**, *171*, 61–69.

[110] S. Alvarez, P. Alemany, D. Casanova, J. Cirera, M. Llunell, D. Avnir, *Coord. Chem. Rev.* **2005**, *249*, 1693–1708.

[111] S. Alvarez, M. Llunell, *J. Chem. Soc., Dalton Trans.* **2000**, 3288–3303.

[112] S. Alvarez, J. Cirera, *Angew. Chem. Int. Ed.* **2006**, *45*, 3012–3020.

[113] S. Alvarez, *Eur. J. Inorg. Chem.* **2021**, 3632–3647.

[114] T. Bianco, M. Rossi, L. Uva, *Inorg. Chim. Acta* **1969**, *3*, 443–446.

[115] G. Booth, J. Chatt, *J. Chem. Soc.* **1962**, 2099–2106.

[116] W. Hieber, K. Heinicke, *Z. Anorg. Allg. Chem.* **1962**, *316*, 305–320.

[117] J. P. Collman, P. H. Farnham, G. Dolcetti, *J. Am. Chem. Soc.* **1971**, *93*, 1788–1790.

[118] C. Pratt Brock, J. P. Collman, G. Dolcetti, P. H. Farnham, J. A. Ibers, J. E. Lester, C. A. Reed, *Inorg. Chem.* **1973**, *12*, 1304–1313.

[119] A. Vlček, A. A. Vlček, *Inorg. Chim. Acta* **1974**, *9*, 165–170.

[120] D. B. Soria, M. E. Chacón Villalba, O. E. Piro, P. J. Aymonino, *Polyhedron* **2002**, *21*, 1767–1774.

[121] S. Ohba, M. Tsuchimoto, S. Kurachi, *Acta Cryst. E* **2018**, *74*, 1526–1531.

[122] Y. Sun, Y. Guo, D. Sun, M. Zhu, F. Ding, Y. Liu, E. Gao, S. Wang, G. Xiong, I. Dragutan, V. Dragutan, *Eur. J. Inorg. Chem.* **2014**, 5741–5751.

[123] Z.-H. Liu, J.-J. Zhang, W.-J. Zhang, *Inorg. Chim. Acta* **2006**, *359*, 519–524.

[124] C. Neumann, private communication, Ludwig-Maximilians-Universität München, **2021**.

[125] J.-L. Roustan, N. Ansari, Y. Le Page, J.-P. Charland, *Can. J. Chem.* **1992**, *70*, 1650–1657.

[126] S. A. Hilderbrand, S. J. Lippard, *Inorg. Chem.* **2004**, *43*, 5294–5301.

[127] A. G. Tennyson, S. Dhar, S. J. Lippard, *J. Am. Chem. Soc.* **2008**, *130*, 15087–15098.

[128] Z. J. Tonzetich, F. Héroguel, L. H. Do, S. J. Lippard, *Inorg. Chem.* **2011**, *50*, 1570–1579.

[129] H. Kurihara, A. Ohta, K. Fujisawa, *Inorganics* **2019**, *7*:116.

[130] A. M. Wright, G. Wu, T. W. Hayton, *J. Am. Chem. Soc.* **2012**, *134*, 9930–9933.

[131] N. Arulsamy, D. S. Bohle, J. A. Imonigie, S. Levine, *Angew. Chem. Int. Ed.* **2002**, *41*, 2371–2373.

[132] S. Bhaduri, B. F. G. Johnson, A. Pickard, P. R. Raithby, G. M. Sheldrick, C. I. Zuccaro, *J. Chem. Soc., Chem. Commun.* **1977**, 354–355.

[133] N. Arulsamy, D. S. Bohle, J. A. Imonigie, R. C. Moore, *Polyhedron* **2007**, *26*, 4737–4745.

[134] F. Weigend, R. Ahlrichs, *Phys. Chem. Chem. Phys.* **2005**, *7*, 3297–3305.

[135] F. Weigend, *Phys. Chem. Chem. Phys.* **2006**, *8*, 1057–1065.

[136] S. Grimme, J. Antony, S. Ehrlich, H. Krieg, *J. Chem. Phys.* **2010**, *132*:154104.

[137] S. Grimme, S. Ehrlich, L. Goerigk, *J. Comput. Chem.* **2011**, *32*, 1456–1465.

[138] E. Caldeweyher, S. Ehlert, A. Hansen, H. Neugebauer, S. Spicher, C. Bannwarth, S. Grimme, *J. Chem. Phys.* **2019**, *150*:154122.

[139] V. Barone, M. Cossi, *J. Phys. Chem. A* **1998**, *102*, 1995–2001.

[140] F. Neese, F. Wennmohs, A. Hansen, U. Becker, *Chem. Phys.* **2009**, *356*, 98–109.

[141] E. van Lenthe, E. J. Baerends, J. G. Snijders, *J. Chem. Phys.* **1993**, *99*, 4597–4610.

[142] E. van Lenthe, E. J. Baerends, J. G. Snijders, *J. Chem. Phys.* **1994**, *101*, 9783–9792.

[143] J. D. Rolfes, F. Neese, D. A. Pantazis, *J. Comput. Chem.* **2020**, *41*, 1842–1849.

[144] F. Cortés-Guzmán, R. F. W. Bader, *Coord. Chem. Rev.* **2005**, *249*, 633–662.

[145] P. Salvador, E. Ramos-Cordoba, *J. Chem. Phys.* **2013**, *139*:071103.

[146] E. Ramos-Cordoba, V. Postils, P. Salvador, *J. Chem. Theory Comput.* **2015**, *11*, 1501–1508.

[147] I. Mayer, *J. Phys. Chem.* **1996**, *100*, 6249–6257.

[148] V. Postils, C. Delgado-Alonso, J. M. Luis, P. Salvador, *Angew. Chem. Int. Ed.* **2018**, *57*, 10525–10529.

[149] D. Gwost, K. G. Caulton, *Inorg. Chem.* **1973**, *12*, 2095–2099.

[150] D. Gwost, K. G. Caulton, *J. Chem. Soc., Chem. Commun.* **1973**, 64a.

[151] A. In-Iam, M. Wolf, C. Wilfer, D. Schaniel, T. Woike, P. Klüfers, *Chem. Eur. J.* **2019**, *25*, 1304–1325.

[152] T. B. Jackson, M. Jane Baker, J. O. Edwards, D. Tutas, *Inorg. Chem.* **1966**, *5*, 2046–2048.

[153] J. A. Kaduk, J. A. Ibers, *Inorg. Chem.* **1977**, *16*, 3283–3287.

[154] T. S. Piper, R. S. Drago, *J. Chem. Phys.* **1962**, *36*, 241–242.

[155] M. Hippler, J. Pfab, *J. Chem. Soc., Faraday Trans.* **1992**, *88*, 2109–2110.

[156] D. Cremer, E. Kraka, *Angew. Chem. Int. Ed. Engl.* **1984**, *23*, 627–628.

[157] N. V. Cherkashina, S. E. Nefedov, M. A. Uvarova, A. P. Klyagina, A. A. Markov, M. N. Vargaftik, I. I. Moiseev, *Russ. J. Inorg. Chem.* **2014**, *59*, 446–454.

[158] B. R. Clare, C. S. McInnes, A. G. Blackman, *Acta Cryst. E* **2005**, *61*, m2042–m2043.

[159] V. Maheshwari, M. Carlone, F. R. Fronczek, L. G. Marzilli, *Acta Cryst. B* **2007**, *63*, 603–611.

[160] E. C. Constable, C. E. Housecroft, M. Neuburger, P. J. Rösel, S. Schaffner, *Dalton Trans.* **2009**, 4918–4927.

[161] A. Hazell, *Polyhedron* **2004**, *23*, 2081–2083.

[162] A. M. Wright, T. W. Hayton, *Inorg. Chem.* **2015**, *54*, 9330–9341.

[163] D. S. P. Beck, P. Klüfers, *Chem. Eur. J.* **2018**, *24*, 16019–16028.

[164] D. B. Chesnut, *J. Phys. Chem. A* **2000**, *104*, 11644–11650.

[165] B. F. Hoskins, F. D. Whillans, D. H. Dale, D. Crowfoot Hodgkin, *J. Chem. Soc. D* **1969**, 69–70.

[166] B. F. Hoskins, F. D. Whillans, *J. Chem. Soc., Dalton Trans.* **1973**, 607–611.

[167] A. M. Wright, H. T. Zaman, G. Wu, T. W. Hayton, *Inorg. Chem.* **2014**, *53*, 3108–3116.

[168] J. H. Enemark, R. D. Feltham, *Proc. Natl. Acad. Sci. USA* **1972**, *69*, 3534–3536.

[169] J. Popp, P. Klüfers, *Eur. J. Inorg. Chem.* **2022**:e202200374.

[170] J. Chatt, L. A. Duncanson, *J. Chem. Soc.* **1953**, 2939–2947.

[171] D. M. P. Mingos, *J. Organomet. Chem.* **2001**, *635*, 1–8.

[172] G. Frenking, N. Fröhlich, *Chem. Rev.* **2000**, *100*, 717–774.

[173] G. Frenking, I. Fernández, N. Holzmann, S. Pan, I. Krossing, M. Zhou, *JACS Au* **2021**, *1*, 623–645.

[174] E. Kraka, W. Zou, Y. Tao, *WIREs Comput. Mol. Sci.* **2020**, *10*:e1480.

[175] A. S. Goldman, K. Krogh-Jespersen, *J. Am. Chem. Soc.* **1996**, *118*, 12159–12166.

[176] A. J. Lupinetti, S. Fau, G. Frenking, S. H. Strauss, *J. Phys. Chem. A* **1997**, *101*, 9551–9559.

[177] R. J. B. Kalescky, E. Kraka, D. Cremer, *J. Phys. Chem. A* **2013**, *117*, 8981–8995.

[178] J. H. Enemark, R. D. Feltham, *J. Am. Chem. Soc.* **1974**, *96*, 5002–5004.

[179] J. H. Enemark, R. D. Feltham, *J. Am. Chem. Soc.* **1974**, *96*, 5004–5005.

[180] R. D. Feltham, J. H. Enemark, *Theoret. Chim. Acta (Berl.)* **1974**, *34*, 165–167.

[181] K. H. Hopmann, J. Conradie, E. Tangen, Z. J. Tonzetich, S. J. Lippard, A. Ghosh, *Inorg. Chem.* **2015**, *54*, 7362–7367.

[182] S. Tanaka, H. Imoto, T. Kato, K. Naka, *Dalton Trans.* **2016**, *45*, 7937–7940.

[183] H. Imoto, M. Konishi, S. Nishiyama, H. Sasaki, S. Tanaka, T. Yumura, K. Naka, *Chem. Lett.* **2019**, *48*, 1312–1315.

[184] R. Kobayashi, T. Fujii, H. Imoto, K. Naka, *Eur. J. Inorg. Chem.* **2021**, 217–222.

[185] Y. Tanabe, S. Kuriyama, K. Arashiba, Y. Miyake, K. Nakajima, Y. Nishibayashi, *Chem. Commun.* **2013**, *49*, 9290–9292.

[186] A. K. Brisdon, C. J. Herbert, *Coord. Chem. Rev.* **2013**, *257*, 880–901.

[187] J. K. Elinburg, L. H. Doerrer, *Polyhedron* **2020**, *190*:114765.

[188] C. B. Ungermann, K. G. Caulton, *J. Am. Chem. Soc.* **1976**, *98*, 3862–3868.

[189] M. P. Doyle, F. J. van Doornik, C. L. Funckes, *Inorg. Chim. Acta* **1980**, *46*, L111–L113.

[190] M. P. Doyle, R. A. Pickering, R. L. Dykstra, B. R. Cook, *J. Am. Chem. Soc.* **1982**, *104*, 3392–3397.

[191] P. Kumar, Y.-M. Lee, L. Hu, J.-W. Chen, Y. J. Park, J. Yao, H. Chen, K. D. Karlin, W. Nam, *J. Am. Chem. Soc.* **2016**, *138*, 7753–7762.

[192] Z. Wei, Y. Wang, Y. Li, R. Ferraccioli, Q. Liu, *Organometallics* **2020**, *39*, 3082–3087.

[193] L. N. Mendelsohn, C. S. MacNeil, L. Tian, Y. Park, G. D. Scholes, P. J. Chirik, *ACS Catal.* **2021**, *11*, 1351–1360.

[194] Y. Jiang, B. Schirmer, O. Blacque, T. Fox, S. Grimme, H. Berke, *J. Am. Chem. Soc.* **2013**, *135*, 4088–4102.

[195] K. M. Miranda, *Coord. Chem. Rev.* **2005**, *249*, 433–455.

[196] N. Paolocci, M. I. Jackson, B. E. Lopez, K. M. Miranda, C. G. Tocchetti, D. A. Wink, A. J. Hobbs, J. M. Fukuto, *Pharmacol. Ther.* **2007**, *113*, 442–458.

[197] J. C. Irvine, R. H. Ritchie, J. L. Favaloro, K. L. Andrews, R. E. Widdop, B. K. Kemp-Harper, *Trends Pharmacol. Sci.* **2008**, *29*, 601–608.

[198] M. A. Rhine, A. V. Rodrigues, R. J. Bieber Urbauer, J. L. Urbauer, T. L. Stemmler, T. C. Harrop, *J. Am. Chem. Soc.* **2014**, *136*, 12560–12563.

[199] T. Riggenmann, D. Schaniel, priv. communication, Ludwig-Maximilians-Universität München, Université de Lorraine, **2023**.

[200] P. G. Potvin, M. Knapp, U. Jordis, *JASPER – JavaScript Percentage Elemental Results Calculator (Version 2.0)*, https://www.yorku.ca/pgpotvin/public/Jasper/jasper2.htm, York University (visited on 24.03.2023).

[201] W. Kopycki, J. Binkowski, *Microchim. Acta* **1984**, *84*, 149–157.

[202] V. P. Fadeeva, V. D. Tikhova, O. N. Nikulicheva, *J. Anal. Chem.* **2008**, *63*, 1094–1106.

[203] JASCO Corp., *Spectra Manager (Version 2.07.00)*, **2002–2008**.

[204] Mettler-Toledo AutoChem Inc., *iC IR (Version 7.0.297)*, **2016**.

[205] G. M. Sheldrick, Bruker AXS Inc., *SADABS*, **2014**.

[206] Bruker AXS Inc., *APEX3*, **2016**.

[207] G. M. Sheldrick, *Acta Cryst. A* **2015**, *71*, 3–8.

[208] C. B. Hübschle, G. M. Sheldrick, B. Dittrich, *J. Appl. Cryst.* **2011**, *44*, 1281–1284.

[209] A. L. Spek, *J. Appl. Cryst.* **2003**, *36*, 7–13.

[210] A. L. Spek, *Acta Cryst. D* **2009**, *65*, 148–155.

[211] G. M. Sheldrick, *CELL_NOW (Version 2008/4)*, Georg-August-Universität Göttingen, **2008**.

[212] L. J. Farrugia, *J. Appl. Cryst.* **2012**, *45*, 849–854.

[213] C. F. Macrae, P. R. Edgington, P. McCabe, E. Pidcock, G. P. Shields, R. Taylor, M. Towler, J. van de Streek, *J. Appl. Cryst.* **2006**, *39*, 453–457.

[214] Persistence of Vision Pty. Ltd., *POVRay – Persistence of Vision Raytracer (V. 3.6.2)*, **1991–2009**.

[215] F. Neese, *WIREs Comput. Mol. Sci.* **2012**, *2*, 73–78.

[216] F. Neese, *WIREs Comput. Mol. Sci.* **2018**, *8*:e1327.

[217] T. Lu, F. Chen, *J. Comput. Chem.* **2012**, *33*, 580–592.

[218] L. D. Field, B. A. Messerle, M. Rehr, L. P. Soler, T. W. Hambley, *Organometallics* **2003**, *22*, 2387–2395.

[219] F. L. Hirshfeld, *Acta Cryst. A* **1976**, *32*, 239–244.

[220] R. E. Rosenfield, K. N. Trueblood, J. D. Dunitz, *Acta Cryst. A* **1978**, *34*, 828–829.

Publications

J. Popp, P. Klüfers: Bond Strength of a Diatomic Acceptor Ligand: A Reliable Measure of Its Antibond Occupation and Its Charge? (Front-Cover Paper), *Eur. J. Inorg. Chem.* **2022**:e202200374.

J. Popp, T. Riggenmann, D. Schröder, T. Ampßler, P. Salvador, P. Klüfers: Bent and Linear $\{CoNO\}^8$ Entities: Structure and Bonding in a Prototypic Class of Nitrosyls, *Inorg. Chem.* **2021**, *60*, 15980–15996.

T. Ampßler, G. Monsch, J. Popp, T. Riggenmann, P. Salvador, D. Schröder, P. Klüfers: Not Guilty on Every Count: The ''Non-Innocent'' Nitrosyl Ligand in the Framework of IUPAC's Oxidation-State Formalism, *Angew. Chem. Int. Ed.* **2020**, *59*, 12381–12386.

Danksagung

An dieser Stelle möchte ich mich bei allen Leuten bedanken, die mich im Laufe meiner Promotion begleitet und unterstützt haben und ohne die diese Arbeit nicht möglich gewesen wäre:

Zunächst danke ich besonders meinem Doktorvater Prof. Dr. Peter Klüfers für die freundliche Aufnahme in seinen Arbeitskreis, die interessante Themenstellung sowie den gewährten großen wissenschaftlichen Freiraum und die ausgezeichneten Arbeitsbedingungen.

Herrn Prof. Dr. Hans-Christian Böttcher danke ich für die Erstellung des Zweitgutachtens sowie für seine stets herzliche und offene Art.

Prof. Dr. Thomas M. Klapötke, Prof. Dr. Andreas Kornath, Prof. Dr. Wolfgang Schnick und Prof. Dr. Silvija Markic möchte ich für ihr Mitwirken in der Promotionskommission danken.

Lida Holowatyj-den Toom und Annette Rogge danke ich für ihre unermüdliche Hilfe bei allen organisatorischen Dingen und ihre immer positive, besonnene Art. Ein besonderer Dank geht an Lida für die sprachliche Korrektur dieser Arbeit.

Christine Neumann danke ich für die stetige Versorgung mit Schlenkrohren und anderen Glasgeräten, ihre wertvollen Ratschläge zu chemischen Arbeitstechniken und unzählige Chemikalienbestellungen.

Dr. Peter Mayer und Dr. Jan Heinemann danke ich für das Messen meiner Kristalle und ihre stete Hilfsbereitschaft, wenn Probleme beim Lösen von Kristallstrukturen auftraten.

Den AK-Admins Dr. Georg Monsch und Torsten Ampßler sowie Philipp Maier (AK Ivanović-Burmazović) danke ich für die Einrichtung meines PCs, die Installation von funktionierendem WLAN im Labor und ihre Hilfe bei allerlei IT-Problemen, die im Laufe der Jahre aufgetreten sind.

Dem Analytik-Team der Fakultät möchte ich für das Messen meiner Proben danken. Weiterhin danke ich meinen AC3-Praktikanten für ihre fleißige und gewissenhafte Mitarbeit.

Darüber hinaus möchte ich meinen Laborkollegen (von denen es über die Jahre doch einige geworden sind) für die gute Zusammenarbeit und stets lustige Arbeitsatmosphäre danken. In chronologischer Reihenfolge: Dr. Martin Oßberger, Dr. Daniel Beck, Christine Neumann, Dr. Jan Heinemann, Torsten Ampßler und Daniel Schröder sowie Christian Wilhelm, Peter Stahl und Joel Stegmaier vom Arbeitskreis Ivanović-Burmazović. Ein extra ''Danke'' an Dani und Christine für die Unterstützung während meiner Masterarbeit, die mir den Einstand im AK Klüfers wesentlich erleichtert hat.

Des Weiteren möchte ich ganz besonders Jan, Torsten und Daniel danken, mit denen ich zusammen den ''letzten Rest'' des AK Klüfers bilden durfte. Daniel danke ich hierbei insbesondere für die unzähligen quanten-chemischen Rechnungen zu meinen Verbindungen und für das geduldige Erklären von theoretisch-chemischen Sachverhalten (und das gemeinsame Lachen über diese). Torsten danke ich für seine zahlreichen Ratschläge zu finanziellen Themen und seine Ausführungen zu deutschen Verkehrsregeln – ich bin mir sicher, dass ich durch deine Weisheiten irgendwann einmal viel Geld sparen werde! Jan danke ich für den regen Austausch von gewissen Memes, die vielen Unterhaltungen über den einzig wahren Radiosender und die Kneipen-Abende in Obersendling. Vielen Dank auch für das sorgfältige Korrekturlesen meiner Arbeit. Ich hoffe, dass da auch in Zukunft mit euch immer noch ein bisschen was gehen wird!

Ich danke allen Mitgliedern des AK Klüfers, die mich während meiner Promotion begleitet haben, für die hilfsbereite und freundschaftliche Atmosphäre und auch für die schöne Zeit außerhalb des Labors. Die vielen Abende in der Kaffeeküche, Feierabend-Biere sowie die zahlreichen Exkursionen zu Biergärten, Hütten und Tanzlokalen werden mir in sehr guter Erinnerung bleiben. Neben dem ''Rest'' geht ein besonderer Dank dabei auch an Dr. Areenan In-Iam, Dr. Daniel Beck, Dr. Sebastian Brück und Tobias Riggenmann sowie an das AK-Ehrenmitglied Luca Rieder.

Ebenso möchte ich mich herzlich bei den Mitgliedern des AK Ivanović-Burmazović bedanken, die mich als Nachfolger vom AK Klüfers am Ende meiner Promotion begleitet haben und mit denen ich noch eine schöne restliche Zeit an der Uni haben durfte. Ein besonderer Dank geht an meine späten Laborkollegen sowie an Julian Oppelt, Philipp Maier und Sebastian Preussger.

Meinen ehemaligen Kommilitonen Dr. Jürgen Mony und Dr. Florian Zoller danke ich für die schöne Studienzeit und die jahrelange Freundschaft. Die Zeit mit euch war immer der perfekte Ausgleich zu den stressigen Phasen des Studiums.

Dietlinde und Martin Obermaier danke ich für ihre jahrelange Unterstützung und dafür, dass sie mir geholfen haben, in Bayern heimisch zu werden. Vielen Dank für die schöne Zeit in Landshut!

Zuletzt möchte ich noch meiner Familie danken für ihre Unterstützung, allen voran meinen Eltern, die mir nicht nur während meines Studiums sehr geholfen haben. Ohne euch wäre vieles nicht möglich gewesen. Vielen Dank für alles!